TECHNISCHE
UNIVERSITÄT
DARMSTADT

Institute of Electrical Energy Conversion
Electrical Drive Systems

Energy Converters - CAD and System Dynamics

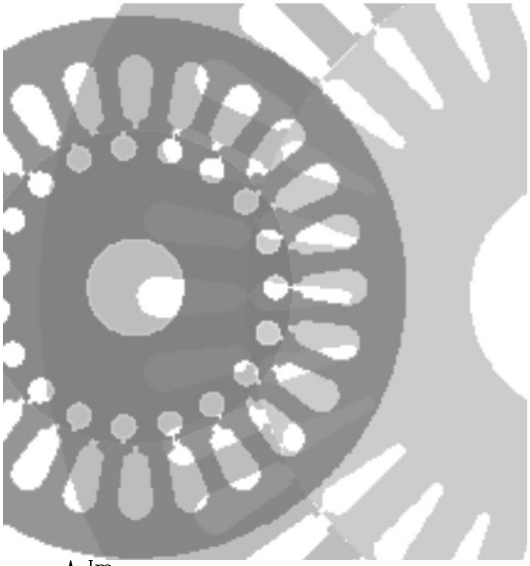

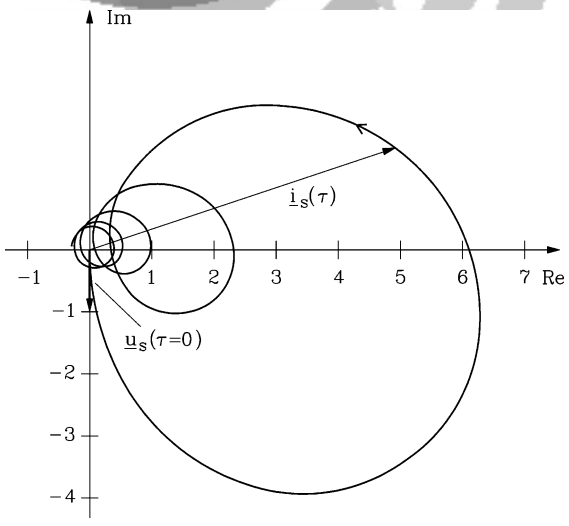

Prof. Dr.-Ing. Yves Burkhardt
Prof. Dr.-Ing. habil. Dr. h. c. Andreas Binder

Issue 2023/24

Dear student,

this text book provides you in detail with the contents of the lecture “Energy Converters - CAD and System Dynamics of Electrical Machines”. This text book is accompanied by the “Collection of Exercises”, which comprises the theoretical questions and calculation examples with detailed solutions for learning for the written exam. The exam comprises three examples and several theoretical questions.
We offer for these lectures in parallel a tutorial, where you get acquainted with calculating examples by hand and by computer software. Computer Aided Design (CAD) of electrical machines is done with the commercial, widely used program package of the SPEED group in UK and for dynamical calculations with the MATLAB/Simulink software. You get an introduction to both programs during the tutorial. Via two mini tests during that tutorial you can gather points, which may help you to get a better final mark. Further details concerning the examination please take from our internet home page or from the black board at our department.

The power point presentation of the lectures may be regarded as the essentials of this course and are a comprehensive “path” through the topics taught during that course. The power point presentation is available at our home page for down load. My assistants and I offer also consulting during our official hours. I do not have fixed official consulting hours. In the case you want to consult me, please make a date with my secretary.

We offer to you in addition to the lectures some experiments during the lecture break and an accompanying excursion to different companies in our vicinity. We invite you to make broad use of these interesting possibilities to get in contact with industry.

As modern CAD comprises also Finite Element methods for design and simulation, we offer a seminar course **“Design of electric machines and actuators with numerical field calculation”** on finite element calculations, where you solve after a short introduction practical tasks on the computer. If you are interested in that course, do not hesitate to contact us.

In case of further questions you are invited to contact our assistants or myself. We wish you good success in taking the main messages of these lectures and a good passing of your examinations.

Yours sincerely

A. Binder Darmstadt, January 2023

Head of Institute for
Electrical Energy Conversion

Contents

The Greek alphabet:

$A\,\alpha$	Alpha	$B\,\beta$	Beta	$\Gamma\,\gamma$	Gamma	$\Delta\,\delta$	Delta
$E\,\varepsilon$	Epsilon	$Z\,\zeta$	Zeta	$H\,\eta$	Eta	$\Theta\,\vartheta$	Theta
$I\,\iota$	Jota	$K\,\kappa$	Kappa	$\Lambda\,\lambda$	Lambda	$M\,\mu$	My (mue)
$N\,\nu$	Ny (nue)	$\Xi\,\xi$	Xi	$O\,o$	Omikron	$\Pi\,\pi$	Pi
$P\,\rho$	Rho	$\Sigma\,\sigma$	Sigma	$T\,\tau$	Tau	$Y\,\upsilon$	Ypsilon
$\Phi\,\varphi$	Phi	$X\,\chi$	Chi	$\Psi\,\psi$	Psi	$\Omega\,\omega$	Omega

Literature

In English:

Design:

[1.1] Fitzgerald, A.E.; Kingsley, C.; Umans, S.D.: Electric machinery, McGraw-Hill, 6th ed., 2003, Boston, USA

[1.2] Gieras, J.F.; Wing, M.: Permanent Magnet Motor Technology, Marcel Dekker, Inc., 2nd ed. 2002, New York, USA

[1.3] Matsch, L.W.: Electromagnetic and Electromechanical Machines, Intext Educational Publishers, Int. Textbook Comp., 1972, Scranton, USA

[1.4] Pyrhonen, J.; Jokinen, T.; Hrabovcova, V.: Design of Rotating Electrical Machines, Wiley, New York, 2009, USA

[1.5] Klempner, G.; Kerszenbaum, I.: Handbook of Large Turbo-Generator Operation and Maintenance, Wiley IEEE-Press, New York, 2008, USA

Dynamics:

[2.1] Adkins, B.: The general theory of Electrical machines, Advanced Engineering Textbooks, Chapman & Hall, 4th ed. 1964, UK

[2.2] Amin, B.: Induction machines – analysis and control, Springer, 2001, Berlin, Germany

[2.3] Boldea, I.; Nasar, S.A.: Electric Drives, CRC Press, 1999, Boca Raton, USA

[2.4] Finney, D.: Variable frequency AC motor drive systems, IEE Power Engineering Series 8, Peter Peregrinus Ltd., 1991, London, UK

[2.5] Jones, C.V.: The Unified Theory of Electrical Machines, Butterworths, 1967, London, UK

[2.6] Krause, P.C.; Wasynczuk, O.; Sudhoff, S.D.: Analysis of Electric machinery and Drive Systems, IEEE series on Power Engineering, John Wiley&Sons, Inc., 2002, USA

[2.7] Leonhard, W.: Control of Electric Drives, Springer, Berlin, 1997

[2.8] Meisel, J.: Pronciples of Electromechanical Energy Conversion, McGraw-Hill, 1966, New York, USA

In German:

Design:

[3.1] Bödefeld, Th.; Sequenz, H.: Elektrische Maschinen, Springer, Wien, 8. Auflage, 1971

[3.2] Böning, W. (Hrsg.) : Hütte – Elektrische Energietechnik – Band 1: Elektrische Maschinen, Springer, Berlin, 1978, 29. Auflage

[3.3] Bohn, Th. (Hrsg.) : Handbuchreihe Energie – Band 4: Elektrische Energietechnik, Verlag TÜV Rheinland, Köln, 1987

[3.4] Fischer, R. : Elektrische Maschinen, Hanser, München – Wien, 9. Auflage, 1995

[3.5] Gotter, G. : Erwärmung und Kühlung elektrischer Maschinen, Springer, Berlin, 1962

[3.6] Nürnberg, W.: Die Asynchronmaschine, Springer, Berlin, 1976

[3.7] Richter, R.; Prassler, H.: Elektrische Maschinen – Band 1: Allgemeine Berechnungselemente und die Gleichstrommaschine, Birkhäuser, Basel, 1967

[3.8] Richter, R.; Brüderlink, R.: Elektrische Maschinen - Band 2: Synchronmaschinen und Einankerumformer, Birkhäuser, Basel, 1963

[3.9] Richter, R. : Elektrische Maschinen – Band 3: Die Transformatoren, Birkhäuser, Basel, 1954

[3.10] Richter, R. : Elektrische Maschinen – Band 4: Die Induktionsmaschinen, Birkhäuser, Basel, 1954

[3.11] Richter, R. : Elektrische Maschine – Band 5: Stromwendermaschinen für ein- und mehrphasigen Wechselstrom, Springer, Berlin, 1950
[3.12] Schuisky, W.: Berechnung elektrischer Maschinen, Springer, Wien, 1960
[3.13] Sequenz, Heinrich (Hrsg.) : Herstellung der Wicklungen elektrischer Maschinen, Springer, Wien, 1973
[3.14] Vogt, K.: Berechnung elektrischer Maschinen, VCH Verlagsgesellschaft, Weinheim, 1996, (überarbeitete Neuauflage 2008: Vogt, K.; Müller, G.; Ponick, B.)
[3.15] Wiedemann, E.; Kellenberger, W.: Konstruktion elektrischer Maschinen, Springer, Berlin, 1967

Dynamics:

[4.1] Bühler, H.-R.: Einführung in die Theorie geregelter Drehstromantriebe, Band 1: Grundlagen, Birkhäuser, Basel, 1977
[4.2] Bühler, H.-R.: Einführung in die Theorie geregelter Drehstromantriebe, Band 2: Anwendungen, Birkhäuser, Basel, 1977
[4.3] Kleinrath, H.: Stromrichtergespeiste Drehfeldmaschinen, Springer, Wien, 1980
[4.4] Kovács, P.; Rácz, I.: Transiente Vorgänge in Wechselstrommaschinen, Verlag der Ungarischen Akademie der Wissenschaften, Budapest, 1959
[4.5] Laible, Th.: Die Theorie der Synchronmaschine im nichtstationären Betrieb, Springer, Berlin, 1952
[4.6] Schröder, D.: Elektrische Antriebe 1: Grundlagen, Springer, Berlin, 1994
[4.7] Späth, H.: Steuerverfahren für Drehstrommaschinen: Theoretische Grundlagen, Springer, Berlin, 1983
[4.8] Wehrmann, C.: Elektronische Antriebstechnik – Dimensionierung von Antrieben mit Mathcad, Vieweg, Braunschweig, 1995
[4.9] Schönfeld, R.; Habiger, E.: Automatisierte Elektroantriebe, Hüthig-Verlag, Heidelberg, 1981
[4.10] Binder, A.: Elektrische Maschinen und Antriebe, Springer, Berlin-Heidelberg, 2012
[4.11] Binder, A.: Elektrische Maschinen und Antriebe - Übungsbuch, Springer, Berlin-Heidelberg, 2012

List of symbols

a	-	number of parallel branches of winding in AC machines, BUT: Half of number of parallel branches of armature winding in DC machines
a_i	-	parallel wires per turn
A	A/m	current layer
A	m^2	area
b	m	breadth
b_p	m	pole width
B	T	magnetic flux density
c	J/(kg·K)	specific heat capacity
C	kVA·min/m^3	*Esson´*s number
C	m	length of integration loop
d_E	m	penetration depth
d_{si}	m	inner stator diameter
E	V/m	electric field strength
f	Hz	electric frequency
F	N	force
g	-	integer number
G_{th}	W/K	thermal conductance
h	m	height
H	A/m	magnetic field strength
i, I	A	electric current
i_f, I_f	A	field excitation current
i	-	per unit current
i	-	counting index
j	-	imaginary unit $\sqrt{-1}$
J	A/m^2	electric current density
J	kgm^2	polar momentum of inertia
k_C	-	*Carter´*s coefficient
k_d	-	distribution factor
k_f	-	slot fill factor, frequency coefficient
k_{Fe}	-	stack fill factor
k_L	-	average decrease of AC inductance
k_n	-	average increase of AC resistance of n conductors
k_p	-	pitch factor, increase of AC resistance of p^{th} conductor
k_R	-	average increase of AC resistance
k_w	-	winding factor
l	m	axial length
L	H	self inductance
L	m	overall length
L	s	life span
m	-	number of phases
m	-	per unit torque
m	kg	mass
M	Nm	torque
M_B	Nm	rated apparent torque
M_b	Nm	asynchronous break down torque
M_{p0}	Nm	synchronous pull out torque
M_s	Nm	shaft torque
M_1	Nm	starting torque

n	1/s	rotational speed
N	-	number of turns per phase
N_c	-	number of turns per coil
N_H	-	number of half oscillations for 95% damping
p	-	number of pole pairs
p	W/kg	power density
P	W	power
q	-	number of slots per pole and phase
q	W/m^2	heat flow density
Q	-	number of slots
r	-	ordinal number of radial force waves, per unit resistance
R	Ohm	electric resistance
R_{th}	K/W	thermal resistance
s	-	slip
s	1/s	*Laplace* operator
s	m	distance
s_Q	m	slot opening
S	VA	apparent power
t	s	time
t_B, t_{St}	s	operating time, stand still time
T	s	time constant, duration of period
T_J	s	starting time constant
T_ϑ	s	thermal time constant
T	K	absolute temperature
u, U	V	electric voltage
u	-	per unit voltage
u_R	V	reactance voltage of commutation
U_f	V	field excitation voltage
U_p	V	back EMF, synchronous generated voltage
$\ddot{u}_I$, $\ddot{u}_U$	-	current / voltage transforming ratio
v	m/s	velocity
v_{10}	W/kg	iron losses at 1.0 T, 50 Hz per 1 kg
v_{15}	W/kg	iron losses at 1.5 T, 50 Hz per 1 kg
V	A	magnetic voltage (m.m.f.)
V	m^3	volume
W	J	energy
W	m	coil width
x	m	circumference co-ordinate
x	-	per unit inductance
X	Ohm	reactance
X_d, X_q	Ohm	direct and quadrature reactance
z	-	total number of conductors
Z	Ohm	impedance
α	rad	firing angle
β	-	slot ripple coefficient
α_e	-	equivalent pole coverage ratio
α , α_k	W·s/m^2	heat transfer coefficient
α_Q	rad	slot angle
γ	rad	circumference angle
γ	kg/m^3	mass density

γ	1/s	inverse armature time constant ($1/T_a$)
δ	m	air gap width
δ	1/s	damping coefficient
η	-	efficiency
ϑ	°C	temperature
$\Delta\vartheta$	K	temperature rise
Θ	A	ampere turns
κ	S/m	electric conductivity
λ	-	"magnetic conductance"
λ_{th}	W/(m·K)	thermal conductivity
μ	-	ordinal number of rotor space harmonics
μ	Vs/(Am)	magnetic permeability
μ_0	Vs/(Am)	magnetic permeability of empty space ($4\pi \cdot 10^{-7}$ Vs/(Am))
ν	-	ordinal number of stator space harmonics
ξ	-	„reduced" conductor height
σ	-	leakage coefficient
σ_0	-	harmonic leakage coefficient
τ	N/m^2	tangential specific thrust
τ_Q, τ_s, τ_r	m	slot pitch (stator, rotor)
τ_p	m	pole pitch
φ	rad	phase angle
Φ	Wb	magnetic flux
ψ, Ψ	Vs	magnetic flux linkage
ω	1/s	electric angular frequency
ω_d	1/s	natural angular frequency ("eigen-frequency")
ω_m, Ω_m	1/s	mechanical angular frequency

Subscripts

a	outer, armature
ad	additional
av	average
amb	ambient
b	asynchronous break down, winding overhang (bobinage)
c	coil
crit	critical
Cu	copper
d	direct axis stator component, DC, distribution, dissipation, dental (tooth)
D	direct axis damper component
e	electric, equivalent
f	field
fr	friction
Fe	iron
Ft	*Foucault* losses (eddy current losses)
h	main-
Hy	hysteresis
i	induced, internal, inner
in	input
k	short circuit-, convective
K	cooling ducts

L	conductor (strand)
mag	magnetic
m	mechanical, magnetising,
max	maximum
N	rated
out	output
p	pole, pitch, synchronous pull-out
ph	phase value
q	quadrature axis stator component
Q	slot, quadrature axis damper component
r	rotor
s	stator
s	shaft
sh	sheet
sk	skew
syn	synchronous
St	stand-still
th	thermal, theoretical
y	yoke
w	winding, windage

δ	air gap
σ	leakage
0	no load, steady state, initial
1	starting ($s = 1$ with induction machine)
∞	infinite

Notation

i	small letters: instantaneous value (e.g.: electric current) or per unit value
I	capital letters: r.m.s. or DC value (e.g.: electric current)
X, x	capital letter: value in physical units e.g. reactance in Ω, small letter: per unit value
$\underline{I}$	underlined: complex values
$\hat{I}$	amplitude
I'	related to stator side winding
Re(.)	real part of ...
Im(.)	imaginary part of ...

German-English translation of important technical items

a	-	Anzahl paralleler Wicklungs-zweige bei Drehfeldmaschinen, aber: HALBE Anzahl paralleler Wicklungszweige bei Gleichstrom-maschinen	number of parallel winding branches of poly-phase machines, however: HALF of the number of parallel winding branches of dc machines
A	A/m	Strombelag	electric loading
A	m^2	Fläche	area
b_s, b_r	m	Nutbreite (Stator, Rotor)	slot width (stator, rotor)
b_p	m	Polschuhbreite	width of pole shoe
b_{Stab}	m	Stabbreite	width of bar
B	T	magnetische Induktion (Flussdichte)	magnetic induction (flux density)
c_d, c_q	-	Feldfaktoren der Längs-, Quer-achse	field factors of d-(direct) and q-(quadrature) axis
c_{ϑ}	Nm/rad	Ersatzfederkonstante der Synchronmaschine	equivalent spring constant of a synchronous machine
d_{si}	m	Bohrungsdurchmesser	bore diameter
D	As/m^2	elektrische Verschiebung (elektrische Flussdichte)	electric displacement (electric flux density)
E	V/m	elektrische Feldstärke	electric field strength
f	Hz	elektrische Frequenz	electric frequency
F	N	Kraft	force
g	-	ganze Zahl	integer
h	m	Höhe	height
H	A/m	magnetische Feldstärke	magnetic field strength
I	A	elektrische Stromstärke	electric current
j	-	imaginäre Einheit	imaginary unit
J	A/m^2	elektrische Stromdichte	electric current density
J	kgm^2	polares Trägheitsmoment	moment of inertia
k	-	Ordnungszahl	ordinal number
k_d	-	Zonenfaktor	distribution factor
k_K	-	Leerlauf-Kurzschluss-Verhältnis	no load - short circuit ratio
k_p	-	Sehnungsfaktor	pitch factor
k_R, k_L	-	Stromverdrängungsfaktoren	current displacement factors
k_R	$V \cdot s/A$	Proportionalitätskonstante der Reaktanzspannung	proportional constant of the reactance voltage
k_w	-	Wicklungsfaktor	winding factor
K	-	Anzahl der Kommutatorsegmente	number of collector segments
l	m	Länge (axial)	length (axial)
L	H	Selbstinduktivität	self inductance
m	-	Strangzahl	number of phases
M	H	Gegeninduktivität	mutual inductance
M	Nm	Drehmoment	torque
M_b	Nm	asynchrones Kippmoment	asynchronous breakdown torque
M_{p0}	Nm	synchrones statisches Kippmoment	synchronous, steady-state break-down torque
M_s	Nm	Kupplungsmoment, Wellenmoment	shaft torque

M_1	Nm	Anfahrmoment	breakaway torque
n	1/s	Drehzahl	motor speed
N	-	Windungszahl je Strang	number of windings per phase
N_c	-	Spulenwindungszahl	number of windings per coil
p	-	Polpaarzahl	number of pole pairs
P	W	Leistung	power
q	-	Lochzahl (Nuten pro Pol und Strang)	number of slots per pole and phase
Q	-	Nutzahl	number of slots
R	Ohm	elektrischer Widerstand	electric resistance
s	-	Schlupf	slip
s	m	Weglänge	distance
t	s	Zeit	time
T	s	Zeitkonstante	time constant
u	-	Spulenseiten je Nut und Schicht	number of coils per slot and layer
U	V	elektrische Spannung	electric voltage
U_p	V	Polradspannung	synchronous internal voltage
$\ddot{u}$, $\ddot{u}_U$	-	Übersetzungsverhältnis (Spannungsübersetzungsverhältnis)	ratio (voltage ratio)
$\ddot{u}_I$	-	Stromübersetzungsverhältnis	current ratio
v	m/s	Geschwindigkeit	velocity
V	A	magnetische Spannung	magneto-motive force (“magnetic voltage”)
V	m^3	Volumen	volume
W	J	Energie	energy
W	m	Spulenweite	coil width
x	m	Umfangskoordinate	circumferential coordinate
X	Ohm	Reaktanz	reactance
X_d, X_q	Ohm	Längs-, Querreaktanz	d-, q-reactance
y	-	Weite einer Spule, gezählt in Nutteilungen	width of a coil in numbers of slots
z	-	gesamte Leiterzahl	total number of conductors
Z	Ohm	Impedanz	impedance
α_e	-	äquivalente Polbedeckung	pole pitch factor
α	rad	Zündwinkel	firing angle
α_Q	rad	Nutenwinkel (elektrischen Grad)	slot angle (electric degrees)
γ	rad	Umfangswinkel (elektrische Grad)	circumferential angle (electric degrees)
δ	m	Luftspalt	air-gap
φ	rad	Phasenwinkel	phase angle
Φ	Wb	magnetischer Fluss (Scheitelwert)	magnetic flux (peak value)
Ψ	Vs	magnetische Flussverkettung (Scheitelwert)	magnetic flux linkage (peak value)
κ	S/m	elektrische Leitfähigkeit	electric conductivity
μ	-	Ordnungszahl	ordinal number
μ	Vs/(Am)	magnetische Permeabilität	magnetic permeability
μ_0	Vs/(Am)	magnetische Permeabilität des Vakuums ($4\pi \cdot 10^{-7}$ Vs/(Am))	magnetic permeability of vacuum ($4\pi \cdot 10^{-7}$ Vs/(Am))

ν	-	Ordnungszahl	ordinal number
ξ	-	„reduzierte“ Leiterhöhe	“reduced” conductor height
η	-	Wirkungsgrad	efficiency
ϑ	rad	Polradwinkel (elektrische Grad)	load angle (electric degrees)
Θ	A	elektrische Durchflutung	Ampere-turns
σ	-	BLONDEL´scher Koeffizient der Gesamtstreuung, Streuziffer	BLONDEL’s leakage coefficient
σ_o	-	Streuziffer der Oberfelderstreuung	leakage coefficient of harmonic leakage
τ_c	m	Kommutatorstegteilung	collector segment pitch
τ_Q, τ_s, τ_r	m	Nutteilung allgemein bzw. Stator- und Rotornutteilung	slot pitch in general, stator / rotor slot pitch
τ_p	m	Polteilung	pole pitch
ω	1/s	elektrische Kreisfrequenz	electric angular frequency
Ω	1/s	elektrische Winkelgeschwindigkeit	electric angular speed
ω_m, Ω_m	1/s	mechanische Winkelgeschwindigkeit	mechanic angular speed
Indizes / Subscripts			
a		Anker	armature
av		Mittelwert	average value
b		Bürste, asynchrones Kippen	brush, asynchronous breakdown
c		Spule, Kommutator	coil, collector
com		Kommutierungs-	collector
C		Koerzitiv-	coercive
d		direct (längs), dc (Gleichgröße), Zone (distribution), Verluste (dissipation)	direct, dc (direct current), phase (distribution), losses (dissipation)
D		Dämpferwicklung in der Längsachse	damper winding in direct axis
e		elektrisch, äquivalent	electric, equivalent
f		Feld	field
Fe		Eisen	steel
h		Haupt-	mutual / magnetising
i		induziert	induced
in		zugeführt	fed -
k		Kurzschluss-	short circuit -
m		Magnetisierungs-, magnetisch	magnetising -, magnetic
m		mechanisch	mechanical
m		maximal	maximum
N		Nenn	rated
out		abgegeben	delivered
o		Oberfelder	harmonics
p		Pol, Polrad, Sehnung	pole, rotor (synchronous machine), pitch
q		quer	quadrature
Q		Dämpferwicklung in der Querachse	damper winding in the quadrature axis

Q		Nut	slot
r		Rotor	rotor
R		Reaktanz- (Gleichstrommaschine), Remanenz, Reibung	reactance (DC machine), remanence, friction
s		Stator	stator
s		Welle	shaft
sch		schalt	switching
syn		Synchron	synchronous
sh		Shunt	shunt
v		Vorwiderstand	external resistance
w		Wicklung	winding
W		Wendepol	commutating
δ		Luftspalt	air-gap
σ		Streu-	leakage
0		Leerlauf	No-load
1		Anfahrpunkt (s = 1 bei Asynchronmaschine)	breakaway (s = 1 with asynchronous machines)
		#	
Notationen / Notations			
i		Kleinbuchstabe: z.B.: elektrische Stromstärke, Augenblickswert	lower case letter: e.g.: electric current, instantaneous value
I		Großbuchstabe: z.B.: elektrische Stromstärke, Effektivwert oder Gleichstrom-Wert	upper case letter: e.g.: electric current, rms or dc value
X, x		Großbuchstabe: z.B. Reaktanz, Kleinbuchstabe: z.B. bezogene Reaktanz (p.u. -Wert)	upper case letter: e.g. reactance, lower case letter: e.g. normalised reactance (p.u.-value)
$\underline{I}$		unterstrichen: komplexe Größen	underlined: complex values
$\hat{I}$		Spitzenwert, Amplitude	peak value, amplitude
I'		auf Ständerwicklungsdaten umgerechnet	as seen from the stator winding
X', X''		transiente, subtransiente Reaktanz	transient, subtransient reactance
$\underline{I}^*$		konjugiert komplexer Wert von $\underline{I}$	conjugated complex value of $\underline{I}$
Re(.)		Realteil von ...	real part of ...
Im(.)		Imaginärteil von ...	imaginary part of ...

1. Basic design rules for electrical machines

1.1 Torque generation and internal power

A rotating electric machine consists of a **stator** and a **rotor**. Magnetic flux density is always arranged in **pole pairs *p*** with at least two poles $2p = 2$ and pole pitch τ_p, yielding rotor circumference $2p\tau_p$. Due to small air gap between stator and rotor, when compared with rotor diameter, stator and rotor diameter are nearly equal, so pole pitch is often calculated frim stator inner diameter $\tau_p = d_{si}\pi/(2p)$. Magnetic flux density B_δ in air-gap, excited by one part (stator or rotor), acts with electric current *i* in winding in the other part by generating a tangential *Lorentz*-force *F*, which forces the rotor to rotate. Due to feeding distributed winding (e.g. distributed in slots) with e.g. AC current the actual current *I* depends at rotor circumference co-ordinate *x* on time *t* . Total number of current carrying conductors *z* along circumference yields in small section *dx* the number of conductors (Fig. 1.1-1)

$$dz = z \cdot \frac{dx}{2p\tau_p} \quad , \tag{1.1-1}$$

if concentration of conductors in slots is neglected, being assumed to be evenly distributed along circumference. With axial length *l* of rotor and perpendicular directions of current flow and air gap flux density, generated *Lorentz*-force at co-ordinate *x* is

$$dF(x,t) = dz \cdot i(x,t) \cdot B_\delta(x,t) \cdot l \quad . \tag{1.1-2}$$

With definition of **current loading (current sheet)**

$$A(x,t) = \frac{z \cdot i(x,t)}{2p\tau_p} \tag{1.1-3}$$

total tangential force is

$$F = l \cdot \int_0^{2p\tau_p} A(x,t) \cdot B_\delta(x,t) \cdot dx \,. \tag{1.1-4}$$

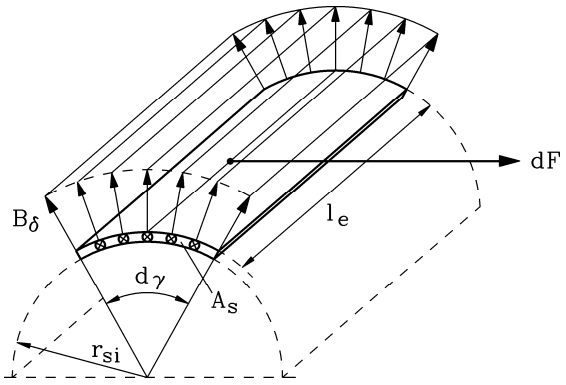

Fig. 1.1-1: Tangential *Lorentz*-force in small section *dx*

If **AC machines**, fed by AC currents with frequency $f = \omega/(2\pi)$ are designed in that way, that the distributed windings generate a sinusoidal distributed rotating current loading

$$A(x,t) = \hat{A} \cdot \cos(x\pi/\tau_p - \omega t) \tag{1.1-5}$$

and a sinusoidal distributed rotating air gap flux density, phase shifted by **internal current angle** φ_i

$$B_\delta(x,t) = \hat{B}_\delta \cdot \cos(x\pi/\tau_p - \omega t + \varphi_i) \quad , \tag{1.1-6}$$

then (1.1-4) yields a constant **total tangential force**

$$F = l \cdot p\tau_p \cdot \hat{A} \cdot \hat{B}_\delta \cdot \cos\varphi_i \quad . \tag{1.1-7}$$

With DC machines, stator excited flux density is (more or less) constant B_δ along pole coverage $\alpha_e \cdot \tau_p$ ($\alpha_e \approx 0.7$) and zero in the pole gaps, whereas current loading A is constant due to commutation of rotor AC current via brushes and commutator. Hence (1.1-4) yields a constant **total tangential force**

$$F = l \cdot 2p\tau_p \cdot A \cdot \alpha_e B_\delta \quad . \tag{1.1-8}$$

Electromagnetic torque results from force with e.g. stator inner diameter as

$$M_e = F \cdot d_{si}/2 \qquad \begin{matrix} M_{e,AC} = l \cdot (p\tau_p)^2 \cdot \hat{A} \cdot \hat{B}_\delta \cdot \cos\varphi_i / \pi \\ M_{e,DC} = l \cdot 2(p\tau_p)^2 \cdot A \cdot \alpha_e B_\delta / \pi \end{matrix} \quad . \tag{1.1-9}$$

Tangential force per stator inner surface is called **specific thrust**

$$\boxed{\tau = F/(d_{si} \cdot \pi \cdot l) \qquad \begin{matrix} \tau_{AC} = \hat{A} \cdot \hat{B}_\delta \cdot \cos\varphi_i / 2 \\ \tau_{DC} = A \cdot \alpha_e B_\delta \end{matrix}} \quad . \tag{1.1-10}$$

Example 1.1-1:
- Air gap flux density peak value 1.0 T,
- Typical maximum current loading for air cooling with open ventilation:
  A = 700 A/cm (DC-machines), corresponding amplitude for AC-machines $\hat{A} = \sqrt{2} \cdot k_{w1} \cdot A$

a) DC-machines: $\alpha_e = 0.7$: $\tau_{DC} = A \cdot \alpha_e B_\delta = 70000 \cdot 0.7 \cdot 1.0 = 49000\ \mathrm{N/m^2} \cong$ 0.5 bar

b) AC-machines: $k_{w1} \approx 0.95$, $\hat{A} = \sqrt{2} \cdot k_{w1} \cdot A = 940$ A/cm, maximum thrust at $\cos\varphi_i = 1$:

$$\tau_{AC} = \hat{A} \cdot \hat{B}_\delta \cdot \cos\varphi_i / 2 = 94000 \cdot 1 \cdot 1/2 = 47000\ \mathrm{N/m^2} \cong 0.5\ \mathrm{bar}$$

In AC machines rotational speed of $A(x,t), B_\delta(x,t)$ is $n_{syn} = f/p$, yielding **internal power (air gap power)** as

$$P_\delta = 2\pi \cdot n_{syn} \cdot M_e \quad . \tag{1.1-11}$$

In DC machines A, B_δ are not rotating, therefore **internal power (air gap power)** is determined by rotational speed of rotor n

$$P_\delta = 2\pi \cdot n \cdot M_e \quad . \tag{1.1-12}$$

Facit:
Electromagnetic torque is determined by air gap flux density and current loading (= ampere-turns per unit length) and corresponds with internal power (air gap power).

1.2 Electromagnetic utilization

Maximum internal power in AC machines is given at $\cos\varphi_i = 1$, which equals **internal apparent power** S_δ. This power per stator bore volume $d_{si}^2(\pi/4)\cdot l$, but usually neglecting $\pi/4$, and per speed n_{syn} is called **electromagnetic utilization or *Esson´*s number *C*.**

$$C = \frac{S_\delta}{d_{si}^2 \cdot l \cdot n_{syn}} = \frac{\pi^2}{2} \cdot \hat{A} \cdot \hat{B}_\delta \tag{1.2-1}$$

From theory of distributed winding we know that current loading A is derivative of ampere-turn distribution V (also called magnetic voltage or "magnetomotive force" m.m.f.).

$$A(x) = dV(x)/dx \tag{1.2-2}$$

Fourier-analysis of spatial ampere-turn distribution for symmetrical three-phase winding (m = 3) with N turns per phase and fundamental winding factor k_{w1}, fed by sinusoidal currents with amplitude $\sqrt{2}I$ and frequency $f = \omega/(2\pi)$, phase shifted each by 120° (= $2\pi/m$), yields fundamental m.m.f. (see lectures: "Electrical machines and drives").

$$V(x,t) = \hat{V} \cdot \sin(x\pi/\tau_p - \omega t) \qquad \hat{V} = \frac{\sqrt{2}}{\pi} \cdot \frac{m}{p} \cdot N \cdot k_{w1} \cdot I \tag{1.2-3}$$

Thus we get with (1.2-2)

$$A(x,t) = \hat{A} \cdot \cos(x\pi/\tau_p - \omega t) \qquad \hat{A} = \sqrt{2} \cdot k_{w1} \cdot A \quad , \tag{1.2-4}$$

where abbreviation

$$\boxed{A = \frac{2 \cdot m \cdot N \cdot I}{2 p \tau_p}} \tag{1.2-5}$$

is the **r.m.s. current loading**, as I is the r.m.s. current per phase, which describes the thermal loading of the conductors. Therefore the usual way to calculate **electromagnetic utilization *C*** of AC machines is

$$\boxed{C_{AC} = \frac{S_\delta}{d_{si}^2 \cdot l \cdot n_{syn}} = \frac{\pi^2}{\sqrt{2}} \cdot k_{w1} \cdot A \cdot B_\delta} \quad . \tag{1.2-6}$$

For air gap flux density always peak value $B_\delta = \hat{B}_\delta$ is used, as it determines saturation of iron parts. For DC machines we get with $S_\delta = P_\delta$ for ***Esson´*s number *C***

$$\boxed{C_{DC} = \frac{P_\delta}{d_{si}^2 \cdot l \cdot n} = \pi^2 \cdot \alpha_e \cdot A \cdot B_\delta} \quad . \tag{1.2-7}$$

Example 1.2-1:
Comparison of electromagnetic utilization of AC and DC machine for the same current loading A and peak air gap flux density $B_\delta = \hat{B}_\delta$:

$$\frac{C_{DC}}{C_{AC}} = \frac{\alpha_e}{k_{w1}/\sqrt{2}} \approx \frac{1}{k_{w1}}.$$

With winding factors ranging between 0.92 to 0.96, even in best case $\cos\varphi_i = 1$ the utilization of DC machines is a little bit higher than of AC machines. With $\cos\varphi_i = 0.8$ as typical value for induction machines this value is higher by about 20%. But note: DC machines need maintenance of brushes, additional inter-poles to minimize sparking (the inter-pole winding causes additional resistive losses) and a mechanical commutator. Therefore nowadays robust induction machines are usually preferred.

Internal power may also be calculated by electric quantities induced voltage (back EMF) and current. For AC machines main flux per pole of air gap sine wave

$$\Phi_h = \frac{2}{\pi} \cdot \tau_p l \cdot B_\delta \tag{1.2-8}$$

induces voltage per phase

$$U_i = \sqrt{2}\pi \cdot f \cdot N \cdot k_{w1} \cdot \Phi_h \quad , \tag{1.2-9}$$

which along with current yields internal apparent power

$$S_\delta = m \cdot U_i \cdot I = C \cdot d_{si}^2 \cdot l \cdot n_{syn} \quad , \tag{1.2-10}$$

which leads with (1.2-5) again to expression (1.2-6). For DC machines main flux per pole

$$\Phi_h = \alpha_e \cdot \tau_p l \cdot B_\delta \tag{1.2-11}$$

induces voltage in the z conductors, which are arranged in $2a$ parallel winding branches

$$U_i = \frac{z \cdot p}{a} \cdot n \cdot \Phi_h \quad . \tag{1.2-12}$$

Along with armature DC current I we get internal power

$$S_\delta = U_i \cdot I = C \cdot d_{si}^2 \cdot l \cdot n \quad , \tag{1.2-13}$$

and with current amplitude per conductor of AC current in rotor armature $I/(2a)$ and current loading

$$A = \frac{z \cdot I/(2a)}{2 p \tau_p} \tag{1.2-14}$$

finally again (1.2-7) is derived.

Facit:

Electromagnetic utilization is given by current loading and air gap flux density amplitude. Latter is limited to about 1 T, as in the rotor and stator teeth flux fringing causes flux densities of about 1.8 ... 2 T, which is saturation limit of iron. Current loading is limited by cooling system, which enables the machine to get rid of winding losses. Big machines with

superior cooling system allow therefore high current loading and high electromagnetic utilization.

Example 1.2-2:
Typical values for electromagnetic utilization, with increased current loading with increasing machine sizes due to improved heat transfer:

a) DC machines: air-cooled, open ventilated, winding temperature rise 105 K

rated power	P	kW	1	10	100	6000
rated speed	n	1/min	1500	1500	1500	400
rated torque	M	Nm	6.4	64	640	143000
pole count	$2p$	-	2	4	4	18
current loading	A	A/cm	150	300	430	600
air gap flux density	B_δ	T	0.7	0.85	0.9	1.05
*Esson´*s number	C	kW·min/m^3	1.2	2.9	4.5	7.3

$\alpha_e = 0.7$

b) AC synchronous machines, $\cos\varphi_i = 0.75$, 50 Hz : winding temperature rise 80 K, air-cooled, open ventilated, except *) ,

rated apparent power	S	kVA	200	800	4000	40000	1000000 *)
rated speed	n	1/min	1500	1500	1500	3000	3000
pole count	$2p$	-	4	4	4	2	2
current loading	A	A/cm	420	440	750	1000	2100
air gap flux density	B_δ	T	0.9	1.0	1.03	1.05	1.1
*Esson´*s number	C	kVA·min/m^3	4.2	4.9	6.1	8.3	25.6

*) Large steam turbine generators with hydrogen gas or conductor direct water cooling

c) AC induction (asynchronous) machines: four poles, winding temperature rise 80 K, air-cooled, open ventilated

rated apparent power	S	kVA	100	1000	10000
current loading	A	A/cm	300	550	1000
air gap flux density	B_δ	T	1.0	1.05	1.1
*Esson´*s number	C	kVA·min/m^3	3.3	6.4	12.2

d) AC induction (asynchronous) machines: four poles, winding temperature rise 105 K, air-cooled, totally enclosed (standard induction motors)

rated apparent power	S	kVA	5	650
current loading	A	A/cm	280	410
air gap flux density	B_δ	T	0.95	1.0
*Esson´*s number	C	kVA·min/m^3	3.0	4.5

The scaling effect of the **rated machine power S_N with machine size** for a given speed (very often used is about 1500 ... 1800 /min) is given by the assumption, that the machine dimensions increase with the machine active length L (including radial ventilation ducts): the proportionality of bore diameter $d_{si} \sim L$ and iron packet length $l \sim L$ lead to a scaling of the machine volume $V \sim (d_{si})^2 l \sim L^3$. Thus we use L as a machine size characterization.

$$S_N \approx S_\delta = C \cdot d_{si}^2 \cdot l \cdot n \sim L^3 \quad . \tag{1.2-15}$$

As power per speed is proportional to torque, we also get

$$\boxed{M_N \sim S_\delta / n = C \cdot d_{si}^2 \cdot l \sim L^3} \quad . \tag{1.2-16}$$

For given electromagnetic utilization machine torque rises with volume of machine. Big torque is achieved better by increasing machine diameter instead increasing machine length.

Note:
According to (1.2-16) torque determines size of machine, NOT power, as for the same torque, but twice speed power is doubled.

1.3 Thermal utilization

Neglecting all other loss components in electric machine, still the losses of armature winding, where current flows, remain. These losses P_{Cu} must be transported off the winding in order to get constant temperature rise $\Delta\vartheta$ in the winding. The coolant (mostly air) flows by the winding, is heated up by the losses, thus absorbing the loss energy, which by coolant flow is transported off to a heat exchanger or is blown into the environment (**convection cooling**). Exchange of winding heat to coolant is raised by

- increased **contact area** A_k between winding and coolant flow $\dot{V}$,
- increased **temperature difference** between winding ϑ_w and ambient ϑ_{amb}

$$\Delta\vartheta = \vartheta_w - \vartheta_{amb} \tag{1.3-1}$$

- improved conditions of heat exchange to coolant such as increased flow velocity of coolant, thus increasing coolant flow $\dot{V}$ and by physical properties of coolant itself (e.g. hydrogen gas has superior parameters for heat absorption than air). These parameters are summarized in **heat transfer coefficient** α_k .

$$\boxed{P_{Cu} = \alpha_k \cdot A_k \cdot \Delta\vartheta} \tag{1.3-2}$$

Assuming the coolant flow in the air gap, as it is the case for machines with internal ventilation, the contact area may be taken as the stator bore surface, increased by the length of the winding overhangs l_b.

$$A_k = d_{si} \cdot \pi \cdot (l_{Fe} + l_b) \tag{1.3-3}$$

Winding losses in the conductors, placed in the slots, are given by the sum of losses per conductor, given by conductor resistance R_c and conductor currents I_c (Fig. 1.3-1). Each conductor per slot with conductivity κ has cross section A_c and length according to iron stack length $l = l_{Fe}$ and length of winding overhang l_b.

$$P_{Cu} = m \cdot R \cdot I^2 = \sum_{i=1}^{z} R_c \cdot I_c^2 = z \cdot R_c \cdot I_c^2 = z \cdot \frac{l_{Fe} + l_b}{\kappa \cdot A_c} \cdot I_c^2 \tag{1.3-4}$$

With **current density per conductor**

$$\boxed{J = I_c / A_c} \tag{1.3-5}$$

we get from (1.3-4)

$$P_{Cu} = z \cdot \frac{l_{Fe} + l_b}{\kappa} \cdot J \cdot I_c = d_{si}\pi \cdot \frac{l_{Fe} + l_b}{\kappa} \cdot J \cdot \frac{z \cdot I_c}{d_{si}\pi} = d_{si}\pi \cdot \frac{l_{Fe} + l_b}{\kappa} \cdot J \cdot A \tag{1.3-6}$$

$$\Delta\vartheta = \frac{P_{Cu}}{\alpha_k \cdot d_{si}\pi \cdot (l_{Fe} + l_b)} = \frac{1}{\alpha_k \cdot \kappa} \cdot J \cdot A \qquad \Rightarrow \qquad \boxed{\Delta\vartheta \sim J \cdot A} \qquad (1.3\text{-}7)$$

Facit:
Thermal utilization of electrical machine (= temperature rise in armature winding for given machine torque) is determined by product of current density and current loading and may be reduced by superior cooling (increased α_k) or decreased losses (increased κ).

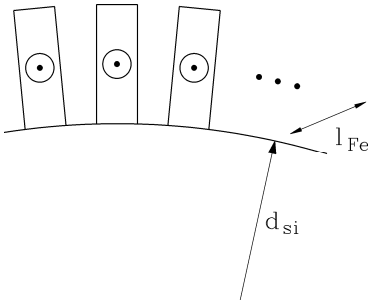

Fig. 1.3-1: Losses in winding (stator slot conductors), cooled via the stator bore surface

Scaling effect with **increasing motor size** is given by considering surface of conductors itself, e.g. $d_c\pi \cdot l_c$ for round conductor wire (cylindrical shape) with wire diameter d_c and wire length l_c , and heat transfer coefficient at conductor surface α_c. With losses per conductor

$$P_{Cu,c} = R_c I_c^2 = \frac{l_c}{\kappa_c A_c} \cdot I_c^2 = \frac{A_c l_c}{\kappa_c} \cdot J^2 \qquad \Rightarrow \qquad P_{Cu} \sim L^3 \qquad (1.3\text{-}8)$$

temperature rise in conductor may be estimated by

$$\Delta\vartheta = \frac{P_{Cu,c}}{\alpha_c \cdot d_c\pi \cdot l_c} = \frac{d_c^2\pi/4 \cdot l_c}{\kappa_c \cdot \alpha_c \cdot d_c\pi \cdot l_c} \cdot J^2 = \frac{d_c}{4 \cdot \alpha_c \cdot \kappa_c} \cdot J^2 \Rightarrow \qquad \Delta\vartheta \sim L \cdot J^2 \qquad (1.3\text{-}9)$$

$$\boxed{J \sim 1/\sqrt{L}} \qquad (1.3\text{-}10)$$

Example 1.3-1:
Typical electromagnetic and thermal utilization and current density of air-cooled asynchronous machines with internal air flow (open ventilated) with temperature rise $\Delta\vartheta$ = 80 K (at ϑ_{amb} = 40 °C) at rated speed of about 1450/min.

Rated power / kW	100	1000	10000
B_δ / T	1.0	1.0	1.0
A / A/cm	300	550	1000
C / kVA·min/m^3	3.3	6.1	11.1
machine volume L^3 / p.u.	1.0	5.4	29.7
machine size L / p.u.	1.0	1.75	3.1
$1/\sqrt{L}$	1.0	0.75	0.55
$J \sim 1/\sqrt{L}$ /A/mm^2	6.8	5.1	3.7
$A \cdot J$ / (A/cm).(A/mm^2)	2040	2850	3700

Example 1.3-2:
Thermal utilization of totally enclosed, air-cooled (standard) AC induction (asynchronous) machines with four poles and shaft-mounted fan.

a) winding temperature rise 105 K:

rated power	P	kW	5	650
current loading	A	A/cm	280	430
current density	J	A/mm^2	7.6	5.0
	$A{\cdot}J$	A/cm·A/mm^2	2100	2150

b) winding temperature rise 80 K:

rated power	P	kW	4	570
current loading	A	A/cm	240	380
current density	J	A/mm^2	6.6	4.4
	$A{\cdot}J$	A/cm·A/mm^2	1580	1670

Losses $P_d \sim I^2$ must reduced by 80 K/105 K = 0.76, compared to a). Therefore power $P \sim U \cdot I$, current I and J and A must be reduced by $\sqrt{80/105} = 0.87$.

Note:
At 80 K temperature rise a open ventilated air-cooled induction machine of about 1 MW has a thermal utilization of typically 2800 (A/cm)(A/mm^2), whereas for totally enclosed, surface cooled machine this value is about 1800 (A/cm)(A/mm^2), thus 35% lower.

Facit:
Machines with increased rated power P at same rated speed have increased geometric dimensions L due to $P \sim L^3$ and increased losses (dissipated power) due to $P_d \sim L^3$. Therefore one must reduce current density J by $1/\sqrt{L}$ to achieve same winding temperature rise $\Delta\vartheta$, if the same cooling conditions (α_c) and the same type of winding material (κ) is assumed. Therefore bigger machines with increased current density need improved cooling systems such as segmented iron cores, internal and external fan or – for big generators – hydrogen gas or direct water cooling.

1.4 Overload capability of AC machines

AC synchronous and asynchronous machines show a maximum torque, when fed with fixed stator voltage system U_s and frequency $f_s = \omega_s/(2\pi)$, which may be influenced by design parameters.

1.4.1 Synchronous machines

The maximum torque and power of grid-operated synchronous machines is the pull-out torque M_{p0}, which for neglected stator resistance and cylindrical rotor machines (no saliency: $L_d = L_q$) occurs at load angle $\vartheta = \pm\pi/2$:

$$M_{p0} = \frac{3 \cdot p}{\omega_s} \cdot \frac{U_s \cdot U_p}{X_d} \quad , \quad P_{p0} = 3 \cdot \frac{U_s \cdot U_p}{X_d} \quad . \qquad (1.4.1\text{-}1)$$

Big overload capability at rated voltage U_{sN} means big ratio of pull-out power versus rated apparent power

$$\frac{P_{p0}}{S_N} = \frac{1}{3 \cdot U_{sN} \cdot I_{sN}} \cdot \frac{3 \cdot U_{sN} \cdot U_p}{X_d} = \frac{U_p}{U_{sN}} \cdot \frac{1}{X_d / Z_N} = \frac{u_p}{x_d} \ . \tag{1.4.1-2}$$

Thus the synchronous reactance $X_d = \omega_s L_d$ as per unit value $x_d = X_d / Z_N$ with the rated impedance $Z_N = U_{sN} / I_{sN}$ should by small.

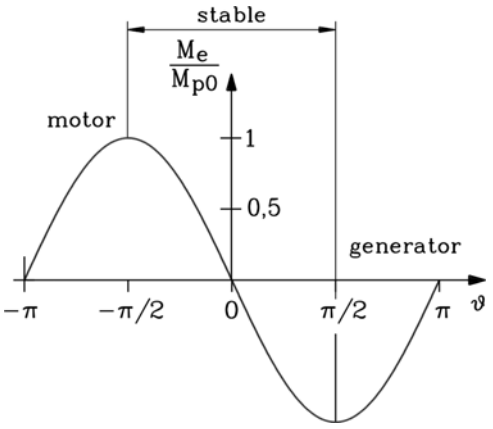

Fig. 1.4.1-1

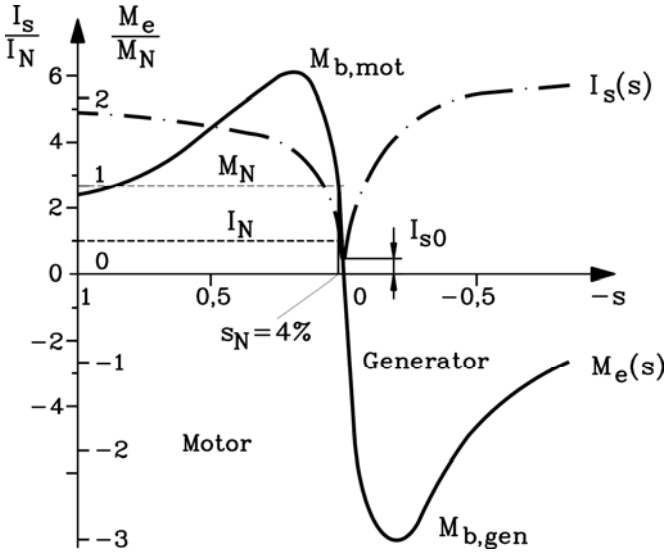

Fig. 1.4.2-1

Fig. 1.4.1-1: Torque versus load angle of synchronous machine when fed from fixed voltage system with pull-out torque at load angle $\vartheta = \pm\pi/2$

Fig. 1.4.2-1: Torque M_e and stator current I_s of induction machine depending on rotor slip s (resp. speed), when operated with fixed stator voltage system

Synchronous reactance consists of magnetizing reactance X_h and stray reactance X_σ, of which the latter may be neglected here. Formula for X_h (from lectures "Electrical machines and drives") shows that magnetizing inductance depends on geometric parameters like air gap δ, pole pitch and stack length, but also on square of number of turns per phase.

$$X_d = X_h + X_\sigma \approx X_h = 2\pi f_s \cdot \mu_0 N^2 k_{w1}^2 \frac{2m}{\pi^2} \frac{l \tau_p}{p \cdot \delta} \tag{1.4.1-3}$$

$$\frac{1}{x_d} = \frac{1}{X_d} \cdot \frac{U_{sN}}{I_{sN}} \sim \frac{U_{sN}}{\sqrt{2}\pi f_s \cdot N \cdot k_{w1} \cdot (2/\pi)\tau_p l} \cdot \frac{1}{\frac{2mN \cdot I_{sN}}{2p\tau_p}} \cdot \frac{\delta}{\tau_p} = \frac{B_\delta}{A} \cdot \frac{\delta}{\tau_p} \tag{1.4.1-4}$$

Big overload capability is achieved by big air gap flux density and small current load.

$$\boxed{\frac{P_{p0}}{S_N} = \frac{u_p}{x_d} \sim \frac{B_\delta}{A} \cdot \frac{\delta}{\tau_p}} \ . \tag{1.4.1-5}$$

Turbo generators for thermal power plants have a high electromagnetic utilization, so A is very big due to elaborate cooling systems. Moreover pole pitch is big, as pole count is only 2:

$\tau_p = d_{si}\pi/(2p) = d_{si}\pi/2$. Therefore overload capability is poor. To increase it, the air gap δ is increased up to several cm or even dm.

Example 1.4.1-1:
Large synchronous generators:

Hydro generators (high pole count: $2p \geq 4$ up to typical 100)	$x_d = 0.8 \ldots 1.2$
Turbo generators ($2p = 2$)	$x_d = 2.0 \ldots 2.3$

Synchronous motors operated from grid:
International standard IEC 34-1 demands minimum overload capability $M_{p0}/M_N = 1.35$.

1.4.2 Induction machines

Breakdown torque M_b at breakdown slip is maximum torque of induction machine in generator or motor mode and defines its overload capability. In Fig. 1.4.2-1 this value is $M_b/M_N = 2.3$ at motor operation. International standard IEC 34-1 demands minimum motor overload capability $M_b/M_N = 1.6$.
With neglected stator winding resistance, absolute value of breakdown torque for generator and motor mode is equal and increases with decreasing stray reactance σX_s (formula acc. to lecture "Electrical machines and drives"):

$$R_s = 0: \quad M_b = \frac{m_s}{2}\frac{p}{\omega_s}U_s^2\frac{1-\sigma}{\sigma X_s} \tag{1.4.2-1}$$

So, in the same way as for synchronous machines, we get for overload capability at rated voltage U_{sN}

$$\frac{P_b}{S_N} \cong \frac{M_b \cdot \omega_s / p}{m_s \cdot U_{sN} \cdot I_{sN}} = \frac{1-\sigma}{2\sigma} \cdot \frac{1}{X_s/Z_N} \sim \frac{1}{\sigma} \cdot \frac{1}{x_s} \quad . \tag{1.4.2-2}$$

Small total stray flux $\sigma = \Phi_\sigma/(\Phi_\sigma + \Phi_h)$, but also small per unit value of stator reactance yield big overload capability. As X_s of induction machine is the corresponding reactance to X_d of synchronous machine

$$X_s = X_h + X_{s\sigma} \approx X_h = 2\pi f_s \cdot \mu_0 N^2 k_{w1}^2 \frac{2m_s}{\pi^2}\frac{l\tau_p}{p \cdot \delta} \quad , \tag{1.4.2-3}$$

we get the same result for big overload capability

$$\frac{P_b}{S_N} \sim \frac{1}{\sigma} \cdot \frac{1}{x_s} \sim \frac{B_\delta}{A} \cdot \frac{\delta}{\tau_p} \quad . \tag{1.4.2-4}$$

Facit:
Big overload capability of AC machines is achieved both for synchronous and induction machines by big air gap flux density and small current load, as well as by small pole pitch and big air gap. Thus machines with low electromagnetic utilization usually have big overload capability, which means that the machine is capable of much more power than actually used one.

2. Design of induction machines

2.1 Motor requirements

Aim is to design a three-phase induction machine, being operated from grid with fixed stator voltage and stator frequency. For grid operation asynchronous start-up torque and stator current must be calculated (Fig.2.1-1) in advance as well as parameters at rated speed such as rated current, power factor, losses and efficiency.

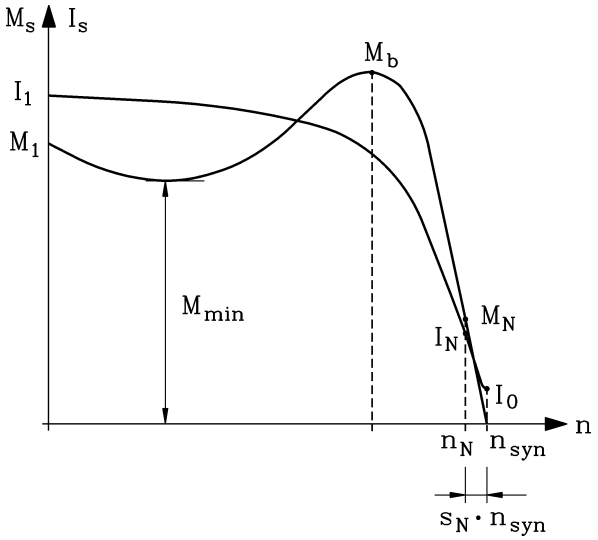

Fig. 2-1: Typical start-up shaft torque and stator current of cage induction machine with increase of starting current due to rotor current displacement

Line operated **cage induction motors** cover about 80% of motor application world wide, as it is a robust cheap motor and many drive applications need only fixed speed (e.g. many pump applications, mills, fan drives, saws, conveyors). Nowadays also many wind mills operated with cage induction machines at fixed speed with a gear between wind turbine and generator. Due to its enormous economical significance, many features of cage induction machines are standardized. Calculated values of machine, which are handed over to customer or are printed on motor name plate, must lie within specified tolerances according to IEC 34-1.

Rated operation:	*Tolerances for measured values:*
Measured rated slip s_N	±20% of calculated rated slip $s_{N,calc}$
Measured power factor $\cos\varphi_N$	$-(1-\cos\varphi_{N,calc})/6$
Measured efficiency η_N	$-0.15\cdot(1-\eta_{N,calc})$ for $P_N \le 50$ kW $-0.10\cdot(1-\eta_{N,calc})$ for $P_N > 50$ kW
Overload capability:	
Measured breakdown torque M_b: Demand: $M_b / M_N \ge 1.6$ for 15 s	-10% of calculated breakdown torque $M_{b,calc}$
Starting parameters (at s = 1):	
Measured starting torque M_1	-15% ... +25% of calculated starting torque $M_{1,calc}$
Measured starting current I_1	+20% of calculated starting current $I_{1,calc}$
Measured minimum torque M_{min} ("saddle" torque):	
Demands: $M_{min} \ge 0.5M_1$ $M_{min} \ge 0.5M_N$ for $P_N > 100$ kW $M_{min} \ge 0.3M_N$ for $P_N \le 100$ kW	

Table 2.1-1: Tolerances for measured operational parameters of cage induction machines according to IEC 34-1

Example 2.1-1:
Calculated power factor: $\cos\varphi_{N,calc} = 0.85$, tolerance $-(1-\cos\varphi_{N,calc})/6 = -0.025$. Thus measured power factor must be at least $\cos\varphi_N = 0.85 - 0.025 = 0.825$.
Calculated efficiency of 30 kW-motor: $\eta_{N,calc} = 0.873$, tolerance $-0.15\cdot(1-\eta_{N,calc}) = -0.019$. Thus measured efficiency must be at least $\eta_N = 0.873 - 0.019 = 0.854$.

For starting machine design, **demanded operation parameters** are given:
- mechanical output power (motor) or electrical output power (generator)
- rated stator voltage and frequency
- rated rotor speed.

Starting demands according to Table 2-1 and often further demand to stay with starting current beneath certain limit e.g. $I_1/I_N < 6$ must be taken into account. Solution should be a machine with low mass, high efficiency and power factor. Steady state temperature rise of stator winding must stay within the specified Thermal Class of used insulation system, which according to IEC 34-1 is standardized.

Example 2.1-2:
Thermal Class B: 80 K average temperature rise of stator winding over 40 °C ambient temperature, measured by rise of resistance of hot winding with respect to resistance of cold winding.

Solution of electromagnetic and thermal calculation must comprise geometric data of stator and rotor iron sheets, winding arrangement, rated operational data such as stator current, power factor, efficiency, no-load current and losses, overload capability and starting data according to Fig. 2-1.

Wound rotor induction machines (slip-ring induction machines) are treated in the same way, but starting performance is determined by external rotor three-phase resistance. Therefore voltage between slip-rings at stand still must be known in advance for specifying these external resistors.

2.2 Main dimensions and basic electromagnetic quantities of induction machines

Main dimensions of induction machines:	
inner and outer diameter of stator and rotor iron stack	d_{si} , d_{sa} , d_{ri} , d_{ra}
air gap between stator and rotor iron stack, and pole pitch	δ, τ_p
length of iron stack, number and length of cooling ducts and total stack length	l_{Fe}, z_K, l_K, $L = l_{Fe} + z_K l_K$
Electric and magnetic quantities:	
Stator and rotor current loading (r.m.s.)	A_s, A_r
Flux density in air gap, stator and rotor teeth and yoke (peak values)	B_δ, B_{ds}, B_{dr}, B_{ys}, B_{yr}
Main flux (in air gap) and stray flux (components in slots, winding overhangs, influence of skewing and deviation of air gap flux from sinusoidal distribution)	Φ_h, Φ_σ

Table 2.2-1: Main dimensions and basic electromagnetic quantities

First cage and wound rotor induction motors were designed and built by *Michael Dolivo-Dobrowolsky*, who studied at *Darmstadt University of Technology*, in 1889 in *Germany*,

based on the basic principles of rotating magnetic fields, found first by *Prof. Ferraris* of *University Torino/Italy* in 1885. Since then a huge number of machines have been designed and built with ever increasing performance. So a lot of experience is available, which is summarized in the following to get an easy start for choosing main dimensions, electromagnetic and thermal utilization.

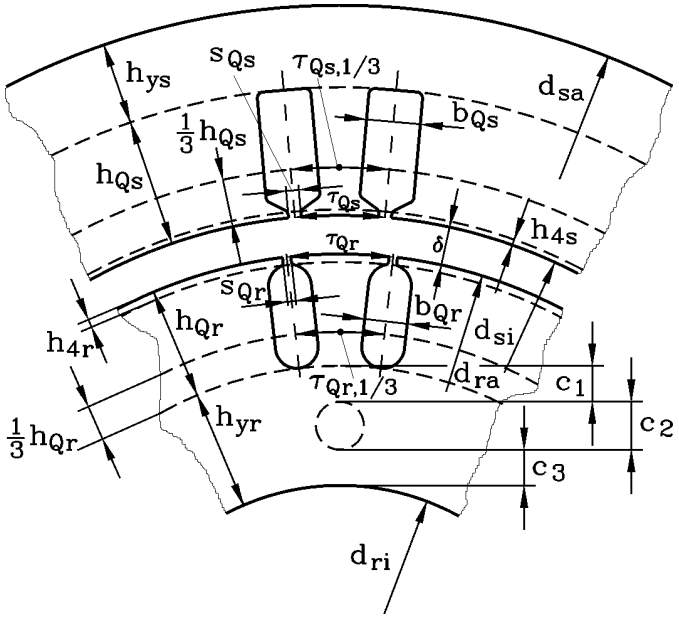

Fig. 2.2-1: Main dimensions and basic electromagnetic quantities of induction machine

Pole count $2p$ is determined by given stator frequency f_s and demanded synchronous speed n_{syn}

$$2p = 2 \cdot f_s / n_{syn} \tag{2.2-1}$$

and determines **pole pitch** τ_p of stator bore

$$\tau_p = d_{si}\pi /(2p) \quad . \tag{2.2-2}$$

Velocity of rotor at synchronous speed at stator bore

$$v_{syn} = 2 f_s \tau_p \tag{2.2-3}$$

may also be taken as being proportional to velocity of air flow in air gap of open ventilated machines with fans mounted shaft. Therefore with increasing pole pitch for given pole count and frequency cooling increases, thus allowing increase of current loading $A \sim \tau_p$. Flux density cannot rise with increasing pole pitch, as it is limited by iron saturation in the teeth and yokes. If no axial cooling ducts are used in iron stack, main air gap flux of fundamental of air gap flux density distribution is

$$\Phi_h = \frac{2}{\pi} \cdot \tau_p \cdot l_{Fe} \cdot B_\delta \quad . \tag{2.2-4}$$

It is excited by coils in slots. In order to get the shape of coils for minimum copper losses for maximum flux, we consider, that the coil must span a surface $\tau_p \cdot l_{Fe}$, resulting in a minimum length per turn of $2 \cdot (\tau_p + l_{Fe})$. This is exact for full pitched coils (coil width W = pole pitch τ_p) with ideally short winding overhangs $l_b = \tau_p$. Maximum flux for given resistance per

winding requires maximum surface $\tau_p \cdot l_{Fe}$ for given length $2 \cdot (\tau_p + l_{Fe}) = const.$, resulting in $\tau_p = l_{Fe}$. This is often realized for 4-pole machines, whereas machines with higher pole count often have $\tau_p < l_{Fe}$ due to the smaller pole pitch. Thus we get for **rated apparent power** S_N with ***Esson´*s equation** and assumed $A \sim \tau_p$, $l_{Fe} \sim \tau_p$ and $d_{si} \sim \tau_p \cdot p$

$$S_N \approx S_\delta = \frac{\pi^2}{\sqrt{2}} \cdot k_{w1} \cdot A \cdot B_\delta \cdot d_{si}^2 \cdot l_{Fe} \cdot \frac{f_s}{p} \sim l_{Fe}^4, \qquad S_N \sim A^4, \qquad S_N \sim \tau_p^4 \tag{2.2-5}$$

Taking $P_N \sim S_N$, we finally arrive at Fig. 2.2-3, 2.2-4 and 2.2-5, showing the increase of pole pitch, iron length and current loading with $\sqrt[4]{P_N}$, whereas average air gap flux density $B_{\delta,av} = (2/\pi) \cdot B_\delta$ is limited by $B_{\delta,av} = (2/\pi) \cdot 1.05 = 0.67\,\mathrm{T}$. As explained in Chapter 1, current density for given cooling system decreases with increasing machine power due to scaling effect (Fig. 2.2-6).

Note:
Two pole machines would require a very big stator and rotor yoke height, as the main flux is twice as big as in four pole machines at the same iron length and stator bore diameter. This would result in very heavy machines. Therefore usually air gap flux density is reduced by about 30% to get smaller machines (Fig. 2.2-5). To compensate this a little, one chooses $\tau_p < l_{Fe}$ to increase power by increased stack length.

As air gap field is magnetized by stator currents, on tries to get **big magnetizing reactance** X_h for small magnetizing current I_m (Fig. 2.2-2). According to Chapter 1 this demands a small air gap δ, which is only limited by mechanical properties of machine such as bending of the rotor. Rotor must not touch stator in any case, so with increasing power and thus heavier rotor the air gap must be increased, as bending increases too (Fig. 2.2-7). Rotor shaft diameter must be increased with bigger machines to increase mechanical stiffness of shaft (Fig. 2.2-8). Rotor iron stack consists of laminated sheets with only a small contribution to rotor stiffness.

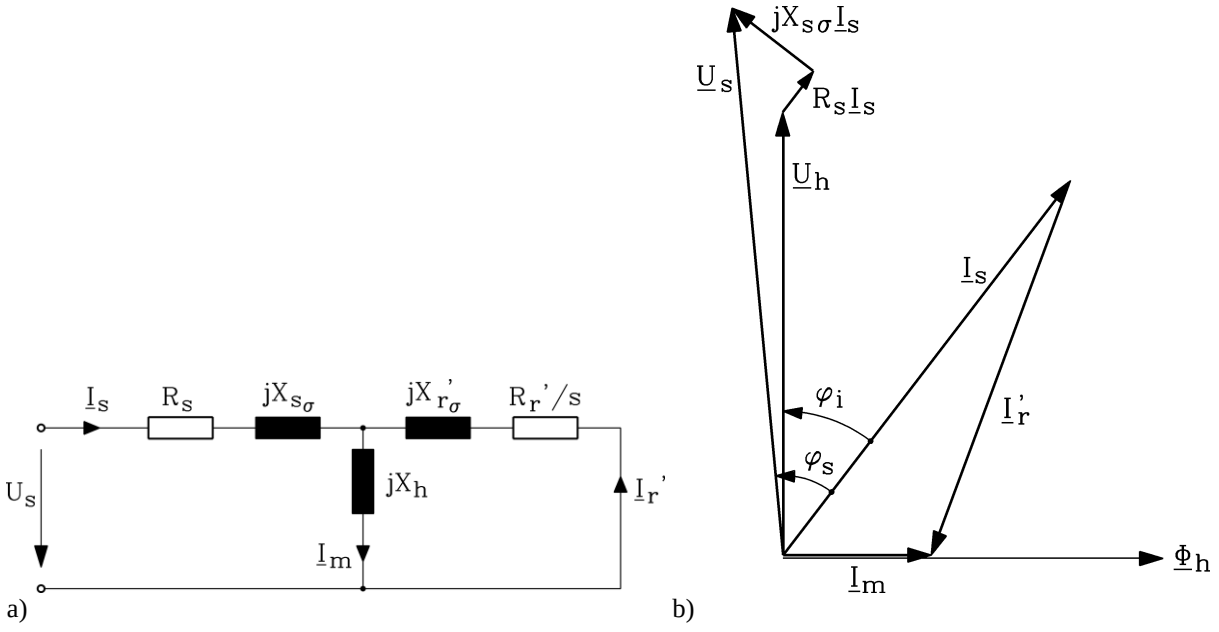

Fig. 2.2-2: Induction machine: a) Equivalent circuit per phase for fundamental air gap flux density distribution, sinusoidal currents and voltages (iron losses $P_{Fe,s}$ neglected, U_s assumed in real axis), b) Corresponding phasor diagram for motor operation

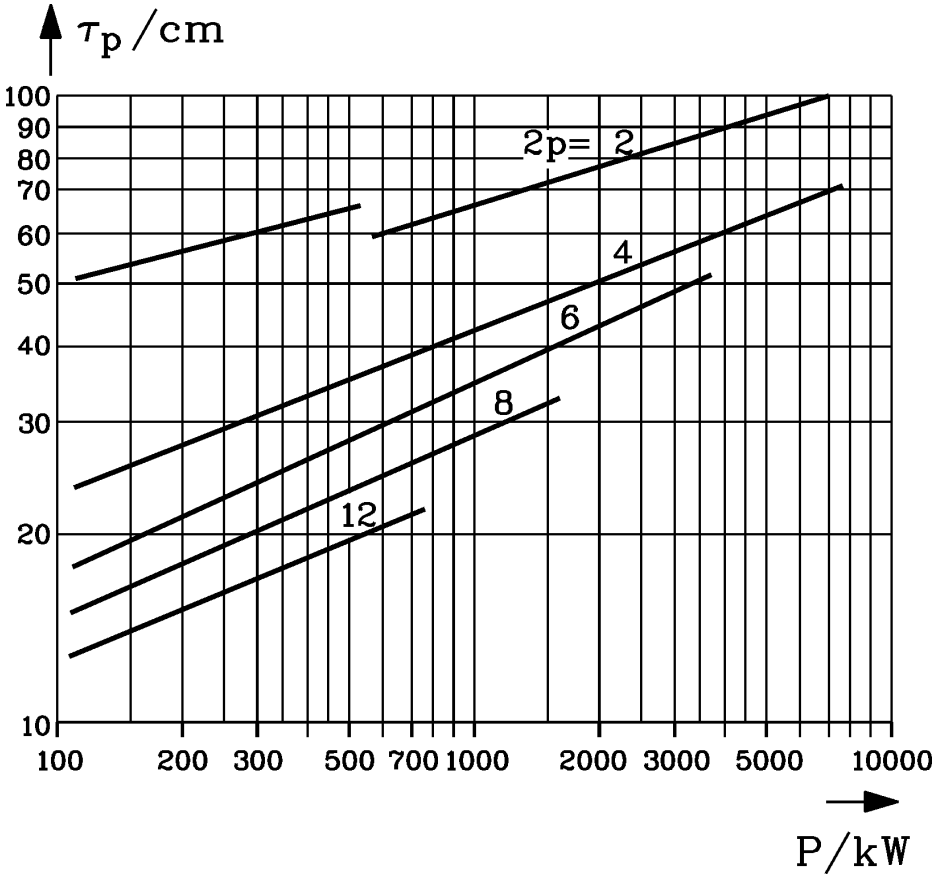

Fig. 2.2-3: Pole pitch of built induction machines for pole numbers 2, 4, 6, 8, 12

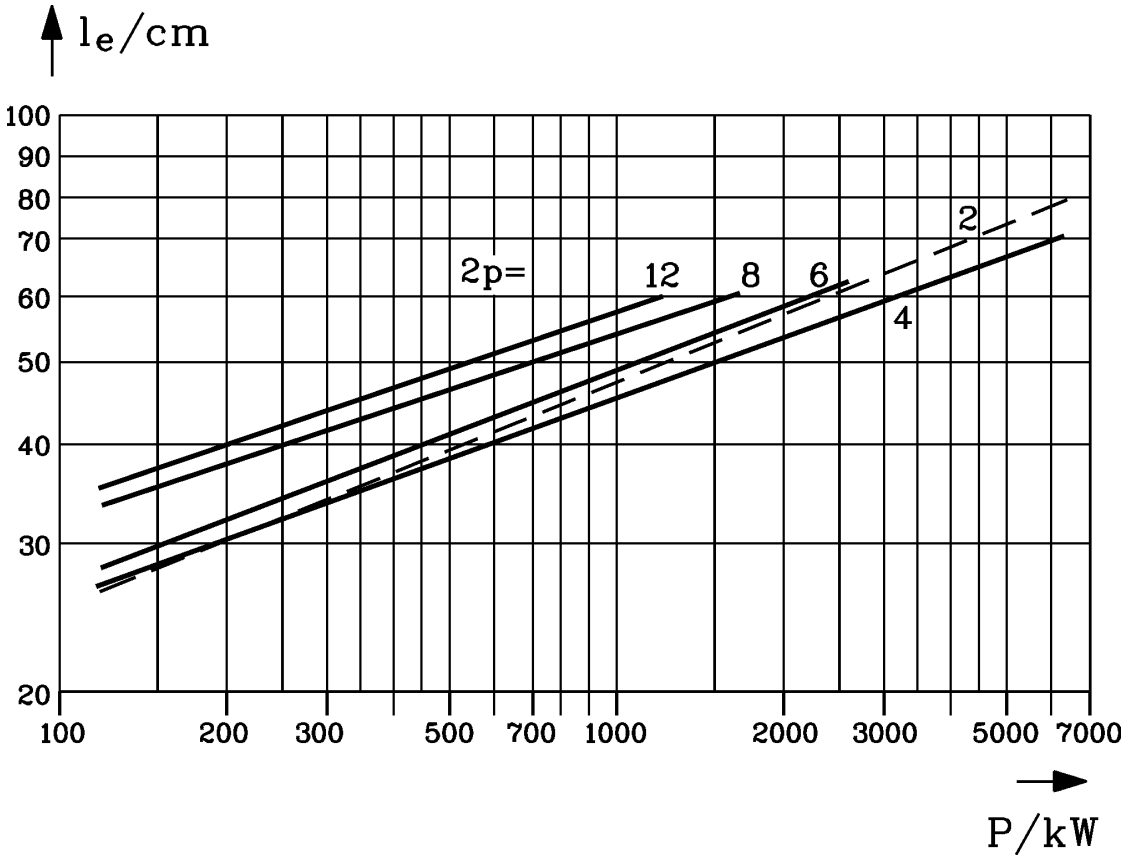

Fig. 2.2-4: Equivalent iron stack length of built induction machines for pole numbers 2, 4, 6, 8, 12

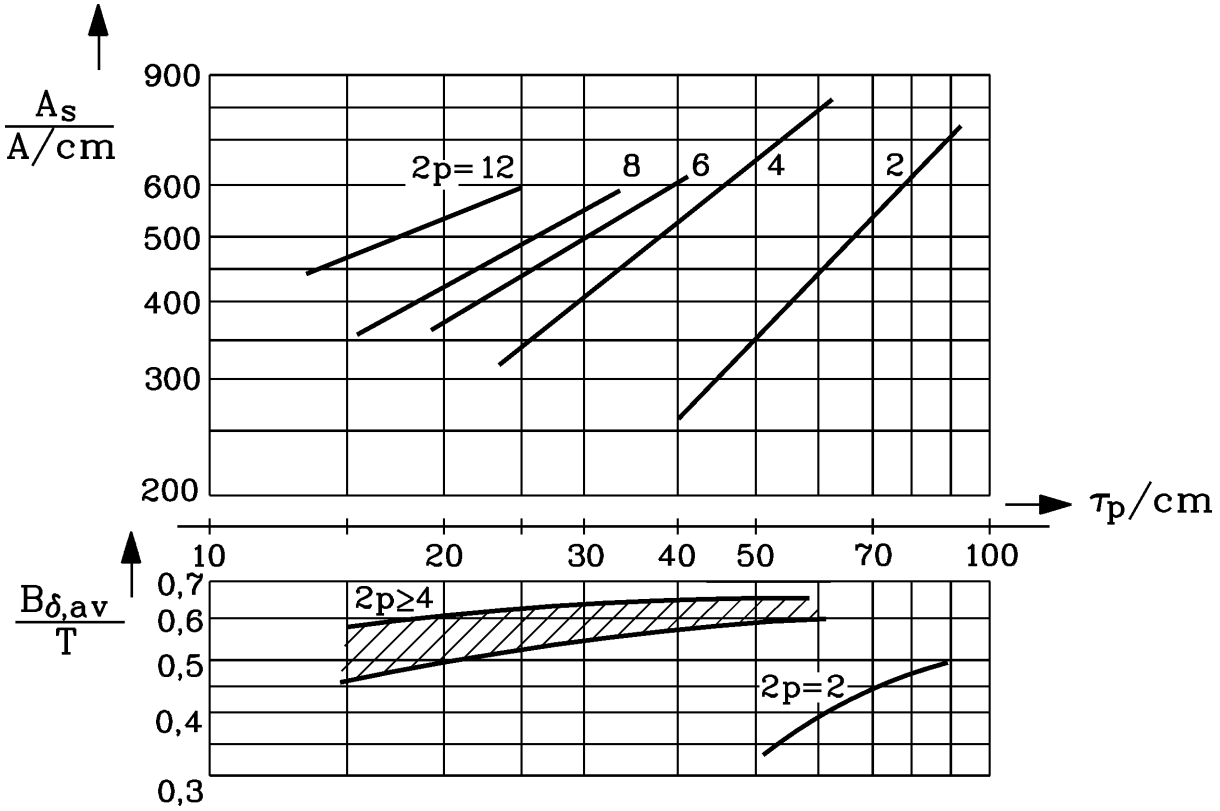

Fig. 2.2-5: Above: Current loading of built induction machines for pole numbers 2, 4, 6, 8, 12; open ventilated air cooled machines, Thermal Class B (temperature rise 80 K over 40 °C ambient); below: Average flux density

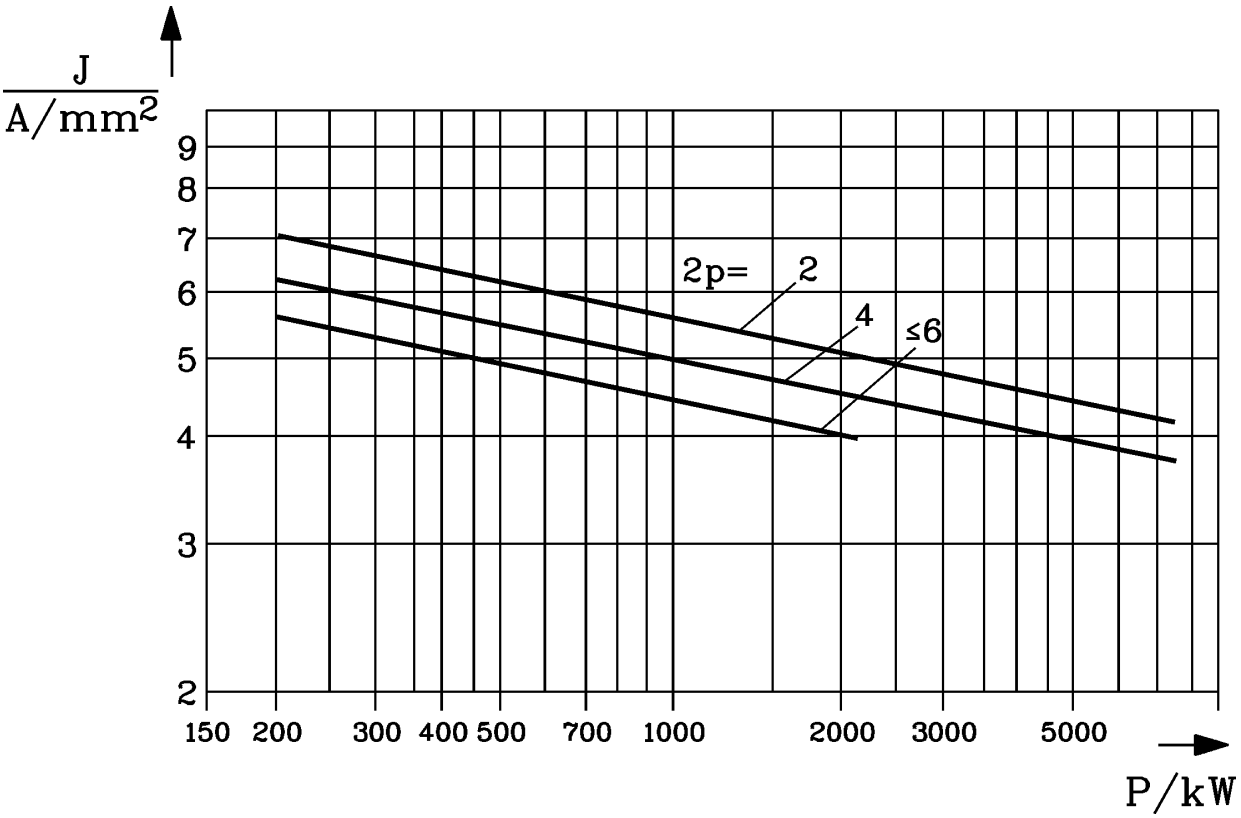

Fig. 2.2-6: Current density of built 6 kV induction machines for pole numbers 2, 4 and ≥ 6; open ventilated air cooled machines, Thermal Class B (temperature rise 80 K over 40 °C ambient)

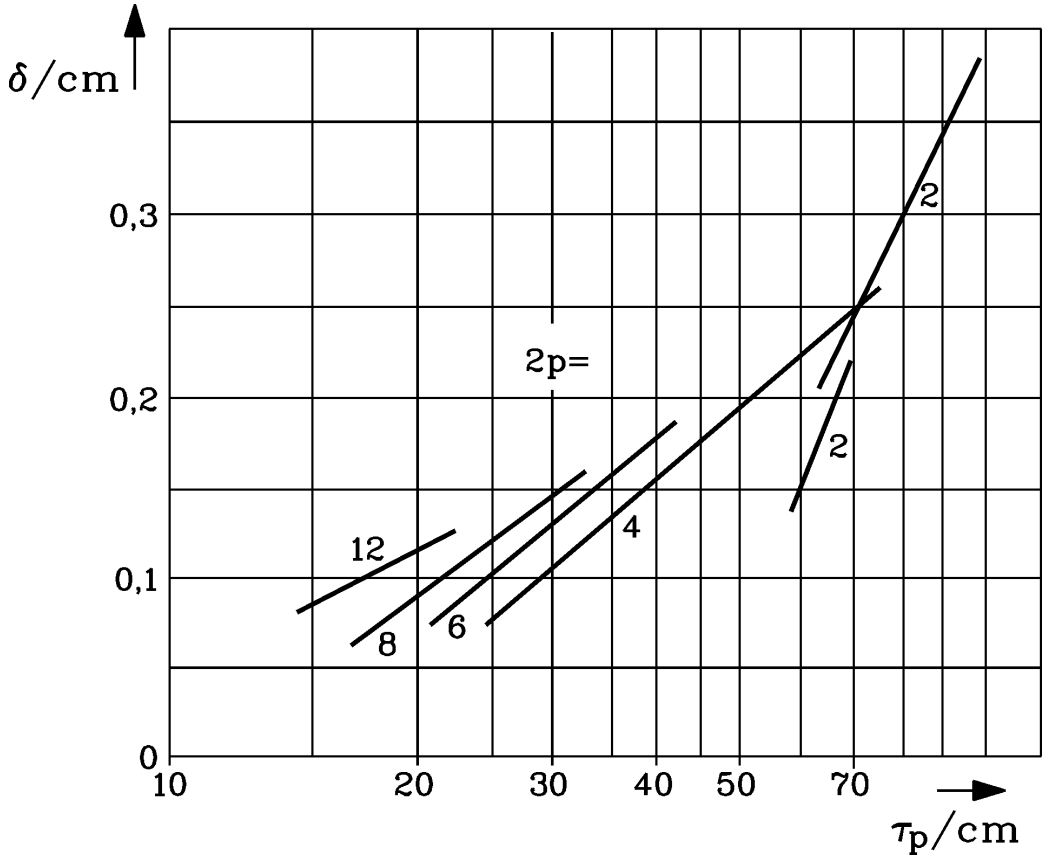

Fig. 2.2-7: Increase of air gap width with increasing induction machine size (pole pitch) for pole numbers 2, 4, 6, 8 and 12

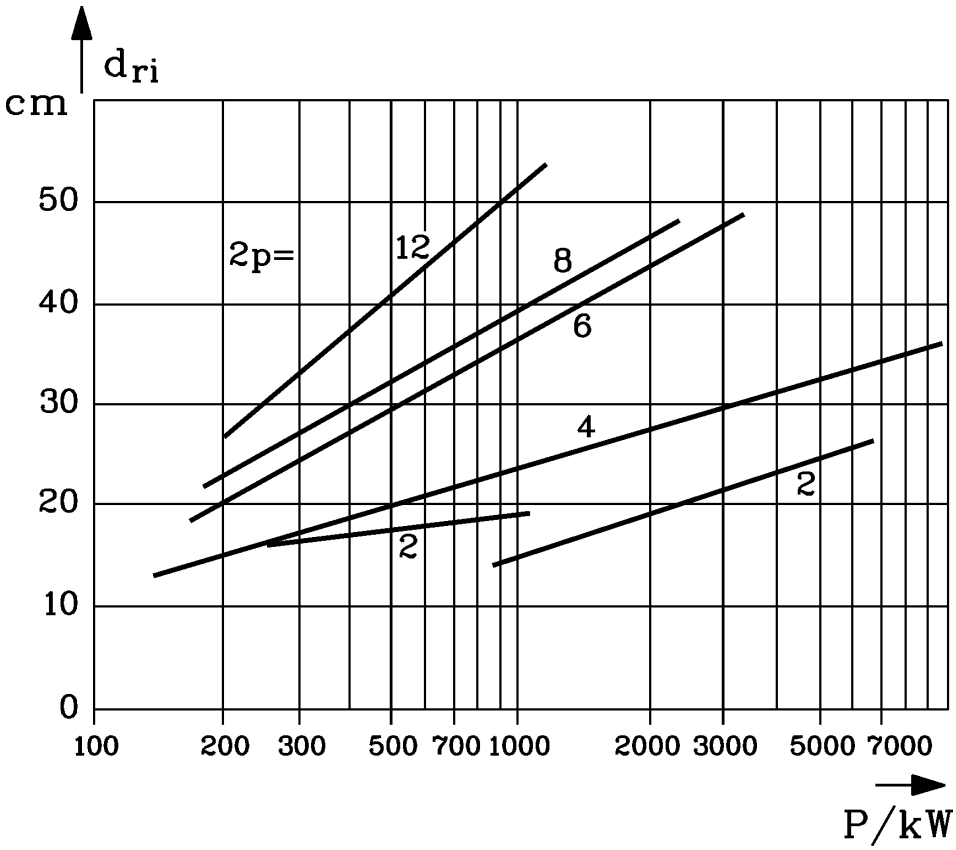

Fig. 2.2-8: Increase of shaft diameter, which is assumed to be equal to inner rotor stack diameter d_{ri}, with increasing induction machine power and size for pole numbers 2, 4, 6, 8 and 12

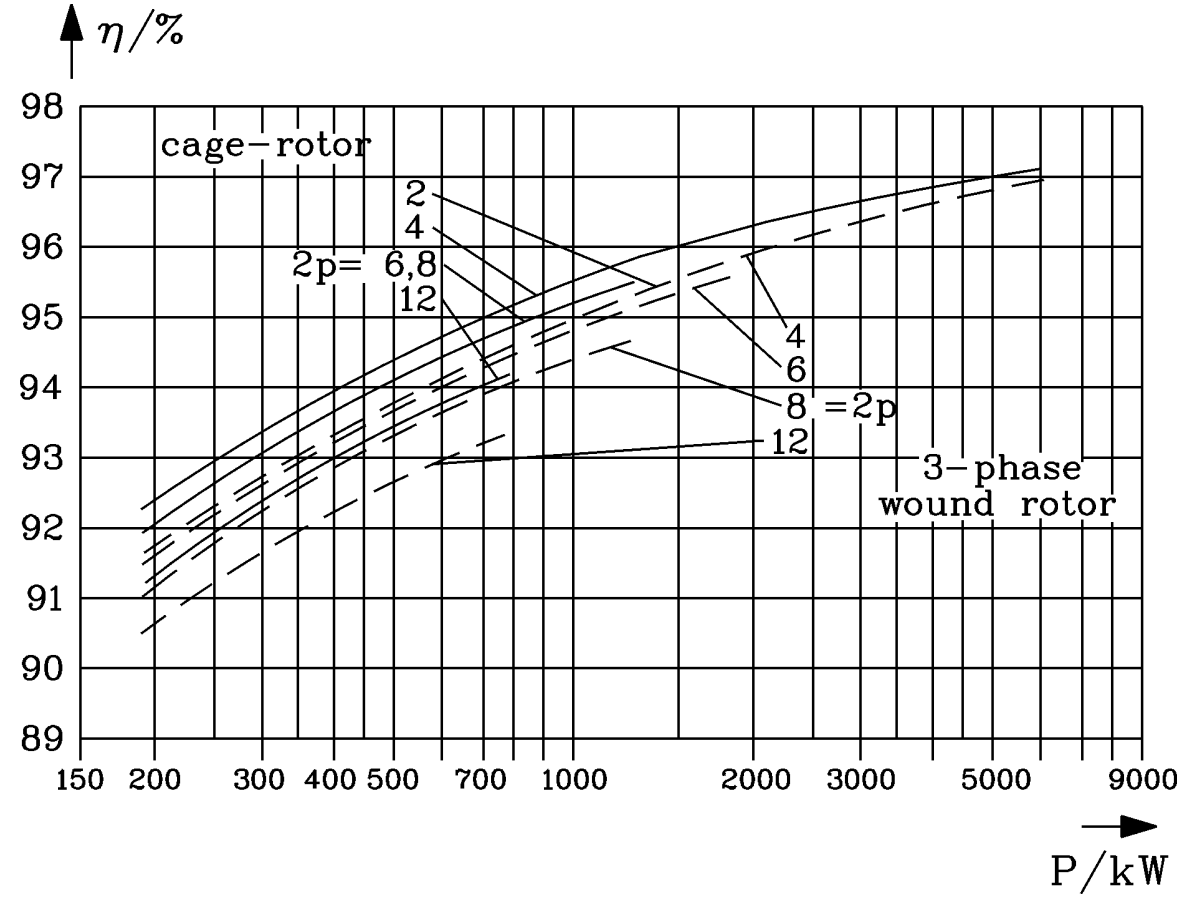

Fig. 2.2-9: Increase of efficiency with increasing induction machine power at pole numbers 2, 4, 6, 8 and 12 for cage and wound rotor, 6 kV, 50 Hz, Thermal Class B, open ventilated machines

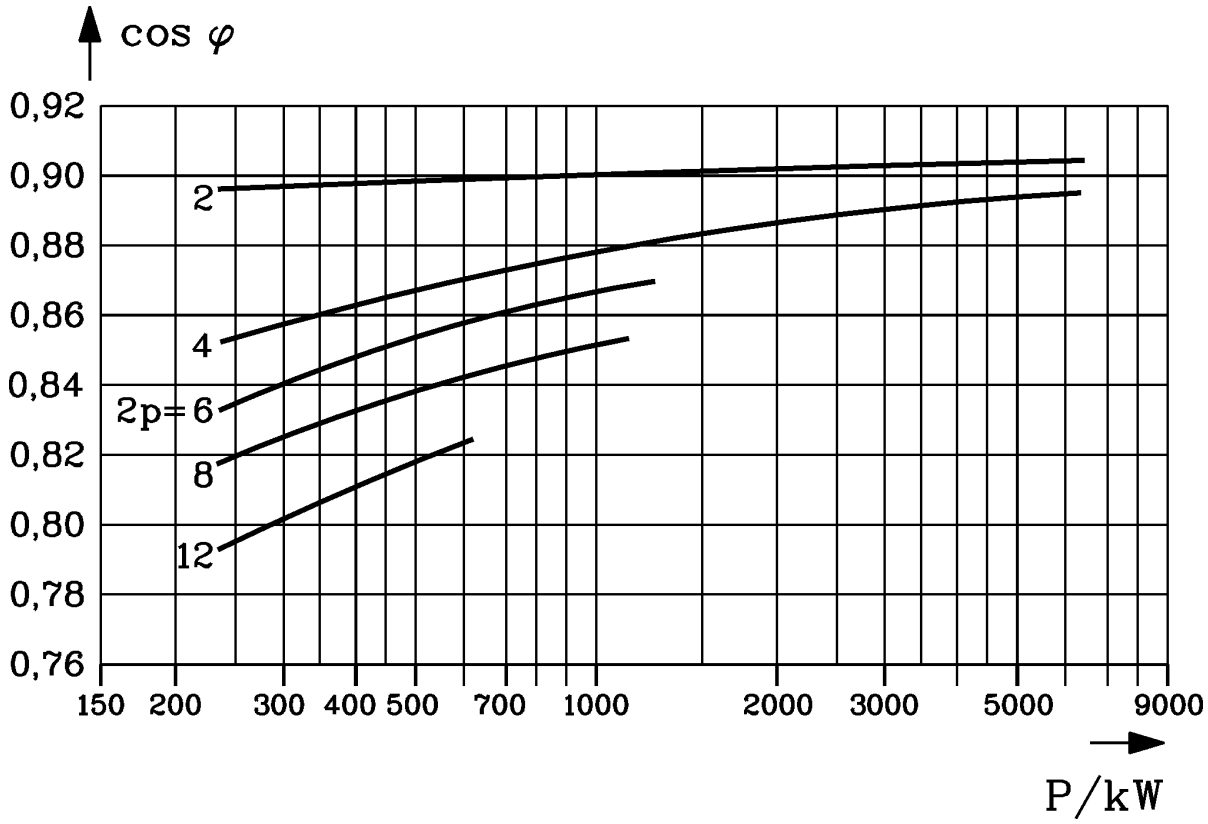

Fig. 2.2-10: Increase of power factor with increasing induction machine power at pole numbers 2, 4, 6, 8 and 12 for cage and wound rotors, 6 kV, 50 Hz, Thermal Class B, open ventilated machines

In Chapter 1 it was shown, that copper losses may described as $P_{Cu} \sim L^3$, which holds also for iron and additional losses $P_d \sim L^3$. Machine output power is according to (2.2-6) $P \sim L^4$, therefore efficiency rises with increased machine size (Fig. 2.2-9):

$$\eta = \frac{P}{P + P_d} = \frac{1}{1 + P_d / P} = \frac{1}{1 + const./L} \quad . \tag{2.2-6}$$

As power rises with speed, machine efficiency rises also with increased speed (or decreased pole count):

Motor: $$\eta = \frac{P}{P + P_d} = \frac{2\pi \cdot n \cdot M}{2\pi \cdot n \cdot M + P_d} \tag{2.2-7a}$$

Generator: $$\eta = \frac{P - P_d}{P} = \frac{2\pi \cdot n \cdot M - P_d}{2\pi \cdot n \cdot M} \quad . \tag{2.2-7b}$$

With increased pole count and therefore reduced pole pitch the ratio τ_p/δ is decreasing, thus decreasing X_h (Chapter 1). Therefore magnetizing current increases with increasing pole count, yielding lower power factor for higher pole numbers (Fig. 2.2-10). With increasing machine size the ratio of stray flux versus main flux Φ_σ/Φ_h may be decreased: Thus power factor rises with increasing machine size (Fig. 2.2-10).

Starting design process from given power, speed and voltage demand has to be done first with some estimates for power factor and efficiency, which can be taken from already built machines. The values in Fig. 2.2-9 and 2.2-10 are valid for rated voltage 6 kV and rated frequency 50 Hz, but may also be taken roughly for other voltage and frequency. Internal apparent power S_δ is smaller/bigger than terminal apparent power S_N in motor/generator operation due to stator stray flux and resistive voltage drop (Fig. 2.2-6b). Neglecting R_s and assuming, that stator leakage is half of total leakage $\sigma_s = \Phi_{\sigma s} / \Phi_h \approx \sigma / 2$, we estimate $U_h = U_s / (1 + \sigma_s)$ for motor and $U_h = U_s \cdot (1 + \sigma_s)$ for generator mode.

$$S_\delta = 3 \cdot U_h \cdot I_s, \quad S = 3 \cdot U_s \cdot I_s, \quad S_\delta = S / (1 + \sigma_s) \text{ (motor mode)} \tag{2.2-8}$$

A good choice for *Blondel´*s stray coefficient is σ = 0.08 ... 0.1.

Example 2.2-1:
Given values for a three-phase induction machine to be designed:
Motor, P_N = 500 kW, 6 kV, 50 Hz, 4 pole.

- Estimated values from Figs. 2.2-9, 2.2-10: η_N = 94.4 %, $\cos\varphi_N$ = 0.868
- Motor output power: 500 kW, apparent power: $S_N = \frac{P_N}{\eta_N \cdot \cos\varphi_N} = 610\,\text{kVA}$
- Motor current: $I_{sN} = \frac{S_{sN}}{\sqrt{3} \cdot U_{sN}} = \frac{610}{\sqrt{3} \cdot 6} = 59\,\text{A}$,
- synchronous speed: $n_{syn} = f_s / p = 1500/\text{min}$
- Pole pitch 360 mm, stack length: 380 mm, air gap: 1.4 mm, shaft diameter: 200 mm,
- Current loading: 500 A/cm, current density: 5.5 A/mm^2,
- Stator bore diameter: $d_{si} = 2p\tau_p / \pi = 458\,\text{mm}$.

- Internal apparent power: (σ_s = 0.08/2 = 0.04): $S_\delta = S/(1+\sigma_s) = 610/1.04 = 587\text{kVA}$
- Electromagnetic utilization: $C = S_\delta/(d_{si}^2 \cdot l_{Fe} \cdot n_{syn}) = 4.9\,\text{kVA·min/m}^3$
- Flux density (k_{w1} = 0.91 estimated): $C = \frac{\pi^2}{\sqrt{2}} \cdot k_{w1} \cdot A \cdot B_\delta \quad \Rightarrow \quad B_\delta = \underline{\underline{0.927}}\,\text{T}$. This value is in the range indicated in Fig.2.2-4: 0.89 ... 0.99 T.
- Thermal utilization: $A \cdot J = 2750\,(\text{A/cm})(\text{A/mm}^2)$

2.3 Stator winding low and high voltage technology

a) Single and two-layer winding:

Three phase windings may be wound as **single layer** or **two layer** windings. For single layer windings usually round wire coils are used, and the *q* coils per pole and phase are often arranged **concentric** (Fig. 2.3-1a). Due to crossing of winding overhangs of coils the coils are bent in the overhang region and are therefore manufactured either in two or three different sizes (Fig. 2.3-2, 2.3-3) to allow bending. Bending of round wire coils is possible, but round wire coils are insulated only for low voltage application (< 1000 V). Note that due to series connection of the coils of different size in a four pole machine (and multiples) according to Fig. 2.3-2 the resistance and stray inductance per phase is identical for all three phases. In case of Fig. 2.3-3 this is not the case.

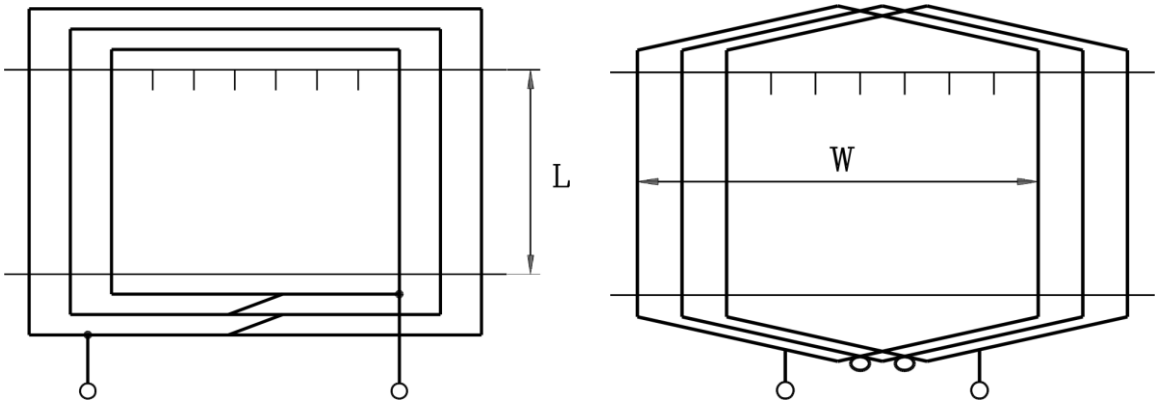

Fig. 2.3-1: Coil groups per pole and phase (here: *q* = 3 per group): left: concentric coils, right: coils with identical span

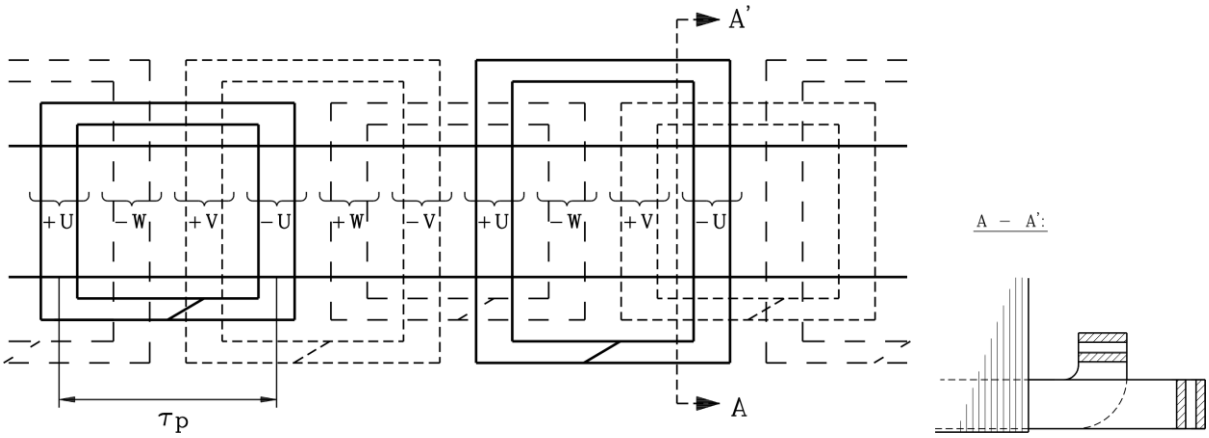

Fig. 2.3-2: Single layer winding: Two different sizes of concentric coil groups (here: *q* = 2 coils per pole and phase): left: coil arrangement (without coil connectors) , right: cross section of winding overhang

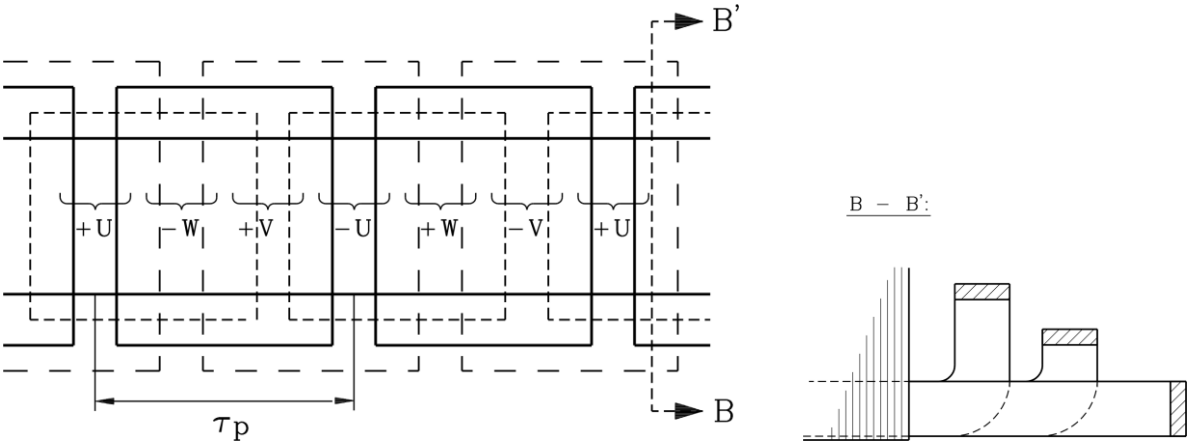

Fig. 2.3-3: Single layer winding: Three different sizes of coils (here: q = 2 coils per pole and phase): left: coil arrangement (without coil connectors), right: cross section of winding overhang

Two layer windings are often manufactured with profile copper (rectangular cross section of conductors), which allow fabrication of form wound coils with high voltage insulation, typically ranging 1 kV ... 24 (30) kV, the latter being used for big synchronous generators. According to Fig. 2.3-4 crossing of coils in winding overhangs is avoided due to two-layer arrangement.

The induced voltages per coil in a coil group, induced by harmonic flux density waves (ordinal number $|\nu| > 1$) with $|\nu| p$ pole pairs, are phase shifted by $\frac{\nu \cdot 2\pi}{m \cdot q}$. Series connection of these coils may therefore lead to cancelling of certain harmonic voltages. Therefore both single and two-layer windings are manufactured with $q > 1$ to allow filtering of inducing harmonic voltage by the **distribution factor**

$$k_{d\nu} = \frac{\sin\left(\frac{\nu \cdot \pi}{2 \cdot m}\right)}{q \cdot \sin\left(\frac{\nu \cdot \pi}{2 \cdot q \cdot m}\right)} \quad . \tag{2.3-1}$$

Example 2.3-1:
Reduction of harmonic induced voltage e.g. for q = 3
- for $\nu = -5 : k_{d,-5} = 0.218$, $\nu = 7 : k_{d,7} = -0.177$.

Note that also fundamental flux linkage is reduced a little bit: $\nu = 1 : k_{d,1} = 0.960$.

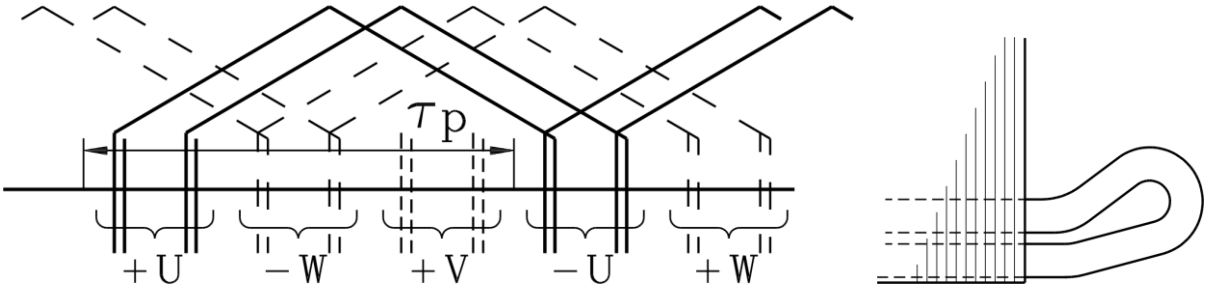

Fig. 2.3-4: Two layer winding: Identical sizes for all coils (here: q = 2 coils per pole and phase): left: coil arrangement with full pitched coils, right: winding overhang

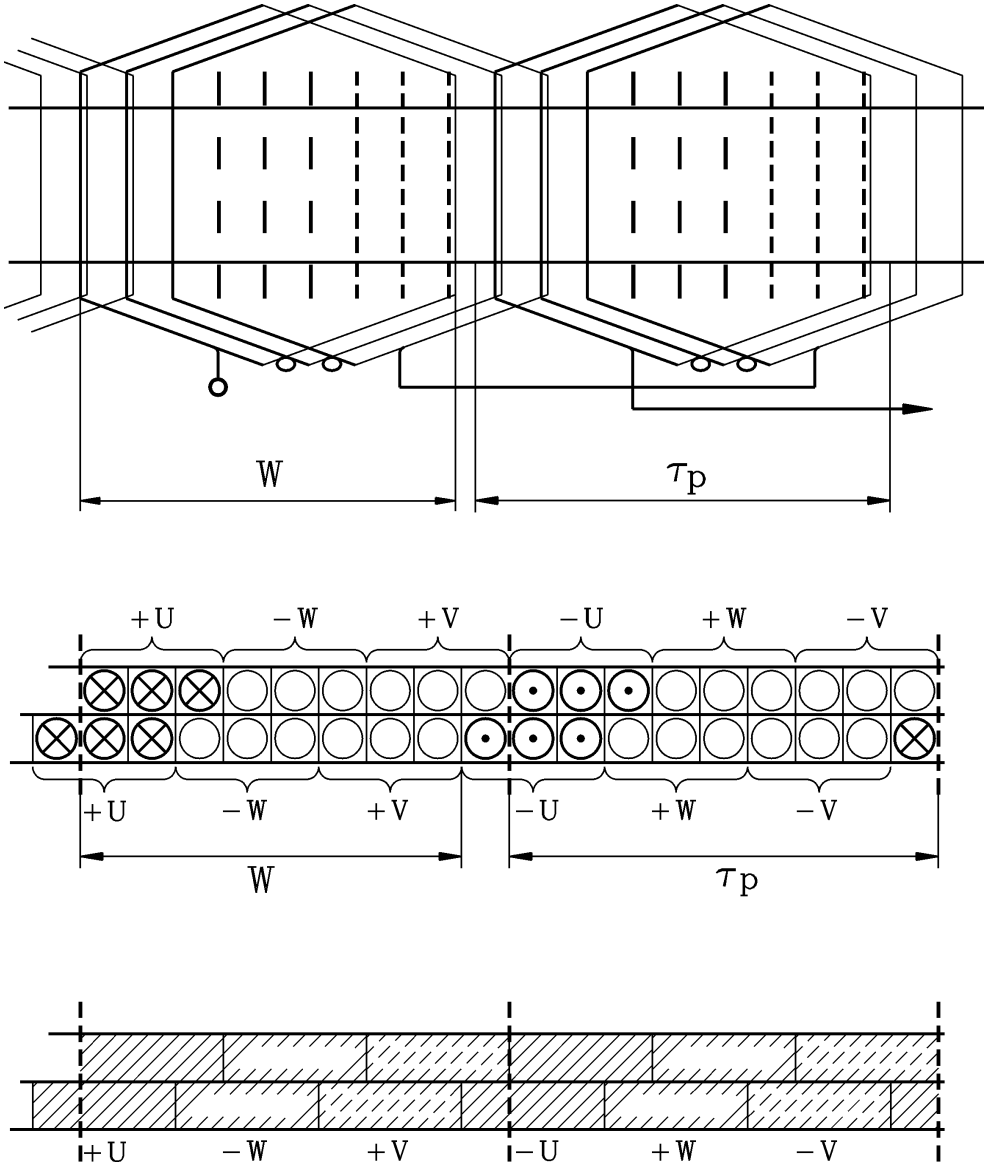

Fig. 2.3-5: Two layer lap-wound winding: Above: Arrangement of pitched coils per phase and connection of coil groups for N- and S-pole (here: q = 3 coils per pole and phase, pitch W/τ_p = 8/9), below: cross section of coil arrangement in slots, showing all three phases U, V, W in upper and lower layer, being symbolized by phase belts (bottom) without depicting single slots

Mostly **lap-wound two layer windings** are used (Fig. 2.3-5), except for large synchronous hydro generators with high pole count, where wave wound windings allow reduction of coil connections in the winding overhang region. Advantage of two-layer winding is pitching of coils, meaning that the coils span W is smaller than pole pitch. This allows electromagnetic filtering of air gap flux density harmonics, which also induce stator winding, which is described by **pitching factor** (chording factor) k_p.

$$k_{p\nu} = \sin(\nu \frac{\pi}{2} \cdot \frac{W}{\tau_p}) \tag{2.3-2}$$

Example 2.3-2:

The flux linkage with stator winding of harmonic flux density waves with $|\nu| p$ pole pairs is reduced for W/τ_p = 8/9 e.g. for $\nu = -5 : k_{p,-5} = 0.64$, $\nu = 7 : k_{p,7} = -0.34$.

Note that also fundamental flux linkage is reduced a little bit: $\nu = 1 : k_{p,1} = 0.984$

Resulting effect of distributed winding and pitching of coils is described by **winding factor**

$$k_{wv} = k_{dv} \cdot k_{pv} \quad . \tag{2.3-3}$$

Further a reduction of amount of copper for winding overhang by W/τ_p is possible. Usually the three phases of two layer winding are arranged in **six sections** of phase belt per pole pair: +U, -W, +V, -U, +W, -V.

b) Slot and coil arrangement and winding insulation:

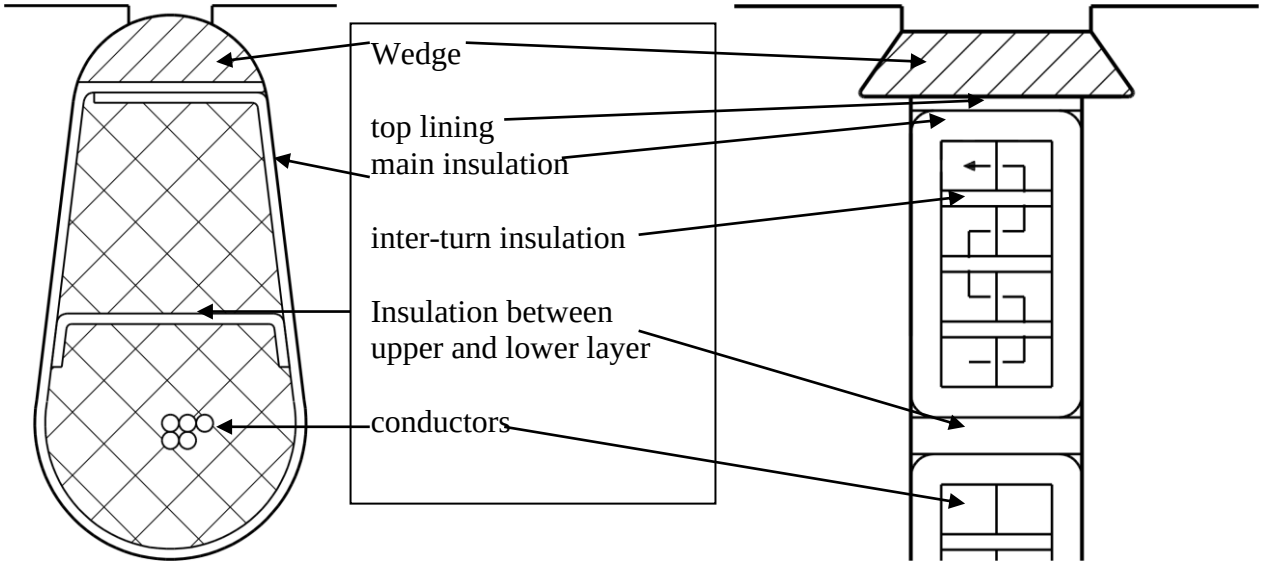

Fig. 2.3-6: Slot geometry: left: Oval semi-closed slot for round wire low voltage, two-layer coil arrangement, right: rectangular slot for form wound high voltage, two-layer coil arrangement with $N_c = 8$ turns per coil

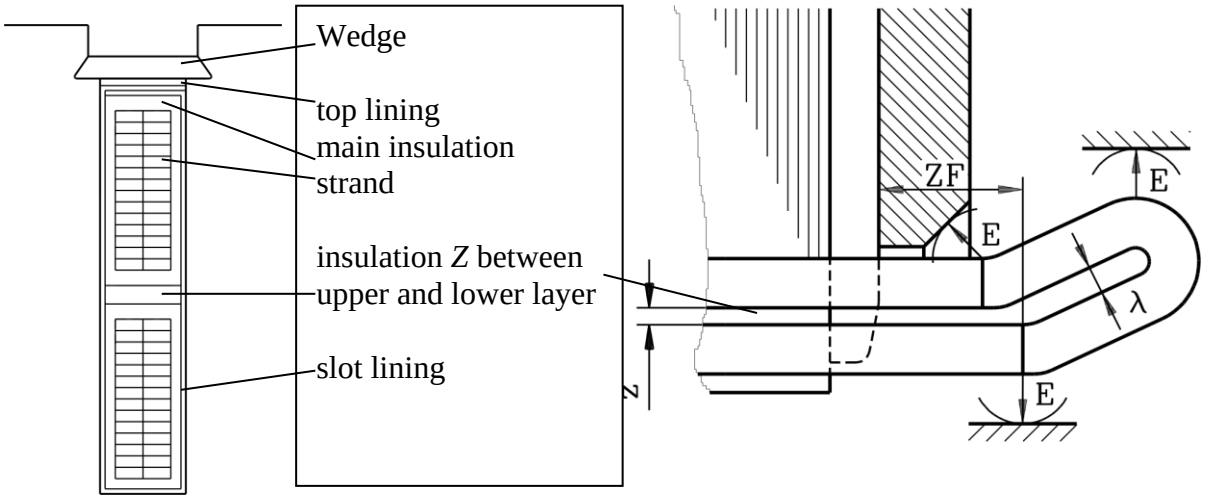

Fig. 2.3-7: *Roebel* bar: left: Cross section in slot with 24 strands per bar, right: winding overhang with clearing *E* to end shields (on earth potential) and clearing *ZF* of end of main insulation from pressing construction of iron stack end

Geometry of slots for **round wire coils** is oval, as round wire coils fill any shape. Oval slots lead to teeth with parallel tooth sides, so tooth flux density is constant within tooth (Fig. 2.3-6). Slot opening may be semi-closed, as each turn of coil is put into coil step by step. Form wound coils, mostly used for high voltage, need slot shape with parallel slot sides. Slots must be open, as the fully impregnated and insulated prefabricated **form-wound coil** is put into the

slot as a whole piece. Parallel slot sides lead to conical tooth shape, so tooth flux density is highest at narrowest part of tooth. Glass fibre wedges are used to close the slots. In case of rectangular slots often magnetically wedges with μ_r = 5 ... 9 are used to reduce influence of slot opening on air gap field.

In **very big machines** the current per conductor is so big, that one conductor per slot and layer (N_c = 1) is needed to get the necessary conductor cross section. Due to the AC current with stator frequency the AC slot leakage flux will induce eddy currents in the conductor, leading to additional losses in the conductor and uneven current density distribution. Whereas this effect of **current displacement** is wanted in cage conductors for increased starting torque (see: Lectures "Electrical machines and Drives"), it is unwanted in stator winding. Therefore the single conductor is segmented into many parallel insulated strands, which are twisted in special way to avoid eddy currents. These conductors (***Roebel* bars**) are used in large synchronous generators (Fig. 2.3-7).

Insulation is necessary between wires of one coil (conductor and inter-turn insulation), between coil and stator core (which is on earth potential for safety reasons) by main insulation and between different phases in the winding overhangs (inter-phase insulation) and in the slots between upper and lower layer. **Low voltage windings** are insulated with special paper or plastic foils or linings, which are impregnated with resin. Conductors are insulated by enamel coating on copper wire, or – for higher temperature – with glass fibre coating. Low voltage winding with 400 V is used mainly for smaller machines up to typically 200 kW. Bigger power is designed with 690 V even up to 3 MW e.g. with wind generators. In that case a lot of parallel winding branches a and parallel strands a_i per conductor are necessary.

Special care must be taken for **high voltage windings,** which is used for bigger power – starting with about 500 kW and reaching to biggest machine power 2000 MVA (4-pole turbo generators for nuclear power plants). High voltage 3.15 kV and 6.3 kV are used between 0.5 MVA and several MVA, 10.5 kV usually above 1 MVA. **Main insulation** is made of many layers of special paper or glass fibre bands, coated with mica (mica foil), which is impregnated by epoxy resin usually under vacuum (pressure < 1 Torr). Admissible average electric strength within main insulation is about 30 kV/cm.

Rated voltage (line-to-line, r.m.s.)	kV	3.3	6.6	11.0	13.8	16.5
Slot main insulation, thickness d	mm	1.5	2.2	3.2	3.8	4.5
Inter-layer insulation, thickness Z	mm	3	4	6	7	8
Top lining thickness	mm	0.3	0.4	0.6	0.7	0.8
Winding overhang main insulation, thickness d_s	mm	2	2.5	3.5	4	4
Clearing of slot main insulation ZF	mm	25	45	80	100	110
Clearing between coils in winding overhang λ	mm	3	4	6	7	8
Clearing from winding overhang to earth potential E	mm	25	35	55	65	75
Total conductor insulation thickness (both sides), glass fibre, inter-turn voltage < 80 V	mm	0.3	0.4	0.4	0.4	0.5
Slot lining thickness in vertical direction and slot play	mm	1	2	2	2	2

Table 2.3-1: High voltage insulation for stator winding

Example 2.3-3:

6.6 kV rated voltage, Y connected winding, phase voltage $6.6/\sqrt{3} = 3.8\,\text{kV}$ (r.m.s.):
Insulation thickness (Table 2.3-1): d = 2.2 mm
$\hat{E} = \hat{U}_s / d = \sqrt{2} \cdot 3.8 / 2.2 = 2.44$ kV/mm = 24.4 kV/cm < 30 kV/cm

Winding overhangs are also insulated with that material. Conductors are insulated with glass fibre coating. Additional **slot linings** protect the coil from sharp edges of iron. **Top linings** protect coils, when wedge is put into slot under pressure to fix the coils mechanically, as they are experiencing AC forces with twice stator frequency due to AC slot stray flux.

In order to put form wound coils into open slots without problem, an additional **play** is necessary. In horizontal direction it must be increased with increasing stack length, as coils sides tend to deviate from parallel due to stacking.

Iron stack length l_{Fe}	m	≤ 0.4	≤ 1.0	≤ 2.0
Slot lining thickness in horizontal direction and slot play	mm	0.4	0.5	0.8

Table 2.3-2: Horizontal slot lining thickness and play

Insulation of conductor increases not only with rated voltage, but also with **inter-turn voltage**, as is shown here for 6.6 kV rated voltage.

Inter-turn voltage	V	≤ 80	≤ 120	≤ 160
Total conductor insulation thickness (both sides), U_N = 6.6 kV	mm	0.4	0.5	0.8

Table 2.3-3: Conductor insulation thickness

Thermal expansion coefficient of insulation material is larger than that of copper and iron. So, duty cycles of electric machine with time varying temperature rise cause a compression of heated insulation with plastic deformation, causing gaps within iron and coils in the slots, when machine is cooled down again. In these small gaps **partial discharge** ("corona") may occur, therefore high voltage coils above 6 kV are covered with an enamel containing graphite to get a conductive layer (of very low conductivity). This **conductive layer band (outer anti-corona screen)** must be in contact with coil surface and slot surface, thus bridging the small gaps (voids) and limiting the voltage at the void to the resistive voltage drop in the conductive band. As this voltage is lower than the partial discharge inception voltage, no partial discharges may occur. In the same way the winding overhangs within the clearing ZF are covered with this "anti-corona layer". Often the conductor surface itself is covered with graphite enamel between conductor insulation and main insulation to get a more homogeneous electric field strength especially at the edges of the copper profiles, thus reducing partial discharge inception voltage within main insulation **(inner anti-corona screen)**.

2.4 Stator winding design

a) Winding arrangement:
Magnetic flux and ampere-turns both need space in the stator, therefore tooth and slot width are most often chosen nearly equal, yielding a ratio slot width versus slot pitch $b_{Qs} / \tau_{Qs} = 0.5 ... 0.6$. Coils in the power range 100 kW ... 10 000 kW are manufactured for slot widths b_{Qs} = 10 mm ... 20 mm. A high number of stator slots Q_s allows a high ratio of cooling coil surface versus coil volume, giving good cooling conditions, but needs more work for manufacturing stator winding (expensive !). A big q allows good filtering of harmonic voltages induced by air gap space harmonics.

Care must be taken concerning stator winding connection. With **star connected winding** the stator phase voltage is $U_{sN} = U_N / \sqrt{3}$, but line current is phase current $I_{sN} = I_N$, whereas with **delta connection** we get $U_{sN} = U_N$, $I_{sN} = I_N / \sqrt{3}$.
Number of turns per phase N_s depend on turns per coil N_c and on how many parallel branches a per phase exist. Parallel branches should be avoided as long as possible, as it must

always be secured that current sharing between parallel branches is correct to avoid overheating of one branch. In case of two-layer winding number of coil groups is equal to number of poles, whereas with single layer winding number of coil groups is only half pole number.

two-layer: $N_s = 2p \cdot q \cdot N_c / a$, single layer: $N_s = p \cdot q \cdot N_c / a$ (2.4-1)

With increasing machine size pole flux increases, demanding lower number of turns per phase for given voltage, with increased conductor cross section for the increased current. Conductor height h_L must be limited at 50 Hz to about 3 ... 4 mm to avoid additional eddy currents being induced by AC slot stray flux. If this limit is reached, parallel branches $a > 1$ are chosen to increase N_c, thus reducing h_L for given slot height. If this is not sufficient, each turn of a winding (conductor) may be split into several (a_i) parallel strands to reduce conductor height further. Details for calculating eddy current losses with stranded conductors are discussed in Lectures: "Large generators and high-power drives". Solving *Maxwell´*s equations for eddy-current generation in conductors due to AC slot flux yield necessary condition for avoiding eddy current losses (n_{ne}: number of conductors aside in slot)

$$\xi = h_L \cdot \sqrt{\frac{\mu_0 \cdot \omega \cdot \kappa \cdot n_{ne} \cdot b_L}{2 \cdot b_Q}} < 0.35 \qquad (2.4\text{-}2)$$

Example 2.4-1:

Data: Induction machine: P_N = 500 kW, 6 kV, Y, 50 Hz, 4 poles, three phases,
pole pitch 360 mm, stack length: 380 mm, stator bore diameter: $d_{si} = 2p\tau_p / \pi = 458\,\text{mm}$.

Stator winding design:

- Chosen number of slots: $q = 5$, $Q_s = 2p \cdot m \cdot q = 4 \cdot 3 \cdot 5 = 60$, leads to 15 slots per pole
- Slot pitch: $\tau_{Qs} = d_{si}\pi / Q_s = 24.0\,\text{mm}$
- Coil pitching is possible in steps of one slot pitch: W/τ_p = 14/15, 13/15 etc., chosen pitch W/τ_p = 12/15 leads to $k_{ps,1} = 0.951$, $k_{ps,-5} = 0$, $k_{ps,7} = 0.588$. The influence of 5th space harmonic is completely eliminated.
- Distribution factor: $k_{ds,1} = 0.957$, stator winding factor: $k_{ws,1} = 0.957 \cdot 0.951 = 0.910$
- With chosen air gap flux density 0.9 T main flux per pole of fundamental $\nu = 1$ is

$$\Phi_h = \frac{2}{\pi} \cdot \tau_p \cdot l_{Fe} \cdot B_{\delta,\nu=1} = \frac{2}{\pi} \cdot 0.36 \cdot 0.38 \cdot 0.9 = 78.4\,\text{mWb}.$$

- Choice of number of turns per phase N_s:

Estimated induced voltage per phase: $U_h = \frac{U_N / \sqrt{3}}{1 + \sigma_s} = \frac{6000/\sqrt{3}}{1.04} = 3330\,\text{V}$

$$U_h = \sqrt{2}\pi f_s \cdot N_s k_{ws1} \cdot \Phi_h \quad \Rightarrow \quad N_s = 210.17$$

$N_c = N_s \cdot a / (2pq) = 210.17 \cdot 1 / (2 \cdot 2 \cdot 5) = 10.5$, so integer value $N_c = \underline{\underline{10}}$ for a = 1 is chosen.

- Final values:

$N_c = 10$, $N_s = 200$, a = 1, for $U_h = 3330\,\text{V}$: $B_{\delta,\nu=1} = 0.946$ T

b) Coil and slot design:

Sizes of round wire copper and profile copper are standardized on the market and are available with single enamel coating (L), double layer coating (2L) for increased voltage stress (Table 2.4-1 and 2.4-2).

wire diameter (mm)	wire cross section (mm^2)	insulated wire diameter (L) (mm)	insulated wire diameter (2L) (mm)
0.1	0.00785	0.121	0.129
0.2	0.03142	0.230	0.245
0.315	0.07793	0.352	0.371
0.4	0.1257	0.442	0.462
0.5	0.1963	0.548	0.569
0.63	0.3117	0.684	0.706
0.71	0.3959	0.767	0.790
0.8	0.5027	0.861	0.885
0.9	0.6362	0.965	0.990
1.0	0.7854	1.068	1.093
1.25	1.227	1.325	1.351
1.4	1.539	1.479	1.506
1.6	2.011	1.683	1.711
1.8	2.545	1.868	1.916
2.0	3.142	2.092	2.120
2.36	4.374	2.459	2.488
2.65	5.516	2.754	2.784
3.0	7.069	3.110	3.142
3.55	9.898	3.676	3.702

Table 2.4-1: Selection of available round copper wire

b_L (mm)	Conductor height h_L (mm)									
	1.8	*2*	*2.24*	*2.5*	*2.8*	*3.15*	*3.55*	*4*	*4.5*	*5*
5	8.637	9.637	10.84	11.95	13.45	15.20	17.22	-	-	-
5.6	9.717	10.84	12.18	13.45	15.13	17.09	19.33	21.54	-	-
6.3	10.98	12.24	13.75	15.20	17.09	19.30	21.82	24.34	27.49	-
7.1	12.42	13.84	15.54	17.20	19.33	21.82	24.66	27.54	31.09	34.64
8	14.04	15.64	17.56	19.45	21.85	24.65	27.85	31.14	35.14	39.14
9	15.84	17.64	19.80	21.95	24.65	27.80	31.40	35.14	39.64	44.14
10	17.64	19.64	22.04	24.45	27.45	30.95	34.95	39.14	44.14	49.14
11.2	19.80	22.04	24.73	27.45	30.81	34.73	39.21	43.94	49.54	55.14
12.5	22.14	24.64	27.64	30.70	34.45	38.83	43.83	49.14	55.39	61.64
14	24.84	27.64	31.00	34.45	38.65	43.55	49.15	55.14	62.14	69.14
16	-	31.64	35.48	39.45	44.25	49.85	56.25	63.14	71.14	79.14

Table 2.4-2: Selection of available profile copper wire: dimensions without enamel coating and cross section (edges of wire rounded by 0.5 mm .... 1.0 mm radius)

Low voltage winding is usually manufactured of round wire, whereas **high voltage** winding is made of profile copper conductors with special main insulation on prefabricated coils. As in low voltage winding copper wires are randomly distributed in slot, it is not possible to make an exact coil design for slot, but one uses **slot fill factor** k_f for calculating slot.

$$k_f = \frac{A_{Cu}}{A_Q} \tag{2.4-3}$$

The whole cross section of conductors per slot is taken as A_{Cu}, whereas A_Q is the cross section of the slot. With single layer winding no inter-layer insulation is necessary, so slot fill factor is slightly higher than for two-layer winding. Theoretical maximum value for fill factor is

$$k_{f,\max,th} = \frac{d_L^2 \cdot \pi / 4}{d_L^2} = \pi / 4 = 0.79 \quad , \tag{2.4-5}$$

but practical values for coils, which are filled in semi-closed slots wire by wire, are much lower, on one hand due to the slot insulation, but also due to irregular positions of wires.

	single layer winding	double layer winding
slot fill factor k_f	≤ 0.45	≤ 0.42

Table 2.4-3: Slot fill factors for low voltage, random wound winding with round copper wire

Example 2.4-2:
Data: Standard induction motor, totally enclosed, shaft mounted-fan, 2-pole, 400 V, D, 50 Hz, 30 kW, power factor 0.87, efficiency 90.6%, insulation Thermal Class B (80 K temperature rise); d_{si} = 180 mm, l_{Fe} = 175 mm, Q_s = 36, oval shaped semi-closed slot (Fig. 2.3-6 left): A_Q = 194 mm^2, σ_s = 0.05, single layer winding with round copper, N_c = 13, a = 1. Each turn per winding consists of a_i = 8 parallel wires with diameter d_{Cu} = 1.0 mm.

Calculation of stator winding design and motor utilization:

- Stator line current: $I_N = \frac{S_N}{\sqrt{3} \cdot U_N} = \frac{P_N / (\cos\varphi_N \cdot \eta_N)}{\sqrt{3} \cdot U_N} = \frac{30000/(0.87 \cdot 0906)}{\sqrt{3} \cdot 400} = 54.9\,\text{A}$
- Stator phase current: $I_{sN} = I_N / \sqrt{3} = 54.9 / \sqrt{3} = 31.7\,\text{A}$
- Induced voltage: $U_h = \frac{U_s}{1+\sigma_s} = \frac{U_N}{1+\sigma_s} = \frac{400}{1.05} = 381\text{V}$
- Slots per pole and phase: $q = Q_s / (2p \cdot m) = 36/(2 \cdot 3) = 6$
- Turns per phase: $N_s = p \cdot q \cdot N_c / a = 1 \cdot 6 \cdot 13/1 = 78$
- Distribution factor: $k_{d,1} = \frac{\sin\left(\frac{\pi}{2 \cdot 3}\right)}{6 \cdot \sin\left(\frac{\pi}{2 \cdot 6 \cdot 3}\right)} = 0.956$, pitching factor: $k_{p,1}$ =1
- Winding factor: $k_{w,1} = k_{d,1} \cdot k_{p,1} = 0.956$
- Flux per pole: $\Phi_h = \frac{U_h}{\sqrt{2} \cdot \pi \cdot f \cdot N_s k_{w,1}} = \frac{381}{\sqrt{2} \cdot \pi \cdot 50 \cdot 78 \cdot 0.956} = 23.0\,\text{mWb}$
- Pole pitch: $\tau_p = d_{si}\pi / (2p) = 282.7\,\text{mm}$, slot pitch: $\tau_Q = d_{si}\pi / Q_s = 15.7\,\text{mm}$
- Flux density: $B_{\delta,\nu=1} = \Phi_h / (\tau_p l_{Fe} \cdot 2/\pi) = \underline{\underline{0.73}}\,\text{T}$
- Conductor: $A_L = a_i \cdot d_{Cu}^2 \cdot \pi / 4 = 8 \cdot 1^2 \cdot \pi / 4 = 6.28\ \text{mm}^2$
- Slot fill factor: $A_{Cu} = N_c \cdot A_L = 13 \cdot 6.28 = 81.7\,\text{mm}^2$, $k_f = 81.7/194 = \underline{\underline{0.421}}$
- Current density: $J = I_{sN} / (a \cdot A_L) = 31.7/(1 \cdot 6.28) = 5.0\,\text{A/mm}^2$

$$A = \frac{2mNI_{sN}}{2p\tau_p} = \frac{2 \cdot 3 \cdot 78 \cdot 31.7}{2 \cdot 28.27} = 262\,\text{A/cm}$$

$A \cdot J = 262 \cdot 5.0 = \underline{\underline{1312}}$ (A/cm)(A/mm^2): fits to limits given in Chapter 1 for totally enclosed machine with 80 K temperature rise.

- Electromagnetic utilization:

$$C = \frac{\pi^2}{\sqrt{2}} \cdot k_{ws} \cdot A \cdot B_\delta = \frac{\pi^2}{\sqrt{2}} \cdot 0.956 \cdot 26200 \cdot 0.73 = 127605\,\text{VAs/m}^3 = \underline{2.12}\ \text{kVA·min/m}^3$$

This rather low utilization is due to 2-pole machine, where flux density is reduced to get lower yoke heights and therefore reduced iron masses.

Example 2.4-3:

Data from Example 2.4-1: Current per phase 59 A, voltage per phase 3460 V, current density limit 5.5 A/mm^2, N_s = 200, N_c = 10, $\tau_{Qs} = 24.0$ mm, a = 1, a_i = 1.

- Conductor cross section: $A_{TL} = I_s/(J_s \cdot a \cdot a_i) = 59/(5.5 \cdot 1 \cdot 1) = 10.73$ mm^2
- Chosen slot breadth: $b_{Qs} = 12.5$ mm (= $0.52 \cdot \tau_{Qs}$)
- Chosen conductor dimensions (Table 2.4-2): $b_L = 7.1$ mm, $h_L = 1.8$ mm
- Inter-turn voltage (neglecting the influence of $1/k_{w,d}$): $U_{turn} \approx U_s / N_s = 3460/200 = 17.3$ V

< 80 V: Table 2.3-3: Conductor insulation thickness d_{ic} = 0.4 mm (both sides)

- Additional inter-turn insulation d_i = 0.3 mm

Slot height design:		**mm**
Number of insulated turns per coil one above the other = 10	$N_c \cdot (h_L + d_{ic}) + (N_c - 1) \cdot d_i =$ $= 10 \cdot (1.8 + 0.4) + 9 \cdot 0.3 = 24.7$	24.7
Main insulation	$2 \cdot d = 2 \cdot 2.2 = 4.4$	4.4
Insulated coil side	24.7 + 4.4 = 29.1	29.1
Two coils per slot	$2 \cdot 29.0 = 58.0$	58.2
Inter-layer insulation	Z = 4.0	4.0
Slot lining (thickness 0.15 mm)	$3 \cdot d_{sl} = 3 \cdot 0.15 = 0.45$	0.45
Wedge + tooth tip height	h_{wedge} = 4.0, h_4 = 0.5	4.5
Top and bottom lining	$2 \cdot d_t = 2 \cdot 0.4 = 0.8$	0.8
Vertical play		1.05
Slot height h_Q		**69.0**

Slot width design:		**mm**
Number of adjacent insulated turns n_{ne} = 1	$n_{ne} \cdot (b_L + d_{ic}) =$ $= 1 \cdot (7.1 + 0.4) = 7.5$	7.5
Main insulation	$2 \cdot d = 2 \cdot 2.2 = 4.4$	4.4
Slot lining (thickness 0.15 mm)	$2 \cdot d_{sl} = 2 \cdot 0.15 = 0.30$	0.3
Play		0.3
Slot width b_Q		**12.5**

Table 2.4-3: Slot design

Check of winding design must comprise:

- height of conductor h_L (or strand) to avoid eddy current losses (current displacement)
- conductor cross section concerning current density : $J < J_{crit}$ (e.g. Fig. 2.2-5)
- coil main insulation thickness with respect to rated voltage (Table 2.3-1)
- conductor insulation with respect to inter-turn voltage (Table 2.3-3)
- sufficient tooth width to avoid increased iron saturation: $B_d < B_{d\,crit} \approx 2 \ldots 2.2$ T
- resulting thermal utilization $A \cdot J$

Example 2.4-3:

- Checking of eddy currents at 20°C: $\kappa_{Cu} = 57 \cdot 10^6$ S/m, f = 50 Hz, n_{ne} = 1, $b_L / b_Q = 7.1/12.5$

$$\xi = h_L \cdot \sqrt{\frac{\mu_0 \cdot \omega \cdot \kappa \cdot n_{ne} \cdot b_L}{2 \cdot b_Q}} = 0.0018 \cdot \sqrt{\frac{4\pi \cdot 10^{-7} \cdot 2\pi \cdot 50 \cdot 57 \cdot 10^6 \cdot 1 \cdot 7.1}{2 \cdot 12.5}} = \underline{\underline{0.144}} < 0.35$$

- Checking of current density and thermal utilization:

$J_s = I_s / (a \cdot a_i \cdot A_{TL}) = 59/(1 \cdot 1 \cdot 12.42) = \underline{\underline{4.75}}\,\text{A/mm}^2 < 5.5\ \text{A/mm}^2$

$$A = \frac{2mN_s I_s}{2p\tau_p} = \frac{2 \cdot 3 \cdot 200 \cdot 59}{4 \cdot 36} = 492\,\text{A/cm}$$

$A \cdot J = 492 \cdot 4.75 = \underline{\underline{2337}}\,(\text{A/cm})(\text{A/mm}^2)$: fits to limits given in Chapter 1 for open ventilated machine with 80 K temperature rise.

- Electromagnetic utilization:

$$C = \frac{\pi^2}{\sqrt{2}} \cdot k_{ws} \cdot A \cdot B_\delta = \frac{\pi^2}{\sqrt{2}} \cdot 0.91 \cdot 49200 \cdot 0.946 = 295585\,\text{VAs/m}^3 = \underline{4.93}\ \text{kVA·min/m}^3$$

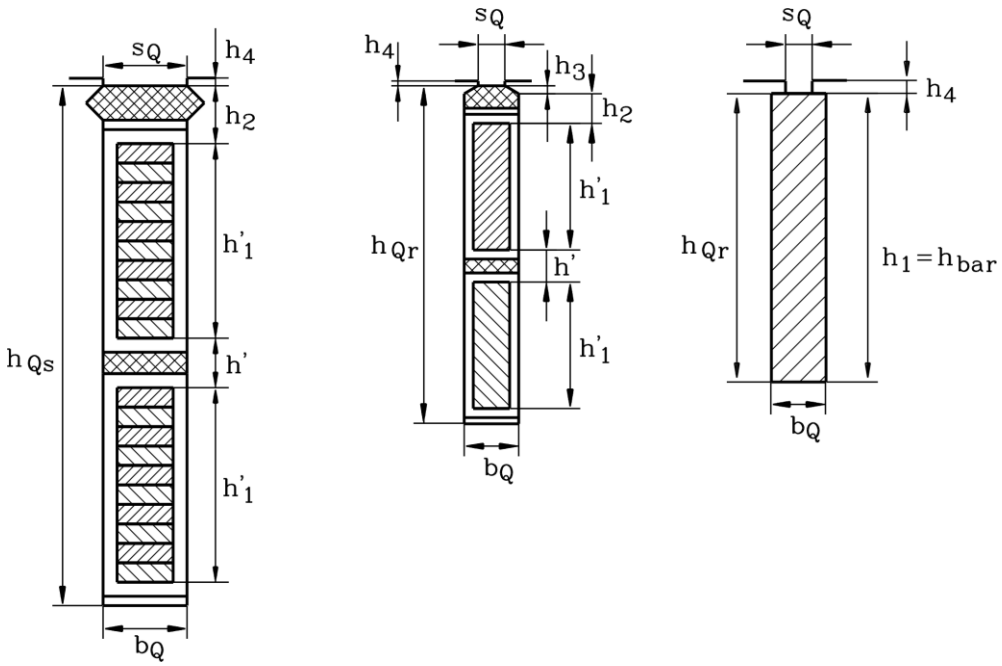

a) b) c)

Fig. 2.4-1: a) Two coils (two-layer winding) in one slot for 6 kV, 500 kW induction machine, b) Wound rotor induction machine: rotor slot design c) Cross section of deep rotor bar in slot

2.5 Rotor cage design

a) Features of squirrel cage:

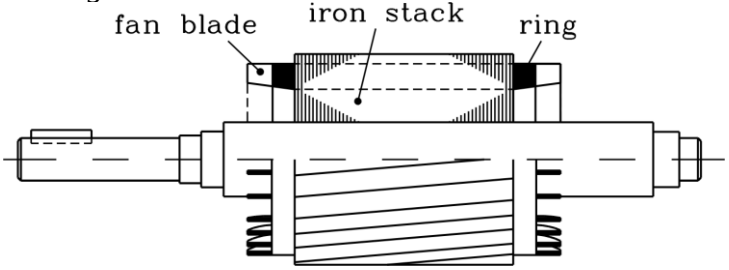

Fig.2.5-1: Die-cast aluminium cage rotor with skewed rotor bars and small fan blades at the rings

The **rotor cage** consists of bars, which are housed in rotor slots usually without any insulation between cage and rotor iron stack. At both ends the bars are short-circuited by rings (squirrel cage). For smaller motors typically up to 200 kW die-cast aluminium cages are used, whereas bigger machines, but also smaller traction motors e.g. for street-cars are fabricated from copper bars, which are soldered to rings.

The stator flux fundamental sine wave induces the rotor cage, when it is rotating with rotational speed *n*, causing a certain slip *s* with respect to fundamental wave speed n_{syn}:

$$s = (n_{syn} - n)/\, n_{syn} \tag{2.5-1}$$

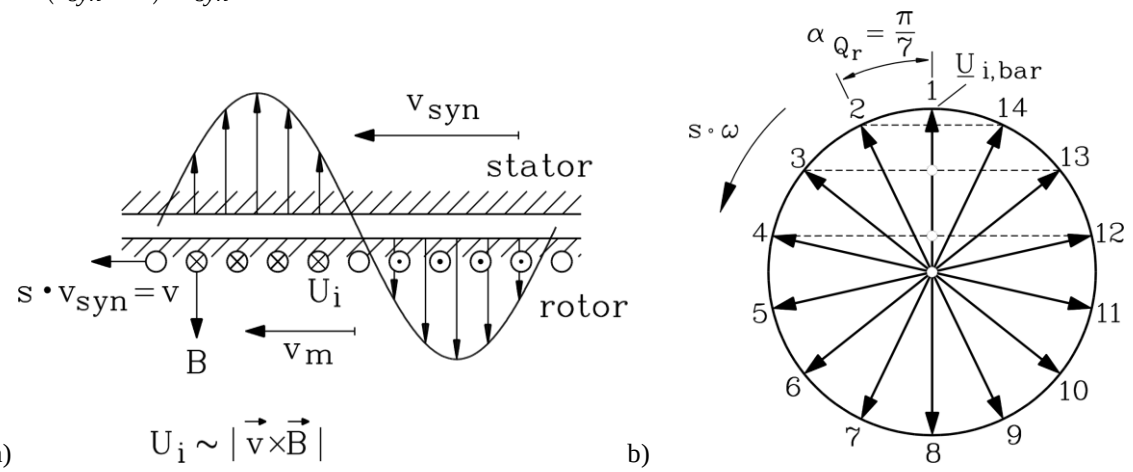

Fig. 2.5-2: a) Stator fundamental flux density wave induces in each bar phase shifted rotor voltages, b) Induced phase shifted voltages for Q_r/p= 14 bars per pole pair

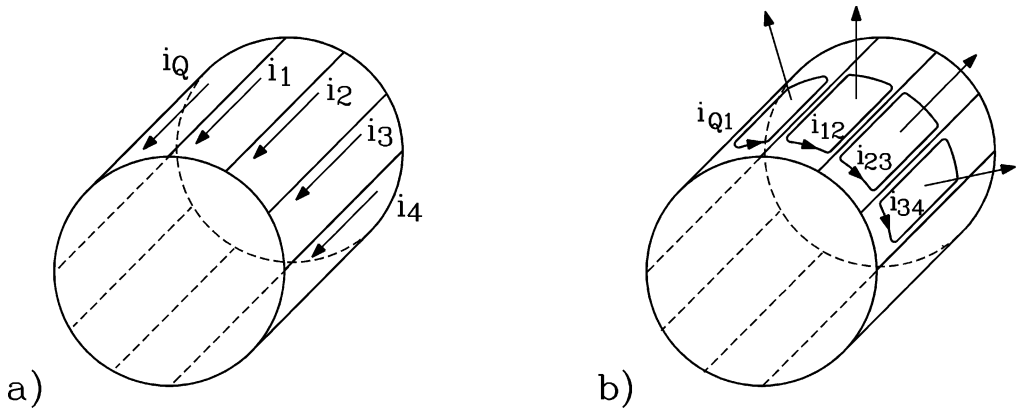

Fig. 2.5-3: Squirrel cage: a) Bar currents, b) Ring currents

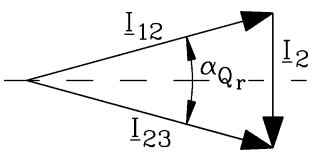

Fig. 2.5-4: *Kirchhoff´s* law for two ring section currents $\underline{I}_{12}$ and $\underline{I}_{23}$ and one bar current $\underline{I}_2$.

Rotor frequency is therefore $f_r = s \cdot f_s$ and usually rather low at rated operation, as rated speed is only in the range of 1% ... 5%, decreasing with increasing machine size. Induced voltage in each bar is phase shifted to the next one by $\alpha_{Q_r} = 2\pi \cdot p / Q_r$ (Fig. 2.5-2). So in each bar flows a different rotor bar current with same r.m.s. value I_r, but with different phase-shift. In the ring sections between two bars flows therefore a ring section current. From

section to section this current is phase shifted by $2\pi \cdot p / Q_r$ (Fig. 2.5-3). According to *Kirchhoff*´s law we get (Fig. 2.5-4)

$$\underline{I}_{12} + \underline{I}_2 - \underline{I}_{23} = 0 \tag{2.5-2}$$

$$I_2 = 2I_{12}\sin(\alpha_{Qr}/2) \quad \Rightarrow \quad I_r = 2I_{Ring}\sin(p\pi/Q_r) \quad . \tag{2.5-3}$$

Thus the resistance of one ring section ΔR_{Ring} may be added as equivalent **series resistance** ΔR^*_{Ring} to the bar resistance R_{bar} for further calculation.

$$P_{Cu,r} = Q_r R_{bar} I_r^2 + 2Q_r \Delta R_{Ring} I_{Ring}^2 = Q_r (R_{bar} + \Delta R^*_{Ring}) I_r^2 = Q_r R_r I_r^2 \qquad \Rightarrow$$

$$\boxed{\Delta R^*_{Ring} = \Delta R_{Ring} \frac{1}{2\sin^2(\pi p / Q_r)}} \tag{2.5-4}$$

b) Shape of rotor bars in rotor slots:

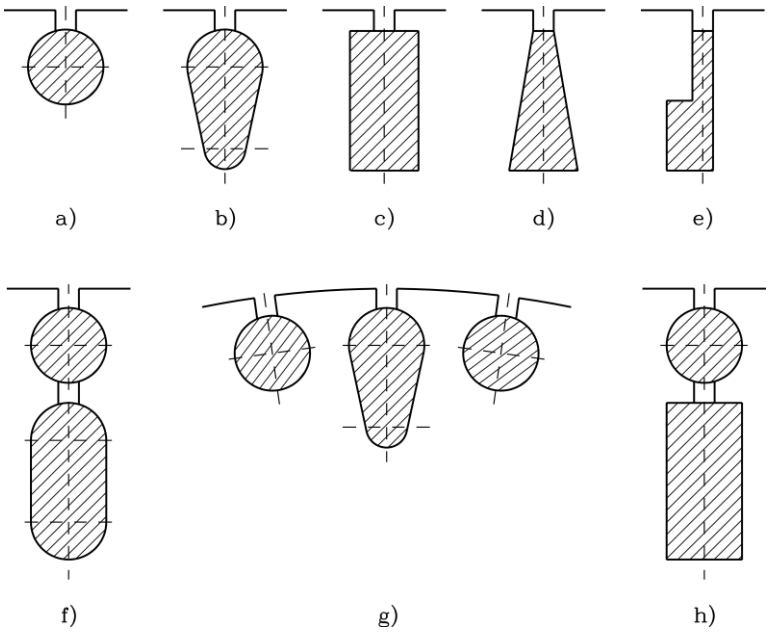

Fig. 2.5-5: Cross section of rotor bars: From a) to h) increasing effective rotor resistance due to current displacement at stand still: a), b) Nearly no current displacement, c) deep bar, f) – h) round bars made of bronze

Raising starting torque is possible by eddy-current effect at stand still, when rotor frequency is identical with stator frequency, thus being large. Rotor AC slot stray flux will therefore induce big eddy currents in rotor bars, which are superimposed to rotor bar current in that way, that bar current density increases at top of bar near rotor slot opening and decreases near bottom of rotor slot ("**current displacement**"). Thus resulting rotor bar current flows mainly in upper half of bar, thereby using only part of rotor bar cross section, which leads to increase of effective rotor bar resistance. According to

$$P_{Cu,r} = Q_r R_r I_r^2 = s \cdot P_\delta \Big|_{s=1} = P_\delta = (\omega_s / p) \cdot M_e \tag{2.5-5}$$

increase of rotor resistance leads to increase of electromagnetic torque at $s = 1$. Additional flux excited by eddy current in rotor bar is in phase opposition to AC slot stray flux and reduces this stray flux component, therefore rotor stray inductance is reduced by current

displacement. With rising speed and decreasing slip rotor frequency decreases also and effect of current displacement vanishes, so no rotor bar eddy currents will occur at rated slip.

Rotor bars with big slot stray flux will generate considerable current displacement, therefore especially shaped rotor bars which are narrow and deep are used (**deep bar**). Further increase of rotor resistance at stand still is achieved by narrowing top of the bar, where main part of rotor bar current flows, or by using double cage, where upper bar is made of bronze instead of copper to increase rotor bar resistance.

c) Choice of rotor slot numbers:

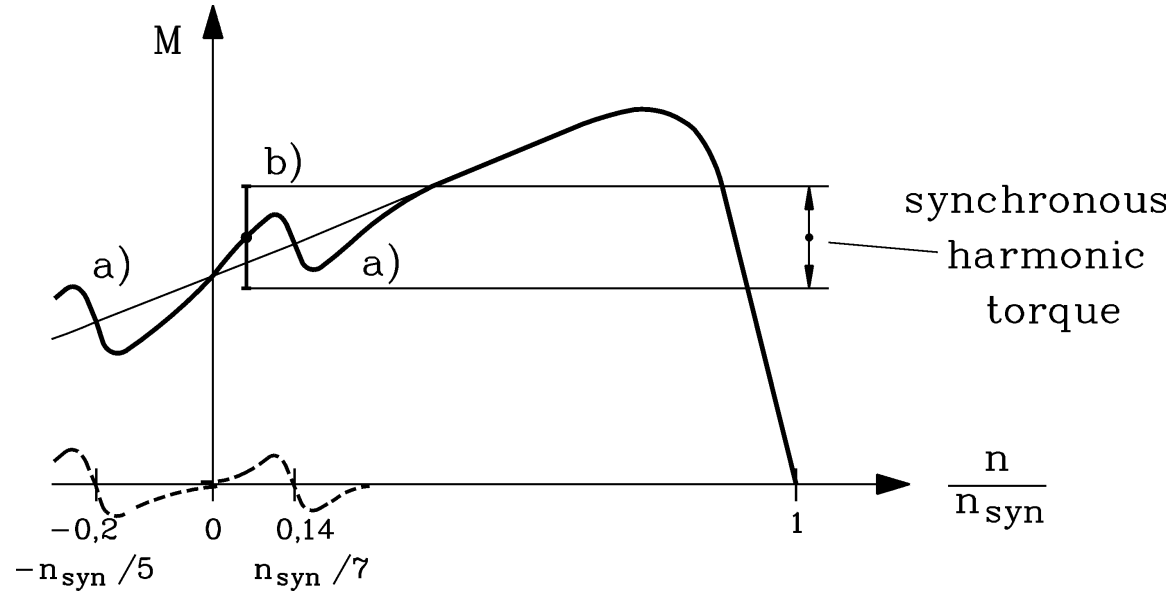

Fig. 2.5-6: a) Asynchronous harmonic torque (here: 5th and 7th space harmonic) and b) synchronous harmonic torque disturb the start up of induction machine. They are reduced by proper stator winding design (few harmonics in generated air gap field) and by rotor skewing

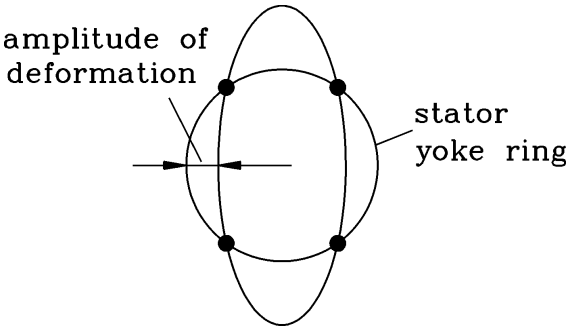

Fig. 2.5-7: Deformation of stator yoke (depicted like a ring) a radial force density distribution with $2r = 4$ nodes

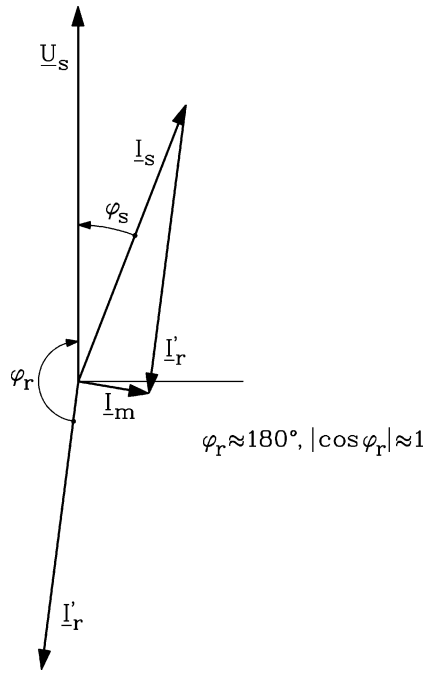

Fig. 2.5-8: Current phasor diagram of induction by motor at rated operation according to equivalent circuit

Line starting motors have usually rotor bars **skewed** by typically one stator slot pitch. Thus stator slot harmonic flux density waves cannot induce the rotor, which otherwise would lead to additional high frequency rotor currents. These currents may cause additional **"asynchronous" harmonic torque** (Fig. 2.5-6), which influence the asynchronous starting curve *M(n)*. This skewing also helps to minimize "synchronous" harmonic torque components, which are generated by space harmonics of stator and rotor flux distribution, excited by I_s and I_r. Further these field space harmonics of stator and rotor flux density distribution may interact not only to generate tangential forces and therefore parasitic torque, but also to generate pulsating radial forces. Radial force distribution along stator circumference is distributed sinusoidal (Fig. 2.5-7) and rotates with tonal frequency, which is determined by stator frequency and stator and rotor ordinal numbers. Deflection of stator is caused, which compresses/decompresses surrounding air, thus generating sound pressure wave (**acoustic noise**) with tonal frequency, which may be significant, if tonal frequency hits a stator yoke bending resonance frequency. Skewing might reduce this radial force, as well as certain choice of slot number ratios.

Choice of rotor slot number Q_r must be done with respect to stator slot number Q_s (details see: Lectures "Motor development for electric drive systems").

1. $Q_s \neq Q_r$: Avoid **cogging** at stand still; good choice is, when Q_s, Q_r have no (or few) common divider.
2. Skewed rotors: $0.8Q_s \leq Q_r < Q_s$ minimizes **inter-bar** currents between bars and iron stack, which cause additional losses and amplify asynchronous harmonic torque.
3. Q_r not below $0.8Q_s$ and not above $1.2\,Q_s$, otherwise slot frequent flux pulsation mainly in rotor teeth due to open stator slots will cause too big additional losses already at no-load.
4. $|Q_s - Q_r| \neq 0, 1, 2, \ldots r^*, 2p, 2p \pm 1, 2p \pm 2, \ldots, 2p \pm r^*$: Avoids radial force waves of node counts $2r^*$, which otherwise might bend the housing and generate vibration and noise. By calculating natural vibrations modes of stator and rotor, those modes r^* with natural frequency < 6 ... 8 kHz, which must not be excited by radial force waves, are determined.
5. Choose Q_r **even** to avoid radial force waves with $2r = 2$ ($r = 1$), which might cause the rotor to perform bending oscillations, which in case of resonance with rotor natural bending frequency might cause the rotor to touch stator or damage the bearings.

Example 2.5-1:
$2p = 4$, $Q_s = 60$, unskewed rotor: $Q_r = (0.8 \ldots 1.2)Q_s = 48 \ldots 72$, taking only even numbers. With $r^* = 4$ the range 52 ... 68 is excluded. The numbers 48, 72 are excluded (common divider 2, 3, 4, 6, 12). Excluding in similar way other slot numbers with common dividers, we get as choice (46), 50, 54, 66, 70, (74).

For **skewed** rotor only slot numbers (46), 50, 54 remain, e.g. $Q_r = 50$ is chosen.

d) Cage design:
Each bar is regarded as a single phase ($m_r = Q_r$), as it is carry its own bar current, with number of turns per phase $N_r = 1/2$; therefore $k_{wr} = 1$. Rotor current transformation ratio $\ddot{u}_I$ must yield same current-loading as stator current:

$$\hat{A}_s = k_{ws} \cdot \sqrt{2} \cdot \frac{2m_s N_s I_s}{2p\tau_p} \qquad \Rightarrow \hat{A}_r = k_{ws} \cdot \sqrt{2} \cdot \frac{2m_s N_s (I_r / \ddot{u}_I)}{2p\tau_p} = k_{wr} \cdot \sqrt{2} \cdot \frac{2m_r N_r I_r}{2p\tau_p}$$

$$\ddot{u}_I = \frac{k_{ws} m_s N_s}{k_{wr} m_r N_r} = \frac{2k_{ws} m_s N_s}{Q_r} \qquad (2.5\text{-}6)$$

Rotor cage is designed according to rotor bar current, which may be taken from Fig. 2.5-8 with the assumption $\cos\varphi_r \cong -1$ ($\varphi_r \cong 180°$) as

$$I'_r = I_r / \ddot{u}_I \approx I_s \cdot \cos\varphi_s \quad . \tag{2.5-7}$$

Rotor bar and ring current density J_r shall be nearly the same and may be a little bit higher than stator current density J_s, as rotor temperature may somewhat higher, as no insulation is in the rotor, which might be damaged by too high temperature.

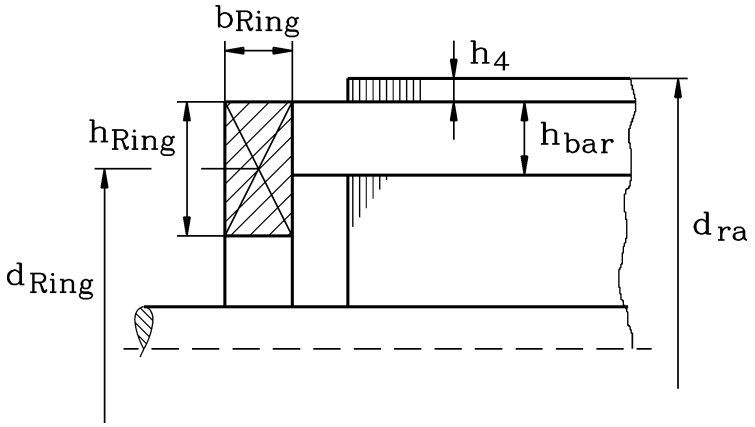

Fig. 2.5-9: Cross section of rotor ring

Example 2.5-2:
Data: Stator current 59 A, $\cos\varphi_N = 0.87$, stator current density: 4.75 A/mm^2, $Q_s/Q_r = 60/50$, $N_s = 200$, $k_{ws} = 0.91$, $m_s = 3$

- $I'_r = I_r / \ddot{u}_I \approx I_s \cdot \cos\varphi_s = 59 \cdot 0.87 = 51.33\text{A},\ \ddot{u}_I = \dfrac{2k_{ws}m_sN_s}{Q_r} = \dfrac{2 \cdot 0.91 \cdot 3 \cdot 200}{50} = 21.84$

  $I_r = \ddot{u}_I \cdot I'_r = 21.84 \cdot 51.33 = \underline{\underline{1121}}\text{A}$
- Deep bar rotor to increase starting torque: ratio $h_{Cu}/b_{Cu} \geq 8$
  Choice: $h_{Cu} = 40$ mm, $b_{Cu} = 5$ mm, cross section: $A_{Cur} = 200$ mm^2 (Fig. 2.4-1c)
- Rotor bar current density: $J_r = I_r / A_{Cur} = 1121/200 = 5.6\,\text{A/mm}^2$
- Semi-closed rotor slot dimensions (Fig. 2.4-1c):
  $h_1 = h_{Cu} = 40$ mm, $b_1 = b_{Cu} = 5$ mm (plus 0.1 mm play each)
  $h_4 = 3.4$ mm, $s_{Qr} = 2.5$ mm
  $h_{Qr} = 40.1 + 3.4 = \underline{43.5}$ mm, $b_{Qr} = \underline{5.1}$ mm
- Rotor ring current $I_{Ring} = I_r / (2 \cdot \sin(p\pi / Q_r)) = 1121/(2 \cdot \sin(2\pi/50)) = \underline{\underline{4472}}\text{A}$
- Ring current density: $J_r = J_{Ring} = 5.6\,\text{A/mm}^2$,
- Necessary ring cross section: $A_{Ring} = I_{Ring} / J_{Ring} = 4472/5.6 = 800\ \text{mm}^2$ (Fig. 2.5-9)
- Ring height is usually at least bar height: $h_{Ring} \geq h_{Cu}$
  Choice: $h_{Ring} = h_{Cu} = \underline{40}$ mm, $b_{Ring} = 800/40 = \underline{20}$ mm

2.6 Wound rotor design

a) Features of wound rotors:
The wound rotor consists – like the stator – of a laminated iron stack with slots, carrying like the stator a three-phase distributed winding, which terminals *x, y, z* are usually connected in star, whereas *u, v, w* are connected to three slip rings. There they may be connected via graphite brushes, running on the slip rings, to three external resistances (which in their turn

are star connected). Thus rotor resistance is increased at stand still for increase of starting torque. After start up the rotor is short circuited at the slip rings, then operating in asynchronous mode as an induction machine.

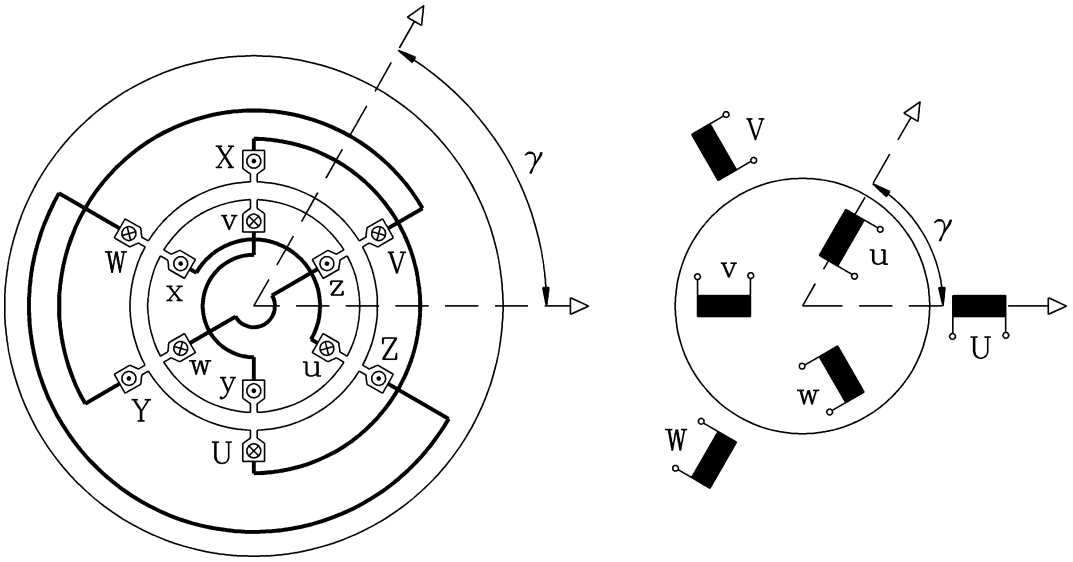

a) b)

Fig. 2.6-1: Wound rotor induction machine: a) Schematic cross section for simplified machine with $2p = 2$, $m_s = m_r = 3$, $q_s = q_r = 1$, $W_s = W_r = \tau_p$ (Note: In reality it must be $Q_s \neq Q_r$). b) Common schematic of wound rotor induction machine

Rotor coils must produce same number of magnet poles like stator winding to generate constant torque, therefore rotor coil span must be (besides of some pitching) the same as stator coil span. Choice of rotor slot number must be $Q_s \neq Q_r$ to avoid cogging, therefore rotor number of coils per pole and phase is chosen (Fig. 2.6-3)

$$q_r = q_s \pm 1, (\pm 2) \quad . \tag{2.6-1}$$

Design of rotor winding is done according to the same principles as stator winding with calculation of rotor winding factor k_{wr} (fundamental), numbers of turns per phase N_r, rotor slot design and number of turns per rotor coil N_{cr}. To avoid flash over at slip rings, rotor winding must be **designed in rather low voltage** < 1000 ... 2000 V (line-to-line = between to slip rings). **Voltage transformation ratio** between stator and rotor winding

$$\ddot{u}_U = \frac{N_s k_{ws}}{N_r k_{wr}} = \frac{U'_r}{U_r} \tag{2.6-2}$$

determines at stand still and open rotor **stand still rotor voltage $U_{r,LL,0}$** between two slip rings**.** From equivalent circuit diagram at $s = 1$ and open rotor circuit we get

$$U'_{r0} = \frac{U'_{r,LL,0}}{\sqrt{3}} = U_h = \frac{X_h}{\sqrt{R_s^2 + (X_{s\sigma} + X_h)^2}} \cdot U_s \approx \frac{X_h}{X_{s\sigma} + X_h} \cdot U_s = \frac{U_s}{1 + \sigma_s} \quad . \tag{2.6-2}$$

$$U_{r0} = \frac{U_{r,LL,0}}{\sqrt{3}} = U'_r / \ddot{u}_U \approx \frac{U_s}{1 + \sigma_s} \cdot \frac{N_r k_{wr}}{N_s k_{ws}} \quad . \tag{2.6-3}$$

Rotor winding is usually made as two-layer low voltage wave winding (Fig. 2.6-2) to reduce amount of copper for coil connectors. In order to get low voltage on rotor side, usually $N_s < N_r$, leading to low number of turns per coil (usually $N_{cr} = 1$ or 2).

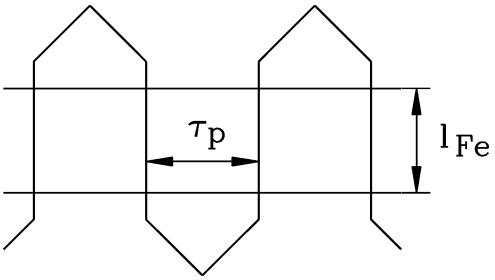

Fig. 2.6-2: Rotor wave winding, full pitched

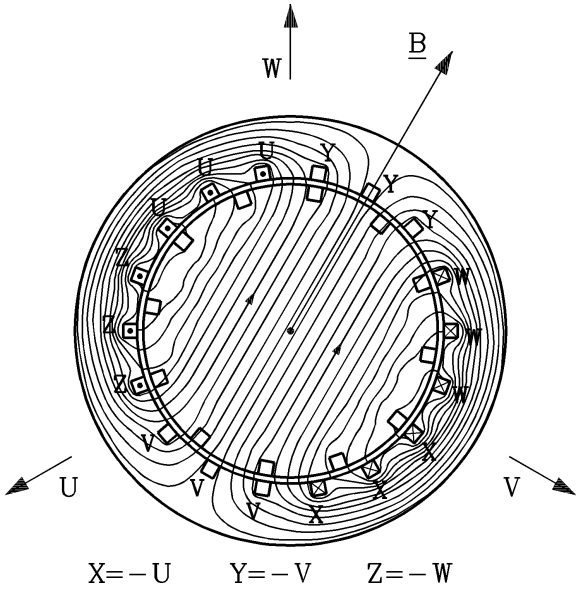

Fig. 2.6-3: Numerically calculated flux lines at $s = 0$ of 2-pole wound rotor induction machine, $m_s = m_r = 3$, at instant, when $i_U = - i_W$, $i_V = 0$. Winding: $q_s = 3$, $q_r = 2$, $W_s = W_r = \tau_p$, $Q_s = 18$, $Q_r = 12$

Slot design for rotor two-layer winding (Fig. 2.6-4) shows deep bar arrangement with semi-closed slots to reduce influence of rotor slot openings on air gap field. Rotor coils are separated in two halves as two bar coil sides, which are inserted into rotor slots, and are afterwards connected by soldering the winding overhangs.

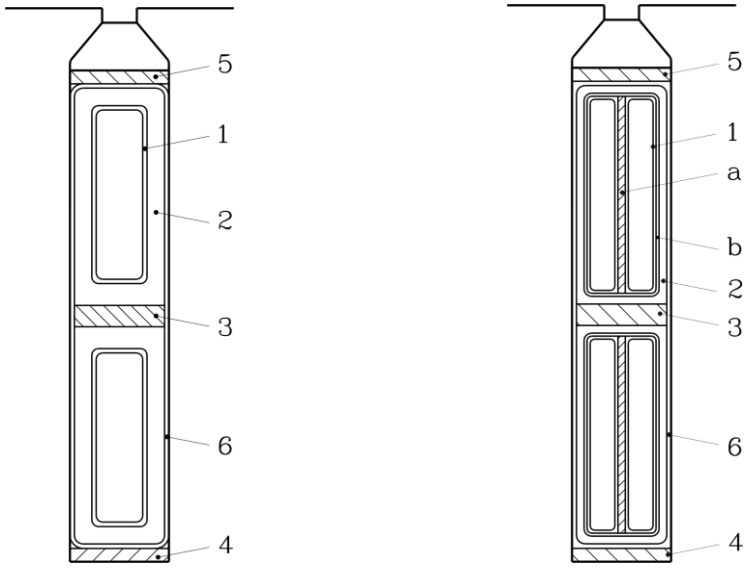

Fig. 2.6-4: Wound rotor slot and two-layer winding design: left: One turn per rotor coil, right: Two turns per rotor coil. 1: Insulation of conductor (glass fibre band), 2: main insulation, 3: inter-layer insulation, 4: bottom lining, 5: top lining, a: vertical inter-turn insulation, b: fixation band

Rotor stand still voltage $U_{r,LL,0}$	-	≤ 800 V	≤ 1500 V	≤ 2000 V
Thickness of main insulation (mm) (one side)	2	0.5	1.0	1.3
Inter-layer insulation (mm)	3	0.5	0.5	1.0
Thickness of winding overhang insulation (mm) *)	-	0.24	0.8	1.0
Vertical inter-turn insulation (mm)	a	0.3	0.3	0.4

*) both sides

Table 2.6-1: Insulation of rotor winding according to rated voltage

Conductor insulation (both sides) (mm)	1	0.3
Slot bottom lining (mm)	4	0.3
Slot top lining (mm)	5	0.5
Fixation band thickness (one side) (mm)	b	0.12

Table 2.6-2: Insulation of conductors and additional linings

b) Rotor winding design:
Rotor slot width should be $b_{Qr} / \tau_{Qr} = 0.4 \ldots 0.5$ and for 100 kW < P < 1000 kW: $b_{Qr} = 10 \ldots 20\,\text{mm}$. Rotor phase current is determined form rotor apparent power

$$S_r = m_r \cdot U_{r0} \cdot I_r \quad , \tag{2.6-4}$$

which is estimated in case of motor operation as

$$S_r = \frac{P_N}{\eta_N \cdot \cos\varphi_r} \tag{2.6-5}$$

with the assumption $\cos\varphi_r \cong -1$ ($\varphi_r \cong 180°$, Fig. 2.5-8). Rotor current loading and rotor current density must fit to the same thermal utilization as stator winding.

Example 2.6-1:
Data: Wound rotor induction motor 500 kW, stator rated voltage 6 kV, Y, stator rated current 59 A, η_N = 0.94, stator current density: 4.75 A/mm^2, q_s = 5, N_s = 200, k_{ws} = 0.91, m_s = 3, d_{si} = 458 mm, air gap δ = 1.4 mm

- Choice: m_r = 3, Y, q_r = 5 + 1 = 6, $Q_r = 2p \cdot m_r \cdot q_r = 4 \cdot 3 \cdot 6 = 72$
- Full pitched wave winding: $W_r = \tau_p$: $k_{pr1} = \sin((W_r / \tau_p) \cdot \pi / 2) = 1$
- Rotor distribution factor: $k_{wr1} = \dfrac{\sin\left(\dfrac{\pi}{2m_r}\right)}{q_r \cdot \sin\left(\dfrac{\pi}{2m_r q_r}\right)} = 0.956$,
- Rotor winding factor: $k_{wr1} = k_{dr1} k_{pr1} = 0.956$
- Choice of number of turns per coil: N_{cr} = 1, series connection per phase: a_r = 1.
- Number of turns per phase: $N_r = 2p \cdot q_r \cdot N_{cr} / a_r = 4 \cdot 6 \cdot 1/1 = 24$
- **Rotor stand still voltage**:

$$U_{r0} \approx \frac{U_s}{1+\sigma_s} \cdot \frac{N_r k_{wr}}{N_s k_{ws}} = \frac{6000/\sqrt{3}}{1+0.04} \cdot \frac{24 \cdot 0.956}{200 \cdot 0.91} = 420\text{V},\ U_{r,LL,0} = \sqrt{3} \cdot 420 = \underline{\underline{727}}\ \text{V}$$

- Rotor rated current:

$$I_r \approx \frac{P_N}{\eta_N \cdot U_{r,LL,0} \cdot \sqrt{3}} = \frac{500000}{0.94 \cdot 727 \cdot \sqrt{3}} = \underline{\underline{423}}\text{A}$$

- Rotor outer diameter: $d_{ra} = d_{si} - 2\delta = 455.2\,\text{mm}$
- Rotor slot pitch: $\tau_{Qr} = d_{ra} \cdot \pi / Q_r = 19.86\,\text{mm}$
- Choice: b_{Qr} = 6.9 mm = 0.35 τ_{Qr}
- Choice of rotor rated current density (nearly the same as in stator): J_r = 5.2 A/mm^2

- Conductor cross section: $A_{Cur} = I_r / (a_r \cdot J_r) = 423/(1 \cdot 5.2) = 81\,\text{mm}^2$

Conductor dimensions:

b_{Lr} = Sloth width – main insulation – conductor insulation – slot lining – play =

$= 6.9 - 2 \cdot 0.5 - 0.3 - 2 \cdot 0.15 - 0.8 = 4.5\,\text{mm}$

$h_{Lr} = A_{Cur} / b_{Lr} = 81/4.5 = 18.0\,\text{mm}$

- Rotor slot opening: s_{Qr} = 2.5 mm, h_4 = 1 mm

Slot height design:		**mm**
Number of insulated turns per coil one above the other = 1	$N_c \cdot (h_{Lr} + d_{ic}) =$ $= 1 \cdot (18 + 0.3) = 18.3$	18.3
Main insulation	$2 \cdot d = 2 \cdot 0.5 = 1.0$	1.0
Insulated coil side	18.3 + 1.0 = 19.3	19.3
Two coils per slot	$2 \cdot 19.3 = 38.6$	38.6
Inter-layer insulation	$Z = 0.5$	0.5
Slot lining (thickness 0.15 mm)	$3 \cdot 0.15 = 0.45$	0.45
Wedge	4.0	4.0
Top and bottom lining	$0.3 + 0.5 = 0.8$	0.8
Vertical play		0.65
Slot height h_{Qr}		**45.0**

Table 2.6-3: Rotor slot height determination (Fig. 2.4-1b)

- Thermal utilization:

$$A_r = \frac{2 m_r N_r I_r}{d_{si} \pi} = \frac{2 \cdot 3 \cdot 24 \cdot 423}{45.8 \pi} = 423\,\text{A/cm}, \quad A_r J_r = 423 \cdot 5.2 = \underline{\underline{2200}}\,(\text{A/cm})(\text{A/mm}^2)$$

2.7 Design of main flux path of magnetic circuit

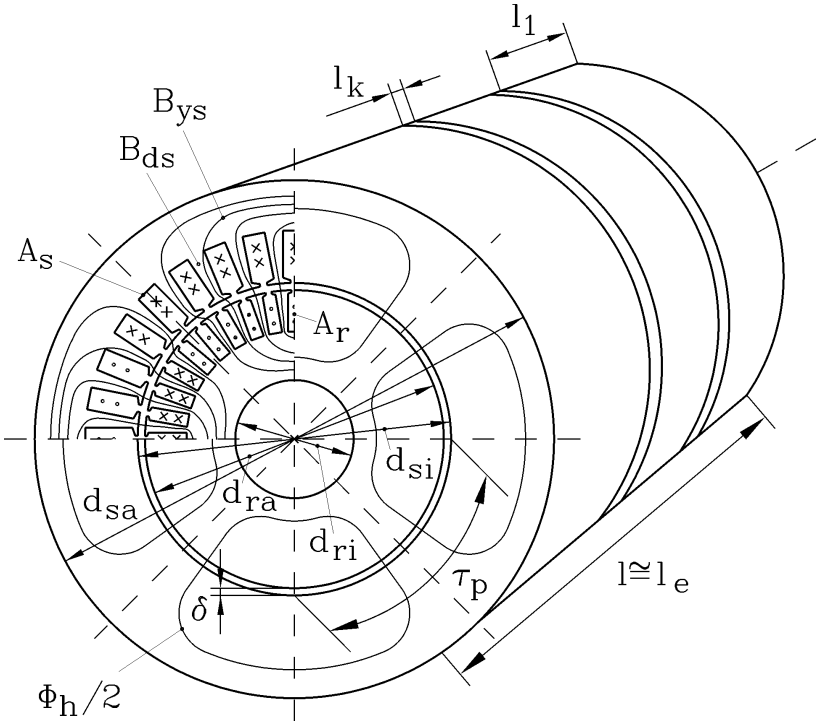

Fig. 2.7-1: Cross section of 4-pole induction machine, showing stator and rotor current distribution and main flux path. Stator and rotor iron stack are subdivided into 3 sections with radial cooling ducts in between.

Fig. 2.7-1 shows cross section of 4 pole induction machines with flux lines of main flux, crossing the air gap, being excited both by stator and rotor ampere-turns of all *m* phases. This may be expressed according to equivalent circuit by **"magnetizing current" I_m** flowing in N_s turns per phase per stator winding, exciting fundamental harmonic ($\nu = 1$) of **magnetizing m.m.f.** per pole pair *p* (see: Lectures "Electrical machines and drives")

$$V_{m,\nu=1} = \frac{\sqrt{2}}{\pi} \cdot \frac{m}{p} \cdot N_s k_{ws1} \cdot I_m = V_m \quad . \tag{2.7-1}$$

Basically, magnetic circuit of main flux is non-linear due to non-linear *B-H*-characteristic of iron. Laminated iron sheets with insulation between sheets are used to suppress eddy currents ant hence reduce **eddy current losses**, which are induced by AC main flux. Stator and rotor iron stack of bigger machines are segmented into axial sections with cooling ducts in between to guide cooling air flow (Fig. 2.7-1). Hysteresis loops of iron sheets must be very small to get low **hysteresis losses**. Eddy current losses and hysteresis losses together are called **iron losses**, which should be small, as they occur already at no-load due to main flux. By adding Si (silicon) to the iron the resistance of iron sheets is increased, thus reducing eddy currents, but on the other hand saturation flux density of these "dynamo sheets" is reduced by this measure. Iron losses are measured according to *Epstein* in so-called *Epstein* frame e.g. at 50 Hz, 1.0 T (Table 2.7-1) as v_{10} losses per kg iron mass. Iron sheet insulation (enamel or oxide layer) is in the range of 3% to 5% of sheet thickness. Sheet thickness is usually 0.5 mm, but special thinner sheets for inverter fed machines (high frequency !) down to 0.35 mm and 0.1 mm are also available. The cross section of iron stack consists therefore only to about

k_{Fe} = 95% ... 97 % **(stacking coefficient)**

of iron, the rest is insulation.

	Si	v_{10}	hysteresis losses	eddy-current losses	*B(H)*-curve Fig. 2.7-2
	%	W/kg	W/kg	W/kg	-
steel-sheet	0	≈ 4.2	*)	*)	*C*
sheet type III	1	2.3	1.6	0.7	*A*
sheet type IV	3.5	1.7	1.3	0.4	*B*

*) not specified, by typically 70% hysteresis losses

Table 2.7-1: Iron losses of typically used iron sheets

Basic method to calculate magnetization current of non-linear iron circuit is shown in basic Fig. 2.7-3, which contains air gap δ and iron part like in the real induction machine, by using *Ampere´*s law.

$$\oint_C \vec{H} \bullet d\vec{s} = N \cdot I \quad \Rightarrow \quad \sum_{i=1}^{n} H_i \cdot s_i = \sum_{i=1}^{n} V_i = N \cdot I \quad . \tag{2.7-2}$$

The closed loop *C* may be taken arbitrarily, but is often used the closed flux line of *B*. In that case $\vec{H}$ is tangential to curve *C*, yielding the scalar product as $\vec{H} \bullet d\vec{s} = H \cdot ds$. By discretization of the integral we get a sum $\sum_{i=1}^{n} H_i \cdot s_i = N \cdot I$.

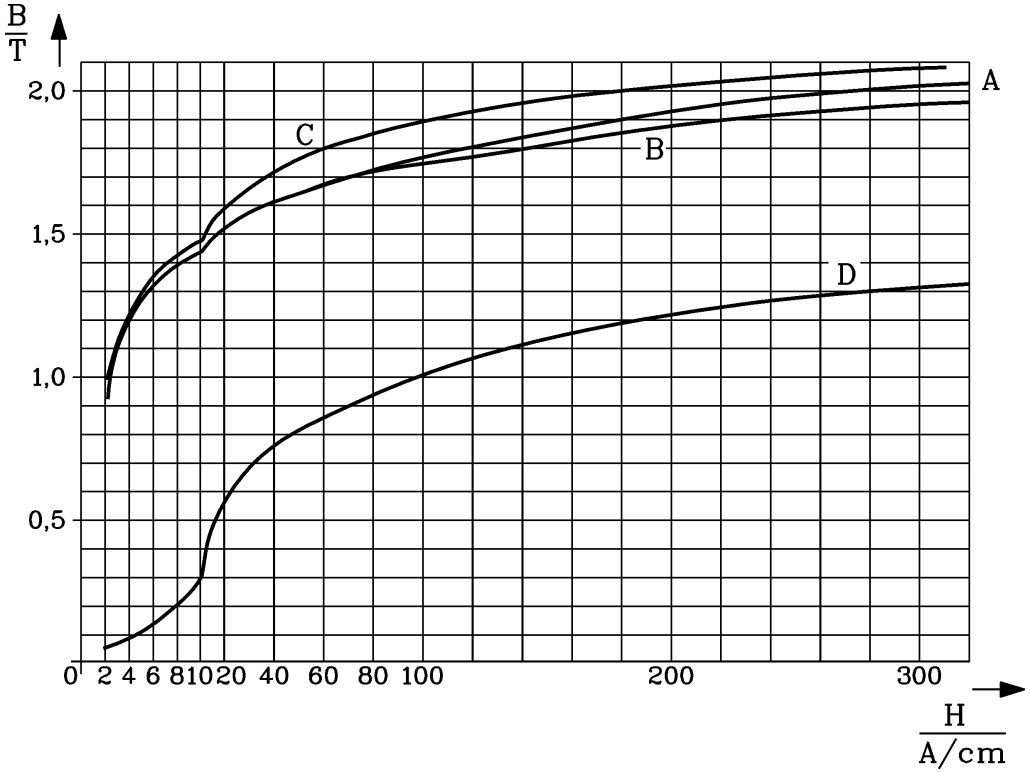

Fig. 2.7-2: Magnetization characteristic $B(H)$ of iron sheets (Manufacturer "a"): A: sheet type III (slightly different to data of Table 2.7-2, different manufacturer), B: sheet type IV, C: steel-sheet, D: cast iron. Hysteresis loops are very narrow and therefore not depicted.

***B* / T**	***H* / A/cm**									
	.,.0	***.,.1***	***.,.2***	***.,.3***	***.,.4***	***.,.5***	***.,.6***	***.,.7***	***.,.8***	***.,.9***
0.5	0.7	0.81	0.83	0.85	0.87	0.89	0.91	0.93	0.95	0.97
0.6	0.99	1.01	1.03	1.05	1.07	1.09	1.11	1.13	1.15	1.17
0.7	1.19	1.21	1.24	1.26	1.28	1.32	1.34	1.36	1.38	1.43
0.8	1.46	1.49	1.53	1.56	1.59	1.64	1.68	1.72	1.75	1.79
0.9	1.83	1.88	1.93	1.98	2.03	2.08	2.13	2.18	2.25	2.3
1.0	2.35	2.4	2.5	2.6	2.7	2.8	2.9	3.0	3.1	3.2
1.1	3.3	3.4	3.5	3.6	3.8	3.9	4.1	4.2	4.4	4.5
1.2	4.7	4.9	5.1	5.2	5.4	5.6	5.8	6.1	6.3	6.6
1.3	6.8	7.1	7.4	7.7	8.1	8.5	9.0	9.5	10.0	10.6
1.4	11.3	12.1	13.0	14.2	15.5	16.8	18.0	19.3	20.5	21.9
1.5	23.3	24.8	26.4	28.1	29.8	31.5	33.4	35.5	37.7	40.0
1.6	42	45	48	51	55	59	62	66	70	74
1.7	78	83	87	92	97	101	106	112	117	123
1.8	129	135	141	148	155	162	170	178	187	196
1.9	206	216	226	236	247	259	272	287	303	320
2.0	339	361	383	408	435	465	495	530	567	605
2.1	650	700	750	810	870	930	1000	1070	1140	1220
2.2	1300	1380	1460	1540	1620	1700	1780	1860	1940	2020
2.3	2100	2180	2260	2340	2420	2500	2580	2660	2740	2820

Table 2.7-2: Magnetization curve $B(H)$ of iron sheet type III (Manufacturer "b"). Hysteresis loop suppressed.

Note that $B(H)$-curves type III of manufacturers "a" and "b" differ. By dividing the magnetic path into n sections of length s_i and taking the cross sections A_i of each section, we start with a certain flux Φ and determine the flux densities $B_i = \Phi / A_i$ per section. For iron sections H_i is taken by $H_i(B_i)$ from Fig. 2.7-2, for air we calculate $H_i = B_i / \mu_0$. The m.m.f. per sections

$$V_i = H_i \cdot s_i \tag{2.7-3}$$

are summed to get the magnetizing ampere-turns $N \cdot I$ and magnetizing current I for given flux Φ. So for different flux values the magnetizing characteristic $\Phi(I)$ of main flux versus magnetizing current is derived. Note that for $\mu_{Fe} \to \infty$ the values H in iron are zero, and $\Phi(I)$ is linear **("air gap characteristic")**.

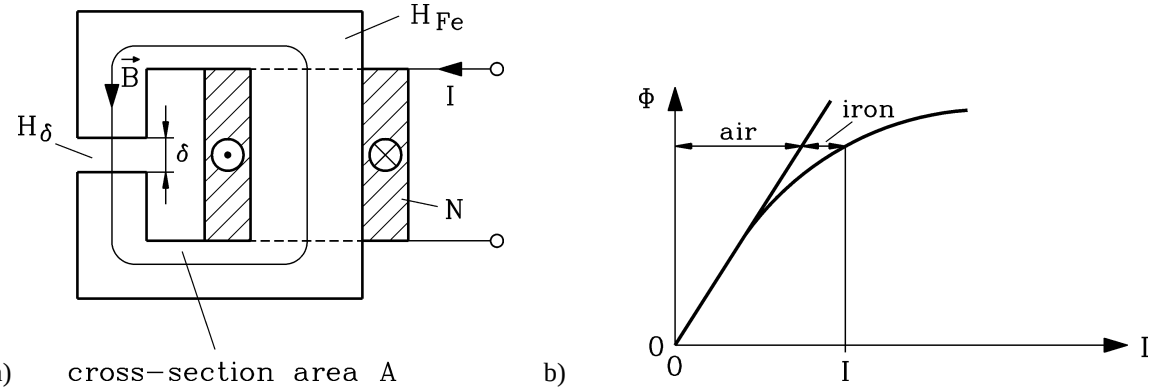

Fig. 2.7-3: Basic arrangement of magnetic circuit with air-gap: a) iron part and exciting coil, b) magnetizing characteristic $\Phi(I)$

Real geometry of induction machine cross section with closed loop C for *Ampere´*s law according to (Fig. 2.7-4), which is following a flux line (Fig. 2.7-5), shows the following sections:
- air gap δ, which is influenced by slot openings s_Q,
- stator and rotor teeth with length l_d, section, and
- stator and rotor yoke with half yoke length l_y.

Instead of determining necessary ampere-turns by numerical field calculation (Fig. 2.7-5), in the following a simplified method according to (2.7-2), (2.7-3) will be presented.

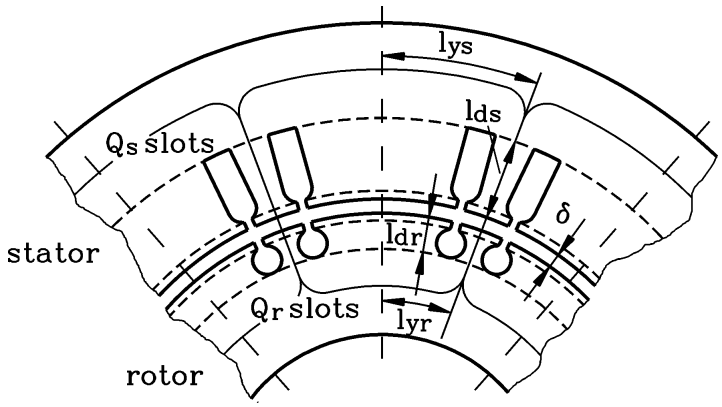

Fig. 2.7-4: Cross section of an 8-pole induction machine with sections of magnetic circuit of main flux

Note that magnetizing ampere-turns per pole is twice m.m.f. amplitude

$$\Theta_m = 2V_m \quad , \tag{2.7-4}$$

so calculating (2.7-2), (2.7-3) with the sections depicted in Fig. 2.7-4 yields

$$\Theta_m = 2 \cdot H_\delta \cdot \delta + 2 \cdot H_{ds} \cdot l_{ds} + 2 \cdot H_{dr} \cdot l_{dr} + 2 \cdot H_{ys} \cdot l_{ys} + 2 \cdot H_{yr} \cdot l_{yr} \quad , \tag{2.7-5}$$

which is often simplified by calculating **"half of magnetic circuit"**

$$\boxed{V_m = H_\delta \delta + H_{ds} l_{ds} + H_{dr} l_{dr} + H_{ys} l_{ys} + H_{yr} l_{yr} = V_\delta + V_{ds} + V_{dr} + V_{ys} + V_{yr}} \quad . \tag{2.7-6}$$

Facit:
Calculation of magnetizing current is done by calculating m.m.f. of sections in iron and air gap step by step.

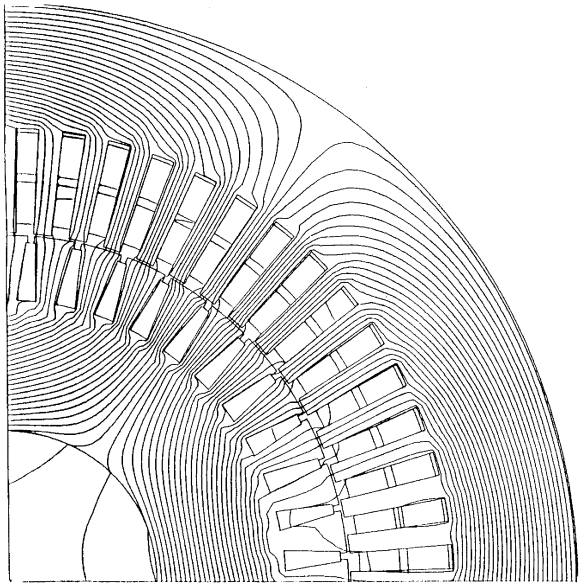

Fig. 2.7-5: Cross section of a three-phase, 4-pole high voltage cage induction machine with wedge rotor slots (Q_s / Q_r = 60/44) induction machine with numerically calculated no-load flux density B at rated voltage and no-load (s = 0, rotor current zero)

2.7.1 Magnetization of air gap

Due to the slot openings the air gap flux density shows a considerable ripple along circumference co-ordinate x, as the flux fringes at the tooth tips (Fig. 2.7.1-1). Especially open stator slots of high voltage machines yield considerable flux density ripple. For unslotted rotor and slotted stator solution of *Maxwell´*s equations (by method of conformal mapping) yield the rippled air gap flux density, from which the **average flux density B_δ per slot pitch** may be derived with respect to the peak value $\hat{B}_\delta$ beneath the tooth tips, called *Carter´*s coefficient $k_C > 1$.

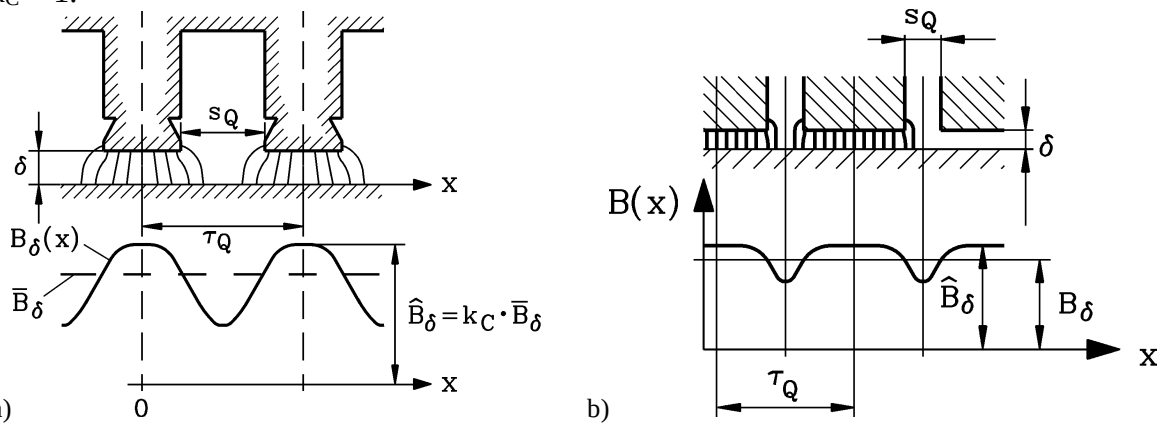

Fig. 2.7.1-1: Flux fringing in air gap due to slotting: a) Real slot geometry, b) Idealized geometry for calculation

$$k_C = \hat{B}_\delta / B_\delta = \frac{\tau_Q}{\tau_Q - \zeta(h) \cdot \delta} \qquad (2.7.1\text{-}1)$$

With increasing slot opening s_Q and/or decreasing air gap δ the influence of slotting on flux ripple increases according to the ratio $h = s_Q / \delta$ (Fig. 2.7.1-2).

$$\zeta(h) = \frac{2}{\pi} \cdot \left[h \cdot \arctan(h/2) - \ln\left(1 + (h/2)^2\right) \right] \approx \frac{h^2}{h+5} \quad . \tag{2.7.1-2}$$

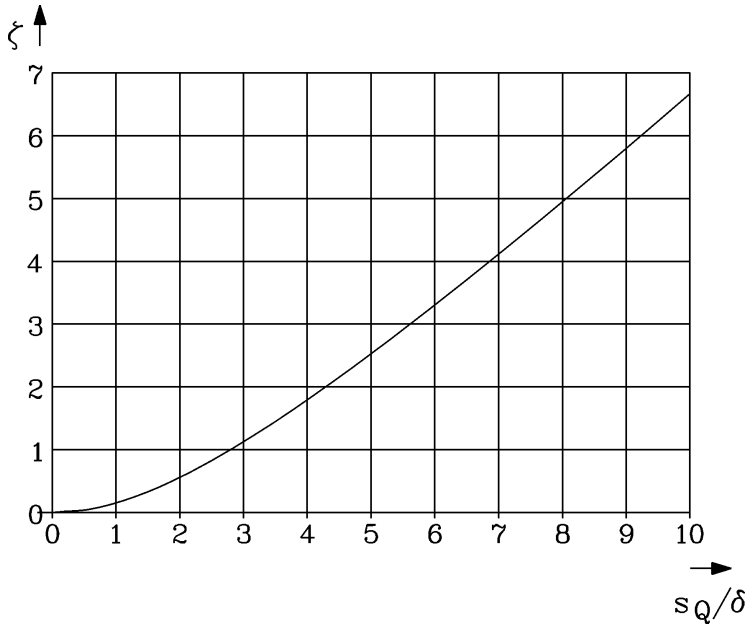

Fig. 2.7.1-2: Influence of ratio s_Q/δ on coefficient ζ to determine *Carter´*s coefficient

The air gap flux per slot pitch is determined with the *average air gap flux density per slot pitch*

$$\Phi_{\delta Q} = B_\delta \cdot \tau_Q \cdot l \quad , \tag{2.7.1-3}$$

but the m.m.f. under the tooth tip, where air gap with is δ, has to be determined with *peak value* $\hat{B}_\delta$

$$V_\delta = \hat{H}_\delta \cdot \delta = \frac{\hat{B}_\delta}{\mu_0} \cdot \delta = \frac{B_\delta}{\mu_0} \cdot k_C \cdot \delta \quad \Rightarrow \quad \boxed{V_\delta = \frac{B_\delta}{\mu_0} \cdot \delta_e \qquad \delta_e = k_C \cdot \delta} \quad . \tag{2.7.1-4}$$

Stator and rotor slotting are considered simultaneously by approximation

$$k_C = k_{Cs} \cdot k_{Cr} \quad , \tag{2.7.1-5}$$

when each of the coefficients k_{Cs}, k_{Cr} are determined for unslotted opposite part.

In the same way **radial ventilation ducts** between sections of iron stack of length l_1 with duct width l_k lead to ripple of air gap flux density in axial direction z (Fig. 2.7.1-3). If we consider ventilation ducts only on stator or rotor side, the relation between average air gap density and peak air gap density is given by (2.7.1-1), if we take $l_k + l_1$ instead of τ_Q and l_k instead of s_Q

$$k'_C = B_\delta / \overline{B}_\delta = \frac{l_1 + l_k}{l_1 + l_k - \zeta(h') \cdot \delta} \tag{2.7.1-6}$$

and for $h' = l_k / \delta$. Without radial ventilation ducts the total iron length of n_k section would be $l_{Fe} = n_k \cdot l_1$ and the air gap flux per slot pitch $\Phi_{\delta Q} = B_\delta \cdot \tau_Q \cdot l_{Fe}$. With ducts the total length is $L = n_k \cdot l_1 + (n_k - 1) \cdot l_k$ and the average air gap flux density decreases to $\overline{B}_\delta < B_\delta$, yielding for flux per slot pitch $\Phi'_{\delta Q} = \overline{B}_\delta \cdot \tau_Q \cdot L$, which is a little bit larger due to some flux passing

through the ducts: $\overline{B}_\delta \cdot L > B_\delta \cdot l_{Fe}$. If we want to use **average flux density per slot pitch** B_δ for calculation, we take according to

$$\boxed{\overline{B}_\delta \cdot L = B_\delta \cdot L / k'_C = B_\delta \cdot l_e \qquad l_e = L / k'_C} \tag{2.7.1-7}$$

equivalent iron length $l_{Fe} < l_e < L$ into account for considering magnetic effect of radial ventilation ducts. Usually radial ventilation ducts are oppositely arranged in stator and rotor, yielding symmetrical fringing of air gap flux density with symmetry line in middle of air gap. So instead of δ only half air gap $\delta/2$ has to be used in (2.7.1-6), (2.7.1-7).

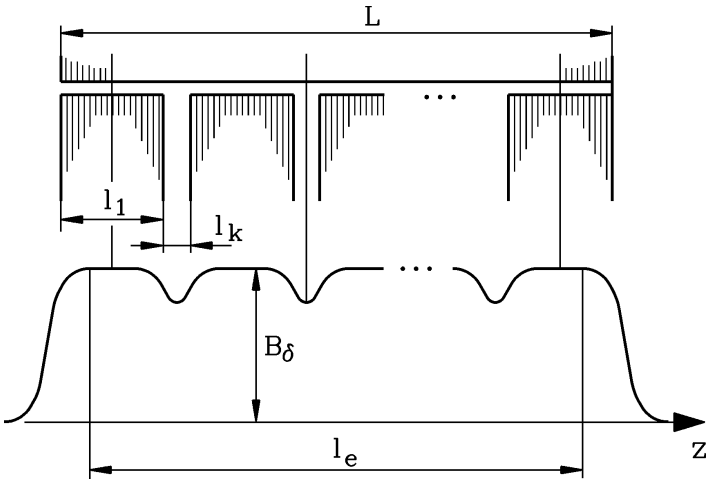

Fig. 2.7.1-3: Ripple of air gap flux density in axial direction due to radial ventilation ducts

$$\Phi_{\delta Q} = B_\delta \cdot \tau_Q \cdot l_e \tag{2.7.1-8}$$

Facit:
*If average air gap flux density B_δ is taken for calculating air gap m.m.f., **equivalent air gap δ_e** has to be used instead of geometrical air gap width δ in order to consider slotting. Magnetic effect of radial ventilation ducts is considered by using **equivalent iron length l_e** instead of real iron length l_{Fe}.*

Example 2.7.1-1:
500 kW, cage induction machine, Q_s/Q_r = 60/50, B_δ = 0.858 T, stator bore diameter: d_{si} = 458 mm, air gap δ = 1.4 mm, high voltage winding: slot width $b_{Qs} = s_{Qs}$ = 12.5 mm, s_{Qr} = 2.5 mm, iron stack of stator and rotor consist of 9 sections with l_1 = 42 mm and 8 radial ducts with width l_k = 10 mm.

	τ_Q / mm	s_Q / mm	s_Q/δ	ζ	k_C
stator	24.0	12.5	8.93	5.72	1.50
rotor	28.8	2.5	1.79	0.47	1.023

*Carter´*s coefficient: $k_C = k_{Cs} \cdot k_{Cr} = 1.5 \cdot 1.023 = \underline{\underline{1.54}}$

Equivalent air gap: $\delta_e = k_C \cdot \delta = 1.54 \cdot 1.4 = 2.156\,\text{mm}$

$$h' = l_k / (\delta/2) = 10/(1.4/2) = 14.28,\ \zeta(h') = 10.58,\ k'_C = \frac{l_1 + l_k}{l_1 + l_k - \zeta(h') \cdot (\delta/2)} = 1.166$$

Total axial length: $L = 9 \cdot l_1 + 8 \cdot l_k = 9 \cdot 42 + 8 \cdot 10 = 458\,\text{mm}$

Iron stack length: $l_{Fe} = 9 \cdot l_1 = 9 \cdot 42 = 378\text{mm}$

Equivalent iron length: $l_e = L / k'_C = 458/1.166 = \underline{\underline{392}}\,\text{mm}$

$$V_\delta = \frac{B_\delta}{\mu_0} \cdot \delta_e = \frac{0.858}{4\pi \cdot 10^{-7}} \cdot 0.002156 = \underline{\underline{1472}}\,\text{A}$$

2.7.2 Magnetization of teeth

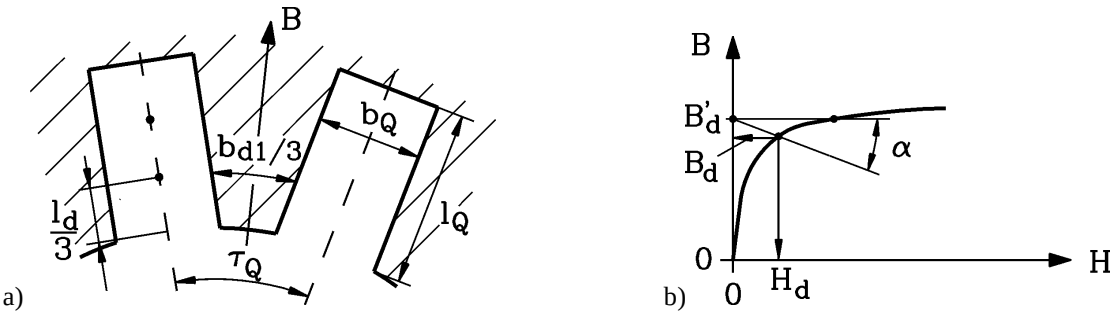

Fig. 2.7.2-1: a) Tooth flux density, b) Determination of magnetic tooth flux density and field strength

Air gap flux per slot pitch $\Phi_{\delta Q} = B_\delta \cdot \tau_Q \cdot l_e$ is quenched into stator and rotor teeth, thus increasing there tooth flux density, which leads to iron saturation. Slots with parallel slot sides lead to teeth, which in stator are narrowest at the tooth tip and in rotor at the slot bottom (Fig. 2.7-1). Thus tooth cross section depends on radius *r*. At a given radius tooth width is $b_d(r)$. If we assume that that air gap flux $\Phi_{\delta Q}$ is completely flowing through iron teeth Φ_d, avoiding the parallel path of slots completely, we get for tooth flux density

$$B'_d(r) = \frac{\Phi_{\delta Q}}{k_{Fe} \cdot b_d(r) \cdot l_{Fe}} \qquad (2.7.2\text{-}1)$$

and via *B(H)*-magnetization curve of iron the tooth magnetic field strength $H'_d(r)$. In reality, some flux Φ_Q also passes **via the parallel slot** and through the insulation of iron sheets (cross section $b_Q(r) l_{Fe} + (1 - k_{Fe}) l_{Fe} \cdot b_d(r)$). This effect is strong especially when iron is strongly saturated. Therefore, **real** tooth flux density $B_d(r)$ is a little bit lower than **apparent** tooth flux density $B'_d(r)$: $B_d(r) < B'_d(r)$, which leads at high saturation to considerable reduction of $H_d(r) < H'_d(r)$. As $H_d(r)$ is directed parallel to tooth side, this magnetic field strength is the **same** in iron and in slot. Slot flux density is therefore $\mu_0 H_d(r)$.

$$\Phi_{\delta Q} = \Phi_d + \Phi_Q = B_d(r) \cdot k_{Fe} b_d(r) l_{Fe} + \mu_0 H_d(r) \cdot l_{Fe} \cdot \left[b_Q(r) + (1 - k_{Fe}) b_d(r) \right] \qquad (2.7.2\text{-}2)$$

Combining (2.7.2-1), (2.7.2-2) leads to

$$B_d(r) = B'_d(r) - \frac{\mu_0}{k_{Fe}} \cdot \left(\frac{b_Q(r)}{b_d(r)} + 1 - k_{Fe} \right) \cdot H_d(r) \quad , \qquad (2.7.2\text{-}3a)$$

being a straight line $B_d(H_d)$ with negative inclination $\tan\alpha$,

$$B_d(r) = B'_d(r) - \tan\alpha \cdot H_d(r) \quad , \qquad (2.7.2\text{-}3b)$$

which can be introduced in *B(H)*-characteristic to determine B_d , H_d (Fig. 2.7.2-1). It is clearly visible, that at low B_d the difference between B_d, B'_d is negligible.

The m.m.f. of teeth with varying width is integral along tooth length l_d, which may be simplified by ***Simpson´*s rule**, taking the values of H_d at tooth tip H_{di}, in the middle of tooth H_{dm} and at tooth bottom H_{da}.

$$V_d = \int_{r_i}^{r_i + l_d} H_d(r) \cdot dr \cong l_d \cdot (H_{di} + 4H_{dm} + H_{da})/6 \qquad (2.7.2\text{-}4)$$

Simplified calculation takes ***H*d at on 1/3 of tooth length** at the narrower side (Fig. 2.7.2-1) for calculating m.m.f. and often also apparent tooth flux density instead of real one:

$$\tau_{Qs,1/3} = (d_{si} + (2/3) \cdot l_{ds}) \cdot \pi / Q_s \quad , \qquad \tau_{Qr,1/3} = \left[d_{si} - 2 \cdot (\delta + (2/3) \cdot l_{dr})\right] \cdot \pi / Q_r$$

$$b_{d,1/3} = \tau_{Q,1/3} - b_Q \quad \Rightarrow \qquad B'_{d,1/3} = \frac{B_\delta \cdot \tau_Q \cdot l_e}{k_{Fe} \cdot b_{d,1/3} \cdot l_{Fe}} \qquad \Rightarrow \qquad H'_{d,1/3}(B'_{d,1/3}) \approx H_{d,1/3}$$

$$\boxed{V_d \cong H_{d,1/3} \cdot l_d} \quad . \qquad (2.7.2\text{-}5)$$

In order to avoid extensive saturation, apparent tooth flux density **should stay below 2.4 T** at narrowest part of tooth.

For **parallel sided teeth** calculation is much simpler, as b_d = const., so (2.7.2-5) can be taken with b_d instead of $b_{d,1/3}$.

Example 2.7.2-1:

Data: 500 kW cage induction motor: B_δ = 0.858 T, k_{Fe} = 0.95, l_e = 392 mm, l_{Fe} = 378 mm, d_{si} = 458 mm, Q_s/Q_r = 60/50, air gap δ = 1.4 mm, τ_{Qs} = 24.0 mm, τ_{Qr} = 28.8 mm, iron sheet type III (Table 2.7-2)

	h_Q, b_Q (mm)	$l_d = h_Q$ (mm)	$b_{d,1/3}$ (mm)	$B'_{d,1/3}$/T	$H'_{d,1/3}$/A/cm	V_d / A
stator	69.0, 12.5	69.0	13.9	1.615	46.5	321
rotor	43.5, 5.1	43.5	19.9	1.35	8.5	37

Check of flux density at narrowest tooth width:

	$b_{d,i}$ (mm)	$B'_{d,1/3}$/T
stator	11.5	1.95 < 2.4
rotor	18.0	1.52 < 2.4

By variation of air gap flux density B_δ from zero to $B_{\delta,max}$ e.g. 1.2 T, one gets corresponding values V_δ , V_{ds} , V_{dr} and thus a non-linear saturation characteristic (Fig. 2.7.3-2).

$$B_\delta = f(V_{\delta+d}) = f(V_\delta + V_{ds} + V_{dr}) \quad . \qquad (2.7.2\text{-}6)$$

2.7.3 Distribution of saturated magnetic air gap flux density

Exciting m.m.f. $V(x)$ and in linear case also magnetic air gap flux density $B_\delta(x)$ is step-like due to conductors being placed in slots (Fig. 2.7-3-1 a). Taking only **fundamental** ν = 1 as

main magnetizing component into account, the m.m.f. $V_{\nu=1}$ and $B_{\delta,\nu=1} = \mu_0 V_{\nu=1} / \delta$ are distributed **sinusoidal.** Due to iron saturation only the percentage of $0 < V_\delta / V_{\nu=1} < 1$ is left for air gap magnetization, whereas the rest is necessary for magnetizing teeth and yokes. As the amount of m.m.f. for magnetizing iron parts increases with increasing B_δ , the shape of saturated magnetic air gap flux density $B_\delta(x)$ is no longer sinusoidal, but **flattened at the top** B_δ (Fig. 2.7-3-1 b).

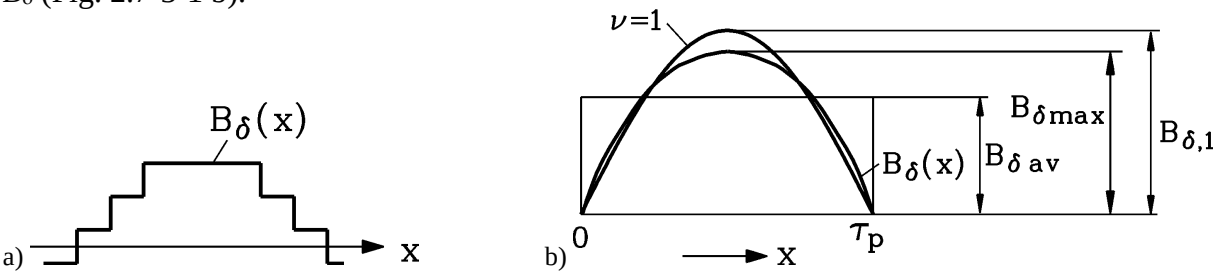

Fig. 2.7.3-1: a) Distribution of air gap field due to coils concentrated in slots (slot openings neglected), b) saturated air gap flux density, excited by sinusoidal fundamental of m.m.f., neglecting steps in field distribution

This flattened distribution may be *Fourier*-analyzed, showing **a fundamental $\nu = 1$**

$$B_{\delta,\nu=1}(x,t) = B_{\delta,\nu=1} \cdot \cos(x\pi / \tau_p - \omega_s t) \tag{2.7.3-1}$$

and a **considerable third harmonic $\nu = 3$**

$$B_{\delta,\nu=3}(x,t) = B_{\delta,\nu=3} \cdot \cos(3(x\pi / \tau_p - \omega_s t)) = B_{\delta,\nu=3} \cdot \cos(3x\pi / \tau_p - 3\omega_s t) \tag{2.7.3-2}$$

and further small space harmonics with **odd ordinal numbers**, dividable by 3: 9, 15, 21, ... These additional harmonics induce phase voltages in stator winding phases U, V, W with frequencies $3f_s$, $9f_s$, $15f_s$, $21f_s$, ... There is **no phase shift** between these harmonic phase voltages of U, V, W due to

$$\begin{aligned} u_{U,3}(t) &= U_3 \cos(3\omega_s t) \\ u_{V,3}(t) &= U_3 \cos(3(\omega_s t - 2\pi/3)) = U_3 \cos(3\omega_s t) = u_{U,3}(t) \\ u_{W,3}(t) &= U_3 \cos(3(\omega_s t - 4\pi/3)) = U_3 \cos(3\omega_s t) = u_{U,3}(t) \end{aligned} \quad , \tag{2.7.3-3}$$

therefore in line-to-line voltage of **star connected stator** winding these harmonics **are not visible**.

$$u_{UV,3}(t) = u_{U,3}(t) - u_{V,3}(t) = 0 \tag{2.7.3-4}$$

No harmonic phase current may flow therefore with frequencies $3f_s$, $9f_s$, $15f_s$, $21f_s$ ... in stator winding, except in that case, when electric connection of star point to ground is used. Then ground current is 3 times phase harmonic current $i_g(t) = 3i_{s,3}(t)$ with frequencies $3f_s$, $9f_s$, $15f_s$, $21f_s$ ... and may be dangerously big in case of high saturation.
In **delta connected stator** winding phase voltage is also line-to-line voltage, so this **harmonic current** $3i_{s3}(t)$ with frequencies $3f_s$, $9f_s$, $15f_s$, $21f_s$ ... circles in delta winding, heating winding up in addition to fundamental current, but is not visible in terminal connections due to 2nd *Kirchhoff*´s law:

$$i_{U,Line,3}(t) = i_{s,U,3}(t) - i_{s,V,3}(t) = i_{s,3}(t) - i_{s,3}(t) = 0 \tag{2.7.3-5}$$

Facit:
In order to avoid harmonic currents with frequencies $3f_s$, $9f_s$, $15f_s$, $21f_s$, ... due to saturation flux density harmonics, stator (and in case of slip ring induction machine also rotor) winding shall be preferably connected in star without any connection of star point to earth. In that case only induced voltage of fundamental of air gap flux density distribution balances terminal voltage of the grid.

Determination of flattened air gap flux density distribution is usually done by only considering saturation of teeth, which due to narrow iron parts dominate in saturation. Taking at $t = 0$ fundamental m.m.f., which is distributed sinusoidal in air gap

$$V_{\delta+d}(x) = \hat{V}_{\delta+d} \cdot \cos(x\pi / \tau_p) \quad , \tag{2.7.3-6}$$

one gets via (2.7.2-6) the corresponding value $B_\delta(x)$, which is **the top-flattened air gap flux density distribution**.

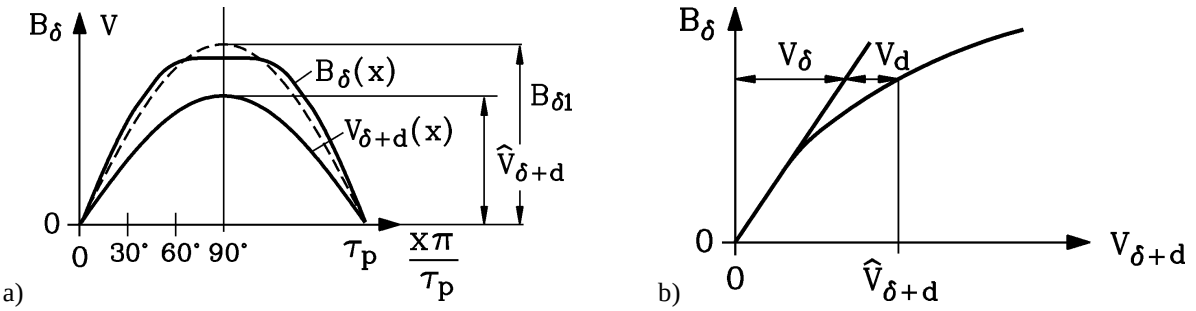

Fig. 2.7.3-2: a) Distribution of sinusoidal m.m.f. $V_{\delta+d}$, saturated air gap flux density B_δ and its fundamental $B_{\delta 1}$, b) non-linear saturation characteristic of teeth and air-gap.

Fourier fundamental of flattened $B_\delta(x)$ is with $\gamma = x\pi / \tau_p$

$$B_{\delta,\nu=1} = \frac{1}{\pi}\int_0^{2\pi} B_\delta(\gamma)\cdot\sin(y)\cdot d\gamma \cong \left[B_\delta(30°) + \sqrt{3}\cdot B_\delta(60°) + B_\delta(90°)\right]/3 \quad . \tag{2.7.3-6}$$

Air gap flux of flattened air gap flux density distribution is nearly the same as of fundamental:

$$\Phi_\delta = l_e \int_0^{\tau_p} B_\delta(x)\cdot dx = l_e\cdot\tau_p\cdot B_{\delta,av} \cong l_e \int_0^{\tau_p} B_{\delta,\nu=1}(x)\cdot dx = \frac{2}{\pi}\cdot l_e\cdot\tau_p\cdot B_{\delta,\nu=1} \quad . \tag{2.7.3-7}$$

Therefore fundamental amplitude may taken from

$$B_{\delta,\nu=1} \cong (\pi/2)\cdot B_{\delta,av} \quad . \tag{2.7.3-8}$$

This procedure of determination of fundamental depending on saturation (2.7.3-6) has been done for iron sheet type III, but is also valid more or less for type IV and similar types of iron sheets. With rising **degree of tooth saturation** V_{ds+dr}/V_δ the ratio of maximum of flattened air gap flux density distribution versus average flux density $B_\delta/B_{\delta,av} = 1/\alpha$ decreases from linear (unsaturated) value $\pi/2 = 1.57$ to typically 1.3 with a theoretical limit 1 at very high saturation (Fig. 2.7.3-3). Once a curve like Fig. 2.7.3-2b has been derived with (2.7.2-4) or (2.7.2-5), only the ratio k is of importance for α (*Arnold´*s method), which is often used instead of method (2.7.3-6). So, if we need a certain $B_{\delta,v=1}$ for inducing the necessary voltage U_h

$$B_{\delta,\nu=1} = \frac{U_h}{\sqrt{2}\pi f_s \cdot N_s k_{ws1} \cdot (2/\pi)\tau_p l_e} \quad , \qquad (2.7.3\text{-}9)$$

how big is the real maximum flux density B_δ in air gap, which determines tooth saturation ? By utilization of Fig. 2.7.3-3 in iterations, this is answered and the correlation of air gap flux $\Phi_\delta = l_e \cdot \tau_p \cdot B_{\delta,av}$, maximum air gap flux density B_δ and fundamental is $B_{\delta,\nu=1}$ is found.

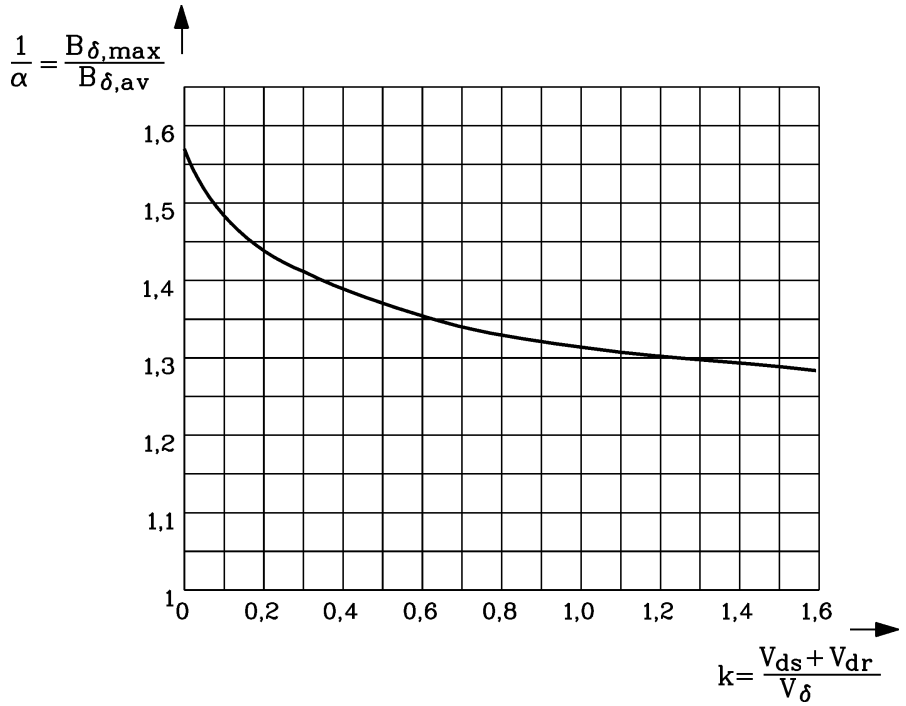

Fig. 2.7.3-3: Ratio of maximum of flattened air gap flux density distribution versus average flux density $B_\delta/B_{\delta,av}$, depending on degree of tooth saturation V_{ds+dr}/V_δ, from many calculated machines acc. to Fig. 2.7.3-2.

Example 2.7.3-1:

550 kW cage induction motor, demanded rated voltage 6.6 kV Y, 50 Hz, motor dimensions according to example 2.7.1-1, 2.7.2-1, σ_s = 0.05, N_s = 200, k_{ws} = 0.91.

$$U_h = U_N/(\sqrt{3}\cdot(1+\sigma_s)) = 6600/(\sqrt{3}\cdot 1.05) = 3629\,\mathrm{V}$$

$$B_{\delta,\nu=1} = \frac{U_h}{\sqrt{2}\pi f_s \cdot N_s k_{ws1} \cdot (2/\pi)\tau_p l_e} = \frac{3629}{\sqrt{2}\pi \cdot 50 \cdot 200 \cdot 0.91 \cdot (2/\pi) \cdot 0.36 \cdot 0.392} = 1.0\,\mathrm{T}$$

$B_{\delta,\nu=1}$ = 1.0 T

$$B_{\delta,av} \cong (2/\pi)\cdot B_{\delta,\nu=1} = (2/\pi)\cdot 1.0 = 0.6366\,\mathrm{T}$$

Assumption (1st iteration):

$B_\delta/B_{\delta,av}$ = 1.41 $\Rightarrow$ V_{ds+dr}/V_δ = 0.3

$$B_\delta = 1.41 B_{\delta,av} = 1.41\cdot 0.6366 = 0.897\,\mathrm{T}$$

$$B'_{ds,1/3} = \frac{B_\delta \cdot \tau_{Qs} \cdot l_e}{k_{Fe} \cdot b_{ds,1/3} \cdot l_{Fe}} = 1.69\,\mathrm{T},\ H'_{ds,1/3} = 74\,\mathrm{A/cm},\ V_{ds} = 74\cdot 6.9 = 511\,\mathrm{A}$$

$$B'_{dr,1/3} = \frac{B_\delta \cdot \tau_{Qr} \cdot l_e}{k_{Fe} \cdot b_{dr,1/3} \cdot l_{Fe}} = 1.42\,\mathrm{T},\ H'_{dr,1/3} = 13\,\mathrm{A/cm},\ V_{dr} = 13\cdot 4.35 = 57\,\mathrm{A}$$

$$V_\delta = \frac{B_\delta}{\mu_0}\cdot\delta_e = \frac{0.897}{4\pi\cdot 10^{-7}}\cdot 0.002156 = \underline{\underline{1539}}\,\mathrm{A}$$

V_{ds+dr}/V_δ = (511+57)/1539 = 0.37

Assumption (2nd iteration): average of old and new value: V_{ds+dr}/V_δ = (0.37 + 0.3)/2 = 0.335

V_{ds+dr}/V_δ	$B_\delta/B_{\delta,av}$	B_δ	$B'_{ds,1/3}$	$B'_{dr,1/3}$	$H'_{ds,1/3}$	$H'_{dr,1/3}$	V_{ds}	V_{dr}	V_δ	V_{ds+dr}/V_δ
-	-	T	T	T	A/cm	A/cm	A	A	A	-
0.3	1.41	0.897	1.69	1.42	74	13	511	57	1539	0.37
0.335	1.40	0.891	1.68	1.41	70	12.1	483	52.6	1529	0.35

Table 2.7.3-1: Iterative determination of flat top B_δ for given air gap flux

As after 2nd iteration values V_{ds+dr}/V_δ at beginning and end of iteration differ only by (0.35-0.335)/0.335 = 4.5% < 5%, iteration is ended, taking as final values B_δ = 0.891 T and V_{ds+dr}/V_δ = 0.35.

2.7.4 Magnetization of yokes

The air gap flux is divided in the yokes into two equal parts, called **yoke flux** (**back iron flux**) (Fig. 2.7.4-1).

$$\Phi_y = \Phi_\delta / 2 \tag{2.7.4-1}$$

The air gap flux as main flux $\Phi_\delta = \Phi_h$ is increased in the stator yoke by the stator stray flux

$$\Phi_{ys} = (\Phi_\delta + \Phi_{\sigma s})/2 = (1+\sigma_s)\cdot\Phi_\delta/2 \quad . \tag{2.7.4-2}$$

Whereas air gap and tooth flux density is oriented radial, the yoke flux density is oriented tangential in circumference direction. The maximum of yoke flux density B_y is in the neutral axis (q-axis), where the air gap flux density is zero, whereas the yoke flux density is zero in d-axis, where air gap flux density is maximum (Fig. 2.7.4-1 a):

$$B_y = \frac{\Phi_y}{h_y \cdot l_{Fe} \cdot k_{Fe}} \tag{2.7.4-3}$$

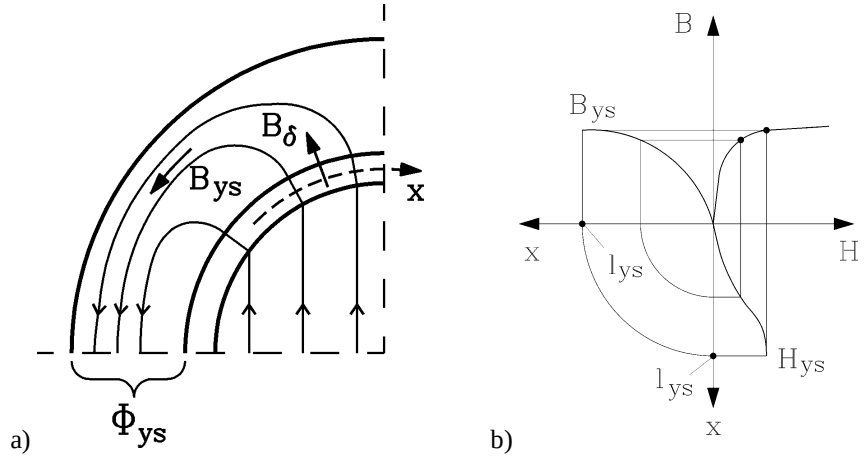

Fig. 2.7.4-1: Yoke flux density: a) Flux density distribution in air gap $B_\delta(x)$and stator and rotor yoke $B_y(x)$ of 2-pole machine, b) Sinusoidal yoke flux density distribution $B_y(x)$ leads to non-sinusoidal distribution of yoke field strength $H_y(x)$ in case of iron saturation

Especially in bigger machines radial cooling ducts are used, which reduce yoke height h_y. In Fig. 2.2-1 e.g. axial round ducts with diameter c_2 are used in rotor iron back. There yoke height is only $c_1 + c_3 < h_{yr}$, whereas in between these ducts yoke height is h_{yr}. By numerical

field calculation of yoke flux flow exact increase of yoke flux density due to ducts is determined. Approximately an **equivalent yoke height** h_{ye} is often taken.

$$h_{ye} = c_1 + c_2/3 + c_3 = h_y - (2/3)\cdot c_2 \qquad (2.7.4\text{-}4)$$

If the rotor iron stack is directly mounted on shaft (Fig. 2.7.4-2), a part of yoke flux will also pass through shaft, thus finding an increased yoke flux cross section. At *ideal no-load* ($s = 0$) rotor frequency is $f_r = s\cdot f_s = 0$ and rotor flux is DC flux, which – in case of 2-pole machine – penetrates rotor shaft completely (Fig. 2.7.4-1). In 4-pole machine (Fig. 2.7-5) yoke flux penetrates rotor shaft only partially. With increasing pole count the flux penetration in the rotor shaft decreases. At *load* (rated slip s_N = 1 ... 5 %) rotor frequency is small (e.g. f_s = 50 Hz: $f_r = s\cdot f_s = 0.5 \ldots 2.5\,\text{Hz}$), but penetrating rotor yoke flux is AC flux, which induces eddy currents in massive rotor shaft. Eddy currents excite additional flux with phase opposition to inducing penetration flux, thus reducing this flux, which only will flow in surface of rotor shaft (Fig 2.7.4-3). **Penetration depth** d_E, determined by solution of *Maxwell´*s equations, may be taken as equivalent depth in shaft, where flux flows:

$$d_E = \frac{1}{\sqrt{\pi\cdot s\cdot f_s\cdot \mu_{Fe}\cdot \kappa_{Fe}}} \qquad (2.7.4\text{-}5)$$

In case of 2- and 4-pole machines rotor yoke height is increased by d_E to consider cross section of rotor yoke flux, whereas with larger pole count effect of flux penetration in shaft is negligible already at DC conditions:

$$h_{yr,e} = h_{yr} + d_E \qquad (2.7.4\text{-}6)$$

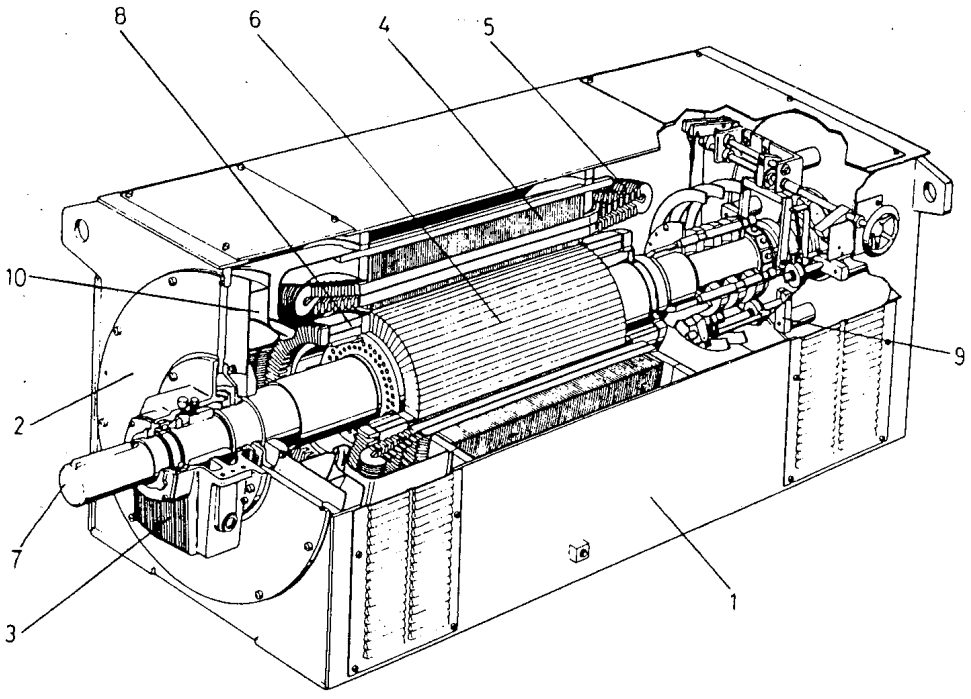

Fig. 2.7.4-2: Open ventilated slip ring induction motor, rotor iron stack directly mounted on shaft, International Mounting IM B3, International Protection IP23
1: stator housing, 2: end shield, 3: oil cooler for sliding bearings, 4: stator iron stack, 5: overhang of two layer form wound stator winding, 6: rotor iron stack with axial ducts in rotor iron back, 7: shaft end, 8: overhang of rotor two layer winding, 9: three phase rotor slip rings with brush contacts and hand wheel to lift brushes and short circuit the rotor, 10: shaft mounted radial fan for generating cooling air flow, which passes through openings in stator housing

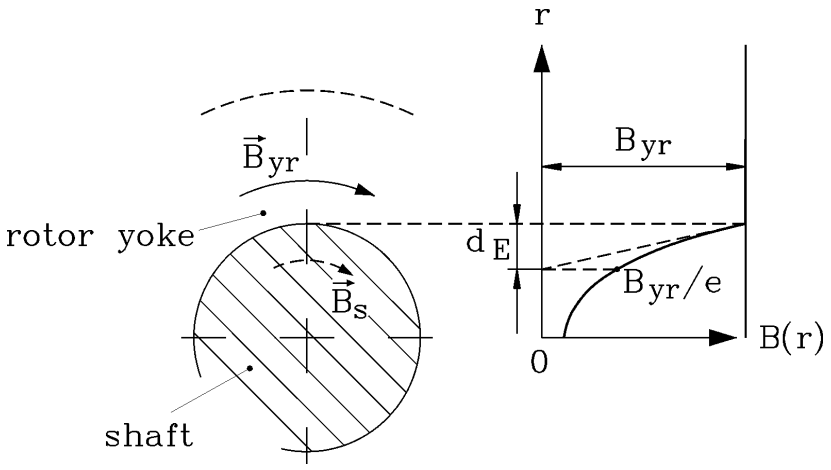

Fig. 2.7.4-3: Penetration of rotor flux into shaft and reduction of shaft flux by shaft eddy currents

Yoke heights must be chosen large enough to avoid high iron saturation. As length of yokes l_y is much larger than length of teeth l_d (especially in machines with low pole count $2p < 10$ ... 12), m.m.f. of yokes would dominate, if yoke flux density is as big as tooth flux density. Therefore **saturation limit** of maximum yoke flux density is chosen lower than for teeth: $B_y < 1.7\,\mathrm{T}$.

Yoke flux density $B_y(x)$ is **integral** of air gap flux density distribution, hence even flat top $B_\delta(x)$-distribution leads to **nearly sinusoidal yoke flux density distribution** $B_y(x)$

$$B_y(x) = \frac{\Phi_y(x)}{A_y} = \frac{l_{Fe} \cdot \int_0^x B_\delta(x) \cdot dx}{A_y} \approx B_y \cdot \sin\left(\frac{x \cdot \pi}{2 l_y}\right) \quad . \tag{2.7.4-7}$$

But non-linear *B(H)*-magnetization of iron therefore yields **non-sinusoidal distribution** of magnetic yoke field strength $H_y(x)$ (Fig. 2.7.4-1, right) along $0 \le x \le l_y$ at average yoke radius r_{ys}, r_{yr} :

$$r_{ys} = (d_{si} + h_{ys})/2 + l_{ds} \qquad r_{yr} = (d_{si} - h_{yr})/2 - l_{dr} - \delta \tag{2.7.4-8}$$

$$l_y = r_y \cdot \pi/(2p) \quad . \tag{2.7.4-9}$$

Deviation of $H_y(x)$ from sinusoidal distribution increases with increasing B_y. Calculation of yoke m.m.f. V_y

$$V_y = \int_0^{l_y} H_y(x) \cdot dx = l_y \cdot \overline{H}_y \tag{2.7.4-10}$$

leads to **average yoke magnetic field strength** $\overline{H}_y(B_y)$, which depends on maximum yoke flux density B_y. This calculation has been done for *B(H)*-magnetization of iron sheet type III for varying $0 < B_y \le 1.8$ T (Table 2.7.4-1), and may be used also roughly for determination of V_y for sheet type IV and similar iron sheets. A similar $B_y(\overline{H}_y)$-characteristic for iron sheets is given in Fig. 2.7.4-4.
Note that $B_y(\overline{H}_y)$-curves of manufacturers “a” and “b” differ somewhat.

B_y / T	$\overline{H}_y$ / A/cm									
	.,.0	.,.1	.,.2	.,.3	.,.4	.,.5	.,.6	.,.7	.,.8	.,.9
0.8	0.83	0.85	0.87	0.89	0.91	0.93	0.95	0.97	0.99	1.01
0.9	1.03	1.05	1.07	1.09	1.1	1.11	1.13	1.15	1.17	1.19
1.0	1.23	1.26	1.29	1.33	1.36	1.39	1.43	1.46	1.49	1.53
1.1	1.56	1.59	1.63	1.68	1.73	1.78	1.83	1.88	1.93	1.98
1.2	2.03	2.08	2.13	2.18	2.23	2.28	2.33	2.38	2.43	2.5
1.3	2.6	2.7	2.8	2.9	3.0	3.1	3.25	3.4	3.55	3.7
1.4	3.9	4.1	4.3	4.5	4.7	5.0	5.3	5.6	5.9	6.2
1.5	6.6	7.0	7.4	7.8	8.3	8.8	9.3	9.8	10.4	11.0
1.6	11.6	12.3	13.0	13.7	14.5	15.4	16.4	17.4	18.4	19.4
1.7	20.4	21.5	22.6	23.9	25.2	26.6	28.0	29.4	31.0	32.7
1.8	34.4	36.1	37.8	39.6	41.4	43.2	45.0	47.2	49.7	52.6

Table 2.7.4-1: Yoke (back iron) average magnetization characteristic of iron sheet type III (Manufacturer "b").

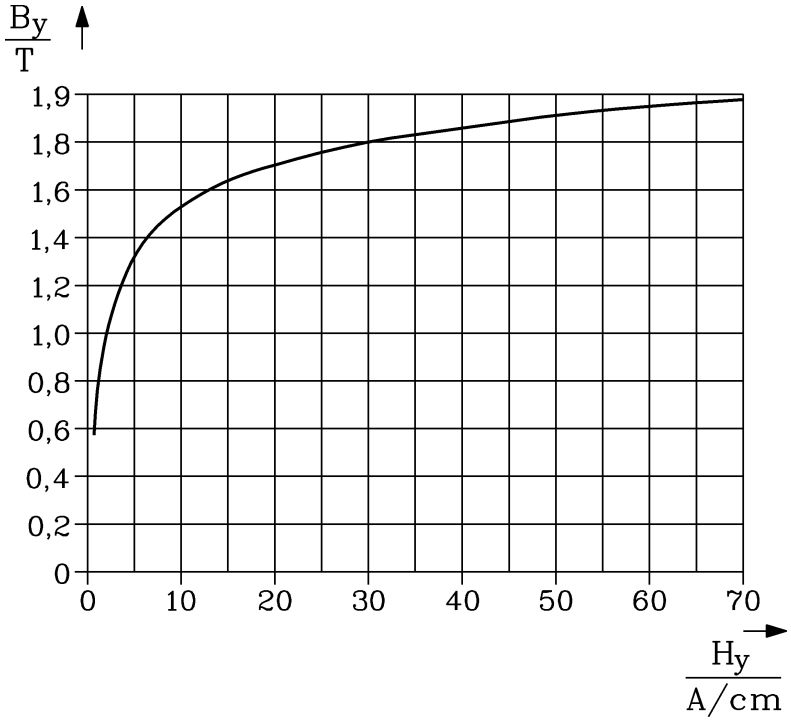

Fig. 2.7.4-4: Yoke average magnetization $B_y(\overline{H}_y)$ for iron sheets type III (Manufacturer "a").

Example 2.7.4-1:

Data: 550 kW 4-pole cage induction motor, demanded rated voltage 6.6 kV Y, 50 Hz, motor dimensions according to example 2.7.1-1, 2.7.2-1: d_{si} = 458 mm, δ = 1.4 mm, l_{ds} = 69 mm, l_{dr} = 43.5 mm, h_{ys} = 77 mm, shaft diameter d_{ri} = 200 mm, c_2 = 30 mm
B_δ = 0.891 T, $B_{\delta,\nu=1}$ = 1.0 T, $B_{\delta,av} = 0.6366\,\mathrm{T}$.

- Stator maximum yoke flux density:

$$B_{ys} = \frac{\Phi_\delta \cdot (1+\sigma_s)/2}{h_{ys} \cdot l_{Fe} \cdot k_{Fe}} = \frac{(2/\pi) \cdot B_{\delta,\nu=1} \cdot \tau_p \cdot l_e \cdot (1+\sigma_s)/2}{h_{ys} \cdot l_{Fe} \cdot k_{Fe}} =$$

$$= \frac{(2/\pi) \cdot 1.0 \cdot 0.36 \cdot 0.392 \cdot 1.05/2}{0.077 \cdot 0.378 \cdot 0.95} = 1.70T$$

$$d_{sa} = d_{si} + 2l_{ds} + 2h_{ys} = 458 + 2 \cdot 69 + 2 \cdot 77 = 750\,\mathrm{mm}$$

$$h_{yr} = \left[d_{si} - 2\delta - 2l_{dr} - d_{ri}\right]/2 = \left[458 - 2 \cdot 1.4 - 2 \cdot 43.5 - 200\right]/2 = 84.1\,\mathrm{mm}$$

- Without flux penetration in shaft:

$$h_{yr,e} = h_{yr} - (2/3)\cdot c_2 = 84.1 - 2/3\cdot 30 = 64.1\,\text{mm}$$

- With flux penetration in shaft at $s_N = 0.015$, $f_s = 50$ Hz, $\mu_{Fe} = 1000\mu_0$,

$$\kappa_{Fe,shaft} = 5\cdot 10^6 \text{ S/m}$$

$$d_E = \frac{1}{\sqrt{\pi \cdot s \cdot f_s \cdot \mu_{Fe} \cdot \kappa_{Fe}}} = \frac{1}{\sqrt{\pi \cdot 0.015 \cdot 50 \cdot 1000 \cdot 4\pi \cdot 10^{-7} \cdot 5 \cdot 10^6}} = 8.2\,\text{mm}$$

$$h_{yr,e} = h_{yr} - (2/3)\cdot c_2 + d_E = 64.1 + 8.2 = 72.3\,\text{mm}$$

- Rotor maximum yoke flux density:

$$B_{yr} = \frac{\Phi_\delta / 2}{h_{yr,e}\cdot l_{Fe}\cdot k_{Fe}} = \frac{(2/\pi)\cdot B_{\delta,\nu=1}\cdot \tau_p \cdot l_e/2}{h_{yr,e}\cdot l_{Fe}\cdot k_{Fe}} = \frac{(2/\pi)\cdot 1.0\cdot 0.36\cdot 0.392/2}{0.0723\cdot 0.378\cdot 0.95} = 1.73\,\text{T}$$

- Yoke radii and lengths :

$$r_{ys} = (d_{si} + h_{ys})/2 + l_{ds} = (458+77)/2 + 69 = 336.5\,\text{mm},\ l_{ys} = r_{ys}\cdot\pi/(2p) = 264.2\,\text{mm}$$

$$r_{yr} = (d_{si} - h_{yr,e})/2 - l_{dr} - \delta = (458 - 72.3)/2 - 43.5 - 1.4 = 148.25\,\text{mm}$$

$$l_{yr} = r_{yr}\cdot\pi/(2p) = 116.4\,\text{mm}$$

- Yoke m.m.f.: According to Table 2.7.4-1: $\overline{H}_{ys} = 20.4$ A/cm, $\overline{H}_{yr} = 23.9$ A/cm,

$$V_{ys} = \overline{H}_{ys} l_{ys} = 20.4\cdot 26.4 = \underline{\underline{539}}\,\text{A},\ V_{yr} = \overline{H}_{yr} l_{yr} = 23.9\cdot 11.64 = \underline{\underline{278}}\,\text{A}$$

2.7.5 Magnetizing reactance

Magnetizing reactance X_h for **infinite iron permeability** is only determined by air gap and may be taken from Lectures: "Electrical machines and drives".

$$X_{h,\infty} = 2\pi f_s \cdot \mu_0 \cdot (N_s k_{ws1})^2 \cdot \frac{2\cdot m_s}{\pi^2 \cdot p} \cdot \frac{l_e \cdot \tau_p}{\delta_e} \qquad (2.7.5\text{-}1)$$

With finite iron permeability X_h is reduced by the ratio $V_{\delta 1}/V_m$ according to (2.7-6) for given voltage and hence flux level. Corresponding magnetizing current is calculated from (2.7-1).

Example 2.7.5-1:

Data: 550 kW 4-pole cage induction motor, demanded rated voltage 6.6 kV Y, 50 Hz, motor dimensions according to example 2.7.1-1, 2.7.2-1. $B_\delta = 0.891$ T, $B_{\delta,\nu=1} = 1.0$ T, $B_{\delta,av} = 0.6366$ T.

- m.m.f.: $V_\delta = 1529$ A, $V_{ds+dr} = 483 + 52.6 = 535.6$ A, $V_{ys} = 539$ A, $V_{yr} = 278$ A

$$V_m = 1529 + 483 + 52.6 + 539 + 278 = 2882\,\text{A},\ V_{\delta 1} = B_{\delta,\nu=1}\cdot\delta_e/\mu_0 = 1716\,\text{A}$$

- unsaturated magnetizing reactance:

$$X_{h,\infty} = 2\pi\cdot 50\cdot 4\pi\cdot 10^{-7}\cdot(200\cdot 0.91)^2\cdot\frac{2\cdot 3}{\pi^2\cdot 2}\cdot\frac{0.392\cdot 0.36}{0.002156} = 260.2\,\Omega$$

$$X_h = \frac{V_{\delta 1}}{V_m}\cdot X_{h,\infty} = \frac{1716}{2882}\cdot 260.2 = \underline{\underline{155.0}}\,\Omega$$

- magnetizing current:

$$I_m = \frac{V_m}{\frac{\sqrt{2}}{\pi}\cdot\frac{m_s}{p}\cdot N_s k_{ws1}} = \frac{2882}{\frac{\sqrt{2}}{\pi}\cdot\frac{3}{2}\cdot 200\cdot 0.91} = \underline{\underline{23.45}}\,\text{A},\quad I_m/I_N = 23.45/59 = \underline{\underline{0.4}}$$

2.8 Stray flux and inductance

Those parts of magnetic field, which do not contribute to generation of electromagnetic torque, are called **stray field** (stray flux). These stray flux components are excited by stator and rotor current, and therefore stator and rotor stray flux has to be considered as **stator and rotor stray inductance in equivalent circuit**. They exist as
- **slot stray flux** in stator and rotor slots,
- **stray flux in winding overhangs** of stator and rotor winding,
- **flux of harmonics of air gap field**, excited by stator current $\nu > 1$ and excited by rotor current $\mu > 1$,
- **stray flux due to skew** between stator and rotor slots in cage induction machines. Usually rotor cage is skewed, thus rotor stray inductance is increased.

2.8.1 Slot stray flux and inductance of stator winding

a) Single layer winding:

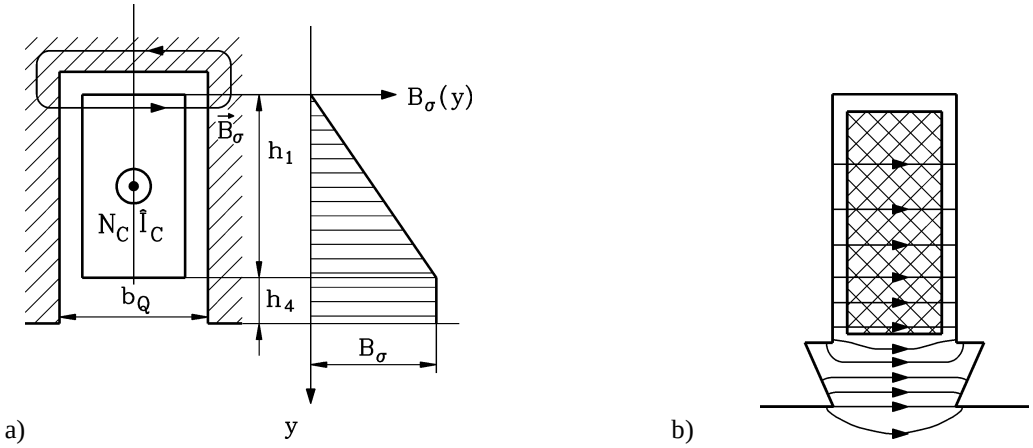

Fig. 2.8.1-1: Slot stray flux of single layer winding in open slot: a) idealized slot shape, b) real slot shape

According to Fig. 2.8.1-1 slot conductor ampere-turns $N_c I_c$ excite the slot stray flux lines, which cross the slot perpendicular. Stray flux density $B_\sigma(y)$ rises linear with co-ordinate y up to $y = h_1$, and remains constant in section h_4, as *Ampere´*s law for closed loop C (taken as closed loop of a stray flux line) yields with $\mu_{Fe} \to \infty$, $H_{Fe} \to 0$:

$$\oint_C \vec{H}_\sigma \bullet d\vec{s} = H_\sigma \cdot b_Q = N_c \hat{I}_c \cdot \frac{y}{h_1} \qquad B_\sigma(y) = \mu_0 H_\sigma(y) = \mu_0 \frac{N_c \hat{I}_c}{b_Q} \cdot \frac{y}{h_1}, \quad 0 \le y \le h_1 \quad (2.8.1\text{-}1)$$

$$\oint_C \vec{H}_\sigma \bullet d\vec{s} = H_\sigma \cdot b_Q = N_c \hat{I}_c \qquad B_\sigma(y) = \mu_0 H_\sigma(y) = \mu_0 \frac{N_c \hat{I}_c}{b_Q}, \quad h_1 \le y \le h_1 + h_4 \quad (2.8.1\text{-}2)$$

Magnetic energy stored in slot stray field of one coil, placed in two slots is determined by slot stray inductance $L_{\sigma c}$ of one coil as well as by energy per volume $B_\sigma^2/(2\mu_0)$, taking volume of the two slots. Axial length of slots in iron stack with radial ventilation ducts is l_e instead of l_{Fe}, considering amount of stray flux in ducts:

$$W_\sigma = \frac{L_{\sigma c} \hat{I}_c^2}{2} = \frac{2 \cdot l_e \cdot b_Q}{2\mu_0} \cdot \int_0^{h_1+h_4} B_\sigma^2(y) \cdot dy \qquad (2.8.1\text{-}3)$$

Solving integral (2.8.1-3) with flux density according to (2.8.1-1), (2.8.1-2) delivers slot stray inductance of one coil in two slots

$$L_{\sigma c} = 2 \cdot \mu_0 \cdot N_c^2 \cdot \lambda_Q \cdot l_e \qquad \lambda_Q = \frac{h_1}{3b_Q} + \frac{h_4}{b_Q} \quad . \tag{2.8.1-4}$$

In single layer winding with series connection of all coils per phase slot stray inductance per phase is $L_{\sigma Q} = p \cdot q \cdot L_{\sigma c}$, in case of a parallel branches per phase it is $L_{\sigma Q} = p \cdot q \cdot L_{\sigma c} / a^2$. With $N_s = p \cdot q \cdot N_c / a$ follows:

$$\boxed{L_{s\sigma Q} = \mu_0 \cdot N_s^2 \cdot \frac{2}{p \cdot q_s} \cdot \lambda_{Qs} \cdot l_e} \tag{2.8.1-5}$$

For **semi-closed slots** (Fig. 2.8.1-2) the influence of geometry on parameter λ_Q is also determined by the width of slot opening s_Q, which increases stray flux:

$$\lambda_{Qs} = \frac{h_1}{3b_Q} + \frac{h_2}{b_Q} + \frac{h_3}{(b_Q + s_Q)/2} + \frac{h_4}{s_Q} \tag{2.8.1-6}$$

In case of **parallel sided tooth** stator slot width at slot bottom b_a is larger than on top b_a, so average slot width $b_{Qav} = (b_i + b_a)/2$ along section h_1 is taken. In case of rounded top of slot with radius $r = b_i/2$ (Fig. 2.8.1-2, right) solution of *Ampere´*s law yields according to *Rothert* $\lambda = 0.685$. The vertical play is usually considered at the slot bottom (no influence on leakage).

$$\lambda_{Qs} = \frac{h_1}{3b_{Qav}} + 0.685 + \frac{h_4}{s_Q} \tag{2.8.1-7}$$

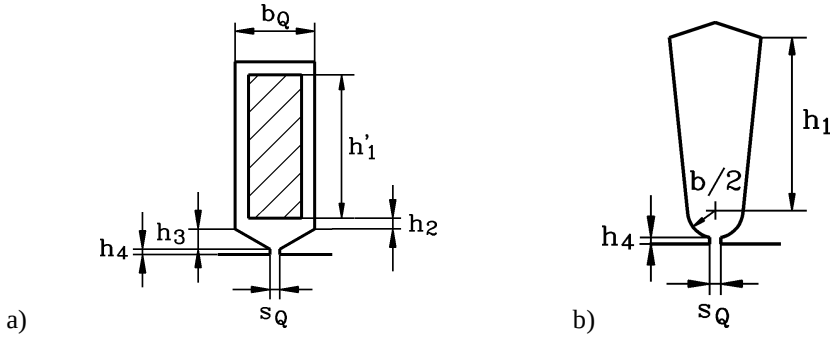

Fig. 2.8.1-2: Slot dimensions for calculating stray flux of single layer winding in semi-closed slots:
a) parallel sided slot, b) parallel sided tooth

b) Two layer winding:
In Fig. 2.8.1-3 phase belt of upper and lower layer is shown for pitched coils. Per phase slots exist, where in upper and lower layer the same phase current flows (Fig. 2.8.1-3 a), but also slots, where in upper layer current of adjacent phase flows, e.g. $\underline{I}_U$ and $-\underline{I}_W$ (Fig. 2.8.1-3 b). Due to phase shift 120° between $\underline{I}_U$ and $\underline{I}_W$ the phase shift between $\underline{I}_U$ and $-\underline{I}_W$ is 60°, so total ampere turns in slot (b) are only 86.6% of slots (a) ($\sqrt{3}/2 = 0.866$!). Therefore they excite a smaller stray flux, thus reducing total slot stray flux (depending on the pitch W/τ_p), which is considered by the **slot stray flux reduction functions**

$$K_1 = \frac{9}{16} \cdot \frac{W}{\tau_p} + \frac{7}{16} \qquad K_2 = \frac{3}{4} \cdot \frac{W}{\tau_p} + \frac{1}{4} \qquad 2/3 \le W/\tau_p \le 1 \quad . \tag{2.8.1-8}$$

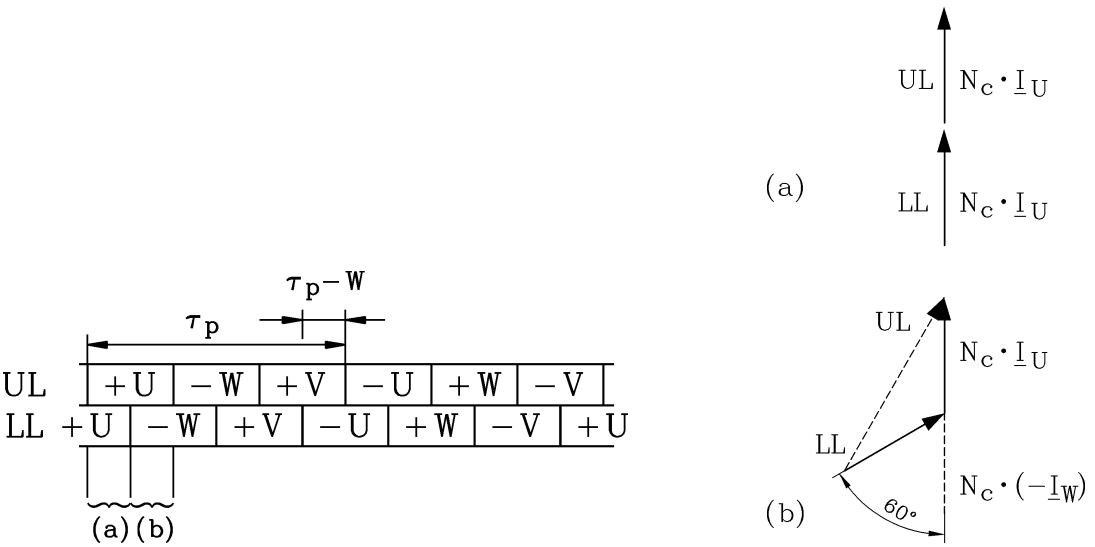

Fig. 2.8.1-3: Left: Phase belt of a two layer winding with coil pitch, Right: Current flow in slots, where upper and lower layer belong (a) to the same phases, (b) to different phases (UL: upper layer, LL: lower layer)

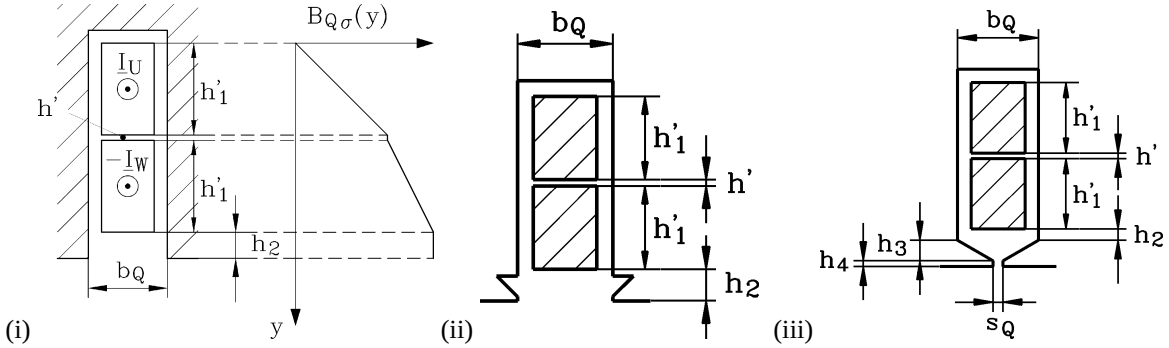

Fig. 2.8.1-4: Slot stray flux of two layer winding, (i) current flow for case (b) of Fig. 2.8.1-3, (ii) open slot geometry, (iii) semi-closed slot geometry

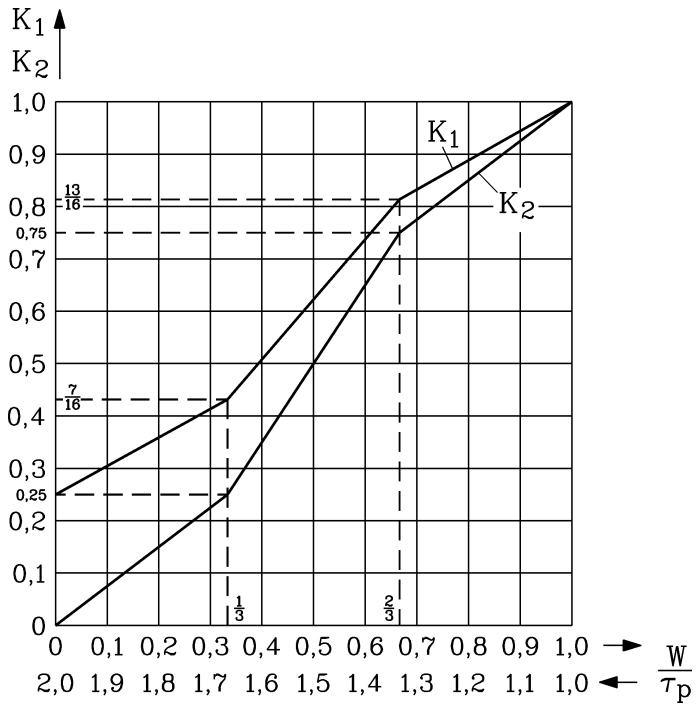

Fig. 2.8.1-5: Function K_1, K_2 for considering reduction of slot stray flux due to coil pitch W/τ_p in two layer winding

For **two-layer** winding the same equation (2.8.1-5) is valid, but λ_Q has to be taken for the slot geometry in Fig. 2.8.1-4:

Open slots:

$$\lambda_{Qs} = K_1 \cdot 2 \cdot \frac{h_1'}{3b_Q} + \frac{h'}{4b_Q} + K_2 \cdot \frac{h_2}{b_Q} \tag{2.8.1-9}$$

Semi-closed slots:

$$\lambda_{Qs} = K_1 \cdot 2 \cdot \frac{h_1'}{3b_Q} + \frac{h'}{4b_Q} + K_2 \cdot \left(\frac{h_2}{b_Q} + \frac{h_3}{(b_Q + s_Q)/2} + \frac{h_4}{s_Q} \right) \tag{2.8.1-10}$$

2.8.2 Slot stray flux and inductance of rotor winding

For **wound rotor induction machines** the same calculation methods as for three-phase stator winding are used (Section 2.8.1).

$$\boxed{L_{r\sigma Q} = \mu_0 \cdot N_r^2 \cdot \frac{2}{p \cdot q_r} \cdot \lambda_{Qr} \cdot l_e} \tag{2.8.2-1}$$

For **cage rotor** slots the different slot shapes have to be taken into account. From (2.8.1-4), which is valid for a coil in two slots, we get for a coil with one winding $N_c = 1$ and further for a bar in one slot $L_{\sigma,bar} = L_{\sigma c} / 2$

$$\boxed{L_{\sigma,bar} = \mu_0 \cdot \lambda_{Qr} \cdot l_e} \tag{2.8.2-2}$$

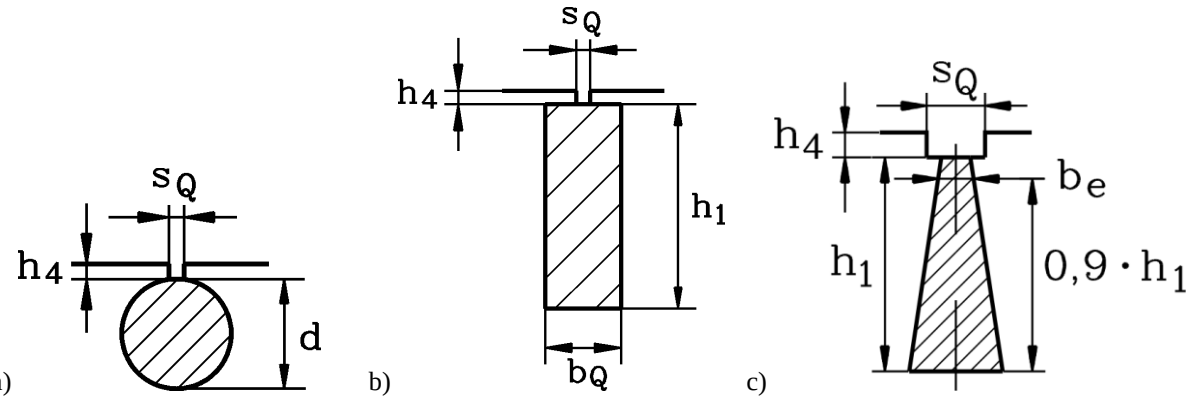

Fig. 2.8.2-1: Cage rotor slot shapes: a) round bar, b) deep bar, c) wedge bar

Due to eddy currents induced in the bar by the AC slot stray flux, the AC resistance of the bar increases by factor k_R with increasing rotor frequency, whereas the stray flux decreases by factor k_L, because the self-field of the eddy currents in the bar opposes the slot stray flux, thus reducing it. This "**current displacement effect**" is used for increase of starting torque due to increase of rotor resistance, whereas decrease of slot stray flux must be considered in that section of slot, where bar is placed (height h_1).

For deep bar (Fig. 2.8.2-1 b), *Maxwell´*s equations yield

$$\xi = h_1 \sqrt{\pi \cdot f_r \cdot \mu_0 \cdot \kappa_{Cu}} \tag{2.8.2-3}$$

$$k_R = \xi \frac{\sinh(2\xi) + \sin(2\xi)}{\cosh(2\xi) - \cos(2\xi)} \tag{2.8.2-4}$$

$$k_L = \frac{3}{2\xi} \cdot \frac{\sinh(2\xi) - \sin(2\xi)}{\cosh(2\xi) - \cos(2\xi)} \quad . \tag{2.8.2-5}$$

Note: $\xi > 2 : k_R \cong \xi,\ k_L \cong 3/(2\xi)$

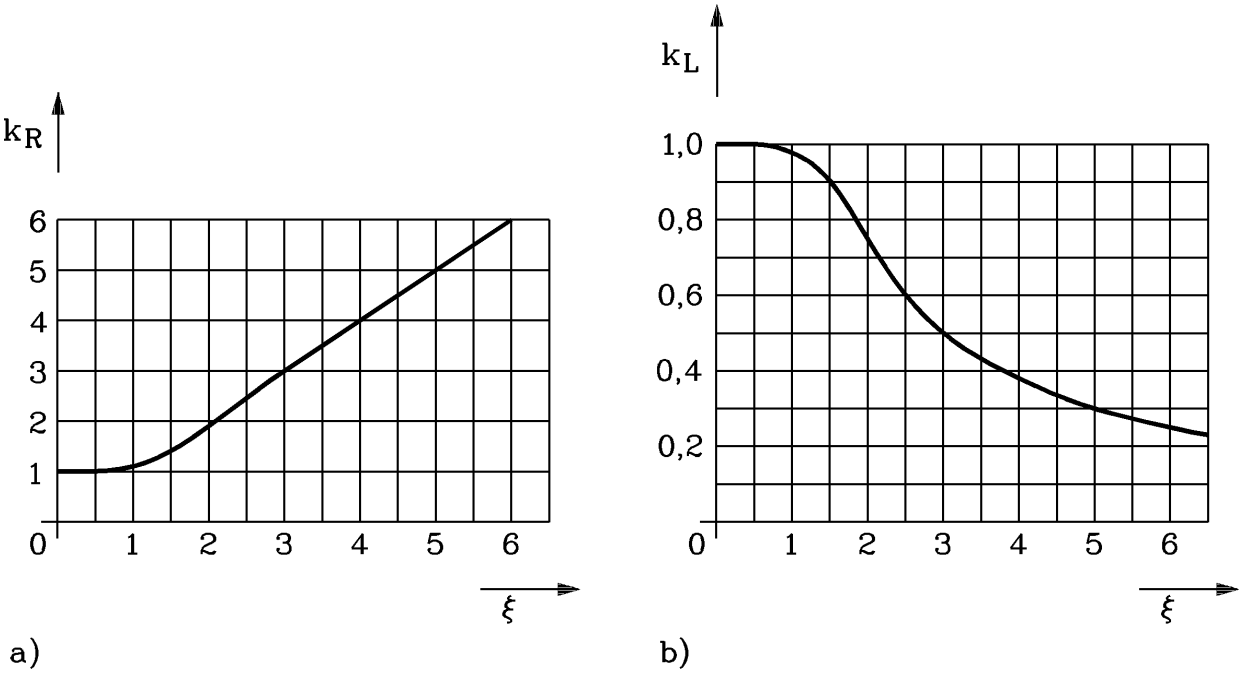

Fig. 2.8.2-2: a) Increase of AC resistance k_R , b) decrease of bar inductance k_L for "deep bar" in dependence of ξ

Example 2.8.2-1:

Deep bar (copper): At 75°C: κ_{Cu} = 50·10^6 S/m, $\mu_0 = 4\pi \cdot 10^{-7}$ Vs/(Am), rotor frequency f_r = 50 Hz, $h_{bar} = h_1$ = 30 mm = 3 cm: ξ = 3, k_R = 3, k_L = 0.5.

Deep bar, semi-closed slot:

$$\lambda_{Qr} = \frac{h_1}{3b_Q} \cdot k_L + \frac{h_4}{s_Q} \tag{2.8.2-6}$$

Round bar, semi-closed slot, $h_1 = d$ ($k_{L,round} \cong 1$):

$$\lambda_{Qr} = \left(\frac{d}{15 s_Q} + 0.47 \right) \cdot k_{L,round} + \frac{h_4}{s_Q} \tag{2.8.2-7}$$

Wedge bar, $b_e = b_o + (b_u - b_o)/10$ ($k_{L,wedge}$ according to Fig. 2.8.2-3):

$$\lambda_{Qr} = \frac{h_1}{3b_e} \cdot k_{L,wedge} + \frac{h_4}{s_Q} \tag{2.8.2-8}$$

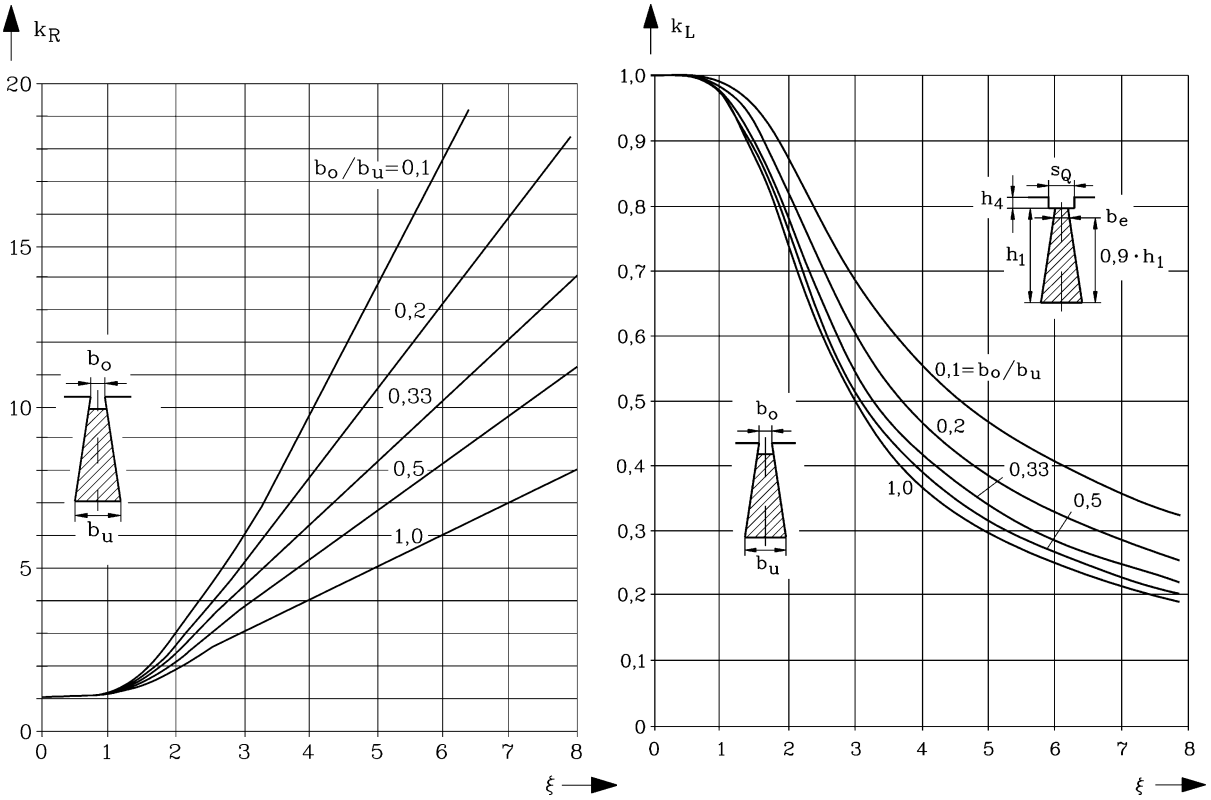

Fig. 2.8.2-3: Increase of AC resistance k_R and decrease of bar inductance k_L for "wedge bar" in dependence of ξ and wedge ratio b_o/b_u

2.8.3 Stray flux and inductance of winding overhangs

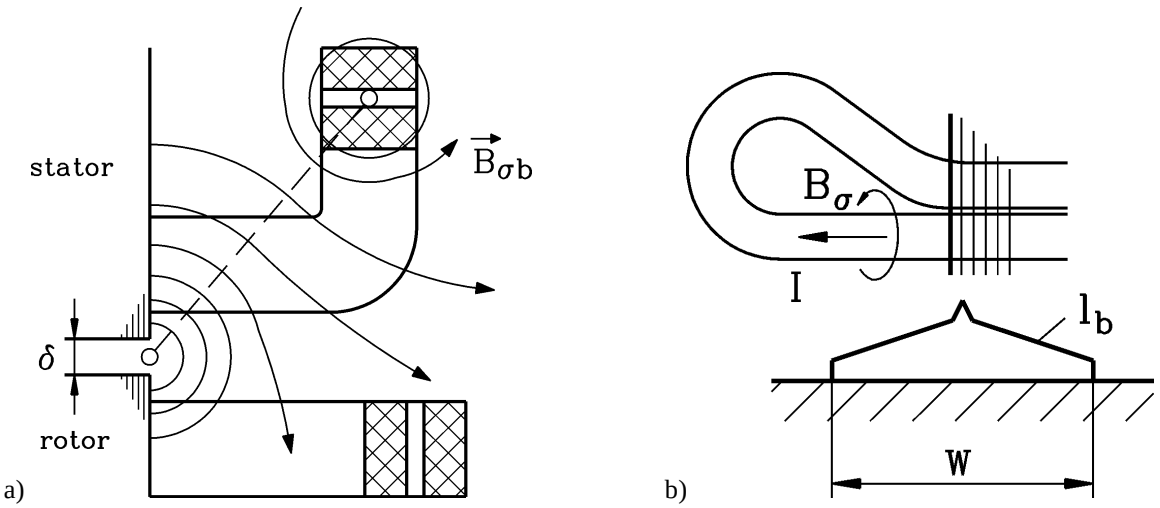

Fig. 2.8.3-1: a) Schematic view of stray field of winding overhang of wound rotor induction machine, b) winding overhang length l_b

Stray flux of winding overhang is inducing voltage at length l_{bs} of turn per coil. As all coils excite in winding overhang the stray flux, no influence of slot number or q respectively, appears. Therefore taking l_{bs} instead of l_e and neglecting q, we get from (2.8.1-5) the expression

$$L_{s\sigma b} = \mu_0 \cdot N_s^2 \cdot \frac{2}{p} \cdot \lambda_{bs} \cdot l_{bs} \qquad (2.8.3\text{-}1)$$

Due to the complicated, three-dimensional field distribution in winding overhangs, λ_{bs} cannot be calculated easily, but is taken from measurements with model coil arrangements according to *Kürzel*. A rough estimate for stator winding of cage induction machine is $\lambda_{bs} \cong 0.3$, where rotor ring stray is already included, whereas more detailed calculation is shown below.

a) Single layer winding:

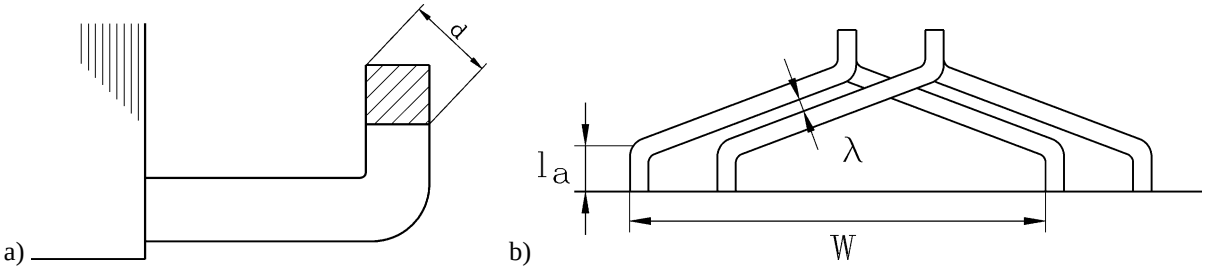

Fig. 2.8.3-2: a) Single layer winding geometry for determining winding overhang stray inductance, b) Two layer winding geometry for determining length of winding overhang

$$\lambda_{bs} = 0.37 \cdot c \cdot \left[1 + 0.9 \cdot \frac{l_b - 10 \cdot d_w}{l_b + 10 \cdot d_w} \right] \qquad (2.8.3\text{-}2)$$

The coefficient c is taking into account the numbers of slots per pole and phase (Table 2.8.3-1), whereas d_w is the diagonal of the cross section of coils in winding overhang.

q	1	2	3	4	5	6	≥ 7
c	1	0.8	0.67	0.6	0.54	0.5	0.47

Table 2.8.3-1: Considering influence of numbers of coils per pole and phase q for stray flux of winding overhangs

b) Two layer winding:

$$\lambda_{bs} = 0.075 \cdot \left(1 + \frac{l_b}{\tau_p} \right) \qquad (2.8.3\text{-}3)$$

c) Ring stray flux of cage rotor:
If the rotor ring stray flux inductance is calculated as transformed value $X'_{r\sigma b} = \ddot{u}_U \ddot{u}_I X_{r\sigma b}$ on stator side with (2.8.3-1), following values are used.

$$\lambda_{br} = 0.12 \quad , \; l_{br} = \tau_p \qquad (2.8.3\text{-}4)$$

It is rather difficult to calculate the length l_{bs} of coils in the winding overhangs. With **round wire coils** an estimate is (Fig. 2.8.3-1a), where l_a is the clearing of main slot insulation in winding overhang *ZF* and some additional length for bending the conductors:

$$l_{bs} = 1.3 \cdot W + 3 \cdot h_Q + 2 \cdot l_a \qquad . \qquad (2.8.3\text{-}5)$$

U_N	V	≤ 690	3300	6600
l_a	mm	20	35	57

For **form wound coils** exact coil geometry is known, from which calculation of l_{bs} is derived. Depending on manufacturing method, some additional length Δl_{bs} is needed for winding arrangement (Fig. 2.8.3-1b).

$$l_{bs} = \frac{W}{\sqrt{1-\frac{(b_Q+\lambda)^2}{\tau_Q^2}}} + \frac{\pi}{2}\cdot\frac{h_Q}{2} + 2\cdot l_a + \Delta l_{bs} \qquad (2.8.3\text{-}6)$$

U_N	kV	≤ 0.69	1	2	3	5	6	8	10	12
l_a	mm	20	23	29	35	50	57	73	91	110
Δl_{bs}	mm	≤ 30	≤ 30	≤ 40	≤ 40	≤ 50	≤ 50	≤ 60	≤ 60	≤ 60

Table 2.8.3-2: Typical dimensions of winding overhangs

2.8.4 Harmonic inductance

a) Single and two-layer windings:

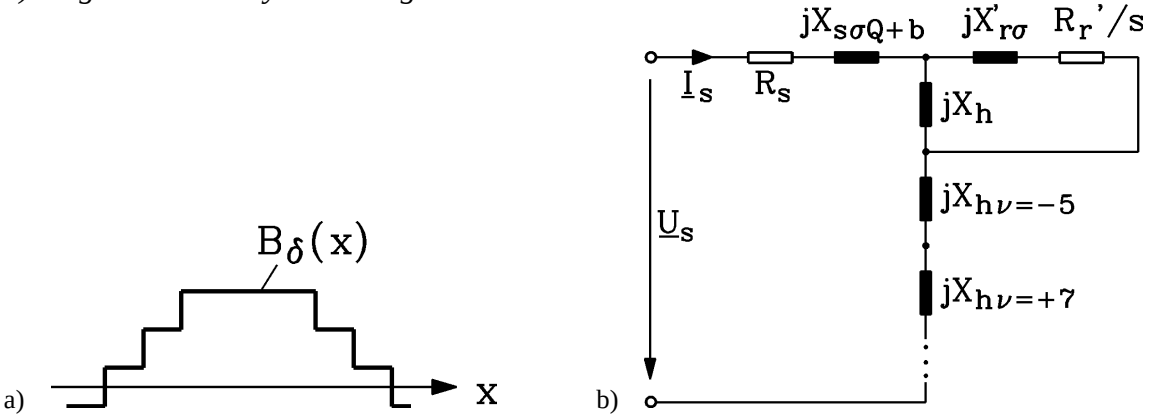

Fig. 2.8.4-1: a) Step-like air gap flux density distribution due to slotting, b) Corresponding equivalent circuit

Step-like stator air gap flux density distribution due to stator slotting – excited by stator current - may be decomposed according to *Fourier* analysis as sum of harmonic flux density waves with ordinal number ν

$$B_\delta(x,t) = \sum_{\nu=1,-5,7,\ldots}^{\infty} \hat{B}_{\delta\nu}\cdot\cos(\nu\pi x/\tau_p - \omega_s t) \qquad (2.8.4\text{-}1)$$

and - neglecting saturation - amplitudes

$$\hat{B}_{\delta\nu} = \frac{\mu_0}{\delta_e}\cdot\frac{\sqrt{2}}{\pi}\cdot\frac{m_s N_s}{p}\cdot\frac{k_{w\nu}}{\nu}\cdot I_s \quad . \qquad (2.8.4\text{-}2)$$

Self-induced stator voltage with stator frequency f_s due to these harmonics is

$$\Delta\underline{U}_{hs} = \sum_{|\nu|>1}\underline{U}_{h\nu} = \sum_{|\nu|>1} jX_{h\nu}\cdot\underline{I}_s \qquad (2.8.4\text{-}3)$$

with **magnetizing reactance per harmonic** $X_{h\nu}$

$$\boxed{X_{h\nu} = 2\pi f_s \cdot \mu_0 \cdot N_s^2 \cdot \frac{k_{ws\nu}^2}{\nu^2} \cdot \frac{2 \cdot m_s}{\pi^2 \cdot p} \cdot \frac{l_e \cdot \tau_p}{\delta_e}} \quad . \tag{2.8.4-4}$$

This **additional self-induced voltage** $\Delta\underline{U}_{hs}$ (Fig. 2.8.4-1, left) may be regarded as additional stray reactance, as the harmonic field waves generate only parasitic asynchronous harmonic torque. From (2.8.4-3), (2.8.4-4) follows

$$\Delta\underline{U}_{hs} = \sum_{|\nu|>1} jX_{h\nu} \cdot \underline{I}_s = jX_{h,\nu=1} \cdot \underline{I}_s \cdot \sum_{|\nu|>1} \left(\frac{k_{ws\nu}}{\nu \cdot k_{ws1}} \right)^2 = jX_{s\sigma O} \cdot \underline{I}_s \quad . \tag{2.8.4-5}$$

Harmonic stray inductance is calculated from fundamental magnetizing inductance (where main flux saturation may be included) by considering **harmonic stray coefficient σ_{Os}**

$$\boxed{L_{s\sigma O} = \sigma_{Os} \cdot L_h} \quad , \qquad \sigma_{Os} = \sum_{|\nu|>1} \left(\frac{k_{ws\nu}}{\nu \cdot k_{ws1}} \right)^2 \quad , \tag{2.8.4-6}$$

which is evaluated by considering the infinite sum of winding factors and is available as exact formula, e.g. for the full-pitched winding with $m_s = 3$ phases

$$\sigma_{Os} = \left(\frac{\pi}{3k_{ws,1}} \right)^2 \cdot \frac{5q_s^2 + 1}{6q_s^2} - 1 \quad . \tag{2.8.4-7}$$

Example 2.8.4-1:
$m_s = 3$, $W/\tau_p = 1$ (e.g. single layer winding): $q_s = 1 : \sigma_{Os} = \underline{\underline{0.097}}$, $q_s = 2 : \sigma_{Os} = \underline{\underline{0.0285}}$, ...

For **pitched winding** $W/\tau_p \neq 1$ with $W = (m_s \cdot q_s - S) \cdot \tau_{Qs}$ more complicated formula is valid, which is given in Table 2.8.4-1.

S/q_s	q_s = 1	2	3	4	5	6	7	8
S = 0	9.662	2.844	1.406	0.890	0.648	0.516	0.437	0.385
1	9.662	2.354	1.149	0.738	0.549	0.446	0.385	0.345
2	9.662	2.844	1.109	0.624	0.437	0.349	0.303	0.276
3		2.844	1.406	0.688	0.411	0.293	0.238	0.212
4		2.844	1.429	0.890	0.500	0.311	0.220	0.176
5		9.662	1.374	0.925	0.648	0.400	0.258	0.181
6			1.406	0.890	0.687	0.516	0.341	0.228
7			3.649	0.830	0.669	0.555	0.437	0.305
8			9.662	0.890	0.622	0.549	0.474	0.385
9				2.062	0.574	0.516	0.476	0.421
10				4.590	0.648	0.469	0.454	0.427
11				9.662	1.398	0.437	0.417	0.413

Table 2.8.4-1: Harmonic stray coefficient $100\sigma_O$ for the pitched 3-phase integer-slot two-layer winding

With increasing slot number per pole and phase q_s harmonic stray inductance decreases, as step like air gap flux density distribution approximates sine wave better. For two-layer

winding for given q_s there exists a minimum harmonic stray inductance for certain pitch between $2/3 < W/\tau_p < 1$, which means that some harmonics are very small.

b) Rotor cage:
Step-like rotor air gap flux density distribution due to rotor slotting – excited by rotor current - may be also decomposed according to *Fourier* analysis as sum of harmonic flux density waves with ordinal number μ. These harmonic waves cause self-induced voltage in rotor cage with rotor frequency $\Delta\underline{U}_{hr}$. In equivalent circuit rotor voltages are given with respect to stator winding data, thus as

$$\Delta\underline{U}'_{hr} = \ddot{u}_U \Delta\underline{U}_{hr} = j \cdot \sigma_{Or} X_h \cdot \underline{I}'_r \quad . \tag{2.8.4-8}$$

With cage data $k_{w\mu} = 1,\ N_r = 1/2,\ m_r = Q_r$ the **rotor stray harmonic coefficient** is derived as

$$\boxed{L'_{r\sigma O} = \sigma_{Or} \cdot L_h} \qquad \boxed{\sigma_{Or} = \frac{1}{\left(\dfrac{\sin(p \cdot \pi / Q_r)}{p \cdot \pi / Q_r}\right)^2} - 1} \quad . \tag{2.8.4-9}$$

According to $\sin(x)/x\big|_{x\to 0} \to 1$ the harmonic stray inductance tends to zero with increasing rotor slot number per pole.

c) Skewed cage winding:

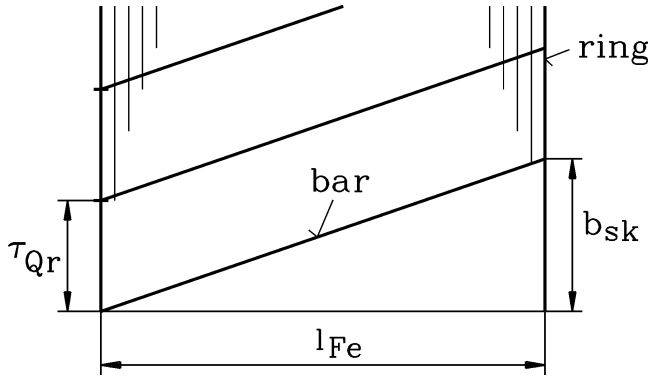

Fig. 2.8.4-2: Skewed rotor bars of cage rotor

By s**kewing** the rotor bars (skew b_{sk}) asynchronous and synchronous harmonic torque due to stator slot harmonic may be significantly reduced, if $b_{sk} \cong \tau_{Qs}$. On the other hand, stator and rotor winding are de-coupled by skewing. Thus a small part of rotor-excited air gap main flux will be de-coupled as skew stray flux. This flux self-induces rotor cage, but not stator winding due to skewing. Hence rotor harmonic stray flux is increased by skewing according to

$$\boxed{\sigma_{O+sk,r} = \frac{1}{\left(\dfrac{\sin(p \cdot \pi / Q_r)}{p \cdot \pi / Q_r}\right)^2 \cdot \left(\dfrac{\sin\left[(p \cdot \pi / Q_r) \cdot (b_{sk} / \tau_{Qr})\right]}{(p \cdot \pi / Q_r) \cdot (b_{sk} / \tau_{Qr})}\right)^2} - 1} \tag{2.8.4-10}$$

Usually $p \cdot \pi / Q_r << 1$, therefore (2.8.4-10) simplifies to

$$\sigma_{O+sk,r} \cong \frac{1}{3} \cdot \left(\frac{p \cdot \pi}{Q_r} \right)^2 + \frac{1}{3} \cdot \left(\frac{p \cdot \pi}{Q_r} \right)^2 \cdot \left(\frac{b_{sk}}{\tau_{Qr}} \right)^2 \quad , \qquad (2.8.4\text{-}11)$$

where first part is harmonic influence of slotting and second part is influence of skew, showing that skew stray flux rises quadratic with skew.

Example 2.8.4-1:
500 kW-cage induction motor:

• *Stray inductance of stator winding :*
Data of Example 2.4-1, 2.4-3, $W/\tau_p = 12/15$, $W = 12\tau_{Qs}$:

Slot: open slot: $b_{Qs} = s_{Qs}$

$$K_1 = \frac{9}{16} \cdot \frac{W}{\tau_p} + \frac{7}{16} = 0.8875 \qquad K_2 = \frac{3}{4} \cdot \frac{W}{\tau_p} + \frac{1}{4} = 0.85 \,, \; b_{Qs} = 12.5 \text{ mm}$$

$$h_1' = N_c \cdot (h_L + d_{ic}) + (N_c - 1) \cdot d_i - d_{ic} = 24.7 - 0.4 = 24.3 \text{ mm}$$

$$h' = Z + 2 \cdot d + 2 \cdot (d_i / 2) = 4 + 2 \cdot 2.2 + 2 \cdot (0.4/2) = 8.8 \text{ mm}$$

$$h_2 = d_{ic}/2 + d + 2 \cdot d_{sl} + d_t + h_{wedge} = 0.4/2 + 2.2 + 2 \cdot 0.15 + 0.4 + 4.0 = 7.1 \text{ mm}$$

$$\lambda_{Qs} = K_1 \cdot 2 \cdot \frac{h_1'}{3 b_{Qs}} + \frac{h'}{4 b_{Qs}} + K_2 \cdot \frac{h_2 + h_4}{b_{Qs}} = 0.8875 \cdot 2 \cdot \frac{24.3}{3 \cdot 12.5} + \frac{8.8}{4 \cdot 12.5} + 0.85 \cdot \frac{7.6}{12.5} = \underline{\underline{1.843}}$$

$$X_{s\sigma Q} = \omega_s L_{s\sigma Q} = 2\pi f_s \cdot \mu_0 N_s^2 \frac{2}{p \cdot q_s} \lambda_{Qs} l_e = 2\pi 50 \cdot 4\pi \cdot 10^{-7} \cdot 200^2 \cdot \frac{2}{2 \cdot 5} \cdot 1.843 \cdot 0.392 = \underline{\underline{2.28}} \, \Omega$$

Winding overhang:

$$l_{bs} = \frac{W}{\sqrt{1 - \frac{(b_{Qs} + \lambda)^2}{\tau_{Qs}^2}}} + \frac{\pi}{2} \cdot \frac{h_{Qs}}{2} + 2 \cdot l_a + \Delta l_{bs} = \frac{12 \cdot 24}{\sqrt{1 - \frac{(12.5 + 4)^2}{24^2}}} + \frac{\pi}{2} \cdot \frac{69}{2} + 2 \cdot 57 + 50 = \underline{\underline{614.8}} \text{ mm}$$

$$\lambda_{bs} = 0.075 \cdot \left(1 + \frac{l_{bs}}{\tau_p} \right) = 0.075 \cdot \left(1 + \frac{614.8}{360} \right) = \underline{\underline{0.203}}$$

$$X_{s\sigma b} = \omega_s L_{s\sigma b} = 2\pi f_s \cdot \mu_0 N_s^2 \frac{2}{p} \lambda_{bs} l_{bs} = 2\pi 50 \cdot 4\pi \cdot 10^{-7} \cdot 200^2 \cdot \frac{2}{2} \cdot 0.203 \cdot 0.6148 = \underline{\underline{1.97}} \, \Omega$$

Harmonic reactance:

$$\sigma_{Os}(q_s = 5, s = 3) = 0.411/100$$

$$X_{s\sigma O} = \omega_s L_{s\sigma O} = \sigma_{Os} \cdot X_h = (0.411/100) \cdot 155.0 = \underline{\underline{0.64}} \, \Omega$$

Resulting stator stray reactance:

$$X_{s\sigma} = X_{s\sigma Q} + X_{s\sigma b} + X_{s\sigma O} = 2.28 + 1.97 + 0.64 = \underline{\underline{4.89}} \, \Omega$$

- *Stray inductance of unskewed rotor cage:*

Data of Example 2.5-2: h_1 = 40 mm, b_{Qr} = 5.1 mm, h_4 = 3.4 mm, s_{Qr} = 2.5 mm

Slot:

$$\lambda_{Qr} = \frac{h_1}{3b_{Qr}} \cdot k_L + \frac{h_4}{s_{Qr}} = \frac{40}{3 \cdot 5.1} \cdot k_L + \frac{3.4}{2.5} = 2.61 k_L + 1.36$$

a) Start slip s = 1 and 20°C: $f_r = 1 \cdot 50 = 50\,\text{Hz}$:

$$\xi = h_1 \sqrt{\pi \cdot f_r \cdot \mu_0 \cdot \kappa_{Cu}} = 0.04 \sqrt{\pi \cdot 50 \cdot 4\pi \cdot 10^{-7} \cdot 57 \cdot 10^6} = 4.24$$

$$k_L = \frac{3}{2 \cdot 4.24} \cdot \frac{\sinh(2 \cdot 4.24) - \sin(2 \cdot 4.24)}{\cosh(2 \cdot 4.24) - \cos(2 \cdot 4.24)} = 0.353\,, \qquad \lambda_{Qr} = \underline{\underline{2.28}}$$

b) Rated slip s = 1.5%: $f_r = 0.015 \cdot 50 = 0.75\,\text{Hz}$: ξ = 0.519, k_L = 0.998, $\lambda_{Qr} = \underline{\underline{3.96}}$

$$\ddot{u}_U = \frac{N_s k_{ws}}{N_r k_{wr}} = \frac{200 \cdot 0.91}{0.5 \cdot 1} = 364, \quad \ddot{u}_I = \ddot{u}_U \cdot \frac{m_s}{Q_r} = 364 \cdot \frac{3}{50} = 21.84$$

a) At stand still:

$$X'_{r\sigma Q} = \ddot{u}_U \ddot{u}_I \omega_s L_{r\sigma Q} = \ddot{u}_U \ddot{u}_I 2\pi f_s \mu_0 \lambda_{Qr} l_e = 364 \cdot 21.84 \cdot 2\pi 50 \cdot 4\pi \cdot 10^{-7} \cdot 2.28 \cdot 0.392 = \underline{\underline{2.80}}\,\Omega$$

b) At rated slip:

$X'_{r\sigma Q} = \underline{\underline{4.87}}\,\Omega$

Winding overhang:

$\lambda_{br} = 0.12$, $l_{br} = \tau_p = 360\,\text{mm}$

$$X'_{r\sigma b} = \omega_s L'_{r\sigma b} = 2\pi f_s \cdot \mu_0 N_s^2 \frac{2}{p} \lambda_{br} l_{br} = 2\pi 50 \cdot 4\pi \cdot 10^{-7} \cdot 200^2 \cdot \frac{2}{2} \cdot 0.12 \cdot 0.36 = \underline{\underline{0.68}}\,\Omega$$

Harmonic reactance:

$$\sigma_{Or} = \frac{1}{\left(\frac{\sin(p \cdot \pi / Q_r)}{p \cdot \pi / Q_r}\right)^2} - 1 = \frac{1}{\left(\frac{\sin(2 \cdot \pi / 50)}{2 \cdot \pi / 50}\right)^2} - 1 = 0.528/100$$

$$X'_{r\sigma O} = \omega_s L'_{r\sigma O} = \sigma_{Or} \cdot X_h = 0.528/100 \cdot 155.0 = \underline{\underline{0.82}}\,\Omega$$

Resulting rotor stray reactance:

a) At stand still (locked rotor): $X'_{r\sigma} = X'_{r\sigma Q} + X'_{r\sigma b} + X'_{r\sigma O} = 2.80 + 0.68 + 0.82 = \underline{\underline{4.30}}\,\Omega$

b) At rated slip: $X'_{r\sigma} = \underline{\underline{6.37}}\,\Omega$

c) For arbitrary slip: $X'_{r\sigma} = \underline{\underline{3.20 \cdot k_L + 3.18}}\,\Omega$

Example 2.8.4-2:

Stray inductance of skewed rotor (Data of Example 2.8.4-1):

Rotor skew b_{sk} = τ_{Qs} = 24 mm, $b_{sk} / \tau_{Qr} = \tau_{Qs} / \tau_{Qr} = Q_r / Q_s = 50/60$

$$\sigma_{O+sk,r} = \frac{1}{\left(\frac{\sin(2\pi / 50)}{2\pi / 50}\right)^2 \cdot \left(\frac{\sin\left[(2\pi / 50) \cdot (50/60)\right]}{(2\pi / 50) \cdot (50/60)}\right)^2} - 1 = 0.896/100$$

$$X'_{r\sigma O} = \omega_s L'_{r\sigma O} = \sigma_{Or} \cdot X_h = (0.896/100) \cdot 155.0 = \underline{\underline{1.39}}\,\Omega$$

Effect of skew: Increase of harmonic stray inductance by 1.39 - 0.82 = 0.57 Ω

2.9 Influence of saturation on inductance

Both magnetizing inductance AND stray inductance are influenced by saturation of iron, decreasing the values from unsaturated to saturated state.

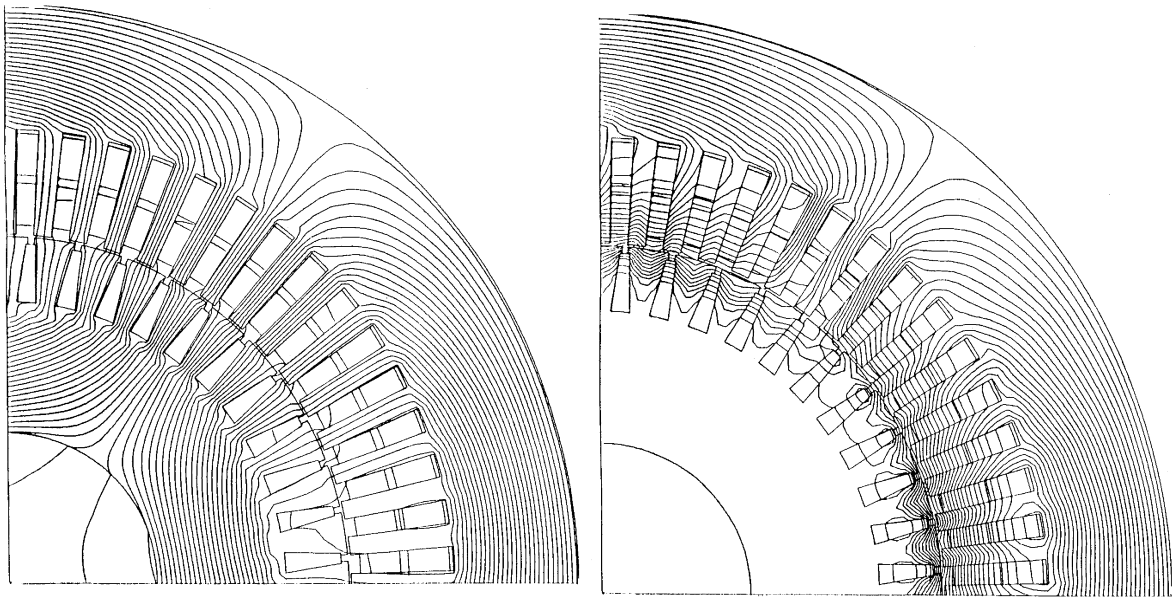

a) b)

Fig. 2.9-1: Numerically calculated two-dimensional magnetic flux density B of a three-phase, 4-pole high voltage cage induction machine with wedge rotor slots (Q_s / Q_r = 60/44) at rated voltage a) at no-load (s = 0, rotor current zero), b) at stand still (locked rotor) s = 1

At **no load** (and rated load) main flux Φ_h dominates and saturates teeth and yokes as described in Chapter 2.7. Main flux saturation can be measured at no-load, operating the electric machine with variable stator voltage U_s, measuring voltage U_s versus no-load current I_{s0} (Fig. 2.9-2).

$$\underline{U}_s = \left(R_s + jX_{s\sigma}\right)\underline{I}_{s0} + \underline{U}_h \approx \underline{U}_h = jX_h\underline{I}_{s0} \tag{2.9-1}$$

This saturation is also valid at **rated slip**, which differs only by few percent from zero slip.

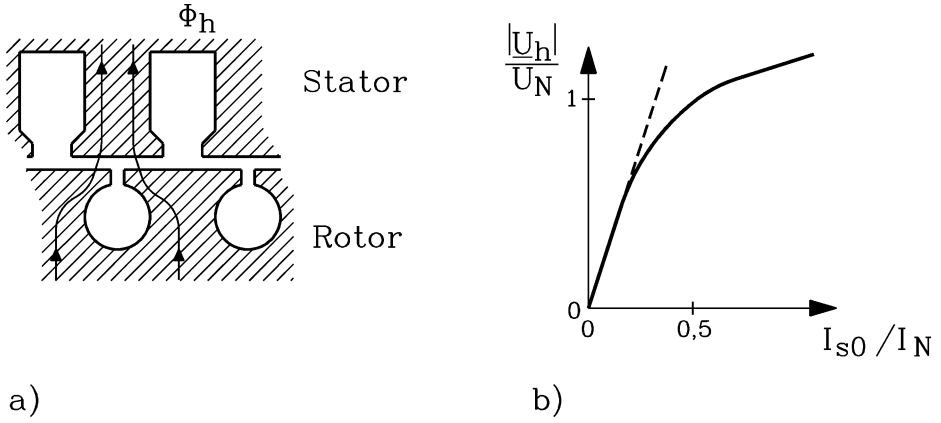

a) b)

Fig. 2.9-2: Saturation of teeth and yokes by main flux: a) Main flux path, b) measured „no-load“-characteristic

At locked rotor (Fig. 2.9-1 b) $s = 1$ rotor and stator current are nearly in phase opposition $s = 1: \underline{I}_s \approx -\underline{I}'_r$, $I_s \cong (5...8)I_N$. Hence magnetic flux is quenched into the air gap

and to the tooth tips Fig. 2.9-3), being directed mainly in circumference direction as stray flux. This effect is supported by rotor current displacement due to bar eddy currents. Main flux Φ_h is reduced strongly and stray flux Φ_σ is increased due to big current. This big **zig-zag stray flux** saturates tooth tips, **therefore at big slip also saturation of stray flux and hence of stray inductance occurs.**

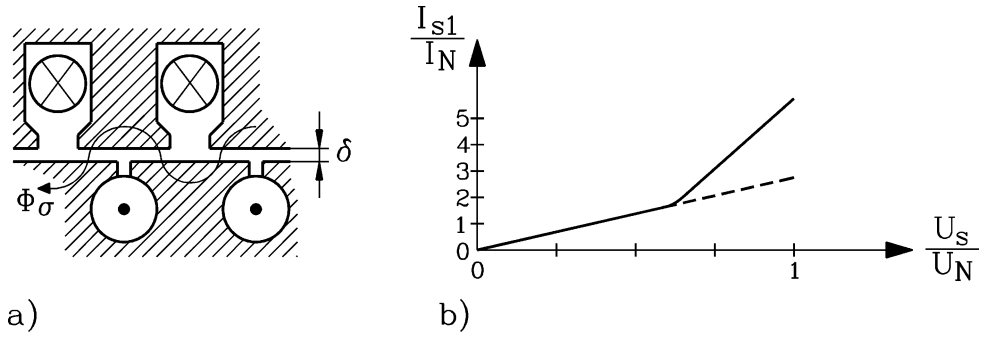

Fig. 2.9-3: Saturation of tooth tips by zig-zag stray flux: a) Zig-zag stray flux path, b) measured „locked rotor"-characteristic

Stray flux saturation can be measured at locked rotor test $s = 1$, operating the electric machine with variable stator voltage U_s, measuring U_s versus locked rotor current I_{s1} (Fig. 2.9-3).

$$s = 1 : \underline{U}_s \cong \left[\left(R_s + R'_r\right) + j\left(X_{s\sigma} + X'_{r\sigma}\right)\right]\underline{I}_{s1} \tag{2.9-2}$$

Calculation of stray inductance saturation is difficult analytically, therefore numerical methods are preferred (Fig. 2.9-1). Saturation influences mainly
- slot bridge component at tooth tip of slot stray flux in case of semi-closed slots and
- harmonic stray flux, as it is an air gap flux component.

A rather simple method to estimate this saturation according to *Norman* uses **zig-zag saturation factor k_{zz}**, which is derived from numerous measurements of built induction machines (Fig. 2.9-4).

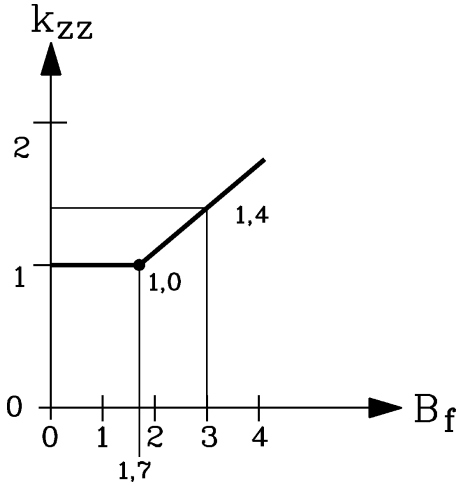

Fig. 2.9-4: Determination of zig-zag saturation factor k_{zz} via "fictive" zig-zag air gap flux density B_f

Zig-zag air gap flux density for unsaturated iron is called "fictive" zig-zag air gap flux density B_f (Fig. 2.9-5a), which is calculated from *Ampere´*s law according to $H_{Fe} = 0$ with Fig. 2.9-5a for one slot by

$$\oint_C \vec{H} \bullet d\vec{s} = (B_f / \mu_0) \cdot 2\delta = \Theta_Q \quad . \tag{2.9-3}$$

Considering the influence of many slots by using stator and rotor slot pitch leads to

$$\boxed{B_f = \mu_0 \cdot \frac{\Theta_Q}{2\delta \cdot \left(2\sqrt{\delta/(\tau_{Qs} + \tau_{Qr})} + 0.5\right)}} \quad . \tag{2.9-4}$$

Slot ampere-turns Θ_Q is taken as average value of stator and rotor slot peak ampere-turn. With N_Q turns per slot (single layer winding: $N_{Qs} = N_c$, two layer winding: $N_{Qs} = 2N_c$, rotor cage: $N_{Qr} = 1$) and *a* parallel branches in stator winding we get for *s* = 1

$$\Theta_Q = \frac{N_{Qs} \cdot \hat{I}_{s1} / a + \hat{I}_{r1}}{2} \tag{2.9-5}$$

or with $N_s = p \cdot q_s \cdot N_{Qs}$, $\hat{I}_{s1} \approx \hat{I}'_{r1} = \ddot{u}_I \hat{I}_r$, $\ddot{u}_I = 2m_s N_s k_{ws} / Q_r$ and $Q_s = 2pm_s q_s$:

$$\Theta_Q = N_{Qs} \cdot (\hat{I}_{s1} / a) \cdot \frac{1 + k_{ws} \cdot Q_s / Q_r}{2} \quad . \tag{2.9-6}$$

In case **of pitched winding** coefficient K_2 (2.8.1-8) considers reduction of stator slot ampere-turns. Influence of arrangement of stator winding in coil groups with q_s coils per group is considered by distribution factor k_{ds}.

$$\boxed{\Theta_Q = N_{Qs} \cdot (\hat{I}_{s1} / a) \cdot \frac{K_2 + k_{ws} \cdot k_{ds} \cdot Q_s / Q_r}{2}} \quad . \tag{2.9-7}$$

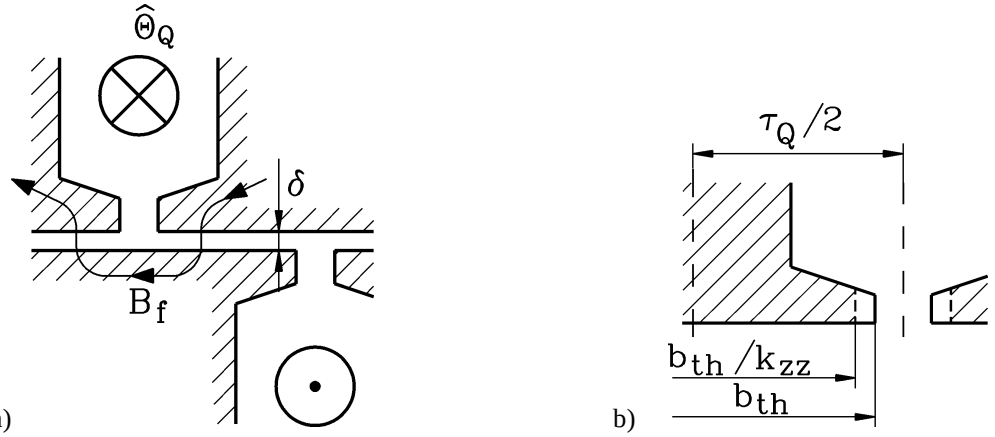

Fig. 2.9-5: a) "Fictive" zig-zag air gap flux density B_f , b) saturation of tooth tips of semi-closed slots by zig-zag stray flux

Below 1.7 T iron does not saturate, hence **zig-zag saturation factor k_{zz}** is determined by

$$\boxed{\begin{aligned} k_{zz} &= 1, & B_f &\le 1.7T \\ k_{zz} &= \frac{B_f + 1.5}{3.2}, & B_f &> 1.7T \end{aligned}} \quad , \tag{2.9-8}$$

leading to **saturated harmonic reactances**

$$\boxed{X_{s\sigma O,sat} = X_{s\sigma O} / k_{zz} \qquad X'_{r\sigma O,sat} = X'_{r\sigma O} / k_{zz}} \quad . \tag{2.9-10}$$

Saturation of slot bridge (breadth b_{bridge}) may be regarded as an increase of slot opening (Fig. 2.9-5b)

$$\boxed{s_{Q,sat} = s_Q + b_{bridge} \cdot \left(1 - \frac{1}{k_{zz}}\right)} \quad , \tag{2.9-11}$$

which leads to a decrease of slot stray flux, e.g. for deep bar slot

$$\lambda_{Qr} = \frac{h_1}{3b_Q} \cdot k_L + \frac{h_4}{s_{Q,sat}} \quad . \tag{2.9-12}$$

Example 2.9-1:
550 kW cage induction machine, I_N = 59 A, $I_{s1} = 5I_N$ = 295 A, slot data of 2.8.4-1:
$K_2 = 0.85,\ k_{ds} = 0.957,\ k_{ws} = 0.91,\ N_{Qs} = 2 \cdot 10 = 20$, $a = 1,\ \tau_{Qs} = 24\,\text{mm},\ \tau_{Qr} = 28.8\,\text{mm}$

$$\Theta_Q = N_{Qs}(\hat{I}_{s1} / a) \frac{K_2 + k_{ws} k_{ds} \cdot Q_s / Q_r}{2} = 20 \cdot (\sqrt{2} \cdot 295/1) \cdot \frac{0.85 + 0.91 \cdot 0.957 \cdot 60/50}{2} = 7906\,\text{A}$$

$$B_f = \frac{\mu_0 \cdot \Theta_Q}{2\delta \cdot \left(2\sqrt{\delta/(\tau_{Qs} + \tau_{Qr})} + 0.5\right)} = \frac{4\pi \cdot 10^{-7} \cdot 7906}{2 \cdot 0.0014 \cdot \left(2\sqrt{1.4/(24 + 28.8)} + 0.5\right)} = 4.29\,\text{T}$$

$$k_{zz} = \frac{B_f + 1.5}{3.2} = \frac{4.29 + 1.5}{3.2} = 1.8$$

$$X_{s\sigma O,sat} = X_{s\sigma O} / k_{zz} = 0.64/1.8 = 0.36\,\Omega, \qquad X'_{r\sigma O,sat} = X'_{r\sigma O} / k_{zz} = 0.82/1.8 = 0.46\,\Omega$$

Stator open slot remains unchanged, as there are no tooth tip horns, which might saturate. Stray inductance of rotor slot (b_{Qr} = 5.1 mm, h_4 = 3.4 mm, s_{Qr} = 2.5 mm) decreases:

$$b_{bridge} = b_{Qr} - s_{Qr} = 5.1 - 2.5 = 2.6\,\text{mm}$$

$$s_{Q,sat} = s_Q + b_{bridge} \cdot \left(1 - \frac{1}{k_{zz}}\right) = 2.5 + 2.6 \cdot \left(1 - \frac{1}{1.8}\right) = 3.66\,\text{mm}$$

At s = 1 and 20°C: $k_L = 0.353$:

$$\lambda_{Qr} = \frac{h_1}{3b_{Qr}} \cdot k_L + \frac{h_4}{s_{Qr,sat}} = \frac{40}{3 \cdot 5.1} \cdot 0.353 + \frac{3.4}{3.66} = 1.85,\ X'_{r\sigma Q} = \underline{\underline{2.27}}\,\Omega$$

$$X_{s\sigma} = X_{s\sigma Q} + X_{s\sigma b} + X_{s\sigma O} = 2.28 + 1.97 + 0.36 = \underline{\underline{4.61}}\,\Omega$$

$$X'_{r\sigma} = X'_{r\sigma Q} + X'_{r\sigma b} + X'_{r\sigma O} = 2.27 + 0.68 + 0.46 = \underline{\underline{3.41}}\,\Omega$$

Facit:
Due to zig-zag stray flux saturation the stray inductance of the 550 kW, high voltage cage induction motor is reduced by 13 % from $X_\sigma = X_{s\sigma} + X'_{r\sigma} = 4.89 + 4.30 = 9.19\,\Omega$ *to* $X_\sigma = 4.61 + 3.41 = 8.02\,\Omega$. *For low voltage machines with semi-closed stator slots, smaller winding overhangs, but increased harmonic stray inductance due to low* q_s *this saturation is much bigger up to 30% ... 40%.*

2.10 Masses and losses

Determination of **efficiency** η for demanded output power P_{out} requires knowledge of losses P_d

$$\eta = \frac{P_{out}}{P_{out} + P_d} \quad . \tag{2.10-1}$$

Loss components are
- stator and rotor ohmic losses,
- friction and windage losses,
- iron losses (mainly in stator iron),
- brush losses in case of slip ring induction machines,
- additional no-load losses such tooth pulsation and surface losses,
- additional load losses such as stator and rotor eddy current losses in conductors.

2.10.1 Stator and rotor winding resistance and mass

a) Stator winding:
According to IEC 34-2 for determining efficiency, a typical **winding temperature** has to be assumed, e.g. for Thermal Class B insulation with maximum winding temperature of 80 K plus 40°C ambient temperature the typical winding temperature is defined as ϑ = 75°C. For copper the increase of specific resistance $\rho = 1/\kappa$ from 20°C ($\kappa_{Cu}(20°C) = 57 \cdot 10^6$ S/m) is

$$\rho(\vartheta) = \rho(20°C) \cdot (1 + \alpha_\vartheta \cdot \Delta\vartheta), \qquad \alpha_\vartheta = 1/255\text{K}^{-1} \qquad \Delta\vartheta = \vartheta - 20°C \tag{2.10.1-1}$$

Stator winding resistance per phase:

$$R_s = \frac{1}{\kappa} \cdot \frac{N_s \cdot 2 \cdot (L + l_b)}{a \cdot a_i \cdot A_{TL}} \tag{2.10.1-2}$$

Total stator winding copper mass (γ_{Cu} = 8900 kg/m^3):

$$m_{Cu,s} = \gamma_{Cu} \cdot m_s \cdot N_s \cdot 2 \cdot (L + l_b) \cdot a \cdot a_i \cdot A_{TL} \tag{2.10.1-3}$$

Example 2.10.1-1:
Stator winding data according to Example 2.4-2, 2.4-3, 2.8.4-1:

$$\rho_{Cu}(75°C) / \rho(20°C) = (1 + (75 - 20)/255) = \underline{\underline{1.22}}$$

$$R_s = \frac{1}{\kappa} \cdot \frac{N_s \cdot 2 \cdot (L + l_b)}{a \cdot a_i \cdot A_{TL}} = \frac{1}{57 \cdot 10^6 / 1.22} \cdot \frac{200 \cdot 2 \cdot (0.458 + 0.6148)}{1 \cdot 1 \cdot 12.42 \cdot 10^{-6}} = \underline{\underline{0.74}}\,\Omega$$

$$m_{Cu,s} = \gamma_{Cu} m_s N_s \cdot 2(L + l_b) \cdot a \cdot a_i A_{TL} =$$

$$= 8900 \cdot 3 \cdot 200 \cdot 2 \cdot (0.458 + 0.6148) \cdot 1 \cdot 1 \cdot 12.42 \cdot 10^{-6} = \underline{\underline{142.3}} kg$$

b) Rotor cage:
The rotor bar at length l_e has increased losses k_R due to current displacement. **Rotor bar and ring segment resistance**

$$R_r = R_{bar} + \Delta R^*_{Ring} = \frac{1}{\kappa} \cdot \frac{(l_e \cdot k_R + (L - l_e))}{A_{Cur}} + \Delta R_{Ring} \frac{1}{2\sin^2(\pi p / Q_r)} \qquad (2.10.1\text{-}4)$$

with average ring diameter (Fig. 2.5-9)

$$d_{Ring} = d_{si} - 2\delta - h_{Ring} - 2h_4 \qquad (2.10.1\text{-}5)$$

and ring segment resistance

$$\Delta R_{Ring} = d_{Ring}\pi / (\kappa \cdot Q_r \cdot A_{Ring}) \qquad (2.10.1\text{-}6)$$

are transformed to stator winding data

$$R'_r = \ddot{u}_U \ddot{u}_I R_r \qquad (2.10.1\text{-}7)$$

and yield **cage losses**

$$P_{Cu,r} = Q_r R_r I_r^2 = m_s R'_r I'^2_r \quad . \qquad (2.10.1\text{-}8)$$

Total cage mass is

$$m_{Cu,r} = \gamma_{Cu} \cdot \left[Q_r \cdot A_{Cur} \cdot L + 2 \cdot A_{Ring} \cdot d_{Ring}\pi \right] \quad . \qquad (2.10.1\text{-}9)$$

Example 2.10.1-2:
Cage data according to Example 2.5-2: 75°C:

Bar:
a) At stand still (locked rotor) s = 1.0: $f_r = 1 \cdot 50 = 50\,\text{Hz}$:

$$\xi = h_1\sqrt{\pi \cdot f_r \cdot \mu_0 \cdot \kappa_{Cu}} = 0.04\sqrt{\pi \cdot 50 \cdot 4\pi \cdot 10^{-7} \cdot (57/1.22) \cdot 10^6} = 3.84$$

$$k_R = 3.84 \cdot \frac{\sinh(2 \cdot 3.84) + \sin(2 \cdot 3.84)}{\cosh(2 \cdot 3.84) - \cos(2 \cdot 3.84)} = 3.844$$

$$R_{bar} = \frac{1}{(57/1.22) \cdot 10^6} \cdot \frac{(0.392 \cdot 3.844 + (0.458 - 0.392))}{200 \cdot 10^{-6}} = 168.32\,\mu\Omega$$

b) Rated slip s = 0.015: $f_r = 0.015 \cdot 50 = 0.75\,\text{Hz}$: $\xi = 0.47$, $k_R = 1.0043$, $R_{bar} = 49.2\,\mu\Omega$

Ring:

$$d_{Ring} = d_{si} - 2\delta - h_{Ring} - 2h_4 = 458 - 2 \cdot 1.4 - 40 - 2 \cdot 3.4 = 408.4\,\text{mm}$$

$$\Delta R_{Ring} = d_{Ring}\pi / (\kappa \cdot Q_r \cdot A_{Ring}) = 0.4084 \cdot \pi / ((57/1.22) \cdot 10^6 \cdot 50 \cdot 800 \cdot 10^{-6}) = 0.69\,\mu\Omega$$

$$\Delta R^*_{Ring} = \Delta R_{Ring} \frac{1}{2\sin^2(\pi p / Q_r)} = 0.69 \cdot \frac{1}{2\sin^2(\pi \cdot 2/50)} = 22.0\,\mu\Omega$$

$$\ddot{u}_U = 364, \quad \ddot{u}_I = 21.84$$

Total cage resistance:
a) At stand still:

$$R_r = R_{bar} + \Delta R^*_{Ring} = 168.32 + 22.0 = 190.3\,\mu\Omega,$$

$$R'_r = \ddot{u}_U \ddot{u}_I R_r = 364 \cdot 21.84 \cdot 0.0001903 = \underline{\underline{1.513}}\,\Omega$$

b) At rated slip:

$R_r = R_{bar} + \Delta R^*_{Ring} = 49.2 + 22.0 = \underline{\underline{71.2}}\,\mu\Omega$

$R'_r = \ddot{u}_U \ddot{u}_I R_r = 364 \cdot 21.84 \cdot 0.0000712 = \underline{\underline{0.566}}\Omega$

c) At arbitrary slip: $R'_r = \underline{\underline{0.3335 \cdot k_R + 0.2325}}\Omega$

Cage mass: Q_r = 50 bars, 2 end rings:

$m_{Cu,r} = 8900 \cdot \left[50 \cdot 200 \cdot 10^{-6} \cdot 0.458 + 2 \cdot 800 \cdot 10^{-6} \cdot 0.4084 \cdot \pi\right] = \underline{\underline{59.0}}\,\text{kg}$

2.10.2 Friction and windage losses

These losses comprise friction losses in bearings and – in case of slip ring machines – brush friction losses. Concerning windage losses, friction of rotating rotor surface in air is usually small. The power consumption of shaft mounted fan usually dominates the windage losses and is much larger than the bearing losses. Bearing losses rise linear with speed, power consumption of fan with third power of speed. A gross estimate of friction and windage losses is given by assuming losses to be proportional to rotor surface and square of surface speed:

$$P_{fr+w} \sim d_{si} \pi L \cdot (d_{si} \cdot \pi \cdot n)^2 \quad \Rightarrow \quad P_{fr+w} \approx 10 \cdot d_{si}^3 \cdot L \cdot \pi^2 \cdot n^2 \qquad (2.10.2\text{-}1)$$

Example 2.10.2-1:

500 kW-induction motor: synchronous speed n = 1500/min

$P_{fr+w} \approx 10 \cdot d_{si}^3 \cdot L \cdot \pi^2 \cdot n^2 = 10 \cdot 0.458^3 \cdot 0.458 \cdot \pi^2 \cdot (1500/60)^2 = \underline{\underline{2714}}\,\text{W}$

2.10.3 Iron losses

a) Basic considerations on eddy current losses in conductive sheets:

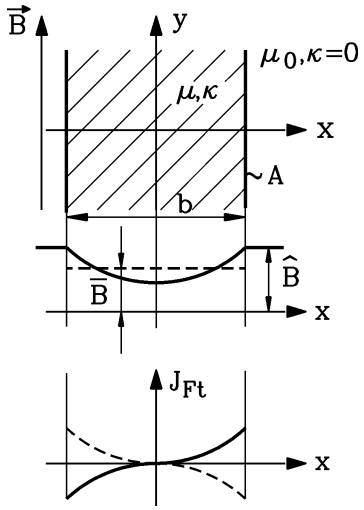

Fig. 2.10.3-1: Eddy current density J_{Ft} and AC flux density distribution in a conductive sheet

If a homogeneous AC flux density

$$B(t) = \hat{B} \cdot \sin(2\pi \cdot f \cdot t) \qquad (2.10.3\text{-}1)$$

penetrates a conductive sheet (breadth b_{sh}, permeability μ, conductivity κ, side surface area A), it induces according to *Faraday´*s law eddy currents with current density $J_{Ft} = U_i/R_{Fe}$. If length of sheet l is assumed infinite, eddy current will flow on left and right sheet side (b_{sh}/2)

in opposite direction, thus forming the eddy. With $U_i = (2\pi f)\cdot(b_{sh} l)\cdot\hat{B}/\sqrt{2}$, the iron sheet resistance $R_{Fe} = 2\cdot l/(\kappa\cdot h\cdot b_{sh}/2)$ and the iron sheet volume $V = b_{sh}\cdot A = b_{sh}\cdot l\cdot h$ we get the eddy current losses per volume: $P_{Ft}/V = U_i^2/(R_{Fe}\cdot V) = (\pi\cdot f\cdot b_{sh}\cdot\hat{B})^2\cdot\kappa/2$. We assumed J_{Ft} to be constant over $b_{sh}/2$. More detailed (Fig. 2.10.3-1), we consider also the self field of the eddy currents. According to *Ampere´*s law eddy currents excite a magnetic field, which opposes the original field, reducing it within the sheet with minimum field in middle of sheet (Fig. 2.10.3-1). Thus the average sheet flux density $\overline{B}$ is lower than peak value $\hat{B}$ at sheet sides. Solving *Maxwell´*s equations yields the **per volume eddy current losses:**

$$P_{Ft}/V = \frac{4\cdot\kappa}{3}\cdot\left(\frac{\pi}{2\sqrt{2}}\cdot f\cdot b_{sh}\cdot\overline{B}\right)^2\cdot k_W \qquad (2.10.3\text{-}2)$$

$$k_W = \frac{3}{\zeta}\cdot\frac{\sinh\zeta-\sin\zeta}{\cosh\zeta-\cos\zeta}\quad,\quad \zeta = b_{sh}/d_E\quad,\quad d_E = 1/\sqrt{\pi\cdot f\cdot\mu\cdot\kappa} \qquad (2.10.3\text{-}3)$$

With **increasing frequency** eddy currents grow strong and reduce internal field much. Field will penetrate only in penetration depth d_E, where the eddy currents flow. If penetration depth is larger than sheet thickness b_{sh}, we speak of **"low frequency"** with respect to sheet thickness b_{sh} ("thin sheet"), resulting in low ζ. At **"high frequency"** with respect to sheet thickness penetration depth is much smaller than b_{sh} ("thick sheet") with big ζ.

"Thin sheet": $\zeta < 2 \;\Rightarrow\; k_W \cong 1 \;\Rightarrow\; \overline{B}\cong\hat{B}$

$$p_{Ft} = P_{Ft}/V = \frac{4\cdot\kappa}{3}\cdot\left(\frac{\pi}{2\sqrt{2}}\cdot f\cdot b_{sh}\cdot\overline{B}\right)^2 = \frac{1}{3}\cdot(\pi\cdot f\cdot b_{sh}\cdot B)^2\cdot\frac{\kappa}{2} \qquad (2.10.3\text{-}4)$$

This is valid for calculating **eddy current losses** in the iron stack of electric machines. The factor 1/3 considers J_{Ft} to rise linear ~ x over $b_{sh}/2$, hence the average of x^2 gives 1/3.

"Thick sheet": $\zeta > 3 \;\Rightarrow\; k_W \cong 3/\zeta \;\Rightarrow\; \overline{B} << \hat{B}$

Losses per volume: $p_{Ft} = P_{Ft}/V = \frac{b_{sh}\cdot\overline{B}^2}{2}\cdot\sqrt{\frac{\pi^3\cdot f^3\cdot\kappa}{\mu}}\qquad V = A\cdot b_{sh}$ (2.10.3-5a)

Losses per sheet surface $P_{Ft}/(2A) = \frac{b_{sh}^2\cdot\overline{B}^2}{4}\cdot\sqrt{\frac{\pi^3\cdot f^3\cdot\kappa}{\mu}}$ (2.10.3-5b)

This equation is valid for calculating **eddy current losses** in massive conductive parts such as iron end shields, rotor shaft or stator housing of electric machine.

Example 2.10.3-1:
Eddy current losses in thin and thick iron sheet at
f = 50 Hz, $\overline{B}$ = 1T, $\kappa_{Fe} = 10^7$ S/m (pure iron), $\mu_{Fe} = 1000\mu_0$, $\gamma_{Fe} = 7850\,\mathrm{kg/m^3}$

	thin sheet b_{sh} = 0.5 mm	thick sheet b_{sh} = 50 mm
ζ	0.7	70
k_W	1	0.043
p_{Ft} / W/dm^3	10.3	4390.5
p_{Ft}/γ_{Fe} / W/kg	1.3	559

Facit:
By using thin insulated sheets, eddy currents may be suppressed significantly.

b) Calculation of iron losses:
Eddy current (Ft) and **hysteresis losses** (Hy) in iron stack are called **iron losses** and are measured at 1.5 T, 50 Hz or 1.0 T, 50 Hz in so-called *Epstein* frame and are given as losses per mass v_{15} or v_{10}. These losses depend on B^2, so $v_{15} = 2.25 \cdot v_{10}$. Hysteresis losses depend on f and eddy current losses on f^2. Further eddy current losses vary with square of sheet thickness (2.10.3-4). Usually sheets with b_{sh} = 0.5 mm or 0.35 mm thickness are used.

$$v_{10} = p_{Hy} \cdot (f/50) + p_{Ft} \cdot (f/50)^2 \cdot (b_{sh}/0.5)^2 \quad (f \text{ in Hz}, b_{sh} \text{ in mm}) \tag{2.10.3-6}$$

e.g. sheet type IV: $p_{Hy} = 1.3\,\text{W/kg},\ p_{Ft} = 0.4\,\text{W/kg}$

Due to different flux density in yoke and teeth losses there are calculated separately. At rated speed rotor frequency is very low, so iron losses there may be neglected. Due to punching the slots in the sheets the punching shear stress in iron increases hysteresis losses. Punching may also destroy insulation of sheets partially, thus bridging the sheets, when stacked. This causes an increase of eddy current losses. As ratio of cutting length versus sheet surface is bigger for teeth than for yoke, the increase of losses due to punching is bigger for teeth than for yokes with typical **loss increase rates**

$k_{Vd} = 1.8 \ldots 2.0$ (teeth), $k_{Vy} = 1.3 \ldots 1.5$ (yoke) ,

leading to **teeth and yoke iron losses**

$$\boxed{P_{Fe,d} = k_{Vd}\left(\frac{B_{d,1/3}}{1.0}\right)^2 v_{10} \cdot k_f \cdot m_d} \qquad \boxed{P_{Fe,y} = k_{Vy}\left(\frac{B_{ys}}{1.0}\right)^2 v_{10} \cdot k_f \cdot m_y} \tag{2.10.3-7}$$

with influence of frequency according to

$$k_f = \frac{p_{Hy}\left(\frac{f}{50}\right) + p_{Ft}\left(\frac{f}{50}\right)^2}{v_{10}} \quad . \tag{2.10.3-8}$$

Calculation of tooth masses (γ_{Fe} = 7800 kg/m^3):

$$m_{ds} = \gamma_{Fe} \cdot \left\{\left[(d_{si} + 2l_{ds})^2 - d_{si}^2\right] \cdot (\pi/4) - Q_s \cdot A_{Qs}\right\} \cdot l_{Fe} \cdot k_{Fe} \tag{2.10.3-9}$$

$$m_{dr} = \gamma_{Fe} \cdot \left\{\left[d_{ra}{}^2 - (d_{ra} - 2l_{dr})^2\right] \cdot (\pi/4) - Q_r \cdot A_{Qr}\right\} \cdot l_{Fe} \cdot k_{Fe} \tag{2.10.3-10}$$

Calculation of yoke masses, neglecting axial ventilation ducts:

$$m_{ys} = \gamma_{Fe} \cdot \left[d_{sa}^2 - (d_{sa} - 2h_{ys})^2\right] \cdot (\pi/4) \cdot l_{Fe} \cdot k_{Fe} \tag{2.10.3-11}$$

$$m_{yr} = \gamma_{Fe} \cdot \left[(d_{ri} + 2h_{yr})^2 - d_{ri}^2\right] \cdot (\pi/4) \cdot l_{Fe} \cdot k_{Fe} \tag{2.10.3-12}$$

Example 2.10.3-2:
550 kW-cage induction motor, 50 Hz, iron sheet type IV, data of Example 2.4-1, 2.4-3, 2.7.4-1: d_{si} = 458 mm, δ = 1.4 mm, l_{ds} = 69 mm, l_{dr} = 43.5 mm, h_{ys} = 77 mm,
shaft diameter d_{ri} = 200 mm, h_{yr} = 84.1 mm

Flux densities:
$B_{ys} = 1.70\,\mathrm{T},\ B_{yr} = 1.73\,\mathrm{T},\ B'_{ds,1/3} = 1.68\ \mathrm{T},\ B'_{dr,1/3} = 1.41\mathrm{T},\ k_{Vd} = 1.8,\ k_{Vy} = 1.5$

Masses:

$$A_{Qs} = b_{Qs} \cdot h_{Qs} = 12.5 \cdot 69 = 862.5\,\mathrm{mm}^2$$

$$m_{ds} = 7800 \cdot \left\{\left[(0.458 + 2 \cdot 0.069)^2 - 0.458^2\right] \cdot (\pi/4) - 60 \cdot 862.5 \cdot 10^{-6}\right\} \cdot 0.378 \cdot 0.95 = 175\,\mathrm{kg}$$

$$A_{Qr} = b_{Qr} \cdot h_1 + s_{Qr} \cdot h_4 = 5.1 \cdot 40.1 + 2.5 \cdot 3.4 = 213\,\mathrm{mm}^2,\ d_{ra} = d_{si} - 2\delta = 0.4552\mathrm{mm}$$

$$m_{dr} = 7800 \cdot \left\{\left[0.4552^2 - (0.4552 - 2 \cdot 0.0435)^2\right] \cdot \frac{\pi}{4} - 50 \cdot 213 \cdot 10^{-6}\right\} \cdot 0.378 \cdot 0.95 = 127.8\,\mathrm{kg}$$

$$m_{ys} = 7800 \cdot \left[0.75^2 - (0.75 - 2 \cdot 0.077)^2\right] \cdot (\pi/4) \cdot 0.378 \cdot 0.95 = 456\mathrm{kg}$$

$$m_{yr} = 7800 \cdot \left[(0.2 + 2 \cdot 0.0841)^2 - 0.2^2\right] \cdot (\pi/4) \cdot 0.378 \cdot 0.95 = 210.2\,\mathrm{kg}$$

Losses:

f = 50 Hz: $k_f = 1$:

$$P_{Fe,ds} = 1.8 \cdot \left(\frac{1.68}{1.0}\right)^2 1.7 \cdot 1 \cdot 175 = \underline{\underline{1511}}\,\mathrm{W}$$

$$P_{Fe,ys} = 1.5 \cdot \left(\frac{1.70}{1.0}\right)^2 1.7 \cdot 1 \cdot 456 = \underline{\underline{3360}}\,\mathrm{W}$$

2.10.4 Surface losses

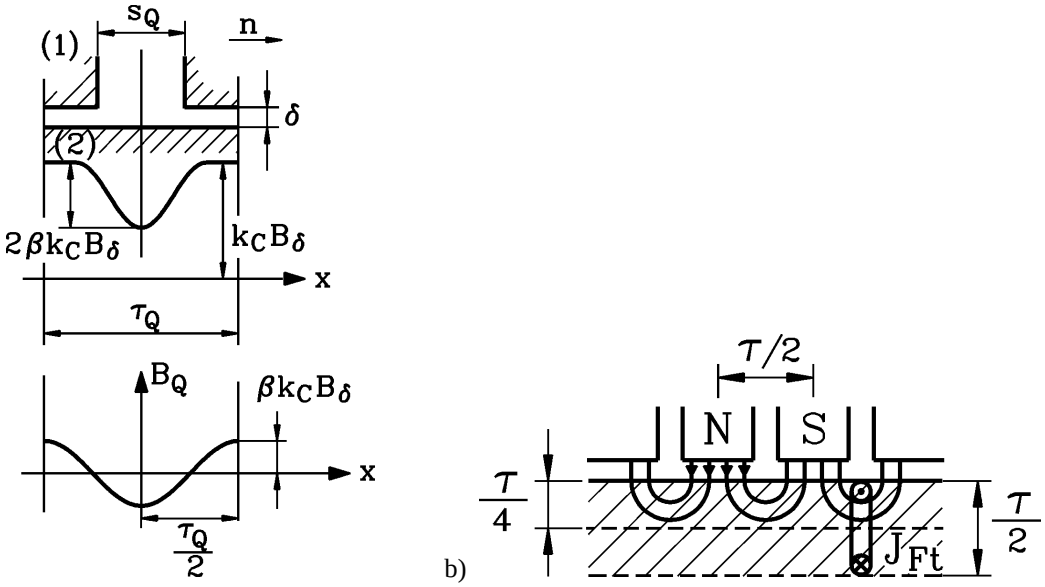

Fig. 2.10.4-1: a) Slot ripple of air gap flux density at rotor surface (2) due to open stator slot (1), b) Penetration of slot-frequent flux ripple into rotor, causing there eddy current density J_{Ft}

As described in Chapter 7, the slot openings cause a slot-frequent ripple of the air gap flux density, especially due to open stator slots of high voltage machines. The rotor surface is usually tooled to adjust the rotor outer diameter. This is necessary to ensure the small air gap which is necessary to limit the magnetization current in induction machines. Due to this tooling the insulated rotor iron sheets may be bridged partially at the rotor tooth tips, leading

to a conductive surface. Here the air gap flux density ripple may induce eddy currents, causing the so-called **rotor surface losses** already at no-load. As rotor slots are usually semi-closed and as stator bore surface is not tooled, stator surface losses are usually negligible.

Solving *Maxwell´*s equation by conform mapping, shape of flux density ripple is derived, yielding field variation under slot opening with average air gap field B_δ, peak value beneath tooth tip with *Carter´*s coefficient $k_C B_\delta$ and minimum value $(1-2\beta)k_C B_\delta$. Hence air gap flux density pulsates with frequency $f_Q = Q_s \cdot n$ (1000 ... 2000 Hz !) with respect to rotor with slot-frequent flux density amplitude

$$\hat{B}_Q = \beta \cdot k_C \cdot B_\delta \qquad (2.10.4\text{-}1)$$

with influence of slot opening versus air gap according to

$$\beta = \frac{1}{2} \cdot \left(1 - \frac{2/h}{\sqrt{1+(2/h)^2}}\right) \qquad h = s_Q / \delta \quad . \qquad (2.10.4\text{-}2)$$

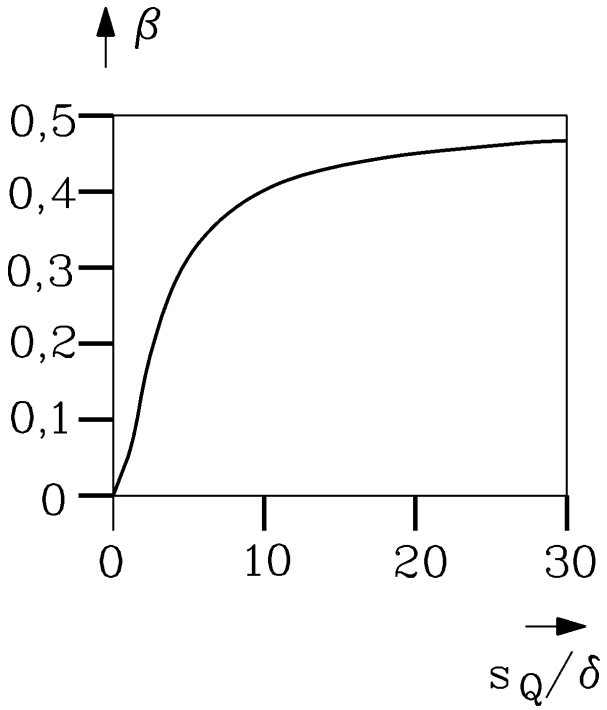

Fig. 2.10.4-2: Slot ripple coefficient β for determining air gap flux density ripple at rotor surface. Note: For infinite s_Q/δ the value of $\beta = 0.5$.

Flux density variation (Fig. 2.10.4-1a) is assumed to be sinusoidal: $\hat{B}_Q \cdot \sin(2x \cdot \pi / \tau_{Qs})$.

Average flux per half wave length (= half slot pitch): $\overline{B} = (2/\pi) \cdot \hat{B}_Q$.

As B_δ itself as fundamental flux wave is sinusoidal distributed along pole pitch, r.m.s. value of B_δ is effective for eddy current losses: $B_\delta / \sqrt{2}$.

In case of **massive rotor iron penetration** of the slot-frequent flux ripple into the rotor, it causes there an induction of the eddy current density J_{Ft} with a penetration of about $\tau_{Qs}/2$. The eddy current density distribution then resembles the calculation model **of the thick sheet**. We take $\tau_{Qs}/2$ as equivalent "sheet thickness" b_{sh} and calculate the rotor surface losses with the rotor surface $A_r = Q_r \cdot (\tau_{Qr} - s_{Qr}) \cdot l_{Fe}$ with the "thick sheet" equation (2.10.3-5b).

$$P_{Or} = A_r \cdot \frac{b_{sh}^2 \cdot \overline{B}^2}{4} \cdot \sqrt{\frac{\pi^3 \cdot f^3 \cdot \kappa}{\mu}} = A_r \cdot \frac{(\tau_{Qs}/2)^2 \cdot \left(\frac{2}{\pi}\beta k_C \frac{B_\delta}{\sqrt{2}}\right)^2}{4} \cdot (Q_s \cdot n)^{1.5} \cdot \sqrt{\frac{\pi^3 \cdot \kappa}{\mu}}$$

Of course **rotor iron is not massive**, but only partially bridged, therefore experiments according to *Richter* show, that measured surface losses of iron stack with 0.5 mm sheet type IV are only k_{exp} = 8 ... 13 % of "thick sheet" equation.

Rotor surface losses:

$$P_{Or} = Q_r \cdot (\tau_{Qr} - s_{Qr}) \cdot l_{Fe} \cdot (\tau_{Qs}/4)^2 \cdot \left(\frac{2}{\pi}\beta k_{Cs} \frac{B_\delta}{\sqrt{2}}\right)^2 \cdot (Q_s \cdot n)^{1.5} \cdot \sqrt{\frac{\pi^3 \cdot \kappa}{\mu}} \cdot k_{exp} \qquad (2.10.4\text{-}3)$$

Example 2.10.4-1:

550 kW, 4-pole cage induction motor, 50 Hz, iron sheet type IV ($\kappa = 4 \cdot 10^6$ S/m), data of Example 2.4-1, 2.4-3, 2.7.4-1: $s_{Qs} = b_{Qs}$ = 12.5 mm, δ = 1.4 mm, B_δ = 0.891 T, $\mu_{Fe} = 1400\mu_0$

$Q_r = 50$, $\tau_{Qr} = 28.8mm$, $s_{Qr} = 2.5mm$, $l_{Fe} = 378mm$, $\tau_{Qs} = 24mm$, $k_{Cs} = 1.5$, $Q_s = 60$, $k_{exp} = 0.08$

a) Pulsation frequency: $f_Q = Q_s \cdot n = 60 \cdot 1500/60 = \underline{\underline{1500}}$Hz

$h = s_{Qs}/\delta = 12.5/1.4 = 8.93$, $\beta = \frac{1}{2} \cdot (1 - \frac{2/8.93}{\sqrt{1 + (2/8.93)^2}}) = 0.391$

b) Flux density amplitude: $\hat{B}_{Qs} = \beta \cdot k_{Cs} \cdot B_\delta = 0.391 \cdot 1.5 \cdot 0.891 = \underline{\underline{0.52}}$T

c) Rotor surface: $A_r = Q_r \cdot (\tau_{Qr} - s_{Qr}) \cdot l_{Fe} = 50 \cdot (0.0288 - 0.0025) \cdot 0.378 = 0.497\,\text{m}^2$

d) Rotor surface losses:

$$P_{Or} = 0.497 \cdot \frac{(0.024/2)^2 \cdot \left(\frac{2}{\pi} \cdot 0.391 \cdot 1.5 \frac{0.891}{\sqrt{2}}\right)^2}{4} \cdot 1500^{1.5} \cdot \sqrt{\frac{\pi^3 \cdot 4 \cdot 10^6}{1400 \cdot 4\pi \cdot 10^{-7}}} \cdot 0.08 = \underline{\underline{1220}}\text{W}$$

2.10.5 Tooth pulsation losses

Stator and rotor slot openings cause a slot-frequent pulsation of the tooth flux density. Especially high voltage machines with open stator slots cause a considerable rotor tooth flux pulsation with frequency $f_Q = Q_s \cdot n$ (1000 ... 2000 Hz !), whereas semi-closed rotor slots usually produce only small stator tooth flux pulsation (Fig. 2.10.5-1).

Rotor tooth flux pulsation depends on slot number ratio Q_s/Q_r (Fig. 2.10.5-1) and is decreasing with $Q_s/Q_r > 1$ (Table 2.10.5-1). Ideal situation for $Q_s/Q_r = 1$ yields no flux pulsation, but produces big cogging torque and is therefore **not** feasible. Minimum and maximum rotor tooth flux $\Phi_{dr,min}$ and $\Phi_{dr,max}$ are shown in Fig. 2.10.5-2, facing either stator slot opening or stator tooth tip.

Rotor tooth flux: $$\Phi_{dr} = l_{Fe} \int_{-\tau_{Qr}/2}^{\tau_{Qr}/2} B_\delta(x) \cdot dx \qquad (2.10.5\text{-}1)$$

Average rotor tooth flux: $\Phi_{dr,av} = \frac{\Phi_{dr,\min} + \Phi_{dr,\max}}{2} = l_{Fe} \cdot \tau_{Qr} \cdot B_\delta$ (2.10.5-2)

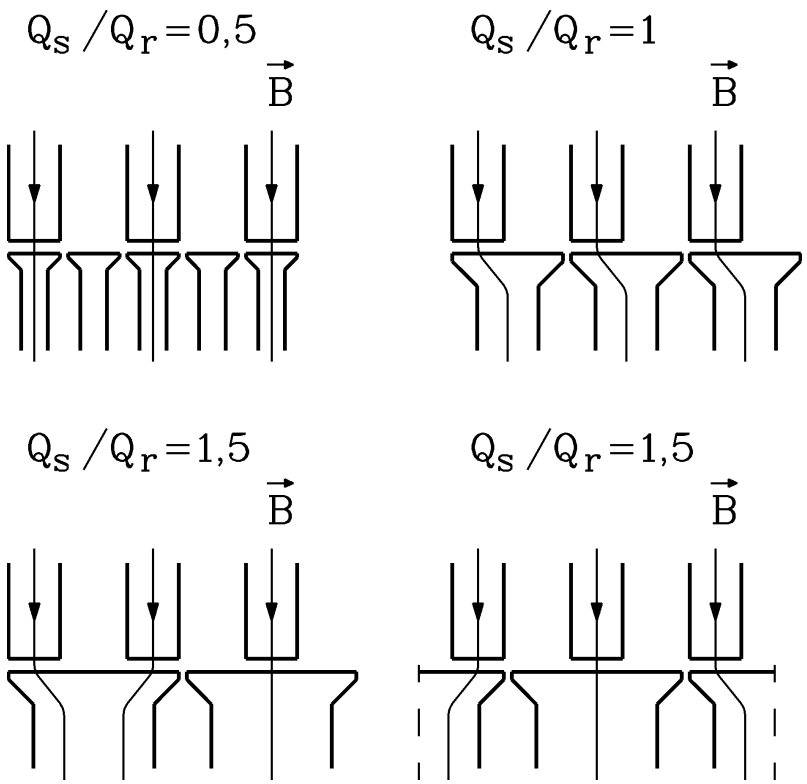

Fig. 2.10.5-1: Influence of slot number ratio Q_s/Q_r on rotor tooth flux pulsation

Q_s/Q_r	
0.5	Each rotor tooth experiences flux pulsation between 0 and 200% due to facing either stator slot opening or stator tooth tip
1.0	Rotor teeth do not experience any flux pulsation, as each rotor tooth tip faces always both stator slot opening and stator tooth tip
1.5	Each rotor tooth experiences flux pulsation between 66% and 133% due to facing either one or two stator slot openings

Table 2.10.5-1: Depending on slot number ratio Q_s/Q_r rotor tooth flux pulsation may vary considerably

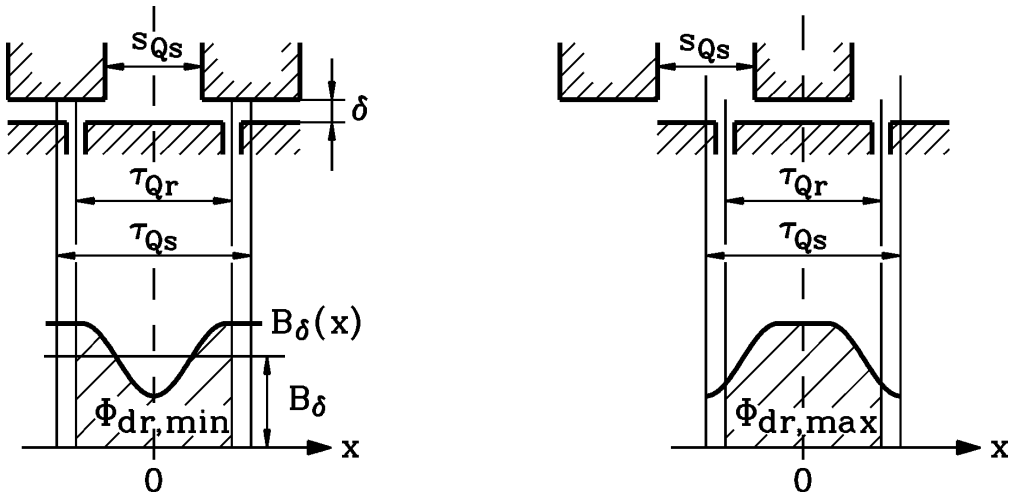

Fig. 2.10.5-2: Variation of air gap flux density causes (left) minimum and (right) maximum rotor tooth flux for a given slot number ratio Q_s/Q_r due to (left) tooth unaligned position, (right) tooth aligned position

With respect to average stator tooth flux $\Phi_{ds,av} = l_{Fe} \cdot \tau_{Qs} \cdot B_\delta$ we get:

$$\Phi_{dr,av} = l_{Fe} \cdot \tau_{Qs} \cdot (Q_s / Q_r) \cdot B_\delta = (Q_s / Q_r) \cdot \Phi_{ds,av} \tag{2.10.5-3}$$

Flux density variation (Fig. 2.10.4-1a) is assumed to be sinusoidal: $\hat{B}_Q \cdot \sin(2x \cdot \pi / \tau_{Qs})$ with $\hat{B}_Q = \beta \cdot k_{Cs} \cdot B_\delta$, so we get for air gap flux density at minimum / maximum rotor tooth flux:

$$B_\delta(x) = B_\delta \mp \hat{B}_Q \cdot \sin(2x \cdot \pi / \tau_{Qs}) \tag{2.10.5-4}$$

With (2.10.5-1) minimum / maximum rotor tooth flux is calculated as

$$\Phi_{dr,\min} = \Phi_{ds,av} \cdot \left[\frac{Q_s}{Q_r} - \frac{\beta \cdot k_{Cs}}{\pi} \cdot \sin\left(\pi \frac{Q_s}{Q_r} \right) \right], \quad \Phi_{dr,\max} = \Phi_{ds,av} \cdot \left[\frac{Q_s}{Q_r} + \frac{\beta \cdot k_{Cs}}{\pi} \cdot \sin\left(\pi \frac{Q_s}{Q_r} \right) \right],$$

hence tooth flux pulsation leads to **pulsation of rotor tooth flux density** according to

$$\frac{\Delta B_{dr}}{B_{dr}} = \frac{\Phi_{dr,\max} - \Phi_{dr,\min}}{2\Phi_{dr,av}} = \beta \cdot k_{Cs} \cdot \frac{\sin(\pi \cdot Q_s / Q_r)}{\pi \cdot Q_s / Q_r} \quad . \tag{2.10.5-5}$$

Even at $f_Q = Q_s \cdot n$ = 1000 ... 2000 Hz iron sheets with thickness 0.35 ... 0.5 mm may be regarded as "thin" sheets ($k_W \cong 1$). Therefore we may use eddy current part of iron loss equation (2.10.3-7) for rotor teeth with frequency $f_Q = Q_s \cdot n$ to calculate **rotor tooth pulsation losses.** As B_δ itself as fundamental flux wave is sinusoidal distributed along pole pitch, r.m.s. value of B_δ is to be used **for tooth pulsation losses**: $B_\delta / \sqrt{2}$.

$$\boxed{P_{puls,r} = k_{Vd} \left(\frac{\Delta B_{d,1/3}}{1.0} \right)^2 \cdot p_{Ft} \cdot \left(\frac{f_Q}{50} \right)^2 \cdot m_{dr}} \tag{2.10.5-6}$$

with slot-frequent tooth flux density amplitude

$$\boxed{\Delta B_{dr,1/3} = \frac{B_{dr,1/3} \cdot \beta \cdot k_{Cs}}{\sqrt{2}} \cdot \frac{\sin(\pi \cdot Q_s / Q_r)}{\pi \cdot Q_s / Q_r}} \quad . \tag{2.10.5-7}$$

Note:
For Q_s/Q_r = 1, 2, 3, ... rotor tooth flux pulsation **is zero**, which fits to Fig. 2.10.5-1.

Example 2.10.5-1:
550 kW, 4-pole cage induction motor, 50 Hz, iron sheet type IV: $p_{Ft} = 0.4\,\text{W/kg}$, data of Example 2.4-1, 2.4-3, 2.7.4-1: $s_{Qs} = b_{Qs} = 12.5$ mm, $\delta = 1.4$ mm, $B_{dr,1/3} = 1.41$ T,
$m_{dr} = 127.8\,\text{kg}$, $Q_r = 50$, $k_{Cs} = 1.5$, $Q_s = 60$, $k_{Vd} = 1.8$, $\beta = 0.391$
Pulsation frequency: $f_Q = Q_s \cdot n = 60 \cdot 1500/60 = \underline{\underline{1500}}\,\text{Hz}$

$$\Delta B_{dr,1/3} = \frac{B_{dr,1/3} \cdot \beta \cdot k_{Cs}}{\sqrt{2}} \cdot \frac{\sin(\pi \cdot Q_s / Q_r)}{\pi \cdot Q_s / Q_r} = \frac{1.41 \cdot 0.391 \cdot 1.5}{\sqrt{2}} \cdot \frac{\sin(\pi \cdot 60/50)}{\pi \cdot (60/50)} = -0.091\text{T}$$

$$P_{puls,r} = 1.8 \cdot \left(\frac{0.091}{1.0}\right)^2 \cdot 0.4 \cdot \left(\frac{1500}{50}\right)^2 \cdot 127.8 = \underline{\underline{688}}\,\mathrm{W}$$

2.10.6 Eddy current losses in stator conductors

In stator slot *n* conductors are arranged along slot height and are exposed to AC stator slot stray flux, which crosses perpendicular (Fig. 2.10.6-1). Each conductor thus suffers eddy current losses due the stray flux, which is excited by the current in the conductor itself. Thus current displacement causes increase of conductor resistance $R_{DC,L}$ by the coefficient $k_R(\xi)$, which is called here $\varphi(\xi)$, to "AC resistance" $R_{AC,L} > R_{DC,L}$. In addition, each p^{th} conductor experiences the stray flux from the p - 1 underneath lying conductors, which causes additional eddy currents and additional increase of resistance by the coefficient $p \cdot (p-1) \cdot \psi(\xi)$. These coefficients have been derived from *Maxwell´*s equations by *Field* and *Emde*.

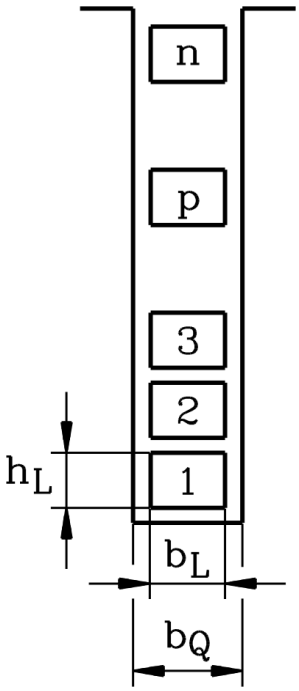

Fig. 2.10.6-1: Arrangement of *n* conductors in stator slot

So total increase of **AC resistance** per p^{th} conductor is (n_{ne}: number of conductors aside in slot)

$$k_p = \varphi(\xi) + p \cdot (p-1) \cdot \psi(\xi) = \frac{R_{AC,L}}{R_{DC,L}} \quad . \qquad (2.10.6\text{-}1)$$

$$\varphi(\xi) = \xi \cdot \frac{\sinh(2\xi) + \sin(2\xi)}{\cosh(2\xi) - \cos(2\xi)} \quad , \quad \psi(\xi) = 2\xi \cdot \frac{\sinh(\xi) - \sin(\xi)}{\cosh(\xi) + \cos(\xi)} \qquad (2.10.6\text{-}2)$$

$$\xi = h_L \cdot \sqrt{\pi \cdot \mu_0 \cdot f_s \cdot \kappa \cdot (n_{ne} \cdot b_L / b_Q)} \qquad (2.10.6\text{-}3)$$

The n^{th} conductor near top of slot experiences **the highest eddy current losses** and will get hottest. In single layer winding all *n* conductors are connected in series, in two layer winding *n*/2 conductors of lower layer are connected with *n*/2 conductors of upper layer of another

slot, so again series connection is given. The average increase of resistance for all *n* series connected conductors is

$$k_n = \frac{1}{n}\sum_{p=1}^{n} k_p = \varphi(\xi) + \frac{n^2-1}{3}\cdot\psi(\xi) \quad . \tag{2.10.6-4}$$

In winding overhangs stray flux is much smaller, so there only negligible eddy currents are induced in conductors. Thus, **average rise of AC resistance** per coil and hence **per phase** is

$$\boxed{k_{R,av} = \frac{k_n \cdot l_e + L - l_e + l_b}{L + l_b}} \quad . \tag{2.10.6-5}$$

By choosing conductor height h_L sufficient small, condition $\xi < 0.35$ ensures that $R_{AC,L} \cong R_{DC,L}$, thus avoiding additional winding losses due to current displacement.

Example 2.10.6-1:

Motor data from Example 2.4-3: f_s = 50 Hz, 20°C: $\kappa_{Cu} = 57\cdot10^6$ S/m, $b_L = 7.1$ mm, $h_L = 1.8$ mm, two layer winding $n = 2N_c = 20$, $n_{ne} = 1$, $b_L / b_Q = 7.1/12.5$

$$\xi = h_L \cdot \sqrt{\pi \cdot \mu_0 \cdot f_s \cdot \kappa \cdot (n_{ne} \cdot b_L / b_Q)} = 0.0018 \cdot \sqrt{\pi \cdot 4\pi \cdot 10^{-7} \cdot 50 \cdot 57 \cdot 10^6 \cdot (1 \cdot 7.1/12.5)} = 0.144$$

$$\varphi(0.144) = 1.0000382,\ \psi(0.144) = 0.0001433$$

$$k_n = 1.0000382 + \frac{20^2-1}{3}\cdot 0.0001433 = \underline{\underline{1.019}}$$

Facit:

Increase of AC resistance is only 1.9% compared to DC resistance and therefore negligible.

2.10.7 Additional losses (stray load losses)

- No-load tooth flux pulsation losses,
- no-load surface losses
- eddy current losses in stator winding due to no-load current

are **additional no-load losses**, which are measured together with iron losses in no-load test. In machine they cannot be measured separately.

Under load increased stator current and rotor current excite increased step-like air gap flux density distribution, causing increase of tooth flux pulsation and surface losses, but also further harmonic currents in rotor cage and in skewed rotor cages inter-bar currents between adjacent bars. These and other eddy current losses in conductive parts such as stator housing or press fingers of stator and rotor iron stack are summarized as **stray load losses (additional load losses)**.

Their calculation is done similar as shown here for additional no-load losses, but always leave a rather big uncertainty concerning the reliable results, when compared to actual measured motor stray load losses. According to IEC 34-2 they may be estimated as 0.5% of electric power of machine, which for smaller motors < 100 kW usually is too low, as measurements show typically 1.5% ... 2%. These stray load losses are eddy current losses, caused by induced

voltage u_i of magnetic field harmonics and stray flux at load in different conductive parts of electric machine. These field components are excited by load current component.

$$\underline{I}_{Load} = \underline{I}_{s0} - \underline{I}_{s} \qquad (2.10.7\text{-}1)$$

With $\varphi_{s0} \cong 90°$ no-load current I_{s0} is a nearly totally inductive component, so load current component is a nearly totally real current, therefore we may put

$$I_{Load}^2 = I_s^2 - I_{s0}^2 \qquad (2.10.7\text{-}2)$$

Therefore we get for stray load losses $P_{ad,1} \sim u_i^2 / R \sim B^2 / R \sim I_{Load}^2 / R$, hence at rated speed

$$\boxed{P_{ad,1} = 0.005 \cdot P_{eN} \cdot (I_s^2 - I_{s0}^2)/(I_{sN}^2 - I_{s0}^2)} \quad . \qquad (2.10.7\text{-}3)$$

At varying speed the frequency of induced eddy currents varies also. In that case additional dependence of speed must be considered.

Example 2.10.7-1:
550 kW motor, efficiency 94.4 %, $P_{in} = P_e = P_{out} / \eta = 550 / 0.944 = 582.6\,\text{kW}$
Stray load losses (IEC 34-2) at rated current: $P_{ad,1} = 0.005 \cdot P_e = 0.005 \cdot 582.6 = \underline{\underline{2.91}}\,\text{kW}$

2.10.8 Total active masses

Stator winding (without winding insulation)	142.3 kg
Rotor cage	59.0 kg
Winding mass:	201.3 kg
Stator teeth	175.0 kg
Stator yoke	456.0 kg
Stator iron mass:	631.0 kg
Rotor teeth	127.8 kg
Rotor yoke	210.2 kg
Rotor iron mass:	338.0 kg
Total active mass:	1170.3 kg

Table 2.10.8-1: Calculated active mass for 550 kW-cage induction machine, open ventilated, Thermal Class B, 50 Hz, four poles

Total active masses comprise stator and rotor iron stack masses and stator and rotor winding masses. **Inactive masses** as mass of rotor shaft, stator housing and end-shield, fan, bearings, terminal box (screws always included) and – for bigger machines – air-air cooler or air-water-cooler must be added to get total mass. Rough estimate for total mass is for standard induction machines (totally enclosed, shaft mounted fan) about 2 ... 3-times active mass.

A typical ratio of **"power per active mass"** is **0.5 kW /kg**:

Thermal Class B: 80 K temperature rise: 550 kW/ 1170.3 kg = 0.47 kW/kg.
Thermal Class F: 105 K temperature rise: $\sqrt{105/80} \cdot 0.47 = 0.54$ kW/kg.

2.10.9 Machine performance

Grid-operated machine performance is calculated from equivalent circuit diagram with the parameters as calculated above, yielding for given stator voltage and frequency U_s and f_s stator and rotor current, electromagnetic torque, shaft torque, all loss components and machine efficiency. Additional thermal calculation based on calculated losses is needed afterwards to check winding temperature rise (see Chapter 3).

No load rotor tooth pulsation losses and surface losses are measured along with stator iron losses at no load and are therefore often taken as total iron losses, which are considered in equivalent circuit as **"equivalent iron resistance"** R_{Fe}. As iron losses are generated by $B^2 \sim \Phi_h^2 \sim U_h^2$ with $U_h = X_h \cdot I_m$, total iron losses are considered by R_{Fe} in parallel to X_{h}. With $U_h = U_s/(1+\sigma_s) \approx U_s$ often for simplification R_{Fe} is put in parallel to feeding voltage U_{s} (Fig. 2.10.9-1). Operation at different frequency f_{s} would lead to dependence of $R_{\mathrm{Fe}}(f_{\mathrm{s}})$.

$$P_{Fe} = m_s \cdot U_h^2 / R_{Fe} \tag{2.10.9-1}$$

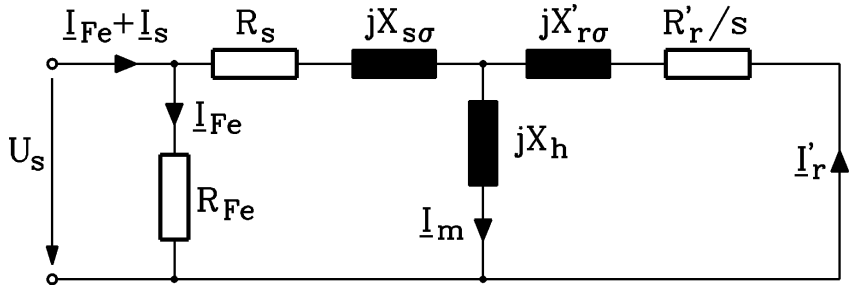

Fig. 2.10.9-1: Equivalent circuit of induction machine with simplified consideration of iron losses

Additional load losses (stray load losses) are proportional to $I_s^2 - I_{s0}^2$.

With $I_{s0}/I_N \approx 0.3 \ldots 0.6$, often simplification $I_s^2 - I_{s0}^2 \approx I_s^2$ is used. In that case, stray load losses may be considered in equivalent circuit as additional **"equivalent series resistance"** $R_{\mathrm{ad,1}}$ in series with stator resistance per phase. Operation at different speed n and / or different frequency f_{s} would lead to dependence of $R_{\mathrm{ad,1}}(f_{\mathrm{s}}, n)$.

$$P_{ad,1} \cong 0.005 \cdot P_{eN} \cdot (I_s / I_N)^2 = m_s \cdot R_{ad,1} \cdot I_s^2 \tag{2.10.9-2}$$

Example 2.10.9-1:
550 kW motor, 6.6 kV, 59 A, 50 Hz:
Total iron losses: $P_{Fe} = P_{Fe,ds} + P_{Fe,ys} + P_{Or} + P_{puls,r} = 1511 + 3360 + 1220 + 688 = 6779\,\mathrm{W}$
Simplified iron resistance consideration:
$R_{Fe} = m_s \cdot U_s^2 / P_{Fe} = 3 \cdot (6600/\sqrt{3})^2 / 6779 = \underline{\underline{6425}}\,\Omega$,
$\underline{I}_{Fe} = \underline{U}_s / R_{Fe} = 3810.5/6425 = 0.59\,\mathrm{A}$ (1% of rated current, thus very small !)
Stray load losses:
$R_{ad,1} = P_{ad,1}/(m_s \cdot I_N^2) = 2910/(3 \cdot 59^2) = \underline{\underline{0.278}}\,\Omega$

In reality, things are little bit more complicated. No load pulsation and surface losses as well as main part of stray load losses occur in rotor due to movement of rotor. Therefore the eddy

current flow of these loss components in rotor leads to braking torque. Thus the loss components must be considered like an eddy current brake, which is acting on shaft in addition to friction and windage losses. Here, for simplification, these losses are all considered on stator side without acting as brake. Neglecting this braking effect yields in most cases only to small errors in relation to rated torque, as Example 2.10.9-2 shows.

Example 2.10.9-2:
550 kW motor, 6.6 kV, 50 Hz, rated speed n = 1490/min:
Rated shaft torque: $M_N = P_N/(2\pi n_N) = 550000/(2\pi \cdot (1490/60)) = \underline{\underline{3525}}\,\text{Nm}$
Braking effect of
- friction and windage losses: $M_{fr+w} = P_{fr+w}/(2\pi n_N) = 2714/(2\pi \cdot (1490/60)) = \underline{\underline{17.4}}\,\text{Nm}$
- tooth pulsation and surface losses:
$M_{puls+O,r} = P_{puls+O,r}/(2\pi n_N) = (688+1220)1/(2\pi \cdot (1490/60)) = \underline{\underline{12.2}}\,\text{Nm}$

According to equivalent circuit the two linear complex equations must solved:

$$\underline{U}_s = R_s\underline{I}_s + jX_{s\sigma}\underline{I}_s + jX_h(\underline{I}_s + \underline{I}'_r) \tag{2.10.9-3}$$

$$0 = \frac{R'_r}{s}\underline{I}'_r + jX'_{r\sigma}\underline{I}'_r + jX_h(\underline{I}_s + \underline{I}'_r) \tag{2.10.9-4}$$

Note that
- stator voltage may be chosen as real number $\underline{U}_s = U_s$,
- $\underline{I}_{Fe} = \underline{U}_s / R_{Fe}$ is constant and that $\underline{I}_s + \underline{I}_{Fe} = \underline{I}_{s,Line} \cong \underline{I}_s$, as $\underline{I}_{Fe}$ is very small.
- instead of R_s we use the equivalent stator resistance $R_{s,e} = R_s + R_{1ad}$.
Unknowns are $\underline{I}_s$, $\underline{I}'_r$ and given parameters are stator voltage, stator frequency, rotor slip and resistance and reactance parameters of equivalent circuit. **Total *Blondel´*s leakage coefficient**

$$\sigma = 1 - \frac{1}{\left(1+\frac{X_{s\sigma}}{X_h}\right)\left(1+\frac{X'_{r\sigma}}{X_h}\right)} \approx 1 - \left(1-\frac{X_{s\sigma}}{X_h}\right)\left(1-\frac{X'_{r\sigma}}{X_h}\right) \approx \frac{X_{s\sigma}+X'_{r\sigma}}{X_h} \tag{2.10.9-5}$$

should be small to ensure big **breakdown torque** M_b. Solution of (2.10.9-3, -4) is for

$$\underline{I}_s = U_s \cdot \frac{R'_r + jsX'_r}{(R_{s,e}R'_r - s\cdot\sigma\cdot X_s X'_r) + j(s\cdot R_{s,e}X'_r + X_s R'_r)} = I_{s,re} + jI_{s,im} \tag{2.10.9-6a}$$

$$\underline{I}'_r = -\underline{I}_s \frac{jX_h}{\frac{R'_r}{s} + jX'_r} \tag{2.10.9-6b}$$

$$P_{e,in} = m_s U_s (I_{s,re} + I_{Fe}) \tag{2.10.9-7}$$

$$P_\delta = P_{e,in} - m_s(R_s + R_{ad,1})I_s^2 - P_{Fe} = P_{e,in} - P_{Cu,s} - P_{ad,1} - P_{Fe} \tag{2.10.9-8}$$

$$M_e = p\frac{P_\delta}{\omega_s} \tag{2.10.9-9}$$

$$P_{Cu,r} = s\cdot P_\delta \tag{2.10.9-10}$$

$$P_{m,out} = P_\delta - P_{Cu,r} - P_{fr+w} \tag{2.10.9-11}$$

Speed n, shaft torque M_s, efficiency η and stator power factor $\cos\varphi_s$ are given by

$$n = (1-s)\cdot f_s / p \qquad (2.10.9\text{-}12)$$

$$M_s = \frac{P_{m,out}}{2\pi m} \qquad (2.10.9\text{-}13)$$

$$\eta = \frac{P_{m,out}}{P_{e,in}} \qquad (2.10.9\text{-}14)$$

$$\cos\varphi_s = \frac{P_{e,in}}{\sqrt{3}U_N \cdot I_{s,Line}} \qquad (2.10.9\text{-}15)$$

Example 2.10.9-3:
550 kW motor, 6.6 kV, 50 Hz, unskewed rotor:
$\underline{U}_s = U_s = 6600/\sqrt{3}\,\mathrm{V}$, $f_s = 50\,\mathrm{Hz}$, at 75°C: R_s = 0.74 Ω, $R_{1,ad}$ = 0.278 Ω, R_{Fe} = 6425 Ω,
$X_{s\sigma}$ = 4.89 Ω, X_h = 155.0 Ω (saturated value), $X'_{r\sigma} = (3.2\cdot k_L(s) + 3.18)\,\Omega$,
$R'_r = (0.3335\cdot k_R(s) + 0.2334)\,\Omega$
For 550 kW output power a slip of s_N = 0.814% is necessary, yielding:
coefficients k_R = 1.0013 and k_L = 0.99963 and $X'_{r\sigma} = 6.379\,\Omega$, $R'_r = 0.5673\,\Omega$, σ = 0.069.
Rated stator current is I_{sN} = 59.04 A (estimated 59 A), rotor current is $I'_r = 51.6\,\mathrm{A}$, $I_m = 23.8\,\mathrm{A}$.

Electrical input power $P_{e,in}$	**574 921 W**
Stator winding losses $P_{Cu,s}$	7 739 W
Total iron losses P_{Fe}	6 779 W
Stray load losses $P_{ad,1}$ (= 0.5% of 574 310 W)	2 875 W
Air gap power P_δ	557 528 W
Rotor cage losses $P_{Cu,r}$	4 538 W
Friction and windage losses P_{fr+w}	2 670 W
Mechanical output power $P_{m,out}$	**550 320 W (≅ 550 kW)**
Efficiency η	95.72 %

$$\cos\varphi_s = \frac{574921}{\sqrt{3}\cdot 6600\cdot 59.04} = 0.852$$

$$P_{Cu,s} = m_s R_s I_s^2 = 3\cdot 0.74\cdot 59.04^2 = 7739\,\mathrm{W}$$

$$P_{Cu,r} = m_s R'_r I'^2_r = 3\cdot 0.5673\cdot 51.6^2 = 4538\,\mathrm{W} \quad \text{or} \quad P_{Cu,r} = sP_\delta = 0.00814\cdot 557528 = 4538\,\mathrm{W}$$

$$M_e = p\frac{P_\delta}{\omega_s} = 2\cdot\frac{557528}{2\pi\cdot 50} = 3549\,\mathrm{Nm}$$

$$M_s = \frac{P_m}{2\pi\cdot n} = \frac{550320}{2\pi\cdot(1487.79/60)} = 3532.2\,\mathrm{Nm}$$

Stator current I_s and electromagnetic torque M_e are calculated with equivalent circuit Fig. 2.10.9-1 in dependence of speed n with the above given equations
a) with considering current displacement (solid line) and
b) without considering current displacement in rotor bars.

Reduction of rotor slot stray inductance due to current displacement leads to increased starting current, whereas increased rotor bar resistance leads to increased starting torque. Below breakdown slip rotor frequency is too low to produce considerable rotor current displacement effect, so between no-load and breakdown slip both calculations a) and b) lead to same values for torque and current (Fig. 2.10.9-2).

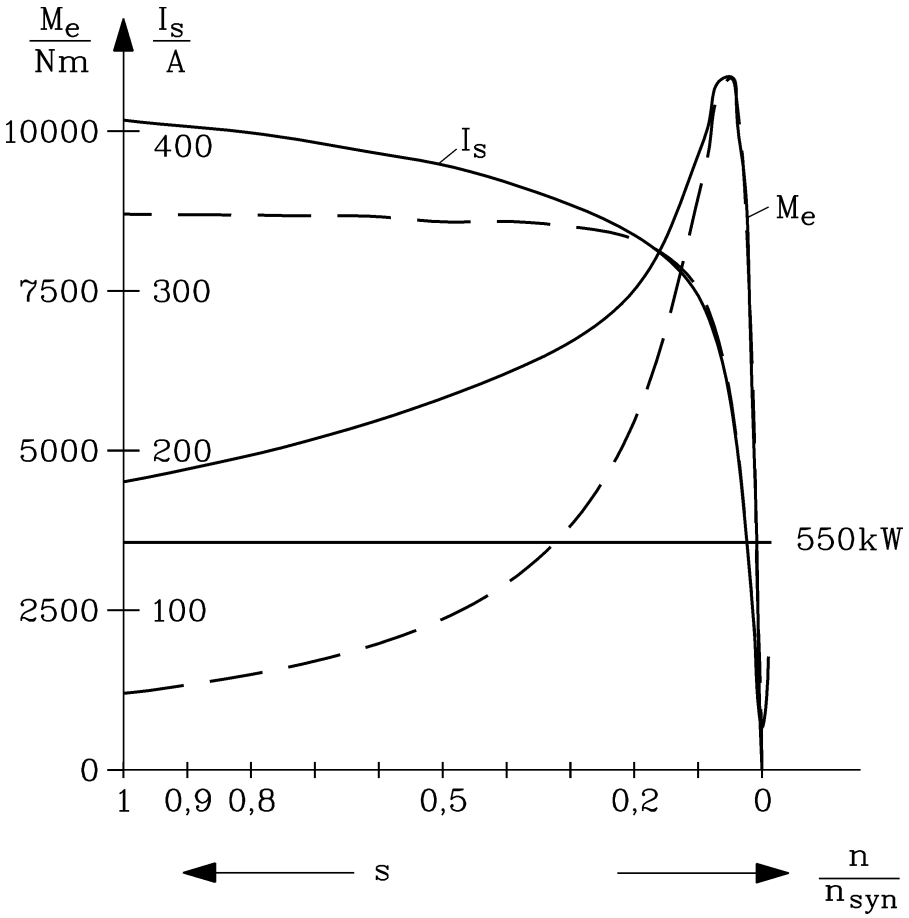

Fig. 2.10.9-2: Calculated stator current and electromagnetic torque versus speed of 550 kW, 4 pole, three phase cage induction motor, 6.6 kV. 50 Hz:
solid lines: with current displacement ($k_L < 1$, $k_R > 1$) in rotor bars considered,
dashed lines: without considering current displacement ($k_L = 1$, $k_R = 1$) too low torque is calculated.

Fig. 2.10.9-3: Cage induction generator (left), 990 kW, 690 V Y, 4 poles, 50 Hz, water jacket cooling, with gear 1:80 (right) coupled to wind turbine (*Source: Winergy, Germany*)

3. Heat transfer and cooling of electrical machines

3.1 Thermal classes, cooling systems, duty types

The losses in copper and iron and the mechanical losses in the bearings cause temperature rise in winding and insulation, iron stack and bearings. Insulation materials are very sensitive to over-temperature, as velocity of chemical decomposition of materials increases exponentially with temperature according to *Arrhenius´* law. For transformer oil and solid insulation materials *Montsinger´s* rule is valid, that insulation life span L decreases by 50% (taken as average of a large number of tested specimen) with increase of temperature ϑ by 10 K.

$$L(\vartheta + 10K) = 0.5 \cdot L(\vartheta) \tag{3.1-1}$$

Example 3.1-1:
Insulation material for Thermal Class F: $L(\vartheta = 155°C) = 100000\,\text{hours} \Rightarrow$
$L(\vartheta = 165°C) = 50000\,\text{hours}$

Thermal classes for different types of insulation materials (organic and inorganic materials such as epoxy resin, glass fibre, mica foil) are defined, which give the maximum permissible temperature limit in hot spot of insulation.

Thermal Class	B	F	H	250
Temperature limit ϑ (°C)	130	155	180	255
Maximum temperature rise $\Delta\vartheta$ (K)	80	105 ($P_N \le 5$ MW) 100 ($P_N > 5$ MW)	125	200

Table 3.1-1: Selected Thermal Classes of insulation systems according to IEC 60034-1

If windings are cooled with air, ambient coolant temperature of ≤ 40°C and height of operation of machine above sea level of ≤ 1000 m are assumed for admissible maximum temperature rise $\Delta\vartheta$. In mountainous regions with height above 1000 m air mass density is decreasing, thus cooling is less efficient, therefore machine power has to be reduced to reduce losses to ensure that temperature stays below the limit.

Open ventilation	*Totally enclosed machines – surface cooling*	*Totally enclosed machines with heat exchanger*	*Hollow conductor cooling*
Coolant air	Coolant air or water jacket	Coolant air Heat exchanger: air-air or air-water	Coolant hydrogen gas, oil or de-ionized water
End shields of machine are open for coolant flow	Increase of machine surface by fins or tubes for air Water jacket cooling	Coolant flow is directed through machine and heat exchanger in closed loop	Pump presses coolant through hollow conductors
Usually up to 500 kW, at higher power acoustic noise is too big	Usually up to 2000 kW	Up to 400 MW ("top air" turbo generators)	Up to biggest machine power (2000 MW)
Often shaft mounted fan	Often shaft mounted fan	Shaft mounted fans, external fans	External pump

Table 3.1-2: Different principles of cooling

Type of cooling system influences mainly thermal utilization of electric machine. With more efficient cooling systems power per mass of electric machine can be raised. With increasing frame size h of electric machine, the ratio "machine surface/ machine volume", which

corresponds with "natural cooling surface versus machine losses", decreases according to $A/V = 1/h$. Thus for bigger machines more sophisticated cooling systems must be used.

No fan	*Shaft mounted fan*	*External fan with fan drive unit*
Cooling only due to natural convection and heat radiation	Speed dependent air flow for cooling	Air flow independent of motor speed
Used for small machines (< 1 kW), e.g. permanent magnet machines due to their lower losses	Used for constant speed drives Big machine power possible	Used for variable speed drives Big machine power possible

Table 3.1-3: Different possibilities of propelling coolant flow

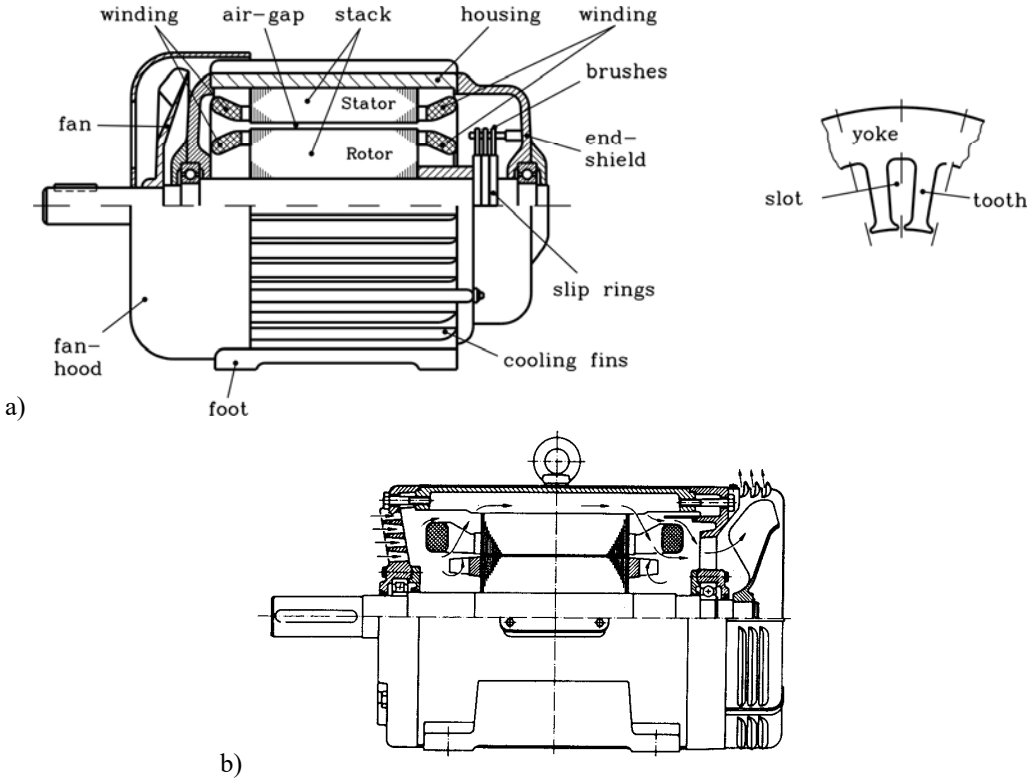

Fig. 3.1-1: Examples of cooling systems: a) IC 41: Shaft mounted fan, fan hood for guiding air flow with air inlet opening, totally enclosed slip-ring induction machine, cooling fins on motor housing, b) IC 01: Shaft mounted fan, open ventilation, cage induction machine, end shields with openings for coolant flow, fan hood for guiding coolant flow with openings for air outlet, additional small fan blades on cage ring for rotor cooling air flow

Type of cooling of machines is abbreviated by code IC (International Cooling) according to IEC 60034-6. First number gives kind of coolant flow according to Table 3.1-2, second number gives information according to Table 3.1-3, how coolant is propelled.

Example 3.1-2:
IC 41: "4": surface cooling, "1": shaft mounted fan
IC 05: "0": Open ventilation, "5": external fan, mounted on machine

For detailed discussion of cooling systems especially for big machines see lectures: "Large generators and high-power drives / Großgeneratoren und Hochleistungsantriebe".

Temperature rise is determined heating up the machine masses and by exchange of heat with coolant, thus leading to **thermal time constants** T_ϑ, ranging between several minutes for

small machines < 1 kW up to about > 1 hour for big machines. So immediate increase of machine power and losses will lead to increased motor temperature with considerable time delay. Therefore short time power overload is possible without surpassing temperature limit. Steady state operation will lead to constant temperature rise, so in that case no overload is possible without surpassing temperature limit. Different duty types of electric machines such as steady state operation (S1) and short time overload (S2) are defined in IEC 60034-2. With steady state operation a **stationary temperature rise** is reached, whereas with varying machine load also **temperature is varying**.

3.2 Elements for calculation of temperature rise

Natural heat flow is only possible from hot to cold region according to *Second fundamental law of Thermodynamics.* Basic principles for heat transfer are
- **conduction** of heat (*Fourier´*s law) by some heat conducting material,
- **convection** of heat by moving coolant, which transports heat energy from hot to cold region (theory of *Blasius, Prandtl* et al.),
- **heat radiation** from hot to cold region, which does not need any medium for heat transfer, but is electromagnetic radiation, mostly in infrared frequency range (law of *Stefan* and *Boltzmann*).

Combining partial differential equation for conduction and convection leads to heat transfer partial differential equation, depending on space co-ordinates and time, being solved by
a) numerical methods with Finite Elements or Finite Integration or by
b) equivalent circuits with concentrated heat transfer elements and losses as heat sources. In that case space co-ordinates are replaced by nodal network, so differential equations depend only on time.

Calculation of heat flow with **equivalent circuit** is discussed here further. Method is:
1. Calculation of heat sources (= losses in electric machine)
2. Design of equivalent circuit of heat transfer elements (conduction, convection, radiation) and heat storage elements (machine masses)
3. By combining 1. and 2., the temperature rise in the nodes of the thermal network may be calculated either
- for **time-varying losses** by solution of nodal time-dependent differential equations or
- for **stationary solution** by simply solving the algebraic equation system without any influence of time.

a) Heat resistance:
In analogy to electrical networks we may take thermal heat flow, which is thermal power P_{th} instead of electric current i, temperature difference $\Delta\vartheta$ instead of electric voltage u (= difference of electric potential) and get an *Ohm´*s law for heat flow:

$$u = R \cdot i \qquad \Rightarrow \qquad \Delta\vartheta = R_{th} P_{th} \tag{3.2-1}$$

Note that electric current density J corresponds with **heat flow density** $q = P_{th}/A$.

a1) Conduction of heat:
Conduction of heat by material is described by ***Fourier´*s law**. In simple case of heat conduction along one axis from hot point 2 to cold point 1 (Fig. 3.2-1a) along distance l in a material with **thermal conductivity** λ_{th} and cross section area A the conducted heat is given by

$$\frac{P_{th}}{A} = \lambda_{th} \cdot (\vartheta_2 - \vartheta_1)/l \qquad \Rightarrow \qquad R_{th} = \frac{l}{\lambda_{th} A} \quad , \qquad (3.2\text{-}2)$$

which allows definition of heat resistance R_{th} due to heat conduction.

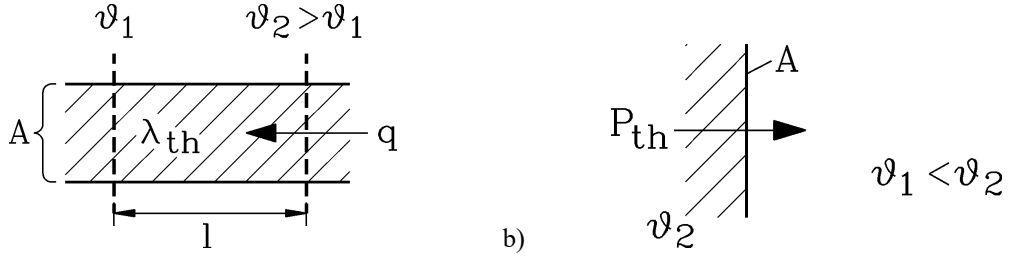

Fig. 3.2-1: Transportation of heat a) by conduction, b) by convection

Material	*Thermal conductivity* λ_{th} W/(m·K)
Air at 20° / 50° / 100°C, 1 bar	0.024 / 0.028 / 0.031
Copper	380
Iron	80
- Iron stack in direction of lamination - Iron stack perpendicular to lamination	20 ... 60 0.5 ... 1.2
Insulation material	0.2
Epoxy resin	0.3

Table 3.2-1: Thermal conductivity for some materials used in electric machines

Example 3.2-1:
550 kW-cage induction machine, 6.6 kV, 60 open stator slots, slot height h_Q = 69 mm, slot width b_Q = 12.5 mm, insulation thickness d = 2.7 mm, stack length: l_{Fe} = 380 mm
Slot surface $A = (2 \cdot h_Q + b_Q) \cdot l_{Fe} = (2 \cdot 69 + 12.5) \cdot 380 = 57190\,\text{mm}^2$

Thermal conductivity resistance from copper to iron: $R_{th} = \frac{d}{\lambda_{th} A} = \frac{0.0027}{0.2 \cdot 0.05719} = \underline{\underline{0.236}}\,\text{K/W}$

a2) Convection:
Heat P_{th} is transferred from hot surface A (Fig. 3.2-1b) to moving coolant, whose temperature is lower by difference $\Delta\vartheta = \vartheta_2 - \vartheta_1$. Coolant is heated up and – by flowing – transports heat off e.g. to some external cooler or to surrounding medium. **Heat transfer coefficient α** describes the cooling effect of flowing ("convection") coolant. Cooling effect depends on kind of coolant (air, hydrogen gas, water, ...), of speed v of coolant and many more parameters such as pressure of gas.

$$\frac{P_{th}}{A} = \alpha \cdot \Delta\vartheta \qquad \Rightarrow \qquad R_{th} = \frac{1}{\alpha A} \qquad (3.2\text{-}3)$$

Here only air as coolant will be considered, which is used in most cases of smaller and medium and even large machines up to 300 MVA.

Coolant & Cooling surface	α in W/(m^{2}K), v in m/s
Nearly not moving air (v = 0 ... 0.5 m/s)	8
Moved air, bare metallic hot surface	$\alpha = 15v^{2/3}$
Moved air, insulated winding	$\alpha = 8v^{3/4}$

Table 3.2-2: Typical values for heat transfer coefficient with air as coolant

Example 3.2-2:
550 kW-cage induction machine, 6.6 kV, open ventilated machine, double-layer winding, velocity of air flow in winding overhang v = 12 m/s = 43 km/h.
Coil height = half slot height $h_Q/2$ = 69/2 = 34.5 mm, coil breadth = slot width b_Q = 12.5 mm, length of winding overhang l_b = 614.8 mm.
- Surface of insulated stator coil in winding overhang:

$$A = 2 \cdot (h_Q / 2 + b_Q) \cdot l_b = (69 + 2 \cdot 12.5) \cdot 614.8 = 57791\,\text{mm}^2$$

- Moved air, insulated winding: $\alpha = 8v^{3/4} = 8 \cdot 12^{3/4} = 51.6\,\text{W/m}^2\text{K}$

$$R_{th} = \frac{1}{\alpha A} = \frac{1}{51.6 \cdot 0.057791} = \underline{\underline{0.335}}\,\text{K/W}$$

a3) Heat radiation:
Heat radiation does not need any medium to transport heat, as also in vacuum infrared electromagnetic waves propagate, thus transporting heat energy. Transferred heat P_{th} from hot (T_1) to cold ($T_2 < T_1$) surface A, where T_1 , T_2 are absolute temperatures, measured in K from absolute zero temperature level –273.15 °C, is calculated with **heat radiation law** of *Stefan* and *Boltzmann*.

$$\frac{P_{th}}{A} = c_s (T_1^4 - T_2^4) \qquad (3.2\text{-}4)$$

Radiation coefficient c_s depends on surface condition and on material condition. The housing of electric machines is often painted in black or grey to increase this coefficient, but painting must also be "grey" or "black" in the infrared frequency range, not only range of visible light. Typical values are c_s = 4...5·10^{-8} W/(m^{2}K^4). Taking typical temperature difference for electric machines $\Delta\vartheta$ = 80...100 K and ambient temperature of T_2 = 300 K (corresponding to about 27 °C) yields a heat transfer, which equals convection heat transfer at α = 7 W/(m^{2}K). Thus heat transfer due to radiation contributes only with rather low values, as temperatures are too low for effective heat radiation.

Example 3.2-3:
Hot heat sink of power electronic device: Radiated losses at c_s = 5·10^{-8} W/(m^{2}K^4)
Temperature difference between heat sink & ambient: $\Delta\vartheta$ = 80 K, ambient temperature 20 °C

T_2 = 20 + 273.15 = 293.15 K
$T_1 = T_2 + \Delta\vartheta$ = 293.15 + 80 = 373.15 K

- Heat flow density: $q = \frac{P_{th}}{A} = c_s (T_1^4 - T_2^4) = 5 \cdot 10^{-8} \cdot (373.15^4 - 293.15^4) = \underline{\underline{600.1}}\,\text{W/m}^2$

How big is an equivalent heat transfer coefficient for convection heat transfer ?

$$\alpha = \frac{P_{th}}{A \cdot \Delta\vartheta} = \frac{q}{\Delta\vartheta} = \frac{600.1}{80} = \underline{\underline{7.5}}\,\text{W/m}^2\text{K}$$

b) Storage of heat energy:

A body with mass m and specific heat capacity c is heated up due to in-flow of thermal power P_{th} , yielding temperature rise (or rise of temperature difference)

$$mc \frac{d\vartheta}{dt} = P_{th} \quad , \quad mc \frac{d\Delta\vartheta}{dt} = P_{th} \quad . \qquad (3.2\text{-}5)$$

In analogy to electric network mc corresponds with electric capacity C.

$$mc\frac{d\Delta\vartheta}{dt} = P_{th} \quad \Rightarrow \quad C\frac{du}{dt} = i \qquad . \tag{3.2-6}$$

Heat is stored in the mass like electric charge is stored in electric capacity.

Material	*Specific heat capacity c* Ws/(kg·K)	*Mass density* γ kg/m^3
Air (at constant pressure)	1009	1.226 (at 25 °C)
Copper	388.5	8900
Iron	502	7850
Epoxy resin	1320 ... 1450	1500

Table 3.2-3: Specific heat capacity for some materials used in electric machines

Example 3.2-4:
Stored heat in volume $V = 1$ dm^3 of a) air, b) copper, c) iron, heated up from 20°C to 100°C:

$$W_{th} = \int_{t=0}^{t} P_{th}\cdot dt = \int_{t=0}^{t} mc\frac{d\Delta\vartheta}{dt}\cdot dt = \int_{\Delta\vartheta=0}^{\Delta\vartheta} mc\cdot d\Delta\vartheta = mc\cdot\Delta\vartheta \quad \Rightarrow \quad W_{th} = \gamma\cdot V\cdot c\cdot\Delta\vartheta$$

$$\Delta\vartheta = 100 - 20 = 80\,\mathrm{K}$$

a) Air: $W_{th} = 1.226\cdot 10^{-3}\cdot 1009\cdot 80 = \underline{\underline{99}}\,\mathrm{J}$

b) Copper: $W_{th} = 8900\cdot 10^{-3}\cdot 388.5\cdot 80 = \underline{\underline{276.6}}\,\mathrm{kJ}$

c) Iron: $W_{th} = 7850\cdot 10^{-3}\cdot 502\cdot 80 = \underline{\underline{315.3}}\,\mathrm{kJ}$

3.3 Heat-source plot

In Fig.3.3-1 cross-section of induction machine is shown with copper losses in slot conductors of stator and rotor $P_{Q,s}$, $P_{Q,r}$, in winding overhangs $P_{b,s}$, $P_{b,r}$ and iron losses in stator and rotor iron stack $P_{Fe,s}$, $P_{Fe,r}$.

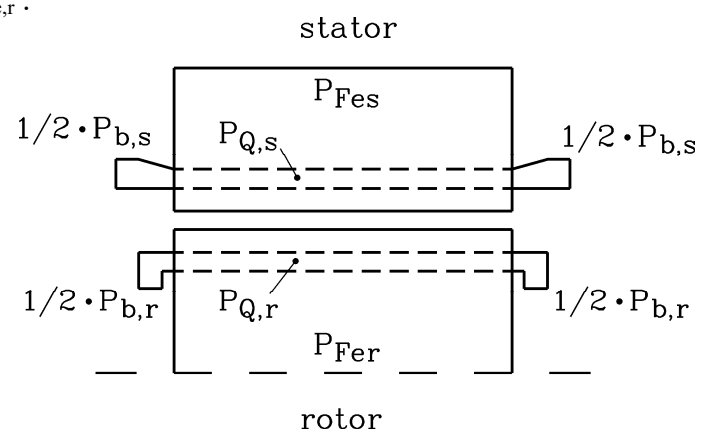

Fig. 3.3-1: Cross-section of induction machine with copper losses in slot conductors of stator and rotor $P_{Cu,Q,s}$, $P_{Cu,Q,r}$, in winding overhangs $P_{Cu,b,s}$, $P_{Cu,b,r}$ and iron losses in stator and rotor iron stack $P_{Fe,s}$, $P_{Fe,r}$

The corresponding **heat-source plot** considers not only the distributed losses as 8 heat sources, given by circles (which correspond with current sources in electrical network), but also the 13 heat resistances between these 8 sources (Fig.3.3-2):

- heat conductance in copper wire of winding R_c from slot to winding overhang,
- heat conductance from copper to iron via slot insulation R_I,
- heat conductance from rotor to stator iron via air gap R_δ,

- heat convection from winding overhang to surrounding air R_b ,
- heat convection from stator and rotor iron to surrounding air R_{Fe} .

Assuming the temperature difference in the surrounding air to be zero, the calculation of temperature difference in the 8 nodes is given by *Kirchhoff*'s laws. Usually calculation of heat resistances in advance is rather uncertain, so measurement of temperature in those 8 nodes of a prototype machine under steady state heating ($d/dt = 0$) with known losses is used to derive the value of the 13 resistances from measurement. By taking only 5 mesh equations and the 8 node equations with known 8 loss components and resistances on gets 13 linear algebraic equations for determination of the 13 resistances. With the geometry parameters of the prototype machine one can determine the values of α and λ_{th}. These values can be used for other machines with similar cooling system, but different geometry parameters to calculate temperature distribution in advance.

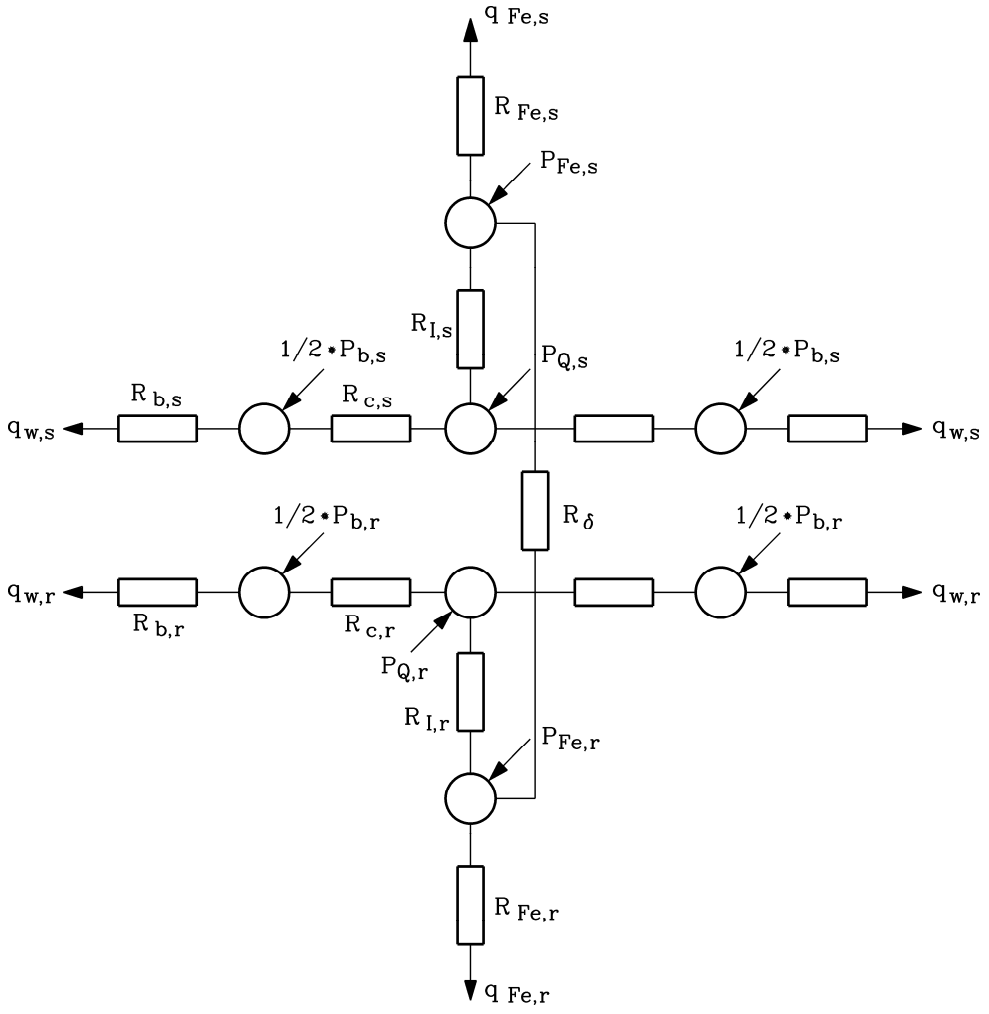

Fig. 3.3-2: Heat-source plot of the cross-section of induction machine of Fig. 3.3-1

Example 3.3-1:

Totally enclosed cage induction machine with shaft mounted fan, 11 kW, 4-pole, 50 Hz, 1450/min rated speed, Thermal Class B:

At rated speed and load the following losses are calculated (Fig. 3.3-3a):

- Copper losses in stator slot conductors and winding overhangs: $P_{Q,s} + P_{b,s} = P_{Cu,s} = 554$ W
- Iron losses in stator: teeth: $P_{Fe,d,s} = 82$ W, yoke: $P_{Fe,y,s} = 178$ W: $P_{Fe,s} = 260$ W
- *Ohmic* losses in rotor cage (= slot conductors and rings): $P_{Q,r} + P_{b,r} = P_{Cu,r} = 556$ W
- Rotor iron losses are very low due to low rotor frequency of 1.7 Hz: $P_{Fe,r} = 0$

Measured temperature differences over ambient (measured with thermo-couples):
- Stator housing surface: 30 K
- Stator end shield, where fan is blowing: 25 K
- Stator iron yoke: 44.5 K
- Stator iron teeth at air gap: 50 K
- Stator copper winding: 67 K
- Rotor iron surface at air gap: 54 K
- Rotor cage bar: 93 K

According to Fig. 3.3-3 the heat flows from rotor cage to stator end shield via air and to stator iron teeth via air gap. Heat flows from the stator winding via the insulation to the stator teeth and via yoke to the stator surface. With measured temperatures and calculated losses the thermal resistances R_{th} or their inverse, the thermal heat conductances $G_{th} = 1/R_{th}$ are derived from the heat-source plot (Fig. 3.3-3b).

a)

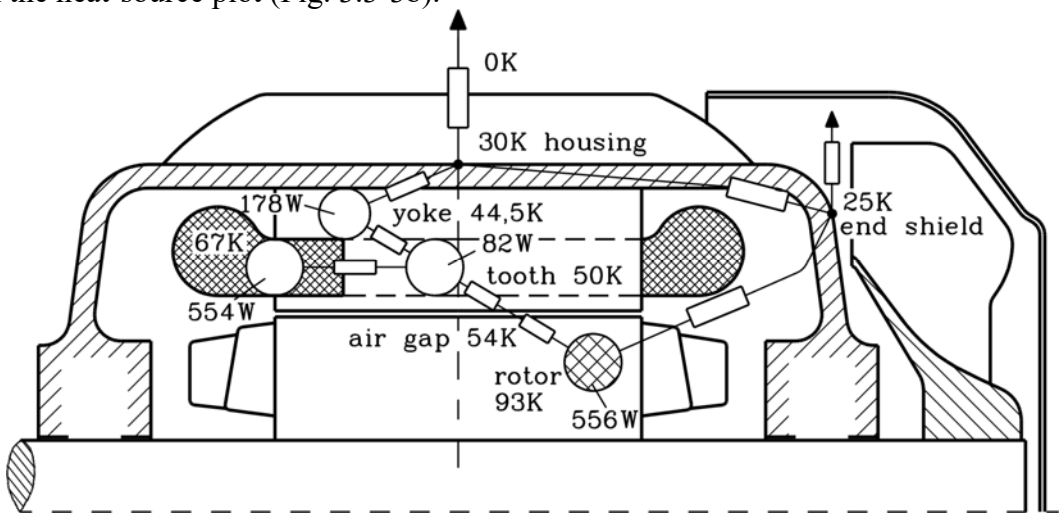

b)

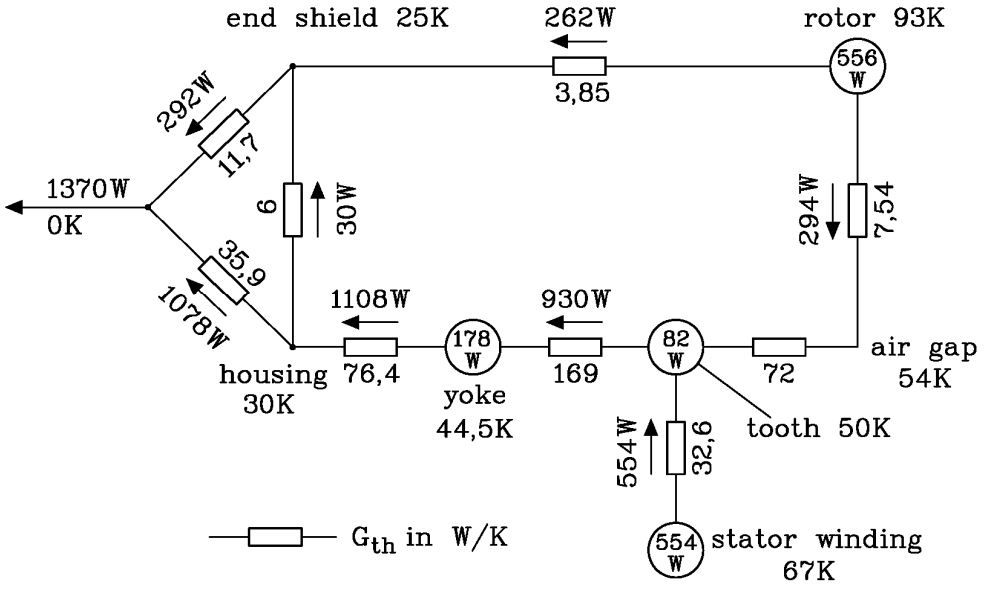

Fig. 3.3-3: Calculation of heat conductances G_{th} from (a) measured temperatures and calculated losses with a (b) heat-source plot

Simplified thermal network is analysed, considering only copper and iron losses in stator and thermal resistance between copper and iron due to slot insulation R_{th2}, heat convection from winding overhang to air R_{th3} and heat convection from iron to air R_{th1} (Fig. 3.3-4).

Loss sources:
Stator copper losses in winding P_{Cu}
Stator iron losses in stator iron stack P_{Fe}

Heat storage:
Copper mass: m_{Cu}
Iron mass: m_{Fe}

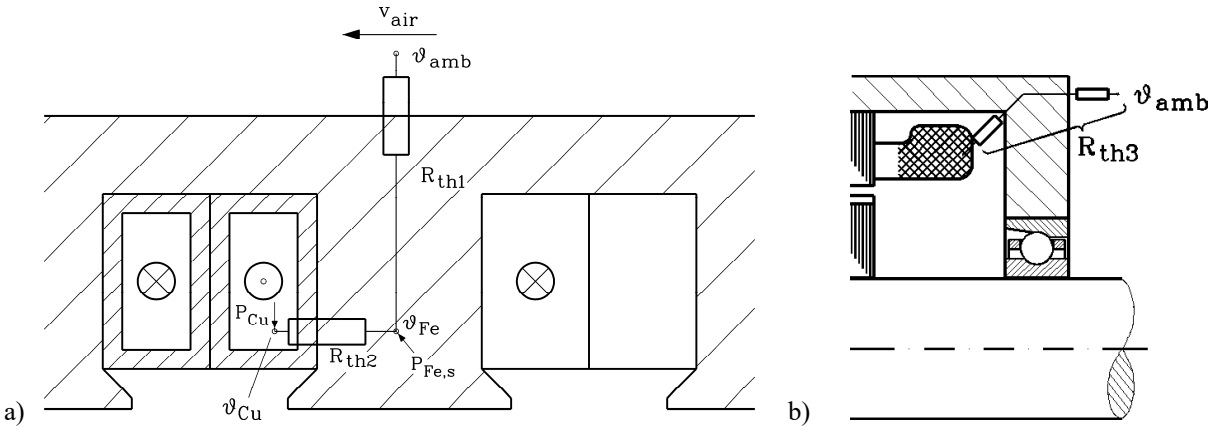

Fig. 3.3-4: Schematic cross section of (a) stator winding in slots and (b) of winding overhang

Heat resistances:

(i) R_{th1} between stator iron and ambient cooling air, given by convection: $R_{th1} = 1/(\alpha A_G)$, where A_G is the surface of the stator iron housing (Fig. 3.3-5).

(ii) R_{th2} between slot conductor copper and iron stack, mainly determined by heat resistance of slot insulation: $R_{th2} = d/(\lambda_{is} A_Q)$, where A_Q is slot surface, λ_{is} is thermal conductivity of slot insulation and d is thickness of slot insulation.

(iii) R_{th3} between winding overhang and surrounding air, given by convection.

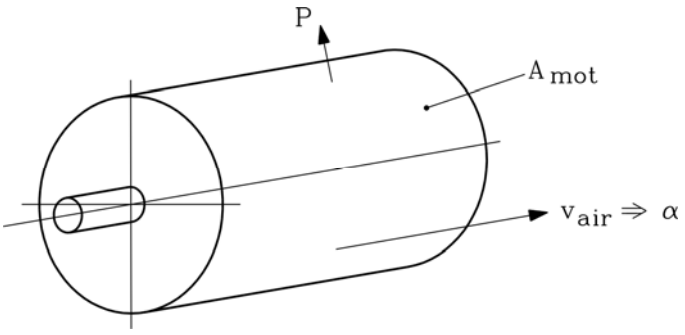

Fig. 3.3-5: Convective heat transfer at motor surface

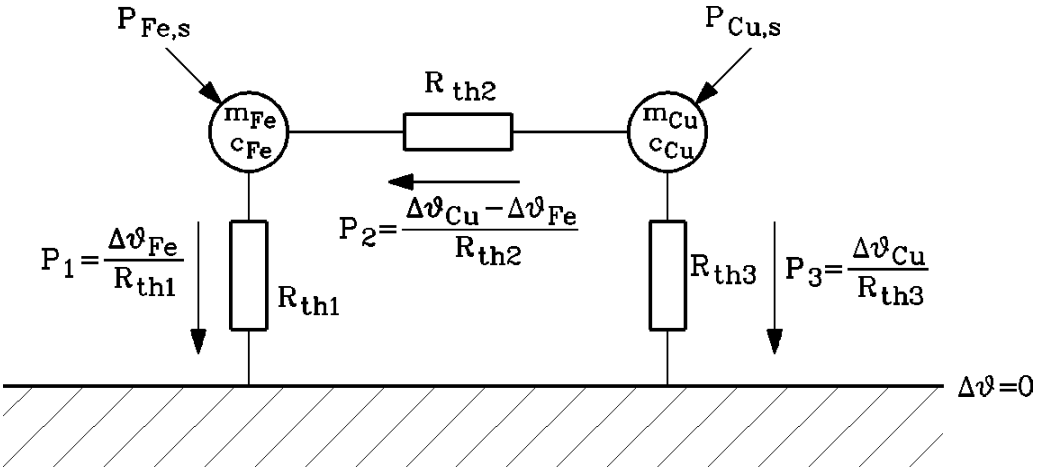

Fig. 3.3-6: Thermal equivalent network for motor cross section of Fig. 3.3-4

Temperature difference between motor local temperature and ambient temperature of surrounding air is $\Delta\vartheta = \vartheta - \vartheta_{amb}$. The two **unknown temperature differences** of copper $\Delta\vartheta_{Cu}$ and iron $\Delta\vartheta_{Fe}$ are determined by one mesh equation and one node equation of *Kirchhoff*´s laws, yielding the two linear differential equations

$$m_{Cu}c_{Cu}\frac{d\Delta\vartheta_{Cu}}{dt} + \frac{\Delta\vartheta_{Cu}}{R_{th3}} + \frac{\Delta\vartheta_{Cu} - \Delta\vartheta_{Fe}}{R_{th2}} = P_{Cu} \tag{3.3-1}$$

$$m_{Fe}c_{Fe}\frac{d\Delta\vartheta_{Fe}}{dt} + \frac{\Delta\vartheta_{Fe}}{R_{th1}} - \frac{\Delta\vartheta_{Cu} - \Delta\vartheta_{Fe}}{R_{th2}} = P_{Fe} \tag{3.3-2}$$

We solve these two equations for several special cases:

a) **„Homogenous-body problem“:** If we put $R_{th3} = \infty$, $\Delta\vartheta_{Fe} = 0$, only the heating of copper winding is considered, where copper is represented by a single, homogenous body.

$$m_{Cu}c_{Cu}\frac{d\Delta\vartheta_{Cu}}{dt} + \frac{\Delta\vartheta_{Cu}}{R_{th2}} = P_{Cu} \tag{3.3-3}$$

Only first order linear differential equation remains. Solution for initial condition $\Delta\vartheta_{Cu}(0) = 0$:

$$\Delta\vartheta_{Cu} = P_{Cu}R_{th2}(1 - e^{-t/T_\vartheta}) \tag{3.3-4}$$

with **thermal time constant**

$$T_\vartheta = m_{Cu}c_{Cu}R_{th2} \quad . \tag{3.3-5}$$

Example 3.3-2:

11 kW cage induction motor, frame size 160 mm, totally enclosed, 50 Hz, four poles, shaft mounted fan, motor mass 76 kg, stator winding copper mass 4.4 kg, ambient temperature 30°C, $P_{Cu,s} = 554W$, $R_{th2} = 0.12$ K/W:

- Steady state over-temperature: $\Delta\vartheta_{Cu,s} = P_{Cu,s}R_{th2} = 554 \cdot 0.12 = \underline{\underline{66.5K}}$
- Steady state winding temperature: $\vartheta_{Cu,s} = \Delta\vartheta_{Cu,s} + \vartheta_{amb} = 66.5K + 30°C = \underline{\underline{96.5°C}}$
- Thermal time constant: $T_\vartheta = 4.4 \cdot 388.5 \cdot 0.12 = 205s = \underline{\underline{3.4}}\,\text{min}$

Facit:

Thermal time constant of copper winding is rather short. Heating up total motor mass takes much longer, which can be estimated by the ratio of motor mass versus copper mass:

$T_{\vartheta,mot} = 76/4.4 \cdot 3.4 = \underline{\underline{35.7}}\,\text{min}$

Note that this time constant corresponds to electric time constant $T = C \cdot R$ in electric capacitive-resistive circuit. Steady state temperature $\Delta\vartheta_\infty = P_{Cu}R_{th2}$ is reached after about three time constants: $\Delta\vartheta_{Cu}(3T_\vartheta) = P_{Cu}R_{th2}(1 - e^{-3}) = 0.95 \cdot \Delta\vartheta_\infty$.

b) **„Two-body problem“**: This corresponds to both equations (3.3-1), (3.3-2) and describes heating up of both copper winding AND iron stack, so TWO thermal time constants are valid, a short one for the copper and a long one for the iron.

c) **Steady state temperature rise:** This corresponds to *d/dt* = 0, as no further change of temperature occurs. One gets this condition e.g. in case a) from (3.3-4) for $t \to \infty$ or in reality for $t > 3T_\vartheta$. With *d/dt* = 0 we get from (3.3-1), (3.3-2) two algebraic linear equations

$$\frac{\Delta\vartheta_{Cu}}{R_{th3}} + \frac{\Delta\vartheta_{Cu} - \Delta\vartheta_{Fe}}{R_{th2}} = P_{Cu} \tag{3.3-6}$$

$$\frac{\Delta\vartheta_{Fe}}{R_{th1}} - \frac{\Delta\vartheta_{Cu} - \Delta\vartheta_{Fe}}{R_{th2}} = P_{Fe} \tag{3.3-7}$$

For totally enclosed machine with shaft mounted fan external air flow on machine surface is big, so convection at housing surface is much better than internal convection at winding overhangs. Thus $R_{th3} >> R_{th1}$, R_{th2}, which leads to simplified solution of (3.3-6), (3.3-7):

$$\Delta\vartheta_{Fe} = (P_{Fe} + P_{Cu})R_{th1} \tag{3.3-8}$$

$$\Delta\vartheta_{Cu} = P_{Cu}R_{th2} + \Delta\vartheta_{Fe} \tag{3.3-9}$$

So copper winding has higher temperature than iron. Insulation temperature is nearly the same as copper temperature and defines Thermal Class. Neglecting heat flow from winding overhangs to surrounding air means, that **HOT SPOT** of temperature distribution occurs in winding overhangs.

Example 3.3-3:
11 kW cage induction motor, Thermal Class F, frame size 160 mm, totally enclosed, 50 Hz, four poles, shaft mounted fan, motor mass 76 kg,
$P_{Cu,s} = 554W$, $P_{Fe,s} = 260W$, $R_{th2} = 0.047K/W$, $R_{th1} = 0.072K/W$:
- Steady state temperature rise:
  - In stator iron: $\Delta\vartheta_{Fe,s} = (P_{Fe,s} + P_{Cu,s})R_{th1} = (260 + 554) \cdot 0.072 = \underline{\underline{58.6K}}$
  - In stator winding: $\Delta\vartheta_{Cu,s} = P_{Cu,s}R_{th2} + \Delta\vartheta_{Fe,s} = 554 \cdot 0.047 + 58.6 = \underline{\underline{84.6K}} < 105K$

  The winding temperature rise does not exceed the Thermal Class F limit.

3.4 Thermal utilization

If only copper losses are considered as heat source, and if only convection heat transfer from machine surface to surrounding air flow is taken into account ($\Delta\vartheta_{Fe}$ = 0, R_{th2} = 0) for determination of steady state temperature rise, then (3.3-8), (3.3-9) yield:

$$\Delta\vartheta_{Cu} = P_{Cu}R_{th1} \quad . \tag{3.4-1}$$

Taking copper losses as

$$P_{Cu} = m \cdot \frac{1}{\kappa} \frac{N \cdot 2(l_{Fe} + l_b)}{a_a A_{Cu}} I^2 \tag{3.4-2}$$

and convection thermal resistance as

$$R_{th1} = \frac{1}{\alpha A_G} \quad , \tag{3.4-3}$$

we get with **current loading** $A = \frac{2mNI}{2p\tau_p}$ and **current density** $J = \frac{I}{a_a A_{Cu}}$ for steady state temperature rise in copper:

$$\Delta\vartheta_{Cu} = A \cdot J \cdot \frac{1}{\alpha \cdot \kappa} \frac{2p\tau_p (l_{Fe} + l_b)}{A_G} \quad \Rightarrow \quad \underline{\Delta\vartheta_{Cu} \sim A \cdot J} \tag{3.4-4}$$

This is the already noted **thermal utilization** of Chapter 1, which defines as a rough estimate stator winding temperature rise.

Example 3.4-1:
For Thermal Class F: (IEC60034-1): $\Delta\vartheta_{Cu}$ = 105 K at ϑ_{amb} = 40°C for standard induction machine (totally enclosed, shaft-mounted fan):
Typical values: A = 250 A/cm, J = 7 A/mm^2: $A{\cdot}J$ = 1750 A/cm·A/mm^2

Influence of machine size (defined by frame size, which may be taken as "characteristic length" l) leads to **„scaling effect**": Bigger machines need for IDENTICAL temperature rise a lower current density and a lower thermal utilization $A{\cdot}J$ than smaller machines, which is easily understood by considering copper volume V_{Cu} and cooling surface A_G:

$$\Delta\vartheta_{Cu} = P_{Cu} R_{th1} = \frac{J^2 V_{Cu}}{\kappa \cdot \alpha A_G} \sim J^2 \frac{V_{Cu}}{A_G} \sim J^2 \frac{l^3}{l^2} = J^2 l = const. \tag{3.4-5}$$

$$J \sim \sqrt{\frac{\Delta\vartheta_{Cu}}{l}} \tag{3.4-6}$$

Example 3.4-2:
Thermal Class F: (IEC60034-1) $\Delta\vartheta_{Cu}$ = 105 K at ϑ_{amb} = 40°C: Totally enclosed machine, shaft-mounted fan: Typical current density: (big machine) 3 ... (small machine) 7 A/mm^2

3.5 Simplified calculation of temperature rise

Simplified calculation for winding temperature rise considers machine as **„Homogenous-body replica":** Total losses P_d within machine are taken as heat source, convection heat transfer from machine surface A to coolant flow is taken as heat resistance: $R_{th} = \frac{1}{\alpha A}$, and total motor mass with equivalent specific thermal capacity is taken for heat storage.

$$m \cdot c \cdot \frac{d\Delta\vartheta_{Cu}}{dt} + \alpha \cdot A \cdot \Delta\vartheta_{Cu} = P_d \tag{3.5-1}$$

Initial condition is winding over-temperature at t = 0: $\Delta\vartheta_{Cu}(0) = \Delta\vartheta_0$. We assume at t = 0 switching on of machine, thus losses follow a step function (Fig. 3.5-1). Solution is

$$\Delta\vartheta_{Cu} = \Delta\vartheta_\infty \cdot (1 - e^{-t/T_\vartheta}) + \Delta\vartheta_0 \cdot e^{-t/T_\vartheta} \quad , \tag{3.5-2}$$

where

$$\Delta\vartheta_\infty = \frac{P_d}{\alpha \cdot A} \tag{3.5-3}$$

is **steady state temperature rise** and

$$T_\vartheta = \frac{m \cdot c}{\alpha \cdot A} \tag{3.5-4}$$

is homogenous-body **thermal time constant**.

Facit:
Thermal time constant increases with mass and decreases with increase of cooling effectiveness. Scaling effect yields with $m \sim l^3$, $A \sim l^2$ *for thermal time constant* $T_\vartheta \sim l$, *so thermal time constant rises with motor size.*

Example 3.5-1:
Shaft-mounted fan, rated speed:
Small machines: $T_\vartheta \cong 10\,\text{min}$ (several 100 W), big machines: $T_\vartheta \cong 3\,\text{h}$ (several MW).

Example 3.5-2:
11 kW cage induction motor, frame size 160 mm, totally enclosed, 50 Hz, four poles, shaft mounted fan, motor mass 76 kg, motor cooling surface (increased surface by cooling fins):
$A_G = 0.9\ \text{m}^2$, velocity of air flow $v = 9\ \text{m/s} = 32\ \text{km/h}$

- Bare metallic surface: $\alpha = 15 v^{2/3} = 15 \cdot 9^{2/3} = 64.9\ \text{W/m}^2\text{K}$
- $T_\vartheta = \frac{m_{mot} \cdot c_{Fe}}{\alpha \cdot A_G} = \frac{76 \cdot 502}{64.9 \cdot 0.9} = 653 s = \underline{\underline{10.9}}\ \text{min}$

Note that **machines with shaft mounted fan** have shorter thermal time constant T_ϑ, when rotating, as fan blows, yielding high heat transfer coefficient α, and longer thermal time constant $T_{\vartheta,St}$ at **stand still**, as air is not moved any longer, yielding low value of α. Typical ratios are

$$T_{\vartheta,St} = (1.5 \ldots 2.0) \cdot T_\vartheta \quad . \tag{3.5-5}$$

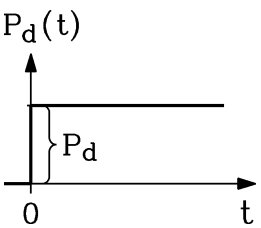

Fig. 3.5-1: Losses in switched-on machine as step function

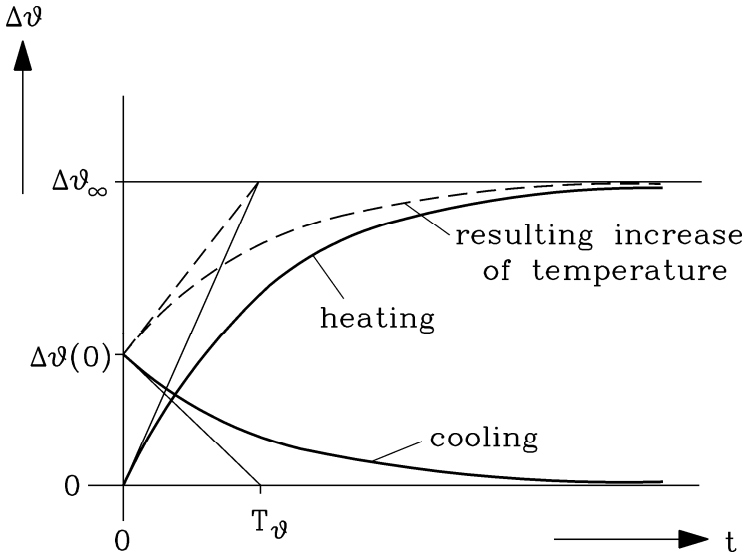

Fig. 3.5-2: Temperature rise from $\Delta\vartheta_0$ may be understood as superposition of temperature rise from $\Delta\vartheta = 0$ due to losses and temperature decrease from $\Delta\vartheta_0$ due to cooling effect

Thus temperature rise from $\Delta\vartheta_0$ may be understood as superposition of temperature rise from $\Delta\vartheta = 0$ due to losses and temperature decrease from $\Delta\vartheta_0$ due to cooling effect (Fig. 3.5-2). So, if losses are zero, one gets as special case from (3.5-2) the cooling of winding from $\Delta\vartheta_0$ down to zero:

$$\Delta\vartheta_{Cu} = \Delta\vartheta_0 \cdot e^{-t/T_\vartheta} \quad , \tag{3.5-6}$$

and if $\Delta\vartheta_0 = 0$, one gets the special case for heating up the winding from zero. This is the case, when electric machines are tested during the thermal load run in the test bay. Steady state temperature rise of winding must stay below maximum admissible temperature rise according to Table 3.1-1. This defines rated power of electric machine for continuous duty S1.

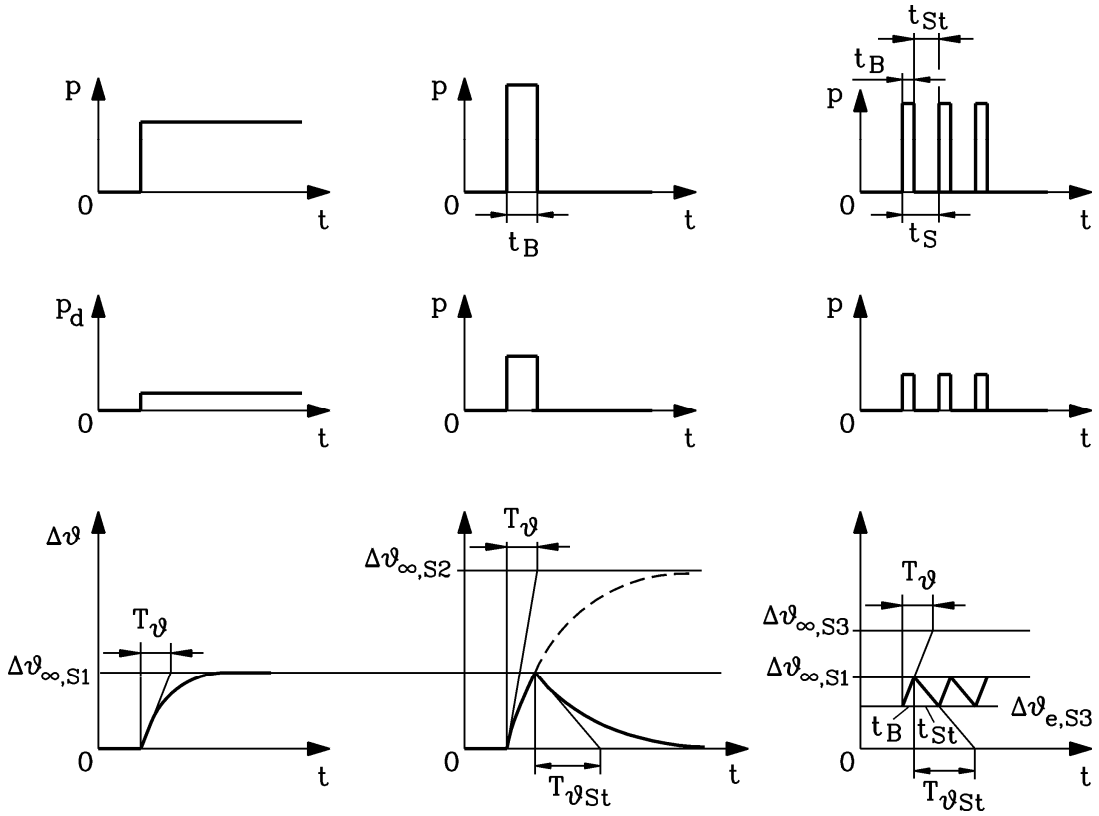

Fig. 3.5-3: Power and loss function and temperature rise and fall for duty type S1 (left), S2 (middle) and S3 (right).

a) Temperature rise at continuous duty S1:
According to Fig. 3.5-3 the S1 operation leads to temperature rise, which under simplified considerations follow one dominant thermal time constant T_ϑ. Machine power $p(t)$ and losses $p_d(t)$ follow at these idealized conditions a step function. Steady state machine power and losses is limited to that value, where temperature rise reaches admissible limit of used Thermal Class $\Delta\vartheta_{\infty,S1}$.

b) Temperature rise at short time duty S2:
Machine is operated only during time t_B (e.g. 10, 30, 60, 90 min.) and is afterwards cooled down to ambient temperature. This duty type is used e.g. for crane motors. Time constant for temperature rise is shorter than time constant for cooling down, if shaft mounted fan is used. Motor power in S2 may be increased over S1 value to such extent, **that Thermal Class temperature rise limit of S1 duty $\Delta\vartheta_{\infty,S1}$ is reached at time $t = t_B$** (Fig. 3.5-3). Continuous

duty is NOT possible with this increased power P_{S2}, because steady state temperature rise $\Delta\vartheta_{\infty,S2}$ would exceed the admissible limit by the ratio of increased losses $P_{d,S2}$ /$P_{d,S1}$.

$$\Delta\vartheta(t_B) = \Delta\vartheta_{\infty,S2} \cdot \left(1 - e^{-t_B/T_\vartheta}\right) \leq \Delta\vartheta_{\infty,S1} \tag{3.5-7}$$

Line-operated machines are supplied with constant voltage U_s. Output power is therefore proportional to stator current I_s, as power factor and efficiency at rated (S1) and overload (S2) conditions are nearly the same.

$$P = 3 \cdot U_s I_s \cdot \cos\varphi_s \cdot \eta \sim I_s \tag{3.5-8}$$

If consider only copper losses, neglecting iron and friction losses, the total losses P_d are proportional to I_s^2 :

$$P_d \approx P_{Cu,s+r} = 3 \cdot (R_s I_s^2 + R_r' I_r'^2) \approx 3 \cdot (R_s + R_r') \cdot I_s^2 \sim I_s^2 \tag{3.5-9}$$

Thus maximum possible overload power P_{S2} for given operation time t_B occurs, if $\Delta\vartheta(t_B) = \Delta\vartheta_{\infty,S1}$. It may be estimated from power P_{S1} with (3.5-7):

$$\frac{P_{S2}}{P_{S1}} = \frac{I_{s,S2}}{I_{s,S1}} = \sqrt{\frac{P_{d,S2}}{P_{d,S1}}} = \sqrt{\frac{\Delta\vartheta_{\infty,S2}}{\Delta\vartheta_{\infty,S1}}} = \frac{1}{\sqrt{1 - e^{-t_B/T_\vartheta}}} \tag{3.5-10}$$

Example 3.5-3:
500 kW cage induction motor, thermal time constant T_ϑ = 40 min. Motor shall be operated in S2 duty with operation time t_B = 30 min.

$$\frac{P_{S2}}{P_{S1}} = \frac{1}{\sqrt{1 - e^{-t_B/T_\vartheta}}} = \frac{1}{\sqrt{1 - e^{-30/40}}} = \sqrt{1.9} = \underline{\underline{1.38}}$$

Motor power may be increased for S2-operation by 38% up to 690 kW.

c) Temperature rise at intermittent periodic duty S3:
Machine is operated periodically during time t_B and is switched of during stand still time t_{St}. **(**Fig. 3.5-3). Staring and braking phase with corresponding losses – which usually last only several seconds - are neglected in that case. Total time of operating period is $t_S = t_B + t_{St}$. Typical relative time of operation, given in percentage of operation period, is

$t_B / t_S = 15\%, 25\%, 40\%, 60\%$.

Usually time t_B and t_{St} last only several minutes and are therefore significantly shorter than thermal time constant: $t_B << T_\vartheta, t_{St} << T_{\vartheta,St}$. So the linear approximation of the temperature curve may be used for heating up and cooling down (Fig. 3.5-4). By combination of linear heating up and cooling down of Fig. 3.5-4, one gets the increase of temperature rise from cold condition according to Fig. 3.5-5. After several periods t_S a stationary temperature cycle is reached. At maximum admissible power P_{S3}, corresponding with maximum admissible losses $P_{d,S3}$, the **upper value of temperature rise** is a the limit $\Delta\vartheta_{\infty,S1}$. The **lower value of temperature rise** at the end of t_{St} is $\Delta\vartheta_{e,S3}$ (Fig. 3.5-6). According to Fig. 3.5-4 and Fig. 3.5-6 we get the following relationships, using linear temperature rise and fall:

$$\Delta\vartheta_{\infty,S1} - \Delta\vartheta_{e,S3} = \Delta\vartheta_{\infty,S1} \cdot \frac{t_{St}}{T_{\vartheta,St}} \tag{3.5-11}$$

$$\Delta\vartheta_{\infty,S1} - \Delta\vartheta_{e,S3} = (\Delta\vartheta_{\infty,S3} - \Delta\vartheta_{e,S3}) \cdot \frac{t_B}{T_\vartheta} \tag{3.5-12}$$

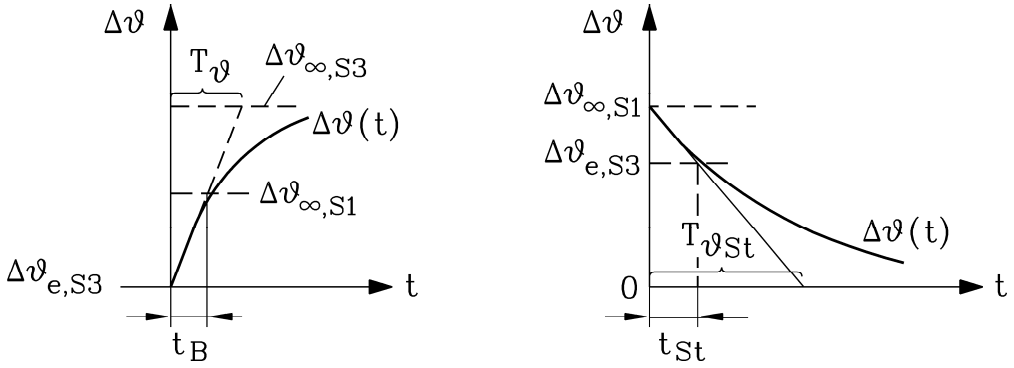

Fig. 3.5-4: If time t_B and t_{St} are much shorter than thermal time constant, linear approximation of temperature curve may be used for heating up (left) and cooling down (right).

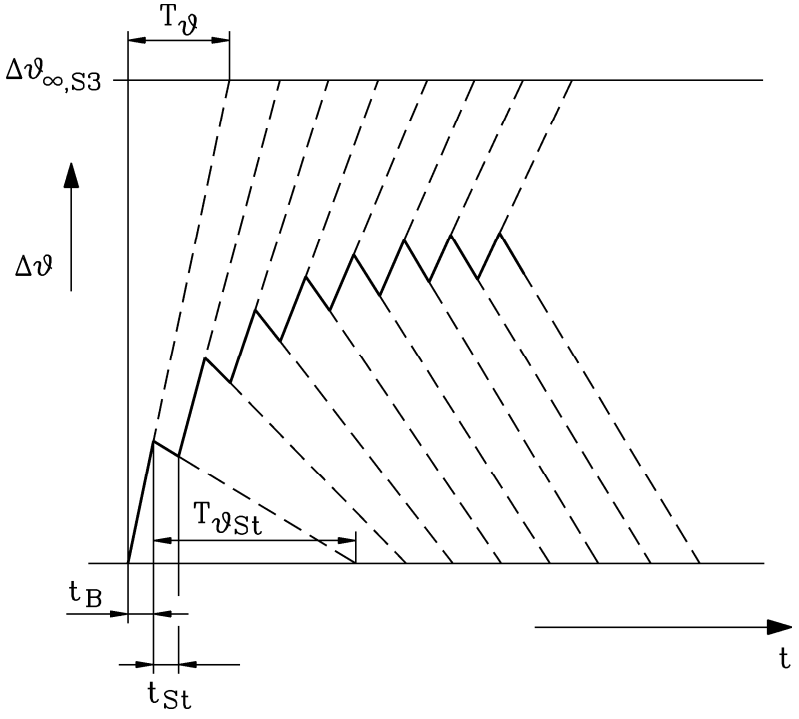

Fig. 3.5-5: Starting cold machine in S3 duty type with time t_B and t_{St} much shorter than thermal time constant. So linear approximation of temperature curve may be used for heating up and cooling down.

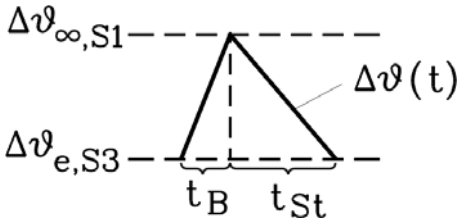

Fig. 3.5-6: Steady state temperature cycle at S3 duty type

By eliminating $\Delta\vartheta_{e,S3}$ from (3.5-11), (3.5-12), the ratio $\Delta\vartheta_{\infty,S3} / \Delta\vartheta_{\infty,S1}$ is derived. With that the relationship of admissible losses in S3 duty versus S1 duty is determined.

$$\frac{P_{d,S3}}{P_{d,S1}} = \frac{\Delta\vartheta_{\infty,S3}}{\Delta\vartheta_{\infty,S1}} = 1 + \frac{T_\vartheta \cdot t_{St}}{T_{\vartheta,St} \cdot t_B} - \frac{t_{St}}{T_{\vartheta,St}} \tag{3.5-13}$$

So increase of power in S3 duty is calculated with

$$\frac{P_{S3}}{P_{S1}} = \frac{I_{s,S3}}{I_{s,S1}} = \sqrt{\frac{P_{d,S3}}{P_{d,S1}}} = \sqrt{\frac{\Delta\vartheta_{\infty,S3}}{\Delta\vartheta_{\infty,S1}}} = \sqrt{1 + \frac{T_\vartheta \cdot t_{St}}{T_{\vartheta,St} \cdot t_B} - \frac{t_{St}}{T_{\vartheta,St}}} \quad . \tag{3.5-14}$$

Example 3.5-4:
500 kW cage induction motor, shaft mounted fan:
Thermal time constants T_ϑ = 40 min, $T_{\vartheta,St}$ = 80 min. Motor shall be operated in S3 duty with operation time t_B = 2 min, t_{St} = 3 min.

- $t_B / t_S = 2/(2+3) = 2/5 = \underline{\underline{40\%}}$
- $\frac{P_{S3}}{P_{S1}} = \sqrt{1 + \frac{T_\vartheta \cdot t_{St}}{T_{\vartheta,St} \cdot t_B} - \frac{t_{St}}{T_{\vartheta,St}}} = \sqrt{1 + \frac{40 \cdot 3}{80 \cdot 2} - \frac{3}{80}} = \sqrt{1.71} = \underline{\underline{1.31}}$

Motor power may be increased for S3-operation by 31% up to 655 kW.

d) Adiabatic temperature rise:
For short time overload, where considered time interval is much shorter than thermal time constant, the tangent at $t = 0$ in Fig. 3.5-2 may be used as approximation for temperature rise. So for that short time temperature rises linear according to $m \cdot c \cdot d\Delta\vartheta_{Cu} / dt = P_d$. For that short time no heat exchange with ambient structure is possible (*adiabatic* state); only the mass m is heated up. Heating up of rotor cage due to starting current may be considered as adiabatic heating, as usually start-up time is much shorter than thermal time constant of rotor cage.

Source: Winergy, Germany

a)

Source: ELIN-EBG Motoren GmbH, Austria

b)

Fig. 3.5-7: Wound rotor 4 pole, 60 Hz induction machines, used as doubly-fed generator in wind power plants:
a) Mounting of air-air heat exchanger with external fan visible during manufacturing, 1500 kW at 1800/min
b) Completed machine 2 MW, 600 V, 60 Hz, 1800/min +/-30% via rotor slip change

4. Dynamics of electrical machines

4.1 Motivation: Why do we need dynamic theory of electrical machines?

Controlled drives:
Modern electric machines are controlled such as speed control or torque control. Dynamic response to quick change of set-point value has to be calculated, so dynamic model of electric machinery is necessary.

Switching of electrical machines in normal operation:
Each industrial motor – controlled or non-controlled – has to be switched to the grid, so switching of machines is a transient operation, which needs dynamic model for calculation. But also sudden change of load, change of supply frequency for AC machines, change of supply voltage for AC and DC machines happen frequently, which have to be simulated for prediction of safe operation, needing dynamic machine models.

Failures in electrical machines:
Sudden short circuit of electrical machines, interruption of phase voltages, broken rotor bars such as in induction machines for electric traction, must be investigated for understanding of mechanical and electric overload of machines and also for the supplied/supplying grid.

Inverter operation:
Inverter operation is a supply of electrical machines with switched voltage, so each switching instant is a transient operation mode, which needs dynamic machine model for understanding non-sinusoidal machine current at inverter operation.

Stability of operation:
DC and AC machines in non-controlled mode tend to run unstable in certain points of operation such as shunt excited or separately excited DC motors without compensation winding, series excited DC generators feeding batteries, AC synchronous machines at big load angle, AC induction machines at big stator resistance or low stator frequency, AC synchronous reluctance machines at low frequency supply. Investigation of stability leads to calculation of oscillation of speed, current and torque, and the correlated damping or amplification of oscillation in case of stable or unstable operation, which needs dynamic modelling of electrical machinery.

Facit:
For switching of motors, sudden failures, for response of machines to controller operation, for inverter operation and for investigation of stability dynamic modelling of electric machines is necessary.

4.2 Methods for calculation of transient machine operation

4.2.1 Differential equations instead of algebraic equations

Dynamics of electric machines means rapid change of speed, torque, voltage and current in case of DC machines, so e.g. for a coil with resistance R and inductance L instead of **constant DC values** U and I we have to consider **"arbitrary" time variation** $u(t)$ and $i(t)$:

$$U = R \cdot I \quad \rightarrow \quad u(t) = R \cdot i(t) + L \cdot di(t)/dt \qquad (4.2.1\text{-}1)$$

Instead of algebraic equation the correlated differential equation has to be solved. For AC machines, instead of sinusoidal time function of $u(t)$ and $i(t)$ with constant amplitude, frequency and phase shift φ , which lead to **complex phasor calculation**, in the same way "arbitrary" time variation $u(t)$ and $i(t)$ has to be taken into account:

$$\underline{U} = R \cdot \underline{I} + j\omega L \cdot \underline{I} \quad \rightarrow \quad u(t) = R \cdot i(t) + L \cdot di(t)/dt \tag{4.2.1-2}$$

As electric machines are electric-mechanical energy converters, the mechanical equations have to consider in dynamic not only constant electromagnetic generated force F_e or torque M_e and constant load F_s (or M_s), but time varying forces and torque $f_e(t)$, $m_e(t)$, $f_s(t)$, $m_s(t)$ and change of speed, called **acceleration** such as e.g. for linear movement of linear motor secondary with mass m:

$$F_e = F_s \quad \rightarrow m \cdot dv(t)/dt = f_e(t) - f_s(t) \tag{4.2.1-3}$$

4.2.2 Solving of linear differential equations

Differential equations in dynamic models have only **time *t* as variable**. So **initial conditions** of e.g. current $i(t = 0) = I_0$ must be known for solving the equations.

Example 4.2.2-2:
A coil with time-depending resistance $R(t)$ and inductance $L(t)$ is energized via an electrical voltage $u(t)$. The coil current $i(t)$ shall be determined. Give the differential equation!

Solution:
Coil flux linkage is time-depending: $\psi(t) = L(t) \cdot i(t)$. The sum of self-induced voltage and of resistive voltage drop must be covered by $u(t)$.

$$d\psi(t)/dt = d(L(t) \cdot i(t))/dt = i \cdot (dL/dt) + L \cdot (di/dt),$$

$$u(t) = R(t) \cdot i(t) + d\psi(t)/dt = R(t) \cdot i(t) + i(t) \cdot (dL/dt) + L(t) \cdot (di/dt),$$

$$u(t) = R_{eq}(t) \cdot i(t) + L(t) \cdot (di/dt) \qquad R_{eq}(t) = R(t) + (dL/dt)$$

If $i_1(t)$ and $i_2(t)$ are solutions of **linear differential equation,** then also $i_3(t) = i_1(t) + i_2(t)$ is a solution, e.g. for

$$R_{eq}(t) \cdot i(t) + L(t) \cdot di(t)/dt = 0 \tag{4.2.2-1}$$

we get as a proof:

$R_{eq}(t) \cdot i_1(t) + L(t) \cdot di_1(t)/dt = 0$ and $R_{eq}(t) \cdot i_2(t) + L(t) \cdot di_2(t)/dt = 0$:

$$R_{eq}(t) \cdot i_3(t) + L(t) \cdot di_3(t)/dt = R_{eq}(t) \cdot \left(i_1(t) + i_2(t)\right) + L(t) \cdot d\left(i_1(t) + i_2(t)\right)/dt =$$

$$= R_{eq}(t) \cdot i_1(t) + L(t) \cdot di_1(t)/dt + R_{eq}(t) \cdot i_2(t) + L(t) \cdot di_2(t)/dt = 0 + 0 = 0$$

In many cases the differential equation consists of non-zero "right side" such as

$$R_{eq}(t) \cdot i(t) + L(t) \cdot di(t)/dt = u(t) \neq 0 \tag{4.2.2-2}$$

and is called **in-homogenous differential equation**. In that cases solution of linear differential equation may be decomposed into two solutions, the **homogenous solution** (for right side is zero, called **homogenous differential equation**) and a partial solution for in-homogenous differential equation. As differential equation is linear, also the sum of homogenous and partial solution is solution, yielding the final solution. For finding solution functions different approaches are known. One method for solving differential equation without decomposition into homogenous and in-homogenous part is *Laplace* transformation, which is discussed below.

Example 4.2.2-2:

Solving $R_{eq}(t) \cdot i(t) + L(t) \cdot di(t)/dt = u(t)$ leads to:

- homogenous differential equation:

$$R_{eq}(t) \cdot i_h(t) + L(t) \cdot di_h(t)/dt = 0$$

- particular solution of in-homogenous differential equation:

$$R_{eq}(t) \cdot i_p(t) + L(t) \cdot di_p(t)/dt = u(t)$$

Final solution: $i(t) = i_h(t) + i_p(t)$

Proof:

$$\left.\begin{aligned} R_{eq}(t) \cdot i_h(t) + L(t) \cdot di_h(t)/dt = 0 \\ R_{eq}(t) \cdot i_p(t) + L(t) \cdot di_p(t)/dt = u(t) \end{aligned}\right\} +$$

$$R_{eq}(t) \cdot \left(i_h + i_p\right) + L(t) \cdot d\left(i_h + i_p\right)/dt = u(t)$$

a) Linear differential equation with constant coefficients:

In (4.2.2-1) the coefficients $R_{eq}(t)$ and $L(t)$ varied with time, thus being not constant. A simpler case is, if coefficients are constant: $R_{eq}(t) = R$, $L(t) = L$. As long as differential equations are linear and have constant coefficients, solutions consist of exponential functions and sine and cosine functions (multiplied with powers of t such as t^{n-1}, t^{n-2}, …, $t^0 = 1$ in case of multiple zeros of the characteristic polynomial of the differential equation).

Example 4.2.2-3:

DC excitation of separately excited DC machine with DC exciting current I_f is short circuited: $u_f(t) = 0$. Decay of $i_f(t)$ due to losses in resistance of field coils R_f has to be calculated:

$R_f \cdot i_f(t) + L_f \cdot di_f(t)/dt = u_f = 0$, initial condition: $i_f(0) = I_f$

- Solving the differential equation:

$$i_f(t) = C \cdot e^{\lambda t}: \quad 0 = R_f \cdot C \cdot e^{\lambda t} + L_f \cdot d\left(C \cdot e^{\lambda t}\right)/dt = R_f \cdot C \cdot e^{\lambda t} + L_f \cdot \lambda \cdot C \cdot e^{\lambda t}$$

$$R_f + L_f \cdot \lambda = 0 \Rightarrow \lambda = -R_f / L_f$$

- Initial condition determines constant C:

$$i_f(0) = I_f = C \cdot e^{\lambda \cdot 0} = C$$

Solution: $\underline{\underline{i_f(t) = I_f \cdot e^{-\frac{t}{T}}}}$, time constant for current decay: $\underline{\underline{T = L_f / R_f}}$.

Example 4.2.2-4

DC excitation of separately excited DC machine switched to DC supply voltage U_f : $u_f(t) = U_f$
Increase of $i_f(t)$ due to that voltage has to be calculated: Initial condition: $i_f(0) = 0$.

$$R_f \cdot i_f(t) + L_f \cdot di_f(t)/dt = u_f(t) = U_f$$

- Solving homogenous differential equation:

$$i_h(t) = C \cdot e^{\lambda t} \rightarrow R_f + L_f \cdot \lambda = 0 \Rightarrow \lambda = -R_f / L_f$$

- Particular solution of in-homogenous differential equation: As "right side" is constant, also particular solution must be constant:

$$i_p(t) = K \rightarrow R_f \cdot K + L_f \cdot dK/dt = U_f \quad \rightarrow \quad K = U_f / R_f$$

- Initial condition determines constant *C*:

$$i_f(0) = i_h(0) + i_p(0) = C \cdot e^0 + K = 0: \quad C = -K$$

Solution: $\underline{\underline{i_f(t) = i_h(t) + i_p(t) = \frac{U_f}{R_f} \cdot \left(1 - e^{-\frac{t}{T}}\right)}}$, time constant: $\underline{\underline{T = L_f / R_f}}$.

b) Laplace transformation:
Mainly for linear differential equations with constant coefficients, *Laplace* transformation may be used, because this transformation is valid for time functions, which are zero for $t \leq 0$. Solving is done by transforming the differential equation depending on time t into an algebraic equation depending on the complex variable $\underline{s} = \alpha + j \cdot \omega$. Initial conditions are included in that algebraic equation. After solution of algebraic equation for variable $\underline{s}$ the inverse *Laplace* transformation delivers solution for time function, depending on t.

***Laplace* transform** of an arbitrary time function $f(t)$, which is zero for $t \leq 0$, is defined by

$$F(\underline{s}) = L\{f(t)\} = \int_{t=0}^{\infty} f(t) \cdot e^{-\underline{s} \cdot t} \cdot dt \quad . \tag{4.2.2-3}$$

Time function $f(t)$ corresponds with *Laplace* transform $F(\underline{s})$:

$$f(t) \leftrightarrow F(\underline{s}) \tag{4.2.2-4}$$

Inverse *Laplace* transformation allows determination of time function $f(t)$ from given complex *Laplace* transform:

$$f(t) = L^{-1}\{F(\underline{s})\} = \frac{1}{2\pi \cdot j} \int_{\underline{s}=\alpha - j\cdot\infty}^{\underline{s}=\alpha + j\cdot\infty} F(\underline{s}) \cdot e^{\underline{s} \cdot t} \cdot d\underline{s} \quad . \tag{4.2.2-5}$$

For many basic functions the *Laplace* transform is known (Table 4.2.2-1). **General rules** for *Laplace* transform are summarized in Table 4.2.2-2.

$f(t)$, $t > 0$ and zero, $t \le 0$	$F(\underline{s})$
K	$K/\underline{s}$
t	$1/\underline{s}^2$
t^n , $n = 1, 2, 3, ...$	$\frac{n!}{\underline{s}^{n+1}}$
$e^{b \cdot t}$	$\frac{1}{\underline{s}-b}$
$\sin(b \cdot t)$	$\frac{b}{\underline{s}^2 + b^2}$
$\cos(b \cdot t)$	$\frac{\underline{s}}{\underline{s}^2 + b^2}$
$\sinh(b \cdot t)$	$\frac{b}{\underline{s}^2 - b^2}$
$\cosh(b \cdot t)$	$\frac{\underline{s}}{\underline{s}^2 - b^2}$

Table 4.2.2-1: *Laplace* transforms of some basic functions

Linearity	$f_1(t) + f_2(t)$	$F_1(\underline{s}) + F_2(\underline{s})$
	$k \cdot f(t)$	$k \cdot F(\underline{s})$
Similarity	$f(t/b)$	$b \cdot F(b \cdot \underline{s})$
	$f(t \cdot c)$	$\frac{1}{c} \cdot F(\underline{s}/c)$
Shifting	$f(t-\tau)$	$e^{-\underline{s} \cdot \tau} \cdot F(\underline{s})$
	$f(t) \cdot e^{-b \cdot t}$	$F(\underline{s}+b)$
Differentiation	$df/dt = f'$	$\underline{s} \cdot F(\underline{s}) - f(0)$
	$d^2 f/dt^2 = f''$	$\underline{s}^2 \cdot F(\underline{s}) - \underline{s} \cdot f(0) - f'(0)$
	$d^n f/dt^n = f^{(n)}$, $n = 1, 2, ...$	$\underline{s}^n F(\underline{s}) - \underline{s}^{n-1} f(0) - \underline{s}^{n-2} f'(0) - - ... - f^{(n-1)}(0)$
Integration	$\int_0^t \int_0^t ... f(t) \cdot dt \cdot dt \cdot ...$, n times	$\frac{1}{\underline{s}^n} \cdot F(\underline{s})$
Convolution	$f_1(t) * f_2(t) = \int_{-\infty}^{\infty} f_1(t-\tau) \cdot f_2(\tau) \cdot d\tau$	$F_1(\underline{s}) \cdot F_2(\underline{s})$
Limits	$\lim_{t \to 0+} f(t)$	$\lim_{\underline{s} \to \infty} \underline{s} \cdot F(\underline{s})$
	$\lim_{t \to \infty} f(t)$	$\lim_{\underline{s} \to 0} \underline{s} \cdot F(\underline{s})$

Table 4.2.2-2: General rules for *Laplace* transform

Example 4.2.2-5

DC excitation of separately excited DC machine switched to DC supply voltage U_f : $u_f(t) = U_f$
Increase of $i_f(t)$ due to that voltage has to be calculated: Initial condition: $i_f(0) = 0$.

$R_f \cdot i_f(t) + L_f \cdot di_f(t)/dt = u_f(t) = U_f$

- *Laplace* transformation:

$L(i_f(t)) = I(\underline{s})$

$L\left(R_f \cdot i_f(t) + L_f \cdot di_f(t)/dt\right) = R_f \cdot I(\underline{s}) + L_f \cdot \left(\underline{s} \cdot I(\underline{s}) - i_f(0)\right) = L(U_f) = U_f / \underline{s}$

- Solution of algebraic equation:

$$R_f I(\underline{s}) + L_f \cdot \underline{s} I(\underline{s}) = \frac{U_f}{\underline{s}} \quad \rightarrow \quad I(\underline{s}) = \frac{U_f}{\underline{s}} \cdot \frac{1}{R_f + \underline{s} L_f} = \frac{U_f}{R_f} \cdot \left(\frac{1}{\underline{s}} - \frac{T}{1 + \underline{s} T} \right)$$

with $T = \frac{L_f}{R_f}$. Initial condition is already implemented in algebraic equation !

- Inverse transformation, using Tables 4.2.2-1 and 4.2.2-2, yields with $1/\underline{s} \leftrightarrow 1$ and $\frac{1}{1+\underline{s}T} \leftrightarrow \frac{e^{-t/T}}{T}$ the solution:

$$\underline{\underline{L^{-1}\left(\underline{I}(\underline{s})\right) = i_f(t) = \frac{U_f}{R_f} \cdot \left(1 - e^{-\frac{t}{T}}\right)}}$$

4.2.3 Solving of non-linear differential equations

Electric machinery contains a lot of non-linear parameter properties, such as iron saturation, where inductance depends on exciting current $L(i)$ or where product of two variables occurs such as in induced voltage $u_i(t) = k \cdot n(t) \cdot \Phi(t)$. **In non-linear equations superposition of two solutions usually does not yield another solution of that equation.**

Example 4.2.3-1:

Solving $R \cdot i(t) + d(L(i) \cdot i(t))/dt = 0$ leads to $R \cdot i(t) + \frac{dL}{di} \cdot \frac{di}{dt} \cdot i + L \cdot \frac{di}{dt} = 0$, hence

$$R \cdot i(t) + \left(\frac{dL(i)}{di} \cdot i(t) + L(i) \right) \cdot \frac{di}{dt} = 0, \quad R \cdot i(t) + L_{eq}(i) \cdot \frac{di}{dt} = 0, \; L_{eq} = \frac{dL}{di} \cdot i + L.$$

Two solutions $i_1(t), i_2(t)$ yield

$R \cdot i_1(t) + L_{eq}(i_1) \cdot (di_1/dt) = 0$ and $R \cdot i_2(t) + L_{eq}(i_2) \cdot (di_2/dt) = 0$.

The sum $i_3 = i_1 + i_2$ is usually no solution, as we get

$R \cdot i_3(t) + L_{eq}(i_3) \cdot (di_3/dt) = R \cdot i_1(t) + L(i_3) \cdot (di_1/dt) + R \cdot i_2(t) + L(i_3) \cdot (di_2/dt) \neq 0$, as

$R \cdot i_1(t) + L(i_3) \cdot (di_1/dt) \neq 0$, $R \cdot i_2(t) + L(i_3) \cdot (di_2/dt) \neq 0$!

Solution of non-linear differential equation usually must be done **numerically** in step-by-step integration with finite step length, starting from $t = 0$ with the value for initial condition. Many different numerical methods are known, the simplest being the integration method of *Euler*, the most used the method of *Runge-Kutta*. These methods imply, that the problem is written as a set of first order differential equations. Then the first order differentiation may be regarded as the slope of the function. By taking with finite step length and the slope the next

value of the function, one gets step by step not an exact new value of the solution, but only an approximation, which of course is more close to the exact solution, if the step is shorter. On the other hand calculation time increases. As per each step also some rounding error occurs in the computer, a too large number of steps due to too small step length might increase the total calculation error due to rounding effects. Thus usually an optimum step length exists, which in numerical programs such as *MATLAB/Simulink*® or *DYMOLA/Modelica*® may be adjusted by the user.

Example 4.2.3-2:

Solving $R \cdot i(t) + d(L(i) \cdot di(t))/dt = 0, \quad \psi(i) = L(i) \cdot i$ numerically with ***Euler´*s method**:

$$\frac{d\psi}{dt} = -R \cdot i(\psi(t)), \quad \psi(i) \rightarrow i(\psi)$$

or with if $L_{eq}(i)$ (see Ex. 4.2.3-1): $\frac{di}{dt} = -\frac{R \cdot i(t)}{L_{eq}(i)}$ resp. $i' = f(i,t)$

with initial condition $i(t_0) = i_0$.

Choosing step length $\Delta t = h$, we get: $\Delta i_0 = f(i_0, t_0) \cdot h$. So new point of solution at $t_1 = t_0 + h$ is: $i_1 = i(t_0 + h) \approx i_0 + \Delta i_0$.

For the next point $t = t_0 + h + h = t_1 + h$ we get in similar way with $\Delta i_1 = f(i_1, t_1) \cdot h$

$i_2 = i(t_1 + h) \approx i_1 + \Delta i_1$ and so on.

General rule is $i_{n+1} = i_n + h \cdot f(i_n, t_n)$ with *n* = 1, 2, 3, ... to be calculated in recursive way. Thus the values i_n at t_n are taken instead of the exact (but unknown) function *i*(*t*).

Example 4.2.3-3:

Solving $R \cdot i(t) + L_{eq}(i) \cdot di(t)/dt = 0$ numerically with ***Runge-Kutta* method**:

$\frac{di}{dt} = -\frac{R \cdot i(t)}{L_{eq}(i)}$ or $i' = f(i,t)$ with initial condition $i(t_0) = i_0$.

Choosing step length $\Delta t = h$, we get at $t_1 = t_0 + h$:

$i_1 \approx i_0 + h \cdot K$, with $K = (k_1 + 2k_2 + 2k_3 + k_4)/6$ and

$$k_1 = f(i_0, t_0)$$

$$k_2 = f(i_0 + \frac{h}{2} \cdot k_1, t_0 + \frac{h}{2})$$

$$k_3 = f(i_0 + \frac{h}{2} \cdot k_2, t_0 + \frac{h}{2})$$

$$k_4 = f(i_0 + h \cdot k_3, t_0 + h)$$

We continue at $t_2 = t_1 + h$ with

$i_2 \approx i_1 + h \cdot K$

and so on.

In comparison to *Euler´*s method the error of *Runge-Kutta* method for the SAME step length *h* is smaller by the ratio h^4 / h.

Example 4.2.3-4:

Comparison of *Euler* and *Runge-Kutta* method for -*R* = *L* = const. (“negative damping”):

$$\frac{di}{dt} = i(t), \quad i(0) = 1$$

For this equation the exact solution is known ($i(t) = e^t$), yielding exponential current rise ("unstable" operation) and can be compared with numerical solution.

T	$i(t)$ ($h = \Delta t = 0.2$)	$i(t)$ ($h = \Delta t = 0.2$)	$i(t)$ (exact solution)
	Euler	*Runge-Kutta*	
0	1.0	1.0	1.0
0.2	1.2	1.2214	1.2214027
0.4	1.44	1.49182	1.4918247
0.6	1.728	1.82211	1.8221188
0.8	2.0736	2.22552	2.2255409
1.0	2.48832	2.71825	2.7182818
1.2	2.98598	3.32007	3.3201169
...	...	...	...

The deviation from exact solution is much smaller with *Runge-Kutta* in comparison with *Euler´*s method.

5. Dynamics of DC machines

5.1 Dynamic system equations of separately excited DC machine

The separately excited DC machine is the most widely used DC machine for converter operation, as field and armature current may be controlled independently. This kind of machine consists of the rotating **armature winding** and the series connected **inter-pole winding** and **compensation winding** in the stator with total resistance R_a (and brush resistance R_{br}, which is neglected in the following) and inductance L_a. The separately excited DC **field winding** in the stator consists of resistance R_f and field inductance L_f. Field winding current i_f magnetizes the *d*-axis of the DC machine with the main flux per pole Φ, whereas the armature current i_a, flowing in armature winding, compensation and inter-pole winding, magnetizes the *q*-axis. **Thus armature and field winding are de-coupled: No mutual inductance between armature and field wind M_{af} exists: $M_{af} = 0$.** The magnetic flux of compensation and inter-pole winding oppose the flux of rotating armature winding, therefore resulting armature inductance L_a is very small. Field winding is made up of many turns N_f to reduce field current i_f for given demand of ampere-turns for certain magnetic flux Φ, yielding big value $L_f \sim N_f^2$.

Voltage equation for armature and field winding as well as mechanical equation for torque and acceleration constitute dynamic system equations of separately excited DC machine according to Fig. 5.1-1.

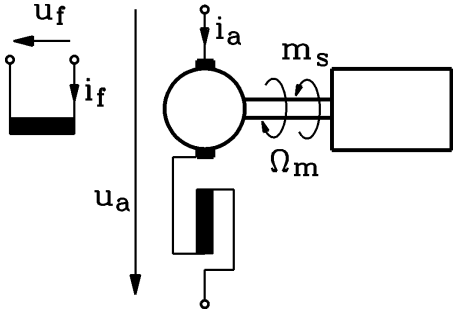

Fig. 5.1-1: Schematic diagram of armature and field circuit and of mechanical load of separately excited DC machine

Induced voltage u_i in rotating armature winding is given with **machine constant**

$$k_2 = \frac{1}{2\pi} \cdot \frac{z \cdot p}{a} \quad , \tag{5.1-1}$$

comprising total number of conductors in rotating armature *z*, number of poles 2*p* and number of parallel branches in rotating armature winding 2*a*, by product of rotor angular speed Ω_m and flux per pole

$$u_i(t) = k_2 \cdot \Omega_m(t) \cdot \Phi(i_f) \quad , \tag{5.1-2}$$

and **electromagnetic torque** is given by product of armature current and flux per pole

$$m_e(t) = k_2 \cdot i_a(t) \cdot \Phi(i_f) \quad . \tag{5.1-3}$$

Voltage equation for armature winding is determined by external armature voltage u_a, resistive voltage drop, induced voltage (back EMF) and self-induced voltage $L_a \cdot di_a / dt$.

$$u_a(t) = R_a \cdot i_a(t) + L_a \cdot \frac{di_a(t)}{dt} + u_i(t) \tag{5.1-4}$$

Acceleration of rotor with angular momentum of inertia J of machine rotor and load is determined by difference of electromagnetic torque and shaft torque $m_s(t)$ due to mechanical load.

$$J \cdot \frac{d\Omega_m}{dt} = m_e(t) - m_s(t) \tag{5.1-5}$$

Voltage equation for field winding is determined by external excitation voltage u_f, resistive voltage drop and self-induced voltage $L_f \cdot di_f / dt$.

$$u_f(t) = R_f \cdot i_f(t) + L_f \cdot \frac{di_f(t)}{dt} \tag{5.1-6}$$

In case of simultaneous change of armature and field current, this set of differential equations **non-linear** due to the products in (5.1-2), (5.1-3). Usually the field current and thus the main flux is kept constant, and only the armature current is changing to adjust torque and speed, because due to $L_a << L_f$ the armature current may be changed much faster than the field current. Thus the flux is kept constant, and the set of differential equations is linear. Moreover (5.1-6) is changing to $u_f(t) = U_f = R_f \cdot I_f$, so that only two differential equations with two variables i_a and Ω_m remain:

$$\boxed{\begin{aligned} u_a(t) &= R_a \cdot i_a(t) + L_a \cdot \frac{di_a(t)}{dt} + k_2 \cdot \Omega_m(t) \cdot \Phi \\ J \cdot \frac{d\Omega_m}{dt} &= k_2 \cdot i_a(t) \cdot \Phi - m_s(t) \end{aligned}} \tag{5.1-7}$$

Substituting either i_a or Ω_m leads to **one linear differential equation of second order with constant coefficients:**

$$\frac{d^2 i_a}{dt^2} + \frac{1}{T_a} \cdot \frac{di_a}{dt} + \frac{1}{T_a \cdot T_m} \cdot i_a = \frac{1}{T_a \cdot R_a} \cdot \frac{du_a}{dt} + \frac{1}{T_a \cdot T_m} \cdot \frac{1}{k_2 \Phi} \cdot m_s \tag{5.1-8}$$

$$\frac{d^2 \Omega_m}{dt^2} + \frac{1}{T_a} \cdot \frac{d\Omega_m}{dt} + \frac{1}{T_a \cdot T_m} \cdot \Omega_m = \frac{1}{T_a \cdot T_m} \cdot \frac{1}{k_2 \Phi} u_a - \frac{1}{T_a} \cdot \frac{1}{J} \cdot m_s - \frac{1}{J} \cdot \frac{dm_s}{dt} \tag{5.1-9}$$

The homogenous differential equation for both variables i_a and Ω_m is identical, containing the **electrical time constant of armature**

$$T_a = L_a / R_a \tag{5.1-10}$$

and **mechanical time constant of machine and load,** which not only depends on mechanical parameter J, but also on flux per pole and armature resistance:

$$T_m = \frac{J \cdot R_a}{(k_2 \Phi)^2} \tag{5.1-11}$$

Facit:

Changing of armature current and rotor speed is ruled by armature voltage and is disturbed by load torque. Both are contained in the "right side" of the system differential equation.

Linear differential equation for constant flux shows, that transient performance of separately excited DC machine may be understood rather simple. Thus DC machine may be controlled in easy way.

5.2 Dynamic response of electrical and mechanical system of separately excited DC machine

Usually electrical time constant is much shorter than mechanical time constant by 1 : 10. For electrical transient situation, where armature current changes quickly and rotor speed does not, only electrical equation has to be considered. On the contrary, when speed changes, usually the current change is already over, so only mechanical equation has to be considered.

5.2.1 Dynamics of mechanical system

Taking $T_a << T_m$ leads to $T_a \to 0$ and thus

$$\frac{d\Omega_m}{dt} + \frac{1}{T_m} \cdot \Omega_m = \frac{1}{T_m} \cdot \frac{1}{k_2 \Phi} u_a - \frac{1}{J} \cdot m_s \quad . \tag{5.2.1-1}$$

a) Steady state condition:
In case of stationary operation $d/dt = 0$ we get from (5.2.1-1)

$$\Omega_m = \frac{1}{k_2 \Phi} u_a - \frac{T_m}{J} \cdot m_s = \Omega_{m0} - \frac{T_m}{J} \cdot m_s \quad , \tag{5.2.1-2}$$

where

$$\Omega_{m0} = \frac{U_a}{k_2 \Phi} \tag{5.2.1-3}$$

is no-load angular speed, which occurs at "no-load" $M_s = 0$. Due to $d/dt = 0$ we also get from Chapter 5.1 $m_e = m_s = k_2 \cdot \Phi \cdot i_a$, so instead of (5.2.1-2) one can also note

$$\Omega_m = \Omega_{m0} - \frac{T_m}{J} \cdot k_2 \cdot \Phi \cdot i_a = \Omega_{m0} - \frac{R_a}{k_2 \cdot \Phi} \cdot i_a \quad , \tag{5.2.1-4}$$

which is the well known steady-state "speed-current characteristic" of separately excited DC machine with negative slope defined by R_a (Fig. 5.2.1-1).

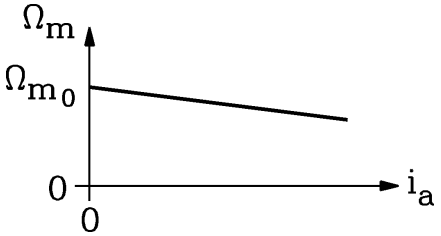

Fig. 5.2.1-1: Steady-state "speed-current characteristic" of separately excited DC machine with negative slope defined by R_a

b) Dynamic operation:
As an example of transient operation the switching on of DC machine at zero speed, rated flux $\Phi = \Phi_N$ and no-load $m_s = 0$ is considered. Armature voltage is switched from zero to rated value $U_a = U_N$ for $t > 0$ (Fig. 5.2.1.2a).

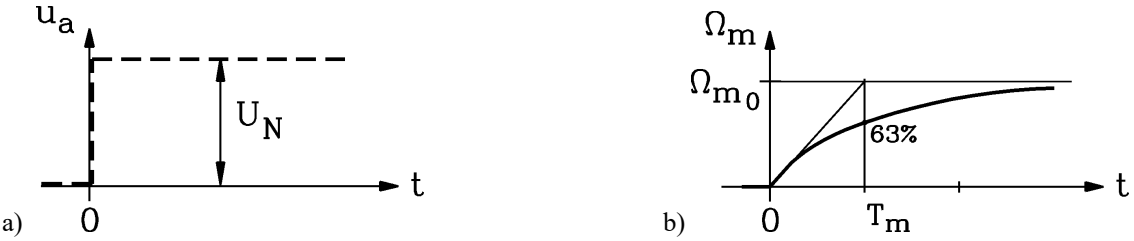

Fig. 5.2.1-2: Dynamic speed response of separately excited DC machine to switching with a) armature voltage step, leading to b) exponential increase of speed

Solving

$$\frac{d\Omega_m}{dt} + \frac{1}{T_m} \cdot \Omega_m = \frac{1}{T_m} \cdot \frac{1}{k_2 \Phi} U_N \tag{5.2.1-5}$$

with initial condition $\Omega_m(0) = 0$ leads to

$$\Omega_m(t) = \Omega_{m0} \cdot \left(1 - \exp(-t / T_m)\right) \tag{5.2.1-6}$$

with no-load angular speed at rated voltage $\Omega_{m0} = U_N / (k_2 \Phi)$ (Fig. 5.2.1-2b). Armature current is given by $i_a = m_e / (k_2 \Phi)$ and electromagnetic torque is due to $m_s = 0$ given by

$$m_e = J \cdot \frac{d\Omega_m}{dt} = J \cdot \frac{\Omega_{m0}}{T_m} \cdot \exp(-t / T_m) \quad . \tag{5.2.1-7}$$

Thus armature current

$$i_a = \frac{U_N}{R_a} \cdot \exp(-t / T_m) \tag{5.2.1-8}$$

"jumps" from value zero up to big value U_N/R_a, as armature time constant T_a has been neglected, and decays with mechanical time constant, as machine is accelerating, as with increasing speed induced voltage increases, thus limiting the current. The result shows, that for usual DC machines with low R_a it is **forbidden** to start DC machine directly rated voltage, as current peak U_N/R_a would be enormous, destroying the machine immediately.

Example 5.2.1-1:

DC machine: $\frac{R_a}{U_N / I_N} = 0.025 \quad \rightarrow \quad \hat{i}_a = \frac{U_N}{R_a} = \frac{I_N}{0.025} = 40 \cdot I_N$!

Armature losses are enormous: $P_{Cu,a} = R_a \hat{i}_a^2 = 40^2 P_{Cu,N} = 1600 \cdot P_{Cu,N}$! Rotor armature winding is over-heated immediately and damaged severely. So, for starting from the grid, an **additional starting resistor R_s** in series with armature is necessary to limit armature current to rated value.

$$\frac{U_N}{R_a + R_s} = I_N \quad \rightarrow \quad R_s = \frac{U_N}{I_N} - R_a \quad \rightarrow \quad \frac{R_s}{R_a} = \frac{U_N}{R_a \cdot I_N} - 1 = \frac{1}{0.025} - 1 = 39$$

So if e.g. R_a = 10 mOhm, the starting resistor should be $R_S = 39 \cdot 10 = 390 m\Omega = \underline{\underline{0.39\Omega}}$.

Facit:
Mechanical time constant rules the dynamic speed and current response to armature voltage steps. For starting machine directly from DC grid (e.g. battery) in most cases a series starting resistor is necessary to limit starting current peak, which otherwise in the first moment at stand still n = 0 is limited only by (small) armature resistance.

5.2.2 Starting time constant of electric machines

The elapsed time T_J to accelerated uncoupled machine with rated torque M_N from stand-still to rated speed n_N, is called "starting time constant".

$$J_M \cdot \frac{d\Omega_m}{dt} = M_N \quad \rightarrow \quad \Omega_m(t) = \frac{M_N}{J_M} \int_{t=0}^{t} dt = \frac{M_N}{J_M} \cdot t \tag{5.2.2-1}$$

$a)\ \Omega_m(t = T_J) = \Omega_{mN} \quad b)\ \Omega_m(t = 0) = 0$

Initial condition: $\Omega_m(t = 0) = 0$. At $t = T_J$ we get $\Omega_m(t = T_J) = \Omega_{mN}$.

$$\boxed{T_J = \frac{J_M \cdot \Omega_{mN}}{M_N} = \frac{J_M \cdot 2\pi \cdot n_N}{M_N}} \tag{5.2.2-2}$$

Example 5.2.2-1:
Comparison of T_m and T_J for DC machine, excited separately with rated flux Φ_N:

If motor runs up with rated torque $M_N = k_2 \Phi_N I_N$ to no-load speed $\Omega_{m0} = \frac{U_N}{k_2 \Phi_N}$, it takes the time $T_{J0} = \frac{J_M \cdot \Omega_{m0}}{M_N}$, which is nearly the same as T_J, as no-load and rated speed are nearly the same. This time MUST not be mixed up with mechanical time constant T_m ! Relationship between these two different time values is given with per unit resistance r_a and flux ϕ:

$$r_a = \frac{R_a}{U_N / I_N},\ \phi = \Phi / \Phi_N : T_{J0} = J_M \cdot \frac{\Omega_{m0}}{M_N} = J_M \cdot \frac{U_N / (k_2 \Phi_N)}{k_2 \Phi_N I_N} = T_m \cdot \frac{1}{r_a} \cdot \left(\frac{\Phi}{\Phi_N} \right)^2$$

$$\boxed{T_{J0} = T_m \cdot \frac{\phi^2}{r_a} \quad \rightarrow \quad T_m = T_{J0} \cdot \frac{r_a}{\phi^2}} \tag{5.2.2-3}$$

Facit:
The mechanical time constant T_m decreases with the square of flux. With flux weakening and with increased stator resistance R_a, which causes voltage drop, thus reducing internal voltage U_i, machines gets "weaker". Therefore mechanical time constant as response to load step increases. Starting time constant is independent of flux and resistance variation.

5.2.3 Dynamics of electrical system of DC machine

Taking $T_a << T_m$ leads to $T_m \rightarrow \infty$, if electrical system only is investigated. From (5.1-8) simplified equation is derived:

$$\frac{di_a}{dt} + \frac{1}{T_a} \cdot i_a = \frac{u_a}{T_a \cdot R_a} - \frac{k_2 \Phi \cdot \Omega_m}{T_a \cdot R_a} = \frac{u_a - u_i}{L_a} \quad . \tag{5.2.3-1}$$

a) Steady state condition:
In case of stationary operation $d/dt = 0$ (5.2.3-1) yields

$$i_a = I_a = \frac{u_a - u_i}{R_a} = \frac{U_a - U_i}{R_a} \quad . \tag{5.2.3-2}$$

For example, in case of generator operation it is $i_a < 0$. So stationary solution is the well-known “voltage-current characteristic” at constant speed for separately excited generator

$$u_a = u_i + i_a \cdot R_a = u_i - (-i_a) \cdot R_a \quad . \tag{5.2.3-3}$$

with negative slope defined by R_a (Fig. 5.2.3-1).

Fig. 5.2.3-1: Steady-state "voltage-current characteristic" at constant speed of separately excited DC machine in generator operation with negative slope defined by R_a

b) Dynamic operation:
As an example of transient operation the switching on of DC machine at zero speed $\Omega_m = 0$, rated flux $\Phi = \Phi_N$ and no-load $m_s = 0$ is considered. Armature voltage is switched from zero to rated value $U_a = U_N$ for $t > 0$ (Fig. 5.2.3-2a).

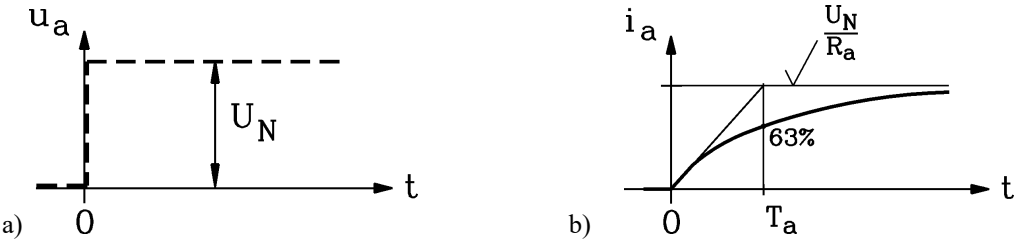

Fig. 5.2.3-2: Dynamic current response of separately excited DC machine at stand still to switching with a) armature voltage step of rated voltage, leading to b) exponential increase of armature current

Solving

$$\frac{di_a}{dt} + \frac{1}{T_a} \cdot i_a = \frac{u_a}{T_a \cdot R_a} - \frac{k_2 \Phi \cdot \Omega_m}{T_a \cdot R_a} = \frac{u_a}{T_a \cdot R_a} \tag{5.2.3-5}$$

with initial condition $i_a(0) = 0$ leads to

$$i_a(t) = \frac{U_N}{R_a} \cdot \left(1 - e^{-t/T_a}\right) \tag{5.2.3-6}$$

with steady-state current $i_a(t \to \infty) = U_N / R_a$. As already stated above, this current is (except for very small machines with rather big armature resistance) much too big, so additional series resistance is needed for starting. Note that with neglecting T_a, the exponential rise of current "degenerates" to current jumping from zero to U_N / R_a, and is only decreasing due to induced voltage at increased speed (see Section 5.2.1).

Facit:
Armature current and therefore electromagnetic torque react to armature voltage steps with short armature time constant T_a. Therefore separately excited DC machines are dynamic drives.

5.3 Dynamics of coupled electric-mechanical system of separately excited DC machine

Taking T_a, T_m into account without any neglecting, the second order differential equation from Section 5.1 has to be solved. Doing this for motor angular speed

$$\frac{d^2\Omega_m}{dt^2} + \frac{1}{T_a} \cdot \frac{d\Omega_m}{dt} + \frac{1}{T_a \cdot T_m} \cdot \Omega_m = \frac{1}{T_a \cdot T_m} \cdot \frac{1}{k_2 \Phi} u_a(t) - \frac{1}{T_a} \cdot \frac{1}{J} \cdot m_s(t) - \frac{1}{J} \cdot \frac{dm_s(t)}{dt} \quad , \qquad (5.3\text{-}1)$$

solution of second order **homogeneous differential equation**

$$\frac{d^2\Omega_m}{dt^2} + \frac{1}{T_a} \cdot \frac{d\Omega_m}{dt} + \frac{1}{T_a \cdot T_m} \cdot \Omega_m = 0 \qquad (5.3\text{-}2)$$

needs two exponential functions as **"eigen-functions"** (C_1, C_2: integration constants):

$$\Omega_{mh}(t) = C_1 \cdot e^{\lambda_1 t} + C_2 \cdot e^{\lambda_2 t} \quad . \qquad (5.3\text{-}3)$$

Putting (5.3-3) into (5.3-2) yields second order algebraic **characteristic equation** for λ:

$$\lambda^2 + \frac{1}{T_a} \cdot \lambda + \frac{1}{T_a \cdot T_m} = 0 \quad \rightarrow \quad \lambda_{1,2} = -\frac{1}{2T_a} \pm \frac{1}{2T_a} \sqrt{1 - \frac{4T_a}{T_m}} \quad . \qquad (5.3\text{-}4)$$

Note that in case of $T_m < 4T_a$ the square root leads to $\sqrt{1 - \frac{4T_a}{T_m}} = j\sqrt{\frac{4T_a}{T_m} - 1}$. As $e^{\pm jx} = \cos x \pm j \cdot \sin x$, the following different solutions may exist for **eigen-values** λ_1, λ_2:

a)	$T_m > 4T_a$	λ_1, λ_2 are real values, so transient speed response contains **TWO time constants** $T_1 = -1/\lambda_1, T_2 = -1/\lambda_2$, a short and a long one.
b)	$T_m = 4T_a$	$\lambda_1 = \lambda_2 = \lambda$ is real value, so transient speed response contains **ONE time constant** $T = -1/\lambda$ **("aperiodic limit").**
c)	$T_m < 4T_a$	$\underline{\lambda}_1, \underline{\lambda}_2$ are complex values $\underline{\lambda}_1 = -\delta + j \cdot \omega_d$, $\underline{\lambda}_2 = -\delta - j \cdot \omega_d$, so transient speed response **oscillates** with **frequency** $f_d = \omega_d / (2\pi)$, which is damped by **damping coefficient** δ.

a) $\Omega_{mh}(t) = C_1 \cdot e^{-t/T_1} + C_2 \cdot e^{-t/T_2}$ (5.3-5)

long time constant: $T_1 = \dfrac{2T_a}{1-\sqrt{1-\dfrac{4T_a}{T_m}}}$, short time constant $T_2 = \dfrac{2T_a}{1+\sqrt{1-\dfrac{4T_a}{T_m}}}$ (5.3-6)

The long time constant is determined mainly by mechanical system, as for $T_a << T_m$ we get $\lim_{T_m \to \infty} T_1 = T_m$. The short time constant is determined mainly by electrical system, as for $T_a << T_m$ we get $\lim_{T_m \to \infty} T_2 = T_a$.

b) $\Omega_{mh}(t) = C_1 \cdot e^{-t/T} + C_2 \cdot t \cdot e^{-t/T}$, $T = 2T_a$ (5.3-7)

c) $\Omega_{mh}(t) = A \cdot e^{-\delta \cdot t} \cdot \cos(\omega_d \cdot t) + B \cdot e^{-\delta \cdot t} \cdot \sin(\omega_d \cdot t)$ *A, B*: integration constants (5.3-8)

Damping coefficient: $\delta = \dfrac{1}{2T_a}$ (5.3-9)

Eigen-frequency: $f_d = \dfrac{1}{2\pi \cdot T_a}\sqrt{\dfrac{T_a}{T_m} - \dfrac{1}{4}} = \dfrac{1}{2\pi \cdot T_a}\sqrt{\dfrac{T_a}{T_J} \cdot \dfrac{\phi^2 \cdot (1-r_a)}{r_a} - \dfrac{1}{4}}$ (5.3-10)

Period of oscillation: $T_d = \dfrac{1}{f_d}$ (5.3-11)

For getting a quick estimate, after which time the oscillation has vanished, we ask: After how many half periods N_H oscillation has been damped down to 5% ?

$$e^{-t^* \cdot \delta} = 0.05 \quad \rightarrow \quad t^* = 3/\delta \quad \rightarrow \quad N_H = \frac{t^*}{T_d/2} = \frac{3/\delta}{\pi/\omega_d} \approx \frac{\omega_d}{\delta}$$

$$\boxed{N_H \approx \frac{\omega_d}{\delta}} \qquad (5.3\text{-}12)$$

Facit:
In case of high dynamic drives (low inertia), the DC machines oscillates in speed and armature current after each load step. Oscillation is stable due to damping by losses in armature resistance. The natural oscillation frequency increases with "stronger" DC machine, thus with reduction of armature resistance and increase of flux.

As in coupled drives total inertia is constituted by motor and load inertia, usually $T_m > 4T_a$, so **no oscillations** occur, but DC machine reacts with two time constants, the shorter being related to electric system and the longer to mechanical system, but due to interaction of mechanical and electrical system both time constants **are influenced by mechanical AND electrical parameters**.

Example 5.3-1:
Separately excited DC machine: Inertia given by T_J = 1 s, electric parameters are T_a = 50 ms, r_a = 0.05, $\Phi = \Phi_N$.

- With $T_J \cong T_{J0}$: Mechanical time constant: $T_m = T_J \cdot \frac{r_a}{\phi^2} = 1 \cdot 0.05/1^2 = \underline{\underline{50}}\,\text{ms}$
- As $T_m = 50ms < 4T_a = 4 \cdot 50 = 200ms$, the DC machine tends to oscillate with frequency $f_d = \frac{1}{2\pi \cdot 0.05} \cdot \sqrt{\frac{0.05}{0.05} - \frac{1}{4}} = \underline{\underline{2.76}}\,\text{Hz}$ and angular frequency $\omega_d = 2\pi f_d = \underline{\underline{17.3}}/\,\text{s}$, yielding an oscillation period of $T_d = 1/\,f_d = 1/2.76 = \underline{\underline{362}}\,\text{ms}$.
- Damping coefficient: $\delta = \frac{1}{2T_a} = \frac{1}{2 \cdot 0.05} = \underline{\underline{10}}/\,\text{s}$
- After $N_H \approx \frac{\omega_d}{\delta} = \frac{17.3}{10} = \underline{\underline{1.73}}$ half-periods the oscillation is damped down to 5% of initial value.

5.4 Linearized model of separately excited DC machine for variable flux

In case of variable flux $\Phi(t)$ both voltage for induced voltage (5.1-2) and electromagnetic torque (5.1-3) are <u>non-linear</u>. For **small transient deviations** $\Delta u_a(t)$, $\Delta i_a(t)$, $\Delta\Omega_m(t)$, $\Delta\Phi(t)$, $\Delta m_s(t)$, $\Delta i_f(t)$, $\Delta u_f(t)$ from steady state operation $U_a, I_a, \Omega_m, \Phi, M_s, I_f, U_f$ the non-linear equations may be linearized. "Small" means that the per unit deviations from steady state are small, e.g. less than 10%: $|\Delta u_a(t)/U_a| << 1$, $|\Delta i_a(t)/I_a| << 1$, $|\Delta\Omega_m(t)/\Omega_m| << 1$, $|\Delta\Phi(t)/\Phi| << 1$ and so on. Thus we get for induced voltage

$$u_i(t) = k_2 \cdot (\Omega_m + \Delta\Omega_m(t)) \cdot (\Phi + \Delta\Phi(t)) = k_2 \cdot \Omega_m \cdot \Phi \cdot (1 + \frac{\Delta\Omega_m(t)}{\Omega_m}) \cdot (1 + \frac{\Delta\Phi(t)}{\Phi}) \quad . \qquad (5.4\text{-}1)$$

Note, that we can **neglect product of small deviations**

$$(1 + \frac{\Delta\Omega_m(t)}{\Omega_m}) \cdot (1 + \frac{\Delta\Phi(t)}{\Phi}) = 1 + \frac{\Delta\Omega_m(t)}{\Omega_m} + \frac{\Delta\Phi(t)}{\Phi} + \frac{\Delta\Omega_m(t)}{\Omega_m} \cdot \frac{\Delta\Phi(t)}{\Phi} \approx 1 + \frac{\Delta\Omega_m(t)}{\Omega_m} + \frac{\Delta\Phi(t)}{\Phi} \;,$$

because of the assumption of SMALL deviations products are VERY SMALL (e.g. one order of magnitude smaller):

$$1.21 = (1 + 0.1) \cdot (1 + 0.1) = 1 + 0.1 + 0.1 + 0.1 \cdot 0.1 = 1 + 0.1 + 0.1 + 0.01 \approx 1 + 0.1 + 0.1 = 1.20 \,,$$

so error with respect to steady state values is less than 1%. For induced voltage therefore one derives

$$u_i(t) \cong k_2 \cdot \Omega_m \cdot \Phi + k_2 \cdot \Delta\Omega_m(t) \cdot \Phi + k_2 \cdot \Omega_m \cdot \Delta\Phi(t) = U_i + \Delta u_{i,\Omega_m}(t) + \Delta u_{i,\Phi}(t) \qquad (5.4\text{-}2)$$

with voltage deviation from steady state value caused by speed deviation and by flux deviation in linear addition. In the same way for electromagnetic torque is derived

$$m_e(t) = k_2 \cdot (i_a + \Delta i_a(t)) \cdot (\Phi + \Delta\Phi(t)) \approx k_2 \cdot I_a \cdot \Phi + k_2 \cdot \Delta i_a(t) \cdot \Phi + k_2 \cdot I_a \cdot \Delta\Phi(t) \quad , \qquad (5.4\text{-}3)$$

showing that torque deviation from steady state value M_e is given in linear addition by speed and current deviation. With splitting up each variable into its steady state and transient component $U_a + \Delta u_a, I_a + \Delta i_a,$ and so on, and substituting this in the system equations of DC machine of Section 5.1, one arrives at

$$\begin{aligned} U_a + \Delta u_a &\approx R_a \cdot (I_a + \Delta i_a) + L_a \cdot \frac{d(I_a + \Delta i_a)}{dt} + U_i + k_2 \cdot \Delta\Omega_m \cdot \Phi + k_2 \cdot \Omega_m \cdot \Delta\Phi \\ J \cdot \frac{d(\Omega_m + \Delta\Omega_m)}{dt} &\approx M_e + k_2 \cdot \Delta i_a \cdot \Phi + k_2 \cdot I_a \cdot \Delta\Phi - M_s - \Delta m_s \end{aligned} \qquad (5.4\text{-}4)$$

or due to $\frac{dI_a}{dt} = 0, \quad \frac{d\Omega_m}{dt} = 0$ one gets

$$\begin{aligned} U_a + \Delta u_a &\approx R_a \cdot (I_a + \Delta i_a) + L_a \cdot \frac{d\Delta i_a}{dt} + U_i + k_2 \cdot \Delta\Omega_m \cdot \Phi + k_2 \cdot \Omega_m \cdot \Delta\Phi \\ J \cdot \frac{d\Delta\Omega_m}{dt} &\approx M_e + k_2 \cdot \Delta i_a \cdot \Phi + k_2 \cdot I_a \cdot \Delta\Phi - M_s - \Delta m_s \end{aligned} \quad . \qquad (5.4\text{-}5)$$

As the steady state conditions are given by

$$U_a = R_a \cdot I_a + U_i \qquad M_e = M_s \quad , \qquad (5.4\text{-}6)$$

only LINEAR **differential equations of deviations** remain:

$$\begin{aligned} \Delta u_a(t) &\approx R_a \cdot \Delta i_a(t) + L_a \cdot \frac{d\Delta i_a(t)}{dt} + k_2 \cdot \Delta\Omega_m(t) \cdot \Phi + k_2 \cdot \Omega_m \cdot \Delta\Phi(t) \\ J \cdot \frac{d\Delta\Omega_m(t)}{dt} &\approx k_2 \cdot \Delta i_a(t) \cdot \Phi + k_2 \cdot I_a \cdot \Delta\Phi(t) - \Delta m_s(t) \end{aligned} \quad . \qquad (5.4\text{-}7)$$

This linear differential equation system can be treated e.g. with *Laplace* transformation, but is only valid within the limits of deviation from steady state operation of about +/- 10 ... 20 %, so it is called "**small signal theory**". Moreover the constant parameters of differential equations (5.4-7) depend on the steady state values Ω_m, I_a, Φ; at a different point of operation, e.g. field weakening with half flux and twice speed the parameters change to $2\Omega_m, I_a, \Phi/2$, thus changing the differential equations.

In case of linear systems NO linearization is necessary, and *Laplace* transformation may be used also for "**large signal theory**". This is the case for separately excited DC machines with constant flux operation $\Phi = const.$, as in that case

$$u_i(t) = U_i + \Delta u_i = k_2 \cdot (\Omega_m + \Delta\Omega_m) \cdot \Phi = k_2 \cdot \Omega_m \cdot \Phi + k_2 \cdot \Delta\Omega_m \cdot \Phi \qquad (5.4\text{-}8)$$

can be exactly decomposed into $U_i = k_2 \cdot \Omega_m \cdot \Phi$ and $\Delta u_i(t) = k_2 \cdot \Delta\Omega_m(t) \cdot \Phi$. The same holds true for electromagnetic torque

$$m_e(t) = M_e + \Delta m_e = k_2 \cdot (I_a + \Delta i_a) \cdot \Phi = k_2 \cdot I_a \cdot \Phi + k_2 \cdot \Delta i_a \cdot \Phi \quad . \qquad (5.4\text{-}9)$$

So LINEAR differential equations of deviations are exact and can be used also for "large signal theory":

$$\begin{aligned} \Delta u_a(t) &= R_a \cdot \Delta i_a(t) + L_a \cdot \frac{d\Delta i_a(t)}{dt} + k_2 \cdot \Delta\Omega_m(t) \cdot \Phi \\ J \cdot \frac{d\Delta\Omega_m(t)}{dt} &= k_2 \cdot \Delta i_a(t) \cdot \Phi - \Delta m_s(t) \end{aligned} \quad . \tag{5.4-10}$$

Facit:
For constant flux operation separately excited DC machine is linear also for large signals, so it is an ideal machine to be controlled, e.g. speed controlled or torque controlled.

5.5 Transfer function of separately excited DC machine

Controlled drives have to be operated by the controller to keep the actual values as close as possible to the set-point values, which may be regarded as the steady state operation. Deviations between actual and set-point values are usually small due to controller actions, so "small signal theory" may be used to describe the controlled machine. The response of the machine to controller actions is determined by the transfer function of the machine, which is derived from the small signal linear differential equation of the machine.

Assuming that at $t = 0$ all deviations are zero,

$$\Delta u_a(0) = 0,\ \Delta i_a(0) = 0,\ \Delta\Omega_m(0) = 0,\ \Delta\Phi(0) = 0,\ \Delta m_s(0) = 0,\ \Delta i_f(0) = 0 \tag{5.5-1}$$

so machine is operating in steady state conditions, leads to **derivation of transfer function** of separately excited DC machine by using *Laplace* transformation. For simplification, complex notation of *Laplace* operator $\underline{s}$ is noted only as s in further context.

$$L\{\Delta i_a(t)\} = \int_0^\infty e^{-s\cdot t} \cdot \Delta i_a(t) \cdot dt = \Delta\breve{i}_a(s) \tag{5.5-2}$$

$$L\left\{\frac{d\Delta i_a(t)}{dt}\right\} = s \cdot \Delta\breve{i}_a(s) - \Delta i_a(0) = s \cdot \Delta\breve{i}_a(s) \tag{5.5-3}$$

Here, constant flux operation is assumed, so results are also valid for large signal theory. Transforming (5.4-10) with *Laplace* theory, we get

$$\begin{aligned} \Delta\breve{u}_a(s) &= R_a \cdot \Delta\breve{i}_a(s) + s \cdot L_a \cdot \Delta\breve{i}_a(s) + k_2 \cdot \Delta\breve{\Omega}_m(s) \cdot \Phi \\ J \cdot s \cdot \Delta\breve{\Omega}_m(s) &= k_2 \cdot \Delta\breve{i}_a(s) \cdot \Phi - \Delta\breve{m}_s(s) \end{aligned} \tag{5.5-4}$$

With abbreviation $\gamma = 1/T_a$ the solution of algebraic equation system (5.5-4) with elimination of current is

$$\Delta\breve{\Omega}_m(s) = \frac{s+\gamma}{s^2 + \gamma \cdot s + \frac{\gamma}{T_m}} \cdot \frac{1}{J} \cdot \left[\frac{\gamma}{s+\gamma} \cdot \frac{k_2\Phi}{R_a} \cdot \Delta\breve{u}_a(s) - \Delta\breve{m}_s(s)\right] \quad . \tag{5.5-5}$$

Armature voltage is the **leading variable,** which acts on DC machine performance, described by characteristic polynomial (5.3-4), via first order time delay of armature time constant $T_a = 1/\gamma$, whereas shaft torque of load is **disturbance variable**, which acts directly on DC machine performance (Fig. 5.5-1).

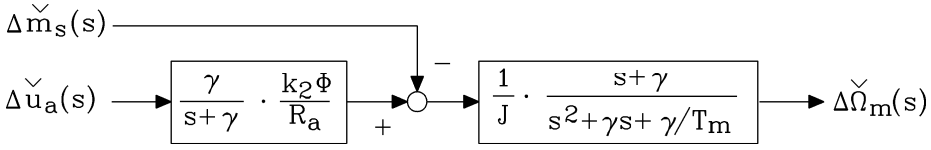

Fig. 5.5-1: Block diagram of DC machine transfer function in *Laplace* transformed description

The transfer behaviour of the separately excited DC machine is given by the polynomial in variable *s* in the denominator

$$P(s) = s^2 + \gamma \cdot s + \frac{\gamma}{T_m} = s^2 + \frac{1}{T_a} \cdot s + \frac{1}{T_a T_m} \quad , \tag{5.5-6}$$

which corresponds to the characteristic polynomial of the second order differential equation, discussed in Section 5.3. The **roots of this polynomial** $\underline{s}_1$, $\underline{s}_2$ are the already described eigenvalues $\underline{\lambda}_1 = -\delta + j \cdot \omega_d = \underline{s}_1$, $\underline{\lambda}_2 = -\delta - j \cdot \omega_d = \underline{s}_2$ of the second order differential operator $\frac{d^2 \cdot}{dt^2} + \frac{1}{T_a} \cdot \frac{d \cdot}{dt} + \frac{1}{T_a T_m}$, which constitutes the second order differential equation:

$$P(s) = 0 = s^2 + \gamma \cdot s + \frac{\gamma}{T_m} = (s - \underline{s}_1) \cdot (s - \underline{s}_2) \tag{5.5-7}$$

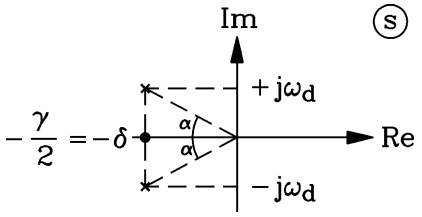

Fig. 5.5-2: Position of conjugate complex roots of DC machine transfer function in *Laplace* complex $\underline{s}$-plane

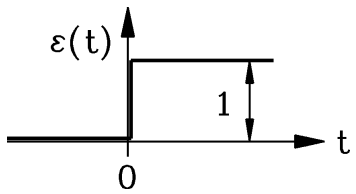

Fig. 5.5-3: *Heaviside* unit step function

Position of these roots in the complex $\underline{s}$-plane (shown in Fig. 5.5-2 for the case of non-vanishing imaginary part $\omega_d > 0$) gives the following information:

- If real part of roots lies in the **left half plane** (Re($\underline{s}$) < 0), then transient response of DC machine is **stable** (= damped solution).
- If **no imaginary part** of roots exist ($\omega_d = 0$), then **no oscillations** occur. Roots are lying then on real axis.
- If real part of roots lies in the far left half plane (Re($\underline{s}$) << 0), then time constants are **very short**; transient response is damped very quickly. In the opposite situation, when real part lies near origin in left half plane, time constant is **very long** and transient response duration is rather long and weakly damped.
- In case of complex roots these occur in **pairs of conjugate complex values**, which means that sine and cosine function will occur in transient response.

- If imaginary part of root is far off origin, then oscillation frequency **is high**. On the contrary, if imaginary part lies in vicinity of origin, then oscillation frequency is very low.
- The **tangent of angle α** between real axis and straight line between origin and root locus is the number N_H of half periods, until transient oscillation is damped down to 5% of initial value.

$$\tan\alpha = \frac{\omega_d}{\delta} = N_H \tag{5.5-8}$$

As **example**, **speed response to mechanical load step**, given by step in shaft torque**, at constant armature voltage** ($u_a(t) = U_a = const.$; $\Delta u_a(t) = 0$) and **no-load operation** may be calculated with *Laplace* transfer function easily. Assuming shaft torque step

$$\Delta m_s(t) = \Delta M_s \cdot \varepsilon(t) \tag{5.5-9}$$

with *Heaviside´*s unit step function (Fig. 5.5-3)

$$\varepsilon(t) = \begin{cases} 0\,, & t < 0 \\ 1\,, & t \geq 0 \end{cases} \quad , \tag{5.5-10}$$

we get as *Laplace* transform

$$L\{\Delta m_s(t)\} = \frac{\Delta M_s}{s} \tag{5.5-11}$$

and immediately with use of the transfer function the speed response

$$\Delta\breve{\Omega}_m(s) = \frac{s+\gamma}{s^2 + \gamma\cdot s + \frac{\gamma}{T_m}} \cdot \frac{1}{J} \cdot \left[\frac{\gamma}{s+\gamma} \cdot \frac{k_2\Phi}{R_a} \cdot 0 - \frac{\Delta M_s}{s} \right] = -\frac{s+\gamma}{s^2 + \gamma\cdot s + \frac{\gamma}{T_m}} \cdot \frac{\Delta M_s}{J\cdot s} \quad . \tag{5.5-12}$$

By decomposing (5.5-12) into single terms for utilization of *Laplace* transformation table of Chapter 4, we get with $\gamma = 2\delta$ and with assumption of conjugate complex roots, which leads to oscillation $s^2 + \gamma\cdot s + \gamma/T_m = (s - \underline{s}_1)(s - \underline{s}_2) = (s + \delta - j\omega_d)(s + \delta + j\omega_d) = (s+\delta)^2 + \omega_d^2$, we get

$$\frac{s+2\delta}{(s+\delta)^2 + \omega_d^2} \cdot \frac{1}{s} = \frac{2\delta}{\delta^2 + \omega_d^2} \cdot \left(\frac{1}{s} - \frac{s+\delta}{(s+\delta)^2 + \omega_d^2} + \frac{\omega_d^2 - \delta^2}{2\delta\cdot\omega_d} \cdot \frac{\omega_d}{(s+\delta)^2 + \omega_d^2} \right),$$

which after inverse *Laplace* transformation yields for $t > 0$:

$$\frac{2\delta}{\delta^2 + \omega_d^2} \cdot \left(1 - e^{-\delta\cdot t} \cdot \cos(\omega_d \cdot t) + \frac{\omega_d^2 - \delta^2}{2\delta\cdot\omega_d} \cdot e^{-\delta\cdot t} \cdot \sin(\omega_d \cdot t) \right) \quad .$$

Note, that we can also write $\dfrac{2\delta}{\delta^2 + \omega_d^2} = \dfrac{\frac{1}{T_a}}{\frac{1}{T_a T_m}} = T_m$! With transformation to $\cos(\omega_d t - \psi)$:

$$\cos(\omega_d t) - \frac{\omega_d^2 - \delta^2}{2\delta \cdot \omega_d} \cdot \sin(\omega_d t) = C \cdot \cos\psi \cos(\omega_d t) + C \cdot \sin\psi \cos(\omega_d t) = C \cdot \cos(\omega_d t - \psi)$$

$$C \cdot \cos\psi = 1$$

$$C \cdot \sin\psi = -\frac{\omega_d^2 - \delta^2}{2\delta \cdot \omega_d} = -\frac{\frac{\omega_d^2 + \delta^2}{2\delta} - \delta}{\omega_d} = -\frac{\frac{1}{T_m} - \frac{1}{2T_a}}{\omega_d}$$

$$C^2 = 1 + \left(\frac{\frac{1}{T_m} - \frac{1}{2T_a}}{\omega_d} \right)^2 = \frac{\frac{1}{T_a^2} \cdot \left(\frac{T_a}{T_m} - \frac{1}{4} \right) + \frac{1}{T_m^2} + \frac{1}{4T_a^2} - \frac{1}{T_a T_m}}{\omega_d^2} = \frac{1}{\omega_d^2 T_m^2}$$

$$\psi = \arccos(1/C) = \arccos(\omega_d T_m)$$

we finally get the solution for transient speed response to load step in case of oscillations

$$\Delta\Omega_m(t) = -\frac{\Delta M_s}{J} \cdot T_m \cdot \left[1 - \frac{1}{\omega_d T_m} \cdot e^{-\frac{t}{2T_a}} \cdot \cos(\omega_d t - \psi) \right] \qquad (5.5\text{-}13)$$

or as per unit values

$$\frac{\Delta\Omega_m(t)}{\Omega_{m0}} = -\frac{\Delta M_s}{M_N} \cdot \frac{r_a}{\phi^2} \cdot \left[1 - \frac{1}{\omega_d T_m} \cdot e^{-\frac{t}{2T_a}} \cdot \cos(\omega_d t - \psi) \right] \qquad (5.5\text{-}14)$$

Example 5.5-1:

Separately excited DC machine with data: $T_J = 1\text{s}, T_a = 50ms, r_a = 0.05, \phi = 1$ with step in shaft torque of $\Delta M_s / M_N = 0.5$ leads to $\omega_d = 17.3/s, T_d = 363ms, T_m = 50ms$ and $\psi = \arccos(17.3 \cdot 0.05) = 0.526$.

The time function of transient speed response with *t* in units of seconds is (Fig. 5.5-4)

$$\frac{\Delta\Omega_m(t)}{\Omega_{m0}} = -0.5 \cdot \frac{0.05}{1} \cdot \left[1 - \frac{1}{0.865} \cdot e^{-\frac{t}{2 \cdot 0.05}} \cdot \cos(17.3 \cdot t - 0.526) \right].$$

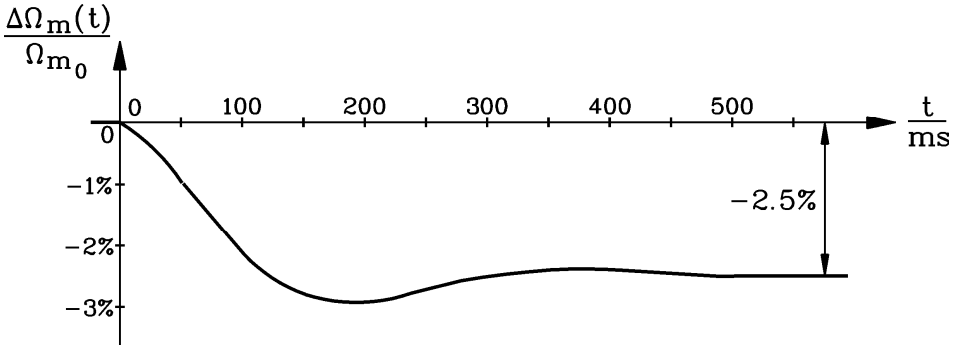

Fig. 5.5-4: Transient speed response to load step of 50% rated torque at rated voltage and no-load

After 1.7 half periods oscillation has nearly vanished. Steady state speed reduction for $t \to \infty$ is $\frac{\Omega_m(t \to \infty)}{\Omega_{m0}} = -0.5 \cdot \frac{0.05}{1} = -0.025 = \underline{\underline{-2.5\%}}$.

5.6 Dynamic simulation of separately excited DC machine

Dynamic simulation of separately excited DC machine (Fig. 5.6-1a) with numerical solver for several examples will be given in the following. Non-linear dependence of main flux per pole due to iron saturation is for simplification linearized according to Fig. 5.6-1b with

$$\Phi(i_f) = k_\Phi \cdot i_f \tag{5.6-1}$$

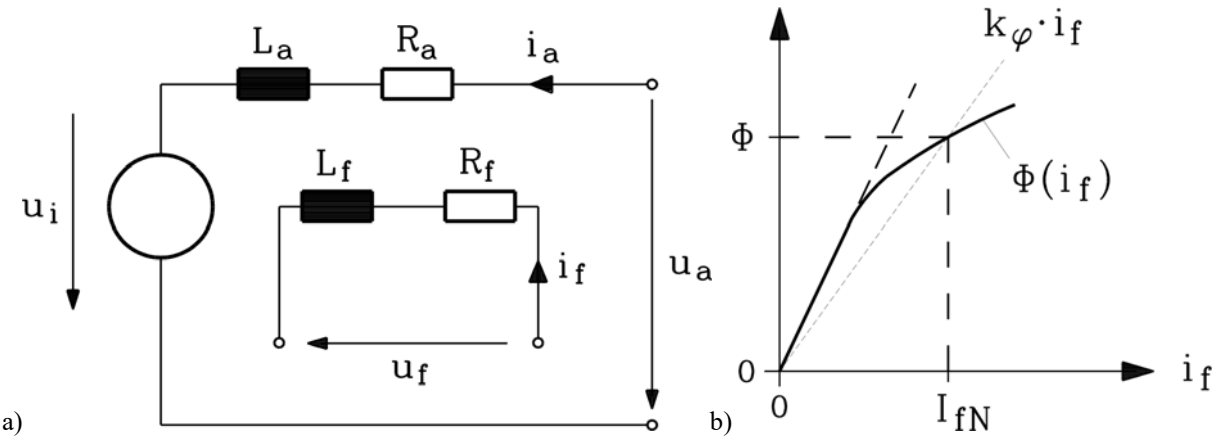

Fig. 5.6-1: Separately excited DC machine: a) Armature and field circuit, b) Non-linear dependence of main flux per pole due to iron saturation is linearized at point of rated field current

For using *Runge-Kutta* solver, the differential equations of Section 5.1 are written **in state space notation** with only first order differentiation occurring, where first order state space variables i_a, i_f, Ω_m are the unknowns, and leading variables u_a, u_f and disturbance variable m_s are to be defined as input along with initial conditions:

$$i_a(0), i_f(0), \Omega_m(0), u_a(0), u_f(0), m_s(0).$$

Large signal theory may be used here, as the differential non-linear equations are solved directly without any restriction.

$$\begin{aligned}
\frac{di_a(t)}{dt} &= \frac{u_a(t)}{L_a} - \frac{R_a}{L_a} \cdot i_a(t) - k_2 \cdot \Omega_m(t) \cdot \frac{k_\Phi}{L_a} \cdot i_f(t) \\
\frac{d\Omega_m}{dt} &= \frac{1}{J} \cdot k_2 \cdot i_a(t) \cdot k_\Phi \cdot i_f(t) - \frac{m_s(t)}{J} \\
\frac{di_f(t)}{dt} &= \frac{u_f(t)}{L_f} - \frac{R_f}{L_f} \cdot i_f(t)
\end{aligned} \tag{5.6-2}$$

Example 5.6-1:
Separately excited DC machine with following **motor** data, fed from ideal DC voltage:
$U_N = 460V, P_N = 142kW, n_N = 625/\min, I_N = 320A, I_{fN} = 6.5A, J_M = 7kg \cdot m^2$
$R_a = 0.05\Omega, L_a = 1.5mH, R_f = 25\Omega, L_f = 64H$. Load inertia: $J_L = 8\ \mathrm{kg \cdot m^2}$

Total inertia is the sum of motor and load inertia J_N = 15 kg·m^2. Note that due to large number of turns in the field winding only a small field current is necessary, but resistance and self-inductance of field winding are big in comparison to armature winding.
Calculation of basic quantities:

- Rated torque: $M_N = \frac{P_N}{2\pi \cdot n_N} = \frac{142000}{2\pi \cdot (625/60)} = 2169.6Nm$
- Induced voltage at rated speed and torque: $U_i = U_N - I_N \cdot R_a = 460 - 320 \cdot 0.05 = 444V$
- Motor constant and flux per pole: $k_2\Phi_N = \frac{U_i}{\Omega_{mN}} = \frac{444}{2\pi \cdot (625/60)} = 6.78Vs$
- Motor constant and flux coefficient: $k_2 k_\Phi = \frac{k_2\Phi_N}{I_{fN}} = \frac{6.78}{6.5} = 1.043H$
- Time constants:
  $T_a = \frac{L_a}{R_a} = \frac{0.0015}{0.05} = 30ms, T_f = \frac{L_f}{R_f} = \frac{64}{25} = 2.56s, T_m = \frac{R_a \cdot J}{(k_2\Phi_N)^2} = \frac{0.05 \cdot 15}{6.78^2} = 0.0163s$
- Motor efficiency: $\eta = \frac{P_N}{U_N \cdot I_N + R_f I_{fN}^2} = \frac{142000}{460 \cdot 320 + 25 \cdot 6.5^2} = 95.78\%$
- No-load speed at rated armature voltage and main flux:
  $n_0 = \frac{U_N}{2\pi \cdot k_2\Phi_N} = \frac{460}{2\pi \cdot 6.78} = 10.8/s = 647.9/\min$

As field time constant is much longer than armature time constant, dynamic torque control is done via armature voltage, not via field voltage.

a) Load step with rated torque at no-load speed, rated armature voltage and flux:
At time t = 0.2 s the machine is loaded at the shaft with rated torque 2169.6 Nm.

(i) Rated inertia:

$J_N = 15\,\mathrm{kg \cdot m^2}$ leads to a small mechanical time constant 16.3 ms. As $T_m = 16.3ms < 4T_a = 120ms$, damped oscillations occur with natural frequency and damping coefficient: $\delta = 1/(2T_a) = 1/(2 \cdot 0.03) = 16.67/s$.

Natural frequency: $f_d = \frac{1}{2\pi \cdot T_a}\sqrt{\frac{T_a}{T_m} - \frac{1}{4}} = \frac{1}{2\pi \cdot 0.03}\sqrt{\frac{0.03}{0.0163} - \frac{1}{4}} = 6.69Hz$

Period of oscillation is $T_d = 1/f_d = 1/6.69 = 149.5ms$

After $N_H = \frac{\omega_d}{\delta} = \frac{2\pi \cdot 6.69}{16.67} = 2.5$ half periods the oscillation is reduced down to 5% of initial value, reaching almost steady state condition.

(ii) Increased inertia:

Now **inertia is increased by 10 via a big load inertia**: $J = 150\,\mathrm{kg \cdot m^2}$, leading to a big mechanical time constant 163 ms. As $T_m = 163ms > 4T_a = 120ms$, no oscillations occur. Transient current and speed response are damped exponential functions with two time constants:

long time constant: $T_1 = \frac{2T_a}{1 - \sqrt{1 - \frac{4T_a}{T_m}}} = \frac{2 \cdot 30}{1 - \sqrt{1 - \frac{4 \cdot 30}{163}}} = 123.3ms$,

short time constant $T_2 = \dfrac{2T_a}{1+\sqrt{1-\dfrac{4T_a}{T_m}}} = \dfrac{2\cdot 30}{1+\sqrt{1-\dfrac{4\cdot 30}{163}}} = 39.6ms$

Electromagnetic torque and armature current have identical transient response, as main flux is kept constant. After three long time constants 95% of steady state condition is reached:
At $3T_1 = 3\cdot 123.3 = 370ms$ we get $0.95\cdot 320 = 304A$ and $0.95\cdot 2169.6 = 2061.4Nm$. Speed is reduced from no-load speed 647.9/min down to rated speed 625/min.

b) Armature voltage step at rated motor operation:
Motor is running with rated armature voltage, rated flux, rated speed and rated torque, thus consuming rated current. At time t = 0.2 s the machine´s armature voltage is increased with voltage step of 20% rated voltage: $\Delta U_a = 0.2U_N = 0.2\cdot 460 = 92V$. Main flux is kept constant. After transient response has vanished, motor´s new steady state values are:

- Shaft torque is still rated torque, so electromagnetic torque and armature current remain at rated value 2169.6 Nm and 320 A.
- Speed is raised according to:

$$n = \frac{1.2U_N + I_N R_a}{2\pi\cdot k_2\Phi_N} = \frac{1.2\cdot 460 - 0.05\cdot 320}{2\pi\cdot 6.78} = 12.58/s = 755/\min$$

(i) Rated inertia:

With rated inertia $J_N = 15\,\mathrm{kg\cdot m^2}$, transient armature current is a damped oscillation with a peak of only 1200 A (or 3.7-times rated current) with a duration of only about 50 ms, as a rather small inertia has to be accelerated. Also speed shows this oscillation, but to much smaller extent than current (and torque), as inertia is smoothing the speed time function. After $N_H = \dfrac{\omega_d}{\delta} = \dfrac{2\pi\cdot 6.69}{16.67} = 2.5$ half periods or 185 ms the oscillation is reduced down to 5% of initial value, reaching almost steady state condition (Fig.5.6-5).

(ii) Increased inertia:

With increased inertia $J = 150\,\mathrm{kg\cdot m^2}$ we get at $3T_1 = 3\cdot 123.3 = 370ms$ nearly steady state speed $0.95\cdot(755-625)+625 = 748/\min$. To accelerate the huge inertia, the armature current rises to about 1750 A or nearly 5.5-times rated current (Fig. 5.6-4).

c) Starting of DC motor at constant battery voltage with starting resistors:
Starting the motor from stand still with constant rated armature voltage e.g. form battery would lead at first moment to armature current peak $\hat{i}_a = U_N / R_a = 460/0.05 = 9200A$, which is nearly 29-times rated current, leading to exorbitant losses: $(9200/320)^2 = 826$-times rated armature losses. Therefore series armature resistor as **starting resistor** has to be used to limit starting current. As starting is rather quick, twice rated current may be permitted to flow, demanding a starting resistor

$$R_{s,1} = \frac{U_N}{2I_N} - R_a = \frac{460}{2\cdot 320} - 0.05 = \underline{\underline{0.67\Omega}} \quad . \qquad (5.6\text{-}3)$$

If the starting of the machine is done under rated load, armature current will first "jump" with armature time constant 30 ms up to twice rated current 640 A and then decline to steady state current 320 A. Starting of motor may be accelerated, if a smaller series resistor $R_{s,2}$ is

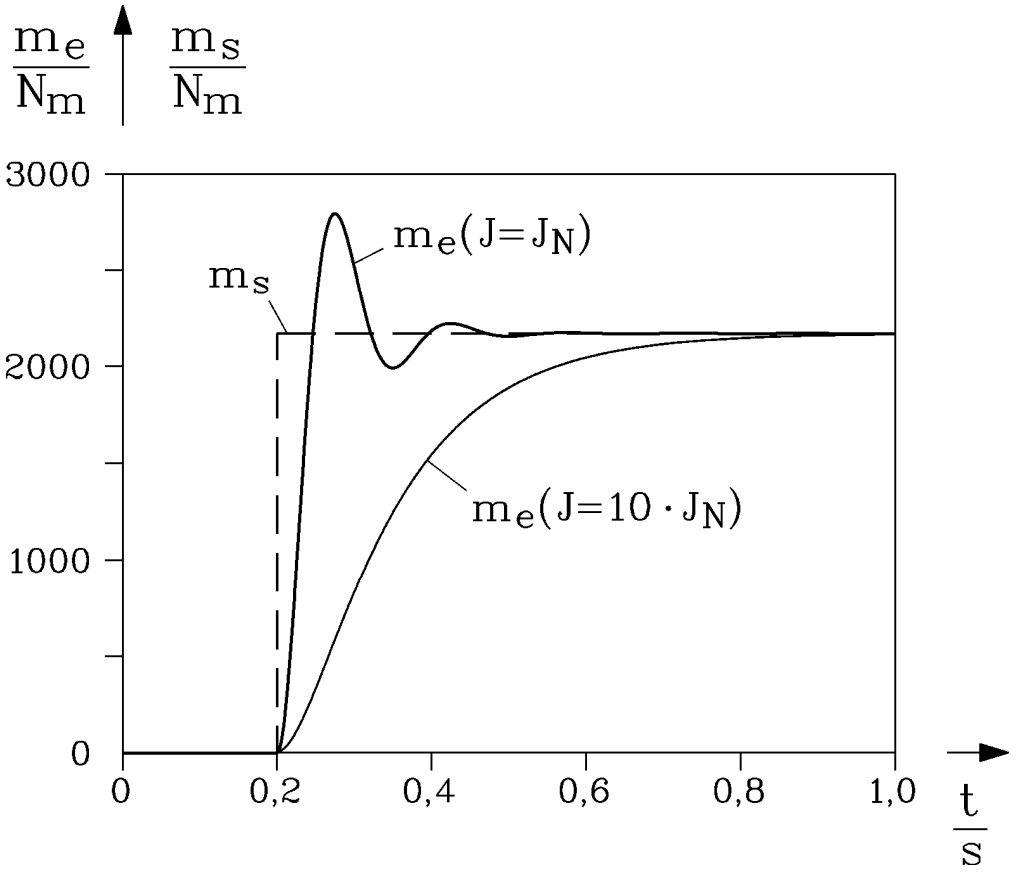

Fig. 5.6-2: Load torque step $m_s(t)$ of rated torque at $t = 0.2$s leads to transient rise of electromagnetic torque $m_e(t)$ a) with oscillations (bold line) at $J_N = 15$ kg·m^2, b) at $10J_N = 150$ kg·m^2 (thin line) without oscillations

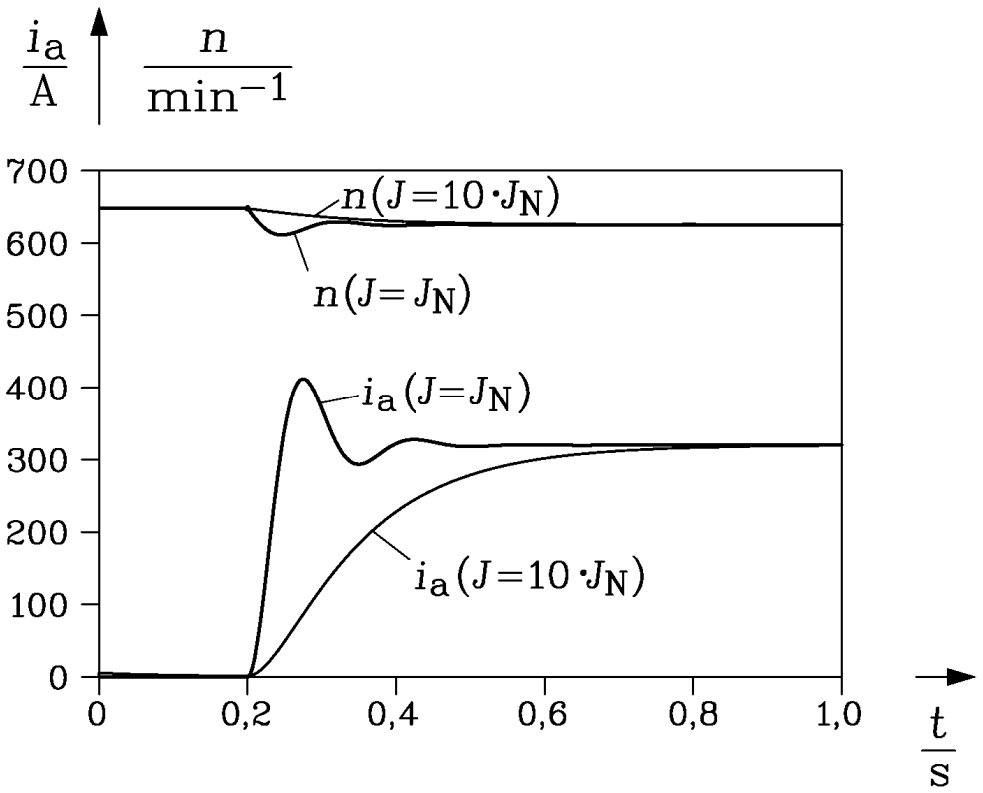

Fig. 5.6-3: Load torque step of rated torque at $t = 0.2$s leads to transient rise of armature current $i_a(t)$ a) with oscillations (bold line) at $J_N = 15$ kg·m^2, b) at $10J_N = 150$ kg·m^2 (thin line) without oscillations

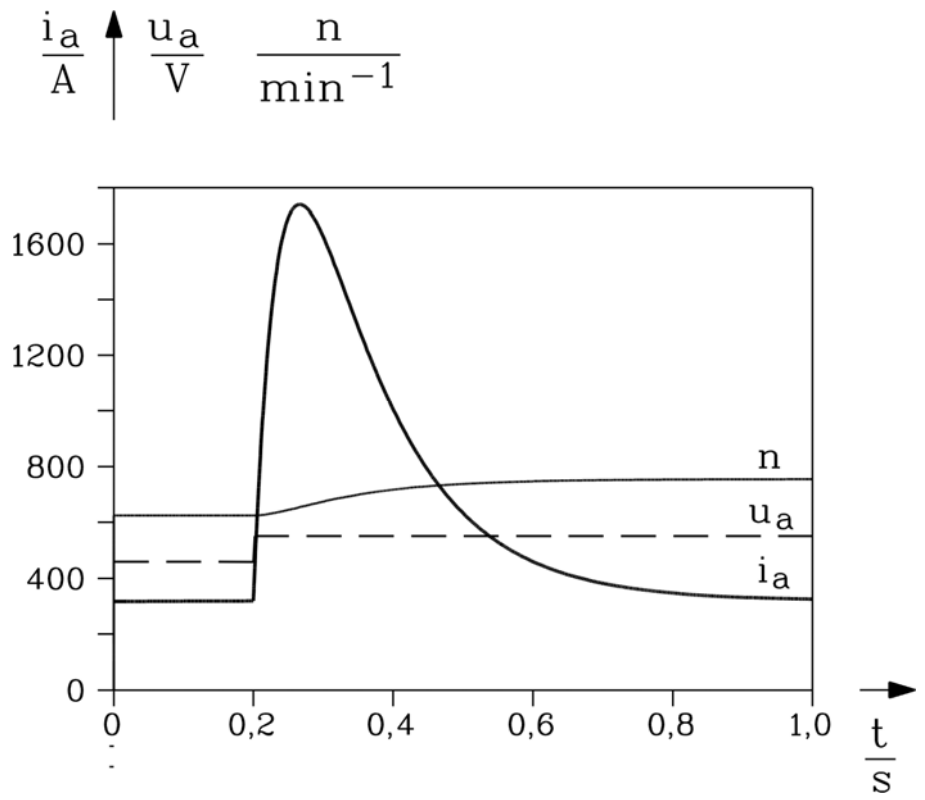

Fig. 5.6-4: Armature voltage step of 20% rated voltage at t = 0.2s (dashed line) and rated operation leads to 550% transient peak of armature current $i_a(t)$ for accelerating inertia $10J_N$ = 150 kg·m^2 (bold line) and steady state rise of speed by 20.8% (thin line)

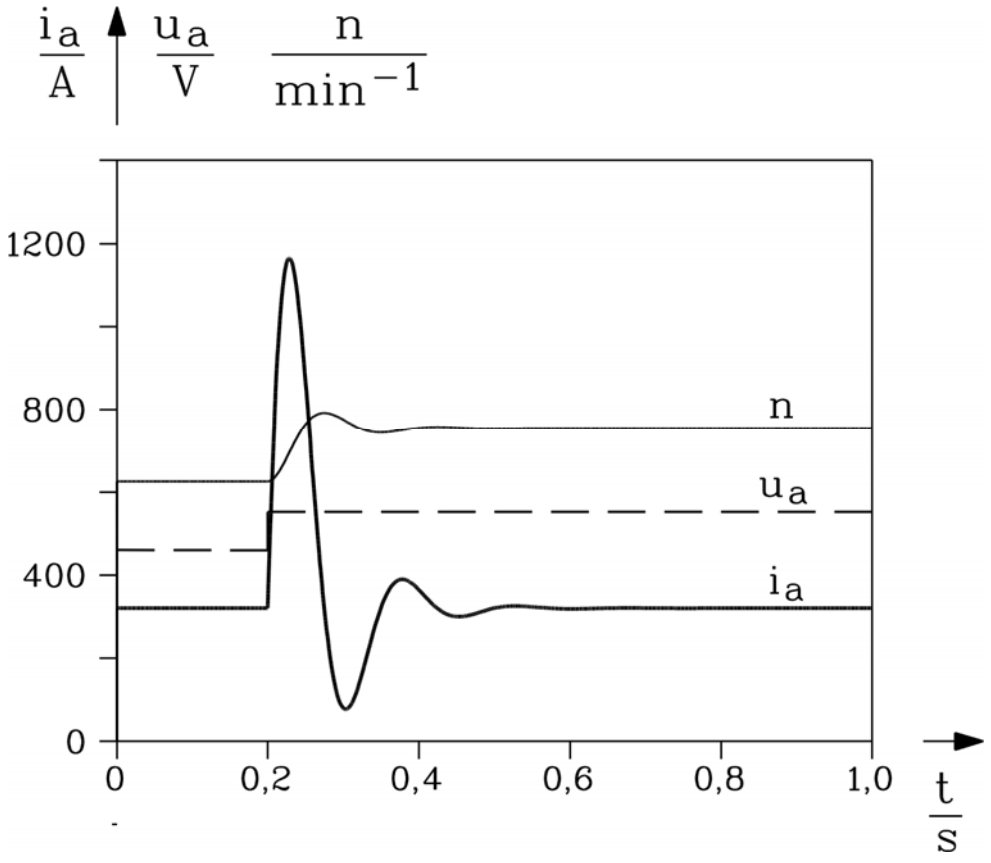

Fig. 5.6-5: Armature voltage step of 20% rated voltage at t = 0.2s (dashed line) and rated operation leads to 375% transient peak of armature current $i_a(t)$ for accelerating the inertia J_N = 15 kg·m^2 (bold line). Steady state rise of speed by 20.8% (dashed line) is independent of inertia and thus the same as in Fig. 5.6-4.

switched instead of $R_{s,1}$, when armature current is just 2% above rated current. With that smaller series resistance, being designed in that way, that next current peak again rises up to 640 A, additional boosting of acceleration is achieved. Repeating this again two times, when current decreases down to 102% rated current, demands two another series resistors $R_{s,3}$, $R_{s,4}$, the latter finally being short circuited to run the motor without any series resistance at rated conditions.
With series resistor $R_{s,1}$ motor would run up with rated torque load only to steady state speed

$$n_{1,\infty} = \frac{U_N - (R_{s,1} + R_a) \cdot I_N}{2\pi \cdot k_2 \Phi_N} = \frac{460 - (0.67 + 0.05) \cdot 320}{2\pi \cdot 6.78} = 5.39/s \qquad (5.6\text{-}4)$$

At that speed induced voltage already limits armature current, so for second series resistor, which allows twice rated current as maximum current peak, we get

$$R_{s,2} = \frac{U_N - 2\pi \cdot n_{1,\infty} \cdot k_2 \Phi_N}{2I_N} - R_a = \frac{460 - 2\pi \cdot 5.39 \cdot 6.78}{2 \cdot 320} - 0.05 = \frac{460 - 229.6}{2 \cdot 320} - 0.5 = \underline{\underline{0.31\Omega}}\,.$$

With that smaller series resistor steady state speed is already higher:

$$n_{2,\infty} = \frac{U_N - (R_{s,2} + R_a) \cdot I_N}{2\pi \cdot k_2 \Phi_N} = \frac{460 - (0.31 + 0.05) \cdot 320}{2\pi \cdot 6.78} = 8.09/s \quad , \qquad (5.6\text{-}5)$$

and therefore next series resistor $R_{s,3}$ is smaller according to

$$R_{s,3} = \frac{U_N - 2\pi \cdot n_{2,\infty} \cdot k_2 \Phi_N}{2I_N} - R_a = \frac{460 - 2\pi \cdot 8.09 \cdot 6.78}{2 \cdot 320} - 0.05 = \frac{460 - 344.6}{2 \cdot 320} - 0.5 = \underline{\underline{0.13\Omega}}\,.$$

Corresponding steady state speed is

$$n_{3,\infty} = \frac{U_N - (R_{3,2} + R_a) \cdot I_N}{2\pi \cdot k_2 \Phi_N} = \frac{460 - (0.13 + 0.05) \cdot 320}{2\pi \cdot 6.78} = 9.45/s \quad , \qquad (5.6\text{-}6)$$

yielding value for last series resistor as

$$R_{s,4} = \frac{U_N - 2\pi \cdot n_{3,\infty} \cdot k_2 \Phi_N}{2I_N} - R_a = \frac{460 - 2\pi \cdot 9.45 \cdot 6.78}{2 \cdot 320} - 0.05 = \frac{460 - 402.6}{2 \cdot 320} - 0.5 = \underline{\underline{0.04\Omega}}\,.$$

After reaching with this series resistor 102% rated armature current, this resistor is short circuited, and motor is running without any series resistor at rated speed and torque.

(i) Rated inertia:

At rated inertia $J_N = 15\,\mathrm{kg \cdot m^2}$, the mechanical time constants are small (Table 5.6-1). Therefore starting is going on rather fast within 2 s (Fig. 5.6-8). Due to dynamical current rise with armature time constant $T_{a,1}$, ..., the current peak at low series resistor values at third and fourth stage and after short-circuiting does not reach twice rated current any longer, but stays below at 400 A ... 580 A. The speed-current-characteristics at these stages therefore deviate from steady state $n(I_a)$ –characteristics (Fig. 5.6-9).

(ii) Increased inertia:

If inertia is increased by factor 10: $J = 150\,\mathrm{kg \cdot m^2}$, the mechanical time constants are bigger by a factor 10 (Table 5.6-1). Therefore starting is going on rather slowly within 20 s instead of

2 s (Fig. 5.6-8). Series resistors increase the mechanical time constant significantly according to Table 5.6-1, for example for first stage, and decrease armature time constant:

$$T_{m,1} = \frac{(R_a + R_{s,1}) \cdot J}{(k_2 \Phi_N)^2} = \frac{(0.05 + 0.67) \cdot 150}{6.78^2} = 2.35s\,. \tag{5.6-7}$$

$$T_{a,1} = \frac{L_a}{R_a + R_{s,1}} = \frac{0.0015}{0.05 + 0.67} = 2.0ms\,. \tag{5.6-8}$$

Series resistor	T_a/ms	(i) Rated inertia $15\,kg \cdot m^2$	(ii) Increased inertia $150\,kg \cdot m^2$
$R_{s,1} = 0.67\Omega$	2.0	$T_{m,1} = 235ms$	$T_{m,1} = 2.35s$
$R_{s,2} = 0.31\Omega$	4.2	$T_{m,2} = 117ms$	$T_{m,2} = 1.17s$
$R_{s,3} = 0.13\Omega$	8.3	$T_{m,3} = 58.7ms$	$T_{m,3} = 587ms$
$R_{s,4} = 0.04\Omega$	16.7	$T_{m,4} = 29.3ms$	$T_{m,4} = 293ms$
0	30	$T_m = 16.3ms$	$T_m = 163ms$

Table 5.6-1: Mechanical time constants for different series resistors and inertia

So with increased inertia and first stage series resistor after about $3T_{m,1} = 3 \cdot 2.35 = 7.05s$ 95% of the steady state speed $n_{1,\infty}$ is reached (Fig. 5.6-6), and at about 10 s the second stage resistor is switched.
After $3T_{m,2} = 3 \cdot 1.17 = 3.5s$ 95% of the steady state speed $n_{2,\infty}$ is reached at 10 + 3.5 = 13.5 s. At about 15 s the third stage is switched, at which after about $3T_{m,3} = 3 \cdot 0.587 = 1.8s$ 95% of the steady state speed $n_{3,\infty}$ is reached at 15 + 1.8 = 16.8 s. At 17 s the fourth stage is switched, at which after about $3T_{m,4} = 3 \cdot 0.293 = 0.9s$ 95% of the steady state speed $n_{4,\infty}$ is reached at 17 + 0.9 = 17.9 s. At about 18.5 s fourth series resistor is short circuited, and after about $3T_m = 3 \cdot 0.163 = 0.5s$ 95% of the steady state speed n_N is reached at 18.5 + 0.5 = 19 s. At 20 s simulation is ended.
Due to these big mechanical time constants the starting of DC motor is **quasi-static**. The speed-current characteristic of starting **is nearly equal** to the steady state speed-current characteristics:

With series resistor $R_{s,1}$: $n_1 = \frac{U_N - (R_{s,1} + R_a) \cdot I_a}{k_2 \Phi_N}$ (5.6-9)

With series resistor $R_{s,2}$: $n_2 = \frac{U_N - (R_{s,2} + R_a) \cdot I_a}{k_2 \Phi_N}$ (5.6-10)

and so on also for $R_{s,3}$, $R_{s,4}$ and finally $n = \frac{U_N - R_a \cdot I_a}{k_2 \Phi_N}$.

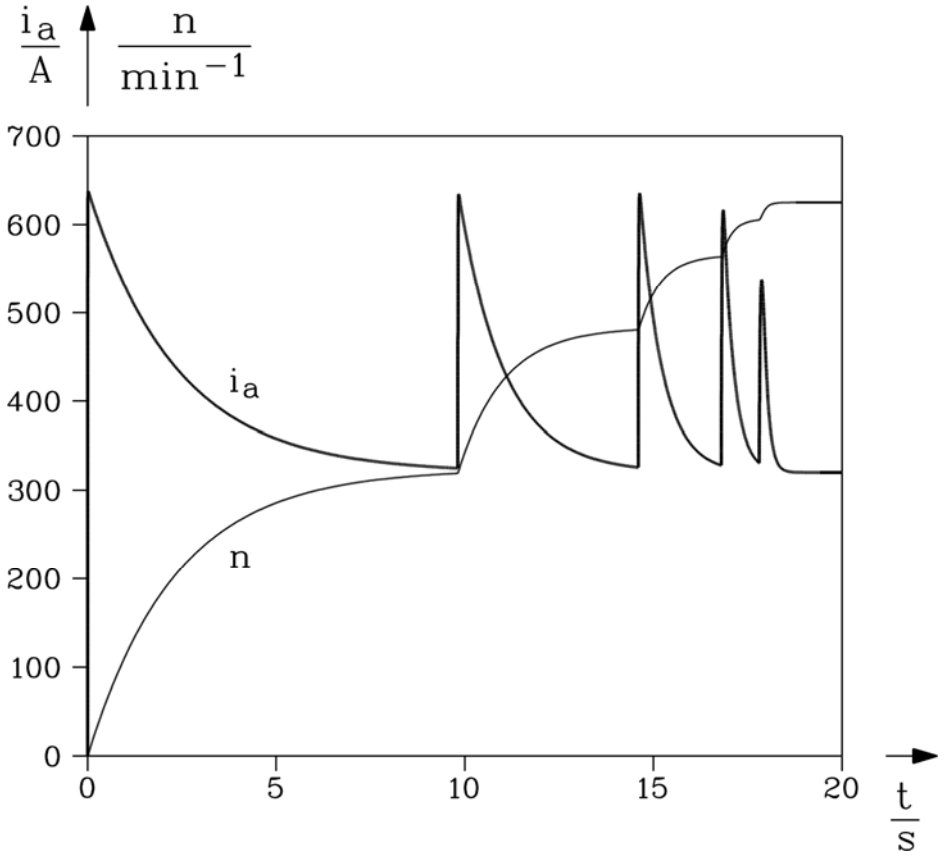

Fig. 5.6-6: Starting of DC machine with rated flux, rated load, rated armature voltage and increased inertia $10J_N$ = 150 kg·m^2 with series resistors 0.67 Ohm, 0.31 Ohm, 0.13 Ohm, 0.04 Ohm, switched one after the other. Series resistors limit armature current peak to twice rated current 640 A (bold line), whereas speed steps up with different steady state speed steps $n_{1,\infty}$, $n_{2,\infty}$, $n_{3,\infty}$, $n_{4,\infty}$, n_N (thin line).

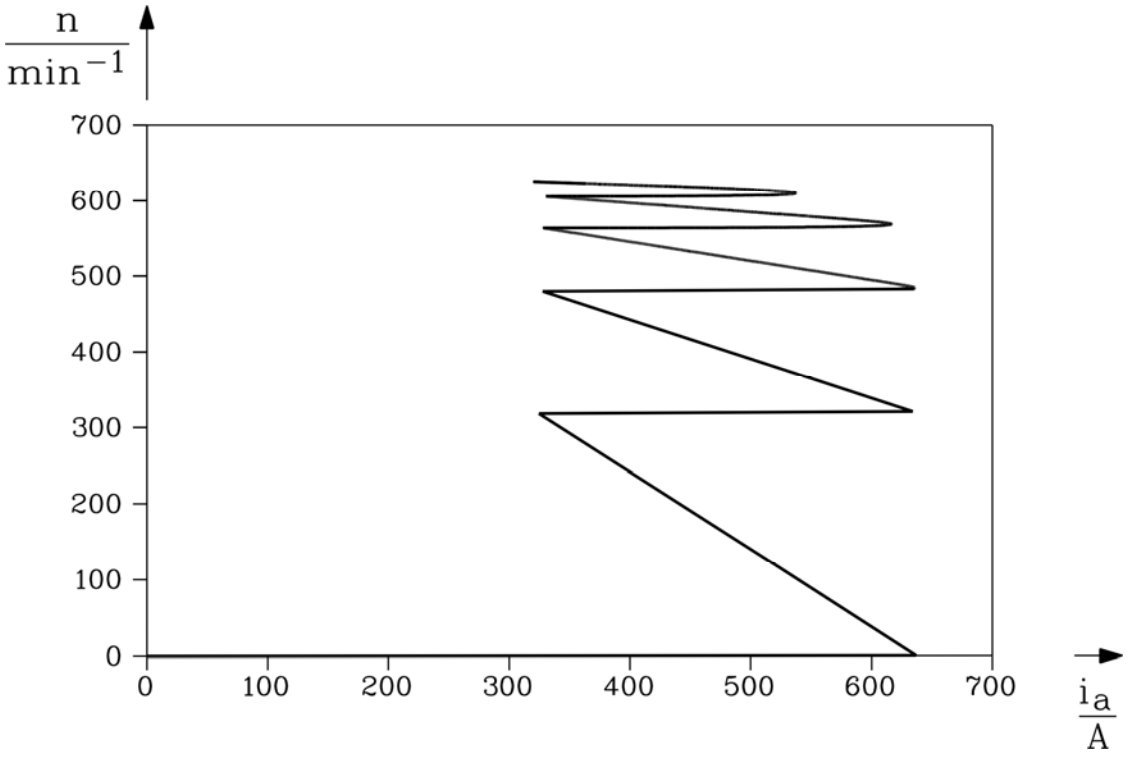

Fig. 5.6-7: Speed-current characteristic of starting of DC machine with rated flux, rated load, rated armature voltage and increased inertia $10J_N$ = 150 kg·m^2 with series resistors 0.67 Ohm, 0.31 Ohm, 0.13 Ohm, 0.04 Ohm, switched one after the other.

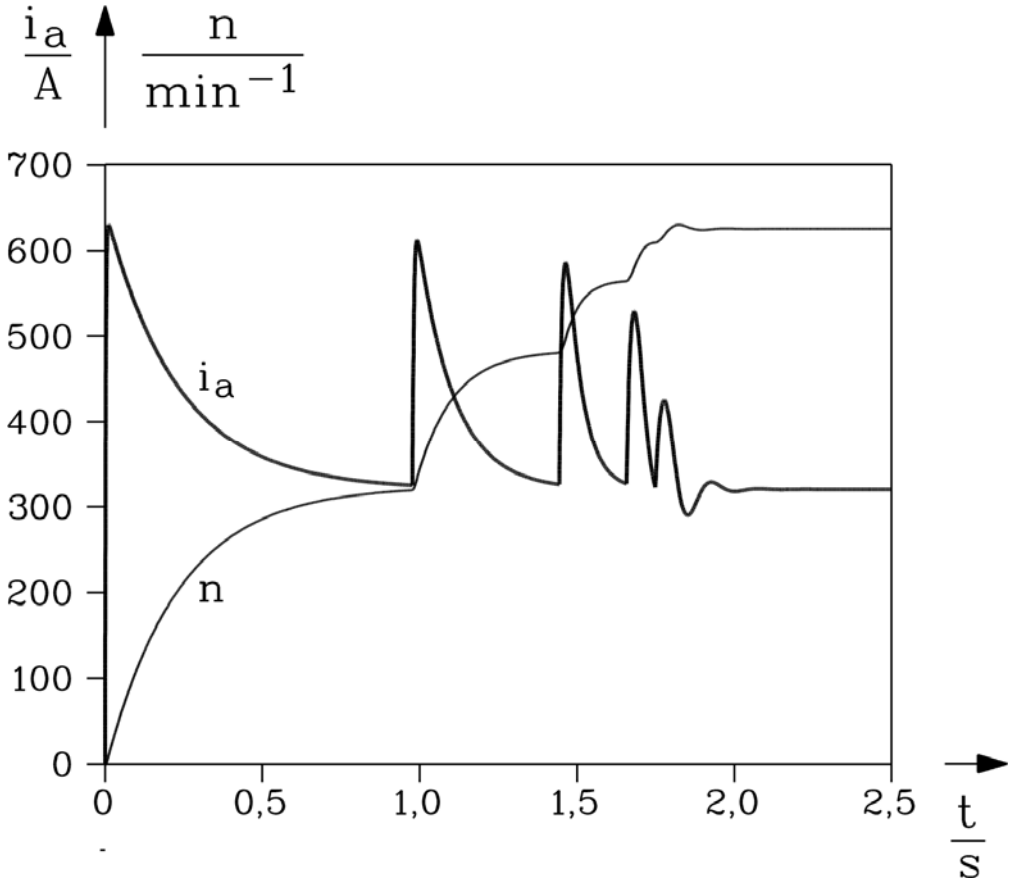

Fig. 5.6-8: Starting of DC machine with rated flux, rated load, rated armature voltage and **rated inertia J_N = 15 kg·m²** with series resistors 0.67 Ohm, 0.31 Ohm, 0.13 Ohm, 0.04 Ohm, switched one after the other. Series resistors limit armature current peak to twice rated current 640 A (bold line), whereas speed steps up with different steady state speed steps $n_{1,\infty}$, $n_{2,\infty}$, $n_{3,\infty}$, $n_{4,\infty}$, n_N (thin line).

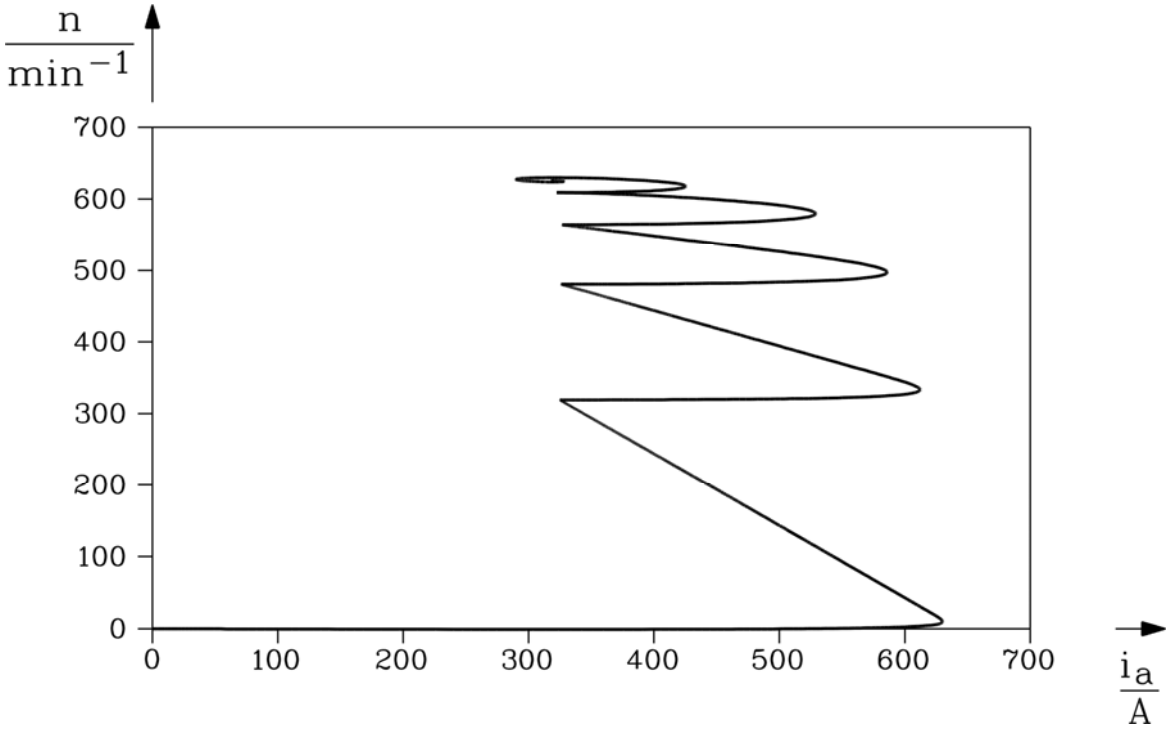

Fig. 5.6-9: Speed-current characteristic of starting of DC machine with rated flux, rated load, rated armature voltage and **rated inertia J_N = 15 kg·m²** with series resistors 0.67 Ohm, 0.31 Ohm, 0.13 Ohm, 0.04 Ohm, switched one after the other.

5.7 Converter operated separately excited DC machine

Usually DC machines are operated from DC converters (Fig. 5.7-1), where three phase AC voltage from the grid is rectified with six pulse voltage-controlled thyristor bridge (B6C). With switch-on angle α of thyristors the voltage is varied between $+U_{d0}$ (at $\alpha = 0°$) and $-U_{d0}$ (at $\alpha = 180°$) according to

$$U_d(\alpha) = U_{d0} \cdot \cos\alpha \qquad U_{d0} = \frac{3}{\pi} \cdot U_{LL} \cdot \sqrt{2} \quad . \tag{5.7-1}$$

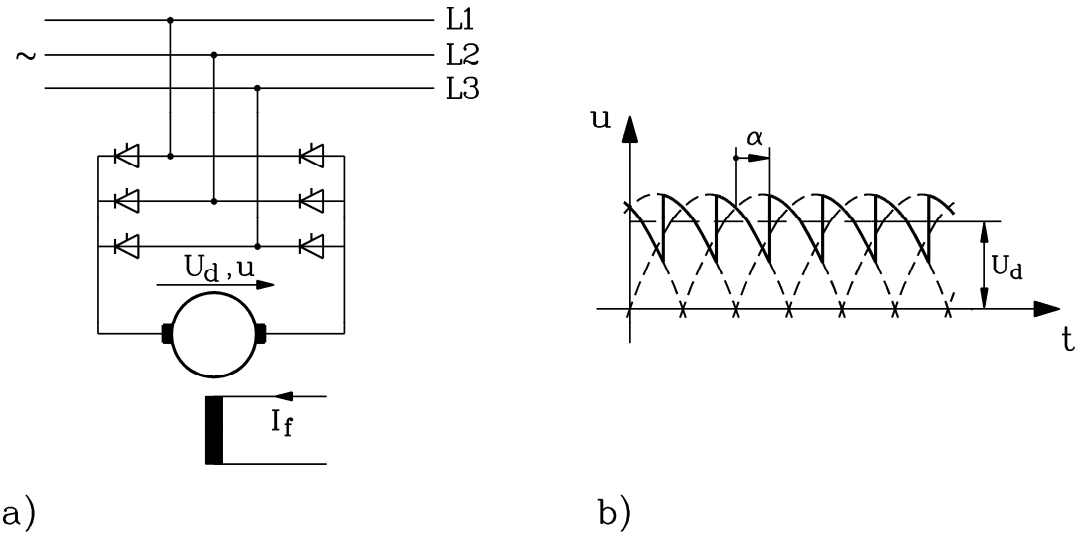

Fig. 5.7-1: Six pulse voltage-controlled thyristor bridge (B6C): With switch-on angle α of thyristors the voltage is varied between $+U_{d0}$ (at $\alpha = 0°$) and $-U_{d0}$ (at $\alpha = 180°$)

$U_a <> 0, I_a > 0$	B6C: One six-pulse, voltage controlled thyristor bridge, 6 thyristors. Voltage and current ripple: $6f$ = 300 Hz. $n \lesseqgtr 0, M \geq 0$, but often only: One quadrant operation: $n \geq 0, M \geq 0$
$U_a <> 0, I_a <> 0$	(B6C)A(B6C): Two anti-parallel six-pulse, voltage controlled thyristor bridges, 12 thyristors Voltage and current ripple: $6f$ = 300 Hz Four quadrants operation: $n <> 0, M <> 0$
$U_f \geq 0, I_f \geq 0$ $\Phi \geq 0$	B2H: One two-pulse, voltage controlled thyristor-diode bridge, 2 thyristors, 2 diodes Voltage and current ripple: $2f$ = 100 Hz
$U_f <> 0, I_f \geq 0$ $\Phi \geq 0$	B2C: One two-pulse, voltage controlled thyristor bridge, 4 thyristors Voltage and current ripple: $2f$ = 100 Hz
$U_f <> 0, I_f \geq 0$ $\Phi \geq 0$	B6C: One six-pulse, voltage controlled thyristor bridge, 6 thyristors Voltage and current ripple: $6f$ = 300 Hz

Table 5.7-1: Different configurations of controlled rectifier bridges for armature and field circuit of separately excited DC machines

As armature current may flow only into one direction, given by thyristor cathode to anode, only positive torque is possible. For positive and negative torque a second, anti-parallel thyristor bridge is connected to DC machine armature (B6C)A(B6C). For separately excited field circuit full (or the cheaper half) controlled thyristor bridges are used, being operated

from one line-to-line voltage in single phase mode as two-pulse field voltage control: B2C or B2H, but also six-pulse voltage control with less current ripple from three-phase AC voltage system is in use. Mostly no anti-parallel bridge is used, so no reversal of field current and main flux is possible.
Armature voltage is used for **speed control**, so rated armature voltage must be lower than maximum armature voltage to have a voltage margin for voltage control.

Example 5.7-1:
Three-phase AC 400 V grid, B6C-bridge:

maximum voltage: $U_d(\alpha = 0) = U_{d0} \cdot \cos 0 = U_{d0} = \frac{3}{\pi} \cdot U_{LL} \cdot \sqrt{2} = \frac{3}{\pi} \cdot 400 \cdot \sqrt{2} = 540V$

rated voltage: $U_d(\alpha = 30°) = U_{d0} \cdot \cos 30° = 540 \cdot \frac{\sqrt{3}}{2} = 460\,\mathrm{V}$

voltage margin for voltage control: $\Delta U_d = 540V - 460V = 80V$

So thyristor bridge is operated between $30° < \alpha < 150°$.

Example 5.7-2:
Three-phase AC 400 V grid, usual rated and maximum voltages:

	Maximum voltage	Rated voltage	
B6C	540 V	460 V	1 quadrant operation
(B6C)A(B6C)	540 V	400 V	4 quadrant operation

Limits of DC machine operation (Fig. 5.7-2) are given by
- armature current limit,
- armature voltage limit,
- commutation limit,
- speed limit n_{max}.

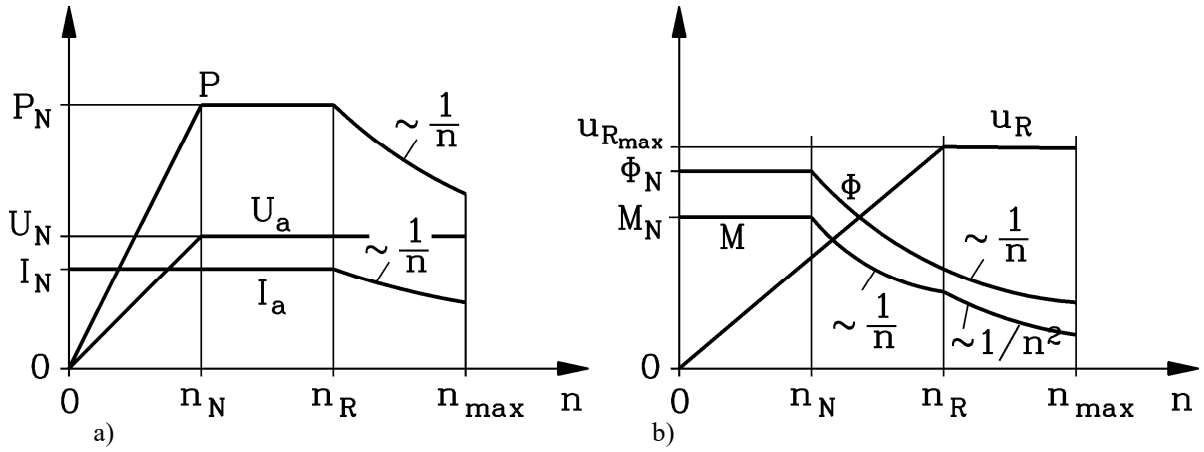

Fig. 5.7-2: Limits of a) armature voltage, armature current, machine power and b) main flux, electromagnetic torque and reactance voltage of commutation u_R

$0 \le n \le n_N$	**Voltage controlled** DC machine: Limits: Maximum armature current, maximum flux
$n_N \le n \le n_R$	Flux controlled DC machine (**Field weakening**): Limits: Maximum armature current and voltage
$n_R \le n \le n_{max}$	Flux controlled DC machine (Field weakening): Limits: Maximum armature and **reactance voltage of commutation**

Table 5.7-2: Limits of DC machine operation

The reactance voltage of commutation u_R, which is induced by reversal of armature current during current commutation, is increasing with current and speed:

$$u_R \sim n \cdot I_a \tag{5.7-2}$$

Usually commutation voltage shall be limited to 12 V to avoid intensive sparking of brushes at trailing edge. This limit is reached for rated current $I_a = I_N$ at speed n_R. Above that speed armature current has to be reduced $I_a \sim 1/n$ to keep commutation voltage constant.

Anti-parallel thyristor bridges may be controlled either
a) by switching off on bridge and operating the other on or
b) by operating both bridges with the same rectified DC voltage, but only one bridge carries the armature current.

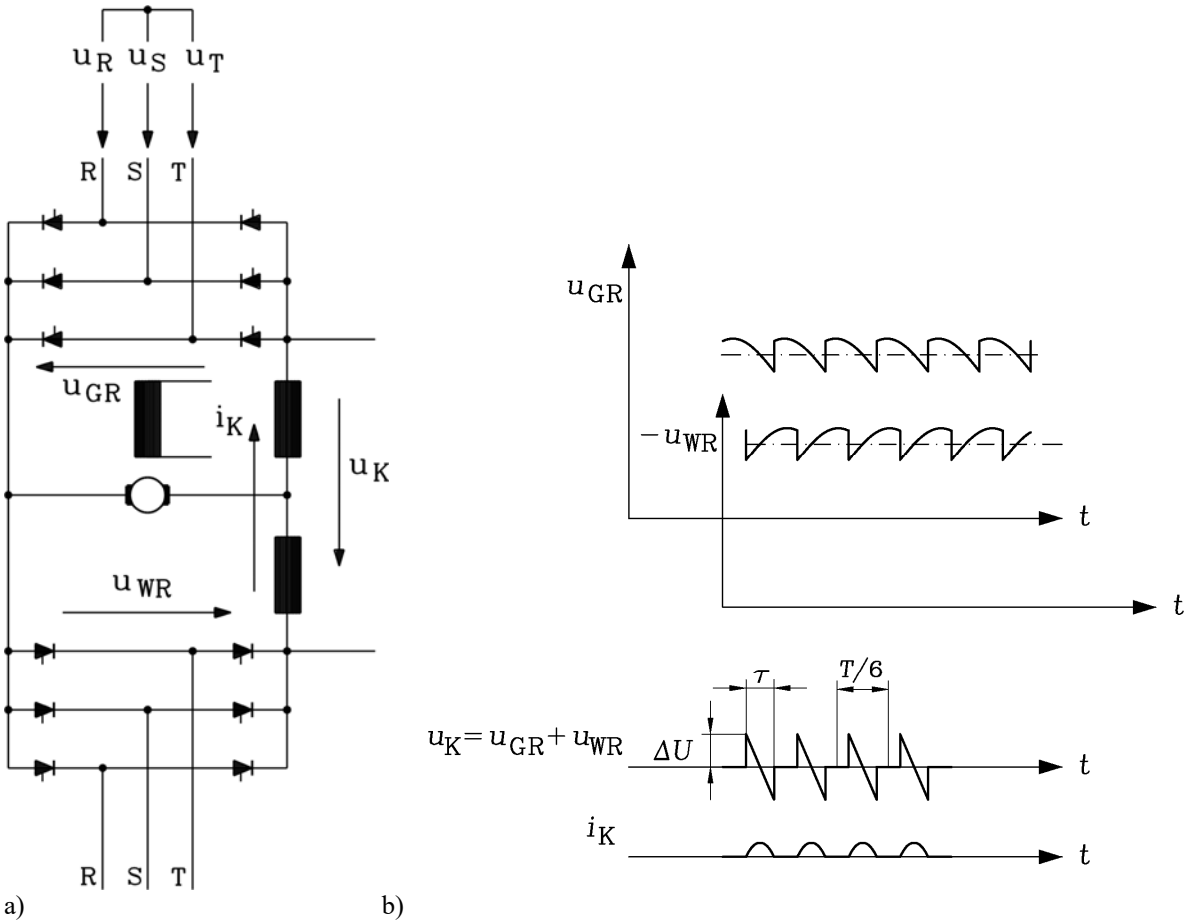

Fig. 5.7-3: a) Anti-parallel (B6C)A(B6C) thyristor bridges operating in parallel with the same DC voltage, which leads to b) parasitic circulating current $i_K(t)$, driven by the difference of momentary voltages of both bridges $u_K(t)$

Method b) has the advantage, that at armature current reversal the other bridge takes over operation very quickly, but has the disadvantage that a parasitic circulating current flows through both bridges (Fig. 5.7-3).

If first bridge (called GR) is operating with ignition angle α_{GR}, leading to DC voltage

$$U_{d,GR} = U_{d0} \cdot \cos(\alpha_{GR}) \quad , \tag{5.7-3}$$

then second anti-parallel bridge (WR) must be operated with $\alpha_{WR} = \pi - \alpha_{GR}$.

$$U_{d,WR} = U_{d0} \cdot \cos(\alpha_{WR}) = U_{d0} \cdot \cos(\pi - \alpha_{GR}) = -U_{d0} \cdot \cos(\alpha_{GR}) \tag{5.7-4}$$

According to Fig. 5.7-3 the voltage $-U_{d,WR} = U_{d0} \cdot \cos(\alpha_{GR})$ is the same as $U_{d,GR}$, but only for average values. The momentary voltages $u_{GR}(t), u_{WR}(t)$ differ, leading to differential voltage

$$u_K(t) = u_{GR}(t) + u_{WR}(t) \quad , \tag{5.7-5}$$

which has a sinusoidal and for $\omega\tau << 1, \omega = 2\pi f$ a more or less triangular shape.

$$u_K(t) = -\Delta U \cdot \sin(\omega t) / \sin(\omega\tau/2) \approx -2\Delta U \cdot t/\tau \qquad -\tau/2 \le t \le \tau/2 \tag{5.7-6}$$

The circulating parasitic current $i_K(t)$ loads both thyristor bridges, but not the DC machine or the grid. With additional chokes L in the DC circuit this current may be reduced, leading to a cosines or nearly **parabola shaped circulating current ripple i_K** for $-\tau/2 \le t \le \tau/2$.

$$i_K(t) = \frac{1}{L}\int_{-\tau/2}^{t} u_K(t) \cdot dt = \frac{U_K}{\omega L_K} \cdot \frac{\cos(\omega t) - \cos(\omega\tau/2)}{\sin(\omega\tau/2)} \approx \frac{\Delta U}{\tau \cdot L} \cdot \left(\left(\frac{\tau}{2}\right)^2 - t^2 \right) \tag{5.7-7}$$

Thyristor bridge operation feeds the DC machine with DC voltage and a voltage ripple, which leads to **armature current ripple i_a** of the same period. The armature inductance L_a is small, so smoothing of current is also small. In case of B6-bridges the armature current shows six parabolic current humps, so armature current consists of DC (average) value and AC harmonics of $6f_s$, $12f_s$, $18f_s$, ..., which at f_s = 50 Hz is 300 Hz, 600 Hz, 900 Hz,...

This **AC current ripple i_a** leads to (Fig. 5.7-4)
- increased armature losses,
- increased sparking at the brushes due to AC current commutation,
- 300 Hz magnetically excited acoustic noise, caused by pulsating armature magnetic field,
- 300 Hz torque ripple.

In the same way a B2H or B2C single phase thyristor bridge for rectifying field voltage leads to DC field voltage with considerable AC voltage ripple with AC harmonics of $2f_s$, $4f_s$, $6f_s$, ... which at f_s = 50 Hz is 100 Hz, 200 Hz, 300 Hz, ... (Fig. 5.7-4).

The big field inductance L_f is smoothing the field current very well, **so field current is nearly ideal DC current.**

In case of **uncompensated DC machines** the armature field adds to the main field and leads at rated current already to increased saturation. Therefore a certain coupling between field and armature circuit occurs, which can be seen in Fig. 5.7-4 as a **300 Hz-ripple** in the field current, which is caused by the changing saturation of changing armature field, which modulates L_f with 300 Hz.

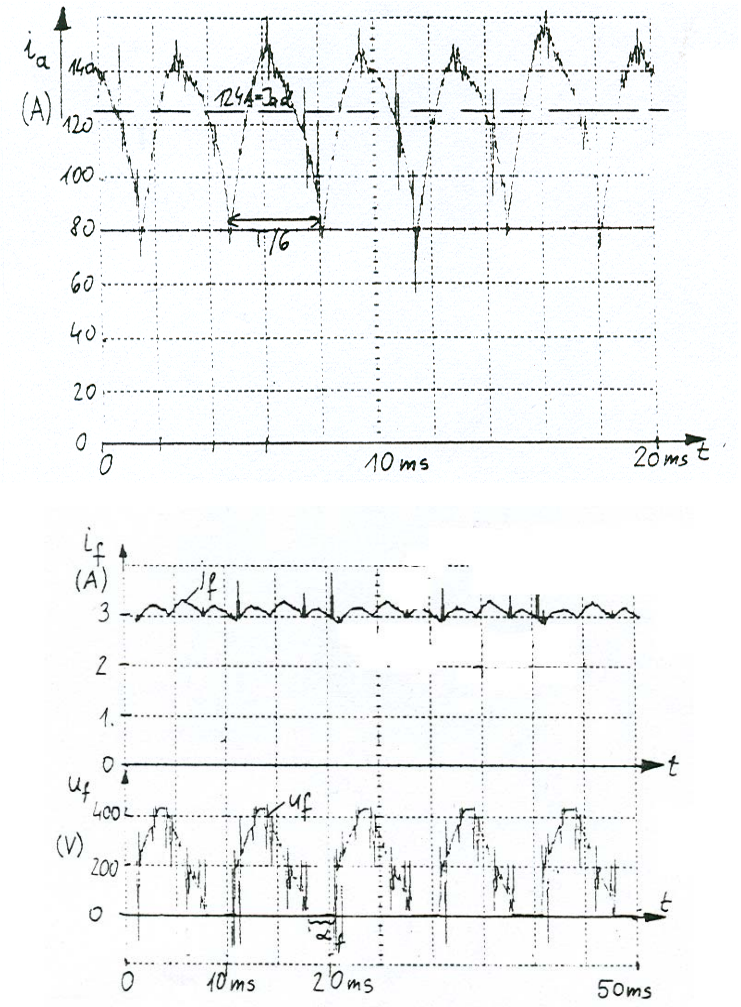

Fig. 5.7-4: Measured armature and field current of a 40 kW separately excited DC motor, fed by B6C armature thyristor bridge and B2H field thyristor bridge: i_a: armature current, u_f: field voltage, i_f: field current.

Example 5.7-3:

4-pole separately excited DC motor, frame size 132 mm, open ventilated, external fan, uncompensated, 40 kW, rated speed 2250/min, maximum speed 5000/min, rated armature current 120 A, rated armature voltage 400 V, rated field current 3 A.

Motor is operated from B6C-thyristor bridge, field is supplied from B2H-bridge. Measured time function with oscilloscope of armature current (Fig. 5.7-4) at rated torque and speed shows average armature current 124 A, but 300 Hz ripple reaches 150 A. Field current has average value of 3.1 A and small AC current ripple of 300 Hz due to armature field, and very small 100 Hz ripple due to 100Hz voltage ripple.

Classic DC machine control concept is based on the fact, that electric time constant T_a is usually significantly smaller than mechanical time constant T_m. So cascaded control circuit is used with inner control loop with PI-controller for armature current, which acts on electric armature circuit with small time constant. Outer control loop for speed is more slowly due to bigger mechanical time constant. So speed controller demands for certain torque to adjust actual speed a certain armature current from inner loop current controller. Current controller commands thyristor bridge via ignition angle α for certain armature voltage to get the necessary actual current.

Measured average current must be measured for at least 1/300 Hz = 3.33 ms to equalize the armature current ripple. So a minimum control time for actual armature current to reach for first time set point current value is 3.3 ms (Fig. 5.7-5).

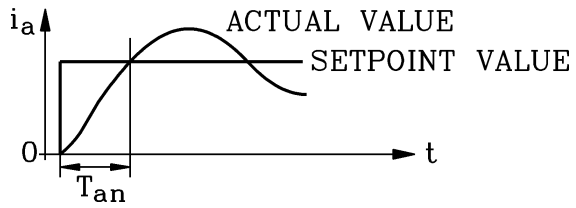

Fig. 5.7-5: Minimum time T_{an} for actual DC armature current to reach set point current is 3.3 ms in B6C bridge controlled DC machines, operated from 50 Hz grid

For **armature current reversal** from $+I_a$ to $-I_a$ (e.g. from motor operation to regenerative braking) different possibilities do exist:
a) Anti-parallel thyristor bridges with both bridges operating in parallel
b) As a), but always only one bridge active
c) Armature polarity changer with mechanical switch.

a) (B6C)A(B6C)	*b) (B6C)A(B6C)*	*c) Mechanical switch*
Both bridges always active	Only one bridge active	Polarity changer
< 0.5 ms	5 ... 10 ms	50 ... 1500 ms

Table 5.7-3: Time for reversal of armature current. The larger numbers correspond with larger drives of several hundreds of kW up to MW range.

For reversing torque not only armature current, but also reversal of main flux is possible, but is not used very often, because dynamical performance is poor due to big field time constant T_f. On the other hand ist is rather cheap, as field current usually is small. For **field current reversal** from $+I_f$ to $-I_f$ different possibilities do exist:
a) Anti-parallel thyristor bridges
b) Field polarity changer with mechanical switch.

a) (B6C)A(B6C)	*b) Mechanical switch*
0.5 ... 2 s	1 ... 2.5 s

Table 5.7-4: Time for reversal of field current. The larger numbers correspond with larger drives of several hundreds of kW up to MW range.

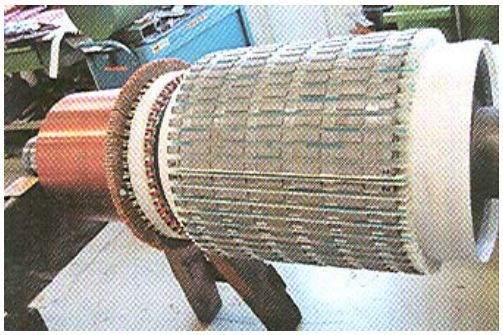

a)

b)

Fig. 5.7-6: DC motors: a) Manufacturing of the rotor of a 200 kW DC machine: Commutator, slots and insulation prepared for inserting the armature winding, b) Small high-precision DC motors of several Watts with permanent magnet excitation and multi-stage gears (operated typically at 5 … 12 V)

6. Space vector theory

6.1 M.m.f. space vector definition

Here **three-phase** AC synchronous and asynchronous machines will be treated, where the three phase currents flow in three different phase windings, which are arranged in stator of AC machine. We consider here only symmetric three-phase windings, where the winding arrangement per phase is identical, but the three phases U, V, W are shifted along stator bore circumference by one third of one pole pair. In Fig. 6.1-1 an example for a single layer, integer slot winding with q = 2 slots per poles and phase is given. In dynamic situation the three phase currents are no longer – as in steady state condition - of sine wave time function, but their values $I_U(t)$, $I_V(t)$, $I_W(t)$ vary arbitrarily.

Steady state condition: fixed frequency, amplitude and phase shift	Dynamic condition: currents change arbitrarily
$I_U(t) = \hat{I} \cdot \cos(\Omega \cdot t)$	$I_U(t)$
$I_V(t) = \hat{I} \cdot \cos(\Omega \cdot t - 2\pi/3)$	$I_V(t)$
$I_W(t) = \hat{I} \cdot \cos(\Omega \cdot t - 4\pi/3)$	$I_W(t)$

In many cases three phase winding is **star-connected**:

$$I_U(t) + I_V(t) + I_W(t) = 0 \qquad (6.1\text{-}1)$$

Delta-connected winding or star-connected winding with **connection of neutral point**

$$I_U(t) + I_V(t) + I_W(t) \neq 0 \qquad (6.1\text{-}2)$$

will be treated later.

Example 6.1-1:

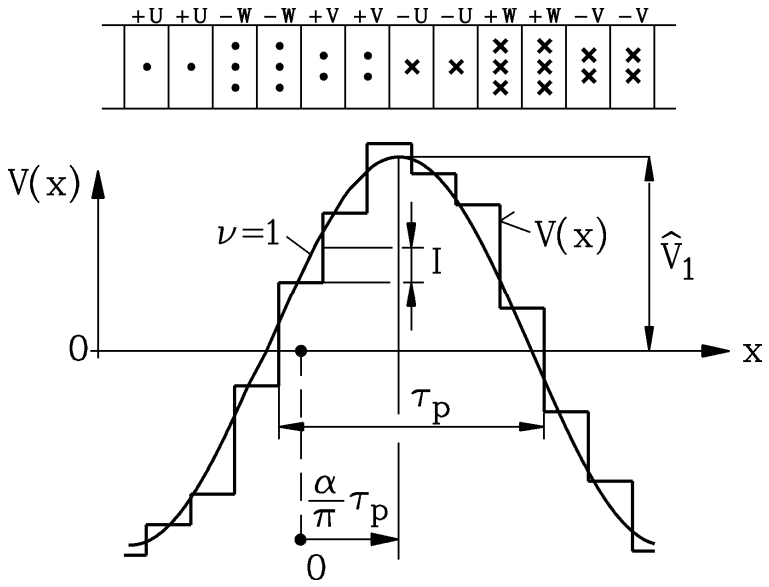

Fig. 6.1-1: Three-phase AC star-connected winding with arbitrary phase currents excites a m.m.f. distribution with a dominant sine wave fundamental (here: q = 2, single layer winding, $I_U(t) = I$, $I_V(t) = 2I$, $I_W(t) = -3I$)

Star-connected three phase single layer winding, q = 2 slots per pole and phase, N_c = 1 turns per coil, dynamic situation with arbitrarily current values:

$I_U(t) = I,\ I_V(t) = 2I,\ I_W(t) = -3I$

Star-connection condition $I_U(t) + I_V(t) + I_W(t) = I + 2I - 3I = 0$ is fulfilled.

Slot ampere turns; $\Theta_{cU} = N_c I_U(t) = 1 \cdot I = I,\ \Theta_{cV} = 2I,\ \Theta_{cW}(t) = -3I$.

The m.m.f. distribution along stator bore circumference *x* is calculated with *Ampere´s* law and is due to slotting a step-like function *V*(*x*), $x = x_s$ stator-fixed coordinate, (Fig.6.1-1, *V*-step height = slot ampere-turns) with symmetric shape of north and south pole. Position of maximum m.m.f. value occurs, where coil currents change polarity.

Facit:

Even with arbitrarily chosen current values a symmetric three-phase AC winding generates an m.m.f. distribution, which contains a dominant sine wave fundamental.

Determination of *Fourier* fundamental m.m.f. wave with amplitude $\hat{V}_1$ (ordinal number $\nu = 1$) is done by determination of sine and cosine wave coefficient

$$\hat{V}_{1s} = \frac{1}{\tau_p} \int_0^{2\tau_p} V(x_s) \cdot \sin\left(\frac{\pi \cdot x_s}{\tau_p}\right) \cdot dx_s \ , \qquad \hat{V}_{1c} = \frac{1}{\tau_p} \int_0^{2\tau_p} V(x_s) \cdot \cos\left(\frac{\pi \cdot x_s}{\tau_p}\right) \cdot dx_s \ , \qquad (6.1\text{-}3)$$

leading to

$$V_1(x_s) = \hat{V}_{1s} \cdot \sin\left(\frac{x_s \pi}{\tau_p}\right) + \hat{V}_{1c} \cdot \cos\left(\frac{x_s \pi}{\tau_p}\right) = \hat{V}_1 \cdot \cos\left(\frac{x_s \pi}{\tau_p} - \alpha\right) = \hat{V}_1 \cdot \cos(\gamma_s - \alpha) \qquad (6.1\text{-}4)$$

with the amplitude $\hat{V}_1$ and the space phase shift α from a chosen origin $x_s = 0$.

$$\hat{V}_1 = \sqrt{\hat{V}_{1s}^2 + \hat{V}_{1c}^2} \ , \qquad \alpha = \arctan\left(\hat{V}_{1s} / \hat{V}_{1c}\right) \qquad (6.1\text{-}5)$$

Example 6.1-2:

Fundamental of m.m.f. wave of Example 6.1-1: $I_U(t) = I,\ I_V(t) = 2I,\ I_W(t) = -3I$, yielding $\hat{V}_1 = \sqrt{\hat{V}_{1s}^2 + \hat{V}_{1c}^2} = 5.69 \cdot I$. Origin $x = 0$ is chosen at coil axis of phase U, that means in the centre between +U, +U and –U, -U, leading to angle α according to Fig. 6.1-1.

Facit:

Amplitude of maximum of fundamental m.m.f. $\hat{V}_1$ *and corresponding air gap magnetic flux density* $B_{\delta 1} = \mu_0 \cdot \hat{V}_1 / \delta$ *(saturation neglected) occurs at position* $x_s = \alpha \tau_p / \pi$ *or at an angle* $\gamma_s = x_s \pi / \tau_p = \alpha$ *, respectively. For further dynamic calculations ONLY fundamental wave will be considered. As only fundamental wave is considered, also only sine wave distribution of coil currents is considered (Fig. 6.1-2b). Maximum value of m.m.f. fundamental occurs, where coil current distribution changes polarity.*

Actual position α and amplitude $\hat{V}_1$ of fundamental m.m.f. wave depends on actual values of $I_U(t)$, $I_V(t)$, $I_W(t)$ and may change rapidly under dynamic conditions with time $\hat{V}_1(t), \alpha(t)$. This actual position of fundamental wave in cross section plane of electric machine (Fig. 6.1-2a) will be described here – according to *Kovacs* – in **complex co-ordinate system** (Fig. 6.1-2b) with $\cos(\gamma_s - \alpha) = \cos(\alpha - \gamma_s)$

$$V_1(x_s) = \hat{V}_1 \cos\left(\frac{x_s \pi}{\tau_p} - \alpha\right) = \hat{V}_1 \cos(\alpha - \gamma_s) = \mathrm{Re}\left\{\hat{V}_1 e^{j\alpha} e^{-j\gamma_s}\right\} = \mathrm{Re}\left\{\underline{V} e^{-j\gamma_s}\right\} \qquad (6.1\text{-}6)$$

as **complex space phasor ("space vector")** $\underline{V} = \hat{V}_1 \cdot e^{j\alpha}$. For machines with higher pole count $2p > 2$ the same notation may be used, counting α only as position of maximum of m.m.f. per pole pair in **electric degrees**: $x_s = 0$ corresponds with $\alpha = 0$, and $x_s = 2\tau_p$ with $\alpha = 2\pi$.

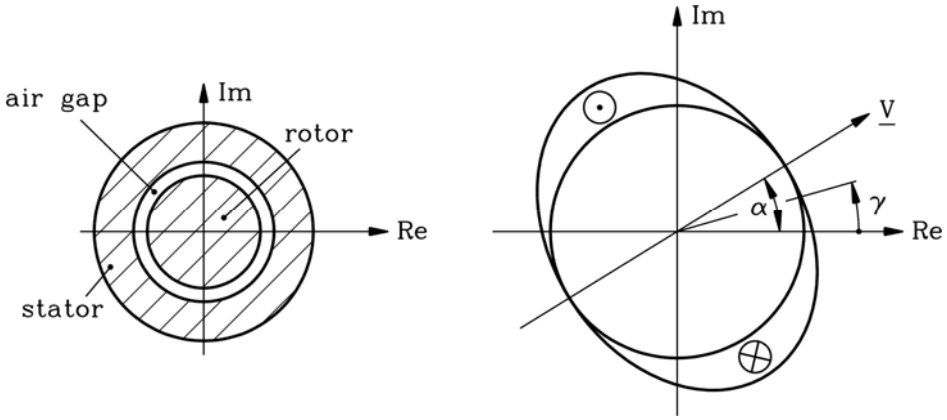

Fig. 6.1-2: Left: Cross-section of AC machine with stator and rotor iron stack and air gap in between; right: actual position α of fundamental of current distribution in coils and of m.m.f. amplitude (here: two-pole arrangement); $\gamma = \gamma_s$ stator-fixed circumference angle.

6.2 M.m.f. space vector and phase currents

Interrelationship between phase current values $I_U(t)$, $I_V(t)$, $I_W(t)$ and their corresponding space vector are derived by considering the m.m.f. distribution of each phase. *Fourier* fundamental wave of m.m.f. distribution of one phase has its maximum (amplitude) $\hat{V}_{1,ph}$ at phase axis, which for phase U is $x_s = 0$ of Fig. 6.1-1, being again depicted in Fig. 6.2-1. Phase winding axis of phase U is chosen as Re-axis of complex co-ordinate system of machine cross-section.

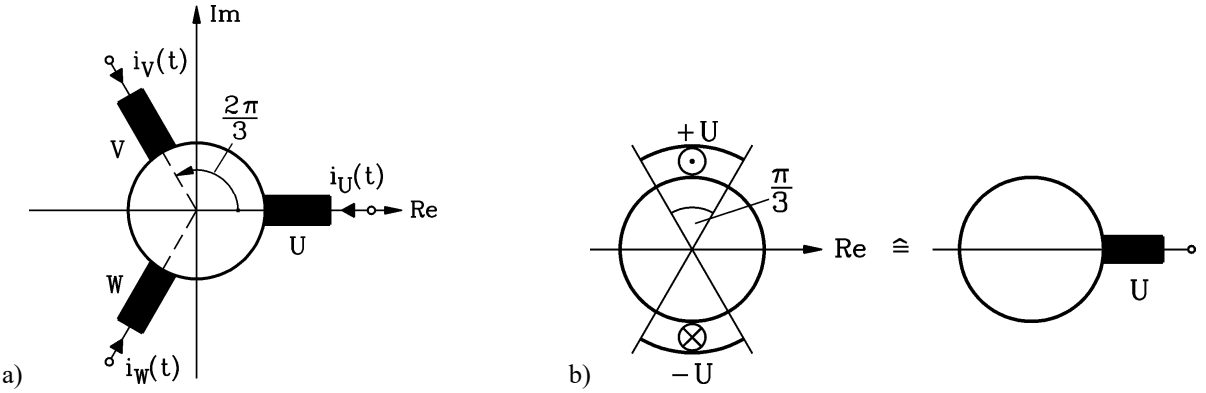

Fig. 6.2-1: Three-phase winding system: a) windings shifted by space phase angle $2\pi/3$, b) coil positions of phase U with coil axis in between.

Fundamental of phase m.m.f. of phase U is directly proportional to phase current value $I_U(t)$:

$$V_{1U}(x_s, t) = \hat{V}_{1U,ph}(t) \cdot \cos\left(\frac{x_s \pi}{\tau_p}\right) = \hat{V}_{1N,ph} \cdot \frac{I_U(t)}{\hat{I}_N} \cdot \cos\left(\frac{x_s \pi}{\tau_p}\right) = \hat{V}_{1N,ph} \cdot i_U(t) \cdot \cos\gamma_s \qquad (6.2\text{-}1)$$

Using amplitude $\hat{V}_{1N,ph}$ for rated current amplitude $\hat{I}_N = \sqrt{2} \cdot I_N$ leads to per unit phase current values $i_U(t), i_V(t), i_W(t),$ and superposition of the three phase fundamental waves to resulting m.m.f. wave:

$$V(\gamma_s, t) = \hat{V}_{1N,ph} \cdot i_U(t) \cdot \cos\gamma_s + \hat{V}_{1N,ph} \cdot i_V(t) \cdot \cos(\gamma_s - \frac{2\pi}{3}) + \hat{V}_{1N,ph} \cdot i_W(t) \cdot \cos(\gamma_s - \frac{4\pi}{3}) \quad (6.2\text{-}2)$$

Axes of V and W phase winding are shifted by $2\pi/3$ and $4\pi/3$, respectively. With star connection we get $i_V(t) + i_W(t) = -i_U(t)$ and from (6.2-2) with

$\cos(\gamma_s - 2\pi/3) = -\frac{1}{2} \cdot \cos\gamma_s + \frac{\sqrt{3}}{2} \cdot \sin\gamma_s$, $\cos(\gamma_s - 4\pi/3) = -\frac{1}{2} \cdot \cos\gamma_s - \frac{\sqrt{3}}{2} \cdot \sin\gamma_s$:

$$V(\gamma_s, t) = \hat{V}_{1N,ph} \cdot \frac{3}{2} \cdot \left[i_U(t) \cdot \cos\gamma_s + \frac{i_V(t) - i_W(t)}{\sqrt{3}} \cdot \sin\gamma_s \right]. \quad (6.2\text{-}3)$$

This is the resulting m.m.f. fundamental wave and must therefore be identical with space vector formulation $\mathrm{Re}\{\hat{V}_1 \cdot e^{j\alpha} \cdot e^{-j\gamma_s}\} = \hat{V}_1 \cdot (\cos\alpha \cdot \cos\gamma_s + \sin\alpha \cdot \sin\gamma_s)$. So the components of a space vector as real and imaginary part may be directly calculated from phase currents by $\underline{V} = \hat{V}_1 \cdot e^{j\alpha} = \hat{V}_1 \cdot (\cos\alpha + j \cdot \sin\alpha)$ with

$$\hat{V}_1 \cdot \cos\alpha = \frac{3}{2} \cdot \hat{V}_{1N,ph} \cdot i_U(t), \quad \hat{V}_1 \cdot \sin\alpha = \frac{3}{2} \cdot \hat{V}_{1N,ph} \cdot \frac{i_V(t) - i_W(t)}{\sqrt{3}} \quad (6.2\text{-}4)$$

By using the abbreviations

$$\underline{a} = e^{j\frac{2\pi}{3}} = -\frac{1}{2} + j\frac{\sqrt{3}}{2}, \quad \underline{a}^2 = e^{j\frac{4\pi}{3}} = e^{-j\frac{2\pi}{3}} = -\frac{1}{2} - j\frac{\sqrt{3}}{2} \quad (6.2\text{-}5)$$

one may also write:

$$\boxed{\underline{V}(t) = \hat{V}_{1N,ph} \cdot \left[i_U(t) + \underline{a} \cdot i_V(t) + \underline{a}^2 \cdot i_W(t) \right]} \quad (6.2\text{-}6)$$

Proof:

$$V(\gamma_s, t) = \hat{V}_1 \cos(\gamma_s - \alpha) = \mathrm{Re}\{\hat{V}_1 e^{j(\alpha - \gamma_s)}\} = \mathrm{Re}\{\underline{V} e^{-j\gamma_s}\} = \mathrm{Re}\{\hat{V}_{1N,ph} \cdot \left[i_U + \underline{a} \cdot i_V + \underline{a}^2 \cdot i_W \right] \cdot e^{-j\gamma_s}\} =$$

$$= \mathrm{Re}\left\{ \hat{V}_{1N,ph} \cdot \left[i_U + \left(-\frac{1}{2} + j\frac{\sqrt{3}}{2} \right) \cdot i_V + \left(-\frac{1}{2} - j\frac{\sqrt{3}}{2} \right) \cdot i_W \right] \cdot \left[\cos\gamma_s - j \cdot \sin\gamma_s \right] \right\} =$$

$$= \hat{V}_{1N,ph} \cdot \left[(i_U - \frac{i_V + i_W}{2}) \cdot \cos\gamma_s + \frac{\sqrt{3}(i_V - i_W)}{2} \cdot \sin\gamma_s \right] = \frac{3}{2} \hat{V}_{1N,ph} \cdot \left[i_U \cdot \cos\gamma_s + \frac{i_V - i_W}{\sqrt{3}} \cdot \sin\gamma_s \right]$$

6.3 Current, voltage and flux linkage space vector

The fundamental wave m.m.f. amplitude at rated current has been already derived in "Electrical machines and drives / Elektrische Maschinen und Antriebe":

$$\hat{V}_{1,N} = \frac{3}{2} \cdot \hat{V}_{1N,ph} = \frac{\sqrt{2}}{\pi} \cdot \frac{3}{p} \cdot N \cdot k_{w,1} \cdot I_N \tag{6.3-1}$$

In the following per unit values of current, voltage and torque will be used, so the **m.m.f. space vector** is calculated as per unit value of rated amplitude $\hat{V}_{1,N}$:

$$\boxed{\underline{v}(t) = \frac{\underline{V}(t)}{\hat{V}_{1N}} = \frac{2}{3} \cdot \left[i_U(t) + \underline{a} \cdot i_V(t) + \underline{a}^2 \cdot i_W(t) \right]} \quad . \tag{6.3-2}$$

In the same formal way a **current space vector** may be defined. In order to get space vector amplitude identical with current amplitude in steady state operation with three phase sine wave current, it must be multiplied with 2/3:

$$\underline{I}(t) = \frac{2}{3} \cdot \left[I_U(t) + \underline{a} \cdot I_V(t) + \underline{a}^2 \cdot I_W(t) \right] \tag{6.3-3}$$

Example 6.3-1:

Calculate current space vector for three phase AC sine wave current system:

$I_U(t) = \hat{I} \cdot \cos(\Omega \cdot t),\ I_V(t) = \hat{I} \cdot \cos(\Omega \cdot t - 2\pi/3),\ I_W(t) = \hat{I} \cdot \cos(\Omega \cdot t - 4\pi/3)$.

With $I_U(t) = \hat{I} \cdot \frac{e^{j\Omega t} + e^{-j\Omega t}}{2}$, $I_V(t) = \hat{I} \cdot \frac{e^{j(\Omega t - 2\pi/3)} + e^{-j(\Omega t - 2\pi/3)}}{2}$

and $I_W(t) = \hat{I} \cdot \frac{e^{j(\Omega t - 4\pi/3)} + e^{-j(\Omega t - 4\pi/3)}}{2}$ one gets

$$\underline{I}(t) = \frac{2}{3} \cdot \left[\hat{I} \cdot \frac{e^{j\Omega t} + e^{-j\Omega t}}{2} + e^{j\frac{2\pi}{3}} \cdot \hat{I} \cdot \frac{e^{j(\Omega t - 2\pi/3)} + e^{-j(\Omega t - 2\pi/3)}}{2} + \right.$$

$$\left. + e^{j\frac{4\pi}{3}} \cdot \hat{I} \cdot \frac{e^{j(\Omega t - 4\pi/3)} + e^{-j(\Omega t - 4\pi/3)}}{2} \right] = \frac{2}{3} \cdot \left[\frac{3\hat{I}e^{j\Omega t}}{2} + \frac{\hat{I}e^{-j\Omega t}}{2} \cdot \left(1 + e^{j\frac{4\pi}{3}} + e^{j\frac{8\pi}{3}} \right) \right] =$$

$$= \underline{\underline{\hat{I} \cdot e^{j\Omega t}}}$$

Facit:

The current space vector of a three phase AC sine wave system is a rotating vector of constant amplitude, which is equal to phase current amplitude. Rotating frequency is electric frequency of phase current.

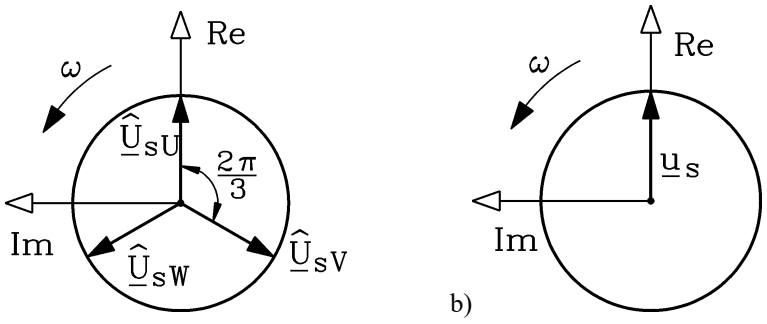

Fig. 6.3-1: Three phase AC sine wave voltage system (stator winding): a) Time phasor representation in complex plane, b) Space vector representation in machine cross-section plane, using a complex co-ordinate system

The per unit current space vector **is identical** with per unit m.m.f. space vector

$$\underline{i}(t) = \frac{\underline{I}(t)}{\hat{I}_N} = \frac{2}{3} \cdot \left[i_U(t) + \underline{a} \cdot i_V(t) + \underline{a}^2 \cdot i_W(t) \right] = \underline{v}(t) \quad . \tag{6.3-3a}$$

Facit:
Physical meaning of per unit current space vector is representation of amplitude and position of per unit m.m.f. fundamental wave.

The same holds true, if instead of three phase AC current system a three phase AC voltage system is taken, with **voltage space vector definition** according to current space vector definition (Fig. 6.3-1).

$$\underline{U}(t) = \frac{2}{3} \cdot \left[U_U(t) + \underline{a} \cdot U_V(t) + \underline{a}^2 \cdot U_W(t) \right] \tag{6.3-4}$$

	Three time phasors	One space vector
Time function	$U_U(t) = \hat{U} \cdot \cos(\Omega \cdot t)$ $U_V(t) = \hat{U} \cdot \cos(\Omega \cdot t - 2\pi/3)$ $U_W(t) = \hat{U} \cdot \cos(\Omega \cdot t - 4\pi/3)$	$U_U(t) = \hat{U} \cdot \cos(\Omega \cdot t)$ $U_V(t) = \hat{U} \cdot \cos(\Omega \cdot t - 2\pi/3)$ $U_W(t) = \hat{U} \cdot \cos(\Omega \cdot t - 4\pi/3)$
Time and phasor correspondence	$U_U(t) = \mathrm{Re}\left\{ \hat{U} \cdot e^{j\Omega \cdot t} \right\}$ $U_V(t) = \mathrm{Re}\left\{ \hat{U} \cdot e^{j(\Omega \cdot t - \frac{2\pi}{3})} \right\}$ $U_W(t) = \mathrm{Re}\left\{ \hat{U} \cdot e^{j(\Omega \cdot t - \frac{4\pi}{3})} \right\}$	$\underline{U}(t) = \frac{2}{3} \cdot \left[U_U(t) + \underline{a} \cdot U_V(t) + \underline{a}^2 \cdot U_W(t) \right]$
Time phasor and space vector	$\underline{\hat{U}}_U = \hat{U}$ $\underline{\hat{U}}_V = \hat{U} \cdot e^{-j\frac{2\pi}{3}}$ $\underline{\hat{U}}_W = \hat{U} \cdot e^{-j\frac{4\pi}{3}}$	$\underline{U}(t) = \hat{U} \cdot e^{j\Omega \cdot t}$

Table 6.3-1: Symmetrical three phase AC sine wave voltage system: Time phasor versus space vector

In unsaturated iron and constant air gap machines according to

$$B_\delta(x) = \mu_0 \cdot V(x) / \delta \tag{6.3-5}$$

magnetic air gap flux density is directly calculated from m.m.f. With constant saturation the necessary m.m.f. for magnetizing iron path may be considered by a fictive increase of air gap: $k_s \cdot \delta, k_s > 1,$ like influence of slot openings may be considered by *Carter´*s coefficient: $k_C \cdot \delta, k_C > 1$. Air gap flux density amplitude $B_{\delta 1} = \mu_0 \cdot \hat{V}_1 / \delta$ leads to **main flux linkage** per phase

$$\Psi_{hN} = k_{w,1} N \cdot \frac{2}{\pi} \cdot \tau_p l_e \cdot B_{\delta 1} = L_h \cdot \hat{I}_N \quad . \tag{6.3-6}$$

$$\Psi_{hU}(t) = L_h \cdot I_U(t) \tag{6.3-7}$$

and allows formal definition of **main flux linkage space vector**

$$\underline{\Psi}_h(t) = \frac{2}{3}\left[\Psi_{hU}(t) + \underline{a}\cdot\Psi_{hV}(t) + \underline{a}^2\cdot\Psi_{hW}(t)\right] \quad . \tag{6.3-8}$$

Example 6.3-2:
AC machine with constant air gap and three phase stator winding, star-connected. Rotor has no winding, so no torque is produced. Only space fundamental $\nu = 1$ is considered. Stator arbitrary phase currents are represented by space sine wave distributed current layer (= current distribution in slots), which – at considered time – lead to corresponding m.m.f. space vector $\underline{V}$ and therefore stator current space vector $\underline{I}$ in Re-axis. The m.m.f. space vector, multiplied by μ_0/δ, marks magnetic air gap field B_δ (Fig. 6.3-2), which is distributed sinusoidal in air gap. As flux density maximum lies in winding axis of phase U, flux linkage of phase U is maximum. Therefore main flux linkage space vector $\underline{\Psi}_h$ is lying in Re-axis aligned with current space vector.

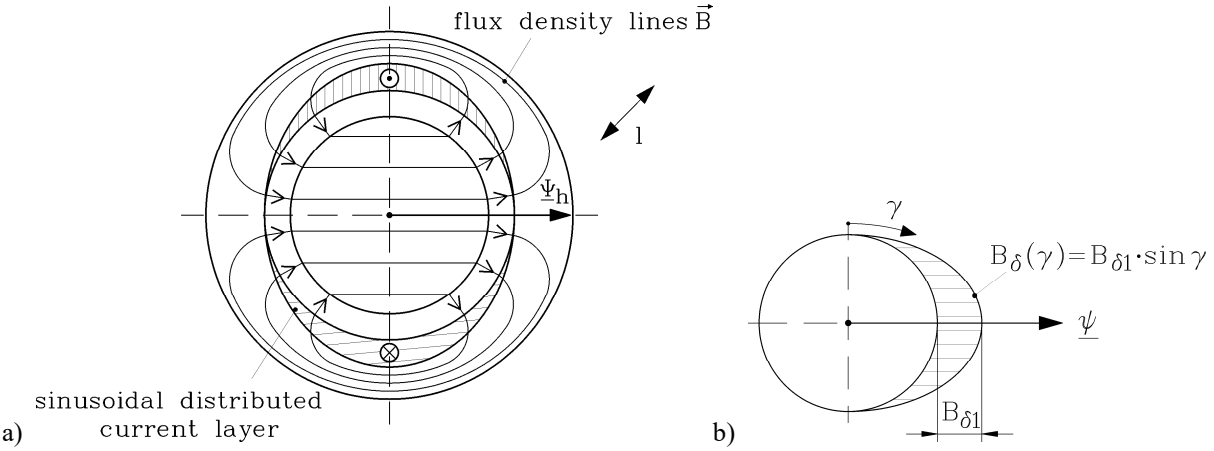

Fig. 6.3-2: Magnetic field excited by three phase AC stator winding with constant air gap, a) magnetic main flux linkage vector and sinusoidal current layer, b) sinusoidal distribution of air gap flux density ($\gamma = \gamma_s$ stator-fixed)

Facit:
Main flux linkage space vector shows position of magnetic space sine wave field in machine cross section. Amplitude of flux linkage space vector is proportional to air gap flux density amplitude (6.3-6), its direction gives direction of N- and S-pole of two pole field, the N-pole being correlated to the arrow symbol of flux linkage space vector.

Relationship between main flux linkage and current space vector is therefore given by main inductance

$$\boxed{\underline{\Psi}_h(t) = L_h \cdot \underline{I}(t) \qquad L_h = \mu_0 \cdot (N \cdot k_{w,1})^2 \cdot \frac{6 \cdot \tau_p l_e}{\pi^2 \cdot p \cdot \delta}} \tag{6.3-9}$$

Proof:

$$\underline{\Psi}_h(t) = \frac{2}{3}\left[\Psi_{hU}(t) + \underline{a}\cdot\Psi_{hV}(t) + \underline{a}^2\cdot\Psi_{hW}(t)\right] = L_h \cdot \frac{2}{3}\left[I_U(t) + \underline{a}\cdot I_V(t) + \underline{a}^2\cdot I_W(t)\right] = L_h \cdot \underline{I}(t)$$

Facit:

The main flux linkage space vector is proportional to current space vector via the air gap main inductance L_h.

The per unit main flux linkage space vector is defined like the current space vector so, that

$$\underline{\psi}_h(t) = \frac{\underline{\Psi}_h(t)}{L_h \hat{I}_N} = \frac{2}{3} \cdot \left[\psi_{hU}(t) + \underline{a} \cdot \psi_{hV}(t) + \underline{a}^2 \cdot \psi_{hW}(t) \right] \tag{6.3-10}$$

Example 6.3-3:

The simple machine of Example 6.3-2 is fed by block-shaped currents, so flux linkage per phase is block shaped (Fig. 6.3-3). How is the movement of resulting magnetic field?

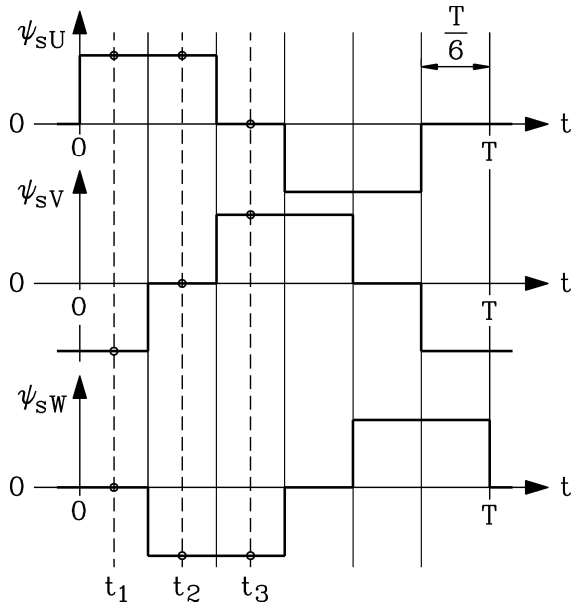

Fig. 6.3-3: Block-shaped flux linkage per phase due to block-shaped stator current supply

For the three time instants t_1, t_2 , t_3 the main flux linkage space vector is calculated according to (6.3-8). In Fig. 6.3-4 the flux linkage space vector is at rest for 1/6 of the period T, then jumping by 60° into next position. In the same way magnetic air gap field is constant for $T/6$ and jumping by 60° six times per period.

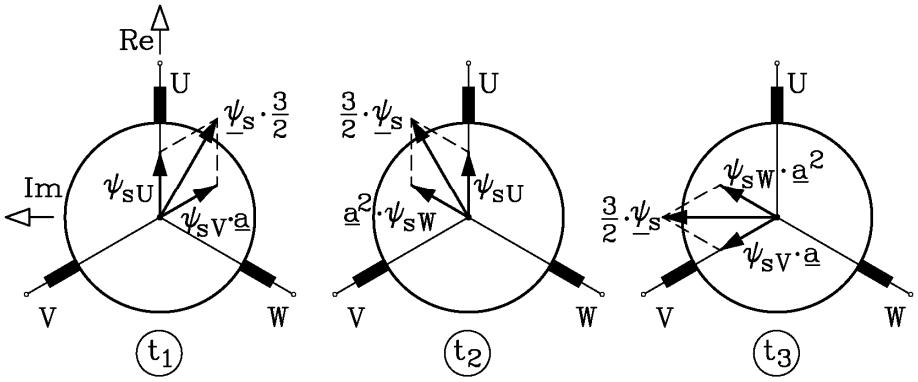

Fig. 6.3-4: Block-shaped flux linkage per phase leads to jumping flux linkage space vector, being in position (1) for $0 \le t \le T/6$, in position (2) for $T/6 \le t \le T/3$, in position (3) for $T/3 \le t \le T/2$ and so on.

In **cage induction and slip-ring induction machines** the rotor bears the Q_r bars or the 3 rotor phase windings, which may be considered as m_r rotor phases (Fig. 6.3-5).

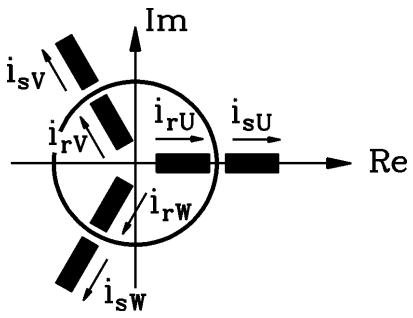

Fig. 6.3-5: Slip-ring induction machine with $m_s = 3$ stator phases and $m_r = 3$ rotor phase windings

Rotor phase currents excite rotor m.m.f. with amplitude

$$\hat{V}_{1,N,r} = \frac{\sqrt{2}}{\pi} \cdot \frac{m_r}{p} \cdot N_r \cdot k_{w,1,r} \cdot I_{N,r} \quad . \tag{6.3-11}$$

With a phase current flow, defined by **current transformation ratio $\ddot{u}_I$,**

$$I'_r(t) = \frac{I_r(t)}{\ddot{u}_I} \qquad \ddot{u}_I = \frac{m_s \cdot N_s \cdot k_{w,1,s}}{m_r \cdot N_r \cdot k_{w,1,r}} \tag{6.3-12}$$

in the stator winding, the same rotor m.m.f. is excited as by the original rotor current flow in the rotor winding. So the **rotor current space vector** is usually defined with transformed rotor currents, using the only three-phase stator winding data for further calculation.

$$\underline{I}'_r(t) = \frac{2}{3} \cdot \left[I'_{rU}(t) + \underline{a} \cdot I'_{rV}(t) + \underline{a}^2 \cdot I'_{rW}(t) \right] \tag{6.3-13}$$

	stator AC winding	rotor cage winding	rotor slip ring winding
phase count	m_s	Q_r	m_r
turns per phase	N_s	1/2	N_r
winding factor ($\nu = 1$)	$k_{w,1,s}$	1	$k_{w,1,r}$

Table 6.3-2: Winding data of cage and slip ring induction machines

6.4 Space vector transformation

The space vector definition (6.3-3) may be formally expressed as transformation from three phase values (e.g. phase currents) to one phase vector value, which is described by two parameters, either by amplitude and angle in complex co-ordinate system, or by two components (real and imaginary part of space vector).

$$\underline{I}(t) = \frac{2}{3} \cdot \left[I_U(t) + \underline{a} \cdot I_V(t) + \underline{a}^2 \cdot I_W(t) \right] = I_\alpha(t) + j \cdot I_\beta(t) \tag{6.4-1}$$

In special case of star-connected winding we hold $I_U(t) + I_V(t) + I_W(t) = 0$. According to (6.2-4) it is

$$I_\alpha(t) = \frac{2}{3} I_U(t) - \frac{1}{3}\left(I_V(t) + I_W(t)\right) = I_U(t), \quad I_\beta(t) = \left(I_V(t) - I_W(t)\right)/\sqrt{3} \tag{6.4-2}$$

or written as **space vector transformation (***Clarke´s* matrix transformation),

$$\begin{pmatrix} I_\alpha(t) \\ I_\beta(t) \end{pmatrix} = \begin{pmatrix} \frac{2}{3} & -\frac{1}{3} & -\frac{1}{3} \\ 0 & \frac{1}{\sqrt{3}} & -\frac{1}{\sqrt{3}} \end{pmatrix} \cdot \begin{pmatrix} I_U(t) \\ I_V(t) \\ I_W(t) \end{pmatrix} = (A) \cdot \begin{pmatrix} I_U(t) \\ I_V(t) \\ I_W(t) \end{pmatrix} \quad . \tag{6.4-3}$$

Inverse matrix operation with $(A)^{-1}$ yields **inverse space vector transformation**

$$\begin{pmatrix} I_U(t) \\ I_V(t) \\ I_W(t) \end{pmatrix} = \begin{pmatrix} 1 & 0 \\ -\frac{1}{2} & \frac{\sqrt{3}}{2} \\ -\frac{1}{2} & -\frac{\sqrt{3}}{2} \end{pmatrix} \cdot \begin{pmatrix} I_\alpha(t) \\ I_\beta(t) \end{pmatrix} = (A)^{-1} \cdot \begin{pmatrix} I_\alpha(t) \\ I_\beta(t) \end{pmatrix} \tag{6.4-4}$$

Note: $(A) \cdot (A)^{-1} = \begin{pmatrix} 1 & 0 \\ 0 & 1 \end{pmatrix}$ (6.4-5)

Facit:
Three-phase currents are transformed into one space vector with two space vector components with perpendicular directions. Thus the space vector theory is also called "two-axes theory".

Example 6.4-1:
Like in Example (6.3-1) space vector transformation is done for symmetrical three phase AC sine wave current system, but now with *Clarke* matrix transformation:

$$\begin{pmatrix} I_\alpha(t) \\ I_\beta(t) \end{pmatrix} = \begin{pmatrix} \hat{I}\cos(\Omega \cdot t) \\ \hat{I}\sin(\Omega \cdot t) \end{pmatrix} = \begin{pmatrix} \frac{2}{3} & -\frac{1}{3} & -\frac{1}{3} \\ 0 & \frac{1}{\sqrt{3}} & -\frac{1}{\sqrt{3}} \end{pmatrix} \cdot \begin{pmatrix} \hat{I}\cos(\Omega \cdot t) \\ \hat{I}\cos(\Omega \cdot t - 2\pi/3) \\ \hat{I}\cos(\Omega \cdot t - 4\pi/3) \end{pmatrix}$$

The matrix operation transforms a three phase sine wave system with 120° phase shift into a two phase sine wave system with IDENTICAL current amplitude, but 90° phase shift. As **apparent power has to be invariant**, the induced voltages are 1.5-times bigger in two phase system:

$$S = 3 \cdot U_{3ph} \cdot I_{3ph} = 3 \cdot U_{3ph} \cdot I = 2 \cdot U_{2ph} \cdot I_{2ph} = 2 \cdot U_{2ph} \cdot I \quad \Rightarrow \quad \frac{U_{2ph}}{U_{3ph}} = \frac{3}{2} \ . \tag{6.4-6}$$

This may be understood easily. The magnetic field in air gap must be the same for three phase and two phase system.

$$B_{\delta,1} = \frac{\mu_0 \hat{V}_{3ph}}{\delta} = \frac{\mu_0 \hat{V}_{2ph}}{\delta} \quad \Rightarrow \quad \hat{V}_{3ph} = \frac{\sqrt{2}}{\pi} \cdot \frac{3}{p} \cdot N_{3ph} k_{w,3ph} \cdot I = \frac{\sqrt{2}}{\pi} \cdot \frac{2}{p} \cdot N_{2ph} k_{w,2ph} \cdot I = \hat{V}_{2ph}$$

So in the fictive two phase system the product of number of turns per winding and winding factor must be bigger by 3/2

$$\frac{N_{2ph}k_{w,2ph}}{N_{3ph}k_{w,3ph}} = \frac{3}{2} \quad , \tag{6.4-7}$$

therefore the induced phase voltage

$$\hat{U}_i = \Omega \cdot N \cdot k_w \cdot \frac{2}{\pi} \tau_p l_e \cdot B_{\delta,1} \tag{6.4-8}$$

is bigger in the two phase system by $\hat{U}_{i,2ph} = (3/2) \cdot \hat{U}_{i,3ph}$.

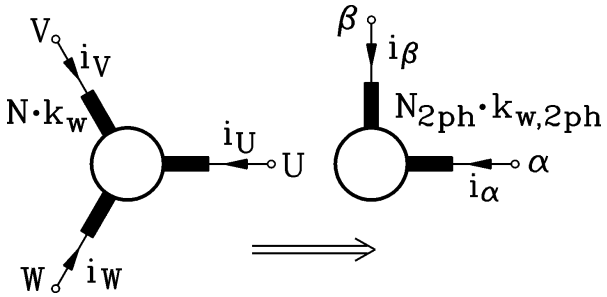

Fig. 6.4-1: Space vector formulation is transformation of 3 phase system U, V, W into fictive two phase system α, β with perpendicular winding axes (**"two-axes theory"**).

Inverse space vector transformation (6.4-4) in complex space vector description is

$$\boxed{\begin{aligned} I_U(t) &= \mathrm{Re}\{\underline{I}(t)\} \\ I_V(t) &= \mathrm{Re}\{\underline{a}^2 \cdot \underline{I}(t)\} \\ I_W(t) &= \mathrm{Re}\{\underline{a} \cdot \underline{I}(t)\} \end{aligned}} \tag{6.4-9}$$

Proof:

$$I_U(t) = \mathrm{Re}\{\underline{I}(t)\} = \frac{2}{3} \cdot \left(I_U(t) + \mathrm{Re}\{\underline{a}\} \cdot I_V(t) + \mathrm{Re}\{\underline{a}^2\} \cdot I_W(t) \right) = \frac{2}{3} \cdot \left(I_U(t) - \frac{I_V(t)}{2} - \frac{I_W(t)}{2} \right)$$

With $I_U(t) + I_V(t) + I_W(t) = 0$ one gets finally $I_U(t)$. In the same way one proofs the other two relationships.

Note that with $\underline{I}(t) = I_\alpha(t) + jI_\beta(t)$ inverse transformation (6.4-9) yields directly:

$$I_U(t) = \mathrm{Re}\{\underline{I}(t)\} = I_\alpha(t)$$

$$I_V(t) = \mathrm{Re}\{\underline{a}^2 \cdot \underline{I}(t)\} = \mathrm{Re}\left\{ \left(-\frac{1}{2} - j\frac{\sqrt{3}}{2} \right) \cdot \left(I_\alpha(t) + jI_\beta(t) \right) \right\} = -\frac{I_\alpha(t)}{2} + \frac{\sqrt{3} \cdot I_\beta(t)}{2}$$

$$I_W(t) = \mathrm{Re}\{\underline{a} \cdot \underline{I}(t)\} = \mathrm{Re}\left\{ \left(-\frac{1}{2} + j\frac{\sqrt{3}}{2} \right) \cdot \left(I_\alpha(t) + jI_\beta(t) \right) \right\} = -\frac{I_\alpha(t)}{2} - \frac{\sqrt{3} \cdot I_\beta(t)}{2}$$

These are the expressions (6.4-4), thus proving the equivalence of *Clarke's* inverse matrix transformation and the complex inverse space vector transformation.

Example 6.4-2:

Space vector transformation for per unit phase current values $i_U = 0.3$, $i_V = 0.5$, $i_W = -0.8$.

The condition due to star connection $i_U + i_V + i_W = 0.3 + 0.5 - 0.8 = 0$ is satisfied.

The per unit current space vector $\underline{i}(t) = \frac{2}{3} \cdot \left[0.3 + \underline{a} \cdot 0.5 - \underline{a}^2 \cdot 0.8\right]$ is shown graphically in Fig. 6.4-2 as an geometric addition of complex vectors $0.3, \underline{a} \cdot 0.5, -\underline{a}^2 \cdot 0.8$, which may regarded as the field contributions of each phase U, V, W. The resulting vector sum is reduced by 2/3 to get the space vector. Inverse transformation (6.4-9) means geometrically the projection of the space vector on the three winding axes of U, V, W, which are given by Re-axis and its shifted values by 120° and 240°. For V-component, the relative position of $\underline{i}$ and of V-axis is the same as of $\underline{a}^2 \cdot \underline{i}$ and Re-axis, therefore the condition for inverse transformation is $i_V(t) = \mathrm{Re}\left\{\underline{a}^2 \cdot \underline{i}(t)\right\}$.

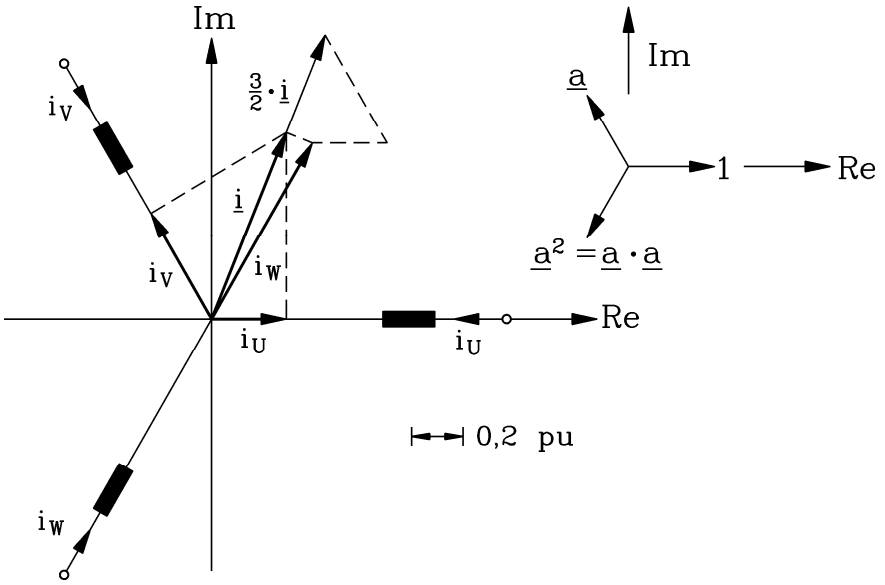

Fig. 6.4-2: Per unit current space vector transformation for the example $i_U = 0.3, i_V = 0.5, i_W = -0.8$

Appendix:

Sometimes space vector is defined slightly different as

$$\underline{I}(t) = \sqrt{\frac{2}{3}} \cdot \left[I_U(t) + \underline{a} \cdot I_V(t) + \underline{a}^2 \cdot I_W(t)\right] = I_\alpha(t) + j \cdot I_\beta(t) \quad ,$$

leading to a symmetrical *Clarke´*s transformation:

$$\begin{pmatrix} I_\alpha(t) \\ I_\beta(t) \end{pmatrix} = \begin{pmatrix} \sqrt{\frac{2}{3}} & -\frac{1}{\sqrt{6}} & -\frac{1}{\sqrt{6}} \\ 0 & \frac{1}{\sqrt{2}} & -\frac{1}{\sqrt{2}} \end{pmatrix} \cdot \begin{pmatrix} I_U(t) \\ I_V(t) \\ I_W(t) \end{pmatrix} = (A_S) \cdot \begin{pmatrix} I_U(t) \\ I_V(t) \\ I_W(t) \end{pmatrix}$$

$$\begin{pmatrix} I_U(t) \\ I_V(t) \\ I_W(t) \end{pmatrix} = \begin{pmatrix} \sqrt{\frac{3}{2}} & 0 \\ -\frac{1}{\sqrt{6}} & \frac{1}{\sqrt{2}} \\ -\frac{1}{\sqrt{6}} & -\frac{1}{\sqrt{2}} \end{pmatrix} \cdot \begin{pmatrix} I_\alpha(t) \\ I_\beta(t) \end{pmatrix} = (A_S)^{-1} \cdot \begin{pmatrix} I_\alpha(t) \\ I_\beta(t) \end{pmatrix}$$

Inverse of transformation matrix is identical with transposed matrix: $(A_S)^{-1} = (A_S)^T$. Applying this symmetric transformation to symmetric three phase AC sine wave system (phase shift 120°), the voltage and current amplitudes in the two phase system (phase shift 90°) are larger by $\sqrt{3/2}$: $U_{2ph} = \sqrt{3/2} \cdot U_{3ph}$, $I_{2ph} = \sqrt{3/2} \cdot I_{3ph}$. Apparent power is of course invariant: $S = 3 \cdot U_{3ph} \cdot I_{3ph} = 3 \cdot \sqrt{2/3} U_{2ph} \cdot \sqrt{2/3} I_{2ph} = 2 \cdot U_{2ph} \cdot I_{2ph}$.

6.5 Influence of the zero sequence current system

Zero sequence current system means, that in each of the three phases U, V, W the same, identical arbitrary current $I_0(t)$ is flowing. This current is also called **common mode current** system. Modern IGBT inverters generate **common mode phase voltages** $U_0(t)$, which will cause under certain circumstances common mode phase currents to flow.

Star connected winding	*Delta connected winding*	*Star connected winding with neutral point connected*
no common mode current	common mode current flows circulating in delta connection, but is not visible in grid connections	common mode current flows in each line and phase and with 3-times in neutral point connection
$I_U(t) + I_V(t) + I_W(t) =$ $= 3 \cdot I_0(t) = 0$ $I_0(t) = 0$	Phase currents: $I_U(t) = I_V(t) = I_W(t) = I_0(t)$ Line currents: $I_{L,UV}(t) = I_U(t) - I_V(t) = 0$	Phase currents: $I_U(t) = I_V(t) = I_W(t) = I_0(t)$ Line currents: $I_{L,U}(t) = I_U(t) = I_0(t)$ Neutral current: $I_n(t) = I_U(t) + I_V(t) + I_W(t) =$ $= 3 \cdot I_0(t)$

Table 6.5-1: Common mode currents for different three phase AC winding connections

An arbitrary current system $I_U(t), I_V(t), I_W(t)$ may always be decomposed into a zero sequence system $I_0(t), I_0(t), I_0(t)$ and a common-mode free system $I_{US}(t), I_{VS}(t), I_{WS}(t)$.

$$I_0(t) = \frac{1}{3} \cdot \left(I_U(t) + I_V(t) + I_W(t)\right) \tag{6.5-1}$$

$$\begin{aligned} I_{US}(t) &= I_U(t) - I_0(t) \\ I_{VS}(t) &= I_V(t) - I_0(t) \\ I_{VS}(t) &= I_U(t) - I_0(t) \end{aligned} \tag{6.5-2}$$

Note that $I_{US}(t) + I_{VS}(t) + I_{WS}(t) = 0$!

Example 6.5-1:
Star connected winding with neutral point connected: At time instant *t* the measured per unit current values are $i_U = 0.3$, $i_V = 0.5$, $i_W = -0.2$ (Note: $i(t) = I(t) / \hat{I}_N$).
How big is zero sequence current in phases and in neutral clamp?

$$i_0(t) = \frac{1}{3} \cdot \left(i_U + i_V + i_W\right) = \frac{1}{3} \cdot \left(0.3 + 0.5 - 0.2\right) = \underline{\underline{0.2}}$$

$$i_n(t) = 3 i_0 = 3 \cdot 0.2 = \underline{\underline{0.6}}$$

Note that in neutral clamp flows 60% of rated current as neutral current!

The common-mode free current values are:

$i_{US} = i_U - i_0 = 0.3 - 0.2 = 0.1$

$i_{VS} = i_V - i_0 = 0.5 - 0.2 = 0.3$

$i_{WS} = i_W - i_0 = -0.2 - 0.2 = -0.4$

Example 6.5-2:

Magnetic air gap field of zero sequence current system, flowing in three phase single layer winding with $q = 2$ slots per pole and phase:

As winding current is identical for all three phases: $I_U(t) = I_V(t) = I_W(t) = I_0(t)$, *Ampere´s* law yields a m.m.f. distribution $V_0(x_s)$, which shows three pole pairs instead of one along double pole pitch $2\tau_p$ (Fig. 6.5-1).

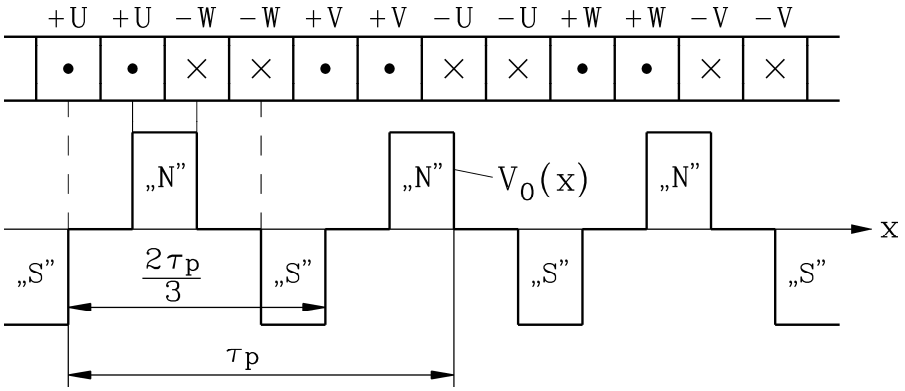

Fig. 6.5-1: Zero sequence current system excites m.m.f. distribution $V_0(x_s)$ with three pole pairs instead of one along double pole pitch $2\tau_p$ ($x = x_s$: stator-fixed coordinate)

Due to different pole count the 3-times pole count **will not** contribute to torque of fundamental field wave. This parasitic additional air gap flux density distribution contains *Fourier* space harmonics of ordinal numbers $\nu = 3, 9, 15, \ldots$, which may cause additional induced voltage in rotor winding and corresponding rotor currents, leading to additional losses and pulsating torque. The *Maxwell* radial pull of these additional space harmonics may cause magnetically excited acoustic noise.

Facit:

Machines for inverter operation, especially with larger rated power, are usually star-connected with insulated star point, in order to avoid common mode phase current.

As zero sequence current excites flux waves, which do not contribute to torque generation of fundamental wave, they should have no effect on space vector formulation, which describes fundamental wave operation. Space vector theory considers this fact automatically, as **space vector of zero sequence current is zero.**

$$\underline{I}_0(t) = \frac{2}{3} \cdot \left(I_0(t) + \underline{a} \cdot I_0(t) + \underline{a}^2 \cdot I_0(t) \right) = \frac{2}{3} \cdot I_0(t) \cdot \left(1 + \underline{a} + \underline{a}^2 \right) = \frac{2}{3} \cdot I_0(t) \cdot \left(1 + e^{j\frac{2\pi}{3}} + e^{j\frac{4\pi}{3}} \right) = 0$$

Thus the space vector of an arbitrary current system $I_U(t), I_V(t), I_W(t)$ is only determined by the common-mode free components $I_{US}(t), I_{VS}(t), I_{WS}(t)$.

$$\underline{I}(t) = \frac{2}{3} \cdot \left[I_U(t) + \underline{a} \cdot I_V(t) + \underline{a}^2 \cdot I_W(t) \right] = \frac{2}{3} \cdot \left[I_{US}(t) + \underline{a} \cdot I_{VS}(t) + \underline{a}^2 \cdot I_{WS}(t) \right] \tag{6.5-3}$$

$$I_\alpha(t) = \frac{2}{3} \cdot \left(I_U(t) - \frac{I_V(t) + I_W(t)}{2} \right) = I_{US}(t) = I_U(t) - I_0(t) \tag{6.5-4}$$

$$I_ß(t) = \frac{1}{\sqrt{3}} \cdot \left(I_V(t) - I_W(t) \right) = \frac{1}{\sqrt{3}} \cdot \left(I_{VS}(t) - I_{WS}(t) \right) \tag{6.5-5}$$

For this general case of arbitrary current system $I_U(t), I_V(t), I_W(t)$ **space vector transformation as** *Clarke´s* matrix transformation is

$$\begin{pmatrix} I_\alpha(t) \\ I_\beta(t) \\ I_0(t) \end{pmatrix} = \begin{pmatrix} \frac{2}{3} & -\frac{1}{3} & -\frac{1}{3} \\ 0 & \frac{1}{\sqrt{3}} & -\frac{1}{\sqrt{3}} \\ \frac{1}{3} & \frac{1}{3} & \frac{1}{3} \end{pmatrix} \cdot \begin{pmatrix} I_U(t) \\ I_V(t) \\ I_W(t) \end{pmatrix} = (A) \cdot \begin{pmatrix} I_U(t) \\ I_V(t) \\ I_W(t) \end{pmatrix} \quad . \tag{6.5-6}$$

$$\begin{pmatrix} I_U(t) \\ I_V(t) \\ I_W(t) \end{pmatrix} = \begin{pmatrix} 1 & 0 & 1 \\ -\frac{1}{2} & \frac{\sqrt{3}}{2} & 1 \\ -\frac{1}{2} & -\frac{\sqrt{3}}{2} & 1 \end{pmatrix} \cdot \begin{pmatrix} I_\alpha(t) \\ I_\beta(t) \\ I_0(t) \end{pmatrix} = (A)^{-1} \cdot \begin{pmatrix} I_\alpha(t) \\ I_\beta(t) \\ I_0(t) \end{pmatrix} \quad . \tag{6.5-7}$$

Fig. 6.5-2: Modern low floor street car (left), driven by water-jacket cooled cage induction motors (right) via gears. Variable speed operation is achieved by inverter feeding of the motors. A very high dynamic torque variation is achieved by space vector control, which is based on the here presented space vector theory.

The **calculation of real instantaneous power *P(t)* with space vectors** must be a formulation, that gives for arbitrary time functions of voltage $U_U(t), U_V(t), U_W(t)$ and current $I_U(t), I_V(t), I_W(t)$ with the arbitrary condition $U_U(t) + U_V(t) + U_W(t) \neq 0$, $I_U(t) + I_V(t) + I_W(t) \neq 0$ the correct expression

$$P(t) = U_U(t) \cdot I_U(t) + U_V(t) \cdot I_V(t) + U_W(t) \cdot I_W(t) \quad . \tag{6.5-8}$$

We consider first a three-phase voltage system $U_U(t), U_V(t), U_W(t)$ and current system $I_U(t), I_V(t), I_W(t)$, that does not contain any zero sequence system: $U_U(t)+U_V(t)+U_W(t)=0$, $I_U(t)+I_V(t)+I_W(t)=0$. Then the real instantaneous power is calculated from the corresponding voltage and current space vectors $\underline{U}(t)=\frac{2}{3}\cdot\left[U_U(t)+\underline{a}\cdot U_V(t)+\underline{a}^2\cdot U_W(t)\right]$ and $\underline{I}(t)=\frac{2}{3}\cdot\left[I_U(t)+\underline{a}\cdot I_V(t)+\underline{a}^2\cdot I_W(t)\right]$ as

$$P(t)=(3/2)\cdot\mathrm{Re}\left\{\underline{U}(t)\cdot\underline{I}(t)^*\right\} \quad . \tag{6.5-9}$$

Proof: With $\underline{a}^*=(e^{j\cdot 2\pi/3})^*=e^{-j\cdot 2\pi/3}=e^{j\cdot 4\pi/3}=\underline{a}^2$, $(\underline{a}^2)^*=e^{-j\cdot 4\pi/3}=\underline{a}$, $\underline{a}^3=1$ we get:

$$P(t)=(3/2)\cdot\mathrm{Re}\left\{\underline{U}(t)\cdot\underline{I}(t)^*\right\}=\frac{3}{2}\mathrm{Re}\left\{\frac{2}{3}\cdot\left[U_U+\underline{a}\cdot U_V+\underline{a}^2\cdot U_W\right]\cdot\frac{2}{3}\cdot\left[I_U+\underline{a}\cdot I_V+\underline{a}^2\cdot I_W\right]^*\right\}=$$

$$=\frac{2}{3}\mathrm{Re}\left\{\left[U_U+\underline{a}\cdot U_V+\underline{a}^2\cdot U_W\right]\cdot\left[I_U+\underline{a}^2\cdot I_V+\underline{a}\cdot I_W\right]\right\}=$$

$$=\frac{2}{3}\mathrm{Re}\left\{U_UI_U+\underline{a}^2U_UI_V+\underline{a}U_UI_W+\underline{a}U_VI_U+U_VI_V+\underline{a}^2U_VI_W+\underline{a}^2U_WI_U+\underline{a}U_WI_V+U_WI_W\right\}=$$

$$=\frac{2}{3}\left\{U_UI_U-\frac{U_UI_V+U_UI_W+U_VI_U}{2}+U_VI_V-\frac{U_VI_W+U_WI_U+U_WI_V}{2}+U_WI_W\right\}=$$

$$=\frac{2}{3}\left\{U_UI_U-\frac{U_U(I_V+I_W)}{2}+U_VI_V-\frac{U_V(I_U+I_W)}{2}+U_WI_W-\frac{U_W(I_U+I_V)}{2}\right\}=$$

$$=\frac{2}{3}\left\{U_UI_U+\frac{U_UI_U}{2}+U_VI_V+\frac{U_VI_V}{2}+U_WI_W+\frac{U_WI_W}{2}\right\}=$$

$$=U_U(t)I_U(t)+U_V(t)I_V(t)+U_W(t)I_W(t)=P(t)$$

Quod erat demonstrandum (What was to be shown!).

In the general case we take the three-phase system of (6.5-9) and add a zero-sequence system $U_0(t)$, $I_0(t)$. Then the real instantaneous power is given by

$$P(t)=(U_U+U_0)\cdot(I_U+I_0)+(U_V+U_0)\cdot(I_V+I_0)+(U_W+U_0)\cdot(I_W+I_0)=$$
$$=U_UI_U+U_UI_0+U_0I_U+U_0I_0+U_VI_V+U_VI_0+U_0I_V+U_0I_0+U_WI_W+U_WI_0+U_0I_W+U_0I_0=$$
$$=U_UI_U+U_VI_V+U_WI_W+I_0(U_U+U_V+U_W)+U_0(I_U+I_V+I_W)+3U_0I_0=$$
$$=U_UI_U+U_VI_V+U_WI_W+I_0\cdot 0+U_0\cdot 0+3U_0I_0=(3/2)\cdot\mathrm{Re}\left\{\underline{U}(t)\cdot\underline{I}(t)^*\right\}+3U_0I_0$$

Facit:

The real instantaneous power is calculated in a three-phase system from the voltage and current space vector according to (6.5-9), adding the zero-sequence power, which in all three phases is equal as U_0I_0.

$$P(t)=(3/2)\cdot\mathrm{Re}\left\{\underline{U}(t)\cdot\underline{I}(t)^*\right\}+3U_0I_0 \tag{6.5-10}$$

Example 6.5-3:

Calculate the I^2R-losses in a three-phase symmetric winding system $R_U = R_V = R_W = R$

a) without zero-sequence system, b) with zero-sequence system.

Solution:

a) *Ohm´*s law yields: $U_U(t) = R \cdot I_U(t), U_V(t) = R \cdot I_V(t), U_W(t) = R \cdot I_W(t)$. Hence we get the space vector equation: $\underline{U}(t) = R \cdot \underline{I}(t)$. With $\underline{z} \cdot \underline{z}^* = |\underline{z}|^2$ we derive:

$$\underline{\underline{P(t)}} = (3/2) \cdot \mathrm{Re}\left\{\underline{U}(t) \cdot \underline{I}(t)^*\right\} = (3/2) \cdot R \cdot \mathrm{Re}\left\{\underline{I}(t) \cdot \underline{I}(t)^*\right\} = (3/2) \cdot R \cdot \mathrm{Re}\left\{|\underline{I}(t)|^2\right\} = (3/2) \cdot R \cdot |\underline{I}(t)|^2 =$$

$$= \frac{3}{2} \cdot R \cdot \left[\mathrm{Re}(\underline{I})^2 + \mathrm{Im}(\underline{I})^2\right] = \frac{3}{2} \cdot R \cdot \left[\left(\frac{2}{3} \cdot (I_U - \frac{I_V + I_W}{2})\right)^2 + \left(\frac{2}{3} \cdot \frac{\sqrt{3}(I_V - I_W)}{2}\right)^2\right] =$$

$$= \frac{2}{3} \cdot R \cdot \left[\left(I_U + \frac{I_U}{2}\right)^2 + \frac{3}{4}\left(I_V^2 - 2I_V I_W + I_W^2\right)\right] = \frac{2}{3} \cdot R \cdot \left[\frac{9}{4} I_U^2 + \frac{3}{4}\left(I_V^2 - (I_V + I_W)^2 + I_V^2 + I_W^2 + I_W^2\right)\right] =$$

$$= R \cdot \left[\frac{3}{2} I_U^2 + \frac{1}{2}\left(2I_V^2 - (-I_U)^2 + 2I_W^2\right)\right] = \underline{\underline{R \cdot \left[I_U^2 + I_V^2 + I_W^2\right]}}$$

b) With an additional zero sequence system I_0 the additional voltage drop in each phase is $U_0 = RI_0$. So the losses are:

$$P(t) = (3/2) \cdot R \cdot \mathrm{Re}\left\{\underline{I}(t) \cdot \underline{I}(t)^*\right\} + 3 \cdot RI_0 \cdot I_0 = \underline{\underline{R \cdot \left[I_U^2 + I_V^2 + I_W^2\right] + 3RI_0^2}}$$

Facit:

The absolute value of current space vector is the square root of the sum of the squares of the phase currents, multiplied with the square-root of 2/3.

$$|\underline{I}(t)| = \sqrt{\underline{I}(t) \cdot \underline{I}(t)^*} = \sqrt{(2/3) \cdot (I_U^2 + I_V^2 + I_W^2)} \qquad (6.5\text{-}11)$$

6.6 Magnetic energy

a) Magnetic energy of a single phase winding:

The magnetic field in electric machines stores magnetic energy. In the basic case of Fig. 6.6-1a a single phase winding current $I(t)$ excites a magnetic flux $\Phi(t)$, which is linked with the winding as flux linkage $\Psi(t)$. The relationship between exciting current and linked flux is the self inductance: $\Psi(t) = L \cdot I(t)$. The **magnetic energy per volume** V is $w_{mag} = \int_0^B \vec{H} \bullet d\vec{B}$, which in case of isotropic materials $\vec{B} = \mu \cdot \vec{H}$ and hence parallel field vectors $\vec{B}, \vec{H}$ is given by $w_{mag} = \int_0^B H \cdot dB = \int_0^B \frac{B}{\mu} \cdot dB = \frac{B^2}{2\mu}$. In case of ideal iron $\mu_{Fe} \to \infty$ the magnetic field with the iron is zero: $H_{\mathrm{Fe}} = 0$. Hence only the air gap volume $V_\delta = A \cdot \delta$ in Fig. 6.6-1 has to be considered, given with assumed constant B_δ in the air gap the magnetic energy $W_{mag} = V_\delta \cdot B_\delta^2 / (2\mu_0)$. In case of saturated iron $H_{\mathrm{Fe}} > 0$ the total volume of the magnetic circuit must be considered. If we assume a constant iron permeability μ_{Fe} and constant field vectors B_{Fe}, H_{Fe}, the magnetic energy is $W_{mag} = V_\delta \cdot B_\delta^2 / (2\mu_0) + V_{Fe} \cdot B_{Fe}^2 / (2\mu_{Fe})$. If we

assume the iron cross section area A in Fig. 6.6-1a to be constant, hence $B_\delta = B_{Fe}$, the magnetic energy stored in the iron versus the air gap is given by the ratio $(V_{Fe}/\mu_{Fe})/(V_\delta/\mu_0)$.

Facit:
Usually the ratio μ_0/μ_{Fe} (e. g. 1/5000) is much smaller than the ratio V_{Fe}/V_δ, so the amount of magnetic energy stored in the air gap is much bigger than in the iron.

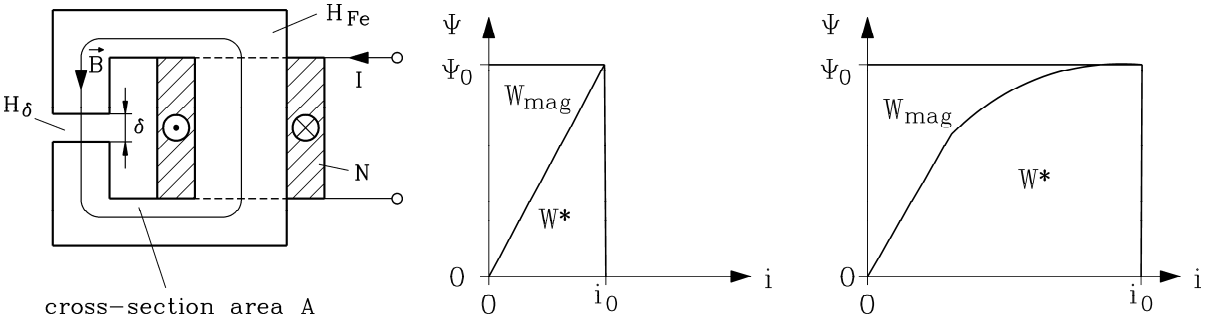

Fig. 6.6-1: a) Magnetic iron-circuit with air gap and single phase excitation winding. Magnetic energy W_{mag} and co-energy W^* for b) linear (unsaturated) and c) non-linear (saturated) flux linkage

Introducing in the unsaturated case the flux $\Phi = B \cdot A$ and via *Ampere´*s law $H_\delta = N \cdot I / \delta$ in $w_{mag} = \int_0^{B_0} H \cdot dB = \int_0^{\Phi_0} \frac{N \cdot I}{\delta} \cdot \frac{d\Phi}{A} = \frac{1}{V_\delta} \int_0^{N\Phi_0} I \cdot d(N\Phi) = \frac{1}{V_\delta} \int_0^{\Psi_0} I \cdot d\Psi$, we get with $W_{mag} = w_{mag} V_\delta$ the alternative formulation for calculating the magnetic energy:

$$W_{mag} = \int_0^{\Psi_0} I \cdot d\Psi = \frac{1}{L} \int_0^{\Psi_0} \Psi \cdot d\Psi = \frac{\Psi_0^2}{2L} = L \frac{I_0^2}{2} \tag{6.6-1}$$

The magnetic energy corresponds in the linear case to the upper triangle area in the Ψ-I-plot Fig. 6.6-1b, whereas the lower triangle area is a fictive energy, called co-energy W^*, which for $\mu_{Fe} \to \infty$ is identical with W_{mag}. It can be shown that also for arbitrary geometries (6.6-1) is correct. In saturated iron the nonlinear case $\Psi(I)$ of Fig. 6.6-1c leads to $W_{mag} = \int_0^{\Psi_0} I(\Psi) \cdot d\Psi < W^*$. As the magnetic energy in the air gap is usually dominating, in the following only the linear case (6.6-1) is considered.
An alternative approach to calculate the magnetic energy is possible from *Faraday´*s law: $U = L \cdot dI/dt$. The magnetic energy is the integral of the reactive power $Q(t) = U(t) I(t)$, which is needed to build up the stored energy:

$$W_{mag} = \int_0^{t_0} Q(t) \cdot dt = \int_0^{t_0} U(t) \cdot I(t) \cdot dt = \int_0^{I_0} L \cdot I \cdot dI = L \cdot I_0^2 / 2 \tag{6.6-2}$$

b) Magnetic energy of a magnetically coupled circuit:
If two windings (e.g. a single phase stator and rotor winding) are magnetically coupled by the mutual inductance M, we distinguish the stator and the rotor self inductances L_s, L_r. From *Faraday´*s law $U_S = L_S \cdot dI_S/dt + M \cdot dI_r/dt$, $U_r = L_r \cdot dI_r/dt + M \cdot dI_S/dt$ we get the

reactive power in the coupled circuit $Q(t) = U_s(t)I_s(t) + U_r(t)I_r(t)$. Its time integration leads to magnetic energy:

$$W_{mag} = \int_0^t Q(t)\cdot dt = \int_0^t (U_s I_s + U_r I_r)dt = \int_0^I (L_s I_s dI_s + L_r I_r dI_r + M I_s dI_r + M I_r dI_s) =$$

$$= L_s \frac{I_s^2}{2} + L_r \frac{I_r^2}{2} + M \cdot I_s I_r$$

Facit:
The magnetic energy in a coupled circuit is given by the stored energy in the two self-inductances and by an additional energy, stored in the mutual inductance.

$$W_{mag} = L_s \frac{I_s^2}{2} + L_r \frac{I_r^2}{2} + 2M \frac{I_s I_r}{2} \qquad (6.6\text{-}3)$$

If an arbitrary transfer ratio $\ddot{u}$ is used with $L_h = \ddot{u}M, L_r' = \ddot{u}^2 L_r, I_r' = I_r/\ddot{u}, U_r' = \ddot{u}U_r$, we get instead of (6.6-3)

$$W_{mag} = L_s \frac{I_s^2}{2} + L_r' \frac{I_r'^2}{2} + 2L_h \frac{I_s I_r'}{2} \qquad . \qquad (6.6\text{-}4)$$

With the definition of the stray inductances $L_{s\sigma} = L_s - L_h, L_{r\sigma}' = L_r' - L_h$ we change (6.6-4):

$$W_{mag} = L_s \frac{I_s^2}{2} + L_r' \frac{I_r'^2}{2} + L_h \frac{2I_s I_r'}{2} = L_s \frac{I_s^2}{2} + L_r' \frac{I_r'^2}{2} + L_h \frac{(I_s + I_r')^2 - I_s^2 - I_r'^2}{2} =$$

$$= L_{s\sigma} \frac{I_s^2}{2} + L_{r\sigma}' \frac{I_r'^2}{2} + L_h \frac{(I_s + I_r')^2}{2}$$

Facit:
The magnetic energy in a coupled circuit can be given also as the stored energy in the two stray-inductances and by an additional energy, stored in the main inductance, due to the fictive "magnetizing" current $I_m = I_s + I'_r$.

$$W_{mag} = L_{s\sigma} \frac{I_s^2}{2} + L_{r\sigma}' \frac{I_r'^2}{2} + L_h \frac{(I_s + I_r')^2}{2} \qquad (6.6\text{-}5)$$

c) Magnetic energy of a magnetically coupled three-phase system:
In a magnetically coupled, symmetrical three phase system with phase windings U, V, W in the stator and U, V, W in the rotor, the stray inductances of all three stator phases $L_{s\sigma}$ and of all three rotor phases $L'_{r\sigma}$ are identical. In the same way the main inductances between the stator and rotor circuits for all three phases U, V, W are of the same magnitude L_h. The magnetic energy in the stator and rotor stray inductances for arbitrary stator and rotor phase currents $I_{sU}(t), I_{sV}(t), I_{sW}(t)$ and $I_{rU}(t), I_{rV}(t), I_{rW}(t)$ is according to (6.6-5)

$$W_{mag,\sigma} = L_{s\sigma}\frac{I_{sU}^2 + I_{sV}^2 + I_{sW}^2}{2} + L'_{r\sigma}\frac{I'^2_{rU} + I'^2_{rV} + I'^2_{rW}}{2} \quad . \tag{6.6-6}$$

With (6.5-11) this magnetic energy may be also written with the stator and rotor current space vector definition:

$$W_{mag,\sigma} = \frac{3}{2}\cdot\left\{\frac{L_{s\sigma}}{2}\cdot\left|\underline{I}_s(t)\right|^2 + \frac{L'_{r\sigma}}{2}\cdot\left|\underline{I}'_r(t)\right|^2\right\}. \tag{6.6-7}$$

In the same way the magnetic energy stored via the magnetizing current is expressed for the three phases as

$$W_{mag,h} = L_h\frac{I_{mU}^2 + I_{mV}^2 + I_{mW}^2}{2} = \frac{3}{2}\cdot\left\{\frac{L_h}{2}\cdot\left|\underline{I}_m(t)\right|^2\right\} .$$

Facit:

The stored magnetic energy in a symmetrical three-phase electrical machine with a magnetically coupled stator and rotor three-phase winding system may be calculated via the stator and rotor current space vector as the stored magnetic energy in the stray and main inductance.

$$W_{mag} = W_{mag,\sigma} + W_{mag,h} = \frac{3}{2}\cdot\left\{\frac{L_{s\sigma}}{2}\cdot\left|\underline{I}_s(t)\right|^2 + \frac{L'_{r\sigma}}{2}\cdot\left|\underline{I}'_r(t)\right|^2 + \frac{L_h}{2}\cdot\left|\underline{I}_s(t) + \underline{I}'_r(t)\right|^2\right\} \tag{6.6-8}$$

7. Dynamics of induction machines

7.1 Per unit calculation

a) Motivation:
Dynamic induction machine models are widely used in the **micro-controller program** of inverters for variable speed drives, consisting of induction machine and inverter. The micro-controller is used for **speed and torque control** of the induction machine, using the same dynamic model of the induction machine for the whole range of small to big induction machines. Thus motor power may vary between typically 1 kW up to 10 MW or 4 orders of magnitude (10^4). Therefore motor parameters vary also within this range, with big parameters (resistance, inductance) for small machines. For limited digits for numbers e.g. for resistance, voltage, current etc. in the controller (16 bit or 32 bit controller) it is unfavourable to calculate at big power with very small numbers. If **per unit numbers** are used, not only the parameters, but also motor voltage, current, speed and torque vary only between typically 0 and 3.0 for all motors of the whole power range, which allows **the same precise controller calculation** for the whole power range.

b) How per unit system works:

Example 7.1-1:
*Ohm´*s law: $U = 10V, R = 2\Omega$: How big is current I ? (Rated voltage and current: $U_N = 5V, I_N = 5A$).
(i) Calculated with physical numbers: $I = U / R = 10V / 2\Omega = \underline{\underline{5A}}$.
Control of physical units: $V / \Omega = V / ((V / A) = A$
(ii) Calculated with per unit numbers: $u = U / U_N = 10 / 5 = 2, Z_N = U_N / I_N = 5 / 5 = 1\Omega$.
$r = R / Z_N = 2 / 1 = 2 \qquad \Rightarrow i = u / r = 2 / 2 = \underline{\underline{1}}$
Note: $i = \underline{\underline{1 p.u.}}$ is equal to $i = I / I_N = \underline{\underline{1}} \quad \Rightarrow \quad I = i \cdot I_N = 1 \cdot 5A = 5A$

Facit:
Per unit values have the physical units 1, so check of results of analytical calculations by physical units check is no longer possible, which is disadvantageous. On the other hand, the calculation result gives directly an impression of the degree of loading of electric device.

In Example 7.1-1 the result "current through resistor" $I = 5A$ does not tell you, if this is heavy or small loading of the resistor, whereas the result "per unit current through resistor" $i = 1 p.u.$ immediately gives information, that the resistor is loaded with its rated current, which is thermally OK. Result of current with e.g. 1.5 p.u. tells immediately: "50% overload" or "125% loss overload" ($P_{Cu} = RI^2 \quad \Rightarrow \quad 1.5^2 = 2.25$) , which means steady state temperature rise up to 225% rated temperature rise, which is unbearable, so only short-time operation is allowed.

- The values for the per unit calculation **for electric machines** are taken from machine data plate such as rated frequency or rated power.
- **In three phase systems (electric machines, transformers, power lines, cables, ...) rated impedance Z_N has to be calculated with phase values,** being defined as ratio of rated **phase** voltage $U_{N,ph}$ versus **rated** phase current $I_{N,ph}$**.**
- The value Z_N is NOT printed on data plate, but has to be calculated separately from data plate values.

- Note that data plate values for voltage and current are ALWAYS line values, namely line-to-line voltage and line current. Electric machine models are usually based on phase values **in order to be independent from kind of winding connection (Y or D)**. **So, for per unit voltage, current and impedance calculation rated <u>phase</u> values are taken.**
- Symbols for per unit values are small letters ($u(t)$, $i(t)$, ...), so for time varying voltage, current etc. in physical units capital letters are used here ($U(t)$, $I(t)$, ...).

<u>Example 7.1-2:</u>
Typical data plates of electric machines:

(i) DC machine:

Type G248	..... Motor Company/2003	
DC-Motor	Nr. 622 085	
440 V	165 A	
65 kW	1000/2350 /min	S1
Excitation: 190 V	1.5 A	
Th.Cl. B	IP 11	

(ii) AC induction machine:

Type MKG-222 M06 F3B-9		Motor Company/2003
AC-Motor	Nr. 691 502	
400 V Y	84 A	
45 kW	1490/3000 /min	S1
75 Hz	$\cos\varphi = 0.88$	
Th.Cl. F	IP 44	

(iii) AC synchronous machine:

Type FL 306/6-6	..... Motor Company/2003	
AC-Generator	Nr. 427 597	
400 V Y	57.7 A	
40 kVA	1000/2000 /min	S1
50 Hz	$\cos\varphi = 0.85$ over-excited	
Excitation: 95 V, 10.1 A		
Th.Cl. B	IP 11	

<u>Example 7.1-3:</u>
Rated impedance of electric machines of Example 7.1-2:
(i) DC machine: $Z_N = U_N / I_N = 440/165 = \underline{\underline{2.67}}\,\Omega$
(ii) AC induction machine: Y connection: $U_{N,ph} = U_N / \sqrt{3} = 400/\sqrt{3} = 230V$, $I_{N,ph} = I_N$
$Z_N = U_{N,ph} / I_{N,ph} = 230/84 = \underline{\underline{2.74}}\,\Omega$
(iii) AC synchronous machine: Y connection:
$U_{N,ph} = U_N / \sqrt{3} = 400/\sqrt{3} = 230V$, $I_{N,ph} = I_N$
$Z_N = U_{N,ph} / I_{N,ph} = 230/57.7 = \underline{\underline{4.0}}\,\Omega$
(iv) AC synchronous machine as (iii), but stator winding in *D connection*:
$U_{N,ph} = U_N = 400V$, $I_{N,ph} = I_N / \sqrt{3} = 57.7/\sqrt{3} = 33.3$ A
$Z_N = U_{N,ph} / I_{N,ph} = 400/33.3 = \underline{\underline{12.0}}\,\Omega$

- Per unit time:
Time *t* is multiplied with rated angular frequency $\omega_N = 2\pi f_N$ to get per unit time τ.

$$\tau = \omega_N \cdot t \tag{7.1-1}$$

- Per unit electric angular frequency:
Electric angular frequency $\Omega_s = 2\pi f_s, \Omega_r = 2\pi f_r$ is divided by rated angular frequency $\omega_N = 2\pi f_N$ to get per unit angular frequency ω_s, ω_r.

$$\omega_s = \Omega_s / \omega_N \qquad \omega_r = \Omega_r / \omega_N \tag{7.1-2}$$

- Per unit mechanical angular frequency:
Mechanical angular frequency $\Omega_m = 2\pi \cdot n$ is divided by rated synchronous angular frequency $\omega_N / p = 2\pi f_N / p$ to get per unit mechanical angular frequency ω_m.

$$\omega_m = \Omega_m \cdot p / \omega_N \tag{7.1-3}$$

- Per unit electric resistance:
Electric resistance R_s, R_r' is divided by rated impedance Z_N to get per unit electric resistance r_s, r_r'.

$$r_s = R_s / Z_N \qquad r_r' = R_r' / Z_N \qquad Z_N = U_{N,ph} / I_{N,ph} \tag{7.1-4}$$

- Per unit inductance:
Inductance L_s, L_h, L_r' etc. is divided by rated impedance-frequency ratio Z_N / ω_N to get per unit inductance l_s, l_h, l_r'. Note that in order to avoid mixing of *l* of per unit inductance with symbol of length l, international standardization **has chosen symbol *x* for per unit inductance** (taken from symbol $X = \omega L$ of reactance).

$$x_s = \omega_N \cdot L_s / Z_N \qquad x_h = \omega_N \cdot L_h / Z_N \qquad x_r' = \omega_N \cdot L_r' / Z_N \tag{7.1-5}$$

- Per unit electric voltage:
Electric phase voltage $U_s(t), U_r'(t)$ is divided by PEAK value of rated sinus phase voltage $\sqrt{2}U_{N,ph}$ to get per unit electric phase voltage $u_s(\tau), u_r'(\tau)$.

$$u_s = U_s / (\sqrt{2}U_{N,ph}) \qquad u_r' = U_r' / (\sqrt{2}U_{N,ph}) \tag{7.1-6}$$

- Per unit electric current:
Electric phase current $I_s(t), I_r'(t)$ is divided by PEAK value of rated sinus phase current $\sqrt{2}I_{N,ph}$ to get per unit electric phase current $i_s(\tau), i_r'(\tau)$.

$$i_s = I_s / (\sqrt{2}I_{N,ph}) \qquad i_r' = I_r' / (\sqrt{2}I_{N,ph}) \tag{7.1-7}$$

- Per unit magnetic flux linkage:
Magnetic flux linkage $\Psi(t)$ is divided by rated flux linkage Ψ_N, which is defined from PEAK value of rated sinus phase voltage and angular frequency, to get per unit magnetic flux linkage $\psi(\tau)$.

$$\psi = \Psi / \Psi_N \qquad \Psi_N = \frac{\sqrt{2} \cdot U_{N,ph}}{\omega_N} \tag{7.1-8}$$

- Per unit torque:
Torque $M(t)$ is divided NOT by rated torque M_N of data plate, but by **rated apparent torque** M_B, which is defined from rated APPARENT power and synchronous speed of data plate, thus including power factor and machine efficiency, to get per unit electromagnetic torque $m(\tau)$.

$$m = M / M_B \qquad M_B = \frac{S_N}{\omega_N / p} = \frac{(3/2) \cdot \sqrt{2} U_{N,ph} \sqrt{2} I_{N,ph}}{\omega_N / p} \tag{7.1-9}$$

Note:
Rated apparent torque is e.g. for motor operation of induction machine bigger than rated torque M_N according to data plate:

$$M_B = \frac{S_N}{\omega_N / p} = \frac{P_N / (\cos\varphi_N \cdot \eta_N)}{\frac{\Omega_{mN}}{1 - s_N}} = \frac{P_N}{\Omega_{mN}} \cdot \frac{1 - s_N}{\cos\varphi_N \cdot \eta_N} = M_N \cdot \frac{1 - s_N}{\cos\varphi_N \cdot \eta_N}$$

$$\boxed{M_B = M_N \cdot \frac{1 - s_N}{\cos\varphi_N \cdot \eta_N}} \tag{7.1-10}$$

- Per unit moment of inertia:
Rotor inertia J is calculated from T_J (see Chapter 5) as per unit starting time constant τ_J.

$$\tau_J = \omega_N \cdot T_J \qquad T_J = J \cdot \frac{\omega_N / p}{M_B} \tag{7.1-11}$$

c) Voltage equation and mechanical equation in per unit system:

The **voltage equation**

$$U(t) = R \cdot I(t) + \frac{d\Psi(t)}{dt} \tag{7.1-12}$$

is transformed into per unit system:

$$u(\omega_N t) = \frac{U(t)}{\sqrt{2} \cdot U_{N,ph}} = \frac{R \cdot I(t)}{\sqrt{2} \cdot U_{N,ph}} \cdot \frac{\sqrt{2} \cdot I_{N,ph}}{\sqrt{2} \cdot I_{N,ph}} + \frac{d\Psi(t)}{\frac{\sqrt{2} \cdot U_{N,ph}}{\omega_N} \cdot d(\omega_N t)} \qquad \rightarrow$$

$$\underline{\underline{u(\tau) = r \cdot i(\tau) + \frac{d\psi(\tau)}{d\tau}}} \tag{7.1-13}$$

In the same way the **mechanical equation**

$$J \cdot \frac{d\Omega_m(t)}{dt} = M_e(t) - M_s(t) \tag{7.1-14}$$

is transformed:

$$\omega_N \cdot J \cdot \frac{\omega_N / p}{M_B} \cdot \frac{d\Omega_m(t)}{\frac{\omega_N}{p} d(\omega_N t)} = \frac{M_e(t) - M_s(t)}{M_B} \quad \rightarrow \quad \underline{\underline{\tau_J \cdot \frac{d\omega_m(\tau)}{d\tau} = m_e(\tau) - m_s(\tau)}} \qquad (7.1\text{-}15)$$

Example 7.1-4:

Given data plate of AC induction **motor** is transformed in per unit data set:

400 V Y	34.5 A	
18.5 kW	1465 /min	S1
50 Hz	$\cos\varphi = 0.84$	$J = 0.054$ kgm^2
Th.Cl. F	IP 54	

- Rated phase voltage: $U_{N,ph} = \frac{400V}{\sqrt{3}} = 230V \quad \rightarrow \quad \hat{U}_{N,ph} = \sqrt{2} \cdot U_{N,ph} = \underline{\underline{325V}}$
- Rated phase current: $\hat{I}_{N,ph} = \sqrt{2} \cdot I_N = \sqrt{2} \cdot 34.5 = \underline{\underline{48.8A}}$
- Rated impedance: $Z_N = U_{N,ph} / I_{N,ph} = 230/34.5 = \underline{\underline{6.67\Omega}}$
- Rated angular frequency: $\omega_N = 2\pi \cdot 50 = \underline{\underline{314/s}}$
- Number of pole pairs: $p = 2$
- Rated motor efficiency:

$$\eta_N = \frac{P_{m,out,N}}{P_{e,in,N}} = \frac{P_N}{\sqrt{3} \cdot U_N \cdot I_N \cdot \cos\varphi_N} = \frac{18500}{\sqrt{3} \cdot 400 \cdot 34.5 \cdot 0.84} = \underline{\underline{0.921}}$$

- Rated torque: $M_N = \frac{P_N}{\Omega_{mN}} = \frac{18500}{2\pi \cdot (1465/60)} = \underline{\underline{120.6Nm}}$
- Rated apparent torque:

$$M_B = \frac{S_N}{\Omega_{syn,N}} = \frac{P_N / (\cos\varphi_N \cdot \eta_N)}{\omega_N / p} = \frac{18500/(0.84 \cdot 0.921)}{314/2} = \underline{\underline{152.3Nm}}$$

Note:

Slip: $s_N = 1 - 1465/1500 = 0.0233$

$$M_B = M_N \cdot \frac{1 - s_N}{\cos\varphi_N \cdot \eta_N} = 120.6 \cdot \frac{1 - 0.0233}{0.84 \cdot 0.921} = \underline{\underline{152.3Nm}}$$

- Rated flux linkage: $\hat{\Psi}_N = \frac{\sqrt{2} \cdot 230}{314} = \underline{\underline{1.036Vs}}$
- Rated starting time: $T_J = 0.054 \cdot \frac{314}{2} \cdot \frac{1}{152.3} = \underline{\underline{0.056s}}, \ \tau_J = \omega_N T_J = 314 \cdot 0.056 = \underline{\underline{17.58}}$

Time period of stator:	$\tau = \omega_N \cdot T = \omega_N / f_s = 314/50 = \underline{\underline{2\pi}}$
Stator voltage in phase U:	$u_{s,U} = 1 \cdot \cos(\tau)$
Stator current in phase U:	$i_{s,U} = 1 \cdot \cos(\tau - \varphi_N)$
Motor torque at rated power:	$m_N = \frac{M_N}{M_B} = \frac{120.6}{152.3} = 0.792$

7.2 Dynamic voltage equations and reference frames of induction machine

Symmetrical machine is assumed, which leads to identical machine parameters per phase, e.g.: $r_{s,U} = r_{s,V} = r_{s,W} = r_s$ and so on. Flux linkage in the three stator phases U, V, W is $\psi_U(\tau), \psi_V(\tau), \psi_W(\tau)$ in per unit formulation, leading to voltage equation per phase:

$$\left.\begin{aligned} u_{s,U}(\tau) &= r_s \cdot i_{s,U}(\tau) + \frac{d\psi_{s,U}(\tau)}{d\tau}\Bigg| \cdot\frac{2}{3} \\ u_{s,V}(\tau) &= r_s \cdot i_{s,V}(\tau) + \frac{d\psi_{s,V}(\tau)}{d\tau}\Bigg| \cdot\frac{2}{3}\cdot\underline{a} \\ u_{s,W}(\tau) &= r_s \cdot i_{s,W}(\tau) + \frac{d\psi_{s,W}(\tau)}{d\tau}\Bigg| \cdot\frac{2}{3}\cdot\underline{a}^2 \end{aligned}\right\} + \left.\begin{aligned} &\cdot\frac{1}{3} \\ &\cdot\frac{1}{3} \\ &\cdot\frac{1}{3} \end{aligned}\right\} +$$

$$\begin{aligned} \underline{u}_s(\tau) &= r_s \cdot \underline{i}_s(\tau) + \frac{d\underline{\psi}_s(\tau)}{d\tau} \\ u_{s0}(\tau) &= r_s \cdot i_{s0}(\tau) + \frac{d\psi_{s0}(\tau)}{d\tau} \end{aligned} \qquad (7.2\text{-}1)$$

In (7.2-1) the definitions for **per unit stator voltage, current and flux linkage space vectors**

$$\begin{aligned} \underline{u}_s(\tau) &= \frac{2}{3}\cdot\left(u_{s,U}(\tau) + \underline{a}\cdot u_{s,V}(\tau) + \underline{a}^2\cdot u_{s,W}(\tau)\right) \\ \underline{i}_s(\tau) &= \frac{2}{3}\cdot\left(i_{s,U}(\tau) + \underline{a}\cdot i_{s,V}(\tau) + \underline{a}^2\cdot i_{s,W}(\tau)\right) \\ \underline{\psi}_s(\tau) &= \frac{2}{3}\cdot\left(\psi_{s,U}(\tau) + \underline{a}\cdot \psi_{s,V}(\tau) + \underline{a}^2\cdot \psi_{s,W}(\tau)\right) \end{aligned} \qquad (7.2\text{-}2)$$

and the **per unit zero sequence stator voltage, current and flux linkage**

$$\begin{aligned} u_{s,0}(\tau) &= \frac{1}{3}\cdot\left(u_{s,U}(\tau) + u_{s,V}(\tau) + u_{s,W}(\tau)\right) \\ i_{s,0}(\tau) &= \frac{1}{3}\cdot\left(i_{s,U}(\tau) + i_{s,V}(\tau) + i_{s,W}(\tau)\right) \\ \psi_{s,0}(\tau) &= \frac{1}{3}\cdot\left(\psi_{s,U}(\tau) + \psi_{s,V}(\tau) + \psi_{s,W}(\tau)\right) \end{aligned} \qquad (7.2\text{-}3)$$

have been used. For three phase **rotor voltage system** the same calculation yields

$$\begin{aligned} \underline{u}'_r(\tau) &= r'_r \cdot \underline{i}'_r(\tau) + \frac{d\underline{\psi}'_r(\tau)}{d\tau}\Bigg|_{(r)} \\ u'_{r0}(\tau) &= r'_r \cdot i'_{r0}(\tau) + \frac{d\psi'_{r0}(\tau)}{d\tau}\Bigg|_{(r)} \end{aligned} \quad . \qquad (7.2\text{-}4)$$

For further considerations the zero sequence system is neglected, thus considering only star connected systems without clamping of neutral. Note that (7.2-4) is valid in the **rotor fixed reference frame**; that means that for an observer in the stator winding (= in the **stator fixed reference frame**) the movement of the rotor space vectors consists of their movement in rotor reference frame and – in addition – the movement of the rotor itself (Fig. 7.2-1).

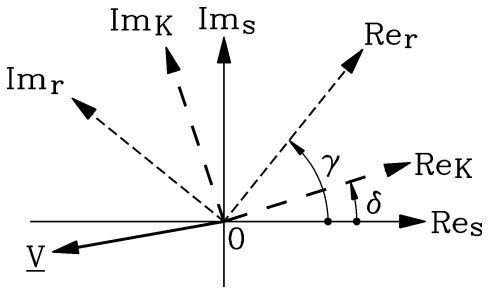

Fig. 7.2-1: An arbitrary space vector $\underline{V}$ has the SAME amplitude, but different co-ordinates (polar angles) in different reference frames.

An arbitrary space vector $\underline{V}$ has the SAME amplitude, but different angles in different reference frames. In Fig. 7.2-1 three reference frames are depicted:

- **stator reference frame *s*:** α-axis is $\mathrm{Re_s}$-axis, β-axis is $\mathrm{Im_s}$-axis.
- **rotor reference frame *r*:** α-axis is $\mathrm{Re_r}$-axis (*d*-axis), β-axis is $\mathrm{Im_r}$-axis (*q*-axis).
- **arbitrary reference frame *K***: α-axis is $\mathrm{Re_K}$-axis, β-axis is $\mathrm{Im_K}$-axis.

Rotor reference frame is shifted by **rotation angle** $\gamma(t)$, measured in "electric degrees",

$$\gamma(t) = p \cdot \int_0^t \Omega_m(t) \cdot dt + \gamma_0 = \int_0^\tau \omega_m(\tau) \cdot d\tau + \gamma_0 = \gamma(\tau) \quad , \tag{7.2-5}$$

with respect to stator reference frame, whereas reference system *K* is shifted by angle $\delta(\tau)$ according the rotational movement of this system. Therefore the SAME space vector is described by different co-ordinates in the different reference frames.

in stator reference frame *s*	**in rotor reference frame *r***	**in reference frame *K***
$\underline{V}_{(s)} = V \cdot e^{j\alpha}$	$\underline{V}_{(r)} = V \cdot e^{j\alpha} \cdot e^{-j\gamma}$	$\underline{V}_{(K)} = V \cdot e^{j\alpha} \cdot e^{-j\delta}$
	$\underline{V}_{(r)} = \underline{V}_{(s)} \cdot e^{-j\gamma}$	$\underline{V}_{(K)} = \underline{V}_{(s)} \cdot e^{-j\delta}$

Table 7.2-1: Space vector $\underline{V}$ has the SAME amplitude, but different co-ordinates (polar angles) in different reference frames.

For solving stator and rotor voltage equation simultaneously, they have to be considered in the SAME reference frame, for example in the reference frame *K*, which is defined by the time function of polar angle $\delta(\tau)$, which we assume here to be given as a certain function. Transformation of stator voltage equation from stator reference frame to reference frame K is done according to $\underline{V}_{(K)} = \underline{V}_{(s)} \cdot e^{-j\delta(\tau)}$ in Table 7.2-1 with multiplication by $\cdot e^{-j\delta(\tau)}$, whereas transformation from rotor reference frame to frame *K* is done by multiplication with $\cdot e^{-j(\delta(\tau)-\gamma(\tau))}$.

Note that **rule for differentiation of product of two functions** has to be obeyed!

$$\begin{aligned} \frac{d\left(\underline{\psi}_s(\tau) \cdot e^{-j\delta(\tau)}\right)}{d\tau} &= e^{-j\delta(\tau)} \cdot \frac{d\underline{\psi}_s(\tau)}{d\tau} + \underline{\psi}_s(\tau) \cdot \frac{d\left(e^{-j\delta(\tau)}\right)}{d\tau} = \\ &= e^{-j\delta(\tau)} \cdot \frac{d\underline{\psi}_s(\tau)}{d\tau} - j \cdot \underline{\psi}_s(\tau) \cdot e^{-j\delta(\tau)} \cdot \frac{d\left(\delta(\tau)\right)}{d\tau} \end{aligned} \tag{7.2-6}$$

$$\underline{u}_{s(K)} = \underline{u}_s \cdot e^{-j\delta} = r_s \cdot \underline{i}_s \cdot e^{-j\delta} + \frac{d\underline{\psi}_s}{d\tau} \cdot e^{-j\delta} = r_s \cdot \underline{i}_{s(K)} + \frac{d\underline{\psi}_{s(K)}}{d\tau} + j \cdot \frac{d\delta}{d\tau} \cdot \underline{\psi}_{s(K)}$$

$$\underline{u}'_{r(K)} = \underline{u}'_r \cdot e^{-j(\delta-\gamma)} = r'_r \cdot \underline{i}'_r \cdot e^{-j(\delta-\gamma)} + \frac{d\underline{\psi}'_r}{d\tau} \cdot e^{-j(\delta-\gamma)} = r'_r \cdot \underline{i}'_{r(K)} + \frac{d\underline{\psi}'_{r(K)}}{d\tau} + j \cdot \frac{d(\delta-\gamma)}{d\tau} \cdot \underline{\psi}'_{r(K)}$$

Stator and rotor equation in arbitrary reference frame *K*:

$$\begin{aligned} \underline{u}_{s(K)} &= r_s \cdot \underline{i}_{s(K)} + \frac{d\underline{\psi}_{s(K)}}{d\tau} + j \cdot \frac{d\delta}{d\tau} \cdot \underline{\psi}_{s(K)} \\ \underline{u}'_{r(K)} &= r'_r \cdot \underline{i}'_{r(K)} + \frac{d\underline{\psi}'_{r(K)}}{d\tau} + j \cdot \frac{d(\delta-\gamma)}{d\tau} \cdot \underline{\psi}'_{r(K)} \end{aligned} \qquad (7.2\text{-}7)$$

Facit:
*The stator voltage per phase consists of resistive voltage drop, induced voltage due to change of flux linkage $d\psi_s/d\tau$ like in transformers **("transformer induced voltage")** and induced voltage due to movement (rotation) of reference frame K relative to stator reference frame $d\delta/d\tau$ **("rotational induced voltage")**. For rotor phase voltage induction the movement of reference frame K relative to rotor $d(\delta - \gamma)/d\tau$ has to be taken into account.*

For practical use formulation of stator and rotor voltage in the following three different reference frames is important (Table 7.2-2).

Reference frame		***Angular rotation of reference frame***
stator reference frame	α-β-frame	$\delta(\tau) = 0 : \omega_K = \frac{d\delta}{d\tau} = 0$
rotor reference frame	*d*-*q*-frame	$\delta = \gamma : \omega_K(\tau) = \frac{d\gamma}{d\tau} = \omega_m$
synchronous reference frame	*a*-*b*-frame	$\omega_K(\tau) = \frac{\Omega_s(\tau)}{\omega_N}$

Table 7.2-2: Mainly used reference frames for voltage equations

Stator and rotor equation in stator reference frame *s*, considering that in induction machines rotor circuit is short-circuited**:**

$$\begin{aligned} \underline{u}_s &= r_s \cdot \underline{i}_s + \frac{d\underline{\psi}_s}{d\tau} \\ 0 &= r'_r \cdot \underline{i}'_r + \frac{d\underline{\psi}'_r}{d\tau} - j \cdot \omega_m \cdot \underline{\psi}'_r \end{aligned} \qquad (7.2\text{-}8)$$

7.3 Dynamic flux linkage equations

As stator and rotor per unit space current vectors

$$\underline{i}_s(\tau) = \frac{2}{3}\left(i_{s,U}(\tau) + \underline{a} \cdot i_{s,V}(\tau) + \underline{a}^2 \cdot i_{s,W}(\tau)\right) \quad \underline{i}'_r(\tau) = \frac{2}{3}\left(i'_{r,U}(\tau) + \underline{a} \cdot i'_{r,V}(\tau) + \underline{a}^2 \cdot i'_{r,W}(\tau)\right) \qquad (7.3\text{-}1)$$

are transformed into the same reference frame, they may be added as resulting **magnetizing space current vector** by vector addition law (Fig. 7.3-1a):

$$\underline{i}_m(\tau) = \underline{i}_s(\tau) + \underline{i}'_r(\tau) \quad . \tag{7.3-2}$$

This magnetizing space current vector excites with **magnetizing inductance**

$$x_h = \frac{\omega_N \cdot L_h}{Z_N} \tag{7.3-3}$$

the **main flux linkage** between stator and rotor winding

$$\underline{\psi}_h(\tau) = x_h \cdot \underline{i}_m(\tau) \quad . \tag{7.3-4}$$

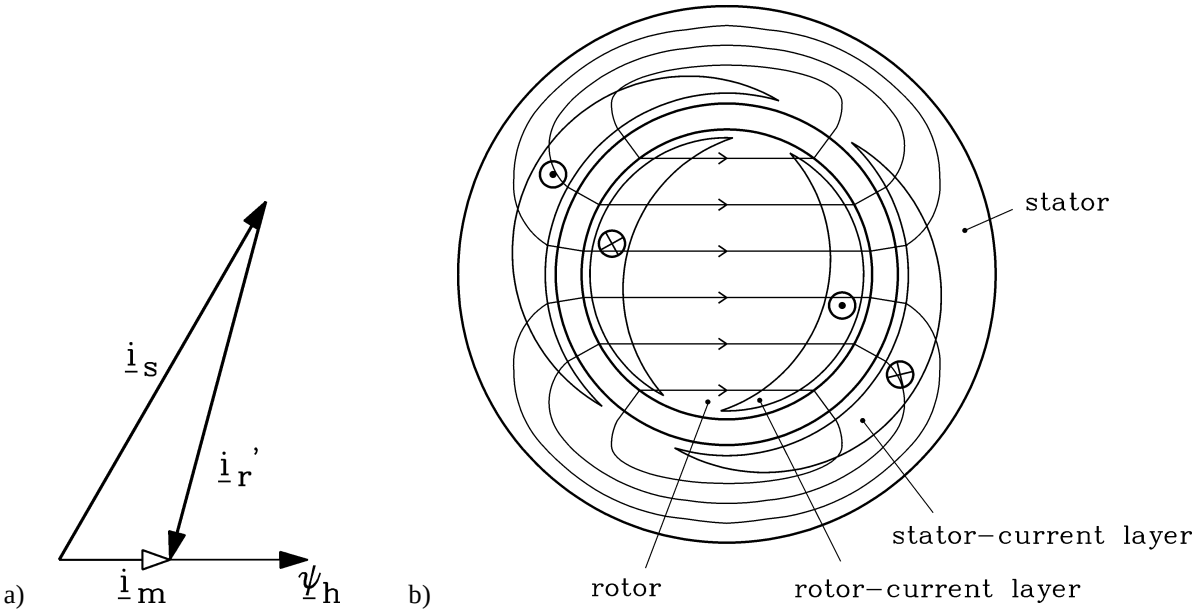

Fig. 7.3-1: Flux linkage in induction machine: a) Vector addition of stator and rotor current space vector yields magnetizing current space vector, b) Stator and rotor sinusoidal distributed current layer correspond with stator and rotor space current vector. Resulting main flux density distribution *B* corresponds with magnetizing space current vector and main flux linkage space vector.

Further, stator and rotor space current vector excite **stator and rotor leakage flux linkage**,

$$\underline{\psi}_{s\sigma}(\tau) = x_{s\sigma} \cdot \underline{i}_s(\tau) \quad , \quad \underline{\psi}'_{r\sigma}(\tau) = x'_{r\sigma} \cdot \underline{i}'_r(\tau) \quad , \tag{7.3-5}$$

$$x_{s\sigma} = \frac{\omega_N \cdot L_{s\sigma}}{Z_N} \quad , \quad x'_{r\sigma} = \frac{\omega_N \cdot L'_{r\sigma}}{Z_N} \tag{7.3-6}$$

consisting of
- slot leakage flux,
- leakage flux of winding overhangs and
- flux linkage of air gap flux density space harmonics.

Facit:
By considering self-inductance of space harmonic flux waves the influence of slotting on air gap flux density distribution, which leads to step-like air gap field curve $B_\delta(x)$, is included in dynamic model.

Vector addition of main and leakage flux linkage space vectors yields **stator and rotor flux linkage space vectors**, considered in the same reference frame.

$$\boxed{\begin{aligned}\underline{\psi}_s &= (x_h + x_{s\sigma})\cdot \underline{i}_s + x_h \cdot \underline{i}'_r = x_s \cdot \underline{i}_s + x_h \cdot \underline{i}'_r = x_{s\sigma} \cdot \underline{i}_s + x_h \cdot \underline{i}_m = \underline{\psi}_{s\sigma} + \underline{\psi}_h \\ \underline{\psi}'_r &= x_h \cdot \underline{i}_s + (x_h + x'_{r\sigma})\cdot \underline{i}'_r = x_h \cdot \underline{i}_s + x'_r \cdot \underline{i}'_r = x_h \cdot \underline{i}_m + x'_{r\sigma} \cdot \underline{i}'_r = \underline{\psi}_h + \underline{\psi}'_{r\sigma}\end{aligned}} \qquad (7.3\text{-}7)$$

Total leakage flux space vector $\underline{\psi}_\sigma$ is described by *Blondel´*s total leakage coefficient

$$\sigma = 1 - \frac{x_h^2}{x_s \cdot x'_r} \qquad (7.3\text{-}8)$$

as

$$\boxed{\left|\underline{\psi}_\sigma\right| = x_{s\sigma} \cdot \left|\underline{i}_s\right| + x'_{r\sigma} \cdot \left|\underline{i}'_r\right| \approx \sigma \cdot x_s \cdot \underline{i}_s} \text{ . Note: } |s| \to \infty : \left|\underline{\psi}_\sigma\right| = \sigma \cdot x_s \cdot \underline{i}_s \qquad (7.3\text{-}9)$$

Example 7.3-1:

Induction machine, resistances neglected, stator reference frame, $|s| >> 1$:

inductance data: $x_h = 2.5, \quad x_s = 2.6, \quad x'_r = 2.58$,

Machine operated at three-phase symmetrical sinus voltage system (u_s = 1) with rated frequency $\omega_s = 1$. Currents at big slip: $|s| >> 1 : \underline{i}'_r = -(x_h / x'_r)\cdot \underline{i}_s = -0.97 \cdot \underline{i}_s \quad \Rightarrow \quad \underline{i}_s \approx -\underline{i}'_r$.

- **Leakage inductances**:

$x_{s\sigma} = x_s - x_h = 2.6 - 2.5 = \underline{\underline{0.1}}, \quad x'_{r\sigma} = x'_r - x_h = 2.58 - 2.5 = \underline{\underline{0.08}}$

- Total leakage coefficient: $\sigma = 1 - \dfrac{x_h^2}{x_s \cdot x'_r} = 1 - \dfrac{2.5^2}{2.6 \cdot 2.58} = \underline{\underline{0.068}}$

- At $|s| >> 1$ stator flux linkage is $\left|\underline{\psi}_s\right| = \sigma \cdot x_s \cdot \left|\underline{i}_s\right| = 0.068 \cdot 2.6 \cdot \left|\underline{i}_s\right| = \underline{\underline{0.177 \cdot \left|\underline{i}_s\right|}}$ or

$$\left|\underline{\psi}_s\right| = \left|\underline{\psi}_\sigma\right| = \left|x_{s\sigma} \cdot \underline{i}_s - x'_{r\sigma} \cdot \underline{i}'_r\right| = \left|0.1 - 0.08 \cdot (-0.97)\right| \cdot \left|\underline{i}_s\right| = \underline{\underline{0.177 \cdot \left|\underline{i}_s\right|}}$$

- **No-load current**:

stator voltage space vector: $\underline{u}_s = 1 \cdot e^{j\tau}$, stator flux linkage $\underline{\psi}_s = x_s \cdot \underline{i}_{s0}$

$$\underline{u}_s = r_s \cdot \underline{i}_s + \frac{d\underline{\psi}_s}{d\tau} \approx \frac{d\underline{\psi}_s}{d\tau} = x_s \cdot \frac{d\underline{i}_{s0}}{d\tau} = e^{j\tau} \quad \rightarrow \quad \underline{\underline{\underline{i}_{s0} = -j \cdot \frac{1}{x_s} \cdot e^{j\tau}}} \quad i_{s0} = \frac{1}{2.6} = \underline{\underline{0.38}},$$

Example 7.3-2:

Induction machine, data from Example 7.3-1:

- **Starting current**:

stator voltage space vector: $\underline{u}_s = 1 \cdot e^{j\tau}$

stator flux linkage $\underline{\psi}_s = \sigma \cdot x_s \cdot \underline{i}_{s1}$

$$\underline{u}_s \cong \frac{d\underline{\psi}_s}{d\tau} = \sigma \cdot x_s \cdot \frac{d\underline{i}_{s1}}{d\tau} = e^{j\tau} \quad \rightarrow \quad \underline{\underline{\underline{i}_{s1} = -j \cdot \frac{1}{\sigma \cdot x_s} \cdot e^{j\tau}}} \quad i_{s1} = \frac{1}{0.068 \cdot 2.6} = \underline{\underline{5.66}},$$

Facit:

The no-load current space vector is phase shifted to stator voltage space vector by 90° (exact, if stator resistance is neglected). No-load current ranges at rated voltage typically between

30% to 50% of nominal current. Starting current at rated voltage ranges between typically 5- to 8-times nominal current.

7.4 Torque equation

The *Lorentz* force of magnetic flux density B_δ on each current-carrying conductor with length *ds* is

$$d\vec{F} = I_c(t) \cdot d\vec{s} \times \vec{B}_\delta \quad . \tag{7.4-1}$$

With perpendicular direction of conductor axis and air gap field (Fig. 7.4-1) this simplifies to a tangential force

$$dF(t) = I_c(t) \cdot B_\delta \cdot ds \quad . \tag{7.4-2}$$

As flux density along motor axial length of iron stack *l* is constant, force is

$$F(t) = \int_0^l dF(t) = I_c(t) \cdot B_\delta \cdot \int_0^l ds = I_c(t) \cdot B_\delta \cdot l \quad . \tag{7.4-3}$$

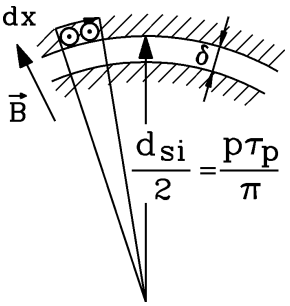

Fig. 7.4-1: Electromagnetic torque generation: tangential forces on current-carrying conductors

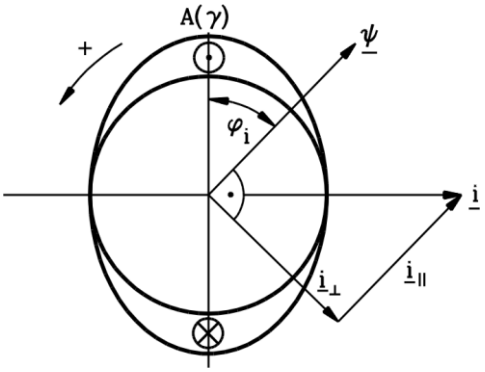

Fig. 7.4-2: Only flux-perpendicular component of current space vector produces torque ($\gamma = \gamma_s$: stator-fixed)

With *a* parallel winding branches per phase we get $I(t) = a \cdot I_c(t)$, and with total number of conductors per machine *z* we have to consider that we have due to the three phases U, V, W a sinusoidal current layer distribution $I(x_s)$ along the stator-fixed machine circumference co-ordinate x_s. Per element dx_s we get with bore diameter d_{si} the torque

$$dM_e(x_s,t) = \frac{I(x_s,t)}{a} \cdot \frac{z \cdot dx_s}{d_{si}\pi} \cdot B_\delta(x_s,t) \cdot l \cdot \frac{d_{si}}{2} \quad . \tag{7.4-4}$$

Total electromagnetic torque is

$$M_e(t) = \int_0^{2p\tau_p} dM_e = \int_0^{2p\tau_p} \frac{I(x_s,t)}{a} \cdot \frac{z}{d_{si}\pi} \cdot B_\delta(x_s,t) \cdot l \cdot \frac{d_{si}}{2} \cdot dx_s \tag{7.4-5}$$

or with definition of **current loading distribution** $A(x_s,t) = \frac{z \cdot I(x_s,t)/a}{d_{si}\pi}$

$$M_e(t) = \int_0^{2p\tau_p} A(x_s,t)\cdot B_\delta(x_s,t)\cdot l\cdot\frac{p\tau_p}{\pi}\cdot dx_s \ . \qquad (7.4\text{-}6)$$

As in space vector theory only sine wave fundamentals $\nu = 1$ are considered, namely

$$B_\delta(x_s) = B_\delta\cdot\cos\left(\frac{x_s\pi}{\tau_p}\right) \ , \ A(x_s) = \hat{A}\cdot\cos\left(\frac{x_s\pi}{\tau_p}-\varphi_i\right) \qquad (7.4\text{-}7)$$

with internal phase shift φ_i between resulting air gap flux density wave and current loading wave (Fig. 7.4-2), (7.4-6) yields

$$M_e = \frac{(p\tau_p)^2}{\pi}\cdot l\cdot\hat{A}\cdot B_\delta\cdot\cos\varphi_i \ . \qquad (7.4\text{-}8)$$

Air gap flux density amplitude is related to **main flux linkage** via

$$\hat{\Psi}_h = N\cdot k_{w1}\cdot\frac{2}{\pi}\tau_p l\cdot B_\delta \qquad (7.4\text{-}9)$$

and current loading wave amplitude is related to **r.m.s. current loading *A*** via

$$\hat{A} = \sqrt{2}\cdot k_{w1}\cdot A \qquad \left(A = \frac{2\cdot m\cdot N\cdot I}{2p\cdot\tau_p}\right) \ . \qquad (7.4\text{-}10)$$

So, for $m = 3$ phases torque is with $\hat{I} = \sqrt{2}\cdot I$ instead of (7.4-8) also

$$M_e = \frac{3}{2}\cdot p\cdot\hat{I}\cdot\hat{\Psi}_h\cdot\cos\varphi_i \qquad (7.4\text{-}11)$$

or in per unit values

$$m_e = \frac{M_e}{M_B} = \frac{\omega_N/p}{3\cdot U_{N,ph}\cdot I_{N,ph}}\cdot\frac{3}{\sqrt{2}\cdot\sqrt{2}}\cdot p\cdot\hat{I}\cdot\hat{\Psi}_h\cdot\cos\varphi_i = i\cdot\psi_h\cdot\cos\varphi_i$$

$$\boxed{m_e = \frac{M_e}{M_B} = i\cdot\psi_h\cdot\cos\varphi_i = i_\perp\cdot\psi_h} \ . \qquad (7.4\text{-}12)$$

In Fig. 7.4-2 the physical meaning of (7.4-12) is depicted: The main flux, excited by stator and rotor currents in induction machines, is corresponding with main flux linkage space vector $\underline{\psi}_h$. It is shifted to e.g. stator current loading fundamental wave, which is corresponding with stator current space vector $\underline{i}$, by angle φ_i. With "right-hand-rule" torque direction on stator currents is given in anti-clockwise direction, so torque on rotor acts according to *Newton´*s "actio est reactio" in clockwise direction. **We define positive torque on rotor in anti-clockwise direction** (= mathematical positive direction of rotation), so example shown in Fig. 7.4-2 yields negative torque on rotor.

If perpendicular **stator** current space vector component $\underline{i}_{s,\perp}$ is 90° **leading** to flux linkage space vector $\underline{\psi}_h$, then torque on rotor is **positive**. If $\underline{i}_{s,\perp}$ is 90° **lagging**, torque on rotor is **negative**.

With rotor space current vector component $\underline{i}'_{r,\perp}$ one gets according to (7.4-16): $\underline{i}'_{r,\perp}$ is 90° leading yields negative rotor torque, $\underline{i}'_{r,\perp}$ is 90° lagging yields positive rotor torque !

Note that only perpendicular component of stator space current vector $i_\perp = i \cdot \cos\varphi_i$ delivers torque, whereas flux-parallel component $i_= = i \cdot \cos\varphi_i$ only adds to magnetization of main flux. **Complex notation** of (7.4-12) is possible with conjugate complex space vector $\underline{i}^*$ or $\underline{\psi}^*$:

$$m_e = i_\perp \cdot \psi_h = -\operatorname{Im}\{\underline{i}^* \cdot \underline{\psi}_h\} = \operatorname{Im}\{\underline{i} \cdot \underline{\psi}_h^*\} \tag{7.4-13}$$

Proof:
By taking space vector $\underline{\psi}_h = \psi_h$ in real axis, current space vector is $\underline{i} = i_= + j \cdot i_\perp$ and its conjugate complex value $\underline{i}^* = i_= - j \cdot i_\perp$: $m_e = -\operatorname{Im}\{\underline{i}^* \cdot \underline{\psi}_h\} = -\operatorname{Im}\{(i_= - j \cdot i_\perp) \cdot \psi_h\} = i_\perp \cdot \psi_h$. In the same way we get with $\underline{\psi}_h^* = \psi_h^* = \psi_h$: $m_e = \operatorname{Im}\{\underline{i} \cdot \underline{\psi}_h^*\} = \operatorname{Im}\{(i_= + j \cdot i_\perp) \cdot \psi_h\} = i_\perp \cdot \psi_h$.

As stator / rotor **stray flux** is not linked with rotor / stator, it cannot produce any torque, therefore one can also write:

$$m_e = \operatorname{Im}\{\underline{i}_s \cdot \underline{\psi}_h^*\} = \operatorname{Im}\{\underline{i}_s \cdot \underline{\psi}_s^*\}. \tag{7.4-14}$$

Proof:
According to $\operatorname{Im}\{\underline{i}_s \cdot x_h \underline{i}_s^*\} = x_h \cdot \operatorname{Im}\{|\underline{i}_s|^2\} = 0$ we get:

$$m_e = \operatorname{Im}\{\underline{i}_s \cdot \underline{\psi}_h^*\} = \operatorname{Im}\{\underline{i}_s \cdot (x_h \underline{i}_s^* + x_h \underline{i}'^*_r)\} = \operatorname{Im}\{\underline{i}_s \cdot (x_{s\sigma} \underline{i}_s^* + x_h \underline{i}_s^* + x_h \underline{i}'^*_r)\} =$$
$$= \operatorname{Im}\{\underline{i}_s \cdot (\underline{\psi}_{s\sigma} + \underline{\psi}_h)^*\} = \operatorname{Im}\{\underline{i}_s \cdot \underline{\psi}_s^*\}$$

Torque can only be produced between STATOR current and ROTOR main flux component or ROTOR current and STATOR flux main flux component. Hence, although $m_e = \operatorname{Im}\{\underline{i}_s \cdot \underline{\psi}_s^*\}$ contains only stator values, on has to note, that stator flux linkage is constituted by stator and rotor current (= magnetizing current).

$$m_e = \operatorname{Im}\{\underline{i}_s \cdot \underline{\psi}_s^*\} = \operatorname{Im}\{\underline{i}_s \cdot (x_s \underline{i}_s^* + x_h \underline{i}'^*_r)\} = \operatorname{Im}\{\underline{i}_s \cdot x_h \underline{i}'^*_r\} \tag{7.4-15}$$

At no-load, where rotor current is zero, also torque is zero. If torque is calculated with rotor variables, then sign of torque equation has to be changed (**"actio est reactio"**):

$$m_e = \operatorname{Im}\{\underline{i}_s \cdot \underline{\psi}_s^*\} = -\operatorname{Im}\{\underline{i}'_r \cdot \underline{\psi}'^*_r\} \tag{7.4-16}$$

Proof:

$$m_e = \operatorname{Im}\{\underline{i}_s \cdot \underline{\psi}_s^*\} = \operatorname{Im}\{\underline{i}_s \cdot (x_s \underline{i}_s^* + x_h \underline{i}'^*_r)\} = \operatorname{Im}\{\underline{i}_s \cdot x_h \underline{i}'^*_r\} = -\operatorname{Im}\{\underline{i}_s \cdot x_h \underline{i}'^*_r\}^* = -\operatorname{Im}\{\underline{i}_s^* \cdot x_h \underline{i}'_r\} =$$
$$= -\operatorname{Im}\{\underline{i}'_r \cdot (x'_{r\sigma} \underline{i}'^*_r + x_h \underline{i}'^*_s)\} = -\operatorname{Im}\{\underline{i}'_r \cdot \underline{\psi}'^*_r\}$$

As stray flux does not contribute to torque, we get in the same

$$m_e = \operatorname{Im}\{\underline{i}_s \cdot \underline{\psi}_h^*\} = -\operatorname{Im}\{\underline{i}'_r \cdot \underline{\psi}'^*_h\} \tag{7.4-17}$$

Component notation $\underline{i} = i_\alpha + j \cdot i_\beta$, $\underline{\psi} = \psi_\alpha + j \cdot \psi_\beta$ yields for torque

$$m_e = \mathrm{Im}\left\{\underline{i}_s \cdot \underline{\psi}_s^*\right\} = \mathrm{Im}\left\{\left(i_{s\alpha} + j \cdot i_{s\beta}\right) \cdot \left(\psi_{s\alpha} + j \cdot \psi_{s\beta}\right)^*\right\} = \psi_{s\alpha} \cdot i_{s\beta} - i_{s\alpha} \cdot \psi_{s\beta}$$

$$m_e = -\mathrm{Im}\left\{\underline{i}'_r \cdot \underline{\psi}'^*_r\right\} = -\mathrm{Im}\left\{\left(i'_{r\alpha} + j \cdot i'_{r\beta}\right) \cdot \left(\psi'_{r\alpha} + j \cdot \psi'_{r\beta}\right)^*\right\} = -\psi'_{r\alpha} \cdot i'_{r\beta} + i'_{r\alpha} \cdot \psi'_{r\beta}$$

$$\boxed{m_e = \psi_{s\alpha} \cdot i_{s\beta} - i_{s\alpha} \cdot \psi_{s\beta} = -\psi'_{r\alpha} \cdot i'_{r\beta} + i'_{r\alpha} \cdot \psi'_{r\beta}} \qquad (7.4\text{-}18)$$

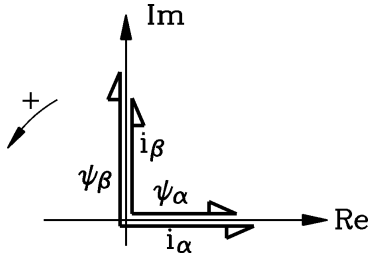

Fig. 7.4-3: Torque generation by flux linkage and current vector components

With Fig. 7.4-3 equation (7.4-18) shows again: Stator current vector β-component is perpendicular to α-component of flux linkage, thus delivering torque. As it is parallel to β-component of flux linkage, it delivers NO torque with that component. Further, stator current vector β-component is leading 90° to α-component of flux linkage, thus producing positive torque on rotor, whereas stator current vector α-component is lagging 90° to flux linkage vector β-component, thus delivering negative rotor torque.

Finally, with electromagnetic torque the mechanical equation of AC machines is

$$\boxed{\tau_J \cdot \frac{d\omega_m}{d\tau} = m_e(\tau) - m_s(\tau) = -\psi'_{r\alpha} \cdot i'_{r\beta} + i'_{r\alpha} \cdot \psi'_{r\beta} - m_s(\tau)} \quad . \qquad (7.4\text{-}19)$$

7.5 Dynamic equations of induction machines in stator reference frame

The complete set of
a) stator and rotor voltage equation – including *Faraday´*s law for voltage induction - in complex space vector notation (comprising all three phases !),
b) stator and rotor flux linkage equation (induction machine acts as transformer !),
c) mechanical equation for rotor in per unit notation – in stator reference frame - allows to calculate dynamic performance or induction machines.

$$\boxed{\begin{aligned}
&\underline{u}_s = r_s \cdot \underline{i}_s + \frac{d\underline{\psi}_s}{d\tau} \\
&0 = r'_r \cdot \underline{i}'_r + \frac{d\underline{\psi}'_r}{d\tau} - j \cdot \omega_m \cdot \underline{\psi}'_r \\
&\underline{\psi}_s = x_s \cdot \underline{i}_s + x_h \cdot \underline{i}'_r \\
&\underline{\psi}'_r = x_h \cdot \underline{i}_s + x'_r \cdot \underline{i}'_r \\
&\tau_J \cdot \frac{d\omega_m}{d\tau} = -\mathrm{Im}\left\{\underline{i}'_r \cdot \underline{\psi}'^*_r\right\} - m_s(\tau)
\end{aligned}} \qquad (7.5\text{-}1)$$

Iron losses and variable saturation, leading to variable inductance $x_h(i_m)$, are not included in this model, but this can be done easily. For many numerical programs equations have to be

written not in complex notation, but only with real values. In that case set (7.5-1) is decomposed by

$$\begin{aligned} \underline{u}_s &= u_{s\alpha} + j \cdot u_{s\beta} \\ \underline{i}_s &= i_{s\alpha} + j \cdot i_{s\beta} \qquad \underline{i}'_r = i'_{r\alpha} + j \cdot i'_{r\beta} \\ \underline{\psi}_s &= \psi_{s\alpha} + j \cdot \psi_{s\beta} \qquad \underline{\psi}'_r = \psi'_{r\alpha} + j \cdot \psi'_{r\beta} \end{aligned} \tag{7.5-2}$$

into 9 equations instead of 5, with 9 unknowns $i_{s\alpha}, i_{s\beta}, i'_{r\alpha}, i'_{r\beta}, \psi_{s\alpha}, \psi_{s\beta}, \psi'_{r\alpha}, \psi'_{r\beta}, \omega_m$.

(7.5-3):	(7.5-5):	
$u_{s\alpha} = r_s \cdot i_{s\alpha} + d\psi_{s\alpha}/d\tau$	$u_{s\alpha} = r_s \cdot i_{s\alpha} + d\psi_{s\alpha}/d\tau$	
$u_{s\beta} = r_s \cdot i_{s\beta} + d\psi_{s\beta}/d\tau$	$u_{s\beta} = r_s \cdot i_{s\beta} + d\psi_{s\beta}/d\tau$	
$0 = r'_r \cdot i'_{r\alpha} + d\psi'_{r\alpha}/d\tau + \omega_m \cdot \psi'_{r\beta}$	$0 = r'_r \cdot i'_{r\alpha} + d\psi'_{r\alpha}/d\tau + \omega_m \cdot \psi'_{r\beta}$	
$0 = r'_r \cdot i'_{r\beta} + d\psi'_{r\beta}/d\tau - \omega_m \cdot \psi'_{r\alpha}$	$0 = r'_r \cdot i'_{r\beta} + d\psi'_{r\beta}/d\tau - \omega_m \cdot \psi'_{r\alpha}$	
$\psi_{s\alpha} = x_s \cdot i_{s\alpha} + x_h \cdot i'_{r\alpha}$	$\psi_{s\alpha} = \sigma \cdot x_s \cdot i_{s\alpha} + (x_h / x'_r) \cdot \psi'_{r\alpha}$	(7.5-3/5)
$\psi_{s\beta} = x_s \cdot i_{s\beta} + x_h \cdot i'_{r\beta}$	$\psi_{s\beta} = \sigma \cdot x_s \cdot i_{s\beta} + (x_h / x'_r) \cdot \psi'_{r\beta}$	
$\psi'_{r\alpha} = x_h \cdot i_{s\alpha} + x'_r \cdot i'_{r\alpha}$	$\psi'_{r\alpha} = \sigma \cdot x'_r \cdot i'_{r\alpha} + (x_h / x_s) \cdot \psi_{s\alpha}$	
$\psi'_{r\beta} = x_h \cdot i_{s\beta} + x'_r \cdot i'_{r\beta}$	$\psi'_{r\beta} = \sigma \cdot x'_r \cdot i'_{r\beta} + (x_h / x_s) \cdot \psi_{s\beta}$	
$\tau_J \cdot \frac{d\omega_m}{d\tau} = (\psi'_{r\beta} \cdot i'_{r\alpha} - \psi'_{r\alpha} \cdot i'_{r\beta}) - m_s$	$\tau_J \cdot \frac{d\omega_m}{d\tau} = (\psi'_{r\beta} \cdot i'_{r\alpha} - \psi'_{r\alpha} \cdot i'_{r\beta}) - m_s$	

As rotor voltage equation and torque equation are non-linear due to product of two variables, this system has to be solved numerically. Like in DC machines, the stator voltage $u_{s\alpha}, u_{s\beta}$ is the leading variable, and the shaft torque of the load m_s the disturbing variable, which must be given as time functions to solve the equations. With *Blondel´*s coefficient the four flux linkage equations can be written also as

$$\begin{aligned} \psi_{s\alpha} &= \sigma \cdot x_s \cdot i_{s\alpha} + \frac{x_h}{x'_r} \cdot \psi'_{r\alpha} \qquad \psi_{s\beta} = \sigma \cdot x_s \cdot i_{s\beta} + \frac{x_h}{x'_r} \cdot \psi'_{r\beta} \\ \psi'_{r\alpha} &= \sigma \cdot x'_r \cdot i'_{r\alpha} + \frac{x_h}{x_s} \cdot \psi_{s\alpha} \qquad \psi'_{r\beta} = \sigma \cdot x'_r \cdot i'_{r\beta} + \frac{x_h}{x_s} \cdot \psi_{s\beta} \end{aligned} \quad . \tag{7.5-4}$$

Proof:

$$\psi_{s\alpha} = \sigma \cdot x_s \cdot i_{s\alpha} + \frac{x_h}{x'_r} \cdot \psi'_{r\alpha} = \sigma \cdot x_s \cdot i_{s\alpha} + \frac{x_h}{x'_r} \cdot \left(\sigma \cdot x'_r \cdot i'_{r\alpha} + \frac{x_h}{x_s} \cdot \psi_{s\alpha} \right)$$

$$\psi_{s\alpha} \cdot \left(1 - \frac{x_h^2}{x_s x'_r} \right) = \psi_{s\alpha} \cdot \sigma = \sigma \cdot x_s \cdot i_{s\alpha} + \sigma \cdot x_h \cdot i'_{r\alpha} \quad \Rightarrow \quad \psi_{s\alpha} = x_s \cdot i_{s\alpha} + x_h \cdot i'_{r\alpha}$$

This leads to slightly changed set of dynamic equations (7.5-5), which are given as flow chart for direct input in e.g. simulation program MATLAB/Simulink (Fig. 7.5-1). These equations can of course also be written in **physical units** (7.5-6) (Fig. 7.5-2).

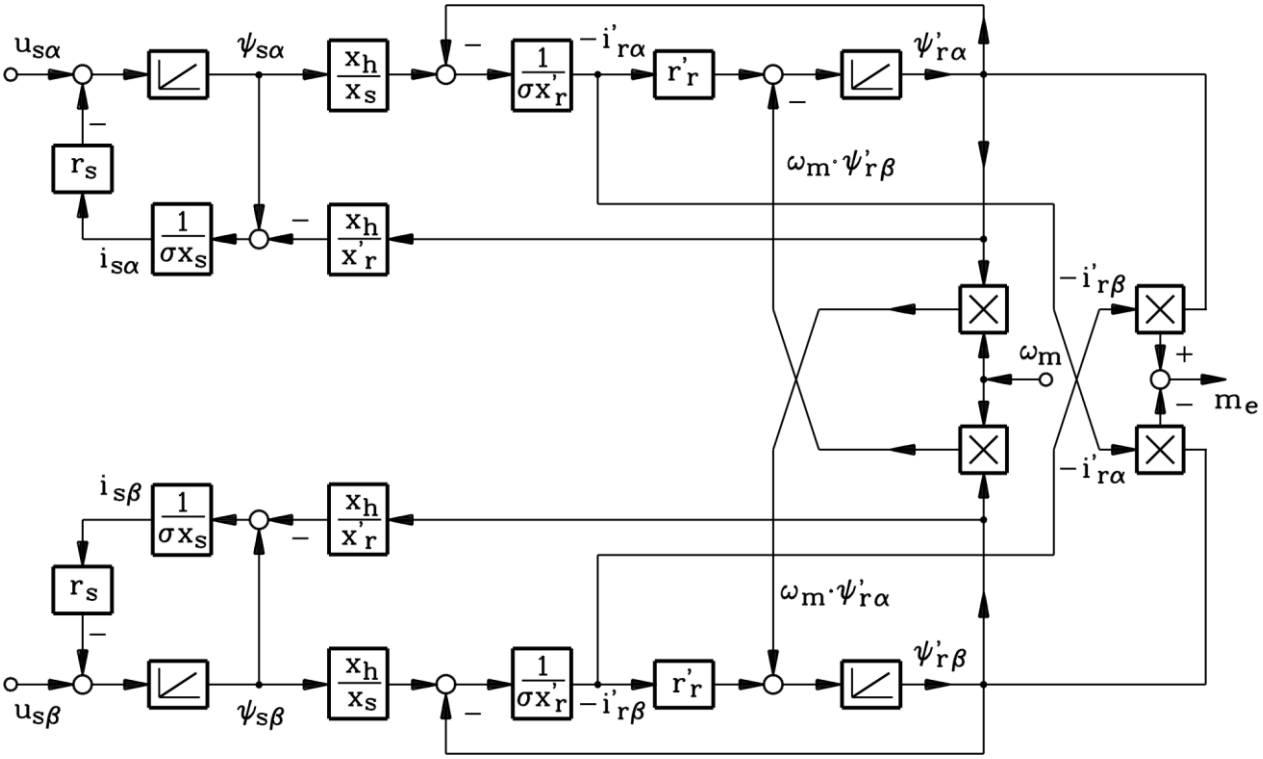

Fig. 7.5-1: Flow chart of per unit dynamic set of 8 equations (voltage and flux linkage equations) for induction machine in stator reference frame. Mechanical equation has to be added. Input is stator voltage and rotor speed, output is induction machine torque, flux linkages and currents.

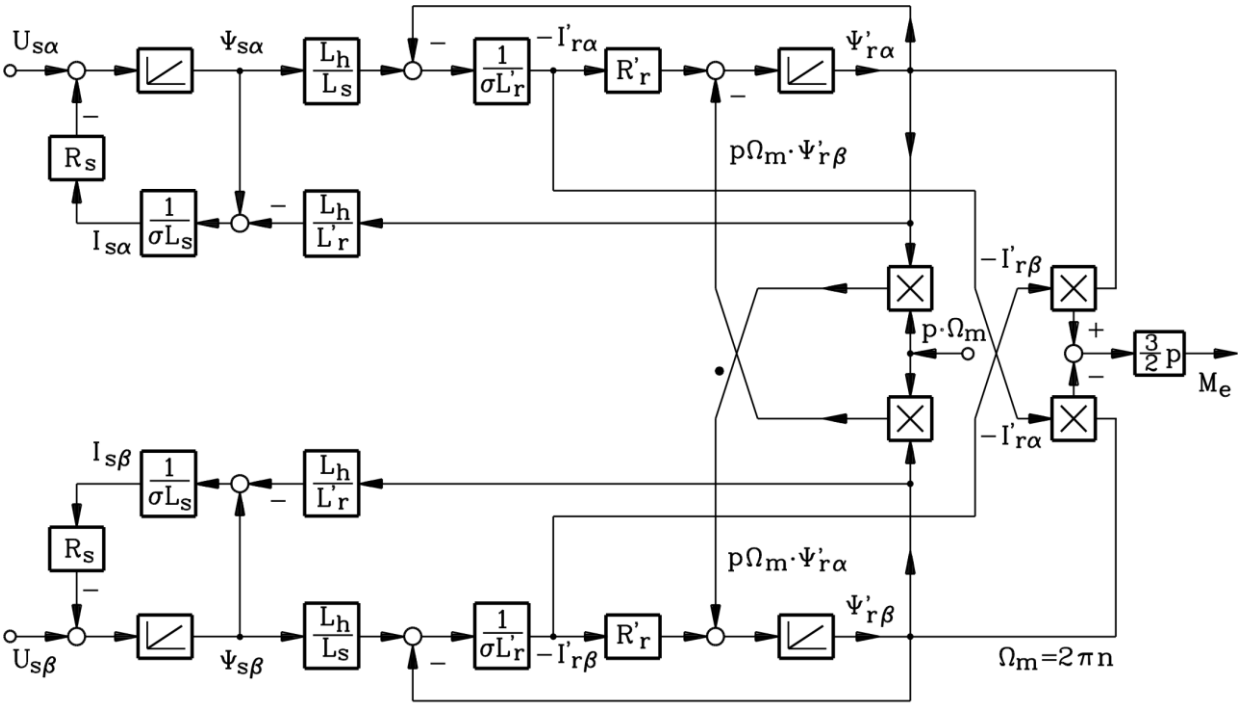

Fig. 7.5-2: Flow chart of dynamic set of 8 equations (voltage and flux linkage equations) for induction machine in stator reference frame **in physical units.** Mechanical equation has to be added.

$$
\begin{aligned}
&U_{s\alpha}(t) = R_s \cdot I_{s\alpha}(t) + d\Psi_{s\alpha}/dt \\
&U_{s\beta}(t) = R_s \cdot I_{s\beta}(t) + d\Psi_{s\beta}/dt \\
&0 = R'_r \cdot I'_{r\alpha}(t) + d\Psi'_{r\alpha}/dt + p \cdot \Omega_m(t) \cdot \Psi'_{r\beta}(t) \\
&0 = R'_r \cdot I'_{r\beta}(t) + d\Psi'_{r\beta}/dt - p \cdot \Omega_m(t) \cdot \Psi'_{r\alpha}(t) \\
&\Psi_{s\alpha}(t) = \sigma \cdot L_s \cdot I_{s\alpha}(t) + (L_h / L'_r) \cdot \Psi'_{r\alpha}(t) \\
&\Psi_{s\beta}(t) = \sigma \cdot L_s \cdot I_{s\beta}(t) + (L_h / L'_r) \cdot \Psi'_{r\beta}(t) \\
&\Psi'_{r\alpha}(t) = \sigma \cdot L'_r \cdot I'_{r\alpha}(t) + (L_h / L_s) \cdot \Psi_{s\alpha}(t) \\
&\Psi'_{r\beta}(t) = \sigma \cdot L'_r \cdot I'_{r\beta}(t) + (L_h / L_s) \cdot \Psi_{s\beta}(t) \\
&J \cdot \frac{d\Omega_m}{dt} = \frac{3}{2} \cdot p \cdot (\Psi'_{r\beta}(t) \cdot I'_{r\alpha}(t) - \Psi'_{r\alpha}(t) \cdot I'_{r\beta}(t)) - M_s(t)
\end{aligned}
\qquad (7.5\text{-}6)
$$

7.6 Solutions of dynamic equations for constant speed

Like with DC machines, the **mechanical time constant** for changing speed is determined by τ_J, whereas for electrical current change the much shorter **electrical time constants** of stator and rotor have to be considered. So for calculating sudden change of voltage and current one may assume **almost constant speed**. In that case the mechanical equation is NOT considered, only voltage and flux linkage equations (4 complex or 8 real equations) remain to be solved, which are linear, so *Laplace*-transformation may be used.

Example 7.6-1:
Switching voltage to an already running motor: This is the case e.g. with **Y-D-start-up**. A motor with stator winding D-connected, is line-started with star connected stator winding, thus reducing starting current and torque to 1/3. After start-up (motor is running with nearly synchronous speed) stator winding is disconnected from grid, switched into D-connection and again switched to the grid, now motor being ready for loading. This second switching in D to the grid with already running motor is treated in this example.

Motor data: $r_s = 0.03,\ r'_r = 0.04,\ x_s = 3,\ x'_r = 3,\ \sigma = 0.0667$

Grid voltage:
Three-phase symmetric voltage system in per unit: $u_s = 1$, grid frequency $\omega_s = 1$:

$u_U(\tau) = u \cdot \cos(\tau),\ u_V(\tau) = u \cdot \cos(\tau - 2\pi/3),\ u_W(\tau) = u \cdot \cos(\tau - 4\pi/3)$

Voltage space vector is rotating with constant amplitude and grid frequency:

$$\underline{u}_s(\tau) = \frac{2}{3} \cdot \left(u_U(\tau) + \underline{a} \cdot u_V(\tau) + \underline{a}^2 \cdot u_W(\tau)\right) = u \cdot e^{j\tau}$$

Laplace transformation yields: $\breve{\underline{u}}_s = \dfrac{u}{s - j}$

Voltage and flux linkage equation in *Laplace*-transformation:

$$
\begin{aligned}
&r_s \cdot \breve{\underline{i}}_s + s \cdot \breve{\underline{\psi}}_s = \breve{\underline{u}}_s + \underline{\psi}_{s0} \\
&r'_r \cdot \breve{\underline{i}}'_r + (s - j \cdot \omega_m) \cdot \breve{\underline{\psi}}'_r = \underline{\psi}'_{r0} \\
&\breve{\underline{\psi}}_s = x_s \cdot \breve{\underline{i}}_s + x_h \cdot \breve{\underline{i}}'_r \\
&\breve{\underline{\psi}}'_r = x_h \cdot \breve{\underline{i}}_s + x'_r \cdot \breve{\underline{i}}'_r
\end{aligned}
\qquad (7.6\text{-}1)
$$

Initial conditions:
At $\tau = 0$ no current flow in winding, so flux linkage is zero: $\underline{\psi}_{s0} = 0, \underline{\psi}'_{r0} = 0$, and (7.6-1) yields by substituting flux linkage two linear equations with stator and rotor current space vector as unknowns. With *Cramer´*s rule these equations are solved:

$$\left(r_s + s \cdot x_s\right) \cdot \breve{\underline{i}}_s + s \cdot x_h \cdot \breve{\underline{i}}'_r = \breve{\underline{u}}_s$$
$$\left(s - j \cdot \omega_m\right) \cdot x_h \cdot \breve{\underline{i}}_s + \left(r'_r + \left(s - j \cdot \omega_m\right) \cdot x'_r\right) \cdot \breve{\underline{i}}'_r = 0$$

$$\breve{\underline{i}}_s = \frac{u}{s - j} \cdot \frac{r'_r + (s - j\omega_m) \cdot x'_r}{(r_s + s \cdot x_s) \cdot (r'_r + (s - j\omega_m) \cdot x'_r) - s \cdot x_h^2 \cdot (s - j\omega_m)} =$$

$$= \frac{u}{s - j} \cdot \frac{r'_r + (s - j\omega_m) \cdot x'_r}{\sigma \cdot x_s \cdot x'_r \cdot \left(s^2 + s \cdot \left(\frac{r_s x'_r + x_s r'_r}{\sigma \cdot x_s \cdot x'_r} - j\omega_m \right) + \frac{r_s \cdot (r'_r - j\omega_m \cdot x'_r)}{\sigma \cdot x_s \cdot x'_r} \right)} = \qquad (7.6\text{-}2)$$

$$= \frac{u}{s - j} \cdot \frac{r'_r + (s - j\omega_m) \cdot x'_r}{\sigma \cdot x_s \cdot x'_r \cdot \left(s - \underline{s}_a\right) \cdot \left(s - \underline{s}_b\right)}$$

For inverse *Laplace* transformation
a) the denominator roots $\underline{s}_a, \underline{s}_b$ have to be determined in dependence of speed with

$$s^2 + s \cdot \left(\frac{r_s x'_r + x_s r'_r}{\sigma x_s x'_r} - j\omega_m \right) + \frac{r_s (r'_r - j\omega_m x'_r)}{\sigma x_s x'_r} = s^2 + s \cdot \left(\alpha_s + \alpha_r - j\omega_m\right) + \alpha_s \cdot \left(\sigma \cdot \alpha_r - j\omega_m\right) = 0$$

We define the **stator and rotor short-circuit time constant,** as $\sigma \cdot x_s$ is the inductance of equivalent circuit at short-circuit (Slip =1):

$$\boxed{\tau_{s\sigma} = \frac{1}{\alpha_s} = \frac{\sigma \cdot x_s}{r_s} \qquad \tau_{r\sigma} = \frac{1}{\alpha_r} = \frac{\sigma \cdot x'_r}{r'_r}} \qquad (7.6\text{-}3a)$$

In the same way we define the **stator and rotor open-circuit time constant,**

$$\boxed{\tau_s = \frac{x_s}{r_s} \qquad \tau_r = \frac{x'_r}{r'_r}} \qquad (7.6\text{-}3b)$$

as x_s is the inductance of equivalent circuit at open secondary (Slip = 0).

b) the solution (7.6-2) has to be separated into

$$\breve{\underline{i}}_s = \frac{\underline{A}}{s - j} + \frac{\underline{B}}{s - \underline{s}_a} + \frac{\underline{C}}{s - \underline{s}_b} \quad . \qquad (7.6\text{-}4)$$

Second task is easily achieved with *Heaviside´*s rule:

$$\boxed{L^{-1}\left\{ \frac{Z(s)}{(s - s_1) \cdot (s - s_2) \cdot \ldots \cdot (s - s_n)} \right\} = \sum_{i=1}^{n} \frac{Z(s_i)}{\prod_{k=1\ldots n \,\wedge\, k \neq i} (s_i - s_k)} \cdot e^{s_i \cdot t}} \qquad (7.6\text{-}5)$$

So we get:

$$i = 1 : \underline{s}_1 = j : \underline{A} = \frac{u \cdot (r'_r + (j - j\omega_m) \cdot x'_r)}{\sigma \cdot x_s \cdot x'_r \cdot \left(j - \underline{s}_a\right) \cdot \left(j - \underline{s}_b\right)}$$

$$i=2:\underline{s}_2=\underline{s}_a:\underline{B}=\frac{u\cdot(r_r'+(\underline{s}_a-j\omega_m)\cdot x_r')}{\sigma\cdot x_s\cdot x_r'\cdot(\underline{s}_a-j)\cdot(\underline{s}_a-\underline{s}_b)}$$

$$i=3:\underline{s}_3=\underline{s}_b:\underline{C}=\frac{u\cdot(r_r'+(\underline{s}_b-j\omega_m)\cdot x_r')}{\sigma\cdot x_s\cdot x_r'\cdot(\underline{s}_b-j)\cdot(\underline{s}_b-\underline{s}_a)}$$

Inverse *Laplace* transformation of (7.6-4) yields:

$\underline{i}_s(\tau)=\underline{A}\cdot e^{j\cdot\tau}+\underline{B}\cdot e^{\underline{s}_a\cdot\tau}+\underline{C}\cdot e^{\underline{s}_b\cdot\tau}$, with the

homogeneous part of solution: $\underline{i}_{s,h}(\tau)=\underline{B}\cdot e^{\underline{s}_a\cdot\tau}+\underline{C}\cdot e^{\underline{s}_b\cdot\tau}$ and the

particular solution: $\underline{i}_{s,p}(\tau)=\underline{A}\cdot e^{j\cdot\tau}$.

Whereas the homogeneous part of solution is decaying with time constants

$$\tau_a=-\frac{1}{\mathrm{Re}(\underline{s}_a)},\ \tau_b=-\frac{1}{\mathrm{Re}(\underline{s}_b)} \quad , \tag{7.6-6}$$

which depend on $\tau_{s\sigma}, \tau_{r\sigma}$, thus representing the transient response of current, the particular solution does not vanish. It represents the steady-state solution, thus the current vector in **steady-state operation.**

Discussion of steady state solution:

$$\underline{i}_{s,p}(\tau)=\frac{u\cdot(r_r'+(j-j\omega_m)\cdot x_r')}{\sigma\cdot x_s\cdot x_r'\cdot(j-\underline{s}_a)\cdot(j-\underline{s}_b)}\cdot e^{j\cdot\tau}$$

With

$$\boxed{1-\omega_m=1-\frac{\Omega_m}{\Omega_{syn}}=Slip} \tag{7.6-7}$$

and

$$\sigma x_s x_r'\cdot(j-\underline{s}_a)\cdot(j-\underline{s}_b)=\sigma x_s x_r'\cdot(j^2+j\cdot(\alpha_s+\alpha_r-j\omega_m)+\alpha_s\cdot(\sigma\cdot\alpha_r-j\omega_m))=$$
$$=r_s r_r'-Slip\cdot\sigma\cdot x_s x_r'+j\cdot(Slip\cdot r_s x_r'+x_s r_r')$$

steady state (particular) solution is

$$\underline{i}_{s,p}(\tau)=\frac{u\cdot(r_r'+j\cdot Slip\cdot x_r')}{r_s r_r'-Slip\cdot\sigma\cdot x_s x_r'+j\cdot(Slip\cdot r_s x_r'+x_s r_r')}\cdot e^{j\cdot\tau} \quad . \tag{7.6-8}$$

This is exactly the steady state solution of stator current of equivalent circuit of induction machine, when being fed by sinusoidal voltage:

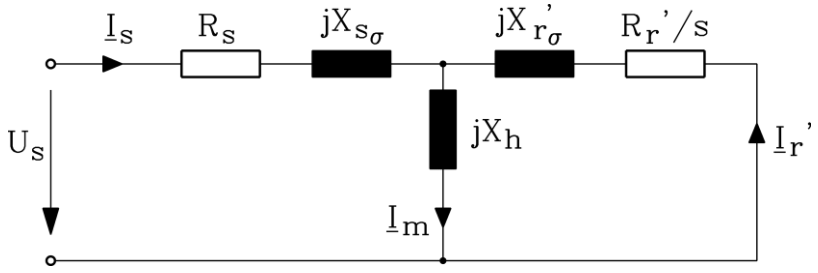

Fig. 7.6-1: Equivalent circuit per phase of induction machine (*s*: Slip) without considering iron and friction losses

$$\boxed{\hat{\underline{I}}_s = \hat{\underline{U}}_s \frac{R'_r + j \cdot Slip \cdot X'_r}{(R_s R'_r - Slip \cdot \sigma \cdot X_s X'_r) + j(Slip \cdot R_s X'_r + X_s R'_r)}} \qquad (7.6\text{-}9)$$

Facit:

Switching on of induction machine to sinusoidal line voltage: After the decay of the transient current the steady state solution of the space vector calculation yields the machine performance, which is described by the steady state equivalent circuit. The stator current space vector rotates around the origin on circle orbit with constant amplitude, given by (7.6-9), with the rotation frequency equal to the grid frequency.

Discussion of transient solution:

For simplification damping is neglected: $r_s = 0, r'_r = 0$: Determination of roots $\underline{s}_a, \underline{s}_b$:

$$s^2 + s \cdot (-j\omega_m) = 0 \quad \rightarrow \quad \underline{s}_a = j\omega_m, s_b = 0$$

$$\underline{i}_s = \frac{u}{s - j} \cdot \frac{r'_r + (s - j\omega_m) \cdot x'_r}{\sigma \cdot x_s \cdot x'_r \cdot (s - \underline{s}_a) \cdot (s - \underline{s}_b)} = \frac{u}{s - j} \cdot \frac{(s - j\omega_m) \cdot x'_r}{\sigma \cdot x_s \cdot x'_r \cdot (s - j\omega_m) \cdot (s - 0)} =$$

$$= \frac{u}{\sigma \cdot x_s \cdot s(s - j)} = \frac{j \cdot u}{\sigma \cdot x_s} \cdot \left(\frac{1}{s} - \frac{1}{s - j} \right)$$

corresponding with $\underline{A} = -\underline{C} = \frac{u}{j \cdot \sigma \cdot x_s}$, $\underline{B} = 0$, yielding with inverse transformation

$$\underline{\underline{i_s(\tau) = \frac{j \cdot u}{\sigma \cdot x_s} \cdot \left(1 - e^{j \cdot \tau}\right)}} \qquad (7.6\text{-}10)$$

Facit:

In transient mode flux changes quickly, inducing the rotor winding. Due to rotor current flow with phase opposite to stator current flow main flux is cancelled, only stray flux remains. So totally effective inductance is total stray inductance $\sigma \cdot x_s$. Stator and rotor current are rather big, as they are only limited by stray inductance. Stator current space vector rotates on circle orbit with constant big amplitude given by short circuit condition. Centre of circle is shifted from origin by current amplitude.

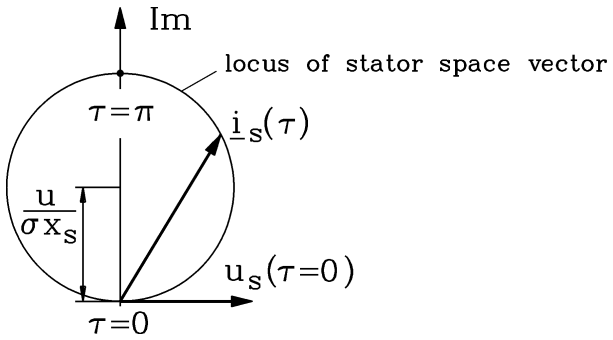

Fig. 7.6-2: Stator current space vector, when running motor is switched to sinusoidal voltage system during Y-D-start-up

Time function of U phase current is (Fig. 7.6-3b)

$$i_U(\tau) = \mathrm{Re}\{\underline{i}_s(\tau)\} = \mathrm{Re}\left\{ \frac{j \cdot u}{\sigma \cdot x_s} \cdot \left(1 - e^{j \cdot \tau}\right) \right\} = \frac{u}{\sigma \cdot x_s} \cdot \mathrm{Re}\{ \cdot (j - j \cdot (\cos\tau + j \sin\tau)) \} = \underline{\underline{\frac{u}{\sigma \cdot x_s} \cdot \sin\tau}}$$

Phase voltage at switching on $\tau = 0$ in phase U is maximum: $u_U(\tau) = u \cdot \cos(\tau) \Rightarrow u_U(0) = u$

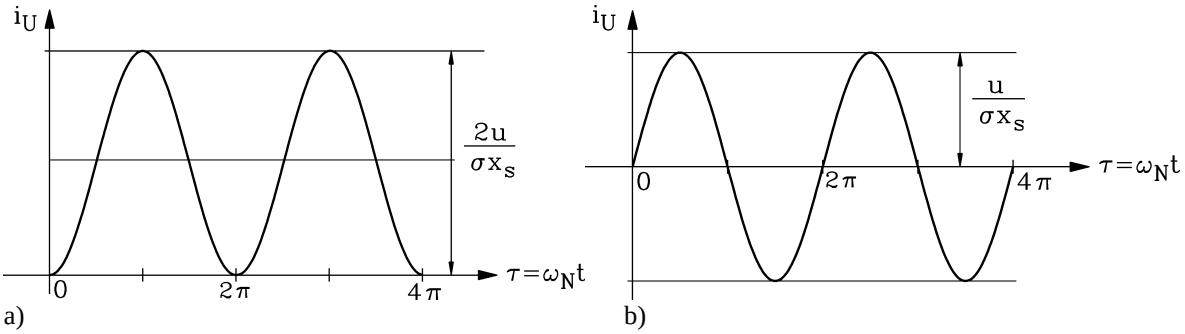

Fig. 7.6-3: Phase current in phase U after switching sinus voltage to running machine, damping neglected: a) Switching on at zero crossing of U phase voltage, b) Switching on at maximum U phase voltage

If switching on is a quarter of grid period later (= shifting of time by $\tau - \pi/2$), voltage and current space vectors are

$$\underline{u}_s(\tau) = u \cdot e^{j(\tau-\pi/2)} = -j \cdot u \cdot e^{j\tau} \qquad \underline{\underline{i_s(\tau) = \frac{u}{\sigma \cdot x_s} \cdot \left(1 - e^{j\cdot\tau}\right)}} \quad , \qquad (7.6\text{-}11)$$

resulting in zero U phase voltage at $\tau = 0$

$$u_U(\tau) = u \cdot \cos(\tau - \pi/2) = u \cdot \sin\tau \quad \rightarrow \quad u_U(\tau = 0) = 0$$

and U phase current (Fig. 7.6-3a)

$$i_U(\tau) = \mathrm{Re}\{\underline{i}_s(\tau)\} = \mathrm{Re}\left\{\frac{u}{\sigma \cdot x_s} \cdot \left(1 - e^{j\cdot\tau}\right)\right\} = \frac{u}{\sigma \cdot x_s} \cdot \mathrm{Re}\{1 - \cos\tau - j\sin\tau\} = \underline{\underline{\frac{u}{\sigma \cdot x_s} \cdot (1 - \cos\tau)}}.$$

Facit:

Switching on of a winding at phase voltage zero yields maximum transient current, which – with neglected damping – is twice pulsating amplitude (200%), occurring at $\tau = \pi$. Offset is a DC component, which is equal to AC amplitude (worst case current peak). Switching on at maximum phase voltage does not yield any DC current component, only an AC component, so the current peak is 100%, occurring at $\tau = \pi/2$.

Switching on at zero voltage	***Switching on at maximum voltage***
Current: DC component = AC component	Current: no DC component
Peak current 200%	Peak current 100%
Peak occurs at half period after switching on	Peak occurs at quarter period after switching on
$i_{s,peak} = 2u_s/(\sigma \cdot x_s) = 2 \cdot 1/(0.0667 \cdot 3) = 10$	$i_{s,peak} = u_s/(\sigma \cdot x_s) = 1/(0.0667 \cdot 3) = 5$
worst case	best case

Table 7.6-1: Transient current peak at switching on of inductive circuit

Note:

- Results of Table 7.6-1 **are valid for any pure inductive circuit**, e.g. hence also valid for switching on of transformer winding, synchronous machine winding etc.
- Transient current amplitude is the same as "short-circuit current" (Slip = 1) of equivalent circuit Fig. 7.6-1 with neglected resistance $R_s = 0$, $R'_r = 0$, which is seen by (7.6-9):

$$\hat{\underline{I}}_s(Slip = 1) = \hat{\underline{U}}_s \frac{j \cdot X'_r}{-\sigma \cdot X_s X'_r} = \frac{\hat{\underline{U}}_s}{j \cdot \sigma \cdot X_s} \quad \rightarrow \quad \left|\hat{\underline{I}}_s(Slip = 1)\right| = \frac{\hat{U}_s}{\sigma \cdot X_s}$$

- Worst case current peak reaches 10-times rated current peak, e.g. with I_N = 100 A we get $i_{peak,s} = 10 \cdot \sqrt{2} \cdot 100 = \underline{\underline{1414A}}$

Discussion of complete solution:

Motor rotates at synchronous speed $\omega_m = 1$. Denominator roots $\underline{s}_a, \underline{s}_b$ are determined by

$$s^2 + s \cdot (\alpha_s + \alpha_r - j\omega_m) + \alpha_s \cdot (\sigma \cdot \alpha_r - j\omega_m) = s^2 + \underline{p} \cdot s + \underline{q} = 0$$

$$\tau_{s\sigma} = 1/\alpha_s = \sigma \cdot x_s / r_s = 0.0667 \cdot 3 / 0.03 = 6.67,\ \tau_{r\sigma} = 1/\alpha_r = \sigma \cdot x'_r / r'_r = 0.0667 \cdot 3 / 0.04 = 5.0$$

$$\underline{p} = 0.35 - j,\ \underline{q} = 0.002 - j0.15$$

$$\underline{s}_{a,b} = -\frac{\underline{p}}{2} \pm \sqrt{\frac{\underline{p}^2}{4} - \underline{q}} = -0.175 + j0.5 \pm \sqrt{-0.22137 - j \cdot 0.25} = -0.175 + j0.5 \pm (-0.0265 + j0.471)$$

$$\underline{s}_a = -0.2015 + j0.971 = -\frac{1}{4.96} + j0.971, \quad \underline{s}_b = -0.1485 + j0.0288 = -\frac{1}{6.73} + j0.0288$$

Transient current space vector decays with **two time constants** due to coupled stator and rotor circuit, **which are more or less stator and rotor short-circuit time constants**.

$$\underline{i}_{s,h}(\tau) = \underline{B} \cdot e^{-\frac{\tau}{4.96}} \cdot e^{j \cdot 0.97 \cdot \tau} + \underline{C} \cdot e^{-\frac{\tau}{6.73}} \cdot e^{j \cdot 0.029 \cdot \tau} \tag{7.6-12}$$

$$\tau_a = -\frac{1}{\mathrm{Re}(\underline{s}_a)} = 4.96 \approx \tau_{r\sigma} = 5.0,\ \tau_b = -\frac{1}{\mathrm{Re}(\underline{s}_b)} = 6.73 \approx \tau_{s\sigma} = 6.67 \tag{7.6-13}$$

Amplitude *B* corresponds to rotor DC current component, decaying with roughly rotor short circuit time constant, delivering due to rotor rotation an eigen-frequency of transient current oscillation of $\omega_{d,a} = 0.971$, which is nearly synchronous speed. Amplitude *C* corresponds to stator DC current component, decaying with roughly stator short circuit time constant, decaying with a very small frequency $\omega_{d,b} = 0.029$.

For **worst case switching** in phase U (at zero voltage) $\underline{u}_s(\tau) = -j \cdot u \cdot e^{j\tau}$ and $\underline{u}_s(0) = -j \cdot u$ complete solution of current space vector is calculated for 5 periods of grid voltage $0 \le \tau \le 10\pi$ with motor running

(i) with synchronous speed $\omega_m = 1, \quad Slip = 0$ (Fig. 7.6-4),

(ii) with rated speed $\omega_m = 0.96, \quad Slip = 0.04$ (Fig. 7.6-5).

In case (ii) time constants remain nearly unchanged, only dominant eigen-frequency $\omega_{d,b} = 0.03$ increases a little bit. Main difference between (i) and (ii) is steady state solution: At (i) steady state current space vector amplitude is **no-load current** $\underline{i}_s(\tau \to \infty) = \underline{A}(Slip = 0) \cdot e^{j\tau} = \underline{i}_{s0} \cdot e^{j\tau}$ with $|\underline{i}_{s0}| = u / \sqrt{r_s^2 + x_s^2} = 1/\sqrt{0.03^2 + 3^2} = 0.33$, whereas in case (ii) steady state current amplitude is rated current: $|\underline{i}_{sN}| = |\underline{A}(rated\ slip)| = 1$.

(i)	(ii)
$\omega_m = 1, \quad Slip = 0$	$\omega_m = 0.96, \quad Slip = 0.04$
$\underline{s}_a = -0.202 + j0.971, \underline{s}_b = -0.149 + j0.029$	$\underline{s}_a = -0.202 + j0.93, \underline{s}_b = -0.149 + j0.03$
Steady state current = no-load current = 0.33	steady state current = rated current = 1
Fig. 7.6-4	Fig. 7.6-5

Table 7.6-2: Solution for "inrush" current of induction machine, being switched to grid when already running (i) at synchronous speed, (ii) at rated speed

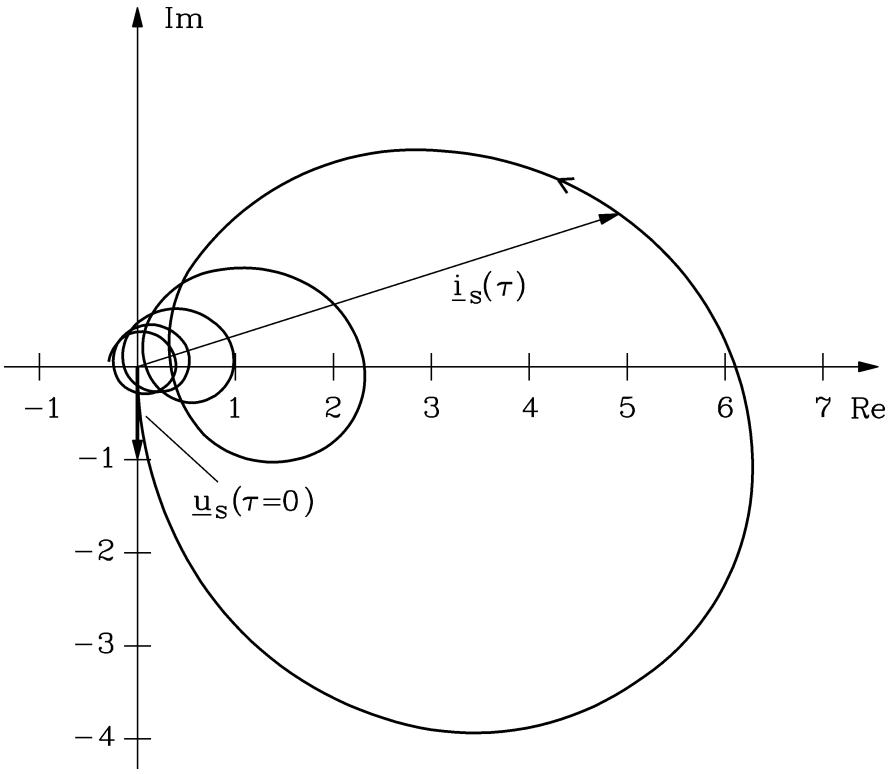

Fig. 7.6-4: Solution for "inrush" current space vector of induction machine, being switched to sinusoidal grid when already running **at synchronous** speed. Worst-case for phase U, where switching occurs at zero voltage, yielding maximum current peak

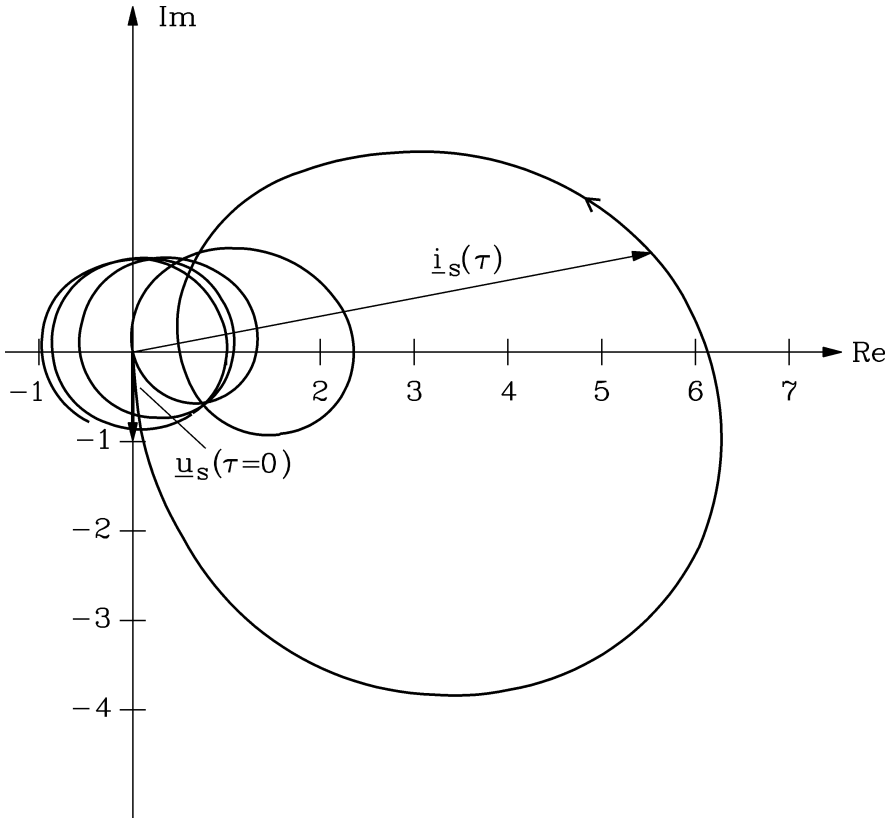

Fig. 7.6-5: Solution for "inrush" current space vector of induction machine, being switched to sinusoidal grid when already running **at rated** speed. Worst-case for phase U, where switching occurs at zero voltage, yielding maximum current peak

Facit:
- Projection of current space vector on Re-Axis yields phase current U, projection on axis 120° yields phase current V and on 240°-axis yields phase current W. Due to position of voltage space vector at $\tau = 0$ in negative Im-axis projection on Re-axis yields voltage zero in phase U, thus maximum transient current in that phase.
- If voltage space vector at $\tau = 0$ has different position, maximum of transient current peak will occur in one of the other phases, but cannot be avoided.
- Influence of damping resistance decreases current peak slightly due to decay of DC link component with rotor short-circuit electric time constant. Projection $\underline{i}_U(\tau) = \mathrm{Re}\{\underline{i}_s(\tau)\}$ in Figs. 7.6-4, 7.6-5 delivers for worst-case current peak in phase U $i_{sU,peak} = 6.3$, which is significantly smaller than for non-damped case.

no damping $r_s = 0, r_r' = 0$	with damping $r_s = 0.03, r_r' = 0.04$
Current peak $i_{sU,peak} = 2u_s/(\sigma \cdot x_s) = 10$	current peak $i_{sU,peak} = 6.3$

An estimation of damping of the stator DC current component $\left|\underline{C} \cdot e^{-\frac{\pi}{4.96}} \cdot e^{j \cdot 0.029 \cdot \pi}\right| = C \cdot 0.53$

yields a 53% reduction of shift of the circle centre in Fig. 7.6-2.

Facit:
Induction machines react to sudden change in voltage with more or less stator and rotor short-circuit time constant. Voltage switching (switching on, but also sudden short-circuit) leads to DC current component, which is largest when switching occurs at zero voltage. The roots $\underline{s}_a, \underline{s}_b$ are the two poles of transfer function of electric circuit in complex s-plane, containing stator and rotor time constant and related eigen-frequency.
Compare: In DC machine only one electric time constant due to armature circuit was given.

Electric transfer function (= stator current vector response to stator voltage vector) for initial condition $\underline{i}_{s0} = 0$:

$$\underline{i}_s(s) = \underline{u}_s(s) \cdot \frac{r_r' + (s - j\omega_m) \cdot x_r'}{\sigma \cdot x_s \cdot x_r' \cdot (s - \underline{s}_a) \cdot (s - \underline{s}_b)} \tag{7.6-14}$$

Stator and rotor current change with **two time constants**

$$\tau_a = -\frac{1}{\mathrm{Re}(\underline{s}_a)}, \tau_b = -\frac{1}{\mathrm{Re}(\underline{s}_b)} \quad , \tag{7.6-15}$$

having **two natural oscillation frequencies**

$$\omega_{d,a} = \mathrm{Im}(\underline{s}_a), \omega_{d,b} = \mathrm{Im}(\underline{s}_b) \quad . \tag{7.6-16}$$

Time constants and oscillation frequencies **depend** not only on resistances and inductances, but also **on rotor speed**, which is quite different to DC machines.

(i) Zero speed operation (stand still): $\omega_m = 0$

Roots $\underline{s}_a, \underline{s}_b$ of denominator of induction machine transfer function:

$$s^2 + s\cdot(\alpha_s + \alpha_r - j\omega_m) + \alpha_s\cdot(\sigma\cdot\alpha_r - j\omega_m) = s^2 + s\cdot(\alpha_s + \alpha_r) + \sigma\cdot\alpha_s\alpha_r = 0$$

$$s_{a,b} = -\frac{\alpha_s + \alpha_r}{2}\cdot\left(1 \pm \sqrt{1 - \frac{4\sigma\alpha_s\alpha_r}{(\alpha_s + \alpha_r)^2}}\right) \approx -\frac{\alpha_s + \alpha_r}{2}\cdot\left(1 \pm \left(1 - \frac{2\sigma\alpha_s\alpha_r}{(\alpha_s + \alpha_r)^2}\right)\right)$$

As $\sigma \sim 0.1$ is small, on can take $\sqrt{1-x} \approx 1 - x/2,\ x << 1$!

$$s_a = -(\alpha_s + \alpha_r) + \frac{\sigma\alpha_s\alpha_r}{\alpha_s + \alpha_r} \approx -(\alpha_s + \alpha_r)$$

$$s_b \approx -\frac{\sigma\alpha_s\alpha_r}{\alpha_s + \alpha_r}$$

So we get a **short and a long electric time constant at speed zero,** the short one being determined by short-circuit time constants, the long one by open-circuit time constants:

short time constant: $$\boxed{\tau_1 = -\frac{1}{s_a} \approx \frac{1}{1/\tau_{s\sigma} + 1/\tau_{r\sigma}} = \frac{1}{\frac{r_s}{\sigma\cdot x_s} + \frac{r_r'}{\sigma\cdot x_r'}}} \quad (7.6\text{-}17)$$

long time constant: $$\boxed{\tau_2 = -\frac{1}{s_b} \approx \tau_s + \tau_r = \frac{x_s}{r_s} + \frac{x_r'}{r_r'}} \quad (7.6\text{-}18)$$

(ii) Synchronous speed operation: $\omega_m = 1$

$$s^2 + s\cdot(\alpha_s + \alpha_r - j) + \alpha_s\cdot(\sigma\cdot\alpha_r - j) = 0$$

As σ, α_s, $\alpha_r \sim 0.1$ are smaller than $\omega_m = 1$, on can take

$$\underline{s}_{a,b} = -\frac{\alpha_s + \alpha_r - j\omega_m}{2}\cdot\left(1 \pm \sqrt{1 - \frac{4\alpha_s\cdot(\sigma\alpha_r - j\omega_m)}{(\alpha_s + \alpha_r - j\omega_m)^2}}\right) \approx -\frac{\alpha_s + \alpha_r - j\omega_m}{2}\cdot\left(1 \pm \sqrt{\left(1 - \frac{j4\alpha_s}{\omega_m}\right)}\right)$$

As $\alpha_s \sim 0.1$ is small, one can take $\sqrt{1-x} \approx 1 - x/2,\ x << 1$!

$$\underline{s}_{a,b} \approx -\frac{\alpha_s + \alpha_r - j\omega_m}{2}\cdot\left(1 \pm (1 - \frac{j2\alpha_s}{\omega_m})\right)$$

$$\underline{s}_a = -\alpha_r + j\left(\omega_m + \frac{\alpha_s(\alpha_s + \alpha_r)}{\omega_m}\right) \approx -\alpha_r + j\omega_m \quad (7.6\text{-}19)$$

$$\underline{s}_b = -\alpha_s - j\frac{(\alpha_s + \alpha_r)\alpha_s}{\omega_m} \approx -\alpha_s \quad (7.6\text{-}20)$$

So we get as **electric time constants more or less the** short-circuit time constants!

$$\boxed{\tau_1 \approx \frac{1}{\alpha_r} = \tau_{r\sigma},\ \tau_2 \approx \frac{1}{\alpha_s} = \tau_{s\sigma}} \quad \boxed{\omega_{d,1} \approx \omega_m,\ \omega_{d,2} \approx 0} \quad (7.6\text{-}21)$$

Example 7.6-2:

Sudden short circuit of induction motor after no-load operation

An induction motor is operating at no load, rated voltage, at the grid and is short-circuited in all three phases between grid fuses and motor terminals. Grid fuses blow, disconnecting short-circuited machine from grid. Magnetic energy of main flux is dissipated in stator and rotor

ohmic losses by the big short circuit current flow. The decay of short-circuit current happens due to $\omega_m = 1$ with electric short-circuit time constant (7.6-19) rather quickly, so speed does not change significantly, and assumption of constant speed is justified.

Motor data	4 pole motor, 50 Hz operation	
Rated power	110.8 kW	
Rated voltage	380 V Y	$u_s = 1$
Rated current	212 A	$i_s = 1$
Rated speed	1470/min	
Rated torque	720 Nm	$M_B = 888.3$ Nm
J	2.8 kgm^2	$\tau_J = 155.5$
R_s	25 mΩ	0.024 p.u.
R'_r	20 mΩ	0.019 p.u.
L_s	9.71 mH	2.95 p.u.
L'_r	9.55 mH	2.90 p.u.
L_h	9.17 mH	2.78 p.u.
σ	0.094	

Initial condition: Motor runs at no load at rated voltage: rotor current is zero:

$$\tau < 0: \quad \underline{u}_s = u \cdot e^{j\tau} = r_s \cdot \underline{i}_s + x_s \frac{d\underline{i}_s}{d\tau} \quad \Rightarrow \quad \underline{i}_s(\tau) = \frac{u \cdot e^{j\tau}}{r_s + j \cdot x_s}$$

At $\tau = 0: \underline{i}_{s0} = \underline{i}_s(0) = \dfrac{u}{r_s + jx_s}$, $\underline{\psi}_{s0} = x_s \underline{i}_{s0}$, $\underline{\psi}'_{r0} = x_h \underline{i}_{s0}$ short circuit occurs:

$$\underline{u}_s(\tau) = 0, \tau > 0$$

$$r_s \cdot \breve{\underline{i}}_s + s \cdot (x_s \cdot \breve{\underline{i}}_s + x_h \cdot \breve{\underline{i}}'_r) = \breve{\underline{u}}_s + \underline{\psi}_{s0} = \underline{\psi}_{s0}$$

$$r'_r \cdot \breve{\underline{i}}'_r + (s - j \cdot \omega_m) \cdot (x_h \cdot \breve{\underline{i}}_s + x'_r \cdot \breve{\underline{i}}'_r) = \underline{\psi}'_{r0}$$

$$(r_s + s \cdot x_s) \cdot \breve{\underline{i}}_s + s \cdot x_h \cdot \breve{\underline{i}}'_r = x_s \underline{i}_{s0}$$

$$(s - j \cdot \omega_m) \cdot x_h \cdot \breve{\underline{i}}_s + (r'_r + (s - j \cdot \omega_m) \cdot x'_r) \cdot \breve{\underline{i}}'_r = x_h \underline{i}_{s0}$$

$$\breve{\underline{i}}_s = \frac{r'_r - j\omega_m x'_r + s \cdot \sigma \cdot x'_r}{\sigma \cdot x'_r \cdot (s - \underline{s}_a) \cdot (s - \underline{s}_b)} \cdot \underline{i}_{s0} = \frac{\underline{D}}{s - \underline{s}_a} + \frac{\underline{E}}{s - \underline{s}_b}$$

$$\breve{\underline{i}}'_r = \frac{(r_s + j\omega_m \cdot x_s) \cdot x_h}{\sigma \cdot x_s \cdot x'_r \cdot (s - \underline{s}_a) \cdot (s - \underline{s}_b)} \cdot \underline{i}_{s0} = \underline{F} \cdot \left(\frac{1}{s - \underline{s}_a} - \frac{1}{s - \underline{s}_b} \right)$$

$$\underline{D} = \frac{r'_r - j\omega_m x'_r + \underline{s}_a \cdot \sigma \cdot x'_r}{\sigma \cdot x'_r \cdot (\underline{s}_a - \underline{s}_b)} \cdot \underline{i}_{s0}, \underline{E} = \frac{r'_r - j\omega_m x'_r + \underline{s}_b \cdot \sigma \cdot x'_r}{\sigma \cdot x'_r \cdot (\underline{s}_b - \underline{s}_a)} \cdot \underline{i}_{s0}, \underline{F} = \frac{(r_s + j\omega_m \cdot x_s) \cdot x_h}{\sigma \cdot x_s x'_r \cdot (\underline{s}_a - \underline{s}_b)} \cdot \underline{i}_{s0}$$

Inverse *Laplace* transformation yields: $\underline{i}_s(\tau) = \underline{D} \cdot e^{\underline{s}_a \tau} + \underline{E} \cdot e^{\underline{s}_b \tau}$ with (7.6-19), (7.6-20):

$$\underline{i}_s(\tau) = \underline{D} \cdot e^{-\tau/\tau_{r\sigma}} \cdot e^{j\omega_m \tau} + \underline{E} \cdot e^{-\tau/\tau_{s\sigma}}, \quad \underline{i}'_r(\tau) = \underline{F} \cdot (e^{-\tau/\tau_{r\sigma}} \cdot e^{j\omega_m \tau} - e^{-\tau/\tau_{s\sigma}}) \qquad (7.6\text{-}22)$$

Facit:

The short circuit current comprises an oscillating AC component with oscillation frequency is rotating frequency and a DC component.

- AC component decays with rotor short-circuit time constant, DC component decays with stator short circuit time constant.
- Current amplitude in worst case is about twice steady state short circuit current amplitude (according to equivalent circuit, Slip = 1).

Worst-case (maximum) and best case (minimum) phase short circuit current:

Non-damped current space vector amplitude is with $r_s = r_r' = 0$: $\underline{D} = \frac{-1+\sigma}{\sigma} \cdot \underline{i}_{s0}$,

$\underline{E} = \frac{1}{\sigma} \cdot \underline{i}_{s0}$, $\underline{F} = \frac{x_h}{\sigma \cdot x_r'} \cdot \underline{i}_{s0}$, $\underline{s}_a = j\omega_m$, $\underline{s}_b = 0$:

$$\underline{i}_s(\tau) = \underline{i}_{s0} \cdot \left(\frac{1}{\sigma} + \left(1 - \frac{1}{\sigma}\right) \cdot e^{j\omega_m \tau} \right) \tag{7.6-23}$$

$$\underline{i}_r'(\tau) = \underline{i}_{s0} \cdot \frac{x_h}{\sigma \cdot x_r'} \cdot \left(e^{j\omega_m \tau} - 1 \right) \tag{7.6-24}$$

Like in Example 7.6-1, maximum current occurs with voltage at zero crossing, when short circuit happens (DC plus AC component), whereas at maximum voltage short circuit DC component is zero, yielding minimum current peak.

Short circuit happens at	***phase voltage zero***	***phase voltage maximum***
Voltage space vector $\tau < 0$	$\underline{u}_s = j \cdot u \cdot e^{j\tau}$	$\underline{u}_s = u \cdot e^{j\tau}$
Current space vector $\tau < 0$	$\underline{i}_s = (u / x_s) \cdot e^{j\tau}$	$\underline{i}_s = -j \cdot (u / x_s) \cdot e^{j\tau}$
Current space vector $\tau = 0$	$\underline{i}_{s0} = (u / x_s)$	$\underline{i}_{s0} = -j \cdot (u / x_s)$
voltage in phase U at $\tau = 0$	$u_U(0) = \mathrm{Re}(j \cdot u \cdot e^{j0}) = 0$	$u_U(0) = \mathrm{Re}(u \cdot e^{j0}) = u$
current in phase U at $\tau = 0$	$i_{sU}(0) = (u / x_s) = 0.34$	$i_{sU}(0) = 0$
maximum short circuit phase current (peak)	$\hat{i}_{s,U} = \frac{u}{x_s} \cdot \left(\frac{2}{\sigma} - 1 \right) = 6.87$	$\hat{i}_{s,U} = \left\| \frac{u}{x_s} \cdot \left(1 - \frac{1}{\sigma} \right) \right\| = 3.27$
occurring at	$\tau = \pi$	$\tau = \pi / 2$

Table 7.6-3: Solution for non-damped short-circuit current of induction machine, being short-circuited after running at no-load, synchronous speed.

Often simplified current formula is used, taking the amplitudes from non-damped calculation, combining them with the time constants from (7.6-22):

$$\underline{i}_s \cong \underline{i}_{s0} \cdot \left(\frac{e^{-\tau/\tau_{s\sigma}}}{\sigma} + \left(1 - \frac{1}{\sigma}\right) \cdot e^{-\tau/\tau_{r\sigma}} \cdot e^{j\omega_m \tau} \right), \quad \underline{i}_r' \cong \frac{x_h}{\sigma \cdot x_r'} \cdot \underline{i}_{s0} \cdot (e^{-\tau/\tau_{r\sigma}} \cdot e^{j\omega_m \tau} - e^{-\tau/\tau_{s\sigma}})$$

$\tau_{s\sigma} = 11.55, \tau_{r\sigma} = 14.35$: After two grid periods $2 \cdot 2\pi = 12.6$ AC and DC short circuit current component have decayed to 37%. Short circuit torque is calculated from

$$m_e(\tau) = -\mathrm{Im}\left\{ x_h \cdot \underline{i}_r' \cdot \underline{i}_s^* \right\} \cong -\frac{x_h^2}{\sigma \cdot x_r'} \cdot i_{s0}^2 \cdot e^{-\tau \cdot \left(\frac{1}{\tau_{r\sigma}} + \frac{1}{\tau_{s\sigma}} \right)} \cdot \sin(\omega_m \tau) \tag{7.6-25}$$

Facit:
The negative torque is braking the rotor. It is oscillating with rotational frequency. Average value is in (7.6-25) zero, as non-damped current amplitudes were taken. With exact values

(7.6-22) average torque is non-zero, being the equivalent of dissipated losses of short circuit stator and rotor current in resistances. Torque is generated by all three phase currents, so there is no influence of switching instant (voltage zero or maximum) on torque function.

Decay of short circuit torque goes with **short circuit time constan**t

$$\tau_{sc} = \frac{1}{\frac{1}{\tau_{s\sigma}} + \frac{1}{\tau_{r\sigma}}} \cong \frac{\sigma \cdot x_s}{r_s + r_r'} \tag{7.6-26}$$

Numerical solution of dynamic equations is given for torque and speed in Fig. 7.6-6. Torque oscillates with 50 Hz, and decays with $T_{sc} \cong \frac{\sigma \cdot L_s}{R_s + R_r'} = \frac{0.094 \cdot 0.00971}{0.025 + 0.02} = 20.2ms$. Peak non-damped torque is $\hat{m}_e = \frac{x_h^2}{\sigma \cdot x_r'} \cdot i_{s0}^2 = \frac{2.78^2}{0.094 \cdot 2.9} \cdot \frac{1}{2.95^2} = 3.25, \hat{M}_e = \hat{m}_e \cdot M_B = 2895Nm$, occurring at $\tau = \pi / 2$ or 5 ms after short circuit, and damped peak torque is $2895 \cdot e^{-5/20.2} = 2260Nm$. Numerical calculation yields 2700 Nm, and shows a slight reduction in speed due to braking.

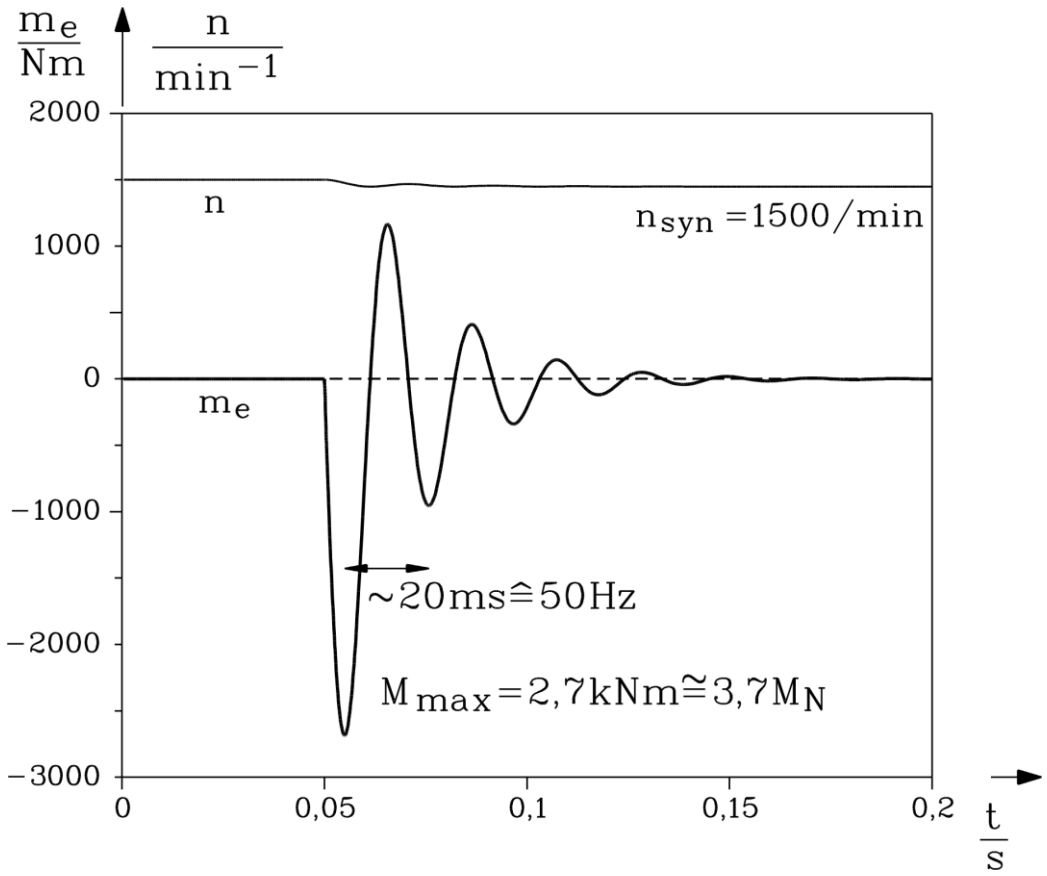

Fig. 7.6-6: Calculated short circuit torque and speed of induction motor, being short circuited at *t* = 0.05ms

7.7 Solutions of dynamic equations for induction machines with varying speed

Solutions of dynamic equations of induction machine for varying speed are only possible numerically, as equation set is non-linear.

Example 7.7-1:
No-load start-up of induction motors and afterwards loading with rated torque is investigated. Example is calculated for a big and a small induction machine 1 and 2.

	Induction machine 1 (big)		Induction machine 2 (small)	
Rated power	110.8 kW		1.18 kW	
Rated voltage	380 V Y		380 V Y	
Rated current	212 A		2.6 A	
Efficiency	93.4 %		85.5 %	
Power factor	0.85		0.81	
Rated slip	2 %		8 %	
Rated speed	1470/min		1380/min	
Rated torque	720 Nm		8.2 Nm	
R_s	25 mΩ	0.024 p.u.	9.5 Ω	0.113 p.u.
R'_r	20 mΩ	0.019 p.u.	6.2 Ω	0.073 p.u.
L_s	9.71 mH	2.95 p.u.	668 mH	2.49 p.u.
L'_r	9.55 mH	2.90 p.u.	662 mH	2.46 p.u.
L_h	9.17 mH	2.78 p.u.	633 mH	2.36 p.u.
σ	0.094		0.094	
J	2.8 kgm^2	$\tau_J = 155.5$	0.00349 kgm^2	$\tau_J = 15.8$
T_J with M_N	611 ms		67 ms	
Starting date	I_1 = 760A $\cos\varphi_1$ = 0.156 M_1 = 205 Nm			

Table 7.7-1: Data of big and small four pole induction machine for start-up calculation at 50 Hz grid

As rotor inertia is given by $J \sim d_{si}^4 l \sim l^5$ and motor power $P \sim d_{si}^3 l \sim l^4$, the scaling ratio of rotor inertia with increasing power is $J_1 / J_2 = (P_1 / P_2)^{5/4}$, delivering in our case $J_1 / J_2 = (110/1.1)^{5/4} = 316$. Real ratio is even bigger with $J_1 / J_2 = 2.8 / 0.00349 = 802$.

Facit:
The 100 times stronger motor 1 needs due to its about factor 1000 bigger inertia about 10 times longer to start up.

In Fig. 7.7-1 numerically calculated electromagnetic torque during start-up (with load shaft torque M_s = 0 = no-load start up) of motor 1 is shown versus time. At t = 1.8 s the motor is loaded with rated torque $M_s = M_N$.

a) Oscillating starting torque:
Due to switching on of stator voltage DC current component occurs in stator and rotor winding, which decays with electric time constant (7.6-18) $x_s / r_s + x'_r / r'_r$ (formula exactly only for zero speed). The 50 Hz AC stator current reacts with the DC flux of rotor DC current in a pulsating 50 Hz-torque. The same does the rotor 50 Hz AC current with the stator DC flux. This **50 Hz-pulsating starting torque** (5 periods per 0.1 s) is superimposed on average starting torque M_1, yielding total torque peak of 1300 Nm. This oscillating torque loads in coupled drive systems the mechanical coupling heavily and might be dangerous, especially for big machines.

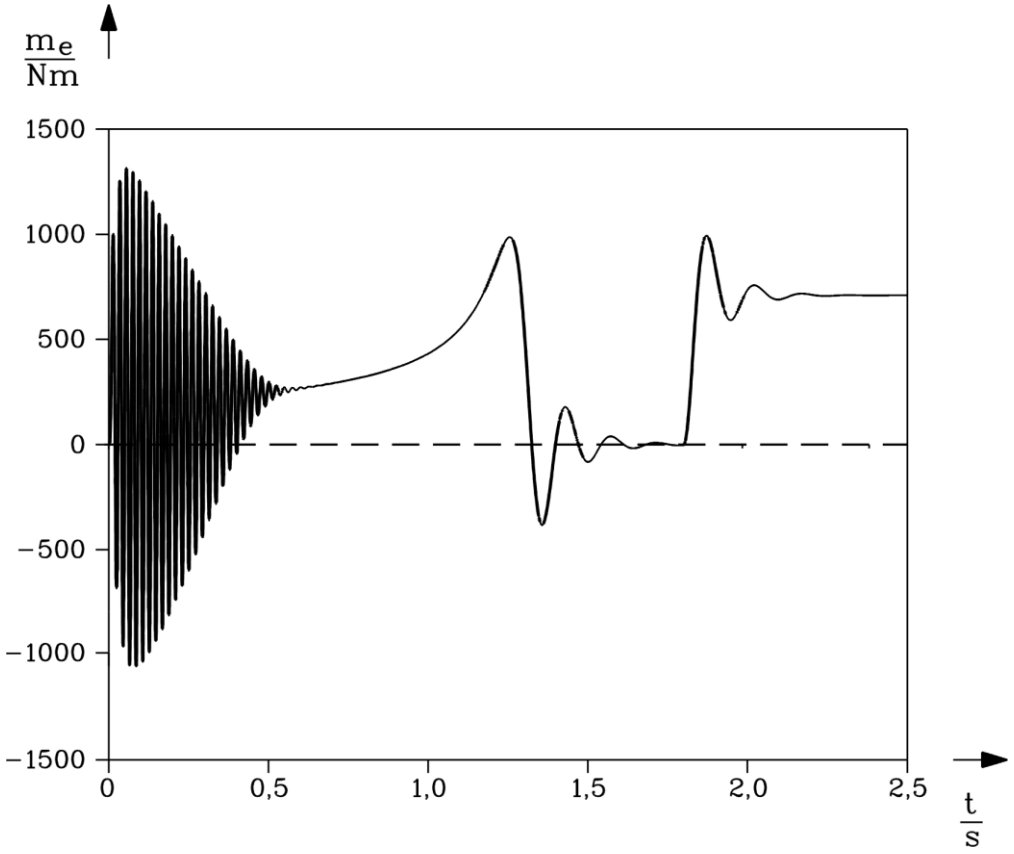

Fig. 7.7-1: Calculated electromagnetic torque of induction machine 1 at no-load starting, being loaded at 1.8 s with rated torque

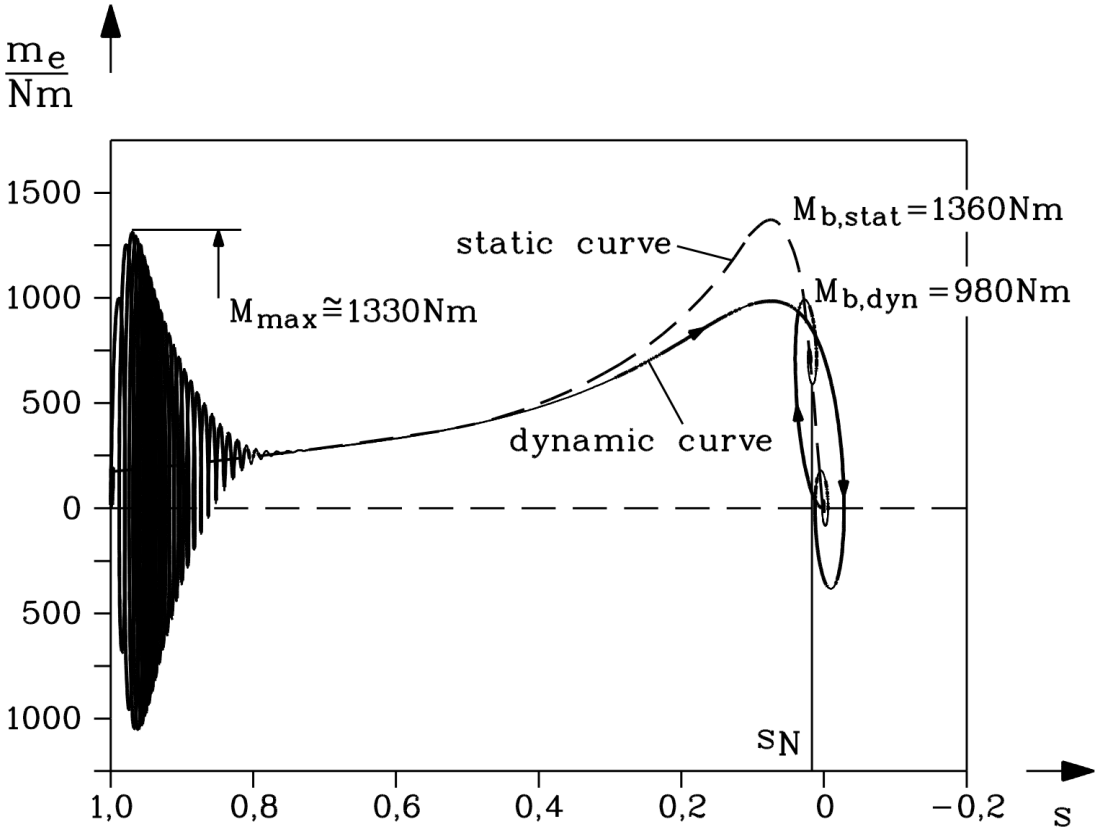

Fig. 7.7-2: Calculated dynamic torque-speed characteristic of induction machine 1 at no-load starting, being loaded at 1.8 s with rated torque. In dashed line static torque-speed characteristic from equivalent circuit diagram is given for comparison.

b) Dynamic break down torque:
Dynamic break down torque $M_{b,dyn}$ = 1000 Nm occurs at 1.2 s and stays well below static break-down torque of motor 1 $M_{b,stat}$ = 1360 Nm due to the dynamic starting (Fig. 7.7-2). The main flux $\underline{\psi}_h = x_h \cdot \underline{i}_m$ is changing with big electric time constant due to slow build up of magnetizing current. For speed zero this time constant is (7.6-18) $x_s / r_s + x'_r / r'_r$, which is $T = L_s / R_s + L'_r / R'_r = 0.388s + 0.478s = 0.866s$. We take as first guess this value also for increasing speed. So, when reaching break down torque at time 1.2 s, still full main flux is not available, being smaller by $1 - e^{-t/T} = 1 - e^{-1.2/0.87} = 0.75$. Thus dynamic break down torque is reduced by 25%; numerical calculation yields 1000/1360 = 0.74.

c) Eigen-frequency of induction machine at synchronous / rated speed:
When the motor reaches synchronous speed, torque decays to zero, but with a damped oscillation of low frequency about 7 Hz. After loading the machine, torque rises to rated torque 720 Nm, again with a damped oscillation of nearly the same natural frequency 7 Hz.

Facit:
Induction machine shows low natural oscillation frequency like in synchronous machines ***("synchronous machine effect in asynchronous machines").*** *Reason for this is that the rotor current does not vanish immediately in the short circuited rotor winding at synchronous speed, but with rotor short circuit time constant. Thus the rotor flux may be regarded as "frozen" for a short time and acts therefore like the electrically excited rotor DC flux in synchronous machines: The rotor flux exerts a force on stator like an elastic connection between stator and rotor, yielding with the rotor mass a natural oscillation system. When loading the machine suddenly. Again the rotor flux can only change with rotor time constant, leading again to natural oscillation.*

The 50 Hz oscillation of starting torque and the natural torque oscillation at synchronous speed leads oscillations in speed (Fig. 7.7-3). According to mechanical equation

$$J \cdot d\Omega_m / dt = \hat{M}_e \cos \omega t \quad \rightarrow \quad \Omega_m(t) = \frac{\hat{M}_e}{\omega \cdot J} \sin \omega t \tag{7.7-1}$$

speed ripple **decreases with increasing inertia and frequency**, so speed ripple at low natural frequency (with lower torque amplitude) is even bigger than speed ripple at starting with about ten times higher frequency 50 Hz and bigger torque amplitude. Increase of inertia increases run up time in almost linear way. As steady state starting torque (200 Nm) is only 30% rated torque, the real run up time is longer than T_J. Whereas speed ripple at starting remains a 50 Hz ripple also with varying inertia, the natural frequency $f_{d,m}$ at synchronous speed decreases with $\sim 1/\sqrt{J}$. This is again understood with mechanical equation: Speed oscillation $\Delta\Omega_m(t)$ is superimposed e.g. at synchronous speed:

$$\Omega_m(t) = \Omega_{syn} + \Delta\Omega_m(t) \tag{7.7-2}$$

Magnetic braking force of "frozen" rotor flux on stator current increases, if angle difference $\Delta\vartheta$ between rotor flux axis and stator space current vector increases: $M_e(\Delta\vartheta) = -c_\vartheta \Delta\vartheta$. As $\Delta\vartheta$ is counted in electric degrees, speed oscillation is given by angle oscillation

$$\frac{d\Delta\vartheta}{dt} = p \cdot \Delta\Omega_m \tag{7.7-3}$$

Mechanical equation yields therefore a second order linear differential equation with constant coefficients

$$J\frac{d\Omega_m}{dt} = M_e(\vartheta) = -c_\vartheta \cdot \Delta\vartheta \qquad \Rightarrow \qquad J\frac{d\Omega_m}{dt} = J\frac{d\Delta\Omega_m}{dt} = -c_\vartheta \cdot \Delta\vartheta$$

$$J\frac{d^2\Delta\vartheta}{dt^2} + p \cdot c_\vartheta \cdot \Delta\vartheta = 0 \tag{7.7-4}$$

with solution $\Delta\vartheta(t) \sim \sin(\omega_{d,m}t)$, $\Delta\Omega_m(t) \sim \cos(\omega_{d,m}t)$ and natural oscillation frequency

$$\boxed{f_{d,m} = \frac{\omega_{d,m}}{2\pi} = \frac{1}{2\pi}\sqrt{\frac{p \cdot |c_\vartheta|}{J}}} \quad . \tag{7.7-5}$$

	$J = 0.5 \cdot J_N$	$J = J_N$	$J = 2 \cdot J_N$
real run up time	0.7 s	1.3 s	2.4 s
T_J	0.3 s	0.6 s	1.2 s
$f_{d,m}$	9.9 Hz	7.0 Hz	4.9 Hz

Table 7.7-2: Influence of motor inertia on start up of induction machine

d) Detailed view on decrease of 50 Hz oscillating torque component:
By increasing inertia further to $J = 10 \cdot J_N$, start up time, but also time of decay of 50 Hz oscillation of starting torque increases (Fig. 7.7-4). In that case start up is so slowly, that during electric transient of switching on the voltage on stator winding the rotor speed changes only minor. So one can take time constant of (7.6-18) for $\omega_m = 0$. After $T_2 = L_s / R_s + L_r' / R_r' = 0.388s + 0.478s = 0.866s$ oscillating torque should have decreased to $1/e$ = 0.37, which fits quite well to Fig. 7.7-4. At lower inertia (quick start up) influence of rising ω_m on time constant is visible, decreasing time constant T_2 and decay of oscillating torque.

	$J = J_N$	$J = 10 J_N$
Time of decay of 50 Hz oscillating torque	0.5 s	2.3 s
	Fig. 7.7-1	Fig. 7.7-4

Table 7.7-3: Influence of motor inertia on time of decay of 50 Hz oscillating torque

The 50 Hz oscillating torque consists of DC and AC current component (see Section 7.6). The AC component delivers steady state starting torque M_1. The DC current component is (damping neglected) equal to AC current component: $I_{DC} \approx \hat{I}_{AC}$. As starting torque is proportional to real part of AC starting current $M_1 \sim \hat{I}_{AC}\cos\varphi_1$, one may estimate peak torque due to DC current component by $M_{1,DC} \sim I_{DC} \sim M_1 / \cos\varphi_1$ and thus **total torque peak at starting**

$$\boxed{M_{1,peak} \approx M_1 \cdot \left(1 + \frac{1}{\cos\varphi_1}\right)} \quad . \tag{7.7-8}$$

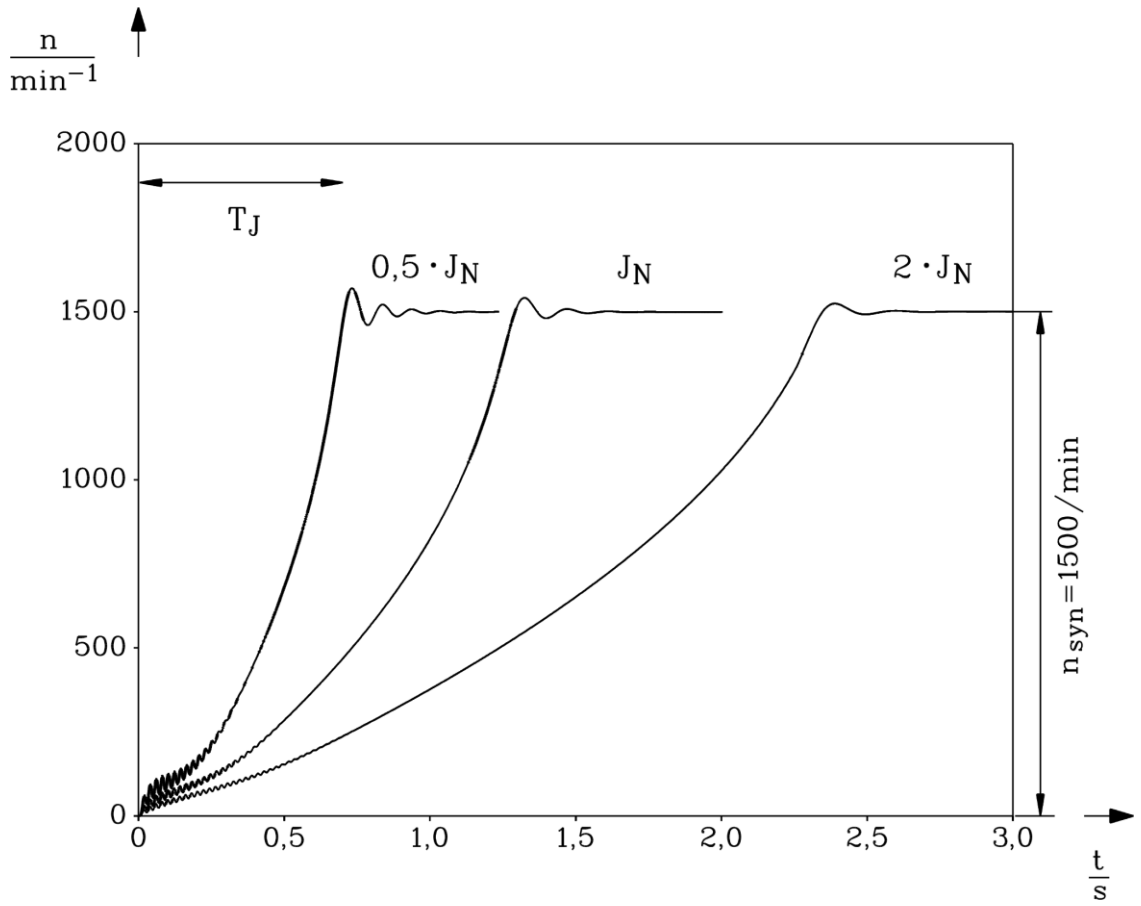

Fig. 7.7-3: Calculated rotational speed of induction machine 1 at no-load starting with a) $0.5J_N$, b) J_N, c) $2J_N$

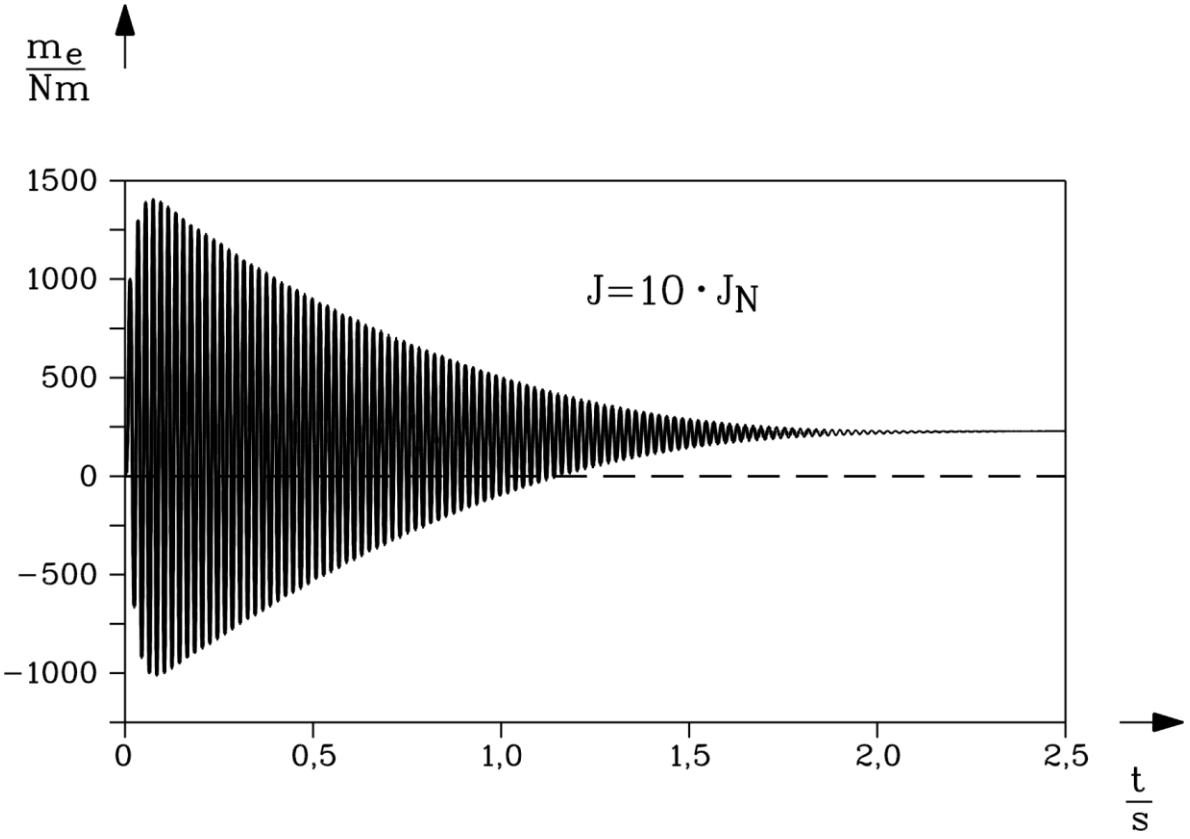

Fig. 7.7-4: Calculated electromagnetic torque of induction machine 1 at no-load starting with ten times increased inertia

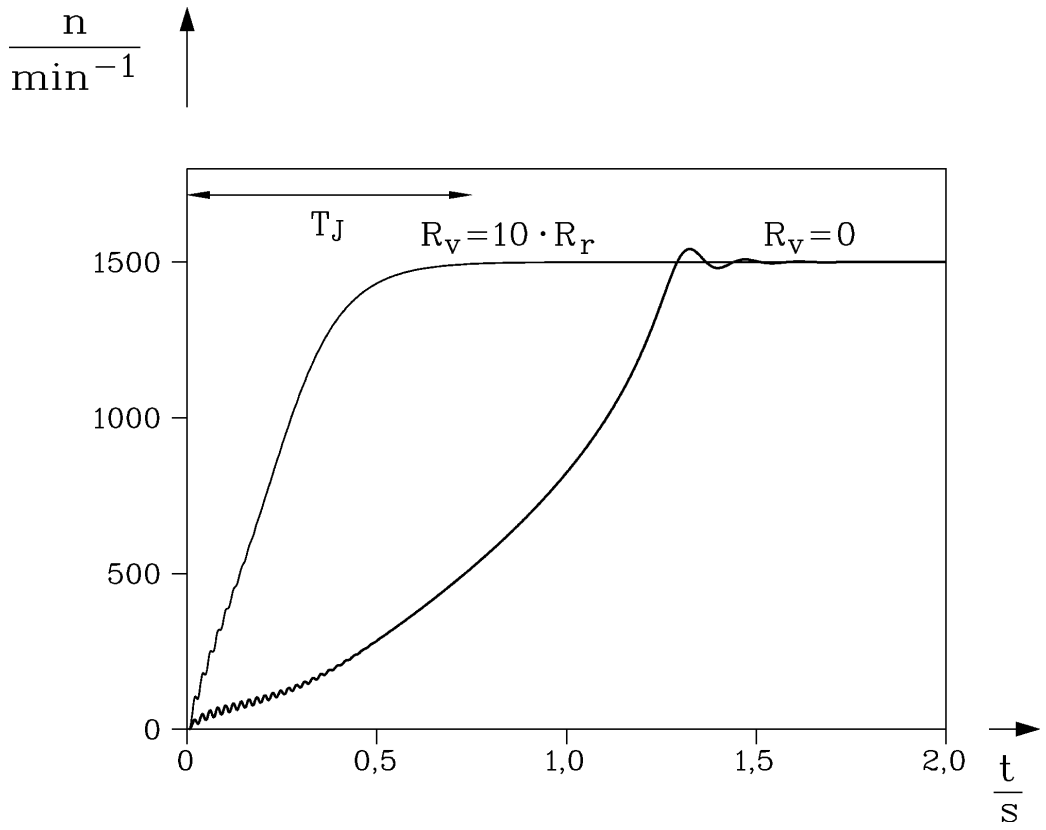

Fig. 7.7-5: Calculated rotational speed of induction machine 1 at no-load starting with rated inertia
a) without additional rotor resistance, b) with 10-times rotor resistance in addition via slip rings in rotor circuit

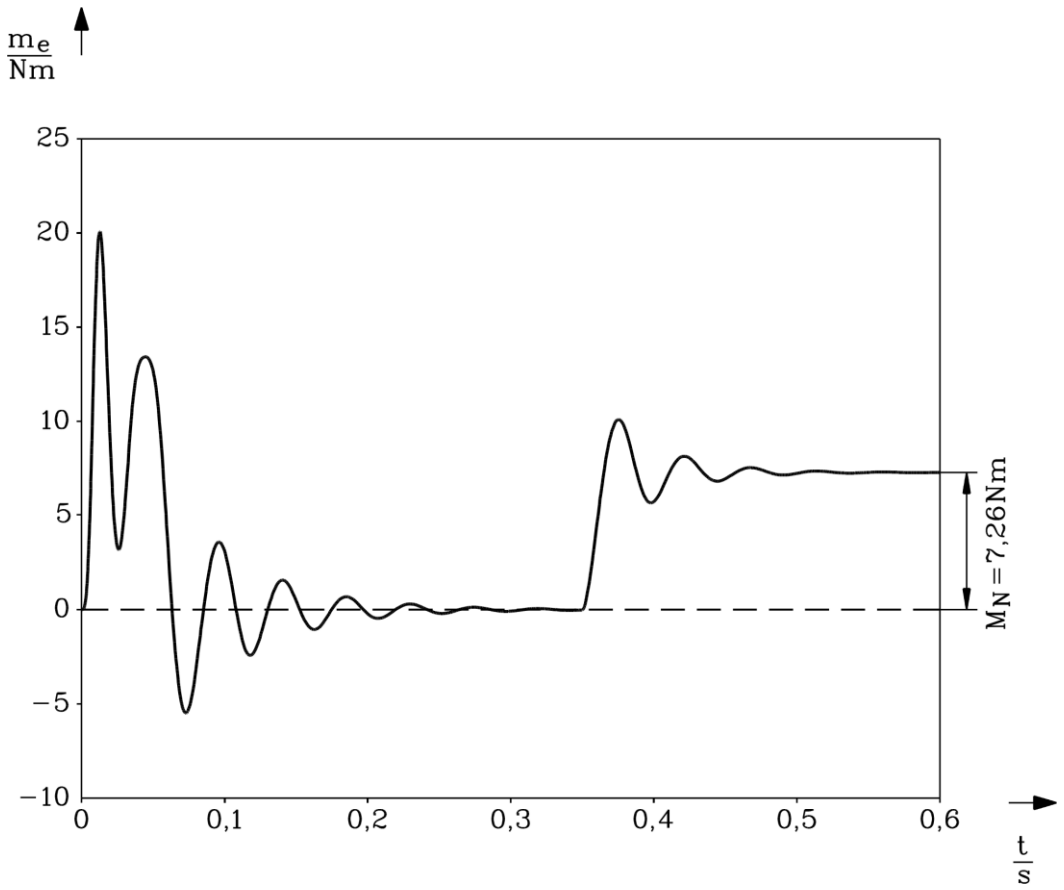

Fig. 7.7-6: Calculated electromagnetic torque of induction machine 2 at no-load starting, being loaded at 0.35 s with nearly rated torque 7.3 Nm

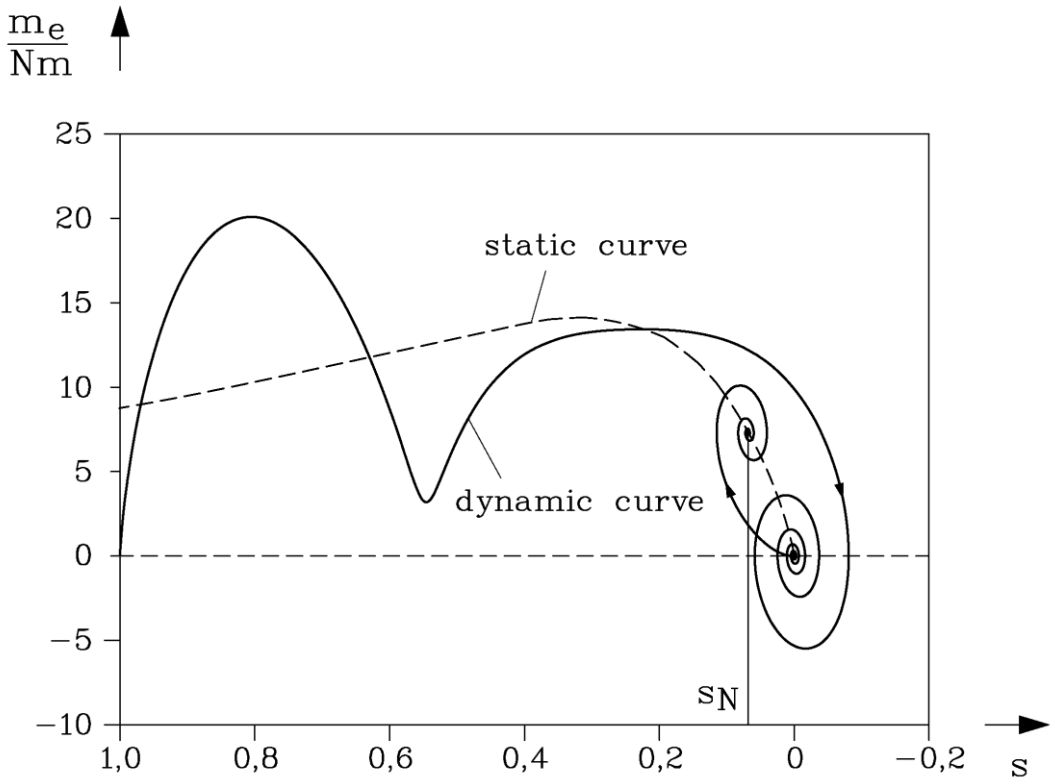

Fig. 7.7-7: Calculated dynamic torque-speed characteristic of induction machine 2 at no-load starting, being loaded at 0.35 s with nearly rated torque 7.3 Nm. In dashed line static torque-speed characteristic from equivalent circuit diagram is given for comparison.

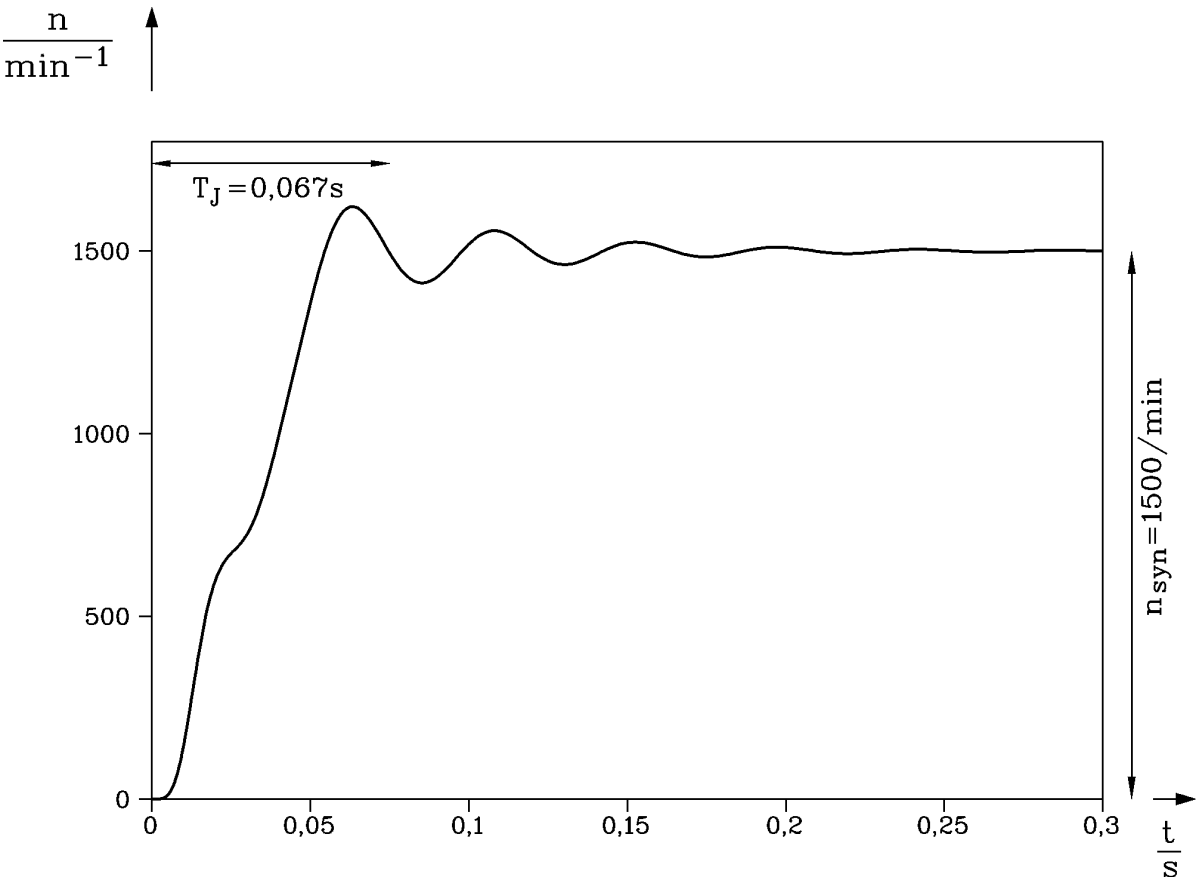

Fig. 7.7-8: Calculated rotational speed of induction machine 2 at no-load starting with J_N

In Fig. 7.7-4 peak torque is 1400 Nm, according to $M_{1,peak} = 205 \cdot \left(1 + \frac{1}{0.156}\right) = 1500Nm$, which fits quite well.

e) Slip ring induction machine: Influence of additional rotor resistance:
If an additional rotor resistance of $R_v = 10R_r$ is added per phase, then break down torque is shifted from slip $s_b = 0.08$ to a 11-times higher slip:

$$\frac{R_r}{s_b} = \frac{R_r + 10R_r}{s_b^*} \quad \rightarrow \quad s_b^* = 11 s_b = 11 \cdot 0.08 = 0.88.$$

Motor now starts nearly with break down torque as starting torque, hence reducing start up time significantly. As break down torque is 1360/720 = 1.89, real run up time is even smaller than T_J (Fig. 7.7-5).

f) Starting performance of small induction motor:
As stated above, the smaller motor 2 will accelerate much faster than motor 1. The DC current component due to switching on voltage is still decaying, while rotor has already gained nearly synchronous speed. So one cannot separate clearly different stages of 50 Hz oscillating torque and of breakdown torque (Fig. 7.7-6). Natural oscillation at no-load and rated point of operation is visible (Fig. 7.7-6 and 7.7-7), whereas shape of dynamic and static torque-speed characteristic differ considerably. But as their average values are nearly the same, the real start up time and rated starting time T_J = 67 ms are about the same.

g) *Pfaff-Jordan* parameter for dynamic break down torque determination:
By solving the dynamic equations for starting of the induction machines with the simplifications r_s = 0 and neglecting the transient dc current component, *G. Pfaff* and *H. Jordan* derived a dimensionless parameter *P*,

$$P = \left(\frac{\omega_s}{u_s} \cdot \frac{x_s}{x_h}\right)^2 \cdot \tau_J \cdot r_r' \cdot s_b = \left(\frac{2\pi f_s}{U_s} \cdot \frac{L_s}{L_h}\right)^2 \cdot J \cdot \frac{R_r' \cdot s_b \cdot 2\pi f_N}{3p^2} \qquad (7.7\text{-}9)$$

which allows – by use of Fig. 7.7-9 – the determination of dynamic breakdown torque from static break down torque.

Example 7.7-2:
Data of induction machine 1 (Example 7.7-1): break down slip s_b = 8%.
Line start at 50 Hz, rated voltage: Calculation of *P* in per unit and physical units, alternatively:

$$P = \left(\frac{\omega_s}{u_s} \cdot \frac{x_s}{x_h}\right)^2 \cdot \tau_J \cdot r_r' \cdot s_b = \left(\frac{1}{1} \cdot \frac{2.95}{2.78}\right)^2 \cdot 155.5 \cdot 0.019 \cdot 0.08 = 0.266$$

$$P = \left(\frac{2\pi f_s}{U_s} \cdot \frac{L_s}{L_h}\right)^2 \cdot J \cdot \frac{R_r' \cdot s_b \cdot 2\pi f_N}{3p^2} = \left(\frac{2\pi 50}{380/\sqrt{3}} \cdot \frac{0.00971}{0.00917}\right)^2 \cdot 2.8 \cdot \frac{0.02 \cdot 0.08 \cdot 2\pi 50}{3 \cdot 2^2} = 0.2696$$

The curve in Fig. 7.7-9 yields $M_{b,dyn} / M_{b,stat} = 0.71$, whereas the numerical solution Fig. 7.7-2 yields 0.74, showing sufficient coincidence.

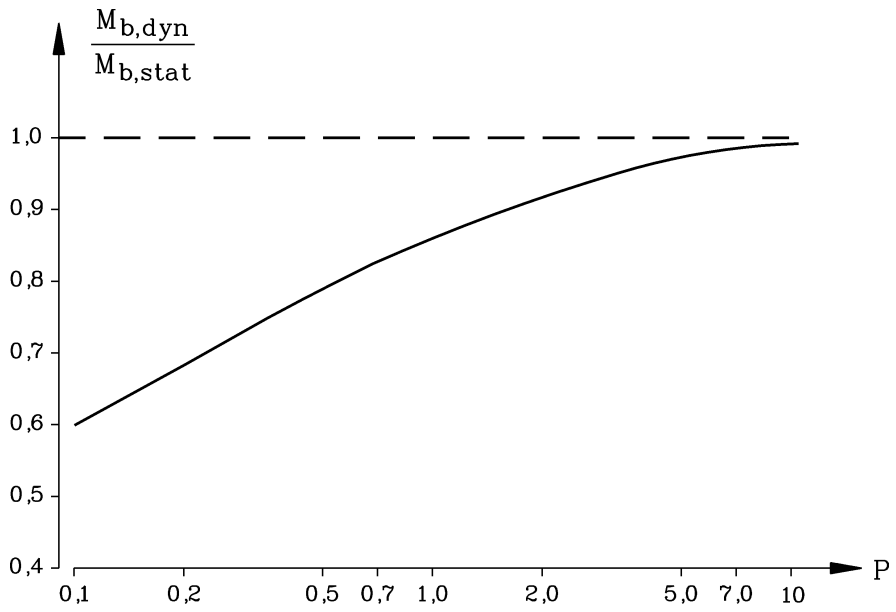

Fig. 7.7-9: Calculated ratio of dynamic versus static break down torque according to *Pfaff* and *Jordan* in dependence of parameter *P*

Understanding the *Pfaff-Jordan*-parameter *P*:
(1) At $R_s = 0$ we get $U_s / \omega_s = \Psi_s$
(2) At no-load we get: $\Psi_s \cdot L_h / L_s = \Psi_h$
(3) Compared to the mechanical time constant of the DC-machine
$T_m = \frac{J \cdot R_a}{(k_2 \Phi)^2} = \frac{J \cdot R_a}{(\frac{p}{2\pi} \frac{z}{a} \Phi)^2} = \frac{J \cdot R_a}{(p \cdot \Psi)^2}$, the expression $T_m = \frac{J \cdot R'_r}{(p \Psi_h)^2}$ may be regarded as the mechanical time constant of the induction machine.
(4) With $s_b \cong R'_r / (\sigma \cdot \omega_s L'_r)$ (for $R_s = 0$) we get for $\omega_{sN} = \omega_s$ the inverse of the rotor short-circuit time constant $1/T_{r\sigma} = \omega_{sN} \cdot s_b = R'_r / (\sigma L'_r)$ of the induction machine.
(5) Hence the *Pfaff-Jordan*-parameter *P* is the ratio of the mechanical time constant versus the rotor time constant: $P = T_m / (3T_{r\sigma})$.

Facit:
The start-up time is – like in DC machines – round-about $3T_m$. If the Pfaff-Jordan-parameter P is big, the duration of the transient current rising in the rotor, described by $3T_{r\sigma}$ at the beginning of the start-up, is much shorter than the start-up time. Hence during most of the time of start-up the rotor current has already reached its steady state value, which depends on slip s according to the OSSANNA circle. So the starting torque, created by stator flux and rotor current, is nearly the steady state value, especially when the break-down slip is reached. The transient current rise has only a small influence on the start-up torque. In case of small P the transient rise time is a big part of the starting time. The rotor current has not reached its steady state value, when the rotor passes the break-down slip. Hence the transient break-down torque is smaller than the steady state break-down torque.

7.8 Linearized transfer function of induction machines in synchronous reference frame

a) Motivation:
For constant speed operation **complex linear transfer function of electrical machine performance** was defined in *Laplace* *s*-plane with two poles (roots) s_a, s_b

$$\underline{s}_a = -\frac{1}{\tau_a} + j\omega_{d,a} \quad , \qquad \underline{s}_b = -\frac{1}{\tau_b} + j\omega_{d,b} \tag{7.8-1}$$

in denominator, describing current output according to voltage input. If transfer function was written not for complex current space vector, but for its two components in α-β-decomposition, then transfer function contains only real numbers. The denominator comprises 4 roots, but each two are conjugate complex:

$$\underline{s}_1 = -\frac{1}{\tau_a} + j\omega_{d,a}, \ \underline{s}_4 = -\frac{1}{\tau_a} - j\omega_{d,a} \tag{7.8-2}$$

$$\underline{s}_2 = -\frac{1}{\tau_b} + j\omega_{d,b}, \ \underline{s}_5 = -\frac{1}{\tau_b} - j\omega_{d,b} \tag{7.8-3}$$

When also mechanical equation shall be considered, speed varies and differential equations are non-linear. Therefore transfer function can only be derived for **small deviations** from chosen point of operation (equilibrium point), thus **linearizing** the equations in that point. Transfer function is then only valid for small amplitudes, typically 10% of considered equilibrium point. With that transfer function **small signal stability investigation** of each equilibrium point of the uncontrolled induction machine is possible. Due to torque equation differential equations have to be written in components, so **small signal transfer function of the electro-mechanical machine performanc**e contains only real numbers, comprising 5 poles (roots) in denominator, four similar to (7.8-2), (7.8-3), which are conjugate complex, and on fifth real root.

b) Why use of "synchronous reference frame"?
Dynamic system equations are considered in **synchronous reference frame**, because in stationary conditions at sinus grid operation all space vectors **do not move** in this reference frame. Decomposition of space vector in real and imaginary part in synchronous reference frame is

$$\underline{u}_{s(syn)}(\tau) = u_{s,a}(\tau) + j \cdot u_{s,b}(\tau) \quad . \tag{7.8-4}$$

Thus we have three reference frames in parallel use (Table 7.8-1).

Stator reference frame	*Rotor reference frame*	*Synchronous reference frame*
Does not rotate	Rotates with $\omega_m = d\gamma / d\tau$	Rotates with $\omega_{syn} = d\delta / d\tau$
Use in induction machines	Use in synchronous machines	Use in induction machines for small signal theory
$\underline{u}_{(s)}(\tau) = u_\alpha(\tau) + ju_\beta(\tau)$	$\underline{u}_{(r)}(\tau) = u_d(\tau) + ju_q(\tau)$	$\underline{u}_{(syn)}(\tau) = u_a(\tau) + ju_b(\tau)$
$\underline{u}_{(s)} = \frac{2}{3}(u_U + \underline{a} \cdot u_V + \underline{a}^2 u_W)$	$\underline{u}_{(r)}(\tau) = \underline{u}_{(s)}(\tau) \cdot e^{-j\cdot\gamma(\tau)}$	$\underline{u}_{(syn)}(\tau) = \underline{u}_{(s)}(\tau) \cdot e^{-j\cdot\delta(\tau)}$

Table 7.8-1: Reference frames in use for space vectors of three-phase AC machines

Example 7.8-1:
Calculate voltage space vector for three phase AC sine wave voltage system
$u_U(\tau) = u \cdot \cos(\omega_s \tau), u_V(\tau) = u \cdot \cos(\omega_s \tau - 2\pi/3), u_V(\tau) = u \cdot \cos(\omega_s \tau - 4\pi/3)$ in
- stator reference frame
- synchronous reference frame:
According to Example 6.3-1 we get in stator reference frame:

$$\underline{u}_s(\tau) = \frac{2}{3}\cdot\left[u_U + \underline{a}\cdot u_V + \underline{a}^2 u_W\right] = u\cdot e^{j\omega_s\tau} = u\cdot(\cos(\omega_s\tau) + j\sin(\omega_s\tau)) = u_{s\alpha} + ju_{s\beta}$$

Transformation into synchronous reference frame yields with angle $\delta = \omega_{syn}\cdot\tau - \delta_0$ between stator and synchronous reference frame, where δ_0 marks the position of synchronous reference frame at $\tau = 0$ (and is chosen zero !):

$$\underline{u}_{s(syn)}(\tau) = \underline{u}_s(\tau)\cdot e^{-j\delta} = u\cdot e^{j\omega_s\tau}\cdot e^{-j\omega_s\tau + j\delta_0} = \underline{\underline{u\cdot e^{j\delta_0}}} = u\cdot(\cos(\delta_0) + j\sin(\delta_0)) = u_{sa} + ju_{sb}$$

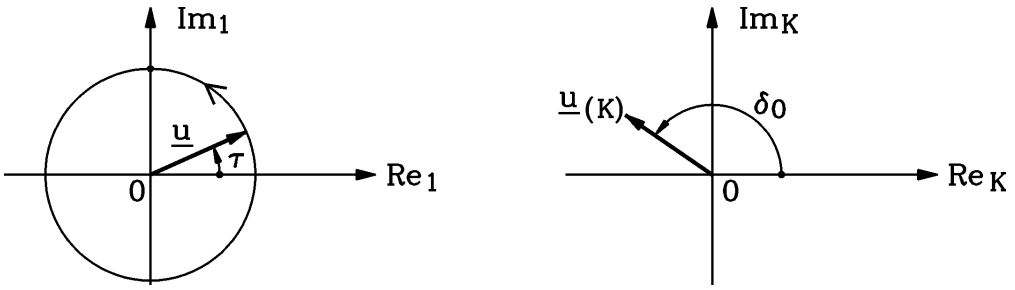

Fig. 7.8-1: Stator voltage space vector of three phase sinus voltage system is rotating in stator reference frame with angular frequency ω_s (left), but does NOT move in synchronous reference frame (right) , *K* =syn. ref. frame

c) Steady state operation at sinusoidal three-phase voltage system:

In **equilibrium points**

- no change of quantities with time occurs: $d\underline{\psi}/d\tau = 0$,
- electromagnetic torque m_e and shaft torque of load m_s are equal, yielding constant speed $d\omega_m/d\tau = 0$. Therefore only voltage and flux linkage equations must be considered for equilibrium points, which is done here in synchronous reference frame. With $d\delta/d\tau = \omega_{syn} = \frac{\Omega_{syn}}{\omega_N/p} = \frac{p\Omega_{syn}}{\omega_N} = \frac{\Omega_s}{\omega_N} = \omega_s$ and $d\gamma/d\tau = \omega_m$.

$$\underline{u}_{s(syn)} = r_s\underline{i}_{s(syn)} + \frac{d\underline{\psi}_{s(syn)}}{d\tau} + j\cdot\frac{d\delta}{d\tau}\cdot\underline{\psi}_{s(syn)} = r_s\underline{i}_{s(syn)} + j\cdot\omega_s\cdot\underline{\psi}_{s(syn)}$$

$$0 = r_r'\underline{i}'_{r(syn)} + \frac{d\underline{\psi}'_{r(syn)}}{d\tau} + j\cdot\frac{d(\delta-\gamma)}{d\tau}\cdot\underline{\psi}'_{r(syn)} = r_r'\underline{i}'_{r(syn)} + j\cdot(\omega_s-\omega_m)\cdot\underline{\psi}'_{r(syn)}$$

$$\underline{\psi}_{s(syn)} = x_s\cdot\underline{i}_{s(syn)} + x_h\cdot\underline{i}'_{r(syn)} \qquad (7.8\text{-}5)$$

$$\underline{\psi}'_{r(syn)} = x_h\cdot\underline{i}_{s(syn)} + x_r'\cdot\underline{i}'_{r(syn)}$$

$$\tau_J\cdot\frac{d\omega_m}{d\tau} = -\mathrm{Im}\left\{\underline{i}^*_{s(syn)}\cdot\underline{\psi}_{s(syn)}\right\} - m_s(\tau) = 0 \quad \Rightarrow m_e(\tau) = m_s(\tau)$$

For simplification the subscript *(syn)* is omitted further, using the abbreviation **slip**

$$Slip = \frac{\Omega_{syn}-\Omega_m}{\Omega_{syn}} = \frac{\omega_s-\omega_m}{\omega_s} \qquad . \qquad (7.8\text{-}6)$$

$$\underline{u}_s = r_s\underline{i}_s + j\cdot\omega_s\cdot(x_s\cdot\underline{i}_s + x_h\cdot\underline{i}'_r) = (r_s + j\omega_s x_s)\cdot\underline{i}_s + j\omega_s x_h\cdot\underline{i}'_r$$

$$0 = r_r'\cdot\underline{i}'_r + j\cdot Slip\cdot\omega_s\cdot(x_h\cdot\underline{i}_s + x_r'\cdot\underline{i}'_r) = j\cdot Slip\cdot\omega_s x_h\cdot\underline{i}_s + (r_r' + j\cdot Slip\cdot\omega_s x_r')\cdot\underline{i}'_r$$

Solution of these linear two equations with unknown currents for given stator voltage is given with use of *Blondel´*s stray coefficient σ

$$\boxed{\underline{i}_s = \underline{u}_s \cdot \frac{r'_r + j \cdot Slip \cdot \omega_s x'_r}{\left(r_s r'_r - Slip \cdot \sigma \cdot \omega_s x_s \cdot \omega_s x'_r\right) + j \cdot \left(r'_r \cdot \omega_s x_s + Slip \cdot r_s \cdot \omega_s x'_r\right)}} \tag{7.8-7}$$

This solution for current space vector for three-phase sinusoidal voltage time function is (of course) identical with the well known solution of sinusoidal stator phase current (7.6-9) from equivalent circuit diagram (Fig. 7.6-1), which defines the **circle diagram** $\underline{i}_s(Slip)$ for locus of space vector for varying slip. It may be taken as particular solution of differential equation system (7.8-5) like (7.6-8).

Note that (7.6-8) was valid in stator reference frame, so current space vector was rotating, whereas here in synchronous reference frame steady state current space vector is a **fixed** complex vector, which is NOT changing with time. This we have like in DC machines for the equilibrium points fixed values for
- voltage,
- current,
- speed,

which in DC machines are real numbers – related to DC values in equilibrium points - and here in AC induction machines are complex numbers – related to sinusoidal AC values with constant frequency and amplitude.

d) Small signal theory in equilibrium points:
Voltage, flux linkage and mechanical equation in *a-b*-components in synchronous reference frame constitute 9 differential equations. By substituting stator and rotor current (4 current components), only 5 equations are left.

$$\boxed{\begin{aligned}\underline{\psi}_s &= x_s \cdot \underline{i}_s + x_h \cdot \underline{i}'_r \\ \underline{\psi}'_r &= x_h \cdot \underline{i}_s + x'_r \cdot \underline{i}'_r\end{aligned}} \quad \Rightarrow \quad \boxed{\begin{aligned}\underline{i}_s &= \frac{1}{\sigma \cdot x_s} \cdot \underline{\psi}_s - \frac{1-\sigma}{\sigma \cdot x_h} \cdot \underline{\psi}'_r \\ \underline{i}'_r &= \frac{1}{\sigma \cdot x'_r} \cdot \underline{\psi}'_r - \frac{1-\sigma}{\sigma \cdot x_h} \cdot \underline{\psi}_s\end{aligned}} \tag{7.8-8}$$

So stator and rotor voltage equations (7.8-5) with (7.8-8) contain as unknowns only flux linkages and rotor speed, whereas leading input is stator voltage and stator frequency and disturbing input is load torque:

$$\begin{aligned}\underline{u}_s &= \left(\frac{r_s}{\sigma \cdot x_s} + j\omega_s\right) \cdot \underline{\psi}_s + \frac{d\underline{\psi}_s}{d\tau} - \frac{r_s}{x_h} \cdot \frac{1-\sigma}{\sigma} \cdot \underline{\psi}'_r \\ 0 &= -\frac{r'_r}{x_h} \cdot \frac{1-\sigma}{\sigma} \cdot \underline{\psi}_s + \left(\frac{r'_r}{\sigma \cdot x'_r} + j(\omega_s - \omega_m)\right) \cdot \underline{\psi}'_r + \frac{d\underline{\psi}'_r}{d\tau} \\ \tau_J \cdot \frac{d\omega_m}{d\tau} &= -\operatorname{Im}\left\{\left(\frac{\underline{\psi}_s}{\sigma \cdot x_s} - \frac{1-\sigma}{\sigma \cdot x_h}\underline{\psi}'_r\right)^* \cdot \underline{\psi}_s\right\} - m_s(\tau) = \frac{1-\sigma}{\sigma \cdot x_h} \cdot \operatorname{Im}\left\{\underline{\psi}_s \cdot \underline{\psi}'^*_r\right\} - m_s(\tau)\end{aligned} \tag{7.8-9}$$

Considering **small deviations**
a) of amplitude for fluxes, voltages, currents in a equilibrium point – which is given by equivalent circuit (7.8-7) as complex numbers, corresponding to sinusoidal AC values with constant amplitude and
b) of speed, load torque and frequency from constant equilibrium values

– we linearize equation set (7.8-9).

Linearization of unknowns:

$$\underline{\psi}_s(\tau) = \underline{\psi}_{s0} + \Delta\underline{\psi}_s(\tau)$$
$$\underline{\psi}'_r(\tau) = \underline{\psi}'_{r0} + \Delta\underline{\psi}'_r(\tau)$$
$$\omega_m(\tau) = \omega_{m0} + \Delta\omega_m(\tau)$$

Linearization of known input:

$$\underline{u}_s(\tau) = \underline{u}_{s0} + \Delta\underline{u}_s(\tau)$$
$$\omega_s(\tau) = \omega_{s0} + \Delta\omega_s(\tau) \qquad (7.8\text{-}10)$$
$$m_s(\tau) = m_{s0} + \Delta m_s(\tau)$$

Starting investigation from steady state equilibrium, the initial conditions for deviations are zero: $\Delta\underline{\psi}_s(0) = \Delta\underline{\psi}'_r(0) = \Delta\omega_m(0) = \Delta\underline{u}_s(0) = \Delta\omega_s(0) = \Delta m_s(0) = 0$

For example, **linearization of stator voltage equation** is with $d\underline{\psi}_{s0}/d\tau = 0$:

$$\underline{u}_{s0} + \Delta\underline{u}_s = \left(\frac{r_s}{\sigma \cdot x_s} + j(\omega_{s0} + \Delta\omega_s)\right) \cdot (\underline{\psi}_{s0} + \Delta\underline{\psi}_s) + \frac{d(\underline{\psi}_{s0} + \Delta\underline{\psi}_s)}{d\tau} - \frac{r_s}{x_h} \cdot \frac{1-\sigma}{\sigma} \cdot (\underline{\psi}'_{r0} + \Delta\underline{\psi}'_r)$$

(i) equilibrium point: $\underline{u}_{s0} = \left(\frac{r_s}{\sigma \cdot x_s} + j\omega_{s0}\right) \cdot \underline{\psi}_{s0} - \frac{r_s}{x_h} \cdot \frac{1-\sigma}{\sigma} \cdot \underline{\psi}'_{r0}$ (7.8-11)

(ii) deviations: $\Delta\underline{u}_s = \frac{r_s}{\sigma \cdot x_s}\Delta\underline{\psi}_s + j\omega_{s0}\Delta\underline{\psi}_s + j\Delta\omega_s\underline{\psi}_{s0} + \underline{\underline{j\Delta\omega_s\Delta\underline{\psi}_s}} + \frac{d\Delta\underline{\psi}_s}{d\tau} - \frac{r_s}{x_h} \cdot \frac{1-\sigma}{\sigma} \cdot \Delta\underline{\psi}'_r$

As long as small deviation are less than 10% to 20% of equilibrium value, neglecting multiplication of two small deviations will lead to an error below 4%, e.g.:

$\frac{\Delta\omega_s \cdot \Delta\psi_s}{\omega_{s0} \cdot \psi_{s0}} = 0.2 \cdot 0.2 = 0.04$, leading to deviations:

$$\Delta\underline{u}_s \cong \frac{r_s}{\sigma \cdot x_s}\Delta\underline{\psi}_s + j\omega_{s0}\Delta\underline{\psi}_s + j\underline{\psi}_{s0}\Delta\omega_s + \frac{d\Delta\underline{\psi}_s}{d\tau} - \frac{r_s}{x_h} \cdot \frac{1-\sigma}{\sigma} \cdot \Delta\underline{\psi}'_r \quad . \qquad (7.8\text{-}12a)$$

This linear differential equation is *Laplace*-transformed to get an algebraic equation:

$$\Delta\breve{\underline{u}}_s \cong \left(\frac{r_s}{\sigma \cdot x_s} + j\omega_{s0} + s\right)\Delta\breve{\underline{\psi}}_s + j\underline{\psi}_{s0}\Delta\breve{\omega}_s - \frac{r_s}{x_h} \cdot \frac{1-\sigma}{\sigma} \cdot \Delta\breve{\underline{\psi}}'_r \qquad (7.8\text{-}12b)$$

In the same way **rotor voltage equation for small deviations** is derived and *Laplace*-transformed, taking $\omega_{s0} - \omega_{m0} = \omega_{r0}$ as rotor frequency:

equilibrium: $0 = -\frac{r'_r}{x_h} \cdot \frac{1-\sigma}{\sigma} \cdot \underline{\psi}_{s0} + \left(\frac{r'_r}{\sigma \cdot x'_r} + j\omega_{r0}\right) \cdot \underline{\psi}'_{r0}$ (7.8-13)

$$0 \cong -\frac{r'_r}{x_h}\frac{1-\sigma}{\sigma}\Delta\underline{\psi}_s + \frac{r'_r}{\sigma \cdot x'_r}\Delta\underline{\psi}'_r + j\omega_{r0}\Delta\underline{\psi}'_r + j(\Delta\omega_s - \Delta\omega_m)\underline{\psi}'_{r0} + \frac{d\Delta\underline{\psi}'_r}{d\tau} \quad \Rightarrow Laplace \Rightarrow$$

$$0 \cong -\frac{r'_r}{x_h}\frac{1-\sigma}{\sigma}\Delta\breve{\underline{\psi}}_s + \left(\frac{r'_r}{\sigma \cdot x'_r} + j\omega_{r0} + s\right)\Delta\breve{\underline{\psi}}'_r + j\underline{\psi}'_{r0}\Delta\breve{\omega}_s - j\underline{\psi}'_{r0}\Delta\breve{\omega}_m \qquad (7.8\text{-}14)$$

Linearization of torque equation demands decomposition of complex space vectors in *a*-*b*-components:

$$\Delta\underline{\psi}_s(\tau) = \Delta\psi_{sa}(\tau) + j\Delta\psi_{sb}(\tau)$$
$$\Delta\underline{\psi}'_r(\tau) = \Delta\psi'_{ra}(\tau) + j\Delta\psi'_{rb}(\tau) \qquad \Delta\underline{u}_s(\tau) = \Delta u_{sa}(\tau) + j\Delta u_{sb}(\tau) \qquad (7.8\text{-}15)$$

$$\tau_J \frac{d\omega_m}{d\tau} = \frac{1-\sigma}{\sigma \cdot x_h}\left(\psi_{sb} \cdot \psi'_{ra} - \psi_{sa} \cdot \psi'_{rb}\right) - m_s \quad \Rightarrow \text{Linearization and } \textit{Laplace}\text{-transformation} \Rightarrow$$

$$\tau_J \frac{d\Delta\omega_m}{d\tau} \cong \frac{1-\sigma}{\sigma \cdot x_h}\left(\psi_{s0b} \cdot \Delta\psi'_{ra} + \Delta\psi_{sb} \cdot \psi'_{r0a} - \psi_{s0a} \cdot \Delta\psi'_{rb} - \Delta\psi_{sa} \cdot \psi'_{r0b}\right) - \Delta m_s \qquad (7.8\text{-}16)$$

$$s \cdot \tau_J \cdot \Delta\breve{\omega}_m \cong \frac{1-\sigma}{\sigma \cdot x_h}\left(\psi_{s0b} \cdot \Delta\breve{\psi}'_{ra} + \psi'_{r0a} \cdot \Delta\breve{\psi}_{sb} - \psi_{s0a} \cdot \Delta\breve{\psi}'_{rb} - \psi'_{r0b} \cdot \Delta\breve{\psi}_{sa}\right) - \Delta\breve{m}_s \qquad (7.8\text{-}17)$$

In the same way stator and rotor voltage equation for small deviations (7.8-12), (7.8-14) are decomposed into *a*-*b*-components, leading to a final linear algebraic set of five equations with five unknowns: $\Delta\breve{\omega}_m, \Delta\breve{\psi}_{sa}, \Delta\breve{\psi}_{sb}, \Delta\breve{\psi}'_{ra}, \Delta\breve{\psi}'_{rb}$, with leading variables $\Delta\breve{\omega}_s, \Delta\breve{u}_{sa}, \Delta\breve{u}_{sb}$ and disturbing variable $\Delta\breve{m}_s$, written as matrix equation.

$$\boxed{(N)\cdot(\Psi) = (U)} \qquad (7.8\text{-}18)$$

Meaning: 5 x 5 system matrix (*N*), 5-dimensional vector of unknowns (Ψ), 5-dimensional vector (*U*) of "right side", containing guiding and disturbing variables. The **induction machine "system response" speed** is got by solving the equation system with *Cramer´*s rule: Replacing the 5th column of matrix (*N*) with vector (*U*) leads to the new matrix (*Z*), leading to

$$\Delta\breve{\omega}_m = \frac{Det(Z)}{Det(N)} = \frac{f(\Delta\breve{u}_{sa}, \Delta\breve{u}_{sb}, \Delta\breve{\omega}_s, \Delta\breve{m}_s)}{P_5(s)} \quad . \qquad (7.8\text{-}19)$$

$$(N) = \begin{pmatrix} s + \frac{r_s}{\sigma \cdot x_s} & -\omega_{s0} & -\frac{r_s(1-\sigma)}{\sigma \cdot x_h} & 0 & 0 \\ \omega_{s0} & s + \frac{r_s}{\sigma \cdot x_s} & 0 & -\frac{r_s(1-\sigma)}{\sigma \cdot x_h} & 0 \\ -\frac{r'_r(1-\sigma)}{\sigma \cdot x_h} & 0 & s + \frac{r'_r}{\sigma \cdot x'_r} & -\omega_{r0} & \psi'_{r0b} \\ 0 & -\frac{r'_r(1-\sigma)}{\sigma \cdot x_h} & \omega_{r0} & s + \frac{r'_r}{\sigma \cdot x'_r} & -\psi'_{r0a} \\ \frac{1-\sigma}{\sigma \cdot x_h}\frac{\psi'_{r0b}}{\tau_J} & -\frac{1-\sigma}{\sigma \cdot x_h}\frac{\psi'_{r0a}}{\tau_J} & -\frac{1-\sigma}{\sigma \cdot x_h}\frac{\psi_{s0b}}{\tau_J} & \frac{1-\sigma}{\sigma \cdot x_h}\frac{\psi_{s0a}}{\tau_J} & s \end{pmatrix} \qquad (7.8\text{-}20)$$

$$(\Psi) = \begin{pmatrix} \Delta\breve{\psi}_{sa} \\ \Delta\breve{\psi}_{sb} \\ \Delta\breve{\psi}'_{ra} \\ \Delta\breve{\psi}'_{rb} \\ \Delta\breve{\omega}_m \end{pmatrix} \qquad (U) = \begin{pmatrix} \Delta\breve{u}_{sa} + \psi_{s0b} \cdot \Delta\breve{\omega}_s \\ \Delta\breve{u}_{sb} - \psi_{s0a} \cdot \Delta\breve{\omega}_s \\ \psi'_{r0b} \cdot \Delta\breve{\omega}_s \\ -\psi'_{r0a} \cdot \Delta\breve{\omega}_s \\ -\frac{\Delta\breve{m}_s}{\tau_J} \end{pmatrix} \qquad (7.8\text{-}21)$$

Det(N) leads to a polynomial expression in *s* of fifth order, the so-called characteristic polynomial with 5 roots as the five poles of the transfer function (7.8-19).

d) Transfer function for typically small motor resistance and frequencies > 0.5·f_N:
Choosing voltage space vector as real: $u_{s0} = u_{s0a}, u_{s0b} = 0$ and investigating transfer function for small deviations

a) from **no-load equilibrium** $\omega_{r0} = 0, \underline{i}'_{r0} = 0$

b) at not **too small stator frequencies** $\omega_{s0} > 0.5...0.6$.

So we can neglect at no-load $r_s << \omega_{s0} x_s$, getting from (7.8-11) with $r_s \approx 0$:

$$u_{s0} = j\omega_{s0}\underline{\psi}_{s0} = jx_s\underline{i}_{s0} \quad \Rightarrow \quad \psi_{s0a} = 0, \psi_{s0b} = -\frac{u_{s0a}}{\omega_{s0}}, i_{s0a} = 0, i_{s0b} = -\frac{u_{s0a}}{\omega_{s0}x_s}$$

$$\underline{\psi}'_{r0} = x_h\underline{i}_{s0} \quad \Rightarrow \quad \psi'_{r0a} = 0, \psi'_{r0b} = -\frac{x_h}{\omega_{s0}x_s}u_{s0a}$$

With **simplifying assumption**

(1) $r_s = r'_r$ and

(2) $x_s = x'_r$

we get identical stator and rotor **short-circuit time constants**:

$$\frac{1}{\tau_{s\sigma}} = \frac{r_s}{\sigma \cdot x_s} = \frac{1}{\tau_{r\sigma}} = \frac{r'_r}{\sigma \cdot x'_r} = \frac{1}{\tau_\sigma} \tag{7.8-22}$$

(3) With **not too small stator frequencies** $r_s << \omega_{s0}x_s$ and

(4) **usually small resistance** $r_s << x_s, r'_r << x'_r$

for calculating deviations from equilibrium we get for denominator of (7.8-19)

$$Det(N) = P_5(s) = (s + \frac{1}{\tau_\sigma}) \cdot \left[\left(s + \frac{1}{\tau_\sigma}\right)^2 + \omega_{s0}^2\right] \cdot \left[\left(s + \frac{1}{2\tau_\sigma}\right)^2 + \omega_{d,m}^2\right] \tag{7.8-23}$$

with **mechanical system natural frequency**

$$\omega_{d,m} = \sqrt{\frac{1}{\tau_J} \cdot \frac{1-\sigma}{\sigma \cdot x_s} \cdot \left(\frac{u_{s0}}{\omega_{s0}}\right)^2 - \frac{1}{(2\tau_\sigma)^2}} \quad , \tag{7.8-24a}$$

$$\Omega_{d,m} = \sqrt{\frac{3p^2}{J} \cdot \frac{1-\sigma}{\sigma \cdot L_s} \cdot \left(\frac{U_{s0}}{\Omega_{s0}}\right)^2 - \frac{1}{(2T_\sigma)^2}} \quad . \tag{7.8-24b}$$

Facit:

The five roots of induction machine electro-mechanical transfer function comprise two pairs of conjugate complex poles and one real pole (Fig. 7.8-2).

$$\begin{aligned} \underline{s}_1 &= -\delta_1 + j\omega_{d,1} \qquad \underline{s}_4 = -\delta_1 - j\omega_{d,1} \\ \underline{s}_3 &= -\delta_3 \\ \underline{s}_2 &= -\delta_2 + j\omega_{d,2} \qquad \underline{s}_5 = -\delta_2 - j\omega_{d,2} \end{aligned} \tag{7.8-25}$$

For our simplifying assumptions the root values are:

$$\begin{aligned} \delta_1 &= \delta_3 = \frac{1}{\tau_\sigma} \qquad \delta_2 = \frac{1}{2\tau_\sigma} \\ \omega_{d,1} &= \omega_{s0} \qquad \omega_{d,2} = \omega_{d,m} \end{aligned} \tag{7.8-26}$$

Inverse *Laplace* transformation of speed deviation due to a small step e.g. of u_{sa} yields

$$\Delta\breve{\omega}_m = \frac{f(\Delta\breve{u}_{sa}, \Delta\breve{u}_{sb}, \Delta\breve{\omega}_s, \Delta\breve{m}_s)}{(s+\frac{1}{\tau_\sigma})\cdot\left[\left(s+\frac{1}{\tau_\sigma}\right)^2+\omega_{s0}^2\right]\cdot\left[\left(s+\frac{1}{2\tau_\sigma}\right)^2+\omega_{d,m}^2\right]} =$$

$$= \frac{\underline{A}(s)}{\left(s+\frac{1}{\tau_\sigma}\right)^2+\omega_{s0}^2} + \frac{\underline{B}(s)}{\left(s+\frac{1}{2\tau_\sigma}\right)^2+\omega_{d,m}^2} + \frac{\underline{C}(s)}{s+\frac{1}{\tau_\sigma}} + \frac{\underline{D}(s)}{s} \quad \Rightarrow \tag{7.8-27}$$

$$\Delta\omega_{m,h}(\tau) = \Delta\omega_{m,1}\cdot e^{-\frac{\tau}{\tau_\sigma}}\cdot\cos(\omega_{s0}\tau+\varphi_1) + \Delta\omega_{m,2}\cdot e^{-\frac{\tau}{2\tau_\sigma}}\cdot\cos(\omega_{d,m}\tau+\varphi_2) + \Delta\omega_{m,3}\cdot e^{-\frac{\tau}{\tau_\sigma}}$$

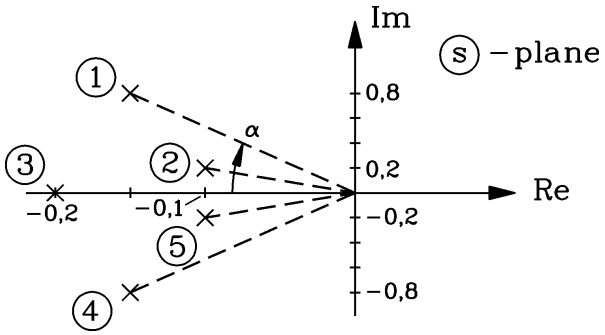

Fig. 7.8-2: The five roots of induction machine electro-mechanical transfer function comprise two pairs of conjugate complex poles and one real pole. The $\tan\alpha$ gives the numbers of half-periods, until natural oscillations have decayed down to 5% of initial value.

Facit:
Disturbances from equilibrium decay with short circuit time constant, thus being ***stable****, if equilibrium is nearly no-load, resistances are small, and stator frequency is not too low. Disturbances oscillate with stator frequency, but also with mechanical system natural frequency. A DC link component occurs, which decays with short circuit time constant.*

Calculation of $\Delta\omega_{m,1}$, $\Delta\omega_{m,2}$, $\Delta\omega_{m,3}$ determines, which of the effects is dominating. Solution of *Det(Z)* is shown in block diagram Fig. 7.8-3.

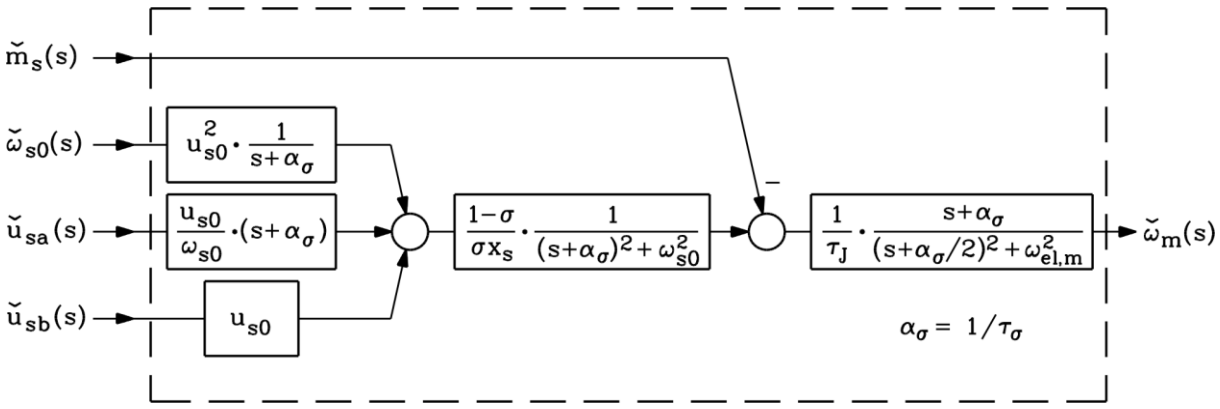

Fig. 7.8-3: Block diagram of induction machine for speed response to small deviations in stator voltage and frequency and load torque from no-load equilibrium (assumptions: small and equal stator and rotor resistance, equal stator and rotor inductance, not too low stator frequency)

Comparing with numerical results of section 7.7 we understand:

- Switching on voltage on machine terminals leads to DC component in current and flux (pole $\underline{s}_3$), which in interaction with steady state current and flux component results in torque and speed oscillation with stator frequency (poles $\underline{s}_1, \underline{s}_4$).
- As rotor flux does not change immediately with stator voltage change, but follows with short circuit time constant, it acts at the first moment of voltage change like "frozen" rotor flux, leading to **"synchronous" machine phenomenon**, causing low frequency change with $\omega_{d,m}$ (poles $\underline{s}_2, \underline{s}_5$).

So with (7.8-24) a simple equation for calculating (7.7-.5) is derived!

Example 7.8-2:
30 kW 4-pole cage induction machine: 400 V Y, 50 Hz, 60.2 A, J = 0.42 kgm^2, T_J = 0.25 s, L_s = 36.5 mH, per unit values: $r_s = r_r' = 0.03, x_s = x_r' = 3.0, \sigma = 0.0667, \tau_J = 75$

$$\tau_{s\sigma} = \tau_{r\sigma} = \frac{\sigma \cdot x_s}{r_s} = \frac{0.0667 \cdot 3}{0.03} = 6.67 \quad T_{s\sigma} = T_{r\sigma} = \tau_{s\sigma} / \omega_N = 6.67/(2\pi 50) = \underline{\underline{21.2}}\,\text{ms}$$

$$\omega_{d,m} = \sqrt{\frac{1}{75} \cdot \frac{1-0.0667}{0.0667 \cdot 3} \cdot \left(\frac{1}{1}\right)^2 - \frac{1}{(2 \cdot 6.67)^2}} = 0.238 \quad f_{d,m} = f_N \cdot \omega_{d,m} = 50 \cdot 0.238 = \underline{\underline{11.9}}\,\text{Hz}$$

or directly

$$f_{d,m} = \frac{\Omega_{d,m}}{2\pi} = \frac{1}{2\pi}\sqrt{\frac{3 \cdot 2^2}{0.42} \cdot \frac{1-0.0667}{0.0667 \cdot 0.0365} \cdot \left(\frac{230}{2\pi 50}\right)^2 - \frac{1}{(2 \cdot 0.0212)^2}} = 11.9\,\text{Hz}$$

e) Transfer function for arbitrary motor resistance and frequencies:
Numerical solution of (7.8-18) shows, that for typical machine parameters and feeding values the characteristic polynomial *Det(N)* comprises also for general case of arbitrary values for resistance and frequency 2 pairs of conjugate complex roots and one real root. Position of the most sensitive conjugate complex pole pair $\underline{s}_{2,5} = -\delta_2 \pm j\omega_{d,2}$ in complex $\underline{s}$-plane is calculated numerically and given in following examples.

Example 7.8-3:
8-pole, three phase cage induction motor, 22 kW, 400 V, Y, 50 Hz, 720/min, efficiency 93%, power factor 0.87, $r_s = 0.03, r_r' = 0.04, x_s = x_r' = 3.0, \sigma = 0.0667, \tau_J = 75.$
Machine is operated **at no-load** from an inverter with **variable stator frequency** ω_{s0}. Only inverter fundamental voltage harmonic u_{s0} is considered. Voltage amplitude is changed $u_{s0} \sim \omega_{s0}$ to keep rotor flux linkage ψ_{r0}' at constant rated value. Numerically calculated $\delta_2(\omega_{s0}), \omega_{d,2}(\omega_{s0})$ is given in Fig. 7.8-4. For rated load values are nearly the same. The other pole values increase with decreasing frequency ω_{s0} from 2.0 down to 0.05:
δ_3 increasing from 0.2 to 0.34, δ_1 increasing from 0.15 to 0.2, ratio $\omega_{d,1} / \omega_{s0}$ increasing from 1.0 to 2.5. Comparison with simple equations of (7.8-26) show:

$$\delta_1 = \delta_3 = \frac{r_s}{\sigma \cdot x_s} = \frac{0.03}{0.0667 \cdot 3} = \underline{\underline{0.15}}$$

$$\delta_2 = \frac{r_s}{2 \cdot \sigma \cdot x_s} = \frac{0.03}{2 \cdot 0.0667 \cdot 3} = \underline{\underline{0.075}}$$

$$\omega_{d,1} / \omega_{s0} = \underline{\underline{1}},\ \omega_{d,2} = \omega_{d,m} = \sqrt{\frac{1}{75} \cdot \frac{1 - 0.0667}{0.0667 \cdot 3} \cdot \left(\frac{1}{1}\right)^2 - 0.075^2} = \underline{\underline{0.238}}$$

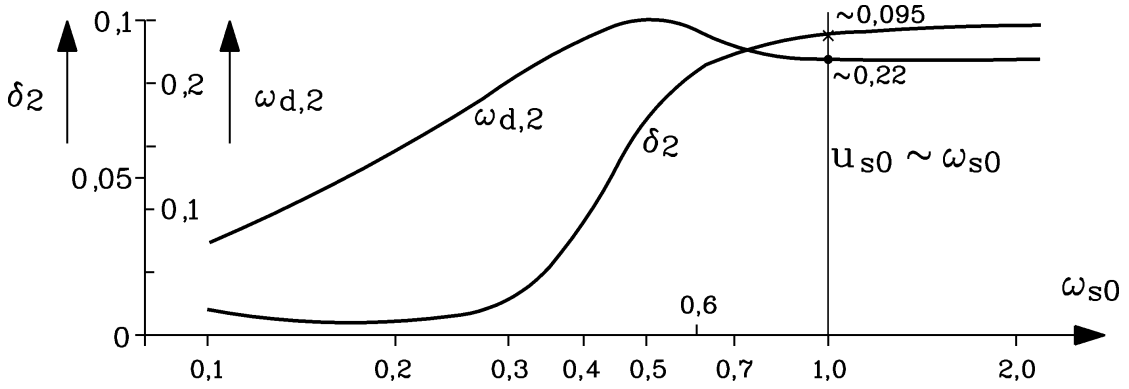

Fig. 7.8-4: Variation of damping δ_2 and natural angular frequency $\omega_{d,2}$ with varying feeding stator frequency and constant rotor flux linkage at rated value, no-load machine operation

Facit:

Simplified equations (7.8-26) are only valid down to stator frequency 60% of rated frequency. At low stator frequencies the damping coefficient gets very small, so induction machines reacts to any change in load torque or disturbance in stator voltage and frequency with long duration of natural oscillation. Natural oscillation frequency decreases with decreasing stator frequency down to below 10% rated frequency. Therefore stability of induction machine, operated by voltage-controlled inverter at low speed, is weak. A speed control is necessary for increased performance of transient response to load steps.

Example 7.8-4:

Motor data from Example 7.8-3:

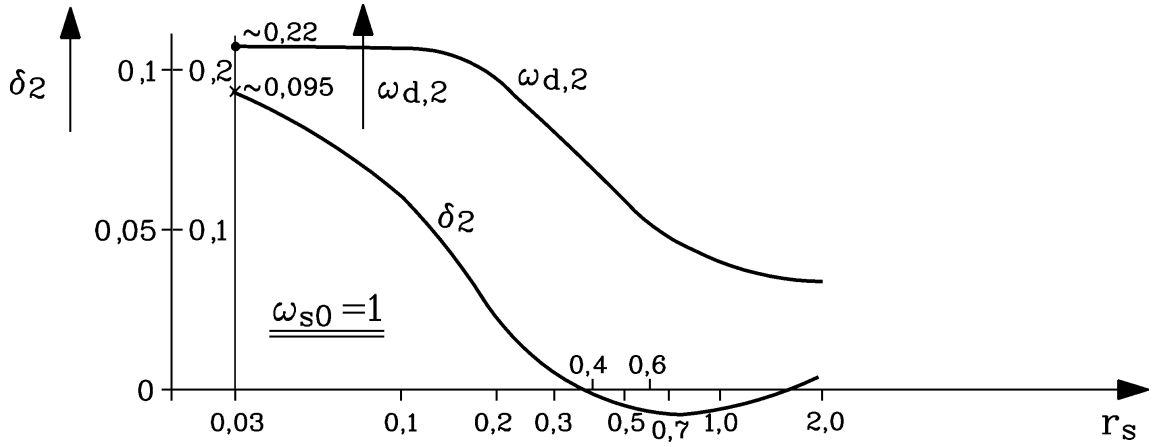

Fig. 7.8-5: Variation of damping δ_2 and natural angular frequency $\omega_{d,2}$ with varying stator resistance at rated stator frequency and constant rotor flux linkage at rated value, no-load machine operation

Machine is operated **at no-load** from grid with **constant stator frequency** $\omega_{s0} = 1$. **Stator resistance r_s varies**, being much increased e.g. by long motor cable between motor and feeding grid terminals. Stator voltage amplitude is increased to compensate stator resistive

voltage drop, so that rotor flux linkage ψ'_{r0} is kept at constant rated value. Numerically calculated $\delta_2(r_s), \omega_{d,2}(r_s)$ is given in Fig. 7.8-5.

Facit:
Between resistance values $0.35 < r_s < 1.8$ *damping is negative,* ***so motor operation gets unstable****. Machine tends to oscillate heavily, thus assumption of small deviations from equilibrium is no longer valid. One has to solve numerically the non-linear set of dynamic equations to get reliable results (see Example 7.8-5). At* ***rated load*** *the damping is also weak, but is still positive, so operation* ***stays stable****.*

f) Numerical solution of non-linear set of dynamic equations ("large signal theory"):
In order to see what happens when machine is operated in unstable conditions, one must return to "large signal theory", as big speed oscillations cannot be treated any longer with small signal theory. This is demonstrated with a numerical example.

Example 7.8-5:
Motor data from Example 7.8-3:
Machine is starting **with no load,** supplied from grid with **constant stator voltage and frequency** $u_{s0} = 1, \omega_{s0} = 1$
a) directly
b) with 13-fold increased stator resistance $r_s = 13 \cdot 0.03 = 0.39$ and by 1/3 reduced rotor inertia: $\tau_J = 75/3 = 25$.

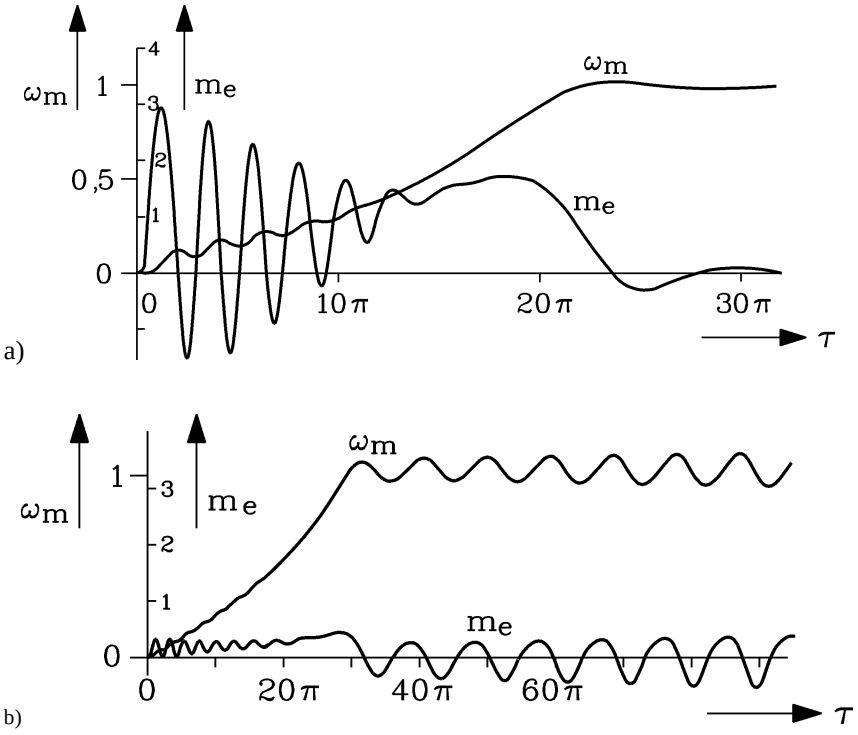

Fig. 7.8-6: Numerically calculated torque and speed during line starting of induction machine a) directly from grid, b) with 13-times additional stator resistance and 0.33 reduced inertia

Facit:
Due to the big voltage drop at stator resistance the torque is reduced to 25%, thus increasing start up time. By reducing inertia to 1/3, increase of start up time is only 50% (30π *instead of*

20π). Torque and speed oscillations due to DC link current component with $f_{d,1} \approx f_N$ *decay in case b) with about 9 grid periods, but amplitude of oscillations with* $f_{d,2} = 11.8\,Hz$ *increase with time due to unstable machine operation at synchronous speed. This amplitude is only limited by non-linear effects in machine.*

7.9 Inverter-fed induction machines with field-oriented control

a) Commonly used inverter systems:

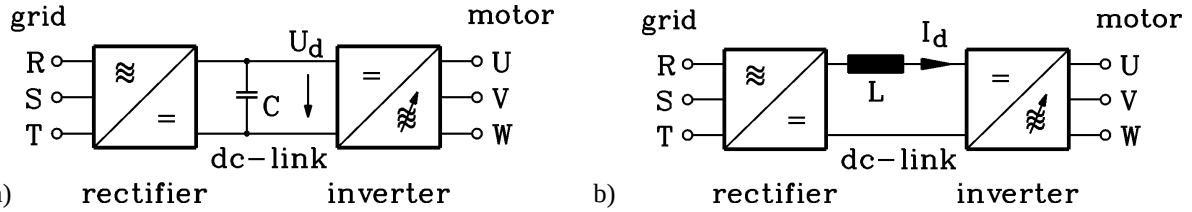

Fig. 7.9-1: Variable speed operation of induction machine with (a) voltage source inverter, (b) current source inverter

Voltage source inverter	***Current source inverter***
DC link capacitor *C*	DC link inductor (choke) *L*
U_d: DC link voltage	I_d: DC link current
motor winding is fed by controlled AC voltage of variable frequency	motor winding is fed by controlled AC current of variable frequency
motor-side inverter operates independently from motor, works also without motor	motor winding is part of motor-side inverter commutation, inverter does not work with disconnected motor
parallel operation of several motors possible	each motor needs a separate inverter
Due to controlled stator voltage motor break down slip is $s_b = \frac{r_r}{\sigma \cdot x_r} = 0.1 \ldots 0.2$. Motor can operate without control within slip range 0 ... s_b	Due to controlled stator current motor break down slip $s_b = \frac{r_r}{x_r} = 0.005 \ldots 0.02$ is very small. Motor is operating in unstable slip range > s_b. Motor control is needed for stable performance.
Stator voltage is pulse width modulated voltage pattern	Stator voltage nearly sinusoidal due to induction by machine flux, which is excited by impressed stator currents
Stator current is smoothened by motor stray inductance to sinusoidal shape with ripple due to voltage switching	Stator current consists of 120° blocks (six step current mode).
Grid side usually diode rectifier, which does not allow power flow to grid, so for electric braking chopped DC link brake resistor is needed. With grid side PWM converter regenerative braking with power flow to grid.	Grid side is converter controlled thyristor bridge for variable rectified voltage U_d for adjusting positive $I_d > 0$. At $U_d < 0$, $\alpha > 90°$ regenerative brake power flow $U_d I_d < 0$ to grid is possible.
With modern IGBTs this inverter type is used in the whole power range 0.1 kW ... 3 MW, low voltage <1k V, and <10 MW, < 6 kV. Bigger power rating with IGCTs or GTOs up to 30 ... 50 MW with medium voltage e.g. 6300 V.	Used for big induction and synchronous motors in MW-range (1 ... 100 MW), thyristor technology. World-wide biggest motor: 100 MW in NASA centre /*Langley/USA* for driving super wind channel for rocket experiments.

Table 7.9-1: Comparison of voltage and current source inverter

Variable speed operation of induction machines is done by inverter operation with variable stator frequency and variable stator voltage amplitude. Today mainly **DC link voltage source inverters** (Fig. 7.9-1a) are used, to generate from e.g. 50 Hz three-phase voltage system of constant amplitude a new motor-side three-phase voltage system of variable frequency and amplitude. A grid-side rectifier and a smoothening DC link capacitor generate a **DC voltage U_d**, which by pulse width modulated chopping (PWM) – done by motor-side inverter – feeds the motor windings, thus generating motor currents of desired frequency and amplitude. For big power also **current source inverters** are available, where in DC link a **DC current I_d** is generated by the rectified line voltage and a big DC link choke L, which is fed to the motor winding via motor-side inverter (Fig. 7.9-1b).

b) Comparison of DC and AC machine control concepts:

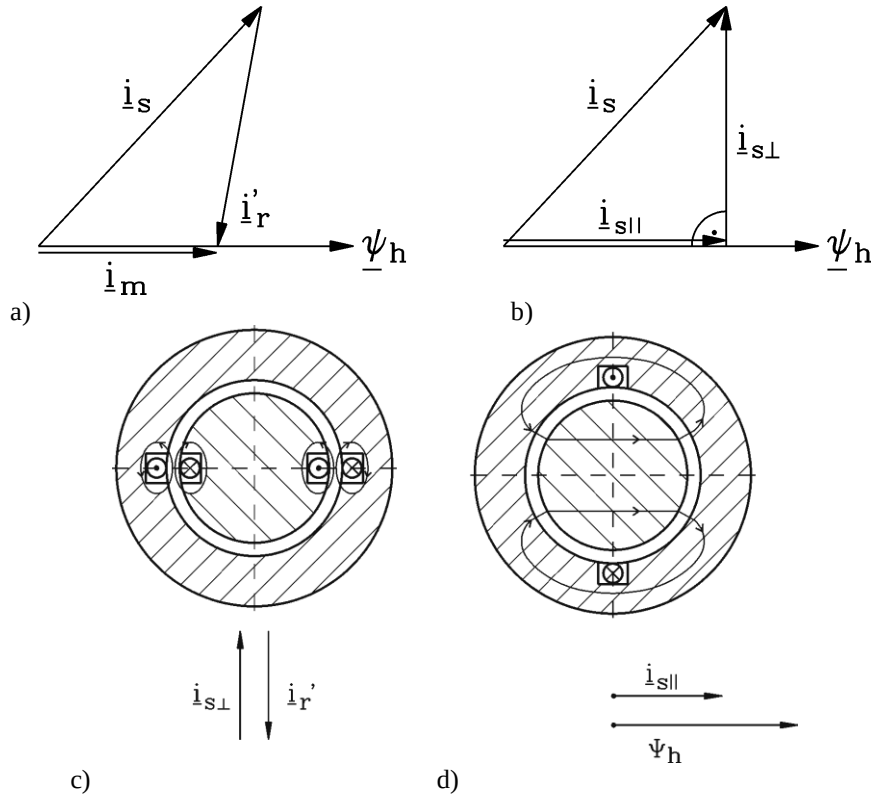

Fig. 7.9-2: Induction machine: a) Main flux excitation by stator and rotor current space vector (= magnetizing current), b) torque generation in induction machine by main flux and perpendicular current component $i_{s\perp}$, c) The load-dependent flux component is mainly a stray flux due to opposing fields, d) The magnetizing flux occurs already at no-load and corresponds to the big main inductance.

With fast switching PWM voltage source inverter dynamic current / torque control is possible. Switching frequency ranges between typically 16 kHz (small inverters in kW-range) down to typically 600 Hz for MW-range. **Speed control** for induction machine requires torque control to cope with changes of load torque. Electromagnetic torque depends on machine main flux, excited by stator and rotor current (= magnetizing current), and stator current (Fig. 7.9-2). To change torque, main flux or perpendicular current component $i_{s\perp}$ have to be changed.

Change of flux linkage AND of stator current is possible by changing voltage amplitude and frequency $\underline{u}_s = r_s \underline{i}_s + \frac{d\underline{\psi}_s}{d\tau}$. By changing stator flux both main and stray flux are changed at

the same time $\underline{\psi}_s = x_s \cdot \underline{i}_s + x_h \cdot \underline{i}'_r = \underline{\psi}_{s\sigma} + \underline{\psi}_h$. Long open circuit time constant for changing main flux is x_s / r_s yields rather **low dynamic performance** of torque control.

Improved dynamic control is possible by changing only perpendicular current space vector component. Only parallel component $\underline{i}_{s=}$ contributes to main flux magnetization, so perpendicular component $\underline{i}_{s\perp}$ excites only stray flux linkage, which changes with much shorter **short-circuit time constant** $\sigma \cdot x_s / r_s$. Therefore *Blaschke* and *Hasse* proposed at the same time a **field-oriented control algorithm**: From voltage and current measurement together with known machine parameters current and flux linkage space vector are determined. Current space vector is "oriented" at flux linkage space vector position, e.g. it is decomposed into parallel and perpendicular component. With dynamic space vector equations it is calculated, how stator voltage space vector has to be changed, so that only $\underline{i}_{s\perp}$ is changed, whereas $\underline{i}_{s=}$ is kept constant in order to keep $\underline{\psi}_h$ constant.

Facit:
With field oriented control – done by micro-controlled inverter operation - it is possible to operate the robust cage induction machine with at least the same dynamic speed and torque performance as silicon-controlled separately excited DC machines. As DC machines are mechanically sensitive due to the commutator, the wound rotor armature and the brush contact, they cannot reach such high speeds as induction machines. Moreover the brush wear requires maintenance. The commutator increases rotor inertia, so the lower cage rotor inertia allows higher dynamic performance. Losses in inter-pole and (in bigger DC machines) compensations windings as well as in brush contact yield lower DC machine efficiency, so induction machines show lower losses and therefore increased torque/mass ratio. For all these reasons modern variable speed drives are inverter-fed induction machine drives.

Type of machine	***DC machine***	***Cage induction machine***
Control	Armature voltage control	Field oriented control
Guiding variable	Armature voltage	Stator voltage
Fixed main flux	Separately excited main flux Φ	Main flux linkage ψ_h
Magnetizing current	Field current i_f	Magnetizing current i_m
Flux time constant	Field time constant L_f/R_f	Open-circuit time constant x_s / r_s
Torque changed by	Armature current i_a	Flux-perpendicular current space vector component $\underline{i}_{s\perp}$
Time constant for torque change	Armature time constant L_a/R_a	Short-circuit time constant $\sigma \cdot x_s / r_s$

Table 7.9-2: Comparison of speed control of DC and AC induction machine

c) Space vector formulation of field orientation with rotor flux linkage:
Often the rotor flux linkage $\underline{\psi}'_r$ is used for the field orientation of the stator current space vector $\underline{i}_s$ in the "rotor flux reference frame" (K), rotating with $\omega_r + \omega_m = \omega_s$, which at steady state is the synchronous reference frame (syn), where space vectors $\underline{u}_s$, $\underline{i}_s$, $\underline{\psi}_s$, $\underline{i}'_r$, $\underline{\psi}'_r$ at sinusoidal operation with stator frequency ω_s are constant, non-rotating complex numbers. The torque equation (7.4-15) $m_e = \mathrm{Im}(x_h \cdot \underline{i}_s \cdot \underline{i}_r^*)$ resp. $m_e = (x_h / x'_r) \cdot \mathrm{Im}(\underline{i}_s \cdot \underline{\psi}'^*_r)$ is due to $\underline{i}_{s(K)} \cdot \underline{\psi}'^*_{r(K)} = \underline{i}_{s(s)} \cdot e^{-j\cdot\delta} \cdot (\underline{\psi}'_{r(s)} \cdot e^{-j\cdot\delta})^* = \underline{i}_{s(s)} \cdot \underline{\psi}'^*_{r(s)}$ independent of the reference frame. Transforming the measured $\underline{i}_s$ from stator into "rotor flux reference frame" with a- and

b-components $\underline{i}_{s(syn)} = \underline{i}_{s(s)} \cdot e^{-j\cdot\delta}$, $\delta = \int \omega_s(\tau)\cdot d\tau + \delta_0$, $\underline{i}_{s(syn)} = i_{s,a} + j\cdot i_{s,b}$, $\underline{i}_{s(syn)}$ is decomposed into rotor-flux-parallel and rotor-flux–perpendicular components $i_{s=}, i_{s\perp}$. Skipping in the following the subscript (syn) and putting $\underline{\psi}'_r = \psi'_{r,a} + j\cdot\psi'_{r,b} = \psi'_r$ into the real axis (a), we get $i_{s,a} = i_{s=}$, $i_{s,b} = i_{s\perp}$ and $\underline{\psi}'^{*}_r = \psi'_r$. With $\underline{i}_s = i_{s=} + j\cdot i_{s\perp}$ the torque is

$$m_e = (x_h / x'_r)\cdot \mathrm{Im}((i_{s,a} + j\cdot i_{s,b})\cdot\psi'_r) = (x_h / x'_r)\cdot i_{s,b}\cdot\psi'_{r,a} = (x_h / x'_r)\cdot i_{s\perp}\cdot\psi'_r \ . \qquad (7.9\text{-}1)$$

So we have to show that $i_{s,b} = i_{s\perp}$ may be changed very fast to get a dynamic change of torque. The determination of the rotor flux linkage space vector from (7.9-2) via e. g. the measured $\underline{i}_s$, measured rotor speed ω_m and known machine parameters yields with the elimination of $\underline{i}'_r$ the 1st order ordinary differential equation (7.9-3).

$$0 = r'_r\underline{i}'_r + \frac{d\underline{\psi}'_r}{d\tau} + j\cdot(\omega_s - \omega_m)\cdot\underline{\psi}'_r, \quad \underline{\psi}'_r = x_h\cdot\underline{i}_s + x'_r\cdot\underline{i}'_r = \psi'_r \qquad (7.9\text{-}2)$$

$$\frac{d\psi'_r}{d\tau} + \left[\frac{r'_r}{x'_r} + j\cdot(\omega_s - \omega_m)\right]\cdot\psi'_r = \frac{r'_r\cdot x_h}{x'_r}\cdot\underline{i}_s = \frac{r'_r\cdot x_h}{x'_r}\cdot(i_{s,a} + j\cdot i_{s,b}) \qquad (7.9\text{-}3)$$

With the rotor open-circuit time constant $\tau_r = x'_r / r'_r$ and field-oriented decomposition of the stator current space vector in (7.9-3) we get (7-9-4) with the definition $\omega_s - \omega_m = Slip\cdot\omega_s$.

$$\frac{d\psi'_r}{d\tau} + \frac{1}{\tau_r}\cdot\psi'_r = \frac{x_h}{\tau_r}\cdot i_{s,=}, \qquad (\omega_s - \omega_m)\cdot\psi'_r = \frac{x_h}{\tau_r}\cdot i_{s,\perp} \text{ or } \quad Slip\cdot\omega_s\cdot\psi'_r = \frac{x_h}{\tau_r}\cdot i_{s,\perp} \qquad (7.9\text{-}4)$$

Facit:
The rotor flux linkage is changed rather slowly by the flux-parallel component of stator current space vector $i_{s,a} = i_{s=}$ via the long rotor open-circuit time constant (low dynamic performance), so it is kept constant. The flux-perpendicular component $i_{s,b} = i_{s\perp}$ directly affects the slip and therefore the steady state torque $m_e = f(Slip)$, which for slip values up to twice rated slip holds $m_e \sim Slip$. According to (7.9-1) a fast change of $i_{s,b} = i_{s\perp}$ is needed for a dynamic change of torque at constant rotor flux linkage.

A dynamic change of the stator current by the stator voltage is calculated with the stator voltage equation in (syn)-reference frame (7.8-5), which, with $\underline{\psi}'_r = \psi'_r$ and combined with stator flux linkage equation (7.5-4) $\underline{\psi}_s = \sigma\cdot x_s\cdot\underline{i}_s + (x_h / x'_r)\cdot\psi'_r$, yields

$$\sigma\cdot x_s\frac{d\underline{i}_s}{d\tau} + (r_s + j\omega_s\cdot\sigma\cdot x_s)\cdot\underline{i}_s = \underline{u}_s - \frac{x_h}{x'_r}\cdot\frac{d\psi'_r}{d\tau} - j\cdot\omega_s\cdot\frac{x_h}{x'_r}\cdot\psi'_r \ . \qquad (7.9\text{-}5)$$

With the rotor voltage equation (7.9-3) $d\psi'_r / d\tau$ is substituted.

$$\sigma\cdot x_s\frac{d\underline{i}_s}{d\tau} + \left(r_s + \frac{(1-\sigma)\cdot x_s}{\tau_r} + j\omega_s\cdot\sigma\cdot x_s\right)\cdot\underline{i}_s = \underline{u}_s + \frac{x_h}{x'_r}\cdot\left(\frac{1}{\tau_r} - j\cdot\omega_m\right)\cdot\psi'_r \ . \qquad (7.9\text{-}6)$$

With the stator and rotor short-circuit time constants

$$\tau_{s\sigma} = \sigma \cdot x_s / r_s = \sigma \cdot \tau_s \ , \ \tau_{r\sigma} = \sigma \cdot x'_r / r'_r = \sigma \cdot \tau_r \tag{7.9-7}$$

and decomposition of (7.9-6) into field-oriented components, the stator voltage equation is

$$\frac{di_{s,=}}{d\tau} + \left(\frac{1}{\tau_{s\sigma}} + \frac{1-\sigma}{\tau_{r\sigma}} \right) \cdot i_{s,=} - \omega_s \cdot i_{s,\perp} = \frac{u_{s,=}}{\sigma \cdot x_s} + (1-\sigma) \cdot \frac{\psi'_r}{\tau_{r\sigma} \cdot x_h} \quad , \tag{7.9-8}$$

$$\frac{di_{s,\perp}}{d\tau} + \left(\frac{1}{\tau_{s\sigma}} + \frac{1-\sigma}{\tau_{r\sigma}} \right) \cdot i_{s,\perp} + \omega_s \cdot i_{s,=} = \frac{u_{s,\perp}}{\sigma \cdot x_s} - (1-\sigma) \cdot \frac{\omega_m}{\sigma \cdot x_h} \cdot \psi'_r \quad , \tag{7.9-9}$$

with the short "resulting" time constant

$$\tau_\sigma = \frac{1}{\frac{1}{\tau_{s\sigma}} + \frac{1-\sigma}{\tau_{r\sigma}}} \approx \frac{1}{\frac{1}{\tau_{s\sigma}} + \frac{1}{\tau_{r\sigma}}} \approx \frac{1}{\frac{2}{\tau_{s\sigma}}} = \frac{\tau_{s\sigma}}{2} \ . \tag{7.9-10}$$

At constant rotor flux operation $d\psi'_r / d\tau = 0$, (7.9-4) yields $i_{s,=} = \psi'_r / x_h$, and (7.9-9) gives

$$\frac{di_{s,\perp}}{d\tau} + \frac{i_{s,\perp}}{\tau_\sigma} = \frac{u_{s,\perp}}{\sigma \cdot x_s} - (1-\sigma) \cdot \frac{\omega_m \cdot \psi'_r}{\sigma \cdot x_h} + \omega_s \cdot i_{s,=} = \frac{u_{s,\perp}}{\sigma \cdot x_s} - \underbrace{(1 - Slip \cdot (1-\sigma))}_{\approx 1} \cdot \frac{\omega_s \cdot \psi'_r}{\sigma \cdot x_h} .$$

Facit:
The flux-perpendicular component of the voltage space vector $u_{s,\perp}$ changes at constant rotor flux linkage $\psi'_r = \text{const.}$ the flux-perpendicular current space vector component $i_{s,\perp}$ via the "50% short-circuit time constant" τ_σ fast, thus changing the torque $m_e = (x_h / x'_r) \cdot i_{s\perp} \cdot \psi'_r$ fast.

For further details on the "field oriented control" see the lecture **"Control of drives"**.
Note that for stationary operation $d./d\tau = 0$ at a given voltage u_s the steady state torque-slip-relationship is derived, as given in the lecture **"Electrical machines and Drives"**. This is proven with $\underline{\psi}'_r = \psi'_r$ for the simplification $r_s = 0$, getting *Kloss* function (7.9-16) for m_e. From (7.9-2) follows then

$$0 = r'_r \underline{i}'_r + \underbrace{\frac{d\psi'_r}{d\tau}}_{=0} + j \cdot \underbrace{(\omega_s - \omega_m)}_{Slip \cdot \omega_s} \cdot \psi'_r \Rightarrow 0 = r'_r \cdot (i'_{ra} + j \cdot i'_{rb}) + j \cdot Slip \cdot \omega_s \cdot \psi'_r \quad ,$$

$$i'_{ra} = 0, \quad i'_{rb} = -Slip \cdot \omega_s \cdot \psi'_r / r'_r \ . \tag{7.9-11}$$

The rotor flux linkage (7.9-2) yields

$$\psi'_r = x_h \cdot (i_{sa} + j \cdot i_{sb}) + x'_r \cdot i'_{rb} \Rightarrow \psi'_r = x_h \cdot i_{sa}, \ i'_{rb} = -(x_h / x'_r) \cdot i_{sb} \ . \tag{7.9-12}$$

The stator voltage equation (7.8-5) and the stator flux linkage $\underline{\psi}_s = x_s \cdot \underline{i}_s + x_h \cdot \underline{i}'_r$ yield

$$\underline{u}_s = \underbrace{r_s \underline{i}_s}_{=0} + \underbrace{\frac{d\underline{\psi}_s}{d\tau}}_{=0} + j\cdot\omega_s\cdot\underline{\psi}_s = j\cdot\omega_s\cdot\underline{\psi}_s = j\cdot\omega_s\cdot(x_s\cdot(i_{sa}+j\cdot i_{sb})+x_h\cdot j\cdot i'_{rb}) = u_{sa}+j\cdot u_{sb} \quad ,$$

which gives with (7.9-12) for the real and imaginary component u_{sa}, u_{sb} via

$$u_{sa} = -\omega_s\cdot x_s\cdot i_{sb} - \omega_s\cdot x_h\cdot i'_{rb} = -\omega_s\cdot x_s\cdot i_{sb} - \omega_s\cdot x_h\cdot(-(x_h/x'_r)\cdot i_{sb}) = -\omega_s\cdot\sigma\cdot x_s\cdot i_{sb}:$$

$$u_{sa} = -\omega_s\cdot\sigma\cdot x_s\cdot i_{sb} \;,\quad u_{sb} = \omega_s\cdot x_s\cdot i_{sa} \;. \tag{7.9-13}$$

From (7.9-11) $i'_{rb} = -Slip\cdot\omega_s\cdot\psi'_r/r'_r$ and (7.9-12) $\psi'_r = x_h\cdot i_{sa}, i'_{rb} = -(x_h/x'_r)\cdot i_{sb}$ we get

$$i_{sb} = (Slip\cdot\omega_s\cdot x'_r/r'_r)\cdot i_{sa} \quad , \tag{7.9-14}$$

and for the given voltage u_s with (7.9-13) and (7.9-14) in dependence of i_{sa}

$$u_s^2 = u_{sa}^2 + u_{sb}^2 = \omega_s^2\cdot x_s^2\cdot(\sigma^2\cdot(Slip\cdot x'_r/r'_r)^2+1)\cdot i_{sa}^2 \;. \tag{7.9-15}$$

The torque $m_e = \mathrm{Im}(x_h\cdot\underline{i}_s\cdot\underline{i}_r^*) = \mathrm{Im}(x_h\cdot(i_{sa}+j\cdot i_{sb})\cdot(j\cdot i'_{rb})^*)) = -x_h\cdot i_{sa}\cdot i'_{rb}$ is with (7.9-12) and (7.9-14)

$$m_e = -x_h\cdot i_{sa}\cdot i'_{rb} = (x_h^2/x'_r)\cdot i_{sa}\cdot i_{sb} = (x_h^2/x'_r)\cdot(Slip\cdot\omega_s\cdot x'_r/r'_r)\cdot i_{sa}^2 = (x_h^2\cdot Slip\cdot\omega_s/r'_r)\cdot i_{sa}^2 \;,$$

and with (7.9-15)

$$m_e = \frac{u_s^2\cdot x_h^2\cdot Slip\cdot\omega_s/r'_r}{\omega_s^2\cdot x_s^2\cdot(\sigma^2\cdot(Slip\cdot\omega_s\cdot x'_r/r'_r)^2+1)} = \frac{(1-\sigma)\cdot u_s^2}{2\sigma\cdot\omega_s^2\cdot x_s}\cdot\frac{2\cdot Slip\cdot\omega_s\cdot\dfrac{r'_r}{\sigma\cdot x'_r}}{((Slip\cdot\omega_s)^2+(\dfrac{r'_r}{\sigma\cdot x'_r})^2)} \;.$$

With the rotor angular frequency $\omega_r = Slip\cdot\omega_s$ and the corresponding "breakdown" value $\omega_{rb} = r'_r/(\sigma\cdot x'_r)$ finally *Kloss* function is derived in dependence of $\omega_r = Slip\cdot\omega_s$.

$$m_e = \frac{(1-\sigma)\cdot u_s^2}{2\sigma\cdot\omega_s^2\cdot x_s}\cdot\frac{2}{\dfrac{\omega_r}{\omega_{rb}}+\dfrac{\omega_{rb}}{\omega_r}} \quad , \tag{7.9-16}$$

with the stationary breakdown torque $m_{b,stat} = \dfrac{(1-\sigma)\cdot u_s^2}{2\sigma\cdot\omega_s^2\cdot x_s}$.

d) Determination of rotor flux linkage for field oriented control:
In order to perform field-oriented control, the actual rotor flux linkage must be known to decompose the stator current space vector into both flux-oriented components. The rotor flux linkage can be determined either
(i) from stator current and voltage measurement or
(ii) from stator current and rotor speed measurement.

(i) Rotor flux linkage space vector determination from stator current and voltage:
In star-connected stator windings we always have $i_U + i_V + i_W = 0$. By measuring two line-to-line voltages u_{UW}, u_{VW} with voltage dividers and two phase currents i_U, i_V with shunts or DC current clamps (Fig. 7.9-3a) one gets the stator voltage space vector from

$$\left.\begin{aligned} \underline{u}_s &= \frac{2}{3}\cdot\left(u_U + \underline{a}\cdot u_V + \underline{a}^2\cdot u_W\right) \\ 0 &= \frac{2}{3}\cdot\left(u_W + \underline{a}\cdot u_W + \underline{a}^2\cdot u_W\right) \end{aligned}\right\} - \qquad (7.9\text{-}17)$$

$$\underline{u}_s = \frac{2}{3}\cdot\left(u_U - u_W + \underline{a}\cdot(u_V - u_W)\right) = \underline{\underline{\frac{2}{3}\cdot\left(u_{UW} + \underline{a}\cdot u_{VW}\right)}}$$

and the current space vector from

$$\underline{i}_s = \frac{2}{3}\cdot\left(i_U + \underline{a}\cdot i_V + \underline{a}^2\cdot i_W\right) = \underline{\underline{\frac{2}{3}\cdot\left(i_U\cdot(1-\underline{a}^2) + i_V\cdot(\underline{a}-\underline{a}^2)\right)}} \qquad (7.9\text{-}18)$$

From the stator voltage equation and flux linkage equation in stator reference frame the rotor flux linkage space vector is derived.

$$\left.\begin{aligned} \underline{u}_s &= r_s\underline{i}_s + d\underline{\psi}_s/d\tau \\ \underline{\psi}_s &= x_s\underline{i}_s + x_h\underline{i}'_r \\ \underline{\psi}'_r &= x_h\underline{i}_s + x'_r\underline{i}'_r \end{aligned}\right\} \Rightarrow \underline{\psi}_s = \frac{x_h}{x'_r}\cdot\underline{\psi}'_r + \sigma\cdot x_s\cdot\underline{i}_s \quad \Rightarrow \underline{\underline{\frac{d\underline{\psi}'_r}{d\tau} = \left(\underline{u}_s - r_s\cdot\underline{i}_s - \sigma\cdot x_s\cdot\frac{d\underline{i}_s}{d\tau}\right)\cdot\frac{x'_r}{x_h}}}$$

(7.9-19)

Facit:
With known machine parameters r_s, x_s, x_h, x'_r (from measurement or calculation) the rotor flux linkage space vector is evaluated by direct integration of stator voltage and current space vector and its derivative. In inverter fed drive the stator voltage varies with stator frequency and speed $u_s \sim \omega_s \sim n$, so at high speed the voltage is big and can be measured with high accuracy. At very low speed the voltage is very low. Measurement errors such as offset or noise will be integrated to big values, so at low speed method (i) is NOT useful.

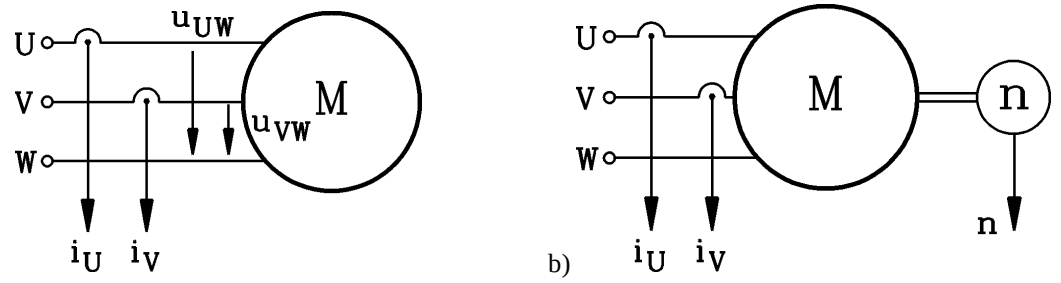

Fig. 7.9-3: Determination of rotor flux linkage space vector a) from stator voltage and current measurement, b) from stator current and rotor speed measurement

(ii) Rotor flux linkage space vector determination from stator current and speed:
This method is very useful also at low speed, but needs an additional rotor speed sensor *n* (Fig. 7.9-3b). Mechanical per unit angular speed is calculated from measured rotor speed *n* by

$$\omega_m = \frac{2\pi \cdot n}{\omega_N / p} \quad . \tag{7.9-20}$$

The measured stator current space vector is transformed into **rotor reference frame** by $\underline{i}_{s(r)} = \underline{i}_{s(s)} \cdot e^{-j \cdot \omega_m \tau}$. The rotor flux linkage space vector is determined in the rotor reference frame with the rotor voltage equation, substituting the rotor current with the rotor flux linkage equation:

$$\left.\begin{aligned} 0 &= r'_{r(r)} \underline{i}'_{r(r)} + d\underline{\psi}'_{r(r)} / d\tau \\ \underline{\psi}'_{r(r)} &= x_h \cdot \underline{i}_{s(r)} + x'_r \cdot \underline{i}'_{r(r)} \end{aligned}\right\} \Rightarrow \quad \underline{\underline{\frac{d\underline{\psi}'_{r(r)}}{d\tau} + \frac{1}{\tau_r} \cdot \underline{\psi}'_{r(r)} = \frac{x_h}{\tau_r} \cdot \underline{i}_{s(r)}}} \tag{7.9-21}$$

Facit:
The rotor flux linkage is derived by integrating the stator current space vector via the rotor open-circuit time constant $\tau_r = x'_r / r'_r$. Due to this PT_1-performance no integration error will occur, so the rotor flux linkage may be determined at any arbitrary speed, e.g. also at n = 0. Machine parameters r'_r, x_h, x'_r must be known. Disadvantage of method (ii) is, that in cage induction machines it is difficult to determine on-line the rotor resistance, which may change between 20°C and e. g. 150°C by 50 %. Usually the stator winding temperature is measured and the rotor cage temperature is estimated from this value via a simple thermal model of the machine (see Chapter 3).

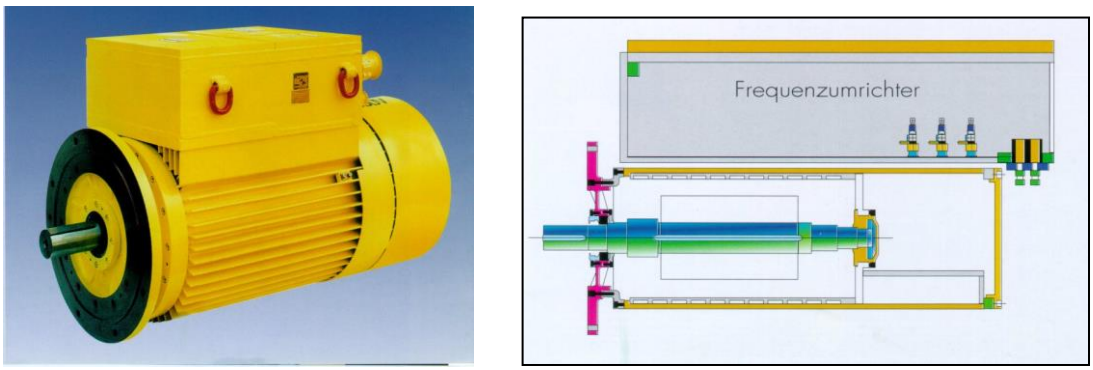

Fig. 7.9-4: Inverter-operated cage induction motor (left) with flange mounting. The inverter is situated within the enlarged motor terminal box on top of the motor (right: cross section of motor and inverter), *Breuer, Germany*.

a) 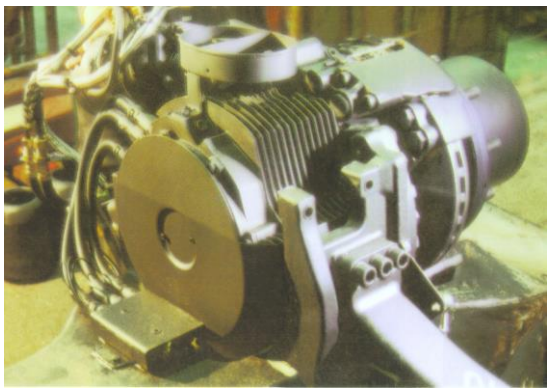

b) 

Fig. 7.9-5: Two different types of inverter-fed induction motors as wheel-hub drives (a) *Daimler-Chrysler, Stuttgart*, b) *Oswald, Miltenberg*) for fuel-cell powered electric busses.

7.10 Appendix: Space vector power balance in the induction machine

The real instantaneous electrical power in physical units and in per unit values, fed into the induction machine, is given as the sum of stator and rotor power.

$$P_e(t) = (3/2)\cdot \mathrm{Re}\left\{\underline{U}_s(t)\cdot \underline{I}_s^*(t) + \underline{U}'_r(t)\cdot \underline{I}'^*_r(t)\right\} \tag{7.10-1}$$

$$p_e = \frac{P_e}{\frac{3}{2}\cdot\sqrt{2}U_{N,ph}\sqrt{2}I_{N,ph}} = \frac{\frac{3}{2}\cdot \mathrm{Re}\left\{\underline{U}_s\cdot \underline{I}_s^* + \underline{U}'_r\cdot \underline{I}'^*_r\right\}}{\frac{3}{2}\cdot\sqrt{2}U_{N,ph}\sqrt{2}I_{N,ph}} = \mathrm{Re}\left\{\underline{u}_s\cdot \underline{i}_s^* + \underline{u}'_r\cdot \underline{i}'^*_r\right\} \tag{7.10-2}$$

Putting the stator reference frame equations $\underline{\psi}_s = x_{s\sigma}\cdot\underline{i}_s + x_h\cdot\underline{i}_m$, $\underline{\psi}'_r = x_h\cdot\underline{i}_m + x'_{r\sigma}\cdot\underline{i}'_r$, $\underline{u}_s = r_s\cdot\underline{i}_s + \frac{d\underline{\psi}_s}{d\tau}$, $\underline{u}'_r = r'_r\cdot\underline{i}'_r + \frac{d\underline{\psi}'_r}{d\tau} - j\cdot\omega_m\cdot\underline{\psi}'_r$ into (7.10-2), the input power – in p.u. - is split up into I^2R-losses $p_{\mathrm{Cu,s}}$ and $p_{\mathrm{Cu,r}}$, change of magnetic energy w_{mag} and mechanical power.

$$p_e(\tau) = \mathrm{Re}\left\{(r_s\cdot\underline{i}_s + \frac{d\underline{\psi}_s}{d\tau})\cdot\underline{i}_s^* + (r'_r\cdot\underline{i}'_r + \frac{d\underline{\psi}'_r}{d\tau} - j\cdot\omega_m\cdot\underline{\psi}'_r)\cdot\underline{i}'^*_r\right\} =$$

$$= \mathrm{Re}\left\{r_s|\underline{i}_s|^2 + r'_r|\underline{i}'_r|^2 + x_{s\sigma}\underline{i}_s^*\frac{d\underline{i}_s}{d\tau} + x'_{r\sigma}\underline{i}'^*_r\frac{d\underline{i}'_r}{d\tau} + (x_h\underline{i}_s^* + x_h\underline{i}'^*_r)\frac{d\underline{i}_m}{d\tau} - j\cdot\omega_m\cdot\underline{\psi}'_r\cdot\underline{i}'^*_r\right\} =$$

$$= r_s|\underline{i}_s|^2 + r'_r|\underline{i}'_r|^2 + \mathrm{Re}\left\{x_{s\sigma}\underline{i}_s^*\frac{d\underline{i}_s}{d\tau} + x'_{r\sigma}\underline{i}'^*_r\frac{d\underline{i}'_r}{d\tau} + x_h\underline{i}_m^*\frac{d\underline{i}_m}{d\tau} - j\cdot\omega_m\cdot\underline{\psi}'_r\cdot\underline{i}'^*_r\right\} =$$

$$= p_{Cu,s} + p_{Cu,r} + \mathrm{Re}\left\{x_{s\sigma}\frac{d(\underline{i}_s\underline{i}_s^*)}{2\cdot d\tau} + x'_{r\sigma}\frac{d(\underline{i}'_r\underline{i}'^*_r)}{2\cdot d\tau} + x_h\frac{d(\underline{i}_m\underline{i}_m^*)}{2\cdot d\tau} - j\cdot\omega_m\cdot\underline{\psi}'_r\cdot\underline{i}'^*_r\right\}$$

With the help of the relation $\mathrm{Re}\left\{\underline{z}^*(\tau)\cdot d\underline{z}(\tau)/d\tau\right\} = (1/2)\cdot d|\underline{z}(\tau)|^2/d\tau$ we get:

$$\mathrm{Re}\left\{x_{s\sigma}\frac{d(\underline{i}_s\underline{i}_s^*)}{2\cdot d\tau} + x'_{r\sigma}\frac{d(\underline{i}'_r\underline{i}'^*_r)}{2\cdot d\tau} + x_h\frac{d(\underline{i}_m\underline{i}_m^*)}{2\cdot d\tau}\right\} = x_{s\sigma}\frac{d|\underline{i}_s|^2}{2\cdot d\tau} + x'_{r\sigma}\frac{d|\underline{i}'_r|^2}{2\cdot d\tau} + x_h\frac{d|\underline{i}_m|^2}{2\cdot d\tau} =$$

$$= \frac{d}{d\tau}\left\{x_{s\sigma}\frac{|\underline{i}_s|^2}{2} + x'_{r\sigma}\frac{|\underline{i}'_r|^2}{2} + x_h\frac{|\underline{i}_m|^2}{2}\right\} = \frac{dw_{mag}(\tau)}{d\tau}$$

Proof: With $\underline{z}(\tau) = x(\tau) + jy(\tau)$ we get:

$$(1/2)\cdot d|\underline{z}(\tau)|^2/d\tau = (1/2)\cdot d(x^2+y^2)/d\tau = x\cdot dx/d\tau + y\cdot dy/d\tau = x\cdot\dot{x} + y\cdot\dot{y} =$$

$$= \mathrm{Re}\left\{x\cdot\dot{x} + y\cdot\dot{y} - j\cdot y\cdot\dot{x} + j\cdot\dot{y}\cdot x\right\} = \mathrm{Re}\left\{(x-jy)(\dot{x}+j\dot{y})\right\} = \mathrm{Re}\left\{\underline{z}^*\cdot d\underline{z}/d\tau\right\}$$

So the power balance is

$$\begin{aligned} p_e(\tau) &= p_{Cu,s} + p_{Cu,r} + dw_{mag}/d\tau - \mathrm{Re}\left\{j\cdot\omega_m\cdot\underline{\psi}'_r\cdot\underline{i}'^*_r\right\} = \\ &= p_{Cu,s} + p_{Cu,r} + dw_{mag}/d\tau + \mathrm{Im}\left\{\omega_m\cdot\underline{\psi}'_r\cdot\underline{i}'^*_r\right\} = p_{Cu,s} + p_{Cu,r} + dw_{mag}/d\tau + p_m \end{aligned} \tag{7.10-3}$$

Hence the electromagnetic torque is given as

$$m_e(\tau) = p_m / \omega_m = \mathrm{Im}\left\{\underline{\psi}'_r \cdot \underline{i}'^{*}_r\right\} = -\mathrm{Im}\left\{\underline{i}'_r \cdot \underline{\psi}'^{*}_r\right\} \quad , \qquad (7.10\text{-}4)$$

which coincides with the expression of (7.4-16).

Facit:
The power balance shows that the electrical input power (motor operation) is consumed for one part as losses in the stator and rotor circuit, for a second part to change the magnetic energy and finally one part to be transformed into mechanical power. Hence the electromagnetic torque may be derived either directly from the Lorentz forces, as shown in section 7.4 or directly from the power balance, as shown in (7.10-4).

8. Dynamics of synchronous machines

8.1 Basics of steady state and significance of dynamic performance of synchronous machines

a) Steady state operation:
Synchronous machines consist of a **rotor with a constant rotor flux**, excited either
- by a field winding with a DC current I_f (Fig. 8.1-1a) or
- by permanent magnets (Fig. 8.1-2a).

The electrically excited synchronous machine usually gets the field current I_f via a plus and minus slip ring from an external DC voltage source such as a controlled B6C rectifier bridge (Fig. 8.1-1b) to adjust the rotor flux to the desired value. In permanent magnet synchronous machines no rotor flux adjustment is possible. The stator of synchronous machines consists of **three phase stator AC winding** like in the induction machine, where a three phase current system excites a synchronously rotating magnetic stator field:

$$\Omega_{syn} = \frac{2\pi \cdot f_s}{p} \tag{8.1-1}$$

If the stator currents are supplied from the grid voltage, the stator field drags the rotor synchronously with mechanical speed equal to synchronous speed

$$\Omega_m = \Omega_{syn} \quad , \tag{8.1-2}$$

so machine is operating as a **motor**. If the rotor is driven by a turbine with that speed, the change of stator flux linkage due to the moving rotor flux will induce **a "synchronous generated voltage"** $\boldsymbol{U_p}$ (r.m.s. phase value) in stator winding, that causes stator currents to flow to the grid (**generator** mode).

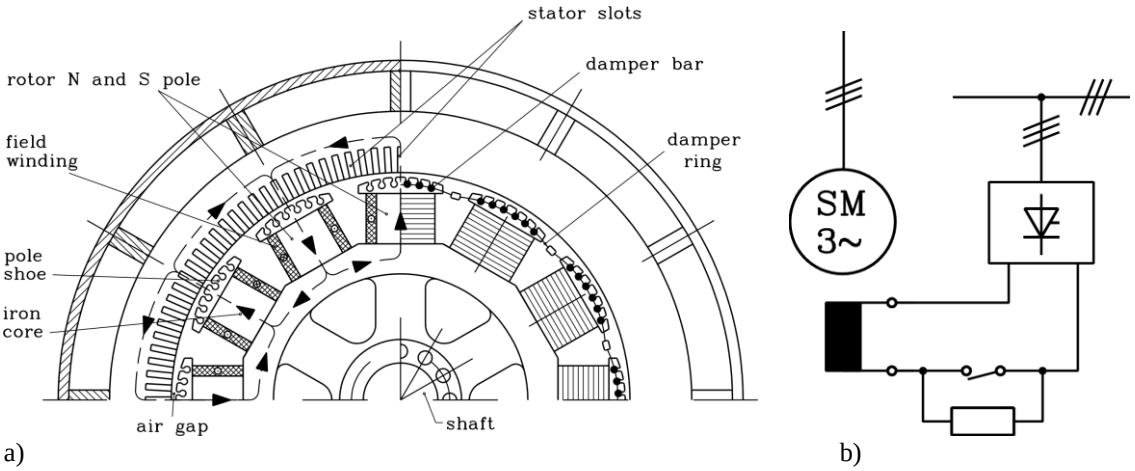

Fig. 8.1-1: Electrically excited synchronous machine: a) Axial cross section of salient 12 pole synchronous machine. The slotted stator bears the three phase stator winding with winding coils placed in the slots like in induction machines, b) DC excitation of electrically excited synchronous machine via slip rings from a DC voltage source such as a silicon controlled rectifier

Synchronous machines are built with different kinds of rotors either as
- **cylindrical rotor synchronous machines** with constant air gap (Fig. 8.1-3a, Fig. 8.1-2a) or as
- **salient pole synchronous machines** with varying air gap (Fig. 8.1-3b, Fig. 8.1-1a) with smallest air gap in the rotor pole axis (**direct axis,** *d*-axis) and with biggest air gap in the centre of inter-pole gap (**quadrature axis**, *q*-axis).

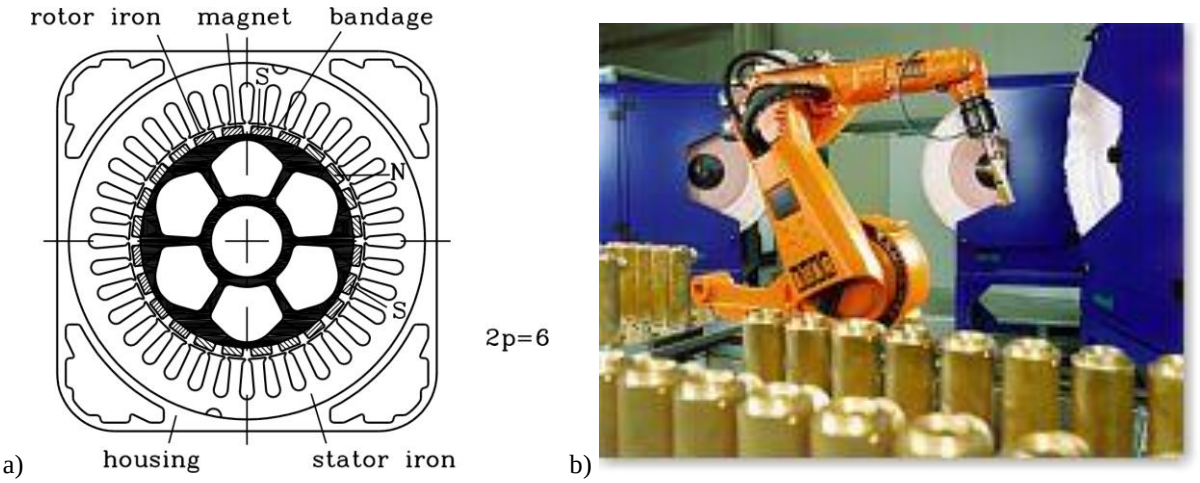

Fig. 8.1-2: Permanent magnet (PM) excited synchronous machine: a) Axial cross section of 6 pole synchronous machine with cylindrical rotor and surface mounted rotor rare earth high energy magnets, b) Application of inverter fed PM machine as adjustable speed drive for driving robots

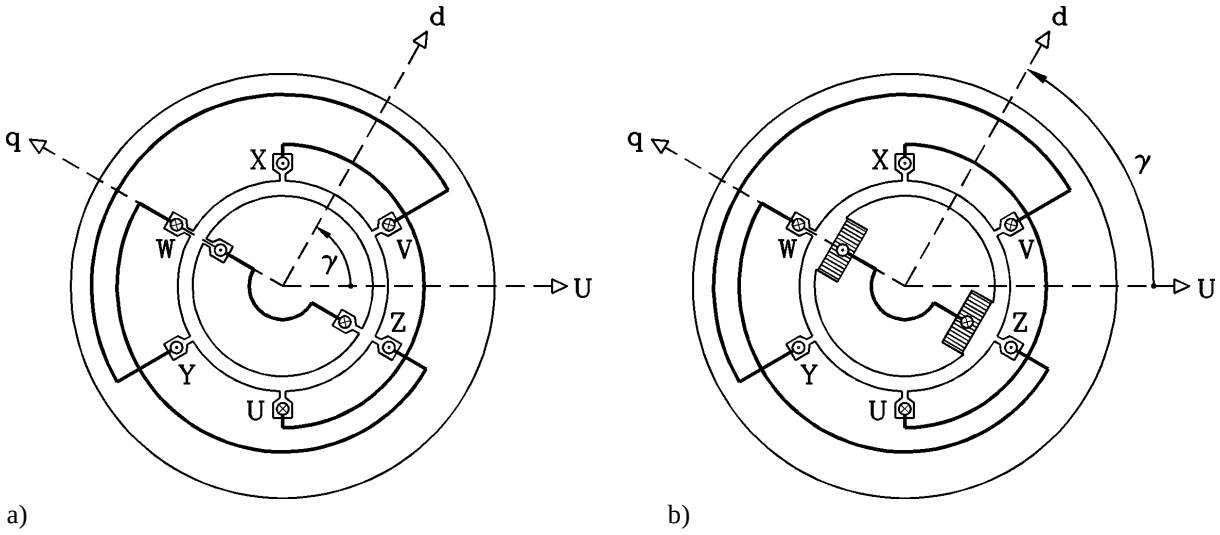

Fig. 8.1-3: Different kinds of synchronous machine rotor constructions: a) Cylindrical rotor synchronous machine with constant air gap, b) Salient pole rotor synchronous machine with non-constant air gap

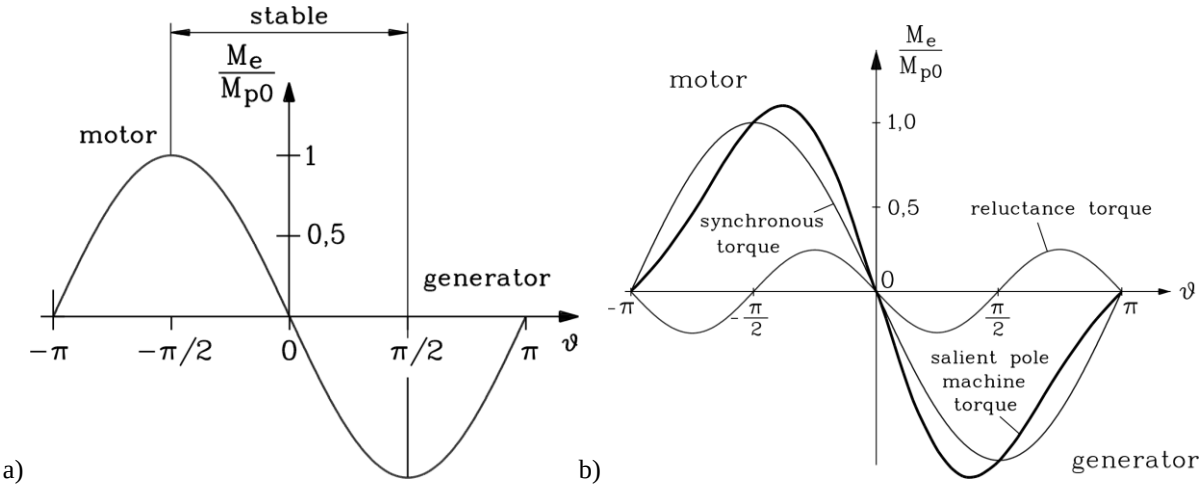

Fig. 8.1-4: Steady state $M_e(\vartheta)$ characteristic for neglected stator losses ($R_s = 0$), constant r.m.s. phase value U_s and constant frequency f_s, constant rotor flux: a) cylindrical rotor synchronous machine, b) salient pole synchronous machine

In motor mode rotor **is lagging** behind the stator field, so a **load angle** ϑ exists between stator field north pole axis and rotor north pole axis. In generator mode the rotor pole axis **is leading** and the stator field is lagging, so load angle has inverse sign. So delivered electromagnetic steady state torque M_e is correlated to load angle, being positive (driving) in motor mode and negative (braking) in generator mode. Please note, that international standardization has defined load angle ϑ positive for generator and negative for motor mode. The correlation of steady state torque and load angle $M_e(\vartheta)$ is non-linear. If the machine is operated from three phase sinusoidal grid voltage with constant r.m.s. phase value U_s and constant frequency f_s, the $M_e(\vartheta)$ characteristic for neglected stator losses ($R_s = 0$) and constant rotor flux is given by Fig. 8.1-4.

In cylindrical rotor synchronous machines torque rises up to **steady state pull out torque** M_{p0} at load angle ±90° and then falls out of synchronism (**"steady state stability limit"**), whereas in salient pole synchronous machines this happens already at a load angle $|\vartheta| < 90°$. The reason for these different characteristics, depending on rotor structure, are understood with Fig. 8.1-5. In cylindrical rotor machines due to constant air gap the stator self inductance per phase L_s (called **synchronous inductance** L_d) is given like in induction machines, which also have constant air gap. It consists of main (magnetizing) inductance due to stator air gap field L_h and of stator stray inductance $L_{s\sigma}$ due to stator leakage flux $\Phi_{s\sigma}$ in slots, winding overhangs and due to stator winding harmonics.

$$L_d = L_h + L_{s\sigma} \tag{8.1-3}$$

In salient pole machines the stator field for a given stator current three phase system with phase r.m.s. value I_s is BIGGER, if stator field is positioned in *d*-axis of rotor, because in that case air gap is smaller (Fig. 8.1-5a), than if stator field is positioned in rotor *q*-axis (Fig. 8.1-5b). So magnetizing inductance in *d*-axis $L_{h,d}$ is bigger than in *q*-axis $L_{h,q}$, leading to different synchronous inductances for *d*- and *q*-axis.

$$L_d > L_q \tag{8.1-4}$$

So even if rotor field excitation current I_f is put to zero, causing rotor flux to vanish, the rotor tends to move its rotor *d*-axis into stator field axis due to the tangential magnetic pull of the stator magnetic field, which is lower in *q*-axis than in *d*-axis. The corresponding so-called **reluctance torque** is biggest at load angle 45° and is superimposed on the synchronous torque related to L_d, causing a shift of steady state pull out torque to smaller values than 90°.

<u>$M_e(\vartheta)$ characteristic for neglected stator losses ($R_s = 0$):</u>

- cylindrical rotor synchronous machine:

$$M_e = -\frac{3 \cdot p \cdot U_s \cdot U_p}{(2\pi \cdot f_s)^2 \cdot L_d} \cdot \sin\vartheta \tag{8.1-5}$$

- salient pole synchronous machine:

$$M_e = -\frac{3 \cdot p}{(2\pi \cdot f_s)^2} \cdot \left[\frac{U_s \cdot U_p}{L_d} \cdot \sin\vartheta + \frac{U_s^2}{2} \cdot \left(\frac{1}{L_q} - \frac{1}{L_d} \right) \cdot \sin(2\vartheta) \right] \tag{8.1-6}$$

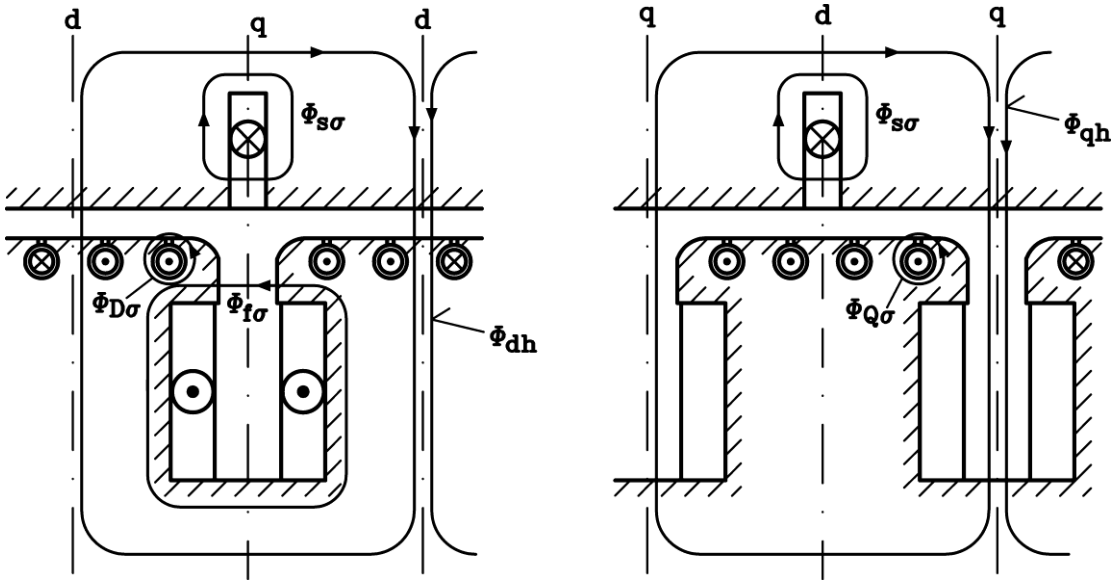

a) b)

Fig. 8.1-5: Flux linkage in salient pole synchronous machine: a) Stator magnetic field excited in parallel with rotor *d*-axis, b) Stator magnetic field excited in parallel with rotor *q*-axis

b) Dynamic operation:

Many synchronous machines are operating as generators, as they are capable of being both **inductive or capacitive**, which is achieved by either low or big field current I_f. Any disturbance in the grid such as

- sudden short circuits,
- voltage dips or oscillations due to switching,
- load steps on turbine or grid side etc.

causes the synchronous machines to operate in the dynamic state. The load angle is then varying very fast, thus the rotor runs for short time not synchronously with stator field. In the same way as explained with induction machines, the tangential magnetic pull of air gap flux on the rotor will cause in case of load steps the rotor speed to oscillate with natural frequency

$$f_{d,m} = \frac{\omega_{d,m}}{2\pi} = \frac{1}{2\pi}\sqrt{\frac{p \cdot |c_\vartheta|}{J}} \quad , \tag{8.1-6}$$

where $c_\vartheta = \frac{dM_e}{d\vartheta}$ is the "stiffness" of the "torsional spring", formed by the tangential magnetic pull (see: Lectures "Elektrische Maschinen und Antriebe"). So the natural frequency depends on the load angle and therefore on the load (Fig. 8.1-6).

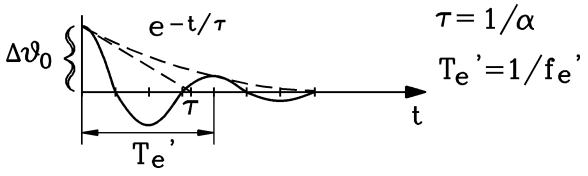

Fig. 8.1-6: Natural oscillations of load angle and rotor speed of synchronous machine after load step

In steady state operation rotor does not experience any change of flux linkage, as it rotates synchronously with stator field. In the dynamic state with mechanical speed different to synchronous speed of stator field rotor flux linkage is changing. With an additional squirrel

cage rotor in the rotor **(damper cage, damper winding)** (Fig. 8.1-5), due to the speed oscillations voltage is induced in that cage by air gap flux with oscillation frequency. The cage currents generate with the air gap field a braking torque, which causes quick decay (damping) of the rotor speed oscillations. Mechanical kinetic energy of speed oscillation is transformed and into *ohm*ic loss energy in damper cage and dissipated into heat.

But also in **rotor excitation winding** voltage is induced, if rotor flux linkage changes due to speed oscillations or due to sudden change of stator flux e.g. at stator sudden short circuit. As rotor field winding consists of many turns $N_f = 2p \cdot N_{f,pole}$ to get low excitation current I_f for the needed rotor ampere-turns $V_f = N_{f,pole} I_f$ to excite the needed rotor air gap field, the induced rotor voltage in field winding may be high at sudden change of flux and might destroy the feeding excitation converter. So fuses or protecting **varistors** (= voltage limiters) are necessary on rotor side. Due to that additional voltage induced in the field winding an additional current will flow in the field winding, which increases the rotor excitation for a short time period, until it decays with rotor time constant. This additional current increases the pull out torque, so (opposite to induction machine) **dynamic pull out torque** is bigger than steady state pull out torque in synchronous machines:

$$M_{p,dyn} > M_{p,0} \quad . \tag{8.1-7}$$

Thus **transient stability limit is higher than steady state stability limit**.

At sudden short circuit e.g. in the grid near the terminals of the synchronous machine the short circuit stator current increases tremendously, reaching much higher peak values than in induction machines, typically 12 to 15 times rated current. Reason for this is that not only the damper cage acts as short circuited secondary winding, which reduces the stator synchronous inductance L_d to short-circuit inductance L_d'', but also the field winding acts as additional secondary short circuit winding in parallel due to the small internal resistance of the DC voltage source, which feeds the field winding.

Permanent magnet machines are mostly operated as motors from inverters **in field oriented control**. Therefore they do not need a damper winding, as the load angle is measured by e.g. an incremental optical encoder and is controlled by the firing angle of the inverter silicon switches, so any oscillation of load angle is immediately cancelled by shifting stator field via the feeding inverter. Hence, without damper and field winding, the dynamic performance of PM synchronous machines is much simpler than for electrically excited synchronous machines. **Linear transfer function** of this kind of machine is needed for designing the speed and torque controller, which is implemented in the micro-processor of the feeding inverter.

We conclude, that **dynamic incidents** occurring with electric machines such as
- switch-on or switch-off,
- rapid change of motor speed or torque,
- sudden short circuits, switching errors or similar operating errors

lead to significantly higher electric and mechanical load than at steady-state operation. All these effects may be calculated with the synchronous machine dynamic equations, which are now introduced.

8.2 Dynamic Flux Linkages of Synchronous Machines

At steady-state operation, the stator field rotates as fast as the rotor and the flux linkage of the stator field with the damper- and the field winding does not change. Therefore, no voltage is

induced in the damper and the field winding. At a dynamic load such as a sudden short-circuit the stator current changes very fast, and so does the amplitude of the stator field. The flux linkage of the damper and the field winding will change, so that a voltage is induced in both windings.

Facit:
At dynamic incidents, the stator and the damper, as well as the damper and the field winding are magnetically coupled via the air gap field like in transformers (Fig. 8.1-5).

Theoretically, the stator current can always be decomposed into a *d*- and a *q*-component. The *d*-component i_{sd} excites a stator field with the main path of the flux along the *d*-axis (Fig. 8.1-5a). This main flux Φ_{dh} couples stator, field and damper winding, which can be represented as a **three winding transformer**. The *q*-component i_{sq} excites a stator field with the main flux path along the *q*-axis (Fig. 8.1-5b). This main flux Φ_{qh} couples only the stator and the damper winding to give a **two winding transformer**. As Fig. 8.1-5b shows, this main flux passes BETWEEN the pole shoes and the pole gap and is therefore NOT linked with the field winding. The magnetic equivalent circuit (Fig. 8.2-1a) shows that the mutual inductance of the *d*-axis equivalent three winding transformer is L_{dh}, whereas L_{qh} is the mutual inductance of the equivalent two winding transformer of the *q*-axis. The leakage flux – drawn schematically in Fig. 8.1-5 – of the field winding $\Phi_{f\sigma}$, the damper winding in *d*- and *q*-axis $\Phi_{D\sigma}$ and $\Phi_{Q\sigma}$ and of the stator winding $\Phi_{s\sigma}$ give the leakage inductances $L_{f\sigma}$, $L_{D\sigma}$, $L_{Q\sigma}$ and $L_{s\sigma}$, respectively the leakage reactances $X_{f\sigma} = \omega_s L_{f\sigma}$, $X_{D\sigma} = \omega_s L_{D\sigma}$, $X_{Q\sigma} = \omega_s L_{Q\sigma}$ and $X_{s\sigma} = \omega_s L_{s\sigma}$.

The damper bars are shorted via the damper rings. The field winding is fed by a dc-voltage source of the excitation system, that has a small internal resistance. Neglecting this resistance, the dc voltage source behaves like a short circuit for the induced alternating voltage so that the field winding can be considered as shorted for dynamic incidences. Therefore, the secondary windings in Fig. 8.2-1 are shorted. If the winding resistances R_s, R_f, R_D and R_Q are also neglected, the following magnetically equivalent reactances are obtained (see Fig. 8.1-2) for the stator winding during dynamic operation:

"Sub-transient reactance of the *d*-axis" X_d''**:**

$$X_d'' = \omega_s L_d'' = \omega_s \left(L_{s\sigma} + \frac{L_{dh} L_{f\sigma} L_{D\sigma}}{L_{dh} L_{f\sigma} + L_{dh} L_{D\sigma} + L_{f\sigma} L_{D\sigma}} \right) \tag{8.2-1}$$

"Sub-transient reactance of the *q*-axis" X_q''**:**

$$X_q'' = \omega_s L_q'' = \omega_s \left(L_{s\sigma} + \frac{L_{qh} L_{Q\sigma}}{L_{qh} + L_{Q\sigma}} \right) \quad . \tag{8.2-2}$$

Example 8.2-1:
Salient pole machine data:
$X_d/Z_N = x_d = 1$ p.u., $X_q/Z_N = x_q = 0.6$ p.u., $X_{s\sigma} = X_{f\sigma} = X_{D\sigma} = X_{Q\sigma} = 0.1\ Z_N$:

$$X_d'' / Z_N = x_d'' = 0.1 + \frac{0.9 \cdot 0.1 \cdot 0.1}{0.9 \cdot 0.1 + 0.9 \cdot 0.1 + 0.1 \cdot 0.1} = \underline{\underline{0.15}}\ \text{p.u.}$$

$$X_q'' / Z_N = x_q'' = 0.1 + \frac{0.5 \cdot 0.1}{0.5 + 0.1} = \underline{\underline{0.18}}\ \text{p.u.}$$

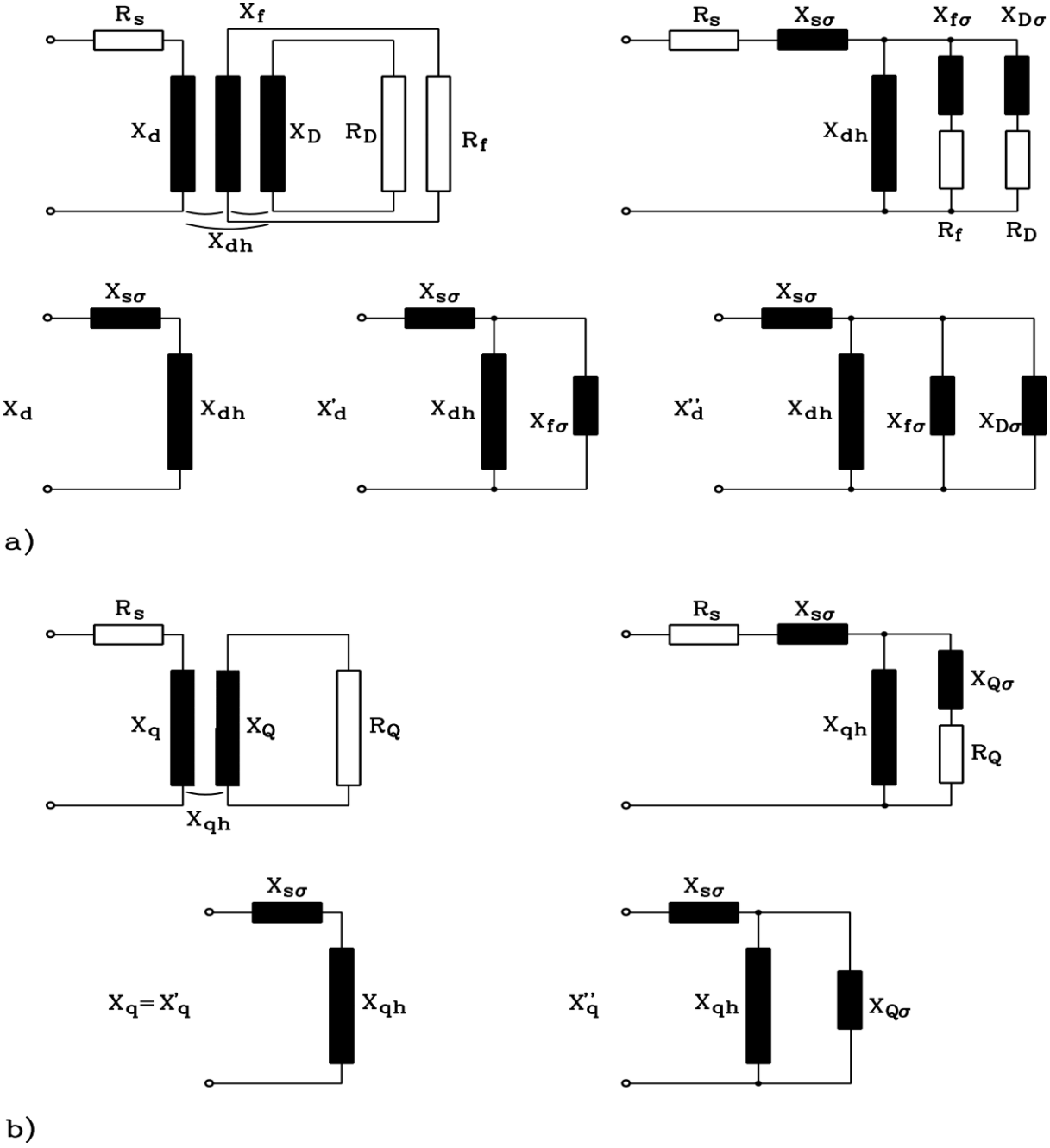

Fig. 8.2-1: **Magnetic coupling** in direct and quadrature axis of a synchronous machine:
a) Direct axis: Three winding transformer, synchronous reactance, transient and sub-transient reactance,
b) Quadrature axis: Two winding transformer, synchronous reactance and sub-transient reactance

Facit:

During the dynamic operation of a synchronous machine, the sub-transient reactances of the direct and the quadrature axis X''_d and X''_q are in effect. They are much smaller than the synchronous reactances X_d and X_q. X''_d and X''_q have almost the same magnitude, even if X_d and X_q are not equal as in the case of a salient-pole machine.

The resistances R_s, R_f, R_D and R_Q cause the decay of the transient currents, which result from the induced transient voltages in the damper, field and stator winding. As the damper winding inductance is smaller, compared with the one of the field winding, the dynamic currents in the damper winding decay faster than the one in the field winding. A typical time constant of the damper winding is 20 ... 50 ms, and of the field winding 0.5 ... 2 s. Therefore, a 3rd state exists

in the *d*-axis, where the damper winding is already at zero current, whereas considerable dynamic current still flows in the field winding in addition to the DC field current. The equivalent reactance of the stator winding is (Fig. 8.2-1) the **"transient reactance of the direct axis"** X'_d **,** that is only slightly bigger than the sub-transient reactance.

$$X'_d = \omega_s L'_d = \omega_s (L_{s\sigma} + \frac{L_{dh} L_{f\sigma}}{L_{dh} + L_{f\sigma}}) \quad . \tag{8.2-.3}$$

After the decay of all dynamic currents, the transformer coupling of stator and rotor winding disappears, and the stator reactances are X_d and X_q again. Fig. 8.2-2 shows a summary of the electromagnetic flux linkage at steady state and at transient and sub-transient operation for direct and quadrature axis. The magnetic field of the dynamic currents in the damper and the field windings counteracts the stator field. The stator field is quenched outside of the rotor, especially at sub-transient state.

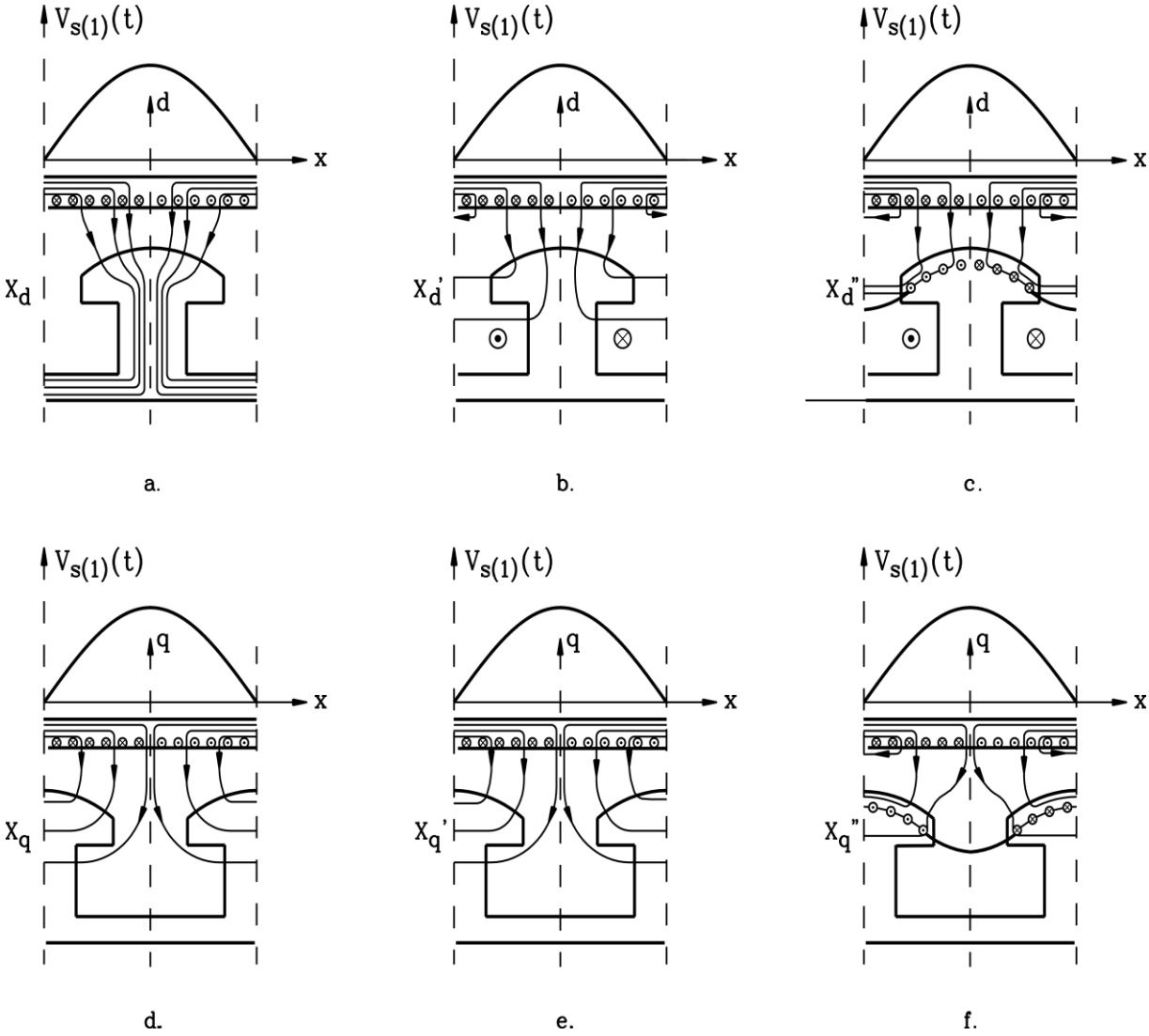

Fig. 8.2-2: Flux linkage at sinusoidal distributed stator winding m.m.f. $V_{s(1)}$ for different time instants:
Direct axis: a) synchronous operation, b) transient operation, c) sub-transient operation
Quadrature axis: d) synchronous operation, e) transient operation, identical with (d)!),
f) sub-transient operation, $x = x_r$: rotor-fixed coordinate in d-q-reference frame.

8.3 Set of dynamic equations for synchronous machines

The p. u. dynamic equations of electrically excited synchronous machines with damper cage are derived from induction machines equations (Chapter 7). In steady state condition of sinusoidal stator three-phase currents the stator fundamental field rotates synchronously with the rotor ($\omega_s = \omega_m$), so no AC voltage is induced on the rotor side. Thus steady state values on rotor side are the DC values U_f, I_f. The field winding rotor flux is in the *d*-axis, but not in the *q*-axis (Fig. 8.1-5a). Hence the dynamic equations are formulated in the *d*-*q*-rotor reference frame with real axis as *d*-axis and imaginary axis as *q*-axis (Fig. 8.3-1).

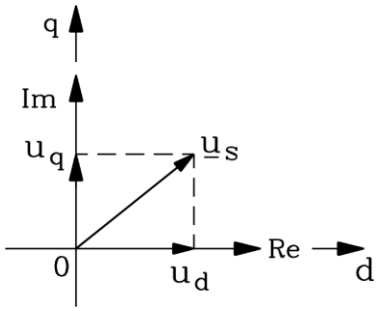

Fig. 8.3-1: Decomposition of space vector in rotor reference frame in *d*- and *q*-component

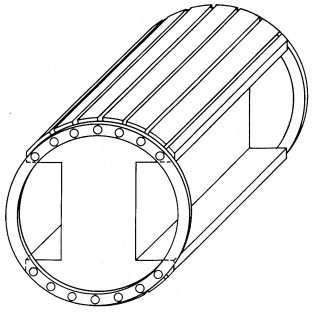

Fig. 8.3-2: Damper cage in 2-pole salient synchronous machine (Note: Usually salient pole machines are built with at least 4 poles !)

In case of the above noted steady state condition the stator voltage and current space vectors DO NOT MOVE in the *d*-*q*-rotor reference frame:

$$\underline{u}_{s(r)} = \underline{u}_{s(s)} \cdot e^{-j\cdot\gamma(\tau)} = \underline{u}_{s(s)} \cdot e^{-j\cdot\omega_m\tau} = u \cdot e^{j\cdot\omega_s\tau} \cdot e^{-j\cdot\omega_m\tau} = u \tag{8.3-1}$$

In dynamic state with arbitrary time dependence of stator voltage and current, stator space vectors are moving in rotor reference frame. Stator equation in rotor reference frame and rotor voltage equation for rotor damper winding are taken from induction machine stator and rotor voltage equation (Chapter 7), skipping the subscript (r) in the following.

$$\underline{u}_{s(r)} = r_s \cdot \underline{i}_{s(r)} + \frac{d\underline{\psi}_{s(r)}}{d\tau} + j \cdot \omega_m \cdot \underline{\psi}_{s(r)}, \qquad 0 = r'_r \cdot \underline{i}'_{r(r)} + \frac{d\underline{\psi}'_{r(r)}}{d\tau} \tag{8.3-2}$$

Decomposition of stator space vectors in *d*- and *q*-components (8.3-3) and of the damper current space vector (8.3-4) shall consider, that in the *q*-axis no field winding exists and that in *d*-axis the main inductance is bigger than in *q*-axis: $x_{dh} > x_{qh}$.

$$\underline{u}_s = u_d + j \cdot u_q, \quad \underline{i}_s = i_d + j \cdot i_q, \quad \underline{\psi}_s = \psi_d + j \cdot \psi_q \tag{8.3-3}$$

$$\underline{i}'_r = i_D + j \cdot i_Q \ . \tag{8.3-4}$$

In salient pole machines the damper bars are missing in the inter-pole gap (Fig. 8.3-2)), so the transferred damper cage resistance $r'_r = \ddot{u}_U \cdot \ddot{u}_I \cdot r_r$ is different for *d*- and *q*-axis: $r'_Q > r'_D$.

$$\ddot{u}_U = \ddot{u}_{UD} = \ddot{u}_{UQ} = \frac{k_{ws} \cdot N_s}{k_{wr} \cdot N_r} = \frac{k_{ws} \cdot N_s}{1 \cdot (1/2)}, \quad \ddot{u}_I = \ddot{u}_{ID} = \ddot{u}_{IQ} = \frac{m_s}{m_r} \cdot \ddot{u}_U = \frac{m_s}{Q_r} \cdot \ddot{u}_U \tag{8.3-5}$$

In the same way damper stray flux linkage is bigger in the *q*-axis: $x'_{Q\sigma} > x'_{D\sigma}$.

We assume that the field winding in *d*-axis is linked to stator and damper winding via the same *d*-axis main flux Φ_{dh} (Fig. 8.1-5a). So the **voltage equation for field winding** has to be added. The transferred field winding resistance $r'_f = \ddot{u}_{Uf} \cdot \ddot{u}_{If} \cdot r_f$, the p. u. transferred field current and field voltage $i'_f = \sqrt{2} \cdot I'_f / \hat{I}_{sN,ph}$, $u'_f = \sqrt{2} \cdot U'_f / \hat{U}_{N,ph}$ with $I'_f = I_f / \ddot{u}_{If}$, $U'_f = \ddot{u}_{Uf} \cdot U_f$ and the p. u. transferred field flux linkage $\psi'_f = \omega_N \Psi'_f / \hat{U}_{N,ph}$, $\Psi'_f = \sqrt{2} \cdot \ddot{u}_{Uf} \cdot \Psi_f$ are calculated with the transformation ratios $\ddot{u}_{Uf} = N_s k_{ws} / (N_f k_{wf} \sqrt{2})$, $\ddot{u}_{If} = m_s \cdot \ddot{u}_{Uf}$, comprising the field winding number of turns N_f and the field winding factor k_{wf}. As the dash notation ´ for damper and field winding values refer to different transformation ratios, they will be skipped in the following (Fig. 8.3-3).

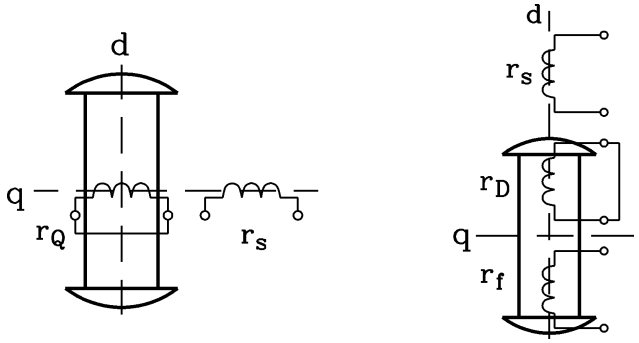

Fig. 8.3-3: Simplified sketch of linked windings in electrically excited synchronous machines

$$u_d = r_s \cdot i_d + \frac{d\psi_d}{d\tau} - \omega_m \cdot \psi_q \qquad u_q = r_s \cdot i_q + \frac{d\psi_q}{d\tau} + \omega_m \cdot \psi_d$$

$$0 = r_D \cdot i_D + \frac{d\psi_D}{d\tau} \qquad 0 = r_Q \cdot i_Q + \frac{d\psi_Q}{d\tau} \qquad (8.3\text{-}6)$$

$$u_f = r_f \cdot i_f + \frac{d\psi_f}{d\tau}$$

In Fig. 8.1-5 the *d*-axis main flux Φ_{dh} is linked to stator winding, damper winding and field winding, whereas the *q*-axis main flux Φ_{qh} is linked ONLY to stator and damper winding. The total flux linkage $\underline{\psi}_s$ in stator winding has to consider in addition stator stray flux $\Phi_{s\sigma}$. Reacting to a changing stator flux in the *d*-axis, the damper bar currents (Fig. 8.1-5) flow per pole in two opposite directions in order to generate an opposing flux. For the same reason as a reaction to a changing stator flux in the *q*-axis, the damper bar currents flow per pole in the SAME direction. The total damper cage flux linkage has to consider damper cage stray flux, which for *d*- and *q*-axis is different in salient pole machines as noted above: $\Phi_{D\sigma}$, $\Phi_{Q\sigma}$. Field winding flux linkage contains in addition to main flux the stray flux $\Phi_{f\sigma}$, which crosses the gap between adjacent poles, yielding finally **flux linkage equations**:

$$\psi_d = x_d i_d + x_{dh} i_D + x_{dh} i_f \qquad \psi_q = x_q i_q + x_{qh} i_Q$$

$$\psi_D = x_{dh} i_d + x_D i_D + x_{dh} i_f \qquad \psi_Q = x_{qh} i_q + x_Q i_Q$$

$$\psi_f = x_{dh} i_d + x_{dh} i_D + x_f i_f$$

$$x_d = x_{dh} + x_{s\sigma} \qquad x_q = x_{qh} + x_{s\sigma} \qquad (8.3\text{-}7)$$

$$x_D = x_{dh} + x_{D\sigma} \qquad x_Q = x_{qh} + x_{Q\sigma}$$

$$x_f = x_{dh} + x_{f\sigma}$$

The electromagnetic torque is calculated like in induction machines:

$$m_e = \mathrm{Im}\{\underline{i}_s \cdot \underline{\psi}_s^*\} = i_q \cdot \psi_d - i_d \cdot \psi_q \quad . \tag{8.3-8}$$

The complete **set of dynamic equations for electrically excited synchronous machines with damper cage and rotor saliency in rotor reference frame** is comprising 11 equations with 11 unknowns: $i_d, i_q, i_D, i_Q, i_f, \psi_d, \psi_q, \psi_D, \psi_Q, \psi_f, \omega_m$, which are determined by the values of u_d, u_q, u_f, m_s . Note that in **generator case** shaft torque is **negative**, as it is driving the machine.

$$\begin{aligned}
&u_d(\tau) = r_s \cdot i_d(\tau) + \frac{d\psi_d(\tau)}{d\tau} - \omega_m(\tau) \cdot \psi_q(\tau) && u_q(\tau) = r_s \cdot i_q(\tau) + \frac{d\psi_q(\tau)}{d\tau} + \omega_m \cdot \psi_d(\tau) \\
&0 = r_D \cdot i_D(\tau) + \frac{d\psi_D(\tau)}{d\tau} && 0 = r_Q \cdot i_Q(\tau) + \frac{d\psi_Q(\tau)}{d\tau} \\
&u_f = r_f \cdot i_f(\tau) + \frac{d\psi_f(\tau)}{d\tau} && \\
&\psi_d(\tau) = (x_{dh} + x_{s\sigma}) \cdot i_d(\tau) + x_{dh} i_D(\tau) + x_{dh} i_f(\tau) && \psi_q(\tau) = (x_{qh} + x_{s\sigma}) \cdot i_q(\tau) + x_{qh} \cdot i_Q(\tau) \\
&\psi_D(\tau) = x_{dh} i_d(\tau) + (x_{dh} + x_{D\sigma}) \cdot i_D(\tau) + x_{dh} i_f(\tau) && \psi_Q(\tau) = x_{qh} i_q(\tau) + (x_{qh} + x_{Q\sigma}) \cdot i_Q(\tau) \\
&\psi_f(\tau) = x_{dh} i_d(\tau) + x_{dh} i_D(\tau) + (x_{dh} + x_{f\sigma}) \cdot i_f(\tau) && \\
&\tau_J \cdot \frac{d\omega_m(\tau)}{d\tau} = i_q(\tau) \cdot \psi_d(\tau) - i_d(\tau) \cdot \psi_q(\tau) - m_s(\tau) && (8.3-9)
\end{aligned}$$

If in addition influence of a **stator zero sequence voltage system** has to be considered, additional stator voltage equation is

$$u_{s0} = r_s \cdot i_{s0} + \frac{d\psi_{s0}}{d\tau} \tag{8.3-10}$$

with the zero sequence stator voltage, current and flux linkage:

$$u_{s0}(\tau) = \left(u_U(\tau) + u_V(\tau) + u_W(\tau)\right)/3 \qquad i_{s0} = \left(i_U + i_V + i_W\right)/3 \qquad \psi_{s0} = \left(\psi_U + \psi_V + \psi_W\right)/3 .$$

Note that the linkage of zero sequence flux with rotor winding and its effects there have to be considered by separate flux linkage and rotor voltage equations similar to (8.3-9), which will not be discussed here further.

For **permanent magnet machines** the equations are much simpler due to the lack of rotor windings. Instead of rotor field current i_f the rotor permanent magnet flux linkage ψ_p has to be introduced in *d*-axis, leading to only 5 equations instead of 11 with 5 unknowns $i_d, i_q, \psi_d, \psi_q, \omega_m$, which are determined by the values of u_d, u_q, ψ_p, m_s .

$$\begin{aligned}
&u_d(\tau) = r_s \cdot i_d(\tau) + \frac{d\psi_d(\tau)}{d\tau} - \omega_m(\tau) \cdot \psi_q(\tau) && u_q(\tau) = r_s \cdot i_q(\tau) + \frac{d\psi_q(\tau)}{d\tau} + \omega_m(\tau) \cdot \psi_d(\tau) \\
&\psi_d(\tau) = x_d \cdot i_d(\tau) + \psi_p && \psi_q(\tau) = x_q \cdot i_q(\tau) \\
&\tau_J \cdot \frac{d\omega_m(\tau)}{d\tau} = i_q(\tau) \cdot \psi_d(\tau) - i_d(\tau) \cdot \psi_q(\tau) - m_s(\tau) && (8.3-11)
\end{aligned}$$

Example 8.3-1:

Steady state operation of synchronous machine as under-excited motor:

In steady state operation ($d./d\tau = 0$) the dynamic equations simplify in rotor reference frame to pure algebraic equations, showing that steady state solutions (= synchronous operation) **are DC values, which may be regarded as the *d*- and *q*-phasor amplitudes of *d*-*q*-phasor diagrams.**

$$u_d = r_s \cdot i_d - \omega_m \cdot \psi_q \qquad u_q = r_s \cdot i_q + \omega_m \cdot \psi_d$$

$$0 = r_D \cdot i_D \qquad 0 = r_Q \cdot i_Q$$

$$u_f = r_f \cdot i_f$$

$$\underline{\underline{i_D = i_Q = 0, \quad i_f = u_f / r_f}}$$

$$\psi_d = x_d i_d + x_{dh} i_f \qquad \psi_q = x_q i_q$$

$$\underline{\underline{u_d = r_s \cdot i_d - \omega_m \cdot x_q i_q}} \qquad \underline{\underline{u_q = r_s \cdot i_q + \omega_m \cdot x_d i_d + \omega_m \cdot x_{dh} i_f}}$$

Facit:

The steady state back emf is $\underline{\underline{u_p = \omega_m \cdot x_{dh} i_f}}$ *, which is directed in q-axis.*

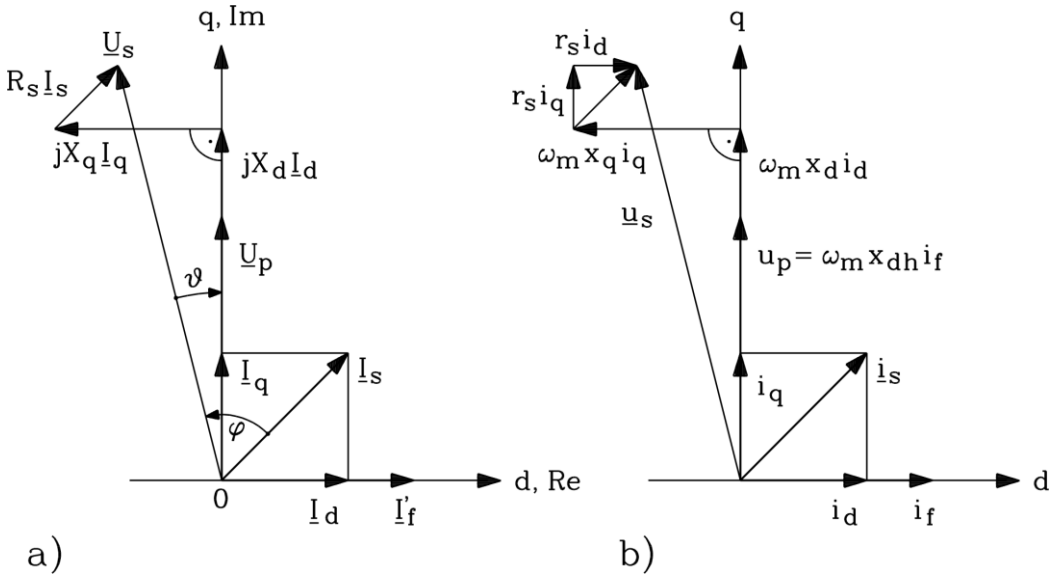

Fig. 8.3-4: Phasor diagram of (a) synchronous under-excited motor and (b) corresponding diagram of steady state *d*- and *q*-components of stator voltage and current: motor: $\vartheta < 0$, under-excited: $\varphi > 0$.

8.4 *Park* transformation

Like the *Clarke* transformation of stator phase values (currents, voltages, flux linkages) from three phase system U, V, W into stator reference frame system $\alpha, \beta, 0$, the transformation into rotor reference frame system $d, q, 0$ (Fig. 8.4-1) is called ***Park* transformation**. It is also written as matrix equation. Transformation of space vector in stator reference frame

$$\underline{u}_{s(S)} = \frac{2}{3} \cdot \left(u_U + \underline{a} \cdot u_V + \underline{a}^2 \cdot u_W \right) \tag{8.4-1}$$

into **rotor reference frame** is

$$u_d + j \cdot u_q = \underline{u}_{s(R)} = \underline{u}_{s(S)} \cdot e^{-j\cdot\gamma} = \frac{2}{3} \cdot \left(u_U + \underline{a} \cdot u_V + \underline{a}^2 \cdot u_W\right) \cdot e^{-j\cdot\gamma} =$$

$$= \frac{2}{3} \cdot \left(u_U + e^{j\frac{2\pi}{3}} \cdot u_V + e^{j\frac{4\pi}{3}} \cdot u_W \right) \cdot e^{-j\cdot\gamma} = \frac{2}{3} \cdot \left(e^{-j\gamma} \cdot u_U + e^{j\left(\frac{2\pi}{3}-\gamma\right)} \cdot u_V + e^{j\left(\frac{4\pi}{3}-\gamma\right)} \cdot u_W \right) =$$

$$= \frac{2}{3} \cdot \left(\cos\gamma \cdot u_U + \cos\left(\frac{2\pi}{3}-\gamma\right) \cdot u_V + \cos\left(\frac{4\pi}{3}-\gamma\right) \cdot u_W \right) -$$

$$- j\frac{2}{3} \cdot \left(\sin\gamma \cdot u_U + \sin\left(\frac{2\pi}{3}-\gamma\right) \cdot u_V + \sin\left(\frac{4\pi}{3}-\gamma\right) \cdot u_W \right)$$

and zero sequence voltage is

$$u_{s0} = \frac{1}{3} \cdot \left(u_U + u_V + u_W\right) \quad .$$

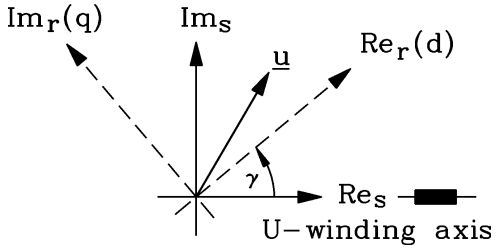

Fig. 8.4-1: Voltage space vector $\underline{u}$ has the same amplitude, but different angle to stator and rotor reference frame real axis and therefore different components in those two different frames. Transformation matrix from phase values u_U, u_V, u_W into stator reference frame components u_α, u_β, u_0 is called *Clarke* transformation, and into rotor reference frame values u_d, u_q, u_0 is called *Park* transformation.

*Park´*s transformation is given by combining both equations to get transformation matrix *(T)* :

$$\begin{pmatrix} u_d \\ u_q \\ u_0 \end{pmatrix} = \begin{pmatrix} \frac{2}{3}\cdot\cos\gamma & \frac{2}{3}\cdot\cos(\gamma-\frac{2\pi}{3}) & \frac{2}{3}\cdot\cos(\gamma-\frac{4\pi}{3}) \\ -\frac{2}{3}\cdot\sin\gamma & -\frac{2}{3}\cdot\sin(\gamma-\frac{2\pi}{3}) & -\frac{2}{3}\cdot\sin(\gamma-\frac{4\pi}{3}) \\ \frac{1}{3} & \frac{1}{3} & \frac{1}{3} \end{pmatrix} \cdot \begin{pmatrix} u_U \\ u_V \\ u_W \end{pmatrix} = (T) \cdot \begin{pmatrix} u_U \\ u_V \\ u_W \end{pmatrix} \qquad (8.4\text{-}2)$$

$$\begin{pmatrix} u_U \\ u_V \\ u_W \end{pmatrix} = \begin{pmatrix} \cos\gamma & -\sin\gamma & 1 \\ \cos(\gamma-\frac{2\pi}{3}) & -\sin(\gamma-\frac{2\pi}{3}) & 1 \\ \cos(\gamma-\frac{4\pi}{3}) & -\sin(\gamma-\frac{4\pi}{3}) & 1 \end{pmatrix} \cdot \begin{pmatrix} u_d \\ u_q \\ u_0 \end{pmatrix} = (T)^{-1} \cdot \begin{pmatrix} u_d \\ u_q \\ u_0 \end{pmatrix} \qquad (8.4\text{-}3)$$

With inverse transformation matrix $(T)^{-1}$ one gets directly to each component u_d, u_q, u_0 the phase values u_U, u_V, u_W. Around 1928/29 with this transformation the dynamic calculation of electric machines began, because by that time electric grids, fed by synchronous generators, were already big enough to cause severe stability problems after load switching, causing the generators to perform speed and load angle oscillations, as described above.

8.5 Equivalent circuits for magnetic coupling in synchronous machines

Before a mathematical solution of the dynamic equations is done, the **physical meaning** of the flux linkages in electrically excited synchronous machines with damper winding is discussed according to the remarks in 8.2. At sudden change of e.g. stator current the stator field changes and therefore the main flux, which also at synchronous rotation of rotor will lead to change of main flux linkage in rotor winding. This changing flux linkage in rotor, decomposed into *d*- and *q*-components ψ_{dh}, ψ_{qh}, induces voltages $d\psi_{dh}/d\tau, d\psi_{qh}/d\tau$ in rotor field winding and in damper cage, giving rise to a dynamic current flow i_f, i_D, i_Q. These currents excite in their turn fluxes, being linked to the stator winding, contributing to the resulting main flux linkage like the magnetizing current in induction machine, and excite additional stray fluxes. For the *d*-axis we get for the resulting flux linkage of stator winding, damper and field winding

$$\begin{aligned}\psi_d &= (x_{dh} + x_{s\sigma}) \cdot i_d + x_{dh} i_D + x_{dh} i_f \\ \psi_D &= x_{dh} i_d + (x_{dh} + x_{D\sigma}) \cdot i_D + x_{dh} i_f \\ \psi_f &= x_{dh} i_d + x_{dh} i_D + (x_{dh} + x_{f\sigma}) \cdot i_f\end{aligned} \quad . \tag{8.5-1}$$

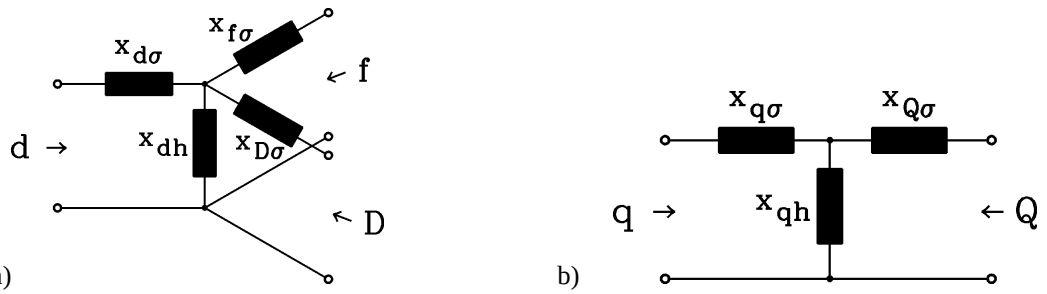

Fig. 8.5-1: Equivalent circuit for flux linkage in electrically excited synchronous machine: a) Three-winding transformer in *d*-axis, b) Two-winding transformer in *q*-axis

The corresponding equivalent circuit is a **three-winding transformer** (Fig. 8.5-1a). The bigger the ***Blondel* stray coefficients $0 \le \sigma \le 1$** of each winding pair "stator-damper", "stator-field", "damper-field", the weaker the coupling between those windings, with total coupling at $\sigma = 0$ and no coupling at $\sigma = 1$.

$$\sigma_{dD} = 1 - \frac{x_{dh}^2}{x_d x_D}, \quad \sigma_{df} = 1 - \frac{x_{dh}^2}{x_d x_f}, \quad \sigma_{fD} = 1 - \frac{x_{dh}^2}{x_f x_D} \tag{8.5-2}$$

$$x_d = x_{dh} + x_{s\sigma}, \quad x_D = x_{dh} + x_{D\sigma}, \quad x_f = x_{dh} + x_{f\sigma} \quad . \tag{8.5-3}$$

In *q*-axis no field winding is arranged, so stator and damper winding act only as a **two-winding transformer** (Fig. 8.5-1b) with the coupling

$$\sigma_{qQ} = 1 - \frac{x_{qh}^2}{x_q x_Q} \qquad x_q = x_{qh} + x_{s\sigma}, \quad x_Q = x_{qh} + x_{Q\sigma} \tag{8.5-4}$$

$$\psi_q = x_q \cdot i_q + x_{qh} \cdot i_D, \quad \psi_Q = x_{qh} \cdot i_q + x_Q \cdot i_Q \quad . \tag{8.5-5}$$

It will be shown by solving the dynamic equations, that the time constant of damper winding for decay of dynamic damper current is much shorter (factor 10) than time constant of field winding for the decay of dynamic field current. This is due to the fact, that the field winding

consists of many turns per pole $N_{f,pole}$, leading to a big field winding inductance $x_f \sim L_f \sim N_{f,pole}^2$ and therefore to a big time constant $T_f = L_f / R_f$, $\tau_f = x_f / r_f$. Thus after ca. 200 ... 500 ms the damper currents vanish, leaving in *d*-axis only a coupling between stator and field winding, hence a two-winding transformer between stator and field winding, whereas in *q*-axis no transformer coupling between stator and rotor exist any longer. After about 1 ... 2 seconds also the transient field winding current has vanished, leaving only the DC field current flow in rotor field winding. No transformer coupling in *d*-axis is active any longer. So the time span after a sudden change of electric quantities is separated into 3 time intervals (Table 8.5-1). The flux plots corresponding to these time sections are shown in Fig. 8.2-2 for sinusoidal distributed air gap m.m.f. of stator winding, being the space fundamental of the step-like m.m.f. distribution due to stator coils in slots, for direct and quadrature axis, assuming that the m.m.f. amplitude has changed rapidly e.g. due to some disturbance in stator winding. The six pictures correspond to the following dynamic states (Table 8.5-2).

Sub-transient time section 0 .... ≈ 0.5 s	Dynamic current flow in stator, damper and field winding
Transient time section 0.5 s .... ≈ 2 s	Dynamic current flow in stator and field winding
Steady state > 2 ... 3 s	Steady state current flow in stator and field winding

Table 8.5-1: Duration of dynamic response to sudden changes in electrically excited synchronous machine with damper cage

	Steady state	**Transient**	**Sub-transient**
Direct axis	Fig. 8.2-2a	Fig. 8.2-2b	Fig. 8.2-2c
Quadrature axis	Fig. 8.2-2d	Fig. 8.2-2e	Fig. 8.2-2f

Table 8.5-2: Flux plots for steady, transient and sub-transient state of operation of electrically excited synchronous machine with damper winding

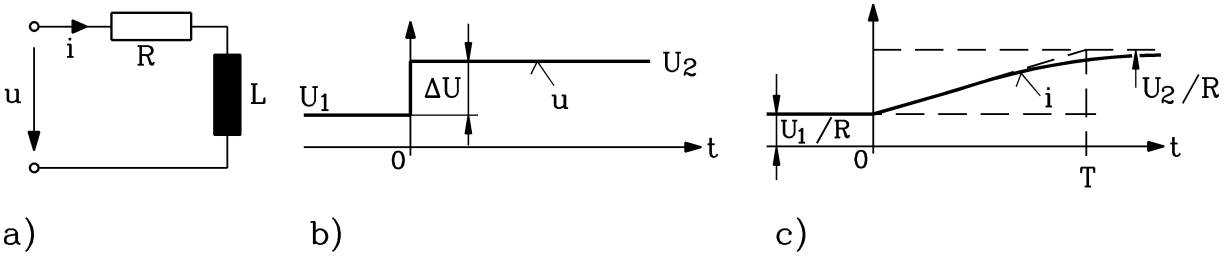

Fig. 8.5-2: Transient current response of a) *R*-*L*-circuit to b) voltage step follows c) system time constant *T*

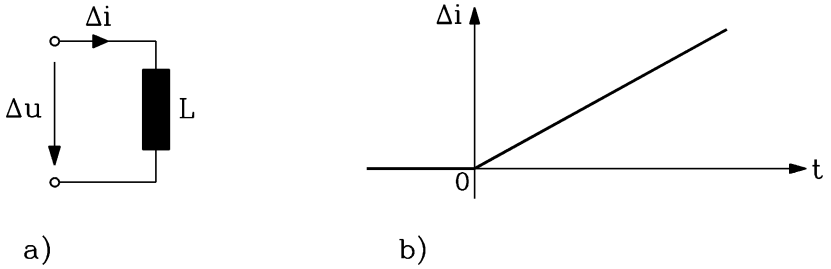

Fig. 8.5-3: For transient current response of *R*-*L*-circuit Fig. 8.5-2 short time after disturbance ($t << T$) it is sufficient to take a) only inductance *L* into account, b) getting current change immediately after disturbance

The **resulting inductance of stator winding** for these different states of operation are derived from the equivalent circuits Fig. 8.5-1. For the calculation of the change of dynamic current IMMEDIATELY after the disturbance only these inductances are needed, as can be seen in Fig. 8.5-2 for a simple *R*-*L*-circuit. If e.g. a step in voltage ΔU at $t = 0$ is applied at this circuit, the current i will change from steady state value U_1 / R, $t < 0$ to new steady state value U_2 / R, $t > 0$ with time constant $T = L / R$:

$$i(t) = \frac{U_1}{R} + \frac{\Delta U}{R} \cdot \left(1 - e^{-t/T}\right) \tag{8.5-6}$$

$$\Delta i(t) = i(t) - \frac{U_1}{R}\bigg|_{t<<T} \approx \frac{\Delta U}{L} \cdot t \tag{8.5-7}$$

Facit:
If one is only interested in the dynamic change of current $\Delta i(t)$ for very short time t << T after disturbance, it is sufficient to know only the resulting inductance for dynamic condition!

	Steady state	**Transient**	**Sub-transient**
Direct axis	Synchronous inductance L_d , x_d	Transient inductance L'_d, x'_d	Sub-transient inductance L''_d, x''_d
Quadrature axis	Synchronous inductance L_q , x_q	Synchronous inductance L_q , x_q	Sub-transient inductance L''_q, x''_q

Table 8.5-3: Equivalent stator inductance per phase for steady, transient and sub-transient state of operation of electrically excited synchronous machine with damper winding

So, for the dynamic *d*- and *q*-axis transformer flux linkages the following equivalent inductances are derived (Fig. 8.5-4, Table 8.5-3). Values belonging to the transient time interval are marked with dash ´, values for the sub-transient time interval with double dash ´´.

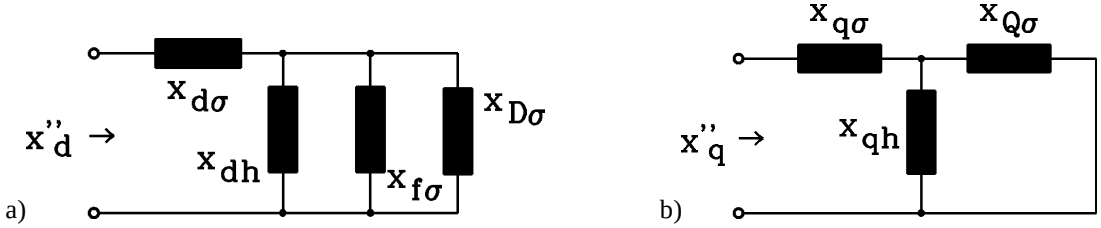

Fig. 8.5-4: Equivalent circuit for sub-transient inductance (per unit) for a) *d*- and b) *q*-axis

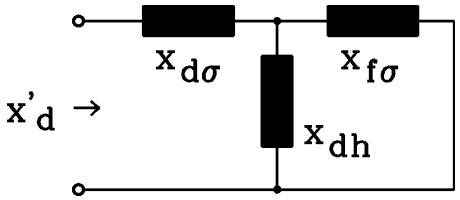

Fig. 8.5-5: Equivalent circuit for p.u. *d*-axis transient inductance. For *q*-axis the transient and synchronous inductances are identical.

Sub-transient inductance of *d*-axis:

$$L''_d = L_{s\sigma} + \frac{L_{dh}L_{f\sigma}L_{D\sigma}}{L_{dh}L_{f\sigma} + L_{dh}L_{D\sigma} + L_{f\sigma}L_{D\sigma}} \qquad x''_d = x_{s\sigma} + \frac{x_{dh}x_{f\sigma}x_{D\sigma}}{x_{dh}x_{f\sigma} + x_{dh}x_{D\sigma} + x_{f\sigma}x_{D\sigma}} \tag{8.5-8}$$

Sub-transient inductance of *q*-axis:

$$L''_q = L_{s\sigma} + \frac{L_{qh}L_{Q\sigma}}{L_{qh} + L_{Q\sigma}} \qquad x''_q = x_{s\sigma} + \frac{x_{qh}x_{Q\sigma}}{x_{qh} + x_{Q\sigma}} \tag{8.5-9}$$

Transient inductance of *d*-axis:

$$L'_d = L_{s\sigma} + \frac{L_{dh} L_{f\sigma}}{L_{dh} + L_{f\sigma}} \qquad x'_d = x_{s\sigma} + \frac{x_{dh} x_{f\sigma}}{x_{dh} + x_{f\sigma}} \tag{8.5-10}$$

Transient inductance of *q*-axis:

$$L'_q = L_q \qquad x'_q = x_q \tag{8.5-11}$$

For **permanent magnet machines** no field winding and often no damper winding exist. The sub-transient and transient inductances are identical with the synchronous inductance: $x_d = x'_d = x''_d$, $x_q = x'_q = x''_q$. For PM machines with surface mounted magnets and cylindrical rotor no inter-pole gaps exist, so *d*- and *q*-axis values are identical: $x_d = x_q$. Note that the relative permeability of ferrite and rare earth magnets such as NdFeB or Sm_2Co_{17} is typically 1.05, so the magnetic "reluctance" of permanent magnets in stator air gap field is nearly the same as the air gap. Thus magnet height h_M has to be added to mechanical air gap δ as well as thickness d_B of glass fibre or carbon fibre bandage, which is fixing the rotor surface-mounted permanent magnets, to get equivalent magnetic air gap:

$$\delta_e = \delta + h_M + d_B >> \delta \tag{8.5-12}$$

As main inductance L_h is proportional to inverse of equivalent air gap, it is rather small in permanent magnet machines with surface mounted rotor magnets, yielding a resulting synchronous reactance of only typically $x_d \approx 0.3 \ldots 0.4$.

Synchronous reactance of direct axis	$x_d = X_d / Z_N$ $X_d = \omega_N L_d$	0.8 ... 1.2: Salient pole synchronous machines with high pole count (e.g. hydro generators with 6 or more poles) 1.2 ... 2.5: 2- and 4-pole cylindrical rotor synchronous machines with high utilization (e.g. steam turbine generators)
synchronous reactance of quadrature axis	$x_q = X_q / Z_N$ $X_q = \omega_N L_q$	$(0.5...0.6)x_d$: Salient pole synchronous machines with high pole count (e.g. hydro generators): Influence of inter-pole gap $(0.8...0.9)x_d$: 2- and 4-pole cylindrical rotor synchronous machines (e.g. steam turbine generators): Influence of rotor slots
Transient reactance of direct axis	$x'_d = X'_d / Z_N$ $X'_d = \omega_N L'_d$	0.2-0.25 ... 0.35-0.4
Transient reactance of quadrature axis	$x'_q = x_q =$ $= X_q / Z_N$	Identical with synchronous reactance due to missing field winding in *q*-axis
Sub-transient reactance of direct axis	$x''_d = X''_d / Z_N$ $X''_d = \omega_N L''_d$	0.1-0.12 ... 0.2-0.3: according to (8.4-8) only slightly bigger than stator stray reactance $x_{\sigma s}$
Sub-transient reactance of quadrature axis	$x''_q = X''_q / Z_N$ $X''_q = \omega_N L''_q$	usually $x''_q > x''_d$, as field winding is missing in *q*-axis, but same order of magnitude 0.1 ... 0.3

Table 8.5-4: Typical magnitudes of per unit inductances resp. reactances for steady state and dynamic state for electrical excited synchronous machines with damper winding

Example 8.5-1:
Electrically excited salient pole synchronous machine with damper cage:
$x_{dh} = 1.2,\ x_{qh} = 0.6,\ x_{s\sigma} = 0.15,\ x_{f\sigma} = 0.2,\ x_{D\sigma} = 0.1,\ x_{Q\sigma} = 0.1$

$$x_d'' = x_{s\sigma} + \frac{x_{dh} x_{f\sigma} x_{D\sigma}}{x_{dh} x_{f\sigma} + x_{dh} x_{D\sigma} + x_{f\sigma} x_{D\sigma}} = 0.15 + \frac{1.2 \cdot 0.2 \cdot 0.1}{1.2 \cdot 0.2 + 1.2 \cdot 0.1 + 0.2 \cdot 0.1} = \underline{\underline{0.21}}$$

$$x_q'' = x_{s\sigma} + \frac{x_{qh} x_{Q\sigma}}{x_{qh} + x_{Q\sigma}} = 0.15 + \frac{0.6 \cdot 0.1}{0.6 + 0.1} = \underline{\underline{0.24}}$$

$$x_d' = x_{s\sigma} + \frac{x_{dh} x_{f\sigma}}{x_{dh} + x_{f\sigma}} = 0.15 + \frac{1.2 \cdot 0.2}{1.2 + 0.2} = \underline{\underline{0.32}}$$

$$x_q' = x_q = x_{qh} + x_{s\sigma} = 0.6 + 0.15 = \underline{\underline{0.75}}$$

$$x_d = x_{dh} + x_{s\sigma} = 1.2 + 0.15 = \underline{\underline{1.35}}$$

8.6 Dynamic performance of synchronous machines at constant speed operation

The non-linear dynamic equations of synchronous machines turn to be linear, if constant speed is assumed. Like in induction machines, electrical time constants of stator and rotor windings are much shorter than mechanical time constant, so for considering only electrical dynamics such as

- sudden short circuits,
- electric load steps with only change of reactive power such as connecting/disconnecting open-end cable or transmission lines (which may be regarded as capacities),
- switching during inverter **operation at constant speed may be assumed.**

The linear equations may be *Laplace* transformed. The mechanical equation is not needed, as speed is constant. Neglecting zero sequence system, we get from Chapter 8.3 with $L\{d\psi / d\tau\} = s \cdot \breve{\psi} - \psi_0$:

$$\begin{aligned}
&\breve{u}_d + \psi_{d0} = r_s \cdot \breve{i}_d + s \cdot \breve{\psi}_d - \omega_m \cdot \breve{\psi}_q \\
&\breve{u}_q + \psi_{q0} = r_s \cdot \breve{i}_q + s \cdot \breve{\psi}_q + \omega_m \cdot \breve{\psi}_d \\
&\psi_{D0} = r_D \cdot \breve{i}_D + s \cdot \breve{\psi}_D \\
&\psi_{Q0} = r_Q \cdot \breve{i}_Q + s \cdot \breve{\psi}_Q \\
&\breve{u}_f + \psi_{f0} = r_f \cdot \breve{i}_f + s \cdot \breve{\psi}_f
\end{aligned} \qquad (8.6\text{-}1)$$

The flux linkage equations are the same in time and in *Laplace* space, and may be written as matrix.

$$\begin{pmatrix} \breve{\psi}_d \\ \breve{\psi}_D \\ \breve{\psi}_f \end{pmatrix} = \begin{pmatrix} x_d & x_{dh} & x_{dh} \\ x_{dh} & x_D & x_{dh} \\ x_{dh} & x_{dh} & x_f \end{pmatrix} \cdot \begin{pmatrix} \breve{i}_d \\ \breve{i}_D \\ \breve{i}_f \end{pmatrix} \qquad (8.6\text{-}2)$$

$$\begin{pmatrix} \breve{\psi}_q \\ \breve{\psi}_Q \end{pmatrix} = \begin{pmatrix} x_q & x_{qh} \\ x_{qh} & x_Q \end{pmatrix} \cdot \begin{pmatrix} \breve{i}_q \\ \breve{i}_Q \end{pmatrix}$$

Mainly the unknowns stator flux linkage and current components $\breve{i}_d, \breve{i}_q, \breve{\psi}_d, \breve{\psi}_q$ in dependence of the stator and field voltages $\breve{u}_d, \breve{u}_q, \breve{u}_f$ are of interest. Please note, that also the initial conditions $\psi_{d0}, \psi_{q0}, \psi_{D0}, \psi_{Q0}, \psi_{f0}$ influence the resulting stator current and flux linkage. Instead of the initial flux linkages the initial values of the current components $i_{d0}, i_{q0}, i_{D0}, i_{Q0}, i_{f0}$ may be used, which are given according to (8.6-2):

$$\begin{pmatrix} \psi_{d0} \\ \psi_{D0} \\ \psi_{f0} \end{pmatrix} = \begin{pmatrix} x_d & x_{dh} & x_{dh} \\ x_{dh} & x_D & x_{dh} \\ x_{dh} & x_{dh} & x_f \end{pmatrix} \cdot \begin{pmatrix} i_{d0} \\ i_{D0} \\ i_{f0} \end{pmatrix} \qquad \begin{pmatrix} \psi_{q0} \\ \psi_{Q0} \end{pmatrix} = \begin{pmatrix} x_q & x_{qh} \\ x_{qh} & x_Q \end{pmatrix} \cdot \begin{pmatrix} i_{q0} \\ i_{Q0} \end{pmatrix} \tag{8.6-3}$$

By eliminating from the 10 unknowns the 6 unknowns damper and field currents and flux linkages $\breve{\psi}_D, \breve{\psi}_Q, \breve{i}_D, \breve{i}_Q, \breve{\psi}_f, \breve{i}_f$, only 4 instead of 10 equations remain with the 4 unknowns $\breve{i}_d, \breve{i}_q, \breve{\psi}_d, \breve{\psi}_q$. Therefore the two already discussed stator voltage equations and two stator flux linkage equations remain, which contain the new abbreviations, called **reactance operators**

$\boxed{x_d(s), x_q(s), x_D(s), x_Q(s), x_f(s)}$:

$$\begin{aligned} \breve{u}_d + \psi_{d0} &= r_s \cdot \breve{i}_d + s \cdot \breve{\psi}_d - \omega_m \cdot \breve{\psi}_q \\ \breve{u}_q + \psi_{q0} &= r_s \cdot \breve{i}_q + s \cdot \breve{\psi}_q + \omega_m \cdot \breve{\psi}_d \\ \breve{\psi}_d - \frac{\psi_{d0}}{s} &= x_d(s) \cdot \left(\breve{i}_d - \frac{i_{d0}}{s} \right) + x_f(s) \cdot \left(\frac{\breve{u}_f}{r_f} - \frac{i_{f0}}{s} \right) - x_D(s) \cdot \frac{i_{D0}}{s} \\ \breve{\psi}_q - \frac{\psi_{q0}}{s} &= x_q(s) \cdot \left(\breve{i}_q - \frac{i_{q0}}{s} \right) - x_Q(s) \cdot \frac{i_{Q0}}{s} \end{aligned} \tag{8.6-4}$$

These **reactance operators** $x_d(s), x_q(s), x_D(s), x_Q(s), x_f(s)$ contain the *Laplace* variable *s*, thus considering the damping influence of the damper and field winding in the dynamic state. The interested reader may follow their derivation from (8.6-1), (8.6-2) in the "Appendix 8.11", resulting in

$$x_d(s) = \frac{s^2 \cdot x_d'' \cdot \sigma_{fD} \cdot \tau_f \cdot \tau_D + s \cdot x_d \cdot \left(\sigma_{df} \cdot \tau_f + \sigma_{dD} \cdot \tau_D \right) + x_d}{s^2 \cdot \sigma_{fD} \cdot \tau_f \cdot \tau_D + s \cdot \left(\tau_f + \tau_D \right) + 1}, \tag{8.6-5}$$

$$x_D(s) = \frac{s \cdot \frac{x_{f\sigma}}{r_f} + 1}{s^2 \cdot \sigma_{fD} \cdot \tau_f \cdot \tau_D + s \cdot \left(\tau_f + \tau_D \right) + 1} \cdot x_{dh} \quad , \tag{8.6-6}$$

$$x_f(s) = \frac{s \cdot \frac{x_{D\sigma}}{r_D} + 1}{s^2 \cdot \sigma_{fD} \cdot \tau_f \cdot \tau_D + s \cdot \left(\tau_f + \tau_D \right) + 1} \cdot x_{dh}, \tag{8.6-7}$$

$$x_q(s) = x_q'' \cdot \frac{s + \dfrac{1}{\sigma_{qQ} \cdot \tau_Q}}{s + \dfrac{1}{\tau_Q}} \quad , \tag{8.6-8}$$

$$x_Q(s) = \frac{\dfrac{1}{\tau_Q}}{s + \dfrac{1}{\tau_Q}} \cdot x_{qh} \quad . \tag{8.6-9}$$

Note that the reactance operators $x_d(s), x_q(s)$ contain the already defined sub-transient inductance of *d*- and *q*-axis x_d'', x_q''. Further the reactance operators depend on **the open-circuit time constants of damper and field winding**

$$\boxed{\tau_D = \frac{x_D}{r_D}, \quad \tau_Q = \frac{x_Q}{r_Q}, \quad \tau_f = \frac{x_f}{r_f}} \quad . \tag{8.6-10}$$

and on *Blondel´*s stray coefficients (8.5-2), (8.5-4). These stray coefficients lead to **short circuit time constants**. For example, in the case of *q*-axis the **short circuit time constant of the damper winding** is (Fig. 8.6-1):

$$\tau_{Q\sigma} = \frac{\sigma_{qQ} \cdot x_Q}{r_Q} \quad . \tag{8.6-11}$$

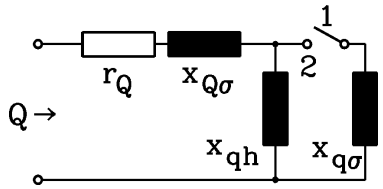

Fig. 8.6-1: Time constant of damper winding in *q*-axis: "1": open circuit time coinstant, "2": short circuit time constant

Facit:
An open circuit time constant considers only resistance and inductance of the winding itself. A short circuit time constant considers the damping influence of a second magnetically linked winding, whose induced current causes a decrease of the total flux linkage. Therefore short-circuit time constant is always shorter than open circuit time constant.

The reactance operator of *d*-axis winding (8.6-5) may also be written as

$$x_d(s) = x_d'' \cdot \frac{s^2 + s \cdot \dfrac{\sigma_{df}\tau_f + \sigma_{dD}\tau_D}{\sigma_{fD}\tau_f\tau_D} \cdot \dfrac{x_d}{x_d''} + \dfrac{1}{\sigma_{fD}\tau_f\tau_D} \cdot \dfrac{x_d}{x_d''}}{s^2 + s \cdot \dfrac{\tau_f + \tau_D}{\sigma_{fD}\tau_f\tau_D} + \dfrac{1}{\sigma_{fD}\tau_f\tau_D}} = x_d'' \cdot \frac{(s + \dfrac{1}{\tau_d'}) \cdot (s + \dfrac{1}{\tau_d''})}{(s + \alpha_{d1}) \cdot (s + \alpha_{d2})}$$

with the solutions of the quadratic equations of numerator and denominator

$$s^2 + s \cdot \frac{\sigma_{df}\tau_f + \sigma_{dD}\tau_D}{\sigma_{fD}\tau_f\tau_D} \cdot \frac{x_d}{x_d''} + \frac{1}{\sigma_{fD}\tau_f\tau_D} \cdot \frac{x_d}{x_d''} = 0 \qquad \Rightarrow \quad s_1 = -\frac{1}{\tau_d'}, s_2 = -\frac{1}{\tau_d''} \quad ,$$

$$s^2 + s \cdot \frac{\tau_f + \tau_D}{\sigma_{fD}\tau_f\tau_D} + \frac{1}{\sigma_{fD}\tau_f\tau_D} = 0 \qquad \Rightarrow \quad s_1 = -\alpha_{d1},\, s_2 = -\alpha_{d2} \quad .$$

As often the **initial conditions are steady state conditions**,

- the damper currents before a dynamic disturbance are zero: $i_{D0} = 0, i_{Q0} = 0$.
- The field voltage is pure DC: $u_f(\tau) = u_{f0}$. In that case is $\frac{\breve{u}_f}{r_f} = \frac{u_{f0}}{s \cdot r_f} = \frac{i_{f0}}{s}$, and therefore $\frac{\breve{u}_f}{r_f} - \frac{i_{f0}}{s} = 0$.

Hence the reactance operators $x_D(s), x_Q(s), x_f(s)$ are NOT needed according to (8.6-4) for calculating deviations from synchronous steady state operation, only $x_d(s), x_q(s)$ remain of interest. Their inverse is needed for calculating stator flux linkage and current. In this inversion of the expressions (8.6-5), (8.6-8) new abbreviations appear:

- the **transient inductance** x'_d of stator winding in *d*-axis,
- the **transient time constant** τ'_d in *d*-axis,
- the **sub-transient time constants** τ''_d, τ''_q in *d*- and *q*-axis.

It is interesting to see that the exact value of the transient inductance is NOT given by (8.6-10), but by the more complicated expression (derivation see Appendix 8.11)

$$\frac{1}{x_d(s)} = \frac{1}{x_d} + \left(\frac{1}{x'_d} - \frac{1}{x_d}\right) \cdot \frac{s}{s + \frac{1}{\tau'_d}} + \left(\frac{1}{x''_d} - \frac{1}{x'_d}\right) \cdot \frac{s}{s + \frac{1}{\tau''_d}}$$

$$\frac{1}{x_q(s)} = \frac{1}{x_q} + \left(\frac{1}{x''_q} - \frac{1}{x_q}\right) \cdot \frac{s}{s + \frac{1}{\tau''_q}} \qquad \text{(8.6-12)}$$

$$x'_d = x''_d \cdot \frac{\frac{1}{\tau''_d} - \frac{1}{\tau'_d}}{\alpha_{d1} + \alpha_{d2} - \frac{1}{\tau'_d} \cdot \left(1 + \frac{x''_d}{x_d}\right)} \quad . \qquad \text{(8.6-13)}$$

$$\alpha_{d1,2} = \frac{\tau_f + \tau_D}{2 \cdot \sigma_{fD} \cdot \tau_f \cdot \tau_D} \mp \sqrt{\left(\frac{\tau_f + \tau_D}{2 \cdot \sigma_{fD} \cdot \tau_f \cdot \tau_D}\right)^2 - \frac{1}{\sigma_{fD} \cdot \tau_f \cdot \tau_D}} \qquad \text{(8.6-14)}$$

$$\frac{1}{\tau'_d}, \frac{1}{\tau''_d} = \frac{x_d \cdot (\sigma_{df}\tau_f + \sigma_{dD}\tau_D)}{x''_d \cdot 2 \cdot \sigma_{fD} \cdot \tau_f \cdot \tau_D} \mp \sqrt{\left(\frac{x_d \cdot (\sigma_{df}\tau_f + \sigma_{dD}\tau_D)}{x''_d \cdot 2 \cdot \sigma_{fD} \cdot \tau_f \cdot \tau_D}\right)^2 - \frac{x_d}{x''_d \cdot \sigma_{fD} \cdot \tau_f \cdot \tau_D}} \qquad \text{(8.6-15)}$$

The **sub-transient time constant of *q*-axis** τ''_q is simply **the short circuit time constant of damper winding in *q*-axis**:

$$\boxed{\tau''_q = \tau_{Q\sigma} = \frac{\sigma_{qQ} \cdot x_Q}{r_Q}} \quad . \tag{8.6-16}$$

In spite of these rather complicated expressions the evaluation of these values for synchronous machines in reality is much simpler, **as the *d*-axis open circuit time constant of damper is much shorter than of field winding,** as already noted in Section 8.5. With $\underline{\underline{\tau_D \ll \tau_f}}$ the solution of (8.6-14) is

$$\alpha_{d1,2} = \frac{\tau_f + \tau_D}{2 \cdot \sigma_{fD} \cdot \tau_f \cdot \tau_D} \mp \sqrt{\left(\frac{\tau_f + \tau_D}{2 \cdot \sigma_{fD} \cdot \tau_f \cdot \tau_D} \right)^2 - \frac{1}{\sigma_{fD} \cdot \tau_f \cdot \tau_D}} =$$

$$= \frac{\tau_f + \tau_D}{2 \cdot \sigma_{fD} \cdot \tau_f \cdot \tau_D} \left[1 \mp \sqrt{1 - \frac{4\sigma_{fD} \cdot \tau_f \cdot \tau_D}{(\tau_f + \tau_D)^2}} \right] \approx \frac{1}{2 \cdot \sigma_{fD} \cdot \tau_D} \left[1 \mp \sqrt{1 - \frac{4\sigma_{fD} \cdot \tau_D}{\tau_f}} \right]$$

With $\sqrt{1-x} \cong 1 - x/2$ for x<<1 we get finally

$$\alpha_{d1,2} \approx \frac{1}{2 \cdot \sigma_{fD} \cdot \tau_D} \left[1 \mp \sqrt{1 - \frac{4\sigma_{fD} \cdot \tau_D}{\tau_f}} \right] \approx \frac{1}{2 \cdot \sigma_{fD} \cdot \tau_D} \left[1 \mp \left(1 - \frac{2\sigma_{fD} \cdot \tau_D}{\tau_f} \right) \right] = \underline{\underline{\frac{1}{\tau_f}, \cong \frac{1}{\sigma_{fD} \cdot \tau_D}}} .$$

The results are called

- **open circuit time constant of damper winding in *d*-axis**

$$\tau''_{d0} = \sigma_{fD} \cdot \tau_D \tag{8.6-17}$$

- **open circuit time constant of field winding** (which is just field winding time constant)

$$\tau'_{d0} = \tau_f \quad . \tag{8.6-18}$$

In the same way we get from (8.6-15)

$$\frac{1}{\tau'_d}, \frac{1}{\tau''_d} = \frac{x_d \cdot (\sigma_{df}\tau_f + \sigma_{dD}\tau_D)}{x''_d \cdot 2 \cdot \sigma_{fD} \cdot \tau_f \cdot \tau_D} \cdot \left[1 \mp \sqrt{1 - \frac{4x''_d \cdot \sigma_{fD} \cdot \tau_f \cdot \tau_D}{x_d \cdot (\sigma_{df}\tau_f + \sigma_{dD}\tau_D)^2}} \right] \approx$$

$$\approx \frac{x_d \cdot \sigma_{df}}{x''_d \cdot 2 \cdot \sigma_{fD} \cdot \tau_D} \cdot \left[1 \mp \sqrt{1 - \frac{4x''_d \cdot \sigma_{fD} \cdot \tau_D}{x_d \cdot \sigma_{df}^2 \tau_f}} \right] \approx \frac{x_d \cdot \sigma_{df}}{x''_d \cdot 2 \cdot \sigma_{fD} \cdot \tau_D} \cdot \left[1 \mp \left(1 - \frac{2x''_d \cdot \sigma_{fD} \cdot \tau_D}{x_d \cdot \sigma_{df}^2 \tau_f} \right) \right] =$$

$$= \underline{\underline{\frac{1}{\sigma_{df} \cdot \tau_f}, \quad \cong \frac{x_d \cdot \sigma_{df}}{x''_d \cdot \sigma_{fD} \cdot \tau_D}}}$$

The results are called

- short circuit time constant of damper winding in *d*-axis or **sub-transient time constant of *d*-axis**

$$\tau''_d = \frac{x''_d \cdot \sigma_{fD} \cdot \tau_D}{x_d \cdot \sigma_{df}} \tag{8.6-19}$$

- short circuit time constant of field winding or **transient time constant of *d*-axis**

$$\tau'_d = \sigma_{df} \cdot \tau_f \quad . \tag{8.6-20}$$

With those values and $\underline{\underline{\tau_D << \tau_f}}$ the expression for the transient inductance (8.6-13) is simplified, leading to the already known equivalent circuit Fig. 8.5-5.

$$x'_d = x''_d \cdot \frac{\frac{1}{\tau''_d} - \frac{1}{\tau'_d}}{\alpha_{d1} + \alpha_{d2} - \frac{1}{\tau'_d} \cdot \left(1 + \frac{x''_d}{x_d}\right)} \approx x''_d \cdot \frac{\frac{x_d \cdot \sigma_{df}}{x''_d \cdot \sigma_{fD} \cdot \tau_D} - \frac{1}{\sigma_{df} \cdot \tau_f}}{\frac{1}{\tau_f} + \frac{1}{\sigma_{fD}\tau_D} - \frac{1}{\sigma_{df} \cdot \tau_f} \cdot \left(1 + \frac{x''_d}{x_d}\right)} \approx$$

$$\approx x''_d \cdot \frac{\frac{x_d \cdot \sigma_{df}}{x''_d \cdot \sigma_{fD} \cdot \tau_D}}{\frac{1}{\sigma_{fD}\tau_D}} = x_d \cdot \sigma_{df} = \underline{\underline{x_{s\sigma} + \frac{x_{dh} x_{f\sigma}}{x_{dh} + x_{f\sigma}}}} \tag{8.6-17}$$

Facit:
Due to the fact, that damper open circuit time constant is much shorter than that of the field winding $\underline{\underline{\tau_D << \tau_f}}$*, the transient inductance* x'_d *may be easily calculated from equivalent circuit Fig. 8.5-5, where the dynamic current in the damper winding has already completely vanished, and only flux linkage of stator and field winding have to be considered.*

Summarizing the results, we conclude that **transfer function for change of flux linkage** – starting from synchronous steady state conditions $i_{D0} = 0, i_{Q0} = 0$, $u_f(\tau) = u_{f0}$ - depends in electrically excited synchronous machines with damper cage on **two rotor time constants in *d*-axis** τ'_d, τ''_d and **one rotor time constant in *q*-axis** τ''_q.

$$\breve{\psi}_d - \frac{\psi_{d0}}{s} = x_d(s) \cdot \left(\breve{i}_d - \frac{i_{d0}}{s}\right)$$

$$\breve{\psi}_q - \frac{\psi_{q0}}{s} = x_q(s) \cdot \left(\breve{i}_q - \frac{i_{q0}}{s}\right)$$

$$\frac{1}{x_d(s)} = \frac{1}{x_d} + \left(\frac{1}{x'_d} - \frac{1}{x_d}\right) \cdot \frac{s}{s + \frac{1}{\tau'_d}} + \left(\frac{1}{x''_d} - \frac{1}{x'_d}\right) \cdot \frac{s}{s + \frac{1}{\tau''_d}}$$

$$\frac{1}{x_q(s)} = \frac{1}{x_q} + \left(\frac{1}{x''_q} - \frac{1}{x_q}\right) \cdot \frac{s}{s + \frac{1}{\tau''_q}}$$

$$\tau'_d = \sigma_{df} \cdot \tau_f$$

$$\tau''_d = \frac{x''_d \cdot \sigma_{fD} \cdot \tau_D}{x_d \cdot \sigma_{df}} \qquad \tau''_q = \tau_{Q\sigma} = \frac{\sigma_{qQ} \cdot x_Q}{r_Q} \tag{8.6-18}$$

Facit:
With Laplace transformation rule, that $\tau \to \infty$ *corresponds with* $s \to 0$ *and vice versa, one concludes:*

*For **short time** after disturbance* $\tau \to 0\ (\Rightarrow s \to \infty)$ *the resultant stator inductance is the sub-transient inductance* $x_d(s \to \infty) = x_d''$, $x_q(s \to \infty) = x_q''$, *thus proving mathematically the equivalent circuits Fig. 8.5-4.*
*For **long time** after disturbance* $\tau \to \infty\ (\Rightarrow s \to 0)$ *the synchronous machine returns to steady state conditions, as the resultant stator inductance is then* $x_d(s \to 0) = x_d$, $x_q(s \to 0) = x_q$.

So **time constant of stator winding** τ_a immediately after disturbance is given by stator resistance r_s and resultant stator inductance x_s'', which in *d*-axis is x_d'' and in *q*-axis is x_q''. As stator field rotates in sub-transient state not synchronously with rotor, it is positioned alternatively in *d*- and *q*-axis position of rotor axes. Therefore resultant stator sub-transient inductance x_s'' may be regarded as parallel connection of *d*- and *q*-axis sub-transient inductance:

$$x_s'' = 2 \cdot \frac{x_d'' \cdot x_q''}{x_d'' + x_q''} \quad , \tag{8.6-19}$$

leading to **stator armature time constant**

$$\tau_a = \frac{2x_d'' \cdot x_q''}{(x_d'' + x_q'') \cdot r_s} \tag{8.6-20}$$

Note that **for a sub-transient symmetrically machine** $x_d'' = x_q''$ we get $x_s'' = x_d'' = x_q''$.
For **permanent magnet machines** without damper cage the dynamic performance is simpler. The sub-transient and transient stator inductances are equal to the synchronous inductance, so no rotor time constants exist. It is $x_d'' = x_d' = x_d$, $x_q'' = x_q$, so we get instead of (8.6-18): $x_d(s) = x_d$, $x_q(s) = x_q$ and $\tau_a = \frac{2x_d \cdot x_q}{(x_d + x_q) \cdot r_s}$.

$$\begin{aligned}
&\breve{u}_d + \psi_{d0} = r_s \cdot \breve{i}_d + s \cdot \breve{\psi}_d - \omega_m \cdot \breve{\psi}_q \\
&\breve{u}_q + \psi_{q0} = r_s \cdot \breve{i}_q + s \cdot \breve{\psi}_q + \omega_m \cdot \breve{\psi}_d \\
&\breve{\psi}_d - \frac{\psi_p}{s} = x_d \cdot \breve{i}_d \qquad\qquad \breve{\psi}_q = x_q \cdot \breve{i}_q \\
&\psi_{d0} = x_d \cdot i_{d0} + \psi_p \qquad\qquad \psi_{q0} = x_q \cdot i_{q0}
\end{aligned} \tag{8.6-21}$$

8.7 Time constants of electrically excited synchronous machines with damper cage

By taking the results of the dynamic equations (Section 8.6), one may derive simplified equivalent circuits in order to understand the dynamic performance of synchronous machine more easily, which are ruled by the corresponding time constants.

Two different states for rotor flux linkage have to be distinguished:
a) **open circuit of stator winding** (= no current flow in stator winding: $i_s = 0$);
b) the stator winding is connected to a feeding voltage source (grid or inverter). In that case a dynamic stator current may flow in case of disturbance **("short-circuit of stator winding").**

For dynamic stator currents with their arbitrary time function the feeding stator voltage source (inverter or grid) with its fixed frequencies has NOT the same time function. So the voltage of the stator voltage source is not limiting the dynamic stator current. Only its inner resistance will be a limiting factor. As it is small, it will be neglected here. So neglecting grid (or inverter) resistance and inductance and – for simplicity – also stator winding resistance r_s, in case b) only stator stray inductance $x_{s\sigma}$ will limit along with main flux linkage the dynamic stator current. Thus in case b) the stator winding for the determination of the dynamic stator current may be regarded as **„short-circuited“.**

a) Field and damper time constant at stator open circuit:
At disturbance in synchronous machine rotor at stator open circuit (such as quick change of damper current) equivalent circuit Fig. 8.7-1 b („state“ 1) has to be used. Flux linkage between field and damper winding is considered, as well as damper resistance. As field winding resistance is much bigger, it leads to a longer time constant is therefore neglected. The resulting open circuit time constant of damper winding in d-axis is T''_{d0}, τ''_{d0} is called "**sub-transient open circuit time constant of direct axis**")

$$T''_{d0} = \frac{L_{D\sigma} + L_{dh} \cdot (L_{f\sigma} / L_f)}{R_D} \qquad \tau''_{d0} = \frac{x_{D\sigma} + x_{dh} \cdot (x_{f\sigma} / x_f)}{r_D} \quad . \tag{8.7-1}$$

After the dynamic damper currents have vanished, only field winding flux linkage remains. In that case the longer open circuit field winding time constant T'_{d0}, τ'_{d0} (Fig. 8.7-1a, „state“ 1), called "**transient open-circuit time constant of *d*-axis“** is simply the time constant of the field winding without any coupling to other windings.

$$T'_{d0} = \frac{L_f}{R_f} = \frac{L_{dh} + L_{f\sigma}}{R_f} = T_f \qquad \tau'_{d0} = \frac{x_f}{r_f} = \tau_f \quad . \tag{8.7-2}$$

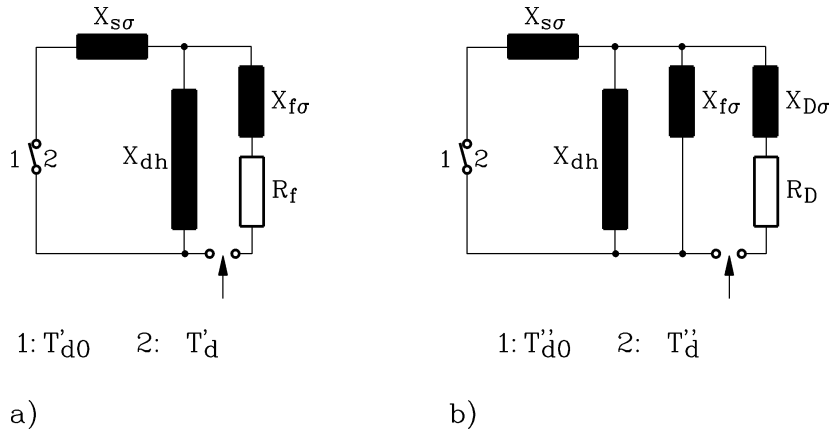

Fig. 8.7-1: **Equivalent circuit** for determination of (1**) open-circuit**- and (2) **short-circuit** time constant of *d*-axis (1: open circuit of stator winding, 2: stator winding connected to stator voltage source = stator winding „short-circuited“)
a) time constant of field winding = transient open circuit and short circuit time constant
b) time constant of damper winding of direct axis = sub-transient open circuit and short circuit time constant

b) Field and damper time constant at stator short circuit:
If the same dynamic change of state on rotor side is considered with operating stator winding, the due to the flux linkage a dynamic stator current is induced, leading to an increased flux damping. Hence much smaller rotor time constants occur. For the damper current the equivalent circuit Fig. 8.7-1b, „state“ 2, is used, leading to a short circuit time constant of the

damper winding in *d*-axis T_d'', τ_d'', called already "**sub-transient short circuit time constant of direct axis**":

$$T_d'' = \frac{L_{D\sigma} + \dfrac{L_{dh}L_{f\sigma}L_{s\sigma}}{L_{dh}L_{f\sigma} + L_{dh}L_{s\sigma} + L_{f\sigma}L_{s\sigma}}}{R_D} \qquad \tau_d'' = \frac{x_{D\sigma} + \dfrac{x_{dh}x_{f\sigma}x_{s\sigma}}{x_{dh}x_{f\sigma} + x_{dh}x_{s\sigma} + x_{f\sigma}x_{s\sigma}}}{r_D} \quad . \text{ (8.7-3)}$$

After decay of the damper bar currents, only the transient flux linkage between field and stator winding exists (Fig. 8.7-1a („state“ 2)), leading to a short circuit time constant of the field winding T_d', τ_d', called already "**transient short-circuit time constant of direct axis**".

$$T_d' = \frac{L_{f\sigma} + L_{dh}\cdot(L_{s\sigma}/L_d)}{R_f} = \frac{L_d\cdot(1-\dfrac{L_{dh}^2}{L_f L_d})}{L_d}\cdot\frac{L_f}{R_f} = \frac{L_d'}{L_d}\cdot T_{d0}', \quad \tau_d' = \frac{x_d'}{x_d}\cdot\tau_{d0}' \quad . \qquad \text{(8.7-4)}$$

As a **proof** for the validity of these equivalent circuits we compare the time constants of Section 8.6, derived from the dynamic equations, with the formulas of this Section, and find identity. Although some of the expressions in the right and left row look quite different, they are **mathematically identical expressions**, thus proving the validity of the equivalent circuits Fig. 8.7-1 for calculating the time constants.

	From dynamic equations of Section 8.6	From equivalent circuit of Section 8.7
τ_{d0}'	$\tau_{d0}' = \tau_f$	$\tau_{d0}' = x_f / r_f = \tau_f$
τ_{d0}''	$\tau_{d0}'' = \sigma_{fD}\cdot\tau_D$	$\tau_{d0}'' = \dfrac{x_{D\sigma} + x_{dh}\cdot(x_{f\sigma}/x_f)}{r_D}$
τ_d'	$\tau_d' = \sigma_{df}\cdot\tau_f$	$\tau_d' = \dfrac{x_d'}{x_d}\cdot\tau_{d0}'$
τ_d''	$\tau_d'' = \dfrac{x_d''\cdot\sigma_{fD}\cdot\tau_D}{x_d\cdot\sigma_{df}}$	$\tau_d'' = \dfrac{x_{D\sigma} + \dfrac{x_{dh}x_{f\sigma}x_{s\sigma}}{x_{dh}x_{f\sigma} + x_{dh}x_{s\sigma} + x_{f\sigma}x_{s\sigma}}}{r_D}$

Table 8.7-1: Transient and sub-transient open circuit and short circuit time constants of *d*-axis

Proof:

$$\underline{\underline{\tau_{d0}''}} = \sigma_{fD}\tau_D = \left(1-\frac{x_{dh}^2}{x_f x_D}\right)\cdot x_D / r_D = \left(x_D - \frac{x_{dh}^2}{x_f}\right)/r_D = \left(x_{D\sigma} + x_{dh} - (x_f - x_{f\sigma})\frac{x_{dh}}{x_f}\right)/r_D =$$

$$= \underline{\underline{\left(x_{D\sigma} + x_{f\sigma}\frac{x_{dh}}{x_f}\right)/r_D}}$$

$$\underline{\underline{\tau_d'}} = \frac{x_d'}{x_d}\cdot\tau_{d0}' = \frac{\sigma_{df}x_d}{x_d}\cdot\tau_{d0}' = \frac{\sigma_{df}x_d}{x_d}\cdot\frac{x_f}{r_f} = \sigma_{df}\frac{x_f}{r_f} = \underline{\underline{\sigma_{df}\cdot\tau_f}},$$

$$\underline{\underline{\tau_d''}} = \frac{x_d''\cdot\sigma_{fD}\cdot\tau_D}{x_d\cdot\sigma_{df}} = x_d''\cdot\frac{1-\dfrac{x_{dh}^2}{x_f x_D}}{1-\dfrac{x_{dh}^2}{x_f x_d}}\cdot\frac{x_D}{x_d}\cdot\frac{1}{r_D} = x_d''\cdot\frac{x_f x_D - x_{dh}^2}{x_f x_d - x_{dh}^2}\cdot\frac{1}{r_D},$$

$$\underline{\underline{\tau''_d}} = \left(x_{s\sigma} + \frac{1}{\frac{1}{x_{f\sigma}} + \frac{1}{x_{D\sigma}} + \frac{1}{x_{dh}}} \right) \cdot \frac{\frac{1}{x_{f\sigma}} + \frac{1}{x_{D\sigma}} + \frac{1}{x_{dh}}}{\frac{1}{x_{f\sigma}} + \frac{1}{x_{s\sigma}} + \frac{1}{x_{dh}}} \cdot \frac{x_{D\sigma}}{x_{s\sigma}} \cdot \frac{1}{r_D} = \left(x_{D\sigma} + \frac{1}{\frac{1}{x_{f\sigma}} + \frac{1}{x_{s\sigma}} + \frac{1}{x_{dh}}} \right) \cdot \frac{1}{r_D} =$$

$$= \underline{\underline{(x_{D\sigma} + \frac{x_{dh} x_{f\sigma} x_{s\sigma}}{x_{dh} x_{f\sigma} + x_{dh} x_{s\sigma} + x_{f\sigma} x_{s\sigma}}) \cdot \frac{1}{r_D}}}$$

Transient open circuit time constant of *d*-axis	$T'_{d0} = L_f / R_f = T_f$	2 ...7 ... 10 s
Transient short circuit time constant of *d*-axis	$T'_d = (L'_d / L_d) \cdot T'_{d0}$	0.6-0.8 ... 1-2 s
Sub-transient open circuit time constant of *d*-axis	T''_{d0}	$T''_{d0} \approx 1.1 \cdot T''_d$
Sub-transient short circuit time constant of *d*-axis	T''_d	0.02 ... 0.1 ... 0.5 s
Sub-transient short circuit time constant of *q*-axis	$T''_q \approx T''_d$	0.02 ... 0.1 ... 0.5 s
Armature time constant	$T_a \approx L''_d / R_s$	0.1 ... 0.4-0.5 s
Acceleration time constant	T_J	3 ... 8-10 s

Table 8.7-2: Magnitudes of time constants of electrically excited synchronous machines with damper cage (range of values for small ... big machines)

8.8 Sudden short circuit of electrically excited synchronous machine with damper cage

A prominent solution of dynamic equations for constant speed is sudden short circuit of all three stator phases.

8.8.1 Sudden Short Circuit at Neglected Resistances

The short circuit current of a synchronous generator, previously running at no-load, following a sudden shortening of all three stator terminals, without consideration of electrical damping by the resistances is calculated in this section (**"three phase sudden short circuit"**). At open stator terminals, the induced phase voltage (e.g. phase U) of a turbine driven synchronous generator at no-load is at constant speed:

$$u_s(t) = \hat{U} \sin(\omega_s t + \varphi_0) = u_{s0}(t) \qquad (8.8.1\text{-}1)$$

If a sudden short circuit of all three terminals occurs, due to the dynamic currents induced in the rotor windings, the sub-transient inductance $L''_d = X''_d / \omega_s$ is effective in the stator windings. For a simplified calculation of the short circuit current $i_s(t)$, the machine is assumed to be symmetrical at sub-transient state ($L''_d = L''_q$) and the stator resistance R_s is neglected, Fig. 8.8.1-1.

According to Fig. 8.8.1-1, with the initial condition $i_s(0) = 0$, $i_s(t)$ is given by:

$$u_s(t) = 0 = u_{s0}(t) + L''_d \cdot di_s / dt \qquad (8.8.1\text{-}2)$$

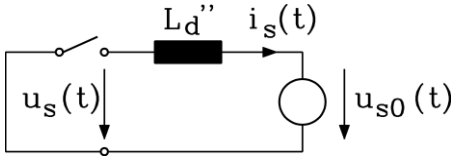

Fig. 8.8.1-1: Simplified equivalent circuit of a synchronous machine, that is symmetrical at sub-transient operation, for calculation of the current following a sudden short circuit of all stator terminals

$$i_s(t) = -\frac{1}{L_d''}\int_0^t u_{s0}(t)dt = \frac{\hat{U}}{\omega_s L_d''}(\cos(\omega_s t + \varphi_0) - \cos\varphi_0) \quad . \tag{8.8.1-3}$$

a) Short Circuit at Zero-Crossing of the Voltage:
If the sudden short circuit occurs at **zero-crossing of the voltage** of phase U, hence at $t = 0$ where $\varphi_0 = 0$, the short circuit current of phase U is (see Fig. 8.8.1-2a):

$$i_s(t) = \frac{\hat{U}}{\omega_s L_d''}(\cos(\omega_s t) - 1) \tag{8.8.1-4}$$

The current rises from 0 (at t = 0) to twice the value of the ac-amplitude $\hat{I}_k''$ (at $t = \pi/\omega_s$). Hence, a **dc-current** with the same amplitude $\hat{I}_k''$ is superimposed to the **sub-transient short circuit ac-component** $\hat{I}_k''$ to give the total current.

$$\hat{I}_k = 2\hat{I}_k'' = 2\sqrt{2}I_k'' = \frac{2\sqrt{2}U}{\omega_s L_d''} = \frac{2\sqrt{2}U}{X_d''} \tag{8.8.1-5}$$

b) Short Circuit at Maximum Voltage:
The case with minimum short-circuit current is the sudden **short circuit at the time of maximum voltage** ($t = 0, \varphi_0 = \pi/2$). Equation (8.8.1-3) gives:

$$i_s(t) = -\frac{\hat{U}}{\omega_s L_d''}\sin(\omega_s t) = -\hat{I}_k''\sin(\omega_s t) \quad . \tag{8.8.1-6}$$

No dc-current exists in that case and the amplitude of the short circuit current is only half of the value of (8.8.1-5).

Example 8.8.1-1:
Parameters: $x_d'' = 0.15 p.u., U_U/U_N = 1,\ f_s = 50Hz$

$$\frac{\hat{I}_k}{I_N} = \frac{2\sqrt{2}U_U/U_N}{X_d''/Z_N} = \frac{2\sqrt{2}\cdot 1}{0.15} = \underline{\underline{18.85}}\,\text{p.u.}$$

Facit:
If the short circuit occurs at zero-crossing of the voltage, the amplitude of the short circuit current in the corresponding phase is very large, because the sub-transient reactance is small and an additional DC-current together with the amplitude of the AC-component occurs.

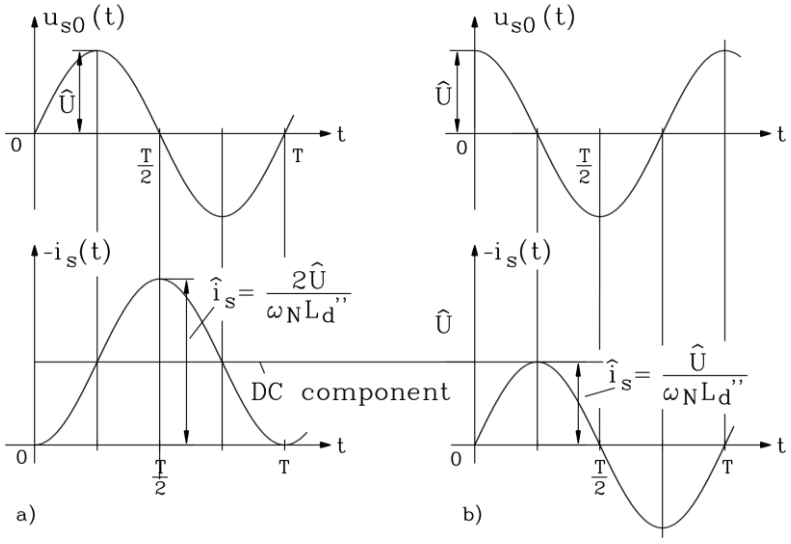

Fig. 8.8.1-2: Undamped current following a sudden short circuit; short circuit occurring at a) zero-crossing of the voltage, b) at maximum voltage.

8.8.2 Sudden Short Circuit with Consideration of Resistances

In the case of a "real" machine the stator resistance R_s must be considered. The dc-current of the stator short circuit current decays with the **stator time constant** $T_a = L_d'' / R_s$ and only the ac-component remains after about $t = 3T_a$. Likewise, the damper currents and the transient current in the field winding decay. Therefore, the synchronous reactance X_d is after the decay of the transient current again the resulting reactance of the stator winding. Then the **steady-state short-circuit current** $I_k = U / X_d$ flows in the stator winding. For the calculation of the time function of the damped sudden short-circuit current, the dynamic equations of the synchronous machines have to be solved. We assume that synchronous machine was

- operating with rated speed $\omega_m = 1$, driven by turbine, as generator
- with open circuit stator winding ($i_s = 0$: $i_{d0} = i_{q0} = 0$)
- in steady state operation $d./d\tau = 0$, $i_{D0} = i_{Q0} = 0$,
- the field winding being excited with DC current $u_{f0} = r_f \cdot i_{f0}$,
- so that at the open stator terminals the no-load voltage is rated voltage: $u_{s0} = u_0$.
- when suddenly short circuit happens.

Initial conditions: Steady state operation (see Example 8.3-1):
$u_{f0} = r_f \cdot i_{f0}$, $\psi_{d0} = x_{dh} i_{f0}, \psi_{q0} = x_q i_{q0} = 0$

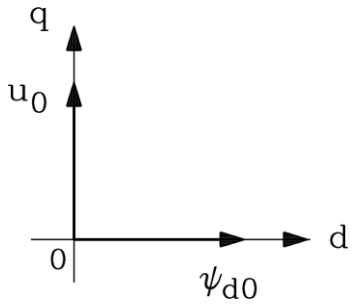

Fig. 8.8.2-1: Steady state no-load voltage in rotor reference frame

$$\underline{\underline{u_{d0} = r_s \cdot i_{d0} - \omega_m \cdot x_q i_{q0} = 0}} \qquad \underline{\underline{u_{q0} = r_s \cdot i_{q0} + \omega_m \cdot x_d i_{d0} + \omega_m \cdot x_{dh} i_{f0} = \omega_m \cdot x_{dh} i_{f0} = u_0}}$$

At a sudden short circuit at $\tau = 0$ stator voltage is zero: $u_d = u_q = 0$. With the dynamic equations in *Laplace* transformation we get:

$$\left.\begin{aligned}
&\breve{u}_d + \psi_{d0} = r_s \cdot \breve{i}_d + s \cdot \breve{\psi}_d - \omega_m \cdot \breve{\psi}_q \Rightarrow \psi_{d0} = r_s \cdot \breve{i}_d + s \cdot \breve{\psi}_d - \breve{\psi}_q \\
&\breve{u}_q + \psi_{q0} = r_s \cdot \breve{i}_q + s \cdot \breve{\psi}_q + \omega_m \cdot \breve{\psi}_d \Rightarrow 0 = r_s \cdot \breve{i}_q + s \cdot \breve{\psi}_q + \breve{\psi}_d \\
&\breve{\psi}_d - \frac{\psi_{d0}}{s} = x_d(s) \cdot \breve{i}_d \\
&\breve{\psi}_q = x_q(s) \cdot \breve{i}_q
\end{aligned}\right\} \Rightarrow$$

$$(r_s + s \cdot x_d(s)) \cdot \breve{i}_d + \psi_{d0} - x_q(s) \cdot \breve{i}_q = \psi_{d0}$$

$$\underline{(r_s + s \cdot x_q(s)) \cdot \breve{i}_q + x_d(s) \cdot \breve{i}_d = -\psi_{d0}/s = -u_0/s}$$

$$\begin{pmatrix} r_s + s \cdot x_d(s) & -x_q(s) \\ x_d(s) & r_s + s \cdot x_q(s) \end{pmatrix} \cdot \begin{pmatrix} \breve{i}_d \\ \breve{i}_q \end{pmatrix} = \begin{pmatrix} 0 \\ -u_0/s \end{pmatrix}$$

Solution:

$$\boxed{\begin{aligned}
&\underline{\underline{\breve{i}_d = -\frac{u_0}{s} \cdot \frac{x_q(s)}{Det}, \quad \breve{i}_q = -\frac{u_0}{s} \cdot \frac{r_s + s \cdot x_d(s)}{Det}}} \\
&Det = (r_s + s \cdot x_d(s)) \cdot (r_s + s \cdot x_q(s)) + x_d(s) x_q(s)
\end{aligned}} \qquad (8.8.2\text{-}1)$$

For inverse *Laplace* transformation we simplify due to $\tau \to 0$:

$$\underline{\tau \to 0:} \quad \frac{r_s}{x_d(s)} \approx \frac{r_s}{x_d(s \to \infty)} = \frac{r_s}{x_d''}, \quad \frac{r_s}{x_q(s)} \approx \frac{r_s}{x_q(s \to \infty)} = \frac{r_s}{x_q''}$$

and due to $r_s << 1$ we put:

$$\underline{r_s << 1:} \quad Det = x_d(s) x_q(s) \left[\left(\frac{r_s}{x_d(s)} + s\right) \cdot \left(\frac{r_s}{x_q(s)} + s\right) + 1 \right] \approx x_d(s) x_q(s) \left[\left(\frac{r_s}{x_d''} + s\right)\left(\frac{r_s}{x_q''} + s\right) + 1 \right] =$$

$$= x_d(s) x_q(s) \left[s^2 + \left(\frac{r_s}{x_d''} + \frac{r_s}{x_q''}\right) s + \frac{r_s^2}{x_d'' x_q''} + 1 \right] \approx x_d(s) x_q(s) \left[\left(s + \frac{r_s \cdot (x_d'' + x_q'')}{2 x_d'' x_q''} \right)^2 + 1 \right]$$

Note that for $x_d'' = x_q''$ the last symbol ≈ is replaced by the identity symbol = !

Facit:

The denominator of current transfer function Det contains the already discussed ***armature time constant*** $\boxed{\tau_a = \frac{2 x_d'' \cdot x_q''}{(x_d'' + x_q'') \cdot r_s}}$*:*

$$Det \approx x_d(s) x_q(s) \left[\left(s + \frac{1}{\tau_a} \right)^2 + 1 \right]$$

$$\breve{i}_d = -\frac{u_0}{s} \cdot \frac{x_q(s)}{x_d(s) x_q(s) \left[\left(s + \frac{1}{\tau_a} \right)^2 + 1 \right]} = -\frac{u_0}{s} \cdot \frac{1}{x_d(s) \left[\left(s + \frac{1}{\tau_a} \right)^2 + 1 \right]}$$

$$\breve{i}_q = -\frac{u_0}{s}\cdot\frac{r_s + s\cdot x_d(s)}{x_d(s)x_q(s)\left[\left(s+\frac{1}{\tau_a}\right)^2+1\right]} \approx -\frac{u_0}{s}\cdot\frac{s}{x_q(s)\left[\left(s+\frac{1}{\tau_a}\right)^2+1\right]}$$

Using the inverse expression for reactance operators yields for inverse *Laplace* transformation for the *d*-axis

$$\frac{1}{s\cdot x_d(s)} = \frac{1}{s\cdot x_d} + \left(\frac{1}{x'_d}-\frac{1}{x_d}\right)\cdot\frac{1}{s+\frac{1}{\tau'_d}} + \left(\frac{1}{x''_d}-\frac{1}{x'_d}\right)\cdot\frac{1}{s+\frac{1}{\tau''_d}} \Rightarrow$$

$$\Rightarrow f_d(\tau) = \frac{1}{x_d} + \left(\frac{1}{x'_d}-\frac{1}{x_d}\right)\cdot e^{-\tau/\tau'_d} + \left(\frac{1}{x''_d}-\frac{1}{x'_d}\right)\cdot e^{-\tau/\tau''_d}$$

and for the *q*-axis

$$\frac{1}{s\cdot x_q(s)} = \frac{1}{s\cdot x_q} + \left(\frac{1}{x''_q}-\frac{1}{x_q}\right)\cdot\frac{1}{s+\frac{1}{\tau''_q}} \Rightarrow f_q(\tau) = \frac{1}{x_q} + \left(\frac{1}{x''_q}-\frac{1}{x_q}\right)\cdot e^{-\tau/\tau''_q}.$$

With the *Laplace* inverse of

$$\frac{1}{\left(s+\frac{1}{\tau_a}\right)^2+1} \Rightarrow g_d(\tau) = e^{-\tau/\tau_a}\cdot\sin\tau$$

$$\frac{s}{\left(s+\frac{1}{\tau_a}\right)^2+1}_{r_s<<1} \approx \frac{s+1/\tau_a}{\left(s+\frac{1}{\tau_a}\right)^2+1} \Rightarrow g_q(\tau) = e^{-\tau/\tau_a}\cdot\cos\tau$$

one has now products of functions for inverse transformation according to

$$\breve{f}(s)\cdot\breve{g}(s) \Rightarrow f(\tau)*g(\tau) = \int_0^\tau f(\tau-\xi)\cdot g(\xi)\cdot d\xi \quad .$$

These products have the following structure:
$1*e^{-\alpha\tau}\cdot\sin\tau, 1*e^{-\alpha\tau}\cdot\cos\tau, e^{-\beta\tau}*e^{-\alpha\tau}\cdot\sin\tau, e^{-\beta\tau}*e^{-\alpha\tau}\cdot\cos\tau$, where $\alpha = 1/\tau_a \sim r_s$ and $\beta = 1/\tau''_d \sim r_D$ or $\beta = 1/\tau'_d \sim r_f$, so we assume $\alpha, \beta << 1$. The solutions of the integrals are

$$e^{-\beta\tau}*e^{-\alpha\tau}\cdot\sin\tau = \int_0^\tau e^{-\beta(\tau-\xi)}e^{-\alpha\xi}\cdot\sin\xi\cdot d\xi =$$

$$= \frac{e^{-\beta\tau}}{1+(\beta-\alpha)^2}\cdot\left[1-e^{(\beta-\alpha)\tau}\cos\tau+(\beta-\alpha)\cdot e^{(\beta-\alpha)\tau}\sin\tau\right]_{\alpha,\beta<<1} \approx e^{-\beta\tau}-e^{-\alpha\tau}\cos\tau$$

and

$$e^{-\beta\tau} * e^{-\alpha\tau} \cdot \cos\tau = \int_0^\tau e^{-\beta(\tau-\xi)} e^{-\alpha\xi} \cdot \cos\xi \cdot d\xi =$$

$$= \frac{e^{-\beta\tau}}{1+(\beta-\alpha)^2} \cdot \left[e^{(\beta-\alpha)\tau} \sin\tau + (\beta-\alpha) \cdot e^{(\beta-\alpha)\tau} \sin\tau - (\beta-\alpha) \right]_{\alpha,\beta<<1} \approx e^{-\alpha\tau} \sin\tau$$

So we conclude for α, $\beta << 1$:

$$e^{-\beta\tau} * e^{-\alpha\tau} \cdot \sin\tau = \int_0^\tau e^{-\beta(\tau-\xi)} e^{-\alpha\xi} \cdot \sin\xi \cdot d\xi \approx e^{-\beta\tau} - e^{-\alpha\tau} \cos\tau$$

$$e^{-\beta\tau} * e^{-\alpha\tau} \cdot \cos\tau = \int_0^\tau e^{-\beta(\tau-\xi)} e^{-\alpha\xi} \cdot \cos\xi \cdot d\xi \approx e^{-\alpha\tau} \sin\tau$$

$$\beta = 0: \quad 1 * e^{-\alpha\tau} \cdot \sin\tau = \int_0^\tau e^{-\alpha\xi} \cdot \sin\xi \cdot d\xi \approx 1 - e^{-\alpha\tau} \cos\tau$$

$$\beta = 0: \quad 1 * e^{-\alpha\tau} \cdot \cos\tau = \int_0^\tau e^{-\alpha\xi} \cdot \cos\xi \cdot d\xi \approx e^{-\alpha\tau} \sin\tau$$

So finally solution of sudden short circuit *d*- and *q*-axis stator current is (for small resistances):

$$i_d(\tau) = -u_0 \cdot \left[\frac{1}{x_d} \left(1 - e^{-\tau/\tau_a} \cos\tau \right) + \left(\frac{1}{x'_d} - \frac{1}{x_d} \right) \cdot \left(e^{-\tau/\tau'_d} - e^{\tau/\tau_a} \cos\tau \right) + \right.$$

$$\left. + \left(\frac{1}{x''_d} - \frac{1}{x'_d} \right) \cdot \left(e^{-\tau/\tau''_d} - e^{-\tau/\tau_a} \cdot \cos\tau \right) \right]$$

$$\boxed{\begin{aligned} i_d(\tau) &= \underline{\underline{-u_0 \cdot \left[\frac{1}{x_d} + \left(\frac{1}{x'_d} - \frac{1}{x_d} \right) \cdot e^{-\tau/\tau'_d} + \left(\frac{1}{x''_d} - \frac{1}{x'_d} \right) \cdot e^{-\tau/\tau''_d} - \frac{1}{x''_d} e^{-\tau/\tau_a} \cdot \cos\tau \right]}} \\ i_q(\tau) &= -u_0 \cdot \left[\frac{1}{x_q} \cdot e^{-\tau/\tau_a} \cdot \sin\tau + \left(\frac{1}{x''_q} - \frac{1}{x_q} \right) \cdot e^{-\tau/\tau_a} \cdot \sin\tau \right] = \underline{\underline{-\frac{u_0}{x''_q} \cdot e^{-\tau/\tau_a} \cdot \sin\tau}} \end{aligned}}$$

The stator phase current in phase U is given as real part of current space vector in stator reference frame, so stator space vector in rotor reference frame $\underline{i}_{s(R)} = i_d + j \cdot i_q$ has to be transformed into stator reference frame by $\underline{i}_{s(S)} = \underline{i}_{s(R)} e^{j\gamma}$ with $\gamma = \omega_m \tau + \gamma_0 = \tau + \gamma_0$:

$$i_U(\tau) = \mathrm{Re}\{\underline{i}_s\} = \mathrm{Re}\{(i_d + j \cdot i_q)(\cos\gamma + j \cdot \sin\gamma)\} = i_d \cdot \cos(\tau + \gamma_0) - i_q \cdot \sin(\tau + \gamma_0)$$

With

$$\cos\tau \cdot \cos(\tau + \gamma_0) = \frac{1}{2} \cdot \left(\cos\gamma_0 + \cos(2\tau + \gamma_0) \right), \; \sin\tau \cdot \sin(\tau + \gamma_0) = \frac{1}{2} \cdot \left(\cos\gamma_0 - \cos(2\tau + \gamma_0) \right)$$

we get

$$i_U(\tau) = -u_0 \cdot \left[\frac{1}{x_d} + \left(\frac{1}{x'_d} - \frac{1}{x_d} \right) \cdot e^{-\tau/\tau'_d} + \left(\frac{1}{x''_d} - \frac{1}{x'_d} \right) \cdot e^{-\tau/\tau''_d} \right] \cdot \cos(\tau + \gamma_0) + \\ + u_0 \cdot \left[\frac{1}{2} \left(\frac{1}{x''_d} + \frac{1}{x''_q} \right) \cdot \cos\gamma_0 + \frac{1}{2} \left(\frac{1}{x''_d} - \frac{1}{x''_q} \right) \cdot \cos(2\tau + \gamma_0) \right] \cdot e^{-\tau/\tau_a} \qquad (8.8.2\text{-}2)$$

Discussion of time function of short circuit current:

- First part $[.] \cdot \cos(\tau + \gamma_0)$ is **AC short circuit current** with frequency $\omega_m = 1$, starting with big amplitude u_0 / x''_d at $\tau = 0$, which decays after three time constants $3\tau''_d$ to the intermediate amplitude u_0 / x'_d and after three time constants $3\tau'_d$ down to the steady state short circuit current u_0 / x_d.
- Second part $[.] \cdot \cos\gamma_0$ is **DC short circuit current**, which decays with armature time constant τ_a and depends on the phase angle γ_0, when sudden short circuit occurs.
- Third part $[.] \cdot \cos(2\tau + \gamma_0)$ is AC short circuit current with **double frequency**, which occurs only, if $x''_d \neq x''_q$ and usually is of minor interest, as it is small.

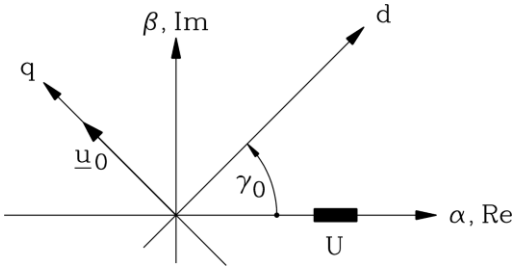

Fig. 8.8.2-2: Steady state no-load voltage in stator reference frame

Influence of phase angle γ_0, when sudden short circuit occurs, is very important: The no-load voltage phasor $\underline{u}_{s(R)} = u_d + j \cdot u_q = j \cdot u_0$ in stator reference frame

$$\underline{u}_{s(S)} = \underline{u}_{s(R)} \cdot e^{j\gamma}$$

leads to stator voltage in phase U (Fig. 8.8.2-2) as

$$u_{s,U}(\tau) = \mathrm{Re}\left\{ \underline{u}_{s(R)} \cdot e^{j\gamma} \right\} = \mathrm{Re}\left\{ j \cdot u_0 \cdot e^{j(\tau+\gamma_0)} \right\} = -u_0 \cdot \sin(\tau + \gamma_0). \qquad (8.8.2\text{-}3)$$

- Worst case: At $\gamma_0 = 0$ the short circuit occurs in phase U at $\tau = 0$, when voltage is zero. This leads to addition of DC and AC component, which for $x''_d = x''_q$ have the same amplitude, so the peak short circuit current is twice the AC amplitude (Fig. 8.8.2-3).

$$\hat{i}_U \approx \frac{2u_0}{x''_d} \qquad . \qquad (8.8.2\text{-}4)$$

- Best case: At $\gamma_0 = \pi/2$ the short circuit occurs in phase U at $\tau = 0$, when voltage is maximum. In that case DC component is zero due to $\cos\gamma_0 = 0$. This leads only to an AC component (Fig. 8.8.2-4)

$$\hat{i}_U \approx \frac{u_0}{x_d''} \quad . \tag{8.7-5}$$

Example 8.8.2-1:
Short circuit of 24-pole synchronous generator after no-load at rated voltage $u_0 = 1$ and rated speed, yielding stator frequency f_N = 50 Hz:
Machine data: S_N = 300 MVA, U_N = 24 kV, I_N = 7217 A, $x_d = 1$, $x_d' = 0.3$, $x_d'' = x_q'' = 0.15$
Time constants: $T_a = 0.03s$, $T_d' = 0.3s$, $T_d'' = 0.05s$ $\Rightarrow$ $\tau_a = 9.42$, $\tau_d' = 94.2$, $\tau_d'' = 15.7$

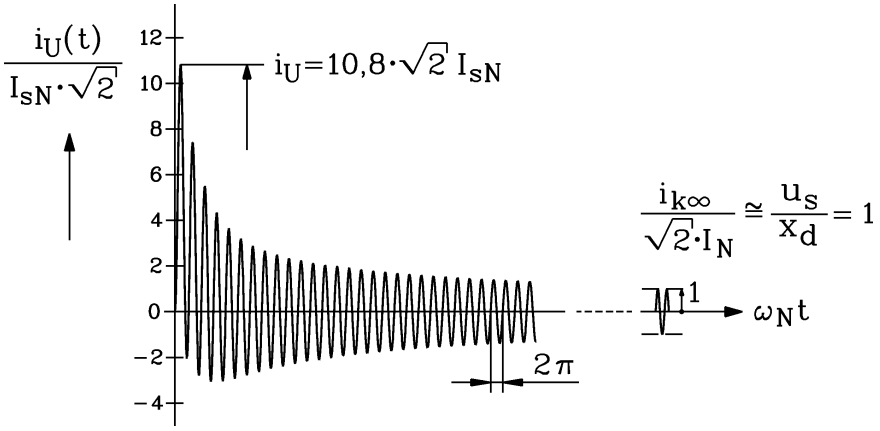

Fig. 8.8.2-3: Sudden short circuit current in phase U in worst case (phase voltage is zero at short circuit: $\gamma_0 = 0$).

The steady state short circuit is for $\tau \to \infty$: $i_s = \hat{I}_{s,U}/(\sqrt{2}I_N) = u_0/x_d = 1/1 = 1$ p.u., which is 7217 A r.m.s. The peak current is with neglecting damping $\hat{i}_U \approx \frac{2u_0}{x_d''} = \frac{2 \cdot 1}{0.15} = 13.3$. Due to the decay of AC and DC current amplitude only 10.8 is reached, which is $10.8 \cdot \sqrt{2} \cdot 7217 = 110.3$ kA (!)

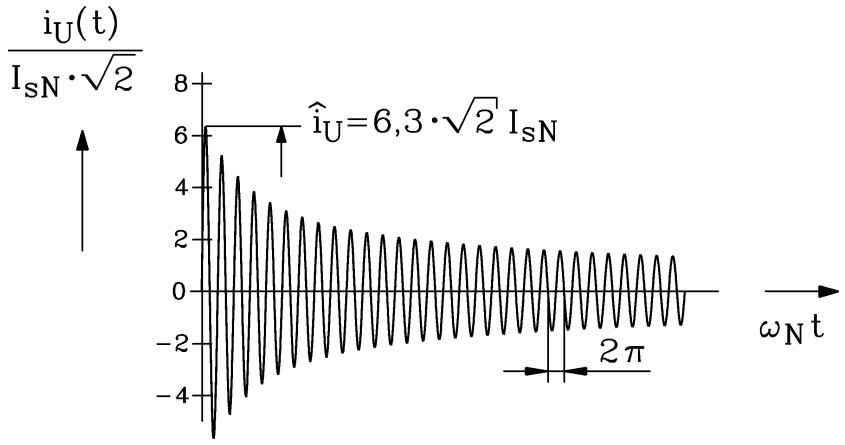

Fig. 8.8.2-4: Sudden short circuit current in phase U in best case (phase voltage is maximum at short circuit: $\gamma_0 = \pi/2$).

Peak current is with neglected damping $\hat{i}_U \approx \frac{u_0}{x_d''} = \frac{1}{0.15} = 6.7$, whereas due to damping only 6.3-times rated current is reached: $6.3 \cdot \sqrt{2} \cdot 7217 = 64.3$ kA

Example 8.8.2-2:
Short circuit of synchronous generator (see Example 8.8.2-1), but with 3-times increased armature time constant and by 2/3 reduced transient and sub-transient time constant:
Time constants: $T_a = 0.1s, T_d' = 0.2s, T_d'' = 0.03s \quad \Rightarrow \quad \tau_a = 31.4, \tau_d' = 62.8, \tau_d'' = 9.4$

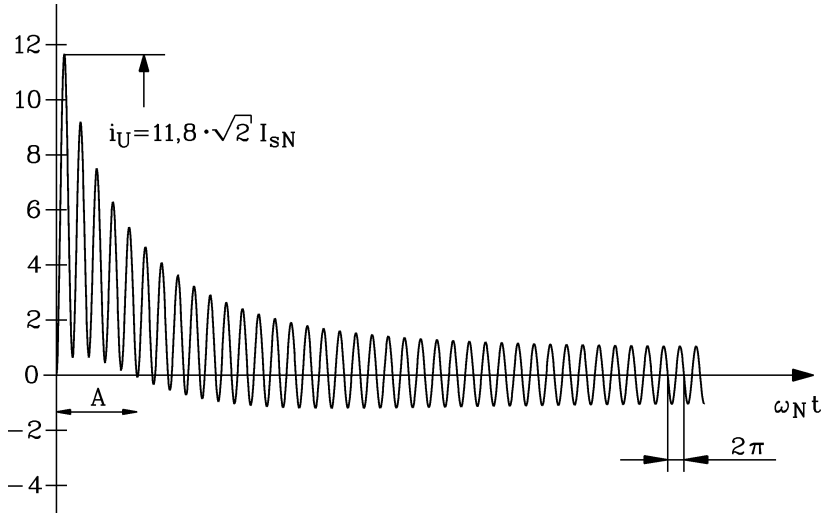

Fig. 8.8.2-5: Sudden short circuit current in phase U in worst case (phase voltage is zero at short circuit: $\gamma_0 = 0$) with armature time constant about 3-times sub-transient time constant

As armature time constant is about 3-times sub-transient time constant, DC current component decays slower than AC component, leading to about five current periods without current zero crossing. AC power switch between generator terminals and location of short circuit cannot extinguish the arc within the switch chamber, as long as no current zero crossing occurs (time span A). So short circuit current can be switched off at the earliest after six periods or $6 \cdot 20 = 120\,\text{ms}$, leading to high mechanical stress during that within the machine due to the big forces between conductors. The peak current is with 11.8 higher than in previous example due to the slower decay of DC short circuit current.

In **permanent magnet machines** the short circuit current is much smaller, as $x_d = x_d' = x_d''$. It is in worst case at maximum twice steady state short circuit current and decays for $x_d = x_q$ with time constant $\tau_a = x_d / r_s$.

8.8.3 Descriptive Explanation of the Behaviour at Sudden Short Circuit

The occurrence of this large stator current following a sudden short circuit due to
a) the DC current component and due to
b) the small sub-transient inductance $L_d'' < L_d$ can be understood from the flux linkages. The **"sudden short circuit at zero-crossing of the voltage"** is used as example for a descriptive explanation, first for the **occurrence of the DC stator current component** (Fig. 8.8.1-2a). Fig. 8.8.3-1a shows a two-pole salient-pole synchronous generator without damper winding at no-load. The rotor is driven at speed Ω_{syn} by a turbine and is excited by permanent magnets. The shown stator coil is at zero current (no load). The voltage $u_{s0}(t)$ with the amplitude according to (8.8.3-1) is induced in this coil due to the change of stator flux linkage ψ_s.

$$\hat{U} = \omega_s \hat{\Psi}_s \quad \text{(e.g. } \omega_s = \omega_N \quad \text{rated frequency)} \tag{8.8.3-1}$$

At the time t = 0, the flux linkage ψ_s of this stator coil is at maximum: $\psi_s = \hat{\psi}_s$, therefore, the induced voltage is zero. Then, the short circuit of this stator coil, representing the stator winding, occurs. Due to (8.8.3-2), the value of $\boxed{\psi_s = const. = \hat{\Psi}_s}$ has to remain constant.

$$R_s \approx 0: \; u_s = d\psi_s / dt = 0 \quad \Rightarrow \quad \psi_s = const. = \hat{\Psi}_s \tag{8.8.3-2}$$

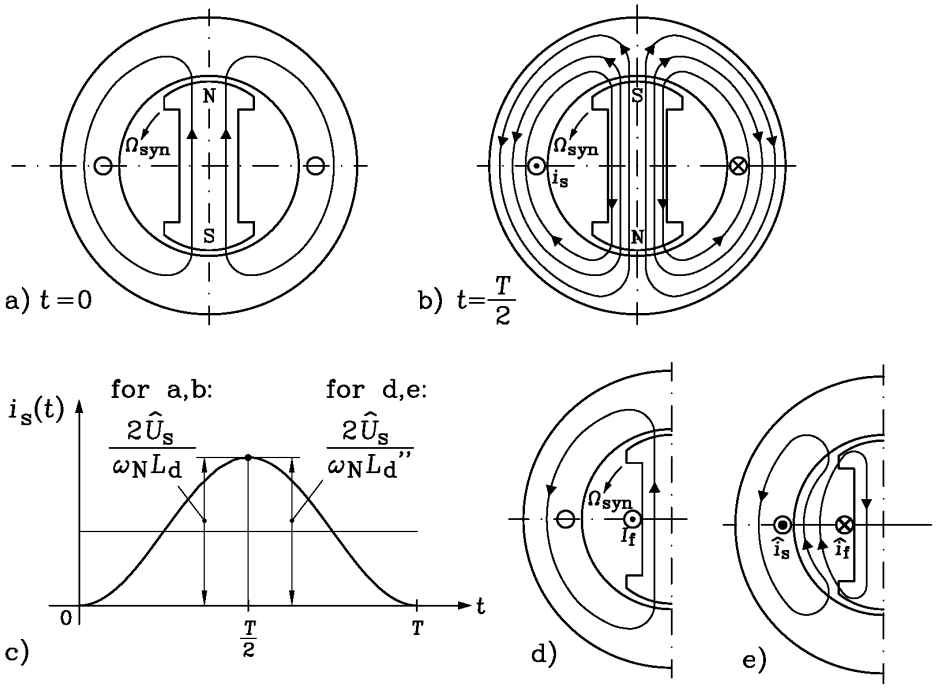

Fig. 8.8.3-1: Flux distribution of a synchronous generator at no-load without damper winding. Rotor with permanent magnet excitation: a) at the time of the short circuit, b) half a revolution of the rotor later, c) qualitative corresponding stator current graph for cases a, b and d, e. Note that in case d, e the current amplitude in A is much higher than in case a, b due to $L_d'' < L_d$. d), e) As a, b, but with electrically excited rotor winding, yielding $L_d' < L_d$, and in case with additional damper $L_d'' < L_d$.

Half a revolution of the rotor later ($\omega_s t = \pi$), the two flux lines of the exciting rotor PM field (which had caused the stator flux linkage $\psi_s = \hat{\Psi}_s$ at t = 0, now causing $-\hat{\Psi}_s$) are linked with opposite sign with the stator coil (Fig. 8.8.3-1b). Therefore, the maximum current i_s has to flow in the coil in a way to excite in addition four flux lines with original polarity (corresponding to $2\hat{\Psi}_s$), so that the overall stator flux linkage remains constant: $2\hat{\Psi}_s - \hat{\Psi}_s = \hat{\Psi}_s = const.$ With the synchronous inductance of the considered stator coil L_d therefore the short circuit current is:

$$L_d \hat{i}_s = 2\hat{\Psi}_s \quad \Rightarrow \quad \hat{i}_s = \frac{2\hat{\Psi}_s}{L_d} = \frac{2\hat{U}}{\omega_s L_d} = i_s(\omega_s t = \pi) \quad . \tag{8.8.3-3}$$

Facit:

The current amplitude (8.8.3-3, Fig. 8.8.3-1c) is derived with a DC component similar to (8.8.1-5), but for L_d due to the PM excitation. A full revolution later, the initial state is obtained again, and the value of the current has to be zero, so that the flux linkage of the stator coil remains constant (Fig. 8.8.3-1c).

In **case of an electrically excited rotor** (Fig. 8.8.3-1d), fed e.g. via two slip rings from a DC voltage source U_f to drive the field current I_f via $U_f = R_f \cdot I_f$, we have to note that the

internal impedance of such voltage sources (e.g. grid voltage with rectifier) is usually very small. Hence also the rotor winding may be regarded as nearly short-circuited, if a change of the rotor winding flux linkage ψ_f occurs, causing a transient field current $i_{f,AC}$.
$U_f = R_f \cdot (i_{f,AC} + I_f) + d\psi_f / dt \Rightarrow 0 = R_f i_{f,AC} + d\psi_f / dt \approx d\psi_f / dt \Rightarrow \psi_f = const. = \hat{\Psi}_f$
So the transient rotor field current $i_f = i_{f,AC} + I_f$ flows in that way to keep the rotor flux linkage (nearly) constant: $\psi_f = const. = \hat{\Psi}_f$. So after half a revolution of the rotor ($\omega_s t = \pi$, Fig. 8.8.1-3e), the two flux lines of the exciting rotor PM field (causing the stator flux linkage $\psi_s = \hat{\Psi}_s$ at $t = 0$ and now $-\hat{\Psi}_s$) are "frozen" and opposite to Fig. 8.8.3-1d. Therefore i_f and i_s have opposite sign, so their excited stator and rotor magnet fields must close the *B*-field lines via the air gap, causing a strong reduction of the corresponding winding inductances. The stator inductance drops from L_d to $L'_d < L_d$, and in case with additional damper to $L''_d < L_d$. The maximum current i_s has to flow in the coil in a way to keep $\psi_s = const. = \hat{\Psi}_s$. So it has to excite $L''_d \hat{i}_s = 2\hat{\Psi}_s$, so that the overall stator flux linkage remains constant: $2\hat{\Psi}_s - \hat{\Psi}_s = \hat{\Psi}_s = const.$ With the small sub-transient inductance L''_d of the considered stator coil therefore the short circuit current is:

$$L''_d \hat{i}_s = 2\hat{\Psi}_s \quad \Rightarrow \quad \hat{i}_s = \frac{2\hat{\Psi}_s}{L''_d} = \frac{2\hat{U}}{\omega_s L''_d} = i_s(\omega_s t = \pi) \quad , \tag{8.8.3-4}$$

which is now much bigger as in the case with rotor permanent magnet excitation, because in addition to the DC current component also the small sub-transient inductance occurs. Also the rotor transient field current is much bigger than the DC field current $i_f > I_f$ to magnetize the rotor field along the long air-gap path.

Facit:
The current amplitude (8.8.3-4) with its DC component (Fig. 8.8.3-1c) is derived in accordance with (8.8.1-5). A full revolution later, the initial state is obtained again, and the value of the current has to be zero, so that the flux linkage of the stator coil and rotor winding remains constant (Fig. 8.8.3-1c).

8.9 Sudden short circuit torque and measurement of dynamic machine parameters

Neglecting the damping of short circuit current, the initial value of sudden short circuit torque immediately after the short circuit is derived. For $\tau \to 0$ we get from the reactance operators for $s \to \infty$ with $i_{d0} = 0, i_{q0} = 0$ and $x_d(s \to \infty) = x''_d$, $x_q(s \to \infty) = x''_q$.

$$\breve{\psi}_d - \frac{\psi_{d0}}{s} = x_d(s) \cdot \left(\breve{i}_d - \frac{i_{d0}}{s} \right) \quad \Rightarrow \quad \psi_d(\tau) = \psi_{d0} + x''_d \cdot i_d(\tau) \tag{8.9-1a}$$

$$\breve{\psi}_q - \frac{\psi_{q0}}{s} = x_q(s) \cdot \left(\breve{i}_q - \frac{i_{q0}}{s} \right) \quad \Rightarrow \quad \psi_q(\tau) = \psi_{q0} + x''_q \cdot i_q(\tau) \tag{8.9-1b}$$

with $\psi_{d0} = u_0, \psi_{q0} = 0$. The short circuit current components for neglected damping are

$$i_d(\tau) = -\frac{u_0}{x''_d} \cdot [1 - \cos\tau] \qquad i_q(\tau) = -\frac{u_0}{x''_q} \cdot \sin\tau \qquad . \tag{8.9-2}$$

So time function of non-damped *d*- and *q*-flux linkage is

$$\psi_d(\tau) = u_0 + x_d'' \cdot (-\frac{u_0}{x_d''}) \cdot [1 - \cos\tau] = u_0 \cdot \cos\tau$$

$$\psi_q(\tau) = x_q'' \cdot (-\frac{u_0}{x_q''}) \cdot \sin\tau = -u_0 \cdot \sin\tau$$

leading to non-damped **electromagnetic short circuit torque**

$$m_e(\tau) = i_q(\tau) \cdot \psi_d(\tau) - i_d(\tau) \cdot \psi_q(\tau) = -\frac{u_0}{x_d''} \cdot [1 - \cos\tau] \cdot u_0 \cdot \sin\tau - \frac{u_0}{x_q''} \cdot \sin\tau \cdot u_0 \cdot \cos\tau$$

$$\boxed{m_e(\tau) = -\frac{u_0^2}{x_d''} \cdot \sin\tau + \frac{u_0^2}{2}\left(\frac{1}{x_d''} - \frac{1}{x_q''}\right) \cdot \sin(2\tau)} \qquad (8.9\text{-}3)$$

Facit:

For sub-transient symmetric machines $x_d'' = x_q''$ the dynamic short circuit pulsates with frequency $\omega_m = 1$ with a big amplitude u_0^2 / x_d''. Average value is zero. With considering damping the torque decays with armature time constant τ_a. The average value of the torque in that case is larger than zero, as the mechanical input power via the torque is converted into the losses in stator, damper and field winding. Thus the speed will decrease a little bit due the braking electromagnetic torque. In any case the ratio peak torque/average torque is very big. The big peak torque might lead to breaking of the machine shaft.

Note that the short circuit torque does not depend on the angle γ_0, as it is constituted from all three phase currents.

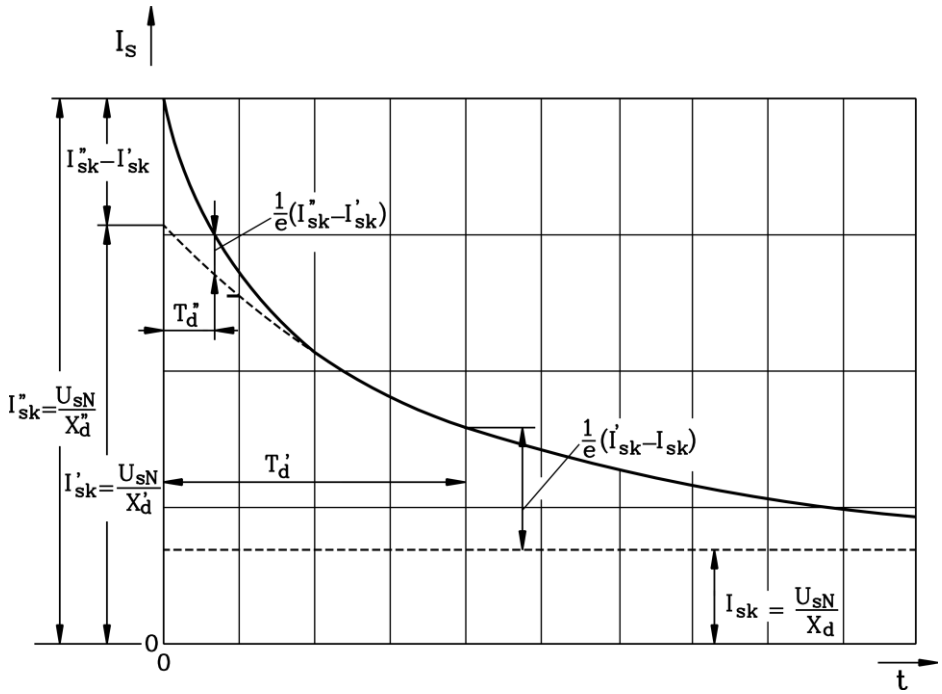

Fig. 8.9-1: Envelope of a symmetrical AC three phase short circuit current for determination of the transient, sub-transient and synchronous reactance and the transient and sub-transient time constant

Example 8.9-1:
Synchronous generator sudden short circuit, data of Example 8.8.2-1:
Peak short circuit torque is $u_0^2 / x_d'' = 1/0.15 = 6.67$.
With $M_B = \frac{S_N}{\omega_N / p} = \frac{300}{2\pi \cdot 50/12} = 11.46\,\text{MNm}$, the peak torque is $6.67 \cdot 11.46 = \underline{\underline{76.43}}\,\text{MNm}$.

From the measured envelope Fig. 8.9-1 of the symmetrical AC short circuit current time function (Fig. 8.8.2-4) the time constants T_d', T_d'' and the reactance X_d, X_d', X_d'' are determined.

$$I_{s,U} = U_{s,N} \cdot \left[\frac{1}{X_d} + \left(\frac{1}{X_d'} - \frac{1}{X_d} \right) \cdot e^{-t/T_d'} + \left(\frac{1}{X_d''} - \frac{1}{X_d'} \right) \cdot e^{-t/T_d''} \right]$$

8.10 Transient stability of electrically excited synchronous machines

After increasing load step it is interesting to notice, that even if this load step would result in a load torque bigger than static pull-out torque $M_s > M_{p0}$, the synchronous machine will not pull out of synchronism, but for the short time of about 3 transient short circuit time constants $3T_d'$ will stay in synchronism. It is reacting with a **dynamical pull-out torque**, which is bigger than the synchronous pull-out torque: $M_{p,dyn} > M_{p0}$. This helps stabilizing the machine, until the field current control will react to increase rotor flux to increase M_{p0}. As this increase of pull-out torque is only active during transient time scale, speed of the machine does not change much and may be considered here constant.

To understand this phenomenon, we start with the steady state solution of the dynamic equations in rotor reference frame at $\tau \le 0$ prior to the load step:

$$u_{d0} = r_s i_{d0} - \omega_s \psi_{q0} = r_s i_{d0} - \omega_s x_q i_{q0} \quad (8.10\text{-}1)$$

$$u_{q0} = r_s i_{q0} + \omega_s \psi_{d0} = r_s i_{q0} + \omega_s x_d i_{d0} + \omega_s x_{dh} i_{f0} \quad (8.10\text{-}2)$$

$$\psi_{d0} = x_d i_{d0} + x_{dh} i_{f0} \quad (8.10\text{-}3)$$

$$\psi_{q0} = x_q i_{q0} \quad , \quad (8.10\text{-}4)$$

where the p.u. **synchronous back EMF** is

$$u_{p0} = \omega_s x_{dh} i_{f0} \quad . \quad (8.10\text{-}5)$$

After a sudden load step the damper bar currents decay within sub-transient time scale $3\tau_d''$. During transient time $3\tau_d'' < \tau < 3\tau_d'$ the transient field current in the field winding flows in addition to the DC field current. For the transient field current flow the field exciter voltage source acts like a short circuit due to its low internal resistance (e.g. a battery or a silicon controlled rectifier).

$$0 = r_f \cdot i_f(\tau) + \frac{d\psi_f(\tau)}{d\tau} \quad (8.10\text{-}6)$$

Neglecting field winding resistance r_f, we get $d\psi_f / d\tau = 0 \Rightarrow \psi_f = const.$. Flux linkage equation of field winding yields

$$\psi_f = x_{dh} i_d + x_f i_f = \text{const.} \tag{8.10-7}$$

Thus the total dynamic field current i_f is a superposition of DC field current i_{f0} and transient field current, which is determined so that the field winding flux linkage ψ_f stays constant.

$$i_f = (\psi_f - x_{dh} i_d) / x_f \tag{8.10-8}$$

As the stator flux linkage of rotor flux prior to load step is $x_{dh} i_{f0}$, the flux linkage $\psi_f = x_{dh} i_{d0} + x_f i_{f0}$ is kept constant during transient operation, if r_f is neglected.

Thus the flux linkage of *d*-axis during transient state is

$$\psi_d = x_d i_d + x_{dh} i_f = x_d i_d - (x_{dh}^2 / x_f) \cdot i_d + (x_{dh} / x_f) \cdot \psi_f = x'_d i_d + (x_{dh} / x_f) \cdot \psi_f \quad , \tag{8.10-9}$$

which is determined by the transient inductance x'_d.

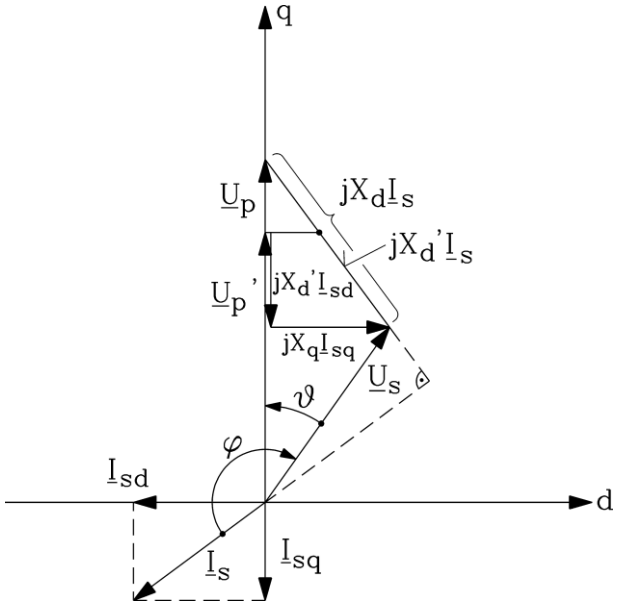

Fig. 8.10-1: Cylindrical rotor synchronous machine: Phasor diagram per phase in physical units in rotor reference frame during transient state: $X'_q = X_q = X_d, X'_d < X_d$, stator resistance neglected (R_s = 0): Phasor diagram for over-excited generator operation

Comparing stator *d*-axis flux linkage (8.10-3) before load step and (8.10-9) after load step, one concludes:

a) Instead of x_d now the **transient inductance** x'_d is acting.
b) Instead of $x_{dh} i_{f0}$, which is the stator flux linkage due to rotor flux and determines synchronous back EMF u_p, the smaller value $(x_{dh} / x_f) \cdot \psi_f$ has to be taken. That means: Instead of synchronous back EMF u_p the smaller **transient back EMF** u'_p has to be taken.

$$u'_p = \frac{x_{dh}}{x_f} \omega_s \psi_f \tag{8.10-10}$$

In quadrature axis due to $x'_q = x_q$ stationary and transient conditions are identical. Thus for cylindrical rotor synchronous machine one can calculate phasor diagrams in rotor reference

frame in transient state in the same way as in synchronous state, if one takes instead of u_p the transient back EMF u'_p and instead of synchronous reactance x_d the transient reactance x'_d.

From the phasor diagram for the **cylindrical rotor synchronous machine** Fig. 8.10-1 the electric machine power $P_{e,dyn}$ and its maximum value, the transient pull-out power, is derived (in physical units):

$$U_d = -X_q I_q = -X_d I_q,\ U_q = X'_d I_d + U'_p \tag{8.10-11}$$

with

$$\underline{U}_s = U_d + jU_q,\ \underline{I}_s = I_d + jI_q \quad . \tag{8.10-12}$$

In dependence of load angle ϑ this may be expressed:

$$U_d = U_s \cdot \sin\vartheta,\ U_q = U_s \cdot \cos\vartheta,\ I_d = (U_q - U'_p)/X'_d,\ I_q = -U_d / X_d \tag{8.10-13}$$

The electrical power during transient state as a function of load angle is therefore

$$P_{e,dyn} = m_s \cdot \mathrm{Re}\{\underline{U}_s \cdot \underline{I}_s{}^*\} = m_s \cdot \mathrm{Re}\{(U_d + jU_q)\cdot(I_d - jI_q)\} = m_s \cdot (U_d I_d + U_q I_q) \tag{8.10-14}$$

$$P_{e,dyn} = m_s \cdot \left(-\frac{U_d U_q}{X_d} - \frac{U_d U'_p}{X'_d} + \frac{U_d U_s}{X'_d} \right) \tag{8.10-15}$$

$$P_{e,dyn} = -m_s \cdot \left(\frac{U_s U'_p}{X'_d}\sin\vartheta - \frac{U_s^2}{2}\left(\frac{1}{X'_d} - \frac{1}{X_d}\right)\sin(2\vartheta) \right) \tag{8.10-16}$$

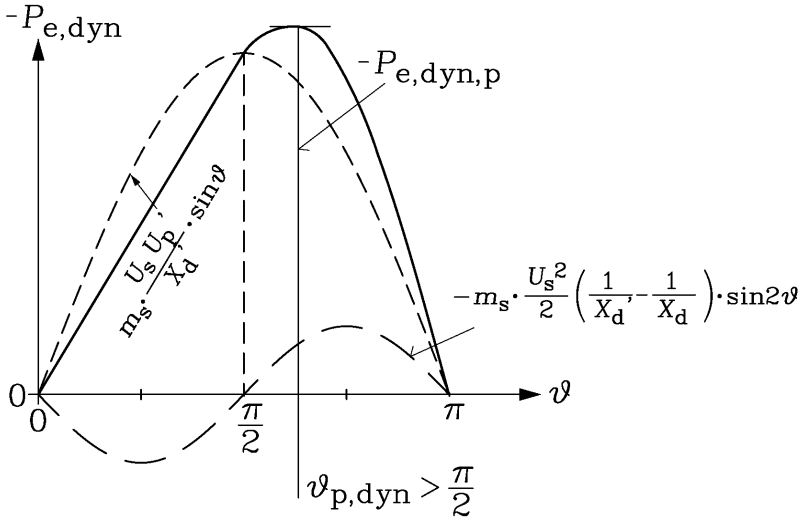

Fig. 8.10-2: Cylindrical rotor synchronous machine: Electrical power during transient state: $X'_q = X_q = X_d$, $X'_d < X_d$, stator resistance neglected $R_s = 0$: Synchronous machine in generator mode

Facit:

During transient state the electric power $P_{e,dyn}(\vartheta)$ in Fig. 8.10-2 ***is determined by U_s and U'_p*** *and* ***NOT by U_p*** *! The similarity of $P_{e,dyn}(\vartheta)$ with synchronous electric power $P_e(\vartheta)$ of salient pole synchronous machine is due to the fact, that in transient state also cylindrical rotor synchronous machine shows saliency, that means difference between direct and quadrature*

axis reactance, according to $X_q = X_d \neq X'_d$. *The hereby caused „dynamic reluctance" torque ~sin2*ϑ *has due to* $X'_d < X_d$ *- that means, direct axis reactance SMALLER than quadrature axis reactance - an opposite sign as the „synchronous reluctance torque" of salient pole synchronous machines. Therefore the load angle, where maximum power (dynamic pull-out power) exists, is bigger than 90° instead of smaller than 90°, as it is the case in salient pole machines under synchronous operation. The* ***transient (or dynamic) pull-out load angle*** $\vartheta_{p,dyn}$ *is larger than* 90°.

Example 8.10-1:
Over-excited synchronous generator with cylindrical rotor:
Data: $u_s = 1$, $i_s = 1$, $\vartheta_N = 45°$, $x_d = 1$, $x'_d = 0.3$, $r_s \approx 0$. Phasor diagram for synchronous rated operation prior to load step is shown in Fig. 8.10-3 a).

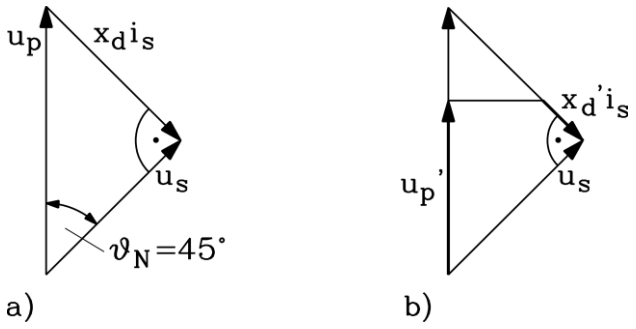

Fig. 8.10-3: Phasor diagram of cylindrical rotor synchronous generator: a) steady state synchronous rated operation, b) transient operation after load step: $X'_q = X_q = X_d$, $X'_d < X_d$, (R_s = 0)

a) Pull-out power in synchronous operation:
From Fig. 8.10-3a we get:
- $u_p = u_s / \sin(\vartheta_N) = 1.41$ p.u., load angle at pull-out: $\vartheta_{p0} = 90°$
- **Synchronous pull-out power** is negative due to generator operation:
  $P_{e,p0} / (m_s U_N I_N) = -u_s u_p / x_d = -1.41$ p.u.

b) Dynamic pull-out power:
From phasor diagram Fig. 8.10-3b we get:
- Transient back EMF:
  $u'_p = U'_p / U_N = u_s \cos\vartheta_N + i_s x'_d \cos(\pi - \vartheta_N) = 0.71 + 0.3 \cdot 0.71 = 0.92$ p.u.
- **Dynamic pull-out load angle** $\vartheta_{p,dyn}$ is derived as the angle at maximum transient power, which is dynamic pull-out power. So derivation *d./d*ϑ of $p_{e,dyn}$

$$p_{e,dyn} = P_{e,dyn} / (m_s U_N I_N) = -A \cdot \sin\vartheta + B \cdot \sin(2\vartheta)$$

with abbreviations $A = u_s u'_p / x'_d = 3.07$, $B = \frac{u_s^2}{2}\left(\frac{1}{x'_d} - \frac{1}{x_d}\right) = 1.17$ yields dynamic pull-out load angle of 117°.

$$dp_{e,dyn} / d\vartheta = 0 \Rightarrow \cos(\vartheta_{p,dyn}) = \frac{A}{8B} \pm \sqrt{\left(\frac{A}{8B}\right)^2 + \frac{1}{2}} \qquad \Rightarrow \qquad \underline{\vartheta_{p,dyn} = 117° > 90°}$$

- Transient (or dynamic) pull-out power:
$p_{e,p,dyn} = P_{e,p,dyn} / (m_s U_N I_N) = -A \cdot \sin\vartheta_{p,dyn} + B \cdot \sin(2\vartheta_{p,dyn}) = -3.68$ p.u.

Facit:
*During transient state the pull-out power of the investigated electrically excited synchronous machine is **2.6-times larger than at steady state operation:** 2.60 = 3.68/1.41. Thus transient stability limit is 2.6-times higher than synchronous stability limit and it occurs at much larger load angle.*

$$\boxed{M_{p,dyn} > M_{p,0} \qquad \vartheta_{p,dyn} > \vartheta_{p,0}}$$

Practical use of this increased dynamic stability limit is, that at **sudden increase** of load (e.g. electrical load on generator mode) cylindrical rotor synchronous machine will not be pull out of synchronism, even if load surpasses synchronous stability limit M_{p0} and pull-out load angle 90°. As long as transient field current flows in the field winding (typically for three transient time constants, e.g. 1 ... 3 s), the significantly higher dynamic stability limit $M_{p,dyn}$ at > 90° is valid. In that short time span the field current controller may react and can increase the DC field current I_f by increasing the field voltage U_f in order to increase synchronous stability limit sufficiently M_{p0}. If this is not possible, after the decay of the transient field current the pull-out torque returns to the stationary stability limit $M_{p0.}$ Hence the synchronous machine will be over-loaded and will be pulled out of synchronism.

Note, that a **slow increase** of load will not lead to induction of transient field current in field winding, so NO increase of stability limit will occur. In that case synchronous stability limit M_{p0} will be the valid limit for synchronous operation.

For **salient pole synchronous machine** the same increase of dynamic stability limit over synchronous limit is observed and a similar equation of dynamic pull-out power and torque may be derived, which is not given here. For rough estimation it is sufficient to take cylindrical rotor dynamic stability limit also for salient pole rotor machines.

8.11 Appendix: Derivation of reactance operators

For *q*-axis the calculation is shorter, as only two windings (stator, damper) are coupled, so this is shown here completely, whereas for *d*-axis it is only shown abbreviated. Rotor side voltage and flux linkage equations shall be eliminated, being substituted by resulting stator flux linkage in for of reactance operators:

<u>*q*-axis voltage and flux linkage equations in *Laplace* domain:</u>

$$\psi_{Q0} = r_Q \cdot \breve{i}_Q + s \cdot \breve{\psi}_Q \tag{8.11-1}$$

$$\begin{pmatrix} \breve{\psi}_q \\ \breve{\psi}_Q \end{pmatrix} = \begin{pmatrix} x_q & x_{qh} \\ x_{qh} & x_Q \end{pmatrix} \cdot \begin{pmatrix} \breve{i}_q \\ \breve{i}_Q \end{pmatrix} \tag{8.11-2}$$

From (8.11-1) we get with $\breve{\psi}_Q = x_{qh}\breve{i}_q + x_Q\breve{i}_Q$ the damper current $\breve{i}_Q$:

$$\psi_{Q0} = r_Q \cdot \breve{i}_Q + s \cdot \breve{\psi}_Q = r_Q \cdot \breve{i}_Q + s \cdot \left(x_{qh}\breve{i}_q + x_Q\breve{i}_Q\right) \quad \Rightarrow \quad \breve{i}_Q = \frac{\psi_{Q0} - s \cdot x_{qh} \cdot \breve{i}_q}{r_Q + s \cdot x_Q} \tag{8.11-3}$$

Thus we get for resulting stator flux linkage in *q*-axis

$$\breve{\psi}_q = x_q\breve{i}_q + x_{qh}\breve{i}_Q = x_q\breve{i}_q + x_{qh} \cdot \frac{\psi_{Q0} - s \cdot x_{qh} \cdot \breve{i}_q}{r_Q + s \cdot x_Q} = \left(x_q - \frac{s \cdot x_{qh}^2}{r_Q + s \cdot x_Q} \right) \cdot \breve{i}_q + \frac{x_{qh} \cdot \psi_{Q0}}{r_Q + s \cdot x_Q} \tag{8.11-4}$$

The expression $x_q(s)$ is called **reactance operator of *q*-axis stator winding**:

$$x_q(s) = x_q - \frac{s \cdot x_{qh}^2}{r_Q + s \cdot x_Q} = \frac{x_q(r_Q + s \cdot x_Q) - s \cdot x_{qh}^2}{r_Q + s \cdot x_Q} = \frac{x_q r_Q + s \cdot \sigma_{qQ} \cdot x_q x_Q}{r_Q + s \cdot x_Q} = \frac{x_q r_Q + s \cdot x_q'' x_Q}{r_Q + s \cdot x_Q}$$

We introduce with *Blondel´*s coefficient $\sigma_{qQ} = 1 - x_{qh}^2/(x_q x_Q)$ the sub-transient reactance of *q*-axis (Fig. 8.11-1b):

$$x_q'' = \sigma_{qQ} \cdot x_q = x_q - x_{qh}^2 / x_Q = x_{qh} + x_{s\sigma} - x_{qh} \cdot (x_Q - x_{Q\sigma}) / x_Q = x_{s\sigma} + \frac{x_{qh} \cdot x_{Q\sigma}}{x_{qh} + x_{Q\sigma}} \qquad (8.11\text{-}5)$$

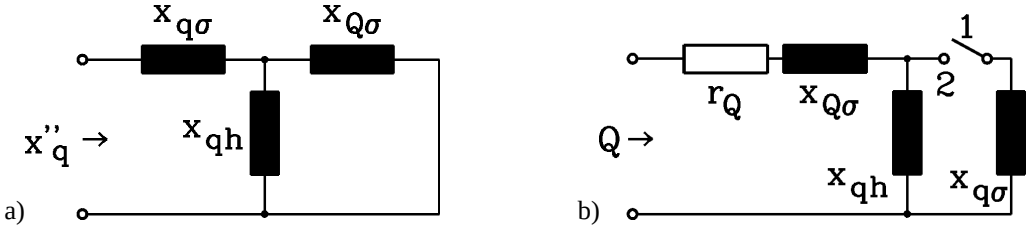

Fig. 8.11-1: Influence of damper cage in *q*-axis: a) reduction of stator inductance in sub-transient state, leading to sub-transient inductance for *q*-axis, b) Time constant of damper cage in *q*-axis (1) at open-circuit of stator winding, (2) at short-circuit of stator winding

Note that *q*-axis reactance operator contains open-circuit and short-circuit time constant $\tau_{Q,}\, \tau_{Q\sigma}$ of *q*-axis damper winding:

$$x_q(s) = \frac{x_q r_Q + s \cdot x_q'' x_Q}{r_Q + s \cdot x_Q} = \frac{\frac{x_q''}{\sigma_{qQ}} r_Q + s \cdot x_q'' x_Q}{r_Q + s \cdot x_Q} = \frac{s + \frac{r_Q}{\sigma_{qQ} x_Q}}{s + \frac{r_Q}{x_Q}} \cdot x_q'' = \frac{s + \frac{1}{\tau_{Q\sigma}}}{s + \frac{1}{\tau_Q}} \cdot x_q''. \qquad (8.11\text{-}6)$$

Introducing **the initial flux linkage conditions**

$$\psi_{Q0} = x_{qh} i_{q0} + x_Q i_{Q0} \qquad \psi_{q0} = x_q i_{q0} + x_{qh} i_{Q0} \qquad (8.11\text{-}7)$$

in stator flux linkage equation (8.1014), by adding $-\psi_{q0}/s$, which fits for further *Laplace* calculations, yields

$$\breve{\psi}_q - \frac{\psi_{q0}}{s} = x_q(s) \cdot \left(\breve{i}_q - \frac{i_{q0}}{s} \right) + \underbrace{\frac{x_{qh} \cdot \psi_{Q0}}{r_Q + s \cdot x_Q} - \frac{\psi_{q0}}{s}}_{-\frac{i_Q}{s} \cdot \frac{r_Q \cdot x_{qh}}{r_Q + s \cdot x_Q} := -\frac{i_{Q0}}{s} \cdot x_Q(s)} + x_q(s) \cdot \frac{i_{q0}}{s}$$

With the abbreviation **"reactance operator of q-axis damper winding"**

$$x_Q(s) = \frac{r_Q x_{qh}}{r_Q + s \cdot x_Q} = \frac{\frac{r_Q}{x_Q}}{\frac{r_Q}{x_Q} + s} \cdot x_{qh} = \frac{\frac{1}{\tau_Q}}{\frac{1}{\tau_Q} + s} \cdot x_{qh} \qquad (8.11\text{-}8)$$

one gets finally a very simple expression of stator *q*-axis flux linkage with included damping effect of *q*-axis damper winding in sub-transient operation in *Laplace* domain:

$$\breve{\psi}_q - \frac{\psi_{q0}}{s} = x_q(s) \cdot \left(\breve{i}_q - \frac{i_{q0}}{s} \right) - \frac{i_{Q0}}{s} \cdot x_Q(s) \tag{8.11-9}$$

Facit:
The damping effect of q-axis damper cage is considered by the q-axis reactance operators of stator and damper winding $x_q(s), x_Q(s)$.

Note:
As in synchronous steady state operations damper current is zero: $i_{Q0} = 0$, for dynamic deviations from synchronous operations only $x_q(s)$ must be considered:

$$\breve{\psi}_q - \frac{\psi_{q0}}{s} = x_q(s) \cdot (\breve{i}_q - \frac{i_{q0}}{s})$$

For *Laplace* transformation back into time domain the inverse $1/x_q(s)$ is needed, which is derived with (8.11-6) and $\tau_{Q\sigma} \cdot x_q = \tau_Q \cdot \sigma_{qQ} x_q = \tau_Q \cdot x_q''$ as

$$\frac{1}{x_q(s)} = \frac{1}{x_q''} \cdot \frac{s + \frac{1}{\tau_Q}}{s + \frac{1}{\tau_{Q\sigma}}} = \frac{1}{x_q} - \frac{1}{x_q} \cdot \frac{s + \frac{1}{\tau_{Q\sigma}}}{s + \frac{1}{\tau_{Q\sigma}}} + \frac{1}{x_q''} \cdot \frac{s + \frac{1}{\tau_Q}}{s + \frac{1}{\tau_{Q\sigma}}} =$$

$$= \frac{1}{x_q} + \left(\frac{1}{x_q''} - \frac{1}{x_q} \right) \cdot \frac{s}{s + \frac{1}{\tau_{Q\sigma}}} + \underbrace{\frac{\frac{1}{\tau_Q x_q''} - \frac{1}{\tau_{Q\sigma} x_q}}{s + \frac{1}{\tau_{Q\sigma}}}}_{0}$$

$$\frac{1}{x_q(s)} = \frac{1}{x_q} + \left(\frac{1}{x_q''} - \frac{1}{x_q} \right) \cdot \frac{s}{s + \frac{1}{\tau_{Q\sigma}}} \tag{8.11-10}$$

For deriving reactance operator in *d*-axis, we start with <u>*d*-axis rotor voltage and flux linkage equations in *Laplace* domain:</u>

$$\begin{aligned} \psi_{D0} &= r_D \cdot \breve{i}_D + s \cdot \breve{\psi}_D \\ \breve{u}_f + \psi_{f0} &= r_f \cdot \breve{i}_f + s \cdot \breve{\psi}_f \end{aligned} \tag{8.11-11}$$

$$\begin{pmatrix} \breve{\psi}_d \\ \breve{\psi}_D \\ \breve{\psi}_f \end{pmatrix} = \begin{pmatrix} x_d & x_{dh} & x_{dh} \\ x_{dh} & x_D & x_{dh} \\ x_{dh} & x_{dh} & x_f \end{pmatrix} \cdot \begin{pmatrix} \breve{i}_d \\ \breve{i}_D \\ \breve{i}_f \end{pmatrix} \tag{8.11-12}$$

Substituting $\breve{\psi}_f, \breve{\psi}_D$ in (8.11-11) leads to

$$\begin{aligned}\psi_{D0} &= r_D \cdot \breve{i}_D + s \cdot \underbrace{(x_{dh} \cdot \breve{i}_d + x_{dh} \cdot \breve{i}_f + x_D \cdot \breve{i}_D)}_{\breve{\psi}_D} \\ \breve{u}_f + \psi_{f0} &= r_f \cdot \breve{i}_f + s \cdot \underbrace{(x_{dh} \cdot \breve{i}_d + x_f \cdot \breve{i}_f + x_{dh} \cdot \breve{i}_D)}_{\breve{\psi}_f}\end{aligned} \qquad \text{(8.11-13a)}$$

Solving that linear equation system by *Cramer´*s rule – using determinant *Det* of equation system - in dependence of stator current

$$\begin{pmatrix} r_f + s \cdot x_f & s \cdot x_{dh} \\ s \cdot x_{dh} & r_D + s \cdot x_D \end{pmatrix} \cdot \begin{pmatrix} \breve{i}_f \\ \breve{i}_D \end{pmatrix} = \begin{pmatrix} \breve{u}_f + \psi_{f0} - s \cdot x_{dh} \cdot \breve{i}_d \\ \psi_{D0} - s \cdot x_{dh} \cdot \breve{i}_d \end{pmatrix} \qquad \text{(8.11-13b)}$$

leads to the solutions $\breve{i}_f(\breve{i}_d, \breve{u}_f, \psi_{f0}, \psi_{D0})$, $\breve{i}_D(\breve{i}_d, \breve{u}_f, \psi_{f0}, \psi_{D0})$:

$$\breve{i}_f = \frac{1}{Det} \cdot \left\{ \left[-s \cdot x_{dh} \cdot (r_D + s \cdot x_D) + s^2 x_{dh}^2 \right] \cdot \breve{i}_d + (\breve{u}_f + \psi_{f0}) \cdot (r_D + s \cdot x_D) - s \cdot x_{dh} \cdot \psi_{D0} \right\}$$

$$\breve{i}_D = \frac{1}{Det} \cdot \left\{ \left[-s \cdot x_{dh} \cdot (r_f + s \cdot x_f) + s^2 x_{dh}^2 \right] \cdot \breve{i}_d - (\breve{u}_f + \psi_{f0}) \cdot s \cdot x_{dh} - (r_f + s \cdot x_f) \cdot \psi_{D0} \right\}$$

$$Det = (r_f + s \cdot x_f) \cdot (r_D + s \cdot x_D) - s^2 x_{dh}^2 = r_f \cdot r_D \cdot \left(1 + s \cdot (\tau_f + \tau_D) + s^2 \cdot \sigma_{fD} \cdot \tau_f \cdot \tau_D\right)$$

The open-circuit time constants of *d*-axis damper winding $\tau_D = x_D / r_D$ and of field winding $\tau_f = x_f / r_f$ are introduced in *Det*, which may be written as

$$Det = r_f \cdot r_D \cdot \Delta \qquad \text{with} \qquad \Delta = 1 + s \cdot (\tau_f + \tau_D) + s^2 \cdot \sigma_{fD} \cdot \tau_f \cdot \tau_D \,. \qquad \text{(8.11-14)}$$

Stator flux linkage equation can now be expressed only by stator current, using these solutions:

$$\breve{\psi}_d = x_d \cdot \breve{i}_d + x_{dh} \cdot \breve{i}_f(\breve{i}_d, \breve{u}_f, \psi_{f0}, \psi_{D0}) + x_{dh} \cdot \breve{i}_D(\breve{i}_d, \breve{u}_f, \psi_{f0}, \psi_{D0}) \qquad \text{(8.11-15)}$$

By the way, in (8.11-15) also the initial conditions of field and damper flux linkage are substituted by the corresponding initial conditions of field and damper current according to

$$\psi_{f0} = x_{dh} \cdot i_{d0} + x_f \cdot i_{f0} + x_{dh} \cdot i_{D0}, \qquad \psi_{D0} = x_{dh} \cdot i_{d0} + x_{dh} \cdot i_{f0} + x_D \cdot i_{D0} \quad . \qquad \text{(8.11-16)}$$

Like in *q*-axis, the initial condition $-\psi_{d0}/s$ is added to $\breve{\psi}_d$. After about one page of calculation one ends up instead of (8.11-15) with the equation

$$\boxed{\breve{\psi}_d - \frac{\psi_{d0}}{s} = x_d(s) \cdot \left(\breve{i}_{d0} - \frac{i_{d0}}{s} \right) + x_f(s) \cdot \left(\frac{\breve{u}_f}{r_f} - \frac{i_{f0}}{s} \right) - x_D(s) \cdot \frac{i_{D0}}{s}} \quad , \qquad \text{(8.11-17)}$$

where as abbreviations the **reactance operators of *d*-axis stator winding, of field winding and of *d*-axis damper winding** are used, which are given by

$$x_d(s) = \frac{1}{\Delta} \cdot \left[x_d + s \cdot x_d \cdot (\sigma_{df} \cdot \tau_f + \sigma_{dD} \cdot \tau_D) + s^2 \cdot x_d'' \cdot \sigma_{fD} \cdot \tau_f \cdot \tau_D \right] \qquad \text{(8.11-18)}$$

$$x_f(s) = \frac{1}{\Delta} \cdot (1 + s \cdot x_{D\sigma} / r_D) \cdot x_{dh} \qquad \text{(8.11-19)}$$

$$x_D(s) = \frac{1}{\Delta} \cdot (1 + s \cdot x_{f\sigma} / r_f) \cdot x_{dh} \quad . \tag{8.11-20}$$

For *Laplace* transformation back into time domain the inverse $1/x_d(s)$ is needed, which is derived with (8.11-18) as

$$\frac{1}{x_d(s)} = \frac{1 + s \cdot (\tau_f + \tau_D) + s^2 \cdot \sigma_{fD} \cdot \tau_f \cdot \tau_D}{\frac{x_d}{x_d''} + s \cdot \frac{x_d}{x_d''} \cdot (\sigma_{df} \cdot \tau_f + \sigma_{dD} \cdot \tau_D) + s^2 \cdot \sigma_{fD} \cdot \tau_f \cdot \tau_D} \cdot \frac{1}{x_d''} =$$

$$= \frac{\frac{1}{\sigma_{fD}\tau_f\tau_D} + s \cdot \frac{\tau_f + \tau_D}{\sigma_{fD}\tau_f\tau_D} + s^2}{\frac{x_d}{x_d''} \cdot \frac{1}{\sigma_{fD}\tau_f\tau_D} + s \cdot \frac{x_d}{x_d''} \cdot \frac{\sigma_{df} \cdot \tau_f + \sigma_{dD} \cdot \tau_D}{\sigma_{fD}\tau_f\tau_D} + s^2} \cdot \frac{1}{x_d''}$$

The quadratic equations in numerator and denominator have the already in Section 8.6 discussed solutions

$$s_{1,2} = -\alpha_{d1,2} = -\frac{\tau_f + \tau_D}{2 \cdot \sigma_{fD} \cdot \tau_f \cdot \tau_D} \pm \sqrt{\left(\frac{\tau_f + \tau_D}{2 \cdot \sigma_{fD} \cdot \tau_f \cdot \tau_D}\right)^2 - \frac{1}{\sigma_{fD} \cdot \tau_f \cdot \tau_D}} \tag{8.11-21}$$

$$s_{1,2} = \frac{-1}{\tau_d'}, \frac{-1}{\tau_d''} = -\frac{x_d(\sigma_{df}\tau_f + \sigma_{dD}\tau_D)}{x_d'' \cdot 2\sigma_{fD}\tau_f\tau_D} \pm \sqrt{\left(\frac{x_d(\sigma_{df}\tau_f + \sigma_{dD}\tau_D)}{x_d'' \cdot 2\sigma_{fD}\tau_f\tau_D}\right)^2 - \frac{x_d}{x_d'' \cdot \sigma_{fD}\tau_f\tau_D}} \tag{8.11-22}$$

So if we decompose into single terms

$$\frac{1}{x_d(s)} = \frac{(s + \alpha_{d1})(s + \alpha_{d2})}{(s + \frac{1}{\tau_d'})(s + \frac{1}{\tau_d''})} \cdot \frac{1}{x_d''} = \frac{1}{x_d} + \left(\frac{1}{x_d'} - \frac{1}{x_d}\right) \cdot \frac{s}{s + \frac{1}{\tau_d'}} + \left(\frac{1}{x_d''} - \frac{1}{x_d}\right) \cdot \frac{s}{s + \frac{1}{\tau_d''}} \quad , \tag{8.11-23}$$

where we define the abbreviation x_d' as an inductance, which is related to transient time constant τ_d' and is therefore called **transient inductance**, we see, that (8.11-23) defines this transient inductance. By comparing the single terms in (8.11-23), one ends for x_d' with the expression (8.11-24), already noted in Section 8.6.

$$\boxed{x_d' = x_d'' \cdot \frac{\frac{1}{\tau_d''} - \frac{1}{\tau_d'}}{\alpha_{d1} + \alpha_{d2} - \frac{1}{\tau_d'} \cdot \left(1 + \frac{x_d''}{x_d}\right)}} \tag{8.11-24}$$

a) 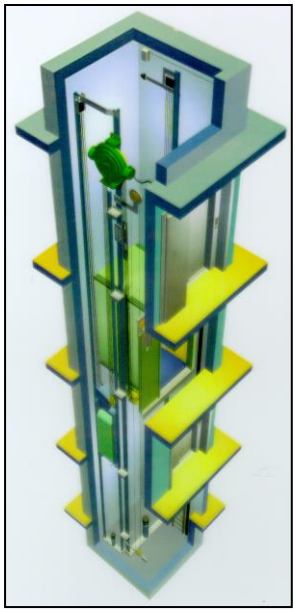 b) 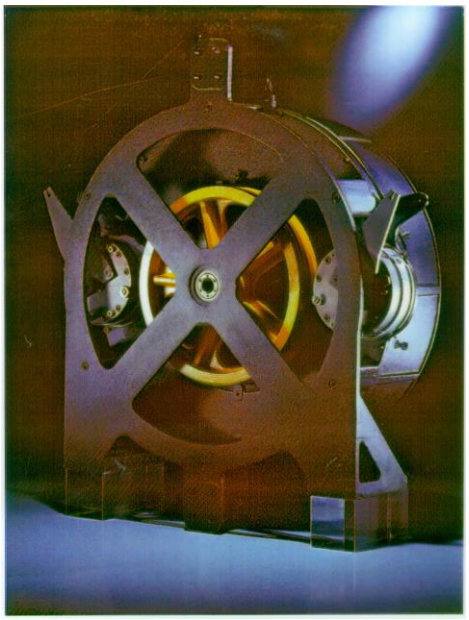

Fig. 8.11-2: Gearless direct drive for elevators with permanent magnet synchronous motors, powered by IGBT-inverter supply and speed control: a) Three stores elevator with cabin, counter-mass and on top an axial-flux disc-like PM synchronous motor, b) Integration of rope drum and PM synchronous motor with emergency brake (left and right)

a) 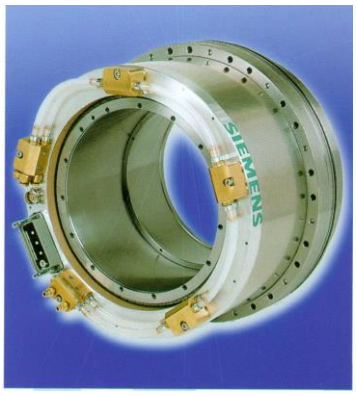

b) 

Fig. 8.11-3: a) Permanent magnet synchronous motors with hollow shaft, low speed, high torque for gearless drive, b) Printing machine with seven printing stations for different colours. Each station contains a printing cylinder, which is driven gearless by an inverter-fed PM synchronous motor. Movement of all cylinders has to be synchronized to ensure exact printing position for the different colours.

Appendix A1: Analytical design of a cage induction machine

Main dimensions and basic electromagnetic quantities of induction machines

Main dimensions of induction machines:	
inner and outer diameter of stator and rotor iron stack	d_{si} , d_{sa} , d_{ri} , d_{ra}
air gap between stator and rotor iron stack, and pole pitch	δ, τ_p
length of iron stack, number and length of cooling ducts and total stack length	l_{Fe}, z_K, l_K, $L = l_{Fe} + z_K l_K$
Electric and magnetic quantities:	
Stator and rotor current loading (r.m.s.)	A_s, A_r
Flux density in air gap, stator and rotor teeth and yoke (peak values)	B_δ, B_{ds}, B_{dr}, B_{ys}, B_{yr}
Main flux (in air gap) and stray flux (components in slots, winding overhangs, influence of skewing and deviation of air gap flux from sinusoidal distribution)	Φ_h, Φ_σ

Table A1-1: Main dimensions and basic electromagnetic quantities

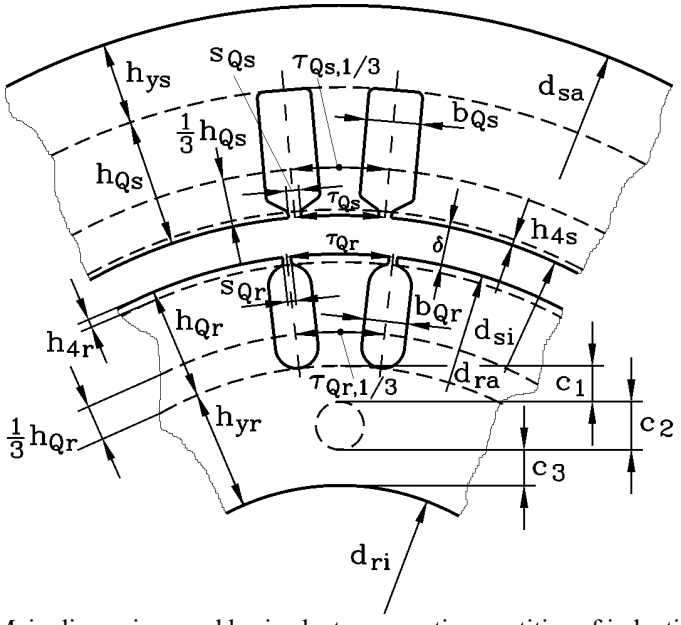

Fig. A1-1: Main dimensions and basic electromagnetic quantities of induction machine

Given values for a three-phase induction machine to be designed with cage rotor:
Motor operation, P_N = 500 kW, 6 kV, 50 Hz, 4 pole.

- Estimated values from graphs of text book (Figs. 2.2-9, 2.2-10):
  η_N = 94.4 %, $\cos\varphi_N$ = 0.868
- Motor output power: 500 kW, apparent power: $S_N = \dfrac{P_N}{\eta_N \cdot \cos\varphi_N} = 610\,\text{kVA}$
- Motor current: $I_{sN} = \dfrac{S_{sN}}{\sqrt{3} \cdot U_{sN}} = \dfrac{610}{\sqrt{3} \cdot 6} = 59\,\text{A}$,
- Synchronous speed: $n_{syn} = f_s / p = 1500\,/\text{min}$
- Pole pitch 360 mm, stack length: 380 mm, air gap: 1.4 mm, shaft diameter: 200 mm,
- Current loading: 500 A/cm, current density: 5.5 A/mm^2,
- Stator bore diameter: $d_{si} = 2p\tau_p / \pi = 458\,\text{mm}$.

- Internal apparent power: ($\sigma_s = 0.08/2 = 0.04$): $S_\delta = S/(1+\sigma_s) = 610/1.04 = 587\,\text{kVA}$
- Electromagnetic utilization: $C = S_\delta/(d_{si}^2 \cdot l_{Fe} \cdot n_{syn}) = 4.9\,\text{kVA·min/m}^3$
- Flux density ($k_{w1} = 0.91$ estimated): $C = \frac{\pi^2}{\sqrt{2}} \cdot k_{w1} \cdot A \cdot B_{\delta,1} \quad \Rightarrow \quad B_{\delta,1} = \underline{\underline{0.927}}\,\text{T}$. This value is in the range indicated in Fig.2.2-4 of the text book: 0.89 ... 0.99 T.
- Thermal utilization: $A \cdot J = 2750\,(\text{A/cm})(\text{A/mm}^2)$

Stator winding design:

- Chosen number of slots: $q = 5$, $Q_s = 2p \cdot m \cdot q = 4 \cdot 3 \cdot 5 = 60$, leads to 15 slots per pole
- Slot pitch: $\tau_{Qs} = d_{si}\pi / Q_s = 24.0\,\text{mm}$
- Coil pitching is possible in steps of one slot pitch: $W/\tau_p = 14/15$, 13/15 etc., chosen pitch $W/\tau_p = 12/15$ leads to $k_{ps,1} = 0.951$, $k_{ps,-5} = 0$, $k_{ps,7} = 0.588$. The influence of 5th space harmonic is completely eliminated.
- Distribution factor: $k_{ds,1} = 0.957$, stator winding factor: $k_{ws,1} = 0.957 \cdot 0.951 = 0.910$
- With chosen air gap flux density 0.9 T main flux per pole of fundamental $\nu = 1$ is

$$\Phi_h = \frac{2}{\pi} \cdot \tau_p \cdot l_{Fe} \cdot B_{\delta,\nu=1} = \frac{2}{\pi} \cdot 0.36 \cdot 0.38 \cdot 0.9 = 78.4\,\text{mWb}.$$

- Choice of number of turns per phase N_s:

Estimated induced voltage per phase: $U_h = \frac{U_N/\sqrt{3}}{1+\sigma_s} = \frac{6000/\sqrt{3}}{1.04} = 3330\,\text{V}$

$$U_h = \sqrt{2}\pi f_s \cdot N_s k_{ws1} \cdot \Phi_h \quad \Rightarrow \quad N_s = 210.17$$

$N_c = N_s \cdot a/(2pq) = 210.17 \cdot 1/(2 \cdot 2 \cdot 5) = 10.5$, so integer value $N_c = \underline{\underline{10}}$ for $a = 1$ is chosen.

- <u>Final values:</u>

$N_c = 10$, $N_s = 200$, $a = 1$, for $U_h = 3330\,\text{V}$: $B_{\delta,\nu=1} = 0.946$ T

Current per phase 59 A, voltage per phase 3460 V, current density limit 5.5 A/mm^2, $N_s = 200$, $N_c = 10$, $\tau_{Qs} = 24.0$ mm, $a = 1$, $a_i = 1$.

- Conductor cross section: $A_{TL} = I_s/(J_s \cdot a \cdot a_i) = 59/(5.5 \cdot 1 \cdot 1) = 10.73\ \text{mm}^2$
- Chosen slot breadth: $b_{Qs} = 12.5\,\text{mm}$ ($= 0.52 \cdot \tau_{Qs}$)
- Chosen conductor dimensions (Table 2.4-2 of the text book): $b_L = 7.1\,\text{mm}$, $h_L = 1.8\,\text{mm}$, $A_{TL} = 12.42\,\text{mm}^2 > 10.73\ \text{mm}^2$
- Inter-turn voltage: $U_s/N_s = 3460/200 = 17.3$ V < 80 V: Table 2.3-3 of text book: Conductor insulation thickness $d_{ic} = 0.4$ mm (both sides)
- Additional inter-turn insulation $d_i = 0.3$ mm

- <u>Checking of eddy currents at 20°C:</u> $\kappa_{Cu} = 57 \cdot 10^6$ S/m, $f = 50$ Hz, $n_{ne} = 1$, $b_L/b_Q = 7.1/12.5$

$$\xi = h_L \cdot \sqrt{\frac{\mu_0 \cdot \omega \cdot \kappa \cdot n_{ne} \cdot b_L}{2 \cdot b_Q}} = 0.0018 \cdot \sqrt{\frac{4\pi \cdot 10^{-7} \cdot 2\pi \cdot 50 \cdot 57 \cdot 10^6 \cdot 1 \cdot 7.1}{2 \cdot 12.5}} = \underline{\underline{0.144}} < 0.35$$

- <u>Checking of current density and thermal utilization:</u>

$$J_s = I_s/(a \cdot a_i \cdot A_{TL}) = 59/(1 \cdot 1 \cdot 12.42) = \underline{\underline{4.75}}\,\text{A/mm}^2 < 5.5\ \text{A/mm}^2$$

$$A = \frac{2mN_s I_s}{2p\tau_p} = \frac{2 \cdot 3 \cdot 200 \cdot 59}{4 \cdot 36} = 492\ \text{A/cm}$$

$A \cdot J = 492 \cdot 4.75 = \underline{\underline{2337}}$ (A/cm)(A/mm^2): fits to limits given in Chapter 1 for open ventilated machine with 80 K temperature rise.

Slot height design:		**mm**
Number of insulated turns per coil one above the other = 10	$N_c \cdot (h_L + d_{ic}) + (N_c - 1) \cdot d_i =$ $= 10 \cdot (1.8 + 0.4) + 9 \cdot 0.3 = 24.7$	24.7
Main insulation	$2 \cdot d = 2 \cdot 2.2 = 4.4$	4.4
Insulated coil side	24.7 + 4.4 = 29.1	29.1
Two coils per slot	$2 \cdot 29.0 = 58.0$	58.2
Inter-layer insulation	$Z = 4.0$	4.0
Slot lining (thickness 0.15 mm)	$3 \cdot d_{sl} = 3 \cdot 0.15 = 0.45$	0.45
Wedge	$h_{\text{wedge}} = 4.5$	4.5
Top and bottom lining	$2 \cdot d_t = 2 \cdot 0.4 = 0.8$	0.8
Vertical play		1.05
Slot height h_Q		**69.0**

Slot width design:		**mm**
Number of adjacent insulated turns $n_{\text{ne}} = 1$	$n_{ne} \cdot (b_L + d_{ic}) =$ $= 1 \cdot (7.1 + 0.4) = 7.5$	7.5
Main insulation	$2 \cdot d = 2 \cdot 2.2 = 4.4$	4.4
Slot lining (thickness 0.15 mm)	$2 \cdot d_{sl} = 2 \cdot 0.15 = 0.30$	0.3
Play		0.3
Slot width b_Q		**12.5**

Table A1-2: Stator slot design

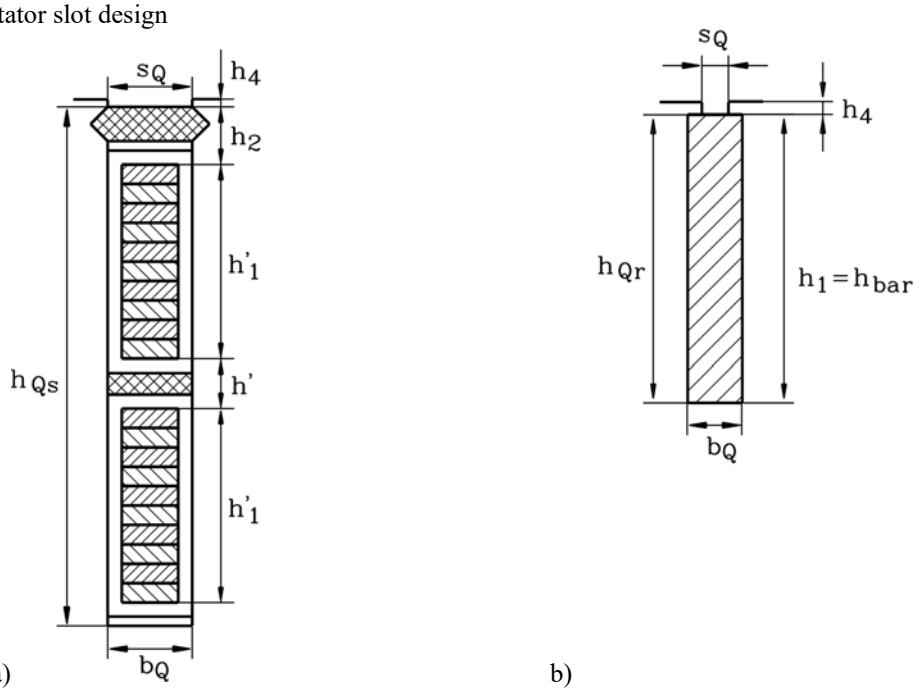

Fig. A1-2: a) Two coils (two-layer winding) in one slot for 6 kV, 500 kW induction machine, b) Cross section of deep rotor bar in slot

- Electromagnetic utilization:

$$C = \frac{\pi^2}{\sqrt{2}} \cdot k_{ws} \cdot A \cdot B_\delta = \frac{\pi^2}{\sqrt{2}} \cdot 0.91 \cdot 49200 \cdot 0.946 = 295585\ \text{VAs/m}^3 = \underline{4.93}\ \text{kVA·min/m}^3$$

Rotor cage design

Choice of rotor slot number Q_r must be done with respect to stator slot number Q_s (details see: Lectures "Motor development for electric drive systems").

$2p = 4$, $Q_s = 60$, unskewed rotor: $Q_r = (0.8 \ldots 1.2)Q_s = 48 \ldots 72$, taking only even numbers. With $r^* = 4$ the range 56 ... 64 is excluded. The numbers 48, 72 are excluded (common divider 2, 3, 4, 6, 12). Excluding in similar way other slot numbers with common dividers, we get as choice (46), 50, 54, 66, 70, (74).

For **skewed** rotor only slot numbers (46), 50, 54 remain, e.g. $Q_r = 50$ is chosen.

- $I'_r = I_r / \ddot{u}_I \approx I_s \cdot \cos\varphi_s = 59 \cdot 0.87 = 51.33\ \text{A},\ \ddot{u}_I = \dfrac{2k_{ws}m_s N_s}{Q_r} = \dfrac{2 \cdot 0.91 \cdot 3 \cdot 200}{50} = 21.84$

  $I_r = \ddot{u}_I \cdot I'_r = 21.84 \cdot 51.33 = \underline{\underline{1121}}\ \text{A}$

- Deep bar rotor to increase starting torque: ratio $h_{Cu}/b_{Cu} \geq 8$
  Choice: $h_{Cu} = 40$ mm, $b_{Cu} = 5$ mm, cross section: $A_{Cur} = 200\ \text{mm}^2$ (Fig. 2.4-1c)
- Rotor bar current density: $J_r = I_r / A_{Cur} = 1121/200 = 5.6\ \text{A/mm}^2$
- Semi-closed rotor slot dimensions (see above Fig. A1-2):
  $h_1 = h_{Cu} = 40$ mm, $b_1 = b_{Cu} = 5$ mm (plus 0.1 mm play each)
  $h_4 = 3.4$ mm, $s_{Qr} = 2.5$ mm
  $h_{Qr} = 40.1 + 3.4 = \underline{43.5}$ mm, $b_{Qr} = \underline{5.1}$ mm
- Rotor ring current $I_{Ring} = I_r / (2 \cdot \sin(p\pi / Q_r)) = 1121/(2 \cdot \sin(2\pi/50)) = \underline{\underline{4472}}\ \text{A}$
- Ring current density: $J_r = J_{Ring} = 5.6\ \text{A/mm}^2$,
- Necessary ring cross section: $A_{Ring} = I_{Ring} / J_{Ring} = 4472/5.6 = 800\ \text{A/mm}^2$ (Fig. 2.5-9)
- Ring height is usually at least bar height: $h_{Ring} \geq h_{Cu}$
  Choice: $h_{Ring} = h_{Cu} = \underline{40}$ mm, $b_{Ring} = 800/40 = \underline{20}$ mm

Design of main flux path of magnetic circuit

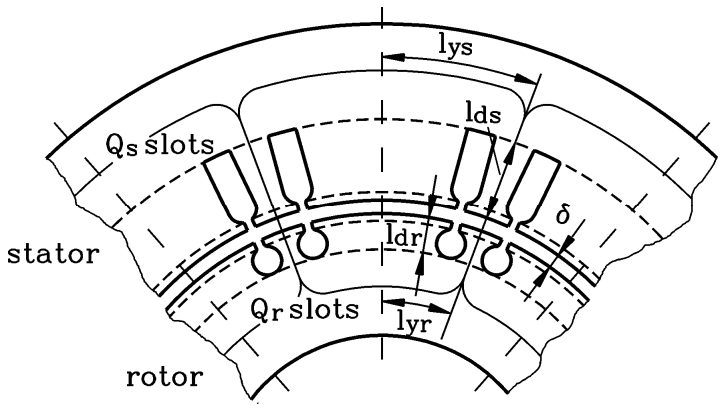

Fig. A1-3: Cross section of an 8-pole induction machine with sections of magnetic circuit of main flux

$k_{Fe} = 95\% \ldots 97\%$ (stacking coefficient)

Q_s/Q_r = 60/50, B_δ = 0.858 T, stator bore diameter: d_{si} = 458 mm, air gap δ = 1.4 mm, high voltage winding: slot width $b_{Qs} = s_{Qs}$ = 12.5 mm, s_{Qr} = 2.5 mm, iron stack of stator and rotor consist of 9 sections with l_1 = 42 mm and 8 radial ducts with width l_k = 10 mm.

Air gap magnetization

	τ_Q / mm	s_Q / mm	s_Q/δ	ζ	k_C
stator	24.0	12.5	8.93	5.72	1.50
rotor	28.8	2.5	1.79	0.47	1.023

Table A1-3: Air-gap influence

*Carter´*s coefficient: $k_C = k_{Cs} \cdot k_{Cr} = 1.5 \cdot 1.023 = \underline{\underline{1.54}}$

Equivalent air gap: $\delta_e = k_C \cdot \delta = 1.54 \cdot 1.4 = 2.156\,\text{mm}$

$$h' = l_k/(\delta/2) = 10/(1.4/2) = 14.28,\ \zeta(h') = 10.58,\ k'_C = \frac{l_1 + l_k}{l_1 + l_k - \zeta(h') \cdot (\delta/2)} = 1.166$$

Total axial length: $L = 9 \cdot l_1 + 8 \cdot l_k = 9 \cdot 42 + 8 \cdot 10 = 458\,\text{mm}$

Iron stack length: $l_{Fe} = 9 \cdot l_1 = 9 \cdot 42 = 378\,\text{mm}$

Equivalent iron length: $l_e = L / k'_C = 458/1.166 = \underline{\underline{392}}\,\text{mm}$

$$V_\delta = \frac{B_\delta}{\mu_0} \cdot \delta_e = \frac{0.858}{4\pi \cdot 10^{-7}} \cdot 0.002156 = \underline{\underline{1472}}\,\text{A}$$

Magnetization of teeth

B_δ = 0.858 T, k_{Fe} = 0.95, l_e = 392 mm, l_{Fe} = 378 mm,
d_{si} = 458 mm, Q_s/Q_r = 60/50, air gap δ = 1.4 mm, τ_{Qs} = 24.0 mm, τ_{Qr} = 28.8 mm, iron sheet type III (see Table 2.7-2 in the text book)

	h_Q, b_Q (mm)	$l_d = h_Q$ (mm)	$b_{d,1/3}$ (mm)	$B'_{d,1/3}$/T	$H'_{d,1/3}$/A/cm	V_d / A
stator	69.0, 12.5	69.0	13.9	1.615	46.5	321
rotor	43.5, 5.1	43.5	19.9	1.35	8.5	37

Check of flux density at narrowest tooth width:

	$b_{d,i}$ (mm)	$B'_{d,1/3}$/T
stator	11.5	1.95 < 2.4
rotor	14.2	1.89 < 2.4

Saturation calculation for operation at 10% elevated voltage of 6.6 kV at no-load s = 0 (ARNOLD´s method)

$U_h = U_N/(\sqrt{3} \cdot (1 + \sigma_s)) = 6600/(\sqrt{3} \cdot 1.05) = 3629\,\text{V}$

$$B_{\delta,\nu=1} = \frac{U_h}{\sqrt{2}\pi f_s \cdot N_s k_{ws1} \cdot (2/\pi)\tau_p l_e} = \frac{3629}{\sqrt{2}\pi \cdot 50 \cdot 200 \cdot 0.91 \cdot (2/\pi) \cdot 0.36 \cdot 0.392} = 1.0\,\text{T}$$

$B_{\delta,\nu=1}$ = 1.0 T

$B_{\delta,av} \cong (2/\pi) \cdot B_{\delta,\nu=1} = (2/\pi) \cdot 1.0 = 0.6366\,\text{T}$

Assumption (1st iteration):

$B_\delta/B_{\delta,av} = 1.41 \Rightarrow V_{ds+dr}/V_\delta = 0.3$

$B_\delta = 1.41 B_{\delta,av} = 1.41 \cdot 0.6366 = 0.897\,\text{T}$

$$B'_{ds,1/3} = \frac{B_\delta \cdot \tau_{Qs} \cdot l_e}{k_{Fe} \cdot b_{ds,1/3} \cdot l_{Fe}} = 1.69\,\text{T},\ H'_{ds,1/3} = 74\,\text{A/cm},\ V_{ds} = 74 \cdot 6.9 = 511\,\text{A}$$

$$B'_{dr,1/3} = \frac{B_\delta \cdot \tau_{Qr} \cdot l_e}{k_{Fe} \cdot b_{dr,1/3} \cdot l_{Fe}} = 1.41\,\text{T},\ H'_{dr,1/3} = 12.1\,\text{A/cm},\ V_{dr} = 12.1 \cdot 4.35 = 52.6\,\text{A}$$

$$V_\delta = \frac{B_\delta}{\mu_0} \cdot \delta_e = \frac{0.897}{4\pi \cdot 10^{-7}} \cdot 0.002156 = \underline{\underline{1539}}\,\text{A}$$

$V_{ds+dr}/V_\delta = (511+57)/1539 = 0.37$

Assumption (2nd iteration): average of old and new value: $V_{ds+dr}/V_\delta = (0.37 + 0.3)/2 = 0.335$

V_{ds+dr}/V_δ	$B_\delta/B_{\delta,av}$	B_δ	$B'_{ds,1/3}$	$B'_{dr,1/3}$	$H'_{ds,1/3}$	$H'_{dr,1/3}$	V_{ds}	V_{dr}	V_δ	V_{ds+dr}/V_δ
-	-	T	T	T	A/cm	A/cm	A	A	A	-
0.3	1.41	0.897	1.69	1.42	74	13	511	57	1539	0.37
0.335	1.40	0.891	1.68	1.41	70	12.1	483	52.6	1529	0.35

Table A1-4: Iterative determination of flat top B_δ for given air gap flux

After 2nd iteration: (0.35-0.335)/0.335 = 4.5% < 5% = iteration is ended, taking as final values $B_\delta = 0.891$ T and $V_{ds+dr}/V_\delta = 0.35$.

Magnetization of yokes at 6.6 kV

$d_{si} = 458$ mm, $\delta = 1.4$ mm, $l_{ds} = 69$ mm,
$l_{dr} = 43.5$ mm, $h_{ys} = 77$ mm, shaft diameter $d_{ri} = 200$ mm, $c_2 = 30$ mm
$B_\delta = 0.891$ T, $B_{\delta,\nu=1} = 1.0$ T, $B_{\delta,av} = 0.6366$ T.

- Stator maximum yoke flux density:

$$B_{ys} = \frac{\Phi_\delta \cdot (1+\sigma_s)/2}{h_{ys} \cdot l_{Fe} \cdot k_{Fe}} = \frac{(2/\pi) \cdot B_{\delta,\nu=1} \cdot \tau_p \cdot l_e \cdot (1+\sigma_s)/2}{h_{ys} \cdot l_{Fe} \cdot k_{Fe}} =$$

$$= \frac{(2/\pi) \cdot 1.0 \cdot 0.36 \cdot 0.392 \cdot 1.05/2}{0.077 \cdot 0.378 \cdot 0.95} = 1.70T$$

$$d_{sa} = d_{si} + 2l_{ds} + 2h_{ys} = 458 + 2 \cdot 69 + 2 \cdot 77 = 750\,\text{mm}$$

$$h_{yr} = \left[d_{si} - 2\delta - 2l_{dr} - d_{ri}\right]/2 = \left[458 - 2 \cdot 1.4 - 2 \cdot 43.5 - 200\right]/2 = 84.1\,\text{mm}$$

- Without flux penetration in shaft:

$$h_{yr,e} = h_{yr} - (2/3) \cdot c_2 = 84.1 - 2/3 \cdot 30 = 64.1\,\text{mm}$$

- With flux penetration in shaft at $s_N = 0.015$, $f_s = 50$ Hz, $\mu_{Fe} = 1000\mu_0$,

$\kappa_{Fe,shaft} = 5 \cdot 10^6$ S/m

$$d_E = \frac{1}{\sqrt{\pi \cdot s \cdot f_s \cdot \mu_{Fe} \cdot \kappa_{Fe}}} = \frac{1}{\sqrt{\pi \cdot 0.015 \cdot 50 \cdot 1000 \cdot 4\pi \cdot 10^{-7} \cdot 5 \cdot 10^6}} = 8.2\,\text{mm}$$

$$h_{yr,e} = h_{yr} - (2/3) \cdot c_2 + d_E = 64.1 + 8.2 = 72.3\,\text{mm}$$

- Rotor maximum yoke flux density:

$$B_{yr} = \frac{\Phi_\delta/2}{h_{yr,e} \cdot l_{Fe} \cdot k_{Fe}} = \frac{(2/\pi) \cdot B_{\delta,\nu=1} \cdot \tau_p \cdot l_e/2}{h_{yr,e} \cdot l_{Fe} \cdot k_{Fe}} = \frac{(2/\pi) \cdot 1.0 \cdot 0.36 \cdot 0.392/2}{0.0723 \cdot 0.378 \cdot 0.95} = 1.73\,\text{T}$$

- Yoke radii and lengths :

$$r_{ys} = (d_{si} + h_{ys})/2 + l_{ds} = (458 + 77)/2 + 69 = 336.5\,\text{mm},\ l_{ys} = r_{ys} \cdot \pi/(2p) = 264.2\,\text{mm}$$

$r_{yr} = (d_{si} - h_{yr,e})/2 - l_{dr} - \delta = (458 - 72.3)/2 - 43.5 - 1.4 = 148.25\,\text{mm}$

$l_{yr} = r_{yr} \cdot \pi/(2p) = 116.4\,\text{mm}$

- Yoke m.m.f.: According to Table 2.7.4-1 of text book: $\overline{H}_{ys} = 20.4$ A/cm, $\overline{H}_{yr} = 23.9$ A/cm,

$V_{ys} = \overline{H}_{ys} l_{ys} = 20.4 \cdot 26.4 = \underline{\underline{539}}$ A, $V_{yr} = \overline{H}_{yr} l_{yr} = 23.9 \cdot 11.64 = \underline{\underline{278}}$ A

Magnetizing reactance at 6.6 kV:

$B_\delta = 0.891$ T, $B_{\delta,\nu=1} = 1.0$ T, $B_{\delta,av} = 0.6366$ T.

- m.m.f.: $V_\delta = 1529$ A, $V_{ds+dr} = 483 + 52.6 = 535.6$ A, $V_{ys} = 534$ A, $V_{yr} = 278$ A

$V_m = 1529 + 483 + 52.6 + 534 + 278 = 2877$ A

- unsaturated and saturated magnetizing reactances $X_{h,\infty}$ and X_h:

$$X_{h,\infty} = 2\pi \cdot 50 \cdot 4\pi \cdot 10^{-7} \cdot (200 \cdot 0.91)^2 \cdot \frac{2 \cdot 3}{\pi^2 \cdot 2} \cdot \frac{0.392 \cdot 0.36}{0.002156} = 260.2\,\Omega$$

$$V_{\delta 1} = B_{\delta,\nu=1} \cdot \delta_e / \mu_0 = 1716\text{A}\,,\; X_h = \frac{V_{\delta 1}}{V_m} \cdot X_{h,\infty} = \frac{1716}{2877} \cdot 260.2 = \underline{\underline{155.2}}\,\Omega$$

- magnetizing current:

$$I_m = \frac{V_m}{\frac{\sqrt{2}}{\pi} \cdot \frac{m_s}{p} \cdot N_s k_{ws1}} = \frac{2877}{\frac{\sqrt{2}}{\pi} \cdot \frac{3}{2} \cdot 200 \cdot 0.91} = \underline{\underline{23.4}}\,\text{A}, \quad I_m / I_N = 23.4/59 = \underline{\underline{0.4}}$$

Stray inductances

Stray inductance of stator winding :

$W/\tau_p = 12/15$, $W = 12\tau_{Qs}$:

Slot:

$$K_1 = \frac{9}{16} \cdot \frac{W}{\tau_p} + \frac{7}{16} = 0.8875 \qquad K_2 = \frac{3}{4} \cdot \frac{W}{\tau_p} + \frac{1}{4} = 0.85\,,\; b_Q = 12.5\text{ mm}$$

$h_1' = N_c \cdot (h_L + d_{ic}) + (N_c - 1) \cdot d_i - d_{ic} = 24.7 - 0.4 = 24.3\,\text{mm}$

$h' = Z + 2 \cdot d + 2 \cdot (d_i/2) = 4 + 2 \cdot 2.2 + 2 \cdot (0.4/2) = 8.8\,\text{mm}$

$h_2 = d_{ic}/2 + d + 2 \cdot d_{sl} + d_t + h_{wedge} = 0.4/2 + 2.2 + 2 \cdot 0.15 + 0.4 + 4.5 = 7.6\,\text{mm}$

$$\lambda_{Qs} = K_1 \cdot 2 \cdot \frac{h_1'}{3b_Q} + \frac{h'}{4b_Q} + K_2 \cdot \frac{h_2}{b_Q} = 0.8875 \cdot 2 \cdot \frac{24.3}{3 \cdot 12.5} + \frac{8.8}{4 \cdot 12.5} + 0.85 \cdot \frac{7.6}{12.5} = \underline{\underline{1.843}}$$

$$X_{s\sigma Q} = \omega_s L_{s\sigma Q} = 2\pi f_s \cdot \mu_0 N_s^2 \frac{2}{p \cdot q_s} \lambda_{Qs} l_e = 2\pi 50 \cdot 4\pi \cdot 10^{-7} \cdot 200^2 \cdot \frac{2}{2 \cdot 5} \cdot 1.843 \cdot 0.392 = \underline{\underline{2.28}}\,\Omega$$

Winding overhang:

$$l_{bs} = \frac{W}{\sqrt{1 - \frac{(b_{Qs} + \lambda)^2}{\tau_{Qs}^2}}} + \frac{\pi}{2} \cdot \frac{h_{Qs}}{2} + 2 \cdot l_a + \Delta l_b = \frac{12 \cdot 24}{\sqrt{1 - \frac{(12.5+4)^2}{24^2}}} + \frac{\pi}{2} \cdot \frac{69}{2} + 2 \cdot 57 + 50 = \underline{\underline{614.8}}\,mm$$

$$\lambda_{bs} = 0.075 \cdot \left(1 + \frac{l_{bs}}{\tau_p}\right) = 0.075 \cdot \left(1 + \frac{614.8}{360}\right) = \underline{\underline{0.203}}$$

$$X_{s\sigma b} = \omega_s L_{s\sigma b} = 2\pi f_s \cdot \mu_0 N_s^2 \frac{2}{p} \lambda_{bs} l_{bs} = 2\pi 50 \cdot 4\pi \cdot 10^{-7} \cdot 200^2 \cdot \frac{2}{2} \cdot 0.203 \cdot 0.6148 = \underline{\underline{1.97}}\,\Omega$$

Harmonic reactance:

$\sigma_{Os}(q_s = 5, s = 3) = 0.411/100$

$X_{s\sigma O} = \omega_s L_{s\sigma O} = \sigma_{Os} \cdot X_h = (0.411/100) \cdot 155.2 = \underline{\underline{0.64}}\,\Omega$

Resulting stator stray reactance:

$X_{s\sigma} = X_{s\sigma Q} + X_{s\sigma b} + X_{s\sigma O} = 2.28 + 1.97 + 0.64 = \underline{\underline{4.89}}\,\Omega$

Stray inductance of unskewed rotor cage:

$h_1 = 40$ mm, $b_{Qr} = 5.1$ mm, $h_4 = 3.4$ mm, $s_{Qr} = 2.5$ mm

Slot:

$$\lambda_{Qr} = \frac{h_1}{3b_{Qr}} \cdot k_L + \frac{h_4}{s_{Qr}} = \frac{40}{3 \cdot 5.1} \cdot k_L + \frac{3.4}{2.5} = 2.61 k_L + 1.36$$

a) Start slip $s = 1$ and 20°C: $f_r = 1 \cdot 50 = 50$ Hz:

$$\xi = h_1 \sqrt{\pi \cdot f_r \cdot \mu_0 \cdot \kappa_{Cu}} = 0.04 \sqrt{\pi \cdot 50 \cdot 4\pi \cdot 10^{-7} \cdot 57 \cdot 10^6} = 4.24$$

$$k_L = \frac{3}{2 \cdot 4.24} \cdot \frac{\sinh(2 \cdot 4.24) - \sin(2 \cdot 4.24)}{\cosh(2 \cdot 4.24) - \cos(2 \cdot 4.24)} = 0.353\,, \qquad \lambda_{Qr} = \underline{\underline{2.28}}$$

b) Rated slip $s = 1.5\%$: $f_r = 0.015 \cdot 50 = 0.75$ Hz: $\xi = 0.519$, $k_L = 0.998$, $\lambda_{Qr} = \underline{\underline{3.96}}$

$$\ddot{u}_U = \frac{N_s k_{ws}}{N_r k_{wr}} = \frac{200 \cdot 0.91}{0.5 \cdot 1} = 364, \quad \ddot{u}_I = \ddot{u}_U \cdot \frac{m_s}{Q_r} = 364 \cdot \frac{3}{50} = 21.84$$

a) At stand still:

$$X'_{r\sigma Q} = \ddot{u}_U \ddot{u}_I \omega_s L_{s\sigma Q} = \ddot{u}_U \ddot{u}_I 2\pi f_s \mu_0 \lambda_{Qr} l_e = 364 \cdot 21.84 \cdot 2\pi 50 \cdot 4\pi \cdot 10^{-7} \cdot 2.28 \cdot 0.392 = \underline{\underline{2.80}}\,\Omega$$

b) At rated slip:

$X'_{r\sigma Q} = \underline{\underline{4.87}}\,\Omega$

Ring stray field (= rotor winding overhang):

$\lambda_{br} = 0.12$, $l_{br} = \tau_p = 360$ mm

$$X'_{r\sigma b} = \omega_s L'_{r\sigma b} = 2\pi f_s \cdot \mu_0 N_s^2 \frac{2}{p} \lambda_{br} l_{br} = 2\pi 50 \cdot 4\pi \cdot 10^{-7} \cdot 200^2 \cdot \frac{2}{2} \cdot 0.12 \cdot 0.36 = \underline{\underline{0.68}}\,\Omega$$

Harmonic reactance:

$$\sigma_{Or} = \frac{1}{\left(\frac{\sin(p \cdot \pi / Q_r)}{p \cdot \pi / Q_r}\right)^2} - 1 = \frac{1}{\left(\frac{\sin(2 \cdot \pi / 50)}{2 \cdot \pi / 50}\right)^2} - 1 = 0.528/100$$

$X'_{r\sigma O} = \omega_s L'_{r\sigma O} = \sigma_{Or} \cdot X_h = 0.528/100 \cdot 155.2 = \underline{\underline{0.82}}\,\Omega$

Resulting rotor stray reactance:

a) At stand still (locked rotor): $X'_{r\sigma} = X'_{r\sigma Q} + X'_{r\sigma b} + X'_{r\sigma O} = 2.80 + 0.68 + 0.82 = \underline{\underline{4.30}}\,\Omega$

b) At rated slip: $X'_{r\sigma} = \underline{\underline{6.37}}\,\Omega$

c) For arbitrary slip: $X'_{r\sigma} = \underline{\underline{3.20 \cdot k_L + 3.18}}\,\Omega$

Alternatively: Stray inductance of skewed rotor:
Rotor skew $b_{sk} = \tau_{Qs} = 24$ mm, $b_{sk} / \tau_{Qr} = \tau_{Qs} / \tau_{Qr} = Q_r / Q_s = 50/60$

$$\sigma_{O+sk,r} = \frac{1}{\left(\frac{\sin(2\pi/50)}{2\pi/50}\right)^2 \cdot \left(\frac{\sin[(2\pi/50)\cdot(50/60)]}{(2\pi/50)\cdot(50/60)}\right)^2} - 1 = 0.896/100$$

$$X'_{r\sigma O} = \omega_s L'_{r\sigma O} = \sigma_{Or} \cdot X_h = (0.896/100)\cdot 155.2 = \underline{\underline{1.39\,\Omega}}$$

Effect of skew: Increase of harmonic stray inductance by 1.39 - 0.82 = 0.57Ω

Saturation of leakage inductance at s = 1 (locked rotor):
A cage induction machine with 10 % increased power of 550 kW instead of 500 kW (due to elevated operating voltage 6.6 kV instead of 6 kV), I_N = 59 A, $I_{s1} = 5I_N$ = 295 A, slot data from above:

$K_2 = 0.85$, $k_{ds} = 0.957$, $k_{ws} = 0.91$, $N_{Qs} = 2\cdot 10 = 20$, $a = 1$, $\tau_{Qs} = 24$ mm, $\tau_{Qr} = 28.8$ mm

$$\Theta_Q = N_{Qs}(\hat{I}_{s1}/a)\frac{K_2 + k_{ws}k_{ds}\cdot Q_s/Q_r}{2} = 20\cdot(\sqrt{2}\cdot 295/1)\cdot\frac{0.85+0.91\cdot 0.957\cdot 60/50}{2} = 7906\text{ A}$$

$$B_f = \frac{\mu_0\cdot\Theta_Q}{2\delta\cdot\left(2\sqrt{\delta/(\tau_{Qs}+\tau_{Qr})}+0.5\right)} = \frac{4\pi\cdot 10^{-7}\cdot 7906}{2\cdot 0.0014\cdot\left(2\sqrt{1.4/(24+28.8)}+0.5\right)} = 4.29\text{ T}$$

$$k_{zz} = \frac{B_f + 1.5}{3.2} = \frac{4.29+1.5}{3.2} = 1.8$$

$$X_{s\sigma O,sat} = X_{s\sigma O}/k_{zz} = 0.64/1.8 = \underline{\underline{0.36\,\Omega}} \qquad X'_{r\sigma O,sat} = X'_{r\sigma O}/k_{zz} = 0.82/1.8 = \underline{\underline{0.46\,\Omega}}$$

Stator open slot remains unchanged, as there are no tooth tip horns, which might saturate. Stray inductance of rotor slot (b_{Qr} = 5.1 mm, h_4 = 3.4 mm, s_{Qr} = 2.5 mm) decreases:

$$b_{bridge} = b_{Qr} - s_{Qr} = 5.1 - 2.5 = 2.6\text{ mm}$$

$$s_{Q,sat} = s_Q + b_{bridge}\cdot\left(1-\frac{1}{k_{zz}}\right) = 2.5 + 2.6\cdot\left(1-\frac{1}{1.8}\right) = 3.66\text{ mm}$$

At s = 1 and 20°C: $k_L = 0.353$:

$$\lambda_{Qr} = \frac{h_1}{3b_{Qr}}\cdot k_L + \frac{h_4}{s_{Qr,sat}} = \frac{40}{3\cdot 5.1}\cdot 0.353 + \frac{3.4}{3.66} = 1.85,\ X'_{r\sigma Q} = \underline{\underline{2.27\,\Omega}}$$

$$X_{s\sigma} = X_{s\sigma Q} + X_{s\sigma b} + X_{s\sigma O} = 2.28 + 1.97 + 0.36 = \underline{\underline{4.61\,\Omega}}$$

$$X'_{r\sigma} = X'_{r\sigma Q} + X'_{r\sigma b} + X'_{r\sigma O} = 2.27 + 0.68 + 0.46 = \underline{\underline{3.41\,\Omega}}$$

Due to the zig-zag stray flux saturation the stray inductance of the 550 kW, high voltage cage induction motor is reduced by 13 % from $X_\sigma = X_{s\sigma} + X'_{r\sigma} = 4.89 + 4.30 = 9.19\,\Omega$ to $X_\sigma = 4.61 + 3.41 = 8.02\,\Omega$.

Masses and losses

Stator winding data:

$$\rho_{Cu}(75°C)/\rho(20°C) = (1 + (75-20)/255) = \underline{\underline{1.22}}$$

$$R_s = \frac{1}{\kappa}\cdot\frac{N_s\cdot 2\cdot(L+l_b)}{a\cdot a_i\cdot A_{TL}} = \frac{1}{57\cdot 10^6/1.22}\cdot\frac{200\cdot 2\cdot(0.458+0.6148)}{1\cdot 1\cdot 12.42\cdot 10^{-6}} = \underline{\underline{0.74\,\Omega}}$$

$$m_{Cu,s} = \gamma_{Cu} m_s N_s \cdot 2(L + l_b) \cdot a \cdot a_i A_{TL} =$$

$$= 8900 \cdot 3 \cdot 200 \cdot 2 \cdot (0.458 + 0.6148) \cdot 1 \cdot 1 \cdot 12.42 \cdot 10^{-6} = \underline{\underline{142.3 kg}}$$

Rotor cage:

Bar:

a) At stand still (locked rotor) $s = 1.0$: $f_r = 1 \cdot 50 = 50$ Hz:

$$\xi = h_1 \sqrt{\pi \cdot f_r \cdot \mu_0 \cdot \kappa_{Cu}} = 0.04 \sqrt{\pi \cdot 50 \cdot 4\pi \cdot 10^{-7} \cdot (57/1.22) \cdot 10^6} = 3.84$$

$$k_R = 3.84 \cdot \frac{\sinh(2 \cdot 3.84) + \sin(2 \cdot 3.84)}{\cosh(2 \cdot 3.84) - \cos(2 \cdot 3.84)} = 3.844$$

$$R_{bar} = \frac{1}{57/1.22 \cdot 10^6} \cdot \frac{(0.392 \cdot 3.844 + (0.458 - 0.392))}{200 \cdot 10^{-6}} = 168.32\ \mu\Omega$$

b) Rated slip s = 0.015: $f_r = 0.015 \cdot 50 = 0.75$ Hz: $\xi = 0.47$, $k_R = 1.0043$, $R_{bar} = 49.2\ \mu\Omega$

Ring:

$$d_{Ring} = d_{si} - 2\delta - h_{Ring} = 458 - 2 \cdot 1.4 - 40 = 415.2 \text{ mm}$$

$$\Delta R_{Ring} = d_{Ring} \pi / (\kappa \cdot Q_r \cdot A_{Ring}) = 0.4152 \cdot \pi / (57/1.22) \cdot 10^6 \cdot 50 \cdot 800 \cdot 10^{-6}) = 0.70\ \mu\Omega$$

$$\Delta R^*_{Ring} = \Delta R_{Ring} \frac{1}{2 \sin^2(\pi p / Q_r)} = 0.70 \cdot \frac{1}{2 \sin^2(\pi \cdot 2/50)} = 22.3\ \mu\Omega$$

$$\ddot{u}_U = 364, \quad \ddot{u}_I = 21.84$$

Total cage resistance:

a) At stand still:

$$R_r = R_{bar} + \Delta R^*_{Ring} = 168.32 + 22.3 = 190.6\ \mu\Omega,$$

$$R'_r = \ddot{u}_U \ddot{u}_I R_r = 364 \cdot 21.84 \cdot 0.0001906 = \underline{\underline{1.515}}\ \Omega$$

b) At rated slip:

$$R_r = R_{bar} + \Delta R^*_{Ring} = 49.2 + 22.3 = \underline{\underline{71.5}}\ \mu\Omega$$

$$R'_r = \ddot{u}_U \ddot{u}_I R_r = 364 \cdot 21.84 \cdot 0.0000715 = \underline{\underline{0.568}}\ \Omega$$

c) At arbitrary slip: $R'_r = \underline{\underline{0.3335 \cdot k_R + 0.2334}}\ \Omega$

Cage mass:

$$m_{Cu,r} = 8900 \cdot \left[60 \cdot 200 \cdot 10^{-6} \cdot 0.458 + 2 \cdot 800 \cdot 10^{-6} \cdot 0.4152 \cdot \pi\right] = \underline{\underline{67.5}}\ \text{kg}$$

Friction and windage losses

at synchronous speed n = 1500/min:

$$P_{fr+w} \approx 10 \cdot d_{si}^3 \cdot L \cdot \pi^2 \cdot n^2 = 10 \cdot 0.458^3 \cdot 0.458 \cdot \pi^2 \cdot (1500/60)^2 = \underline{\underline{2714}}\ \text{W}$$

Iron losses

For lower iron losses, an iron sheet type IV (v_{10} = 1.7 W/kg) with electrical conductivity $\kappa = 4 \cdot 10^6$ S/m, instead of iron sheet type III (v_{10} = 2.3 W/kg), is used: d_{si} = 458 mm, δ = 1.4 mm, l_{ds} = 69 mm, l_{dr} = 43.5 mm, h_{ys} = 77 mm, shaft diameter d_{ri} = 200 mm, h_{yr} = 84.1 mm

Flux densities:

$B_{ys} = 1.70$ T, $B_{yr} = 1.73$ T, $B'_{ds,1/3} = 1.68$ T, $B'_{dr,1/3} = 1.41$T, k_{Vd} = 1.8, k_{Vy} = 1.5

Masses:

$A_{Qs} = b_{Qs} \cdot h_{Qs} = 12.5 \cdot 69 = 862.5\,\text{mm}^2$

$m_{ds} = 7800 \cdot \left\{\left[(0.458 + 2 \cdot 0.069)^2 - 0.458^2\right] \cdot (\pi / 4) - 60 \cdot 862.5 \cdot 10^{-6}\right\} \cdot 0.378 \cdot 0.95 = 175\,\text{kg}$

$A_{Qr} = b_{Qr} \cdot h_1 + s_{Qr} \cdot h_4 = 5.1 \cdot 40.1 + 2.5 \cdot 3.4 = 213\,\text{mm}^2,\ d_{ra} = d_{si} - 2\delta = 0.4552\,\text{mm}$

$m_{dr} = 7800 \cdot \left\{\left[0.4552^2 - (0.4552 - 2 \cdot 0.0435)^2\right] \cdot \frac{\pi}{4} - 50 \cdot 213 \cdot 10^{-6}\right\} \cdot 0.378 \cdot 0.95 = 127.8\,\text{kg}$

$m_{ys} = 7800 \cdot \left[0.75^2 - (0.75 - 2 \cdot 0.077)^2\right] \cdot (\pi / 4) \cdot 0.378 \cdot 0.95 = 456\,\text{kg}$

$m_{yr} = 7800 \cdot \left[(0.2 + 2 \cdot 0.0841)^2 - 0.2^2\right] \cdot (\pi / 4) \cdot 0.378 \cdot 0.95 = 210.2\,\text{kg}$

Iron losses:

f = 50 Hz: $k_f = 1$: stator teeth $P_{Fe,ds} = 1.8 \cdot \left(\frac{1.68}{1.0}\right)^2 1.7 \cdot 1 \cdot 175 = \underline{\underline{1511}}\,\text{W}$

stator yoke: $P_{Fe,ys} = 1.5 \cdot \left(\frac{1.70}{1.0}\right)^2 1.7 \cdot 1 \cdot 456 = \underline{\underline{3360}}\,\text{W}$

Additional no-load losses:

a) Surface losses

$s_{Qs} = b_{Qs} = 12.5$ mm, $\delta = 1.4$ mm, $B_\delta = 0.891$ T, $\mu_{Fe} = 1400\mu_0$ (assumed)

$Q_r = 50,\ \tau_{Qr} = 28.8mm,\ s_{Qr} = 2.5mm,\ l_{Fe} = 378mm,\ \tau_{Qs} = 24mm,\ k_{Cs} = 1.5,\ Q_s = 60, k_{\exp} = 0.08$

- Pulsation frequency: $f_Q = Q_s \cdot n = 60 \cdot 1500 / 60 = \underline{\underline{1500}}\,\text{Hz}$

$h = s_{Qs} / \delta = 12.5 / 1.4 = 8.93,\ \beta = \frac{1}{2} \cdot \left(1 - \frac{2 / 8.93}{\sqrt{1 + (2 / 8.93)^2}}\right) = 0.391$

- Flux density amplitude: $\hat{B}_{Qs} = \beta \cdot k_{Cs} \cdot B_\delta = 0.391 \cdot 1.5 \cdot 0.891 = \underline{\underline{0.52}}\,\text{T}$

- Rotor surface: $A_r = Q_r \cdot (\tau_{Qr} - s_{Qr}) \cdot l_{Fe} = 50 \cdot (0.0288 - 0.0025) \cdot 0.378 = 0.497\,\text{m}^2$

- Rotor surface losses:

$$P_{Or} = 0.497 \cdot \frac{(0.024 / 2)^2 \cdot \left(\frac{2}{\pi} \cdot 0.391 \cdot 1.5 \frac{0.891}{\sqrt{2}}\right)^2}{4} \cdot 1500^{1.5} \cdot \sqrt{\frac{\pi^3 \cdot 4 \cdot 10^6}{1400 \cdot 4\pi \cdot 10^{-7}}} \cdot 0.08 = \underline{\underline{1220}}\,\text{W}$$

b) Tooth pulsation losses

iron sheet type IV: $p_{Ft} = 0.4$ W/kg: $s_{Qs} = b_{Qs} = 12.5$ mm, $\delta = 1.4$ mm, $B_{dr,1/3} = 1.41$ T,

$m_{dr} = 127.8$ kg, $Q_r = 50,\ k_{Cs} = 1.5,\ Q_s = 60, k_{Vd} = 1.8,\ \beta = 0.391$

Pulsation frequency: $f_Q = Q_s \cdot n = 60 \cdot 1500 / 60 = \underline{\underline{1500}}\,\text{Hz}$

$\Delta B_{dr,1/3} = \frac{B_{dr,1/3} \cdot \beta \cdot k_{Cs}}{\sqrt{2}} \cdot \frac{\sin(\pi \cdot Q_s / Q_r)}{\pi \cdot Q_s / Q_r} = \frac{1.41 \cdot 0.391 \cdot 1.5}{\sqrt{2}} \cdot \frac{\sin(\pi \cdot 60 / 50)}{\pi \cdot (60 / 50)} = -0.091\,\text{T}$

$P_{puls,r} = 1.8 \cdot \left(\frac{0.091}{1.0}\right)^2 \cdot 0.4 \cdot \left(\frac{1500}{50}\right)^2 \cdot 127.8 = \underline{\underline{688}}\,\text{W}$

c) Check of eddy currents in stator conductors at 50 Hz:

Motor data from Example 2.4-3: f_s = 50 Hz, 20°C: $\kappa_{Cu} = 57 \cdot 10^6$ S/m, $b_L = 7.1$ mm, $h_L = 1.8$ mm, two layer winding $n = 2N_c = 20$, $n_{ne} = 1$, $b_L / b_Q = 7.1/12.5$

$$\xi = h_L \cdot \sqrt{\pi \cdot \mu_0 \cdot f_s \cdot \kappa \cdot (n_{ne} \cdot b_L / b_Q)} = 0.0018 \cdot \sqrt{\pi \cdot 4\pi \cdot 10^{-7} \cdot 50 \cdot 57 \cdot 10^6 \cdot (1 \cdot 7.1/12.5)} = 0.144$$

$\varphi(0.144) = 1.0000382$, $\psi(0.144) = 0.0001433$

$$k_n = 1.0000382 + \frac{20^2 - 1}{3} \cdot 0.0001433 = \underline{\underline{1.019}}$$

Increase of AC resistance is only 1.9% compared to DC resistance and therefore negligible.

Additional losses at load (stray load losses) at increased load 550 kW motor:
Acc. to IEC 60034-2: $P_{ad,1} = 0.005 \cdot P_e = 0.005 \cdot 582.6 = \underline{\underline{2.91}}$ kW

Total active masses

Stator winding (without winding insulation)	142.3 kg
Rotor cage	67.5 kg
Winding mass:	209.8 kg
Stator teeth	175.0 kg
Stator yoke	456.0 kg
Stator iron mass:	631.0 kg
Rotor teeth	127.8 kg
Rotor yoke	210.2 kg
Rotor iron mass:	338.0 kg
Total active mass:	1178.8 kg

Table A1-5: Calculated active mass for the high voltage cage induction machine, open ventilated, Thermal Class B, 50 Hz, four poles

Machine performance

At increased motor power 550 kW and elevated voltage 6.6 kV, 50 Hz, unskewed rotor, at 75°C winding temperature:

Total iron losses: $P_{Fe} = P_{Fe,ds} + P_{Fe,ys} + P_{Or} + P_{puls,r} = 1511 + 3360 + 1220 + 688 = 6779$ W

Simplified iron resistance consideration:

$R_{Fe} = m_s \cdot U_s^2 / P_{Fe} = 3 \cdot (6600/\sqrt{3})^2 / 6779 = \underline{\underline{6425}}\ \Omega$,

$\underline{I}_{Fe} = \underline{U}_s / R_{Fe} = 3810.5 / 6425 = 0.59$ A (1% of rated current, thus very small !)

Stray load losses:

$R_{ad,1} = P_{ad,1} / (m_s \cdot I_N^2) = 2910 / (3 \cdot 59^2) = \underline{\underline{0.278}}\ \Omega$

rated speed n = 1490/min:

Rated shaft torque: $M_N = P_N / (2\pi n_N) = 550000 / (2\pi \cdot (1490/60)) = \underline{\underline{3525}}$ Nm

Braking effect of

- friction and windage losses: $M_{fr+w} = P_{fr+w} / (2\pi n_N) = 2714 / (2\pi \cdot (1490/60)) = \underline{\underline{17.4}}$ Nm
- tooth pulsation and surface losses:

$M_{puls+O,r} = P_{puls+O,r} / (2\pi n_N) = (688 + 1220)1 / (2\pi \cdot (1490/60)) = \underline{\underline{12.2}}$ Nm

$\underline{U}_s = U_s = 6600/\sqrt{3}$ V, $f_s = 50$ Hz, at 75°C: R_s = 0.74 Ω, $R_{1,ad}$ = 0.278 Ω, R_{Fe} = 6425 Ω,

$X_{s\sigma}$ = 4.89 Ω, X_h = 155.2 Ω (saturated value), $X'_{r\sigma} = (3.2 \cdot k_L(s) + 3.18)\,\Omega$,

$R'_r = (0.3335 \cdot k_R(s) + 0.2334)\,\Omega$

For 550 kW output power a slip of $s_N = 0.814\%$ is necessary, yielding:
coefficients $k_R = 1.0013$ and $k_L = 0.99963$ and $X'_{r\sigma} = 6.379\,\Omega, R'_r = 0.5673\,\Omega, \sigma = 0.069$.
Rated stator current is I_{sN} = 59.04 A (estimated 59 A), rotor current is $I'_r = 51.6\,\text{A}$, $I_m = 23.8\,\text{A}$.

Electrical input power $P_{e,in}$	**574 921 W**
Stator winding losses $P_{Cu,s}$	7 739 W
Total iron losses P_{Fe}	6 779 W
Stray load losses $P_{ad,l}$ (= 0.5% of 574 310 W)	2 875 W
Air gap power P_δ	557 528 W
Rotor cage losses $P_{Cu,r}$	4 538 W
Friction and windage losses P_{fr+w}	2 670 W
Mechanical output power $P_{m,out}$	**550 320 W (≅ 550 kW)**
Efficiency η	95.72 %

Table A1-6: Losses

$$\cos\varphi_s = \frac{574921}{\sqrt{3}\cdot 6600\cdot 59.04} = 0.852\,,\ P_{Cu,s} = m_s R_s I_s^2 = 3\cdot 0.74\cdot 59.04^2 = 7739\,\text{W}$$

$$P_{Cu,r} = m_s R'_r I'^2_r = 3\cdot 0.5673\cdot 51.6^2 = 4538\,\text{W} \quad \text{or} \quad P_{Cu,r} = sP_\delta = 0.00814\cdot 557528 = 4538\,\text{W}$$

$$M_e = p\frac{P_\delta}{\omega_s} = 2\cdot\frac{555528}{2\pi\cdot 50} = 3549\,\text{Nm},\ M_s = \frac{P_m}{2\pi\cdot n} = \frac{550320}{2\pi\cdot(1487.79/60)} = 3532.2\,\text{Nm}$$

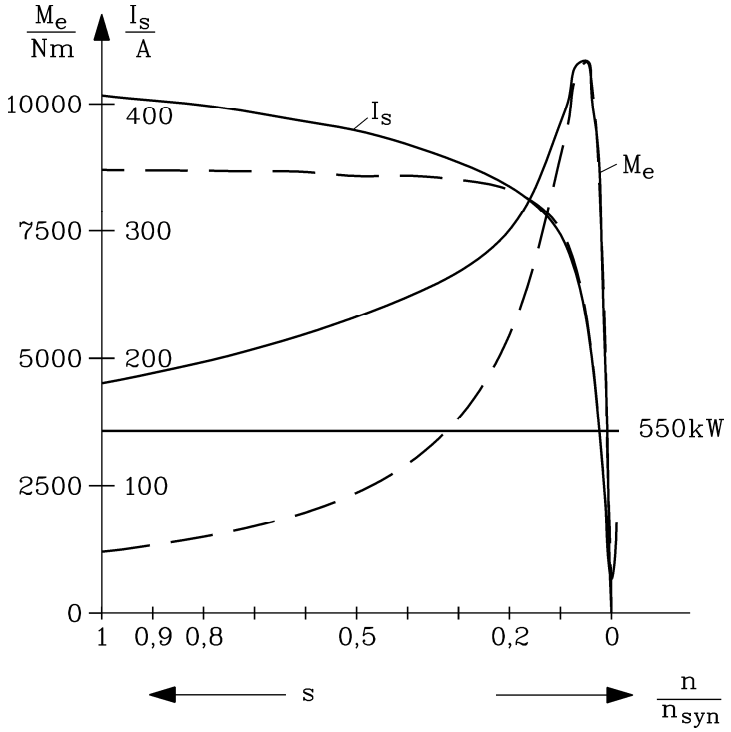

Fig. A1-4: Calculated stator current and electromagnetic torque versus speed of 550 kW, 4 pole, three phase cage induction motor, 6.6 kV. 50 Hz:
solid lines: with current displacement ($k_L < 1$, $k_R > 1$) in rotor bars considered,
dashed lines: without considering current displacement ($k_L = 1$, $k_R = 1$) too low torque is calculated

Comparison of no-load and locked rotor characteristic between analytical calculation and computation results by the SPEED program

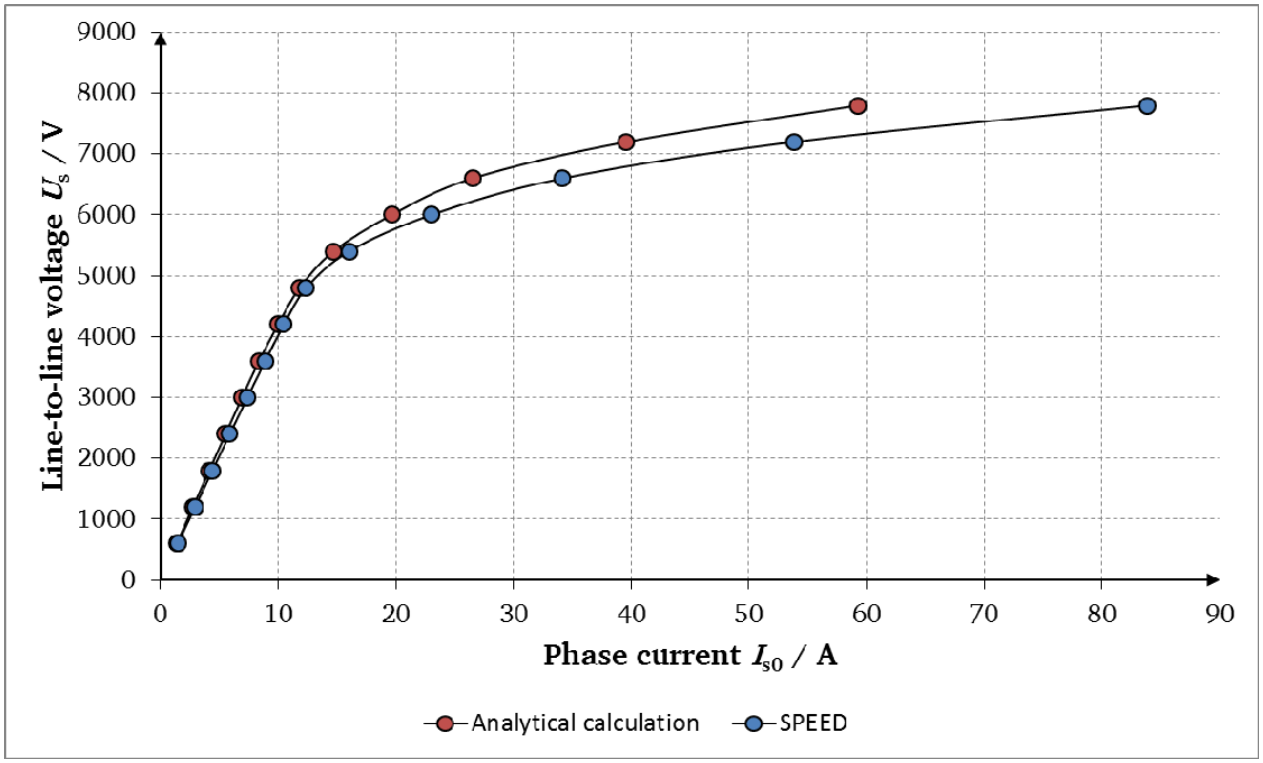

Fig. A1-5: Calculated no-load characteristic of 550 kW, 4 pole, three phase cage induction motor, 50 Hz

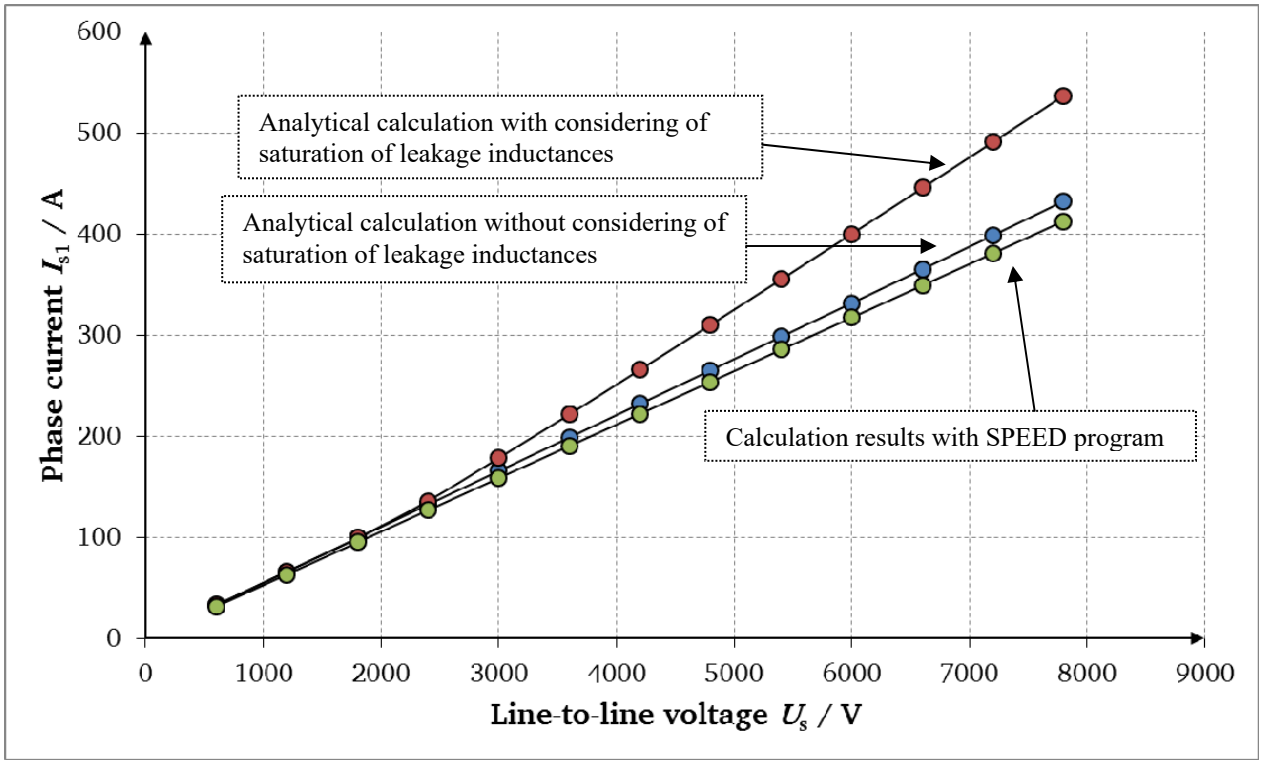

Fig. A1-6: Calculated locked-rotor characteristic of 550 kW, 4 pole, three phase cage induction motor, 50 Hz

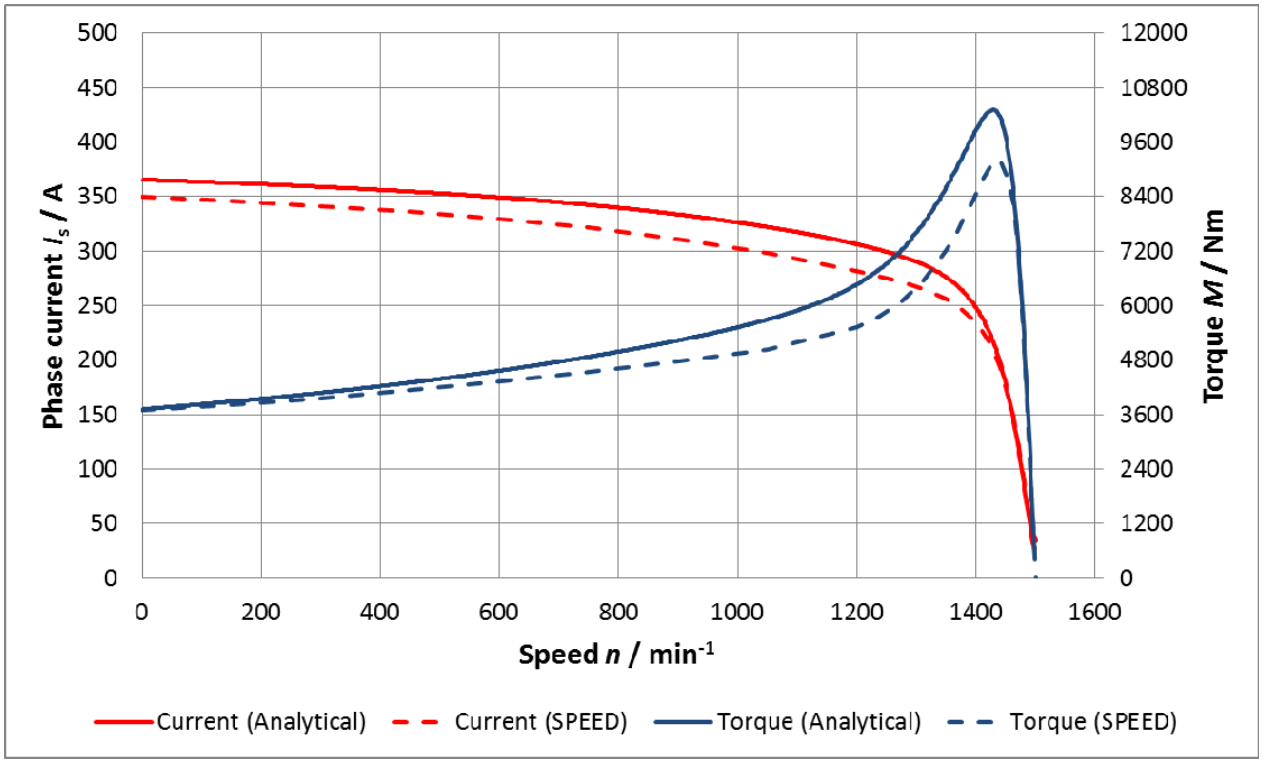

Fig. A1-7: Calculated stator current (red line) and electromagnetic troque (blue line) versus speed for an induction machine with 550 kW, 4 pole, 50 Hz, U_N = 6600 V, dashed lines: Results of analytical calculations without considering of saturation of leakage inductances, solid lines: Calculation results with SPEED program

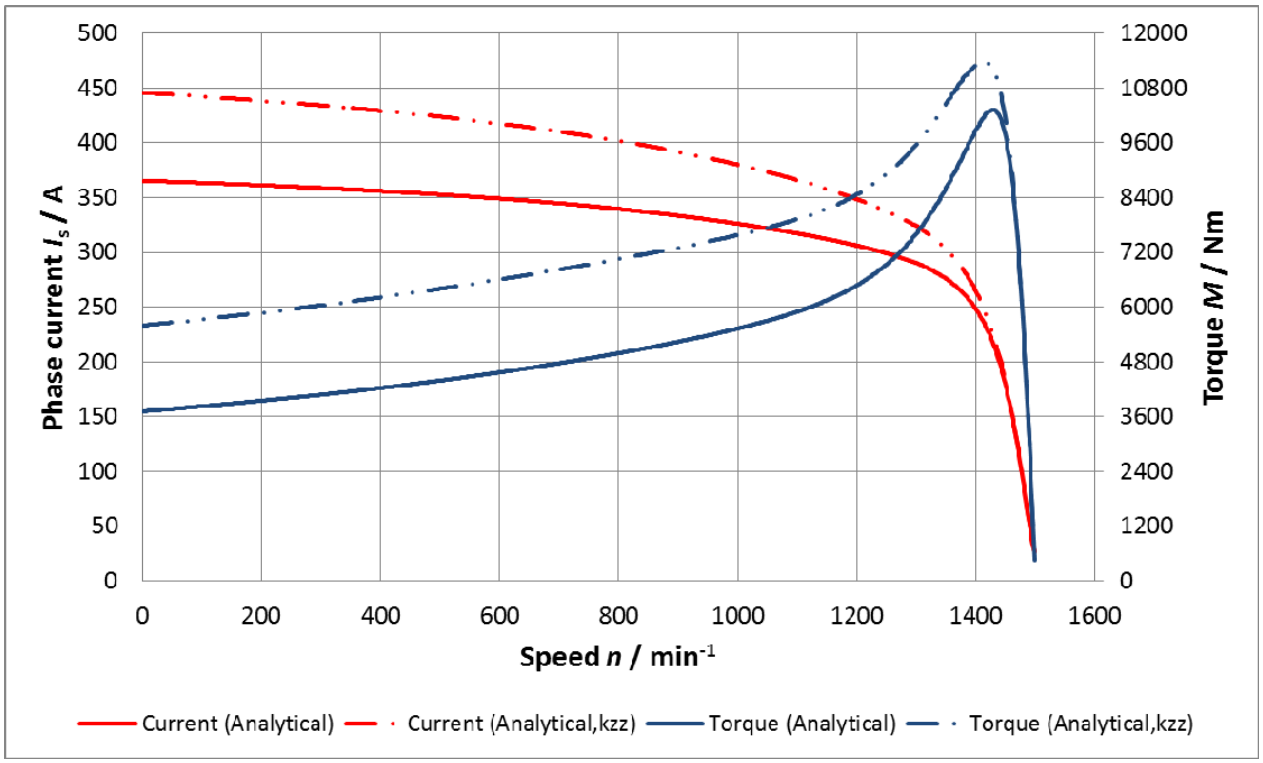

Fig. A1-8: Calculated stator current (red line) and electromagnetic troque (blue line) versus speed for an induction machine with 550 kW, 4 pole, 50 Hz, U_N = 6600 V, solid lines: Results of analytical calculations without considering of saturation of leakage inductances, dashed lines: Results of analytical calculations with considering of saturation of leakage inductances

Appendix A2: Computer Aided Design of the Induction Machine with Program SPEED

This guide is to facilitate the design of the asynchronous machine with the program PC-IMD. The design of the machine model from the lecture script "Energy Converters - CAD and System Dynamics" is presented. The input data, needed by the program, are bold printed indicated in the appropriate places (**variable = value**). In the program PC-IMD there are two important editors, where data have to be specified for the machine calculation. One of them is the **template editor**, where part of the geometric dimensions of the machine, calculation methods and further boundary conditions are chosen. The other one is the **outline editor**, where detailed geometric dimensions of stator, rotor and shaft are specified and also visualized with different view options. In the following the values that have to be specified in the **template editor** are printed as (**TE: variable=value**), while the values that have to be specified in the **outline editor** are printed as (**OE: variable=value**). **Fig. 0** shows where to select the different editors.

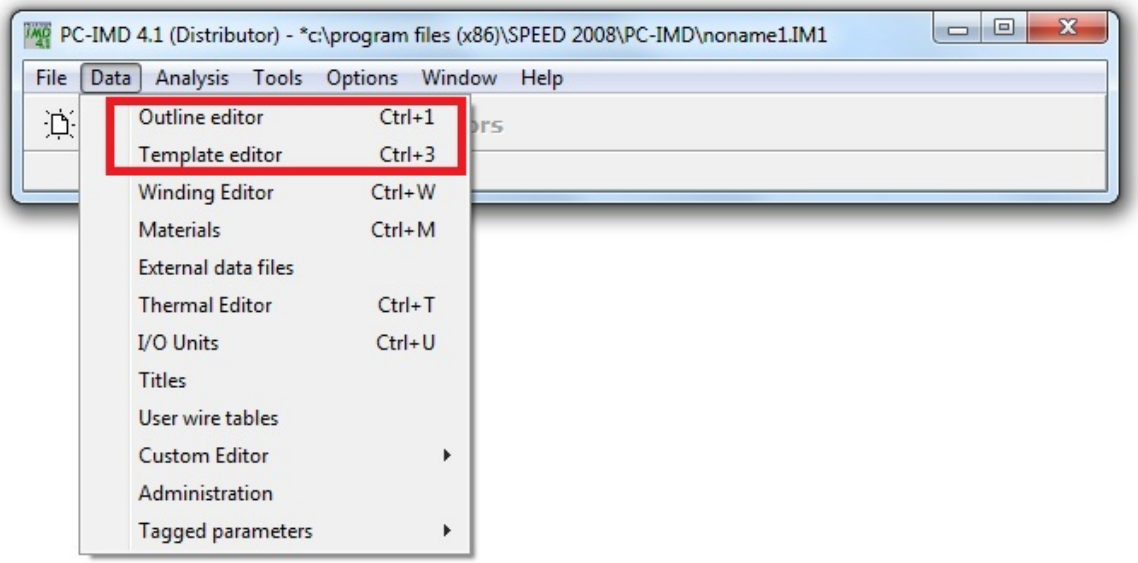

Fig. A2-0: Screenshot PC-IMD menu bar – editor selection

Machine design:

Given data:

Asynchronous motor with squirrel-cage rotor (C-rotor)				(**TE: Bar1 = Type2**)
Rated power:	P_N	=	500 kW	(**TE: PowrSh. = 500 000.0**)
Rated voltage:	U_N	=	6 kV	(**TE: Vs = 6000.0**)
Rated frequency:	f_N	=	50 Hz	(**TE: Freq = 50.0**)
Number of poles:	$2p$	=	4	(**TE: Poles = 4**)

As the frequency and the power at shaft is given we choose the calculation method (**TE: CalcMode=f/PowerSh**) and (**TE: TorqCalc = LR + Brk + NL**) in the template editor.

Aim is to design a machine with efficiency and a power factor as high as possible. By the design some conditions are to be kept:

- Overload capability: $3 > M_b/M_N > 1.6$

- Starting current: $4 < I_1/I_N < 6$

- Starting torque: $0{,}7 < M_1/M_N < 1.6$ (i.e. starting torque should not be too small, however not unnecessarily high)

- Winding temperature rise: ISO-Kl. B

1. Calculation of main design geometry data

1.1. Electromagnetic and thermal utilization

A time-dependent temperature rise calculation is not carried out (**TE: TempCalc = fixed**). The ambient temperature is 20 °C (**TE: Ambient = 20.0**), stator and rotor temperature according to ISO-Kl. B 75 °C (**TE: WdgTemp = 75.0**; **TE: RoTemp = 75.0**). At the beginning of the design several parameters have to be estimated, respectively initial values for these parameters must be chosen, which could change during the design process. For simplification, given curves of optimised machines will be used during the design. From Fig. 2.1-3 to Fig. 2.1-10 (see [1]) the following initial values are extracted:

Table A2-1: Initial values of the design

Notation	**Value**	**To insert as**
Number of poles	$2p = 4$	**TE: Poles = 4**
Efficiency	$\eta_N = 0{,}94$	
Power factor	$\cos\varphi_N = 0{,}868$	
Pole pitch	$\tau_p = 36$ cm	
Equivalent iron stack length	$l_e = 38$ cm	
Current loading	$A_s = 485$ A/cm	
Air gap flux density	$B_{\delta,av} = 0{,}56$ T ... 0,63 T	
Current density	$J_s = 5{,}5$ A / mm^2	
Air gap width	$\delta = 0{,}14$ cm	**OE: Gap = 1.4 mm**
Inner rotor diameter and shaft radius	$d_{ri} = 20$ cm $r_{shaft} \cong r_{ri} = \frac{d_{ri}}{2}$	**OE: RadSh = 100 mm**

From the initial values (Table A2-1) we find:

- Apparent power:

$$S_N = \frac{P_N}{\eta_N \cdot \cos\varphi_N} = \frac{500 \cdot 10^3}{0.944 \cdot 0.868} \cong 610\,\text{kVA}$$

- Motor current:

$$I_N = \frac{S_N}{\sqrt{3} \cdot U_{sN}} = \frac{610 \cdot 10^3}{\sqrt{3} \cdot 6 \cdot 10^3} \cong 59\,\text{A}$$

- Synchronous speed:

$$n_{syn} = f_s / p = 1500\,/\text{min}$$

- Stator bore diameter:

$$d_{si} = 2p\tau_p / \pi = 458\,\text{mm}.$$

Stator inner radius: $r_{si} = d_{si} / 2 = 229\,\text{mm}.$

Rotor outer radius: $r_{ro} = d_{si} / 2 - \delta = 227.6\,\text{mm}$ **(OE: Rad1= 227.6 mm)**

- Internal apparent power for the stator stray coefficient $\sigma_s = 0.08/2 = 0.04$:

$$S_\delta = S/(1+\sigma_s) = 610 \cdot 10^3 / 1.04 = 587\,\text{kVA}$$

- Electromagnetic utilization: $C = S_\delta / (d_{si}^2 \cdot l_{Fe} \cdot n_{syn}) = \dfrac{587 \cdot 10^3}{0.458^2 \cdot 0.38 \cdot 1500} = 4.89\,\text{kVA·min/m}^3$

With the stator stray coefficient $\sigma_s = 0{,}04$ and winding factor $k_{ws} = 0{,}91$ estimated as initial values, the air gap flux density results:

$$C = \frac{\pi^2}{\sqrt{2}} \cdot k_{w1} \cdot A \cdot B_\delta \quad \Rightarrow \quad B_\delta = \frac{\sqrt{2} \cdot C}{k_{w1} \cdot A \cdot \pi^2} = \frac{\sqrt{2} \cdot 4.89 \cdot 10^3 \cdot 60}{\pi^2 \cdot 0.91 \cdot 500 \cdot 100} = 0.954\,\text{T}.$$

and the average:

$$B_{\delta,av} = \frac{2}{\pi} \cdot B_\delta = \frac{2}{\pi} \cdot 0.954 \cong 0.6\,\text{T}$$

Machines of this power class are equipped in axial direction with round cooling ducts. The lamination stack is divided into individual packages. According to [1] we will assume that both iron stacks, stator and rotor, consist of 9 sections with l_1 = 42 mm and 8 radial ducts (switch **OE** to axial view **OE: NSDuct = 8** and **OE: NRDuct = 8**) with width l_k = 10 mm (**OE: WSDuct = 10 mm** and **OE: WRDuct = 10 mm**). The iron stacks length results:

$$l_{Fe} = 9 \cdot l_1 = 9 \cdot 42 = 378\,\text{mm}.$$

The total axial length will be extended in this case by the width of the cooling ducts:

$$L = 9 \cdot l_1 + 8 \cdot l_k = 9 \cdot 42 + 8 \cdot 10 = 458\,\text{mm} \qquad \textbf{(OE: Lstk = 458 mm)}$$

The length of the winding extension at each end of iron stack must be determined and inserted into the program. In dependence of the voltage (Table 2.8.3-2 [1]) the following value will be considered: l_a=5.7 cm (**TE: Ext=57.0**).

1.2. Design of the stator winding

The stator slot pitch τ_{Qs} changes with the number of coils per pole and phase q which is to be chosen. As q has an effect on the harmonic content of the winding it cannot be selected arbitrarily. The influence of q should be clarified within a table. The stator slot pitch consists of the tooth width b_{ds} and the slot width b_{Qs}. The tooth width may not be smaller than a minimum value for which the tooth flux density B_{ds} becomes inadmissibly high. The minimum tooth width $b_{ds,min}$ is determined by linear calculation, without field flattening and for an iron fill factor of k_{Fe} = 0,95 (**OE: Stf = 0.95**).

$$b_{ds,min} = \frac{B_{\delta,av}}{B_{ds,max}} \frac{\pi}{2} \frac{\tau_{Qs}(1+\sigma_s)}{k_{Fe}}$$

The maximum tooth flux density is assumed to 2.4 T (higher value because it is calculated without flattening). Thus the maximal permissible slot width can be indicated and the distribution and pitching factors can be calculated (see Table 2) with expressions:

$$k_{dv} = \frac{\sin\left(\frac{v\pi}{2m_s}\right)}{q\sin\left(\frac{v\pi}{2m_s q}\right)}; \quad k_{pv} = \sin\left(v\frac{m_s q - s}{m_s q}\frac{\pi}{2}\right) = \sin\left(v\frac{W}{\tau_p}\frac{\pi}{2}\right)$$

Table A2-2: Choice of number of coils per pole and phase and short-pitching of the stator winding

					To insert as
Number of slots per pole and phase q:	3	4	***5***	6	**TE: CPP = 5**
Number of stator slots $Q_s = 2\,p\,m_s\,q$:	36	48	***60***	72	**TE: Slots = 60**
Slot pitch $\tau_{Qs} = \tau_p / (m_s\,q)$ in cm:	4,00	3,00	***2,40***	2,00	
Tooth width b_{dsmin} in cm:	1.17	1,31	***1,04***	0,87	
Slot width $b_{Qs} = \tau_s - b_{dsmin}$ in cm:	2.26	1,17	***1,36***	1,13	
Ratio b_{Qs} / τ_{Qs}:	0,56	0,56	***0,56***	0,56	
Pole pitch in slots τ_p:	9	12	15	18	
Distribution factor k_{d1} :	0,9598	0,9577	0,9567	0,9561	
Distribution factor k_{d5} :	0,2176	0,2053	0,2000	0,1972	
Distribution factor k_{d7} :	-0,1774	-0,1576	-0,1494	-0,1453	
Coil pitching with 1 Slot (s = 1):	8	11	14	17	
Pitching factor k_{p1} :	0,9848	0,9914	0,9945	0,9962	
Winding factor k_{w1} :	0,9452	0,9495	0,9514	0,9525	
Pitching factor k_{p5} :	0,6428	0,7934	0,8660	0,9063	
Winding factor k_{w5} :	0,1398	0,1629	0,1732	0,1787	
Pitching factor k_{p7} :	-0,3420	-0,6088	-0,7431	-0,8192	
Winding factor k_{w7} :	0,0607	0,0959	0,1111	0,1190	
Coil pitching with 2 Slots (s = 2):	7	10	13	16	
Pitching factor k_{p1} :	0,9397	0,9659	0,9781	0,9848	
Winding factor k_{w1} :	0,9019	0,9250	0,9358	0,9416	
Pitching factor k_{p5} :	-0,1736	0,2588	0,5000	0,6428	
Winding factor k_{w5} :	-0,0378	0,0531	0,1000	0,1267	
Pitching factor k_{p7} :	0,7660	0,2588	-0,1045	-0,3420	
Winding factor k_{w7} :	-0,1359	-0,0408	0,0156	0,0497	
Coil pitching with 3 Slots (s = 3):	6	9	***12***	15	**TE: Throw = 12**
Pitching factor k_{p1} :	0,8660	0,9239	***0,9511***	0,9659	
Winding factor k_{w1} :	0,8312	0,8848	***0,9099***	0,9236	
Pitching factor k_{p5} :	-0,8660	-0,3827	***0,0000***	0,2588	
Winding factor k_{w5} :	-0,1884	-0,0786	***0,0000***	0,0510	
Pitching factor k_{p7} :	0,8660	0,9239	***0,5878***	0,2588	
Winding factor k_{w7}:	-0,1536	-0,1456	***-0,0878***	-0,0376	

With the choice of q, we are trying to reduce the fifth harmonic wave amplitude of mmf. at an as small as possible value. From Table A2-2, it becomes evident that both $q = 4$ and $q = 5$ provide reasonable results and fulfil the conditions (see [1]): $b_{Qs}/\tau_{Qs} = 0.5 \ldots 0.6$ and 1 cm < b_{Qs} < 2 cm.

Here $q = 5$ is selected with a short-pitching of $s = 3$. The winding diagram created by SPEED is presented in Fig. A2-1 for the chosen case: $q = 5$ and $\frac{W}{\tau_p} = \frac{12}{15}$.

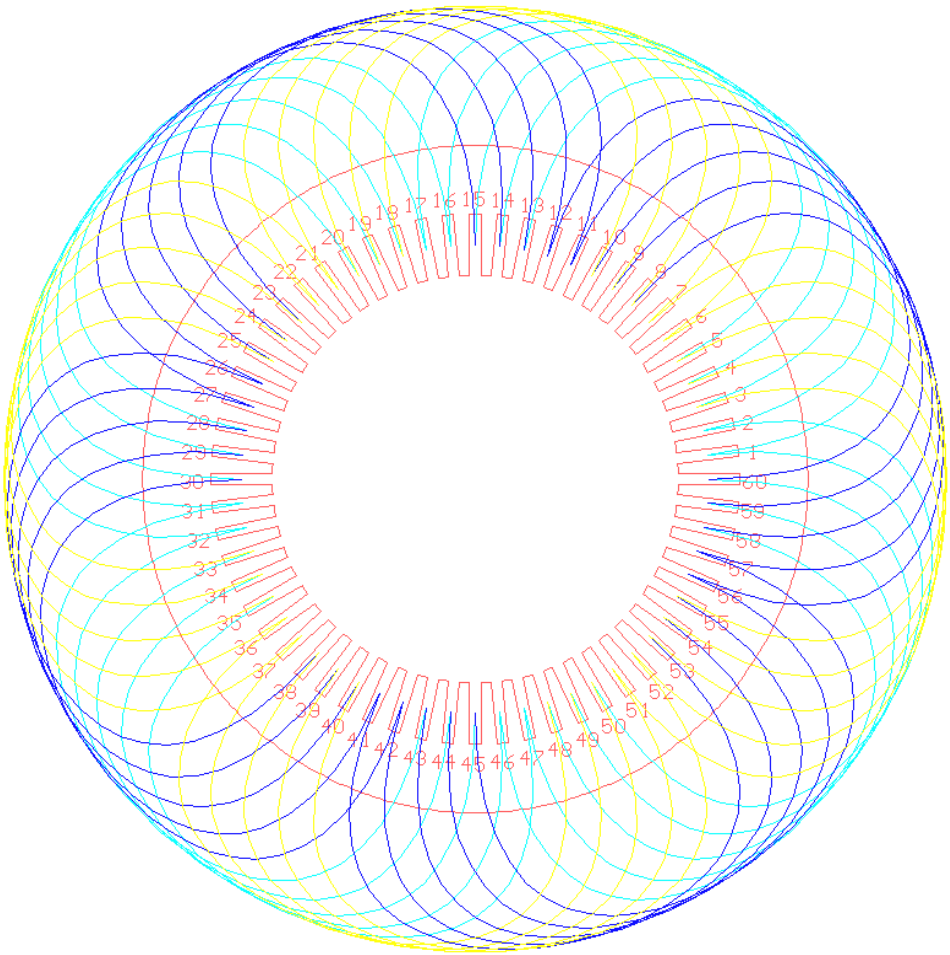

Fig. A2-1: Winding diagram created by SPEED (WdgType = Lap)

1.3. Choice of number of turns

The considered winding is a three-phase, double-layer winding in y-connection (**TE : Connex = 3-PhWye; TE: WdgType = Lap ; TE: CoilForm = None**).

The number of turns per phase is calculated as:

$$N_s = \frac{U_h}{\sqrt{2}\pi f_s \cdot k_{w1} \cdot \Phi_h} = \frac{3330}{\sqrt{2}\pi \cdot 50 \cdot 0.91 \cdot 83.12 \cdot 10^{-3}} \cong 198 \text{ turns /phase}$$

where the estimated induced voltage per phase is:

$$U_h = \frac{U_N / \sqrt{3}}{1 + \sigma_s} = \frac{6000 / \sqrt{3}}{1.04} = 3330 \text{ V}$$

and the main flux per pole of fundamental $\nu = 1$ is for the air gap flux density $B_{\delta,\nu=1} = 0.954\,\mathrm{T}$:

$$\Phi_\mathrm{h} = \frac{2}{\pi} \cdot \tau_\mathrm{p} \cdot l_\mathrm{e} \cdot B_{\delta,\nu=1} = \frac{2}{\pi} \cdot 0.36 \cdot 0.38 \cdot 0.954 = 83.12\,\mathrm{mWb}.$$

By a roughly assumption we have considered, for a preliminary estimation, the stator iron length equal to the equivalent iron length: $l_\mathrm{Fe} \approx l_\mathrm{e} \cong 380\,\mathrm{mm}$.

The number of turns per coil is:

$N_\mathrm{c} = N_\mathrm{s} \cdot a/(2pq) = 198 \cdot 1/(2 \cdot 2 \cdot 5) = 9.9$, so the integer value $N_\mathrm{c} = \underline{\underline{10}}$ (**TE: TC = 10)** for a = 1 (**TE: Ppaths = 1**) is chosen.

The values for the number of turns per phase, flux, flux density and current loading are to be determined thereby again.

Table A2-3: Corrected values

Number of turns per phase	$N_\mathrm{s} = 2pqN_\mathrm{c} = 200$
Flux density	$B_\delta = 0{,}946\,\mathrm{T}$
Air gap flux	$\hat{\Phi}_\mathrm{h} = 82.4\,\mathrm{mWb}$
Current loading	$A = \frac{2m_\mathrm{s}N_\mathrm{s}I_\mathrm{s}}{2p\tau_\mathrm{p}} = 491\,\mathrm{A/cm}$

The thermal utilization is $A \cdot J = 491 \cdot 5.5 = 2700.5\,(\mathrm{A/cm}) \cdot (\mathrm{A \cdot mm^2})$, which is a permissible value for a 500 kW induction machine (see [1]).

Attention:
Since the terminal voltage is an effective constant value, the air gap flux density depends on the number of turns per phase. If the air gap flux density is selected too small, the machine is poorly used and a larger number of turns per phase will be necessary in order to come to the given voltage. Possibly the necessary place is not available in the slot for this number of turns. If the flux density is selected too big, the iron will be strongly saturated and the magnetisation demand becomes too high!

1.4. Slot dimensions

The designed winding is a high-voltage winding. The slot flanks are parallel. The coils are inserted into the slot and then the conductor width must correspond to the slot opening. Because profile copper is used, rectangular conductors are specified in the winding parameters (**TE: Wire_1=Rect**). As can be seen from Table A2-2, for q = 5, the maximal permissible slot width is b_{Qs} = 1.36 cm and the minimal calculate permissible slot is b_{Qs} = 1.04 cm. The slot width is fixed here to b_{Qs} = 1,25 cm and from this, further conductor dimensions and slot dimensions (Table A2-4 and Table A2-6) are determined according to the text script [1]. The initial value for the outer radius of the stator is with 50 mm much smaller than the already chosen radius of the rotor. In order to have a better overview of the change of the stator slots we set the outer radius of the stator arbitrarily to 400 mm (**OE: Rad3 = 400**). The final value of the stator outer radius will be later calculated.

Table A2-4: Conductor and slot width dimensions

Slot geometry	Parallel flanks	**OE: S-Slots = PllSlot**
Slot width b_{Qs}:	12.5 mm	**OE: SWid = 12.5**

Conductor insulation d_{ic}:	0.40 mm		
Slot-lining:	0.15 mm	One-side	**TE: Liner = 0.15**
Main insulation:	2.2 mm	One-side	
Tolerance (slot play) b_{Tol}:	0.3 mm		
Insulation width b_{Is}:	4.7 mm	2times slot-lining + 2times main ins.	
Conductor width b_L	7.1 mm	$b_L = b_{Qs}$ - b_{Is} - b_{Tol}	**TE: wa_1 =7.1**

Conductor cross section is checked: $A_{TL} = I_s/(J_s \cdot a \cdot a_i) = 59/(5.5 \cdot 1 \cdot 1) = 10.73$ mm^2 and for $b_L = 7.1$ mm and for the smallest admissible area of the conductor $A_{TL} = 12.42$ mm^2 (see Table A2-5) the conductor height $h_L = 1.8$ mm is chosen.

Table A2-5: Selection of available profile copper wire: dimensions without enamel coating and cross section (edges of wire rounded by 0.5 mm .... 1.0 mm radius)

b_L (mm)	Conductor height h_L (mm)									
	1.8	*2*	*2.24*	*2.5*	*2.8*	*3.15*	*3.55*	*4*	*4.5*	*5*
5	8.637	9.637	10.84	11.95	13.45	15.20	17.22	-	-	-
5.6	9.717	10.84	12.18	13.45	15.13	17.09	19.33	21.54	-	-
6.3	10.98	12.24	13.75	15.20	17.09	19.30	21.82	24.34	27.49	-
7.1	12.42	13.84	15.54	17.20	19.33	21.82	24.66	27.54	31.09	34.64
8	14.04	15.64	17.56	19.45	21.85	24.65	27.85	31.14	35.14	39.14
9	15.84	17.64	19.80	21.95	24.65	27.80	31.40	35.14	39.64	44.14
10	17.64	19.64	22.04	24.45	27.45	30.95	34.95	39.14	44.14	49.14
11.2	19.80	22.04	24.73	27.45	30.81	34.73	39.21	43.94	49.54	55.14
12.5	22.14	24.64	27.64	30.70	34.45	38.83	43.83	49.14	55.39	61.64
14	24.84	27.64	31.00	34.45	38.65	43.55	49.15	55.14	62.14	69.14
16	-	31.64	35.48	39.45	44.25	49.85	56.25	63.14	71.14	79.14

The wire insulation thickness is set to 0.15 mm **(TE: InsThk1 = 0.150)**.

Table A2-6: Conductor and slot height dimensions

Cond. height h_L:	1,80 mm		**TE: wb_1=1.80**
Inter-turn insulation:	0.3 mm		
Conductor insulation d_{ic}:	0.4 mm		
Coated coil:	24.7 mm	$N_c \cdot (h_L + d_{ic})$ + $(N_c$-1)·inter-turn ins.	
Main insulation	4.4 mm		
Insulated coil upper layer:	29.1 mm		
Two coils per slot	58.2 mm		
Inter-layer insulation:	4,0 mm		
Slot-lining (3 times):	0,45 mm		
Wedge:	4,5 mm		
Top and Bottom lining:	0.8 mm		
Vertical play:	1.05 mm		
Slot height h_{Qs}:	69,0 mm		**TE: SD_S = 69.0**
Stator tang depth h_{4s}	0 mm		**TE: TGD_S = 0.001***

(*Speed Software cannot handle h_{4s} = 0, therefore a small value is inserted)

The magnetic circuit computation assumes parallel-sided stator teeth. Simplified calculation takes H_d on 1/3 of tooth length at the narrower side to calculate the mmf. Then:

$$\tau_{Qs,1/3} = (d_{si} + (2/3)\cdot l_{ds})\cdot \pi / Q_s = (458 + (2/3)\cdot 69)\cdot \pi / 60 = 26.38\,\text{mm}$$
$$b_{ds,1/3} = \tau_{Qs,1/3} - b_{Qs} = 26.38 - 12.5 = 13.9\,\text{mm}$$

1.5. Determination of the rotor winding parameters of the squirrel-cage rotor

Choice of rotor slot number Q_r must be done with respect to stator number Q_s (see Lectures: "Motor development for electric drive systems"). We get as choice the slot numbers from Table A2-7.

Table A2-7: Choice of rotor slot number Q_r

According to the script for and number of pole pairs the following rotor slot numbers Q_r	Q_s = 60 stator slots p = 2	
Are permitted for unskewed rotor bars:	50, 54, 66, 70	**TE: Skew = 0**
Selected number of rotor slots:	Q_r = 50 rotor slots	**TE: R_Bars = 50**

Rotor cage is designed according to rotor bar current:

$$I'_r = I_r / \ddot{u}_I \approx I_s \cdot \cos\varphi_s = 59\cdot 0.868 = 51.21\,\text{A},\ \ddot{u}_I = \frac{2k_{ws}m_s N_s}{Q_r} = \frac{2\cdot 0.91\cdot 3\cdot 200}{50} = 21.84$$
$$I_r = \ddot{u}_I \cdot I'_r = 21.84\cdot 51.33 = 1118\ \text{A}$$

The rotor bar current density results:

$$J_r = I_r / A_{Cu} = 1118/200 = 5.6\,\text{A/mm}$$

Deep bar rotor to increase starting torque should respect the ratio $h_{Cu}/b_{Cu} \geq 8$. Then: h_{Cu} = 40 mm and b_{Cu} = 5 mm with the cross section: A_{Cu} = 200 mm^2 .

The necessary ring cross section:

$$A_{Ring} = I_{Ring} / J_{Ring} = 4462/5.6 = 798\ \text{A/mm}^2$$

Where:

- Rotor ring current: $I_{Ring} = I_r /(2\cdot\sin(p\pi/Q_r)) = 1121/(2\cdot\sin(2\pi/50)) = \underline{\underline{4462}}\,\text{A}$
- Ring current density: $J_{Ring} = J_r = 5.6\,\text{A/mm}^2$,

Table A2-8: Rotor cage dimensions

Conductor dimensions:			
Winding factor k_{wr}:	1	by cage windings	
Choice of bar height and bar width:			
Bar height h_{Cu}:	40 mm		**OE: BarDpth = 40**
Bar width b_{Cu}:	5 mm		**OE: BarWdth = 5**
Set-back h_{4r}:	3.5 mm	acc. To text script [1]	**OE: SetBack = 3.5 mm**

Rotor slot opening s_{Or}	2.5 mm		**OE: SO_R = 2.5 mm**
Ring height and axial width:			
Ring height h_{Ring}	40 mm	Ring height is usually at least bar height: $h_{Ring} > h_{Cu}$	
Additional radial ring height:	0 mm	$h_z = h_{Ring} - h_{Cu}$	**OE: ERLedge1 = 0**
			OE: ERLedge2 = 0
Ring width b_{Ring}:	20 mm		**OE: Erthk1 = 20**
			OE: Erthk2 = 20

The set-backs in the rotor are not filled with copper, therefore (**TE: SBFull = false**).
As copper is used as rotor bars, the cage- and end-ring density is set to the one of copper which is 8900 kg/m³ **(TE: CgDensity = 8900 kg/m³) (TE: ERDensity = 8900 kg/m³)**.

1.6. Yoke radii

The permissible flux density $B_y \le 1{,}7$**I**1.8 T determines the thickness of the stator and rotor back.
For stator:

$$h_{ys} = \frac{\Phi_\delta \cdot (1+\sigma_s)/2}{l_{Fe} \cdot k_{Fe} \cdot B_{ys}} = \frac{82.4 \cdot 10^{-3} \cdot (1+0.04)/2}{0.378 \cdot 0.95 \cdot 1.8} \cong 70 \text{ mm},$$

value which can be increased according to motor performances. Let's accept: $h_{ys} = 77$ mm.
Recalculate value of stator maximum flux density:

$$B_{ys} = \frac{\Phi_\delta \cdot (1+\sigma_s)/2}{h_{ys} \cdot l_{Fe} \cdot k_{Fe}} = 1.54 \text{ T}$$

The stator outer diameter results:

$$d_{so} = d_{si} + 2l_{ds} + 2h_{ys} = 458 + 2 \cdot 69 + 2 \cdot 77 = 750 \text{ mm}$$ **(OE: Rad3= 375 mm)**

Without flux penetration in shaft, the rotor height back is:

$$h_{yr} = \left[d_{si} - 2\delta - 2l_{dr} - d_{ri}\right]/2 = \left[458 - 2 \cdot 1.4 - 2 \cdot 43.5 - 200\right]/2 = 84.1 \text{ mm}$$

For axial cooling four ducts with a diameter of $c_2 = 30$ mm it results: **(OE: NumHoles = 4)**

$$h_{yr,e} = h_{yr} - (2/3) \cdot c_2 = 84.1 - 2/3 \cdot 30 = 64.1 \text{ mm}$$ **(OE: HoleDia=30 mm)**

The radius for the circle, on which the axial cooling ducts lie (pitch circle), is is set to 286.5 mm **(OE: PCDia = 286.5 mm)**.

Rotor maximum yoke flux density is:

$$B_{yr} = \frac{\Phi_\delta/2}{h_{yr,e} \cdot l_{Fe} \cdot k_{Fe}} = \frac{(2/\pi) \cdot B_{\delta,\nu=1} \cdot \tau_p \cdot l_e/2}{h_{yr,e} \cdot l_{Fe} \cdot k_{Fe}} = 1.85 \text{ T}$$

In the reality this value will be much smaller due to the shaft presence (see [1]) and a round cooling duct with $c_2 = 30$ mm may be accepted.

Now all values for the calculation of the machine with the PC-IMD program are available!

In Fig. A2-2 the geometry of the induction machine is given, as it has been generated by SPEED, with details of the stator and rotor slots.

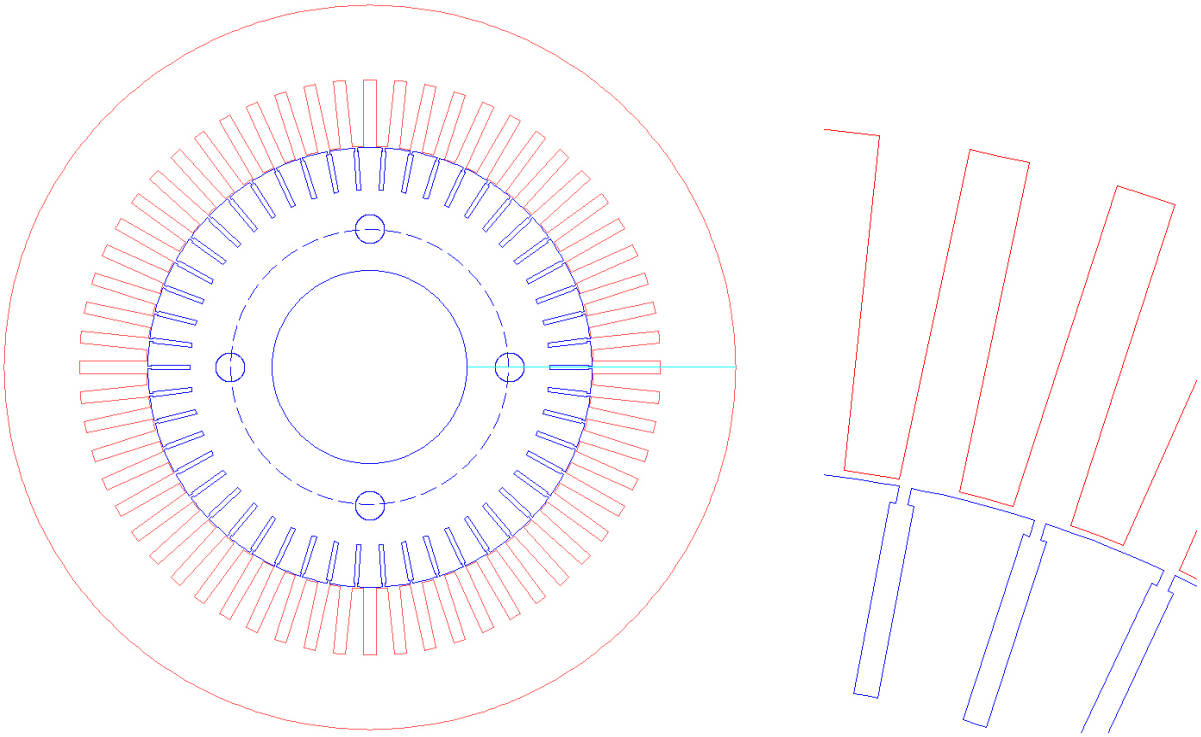

Fig. A2-2: Geometry of 500kW induction machine

1.7 Setting of calculation methods

Before performing the calculation several calculation method settings for simulation have to be set.

Table A2-9: Calculation method settings

Method of calculating X_{diff}	SPEED	**TE: DiffLeak = SPEED**
End-winding leakage reactance calculation method:	*R. Richter*	**TE: EndLeak = RICHTER**
Method of calculating deep-bar factors	Classical	**TE: DeepBar = Classical**
Component of (rotor side) *Carter* factor		**TE: qC_R = 1 (for semi-closed slots)**
Method for calculating iron losses	SPEED	**TE: WFeCalc: SPEED**

2. Numerical computation of machine performances

For a better understanding, all the values, which are necessary for the input into the program, are again presented in Fig. A2-3 to A2-5.

The calculated values for power factor (**P.F.**), torque (**TorqSh**), current densities (**Jrms**, **Jrotor**) etc., are located in design sheets. Beside the specification of a desired power (the program calculates then the associated slip) it is also possible to perform calculations for a given slip value. For this the parameter **CalcMode** (Figure1, Control Parameters) must be changed of **f/PowerSh** on

f/slip and the appropriate slip (**Slip**) to be entered. Thus starting current / rated current ratios can be determined. The ratio pull-out torque / rated torque (**TBrkpu**) can be directly read! Are all values within the demanded range, the recalculation of the design with the values supplied by the program is to be performed.

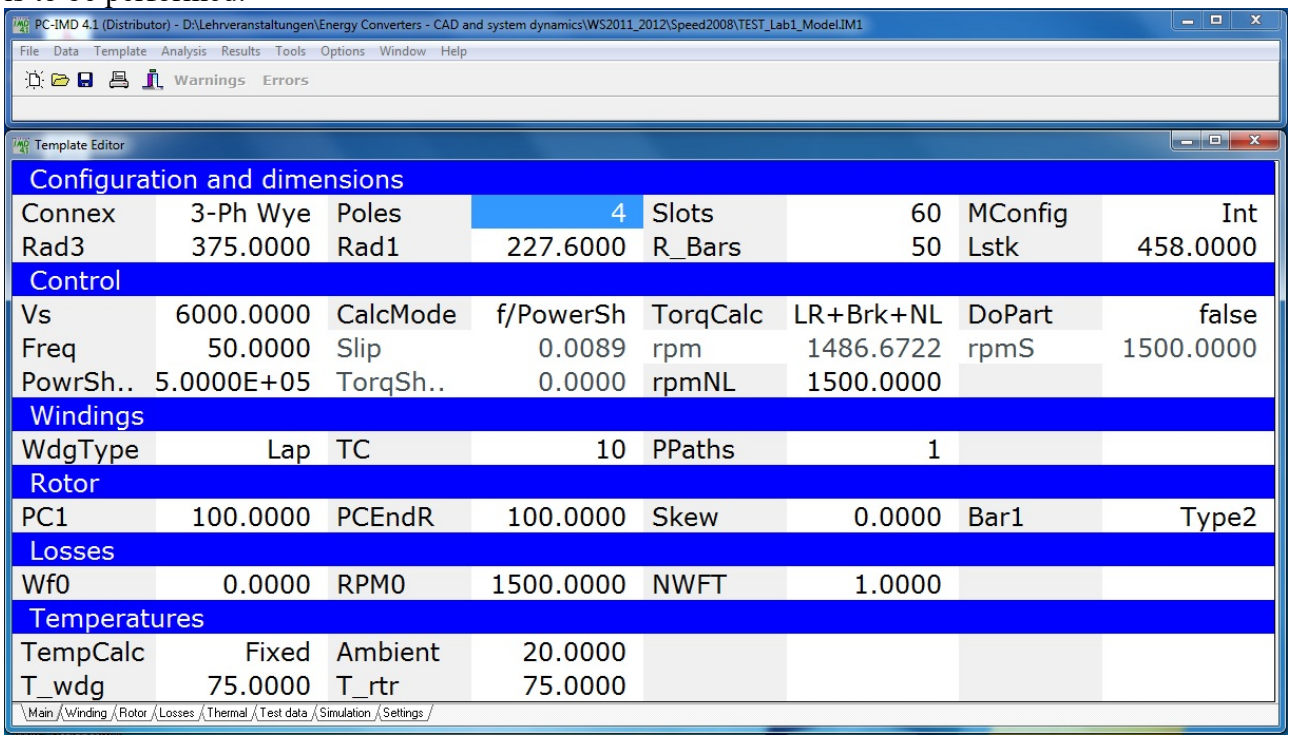

Fig. A2-3: Template Editor: Main specifications

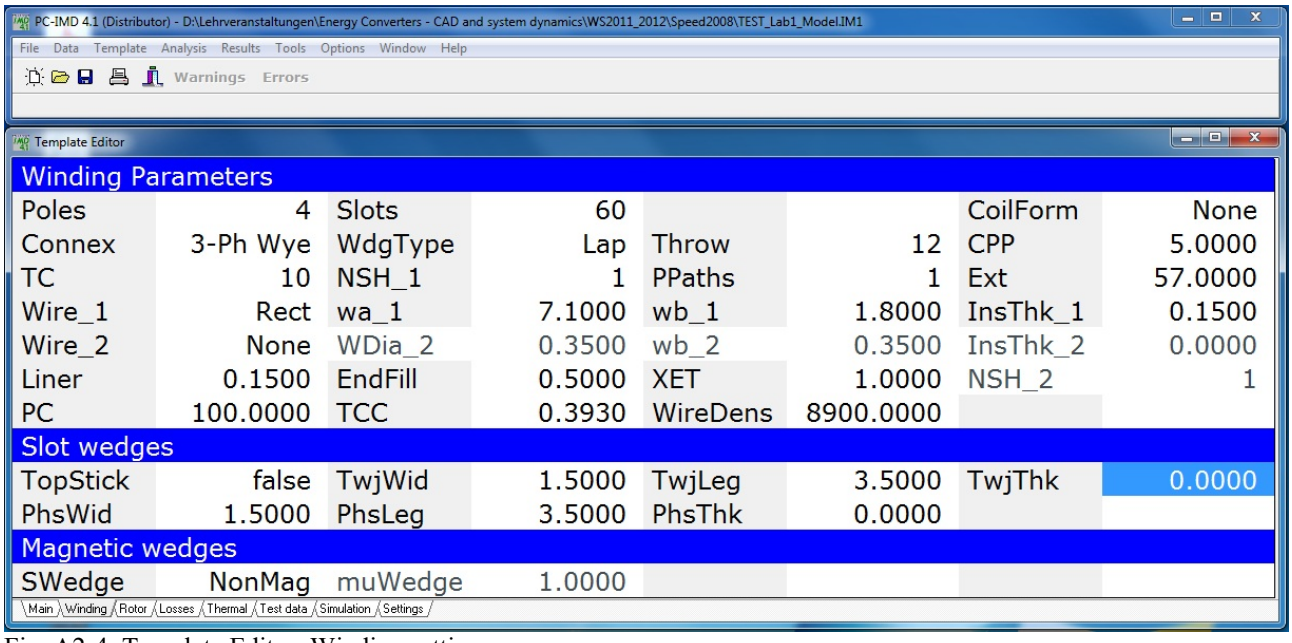

Fig. A2-4: Template Editor: Winding settings

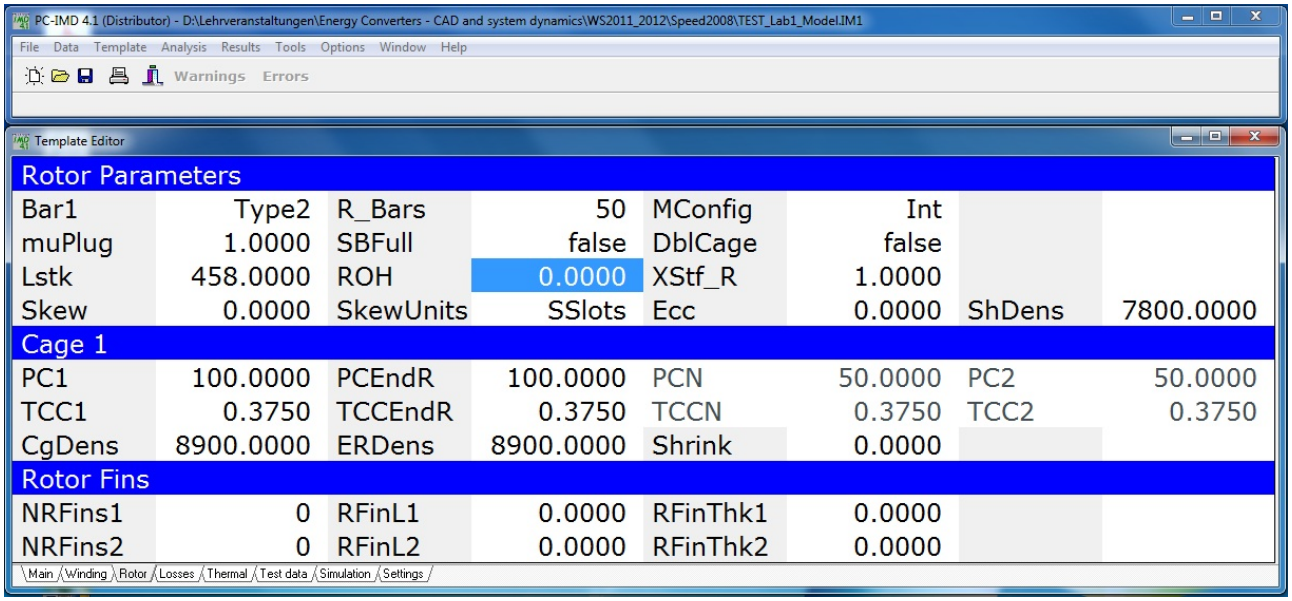

Fig. A2-5: Template editor: Rotor settings

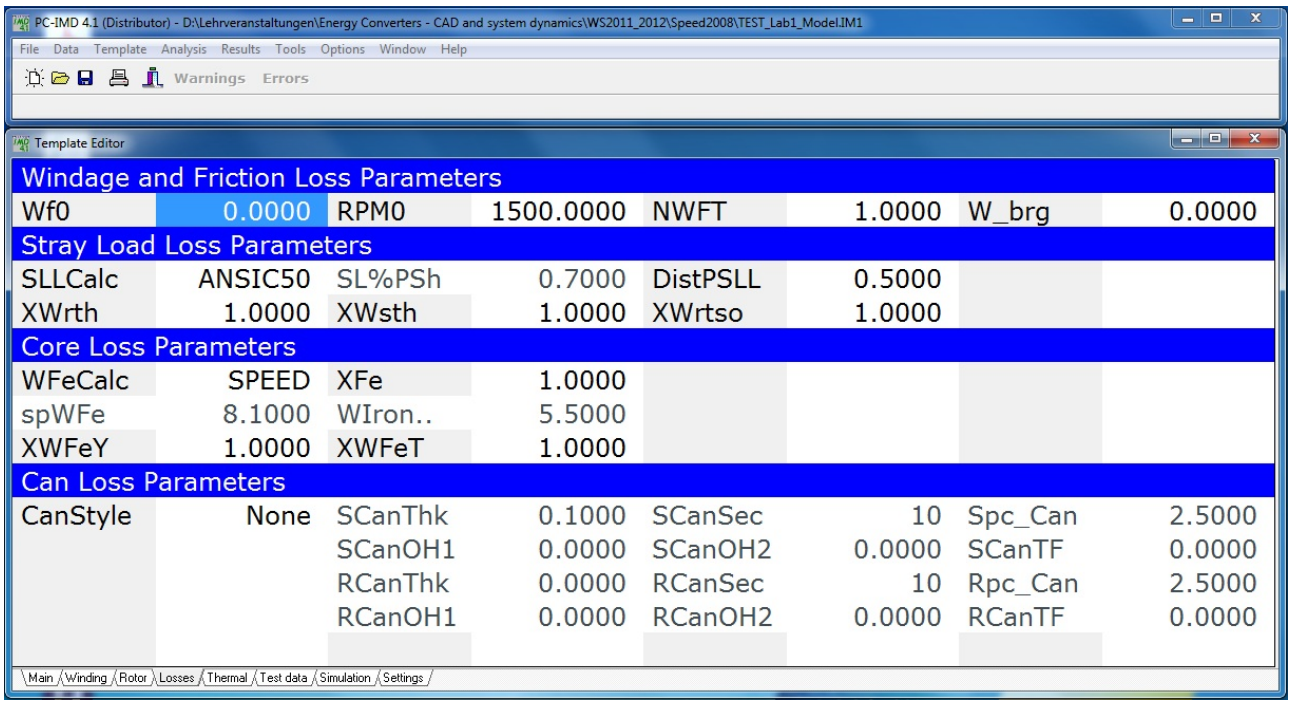

Fig. A2-6: Template editor: Loss calculation settings

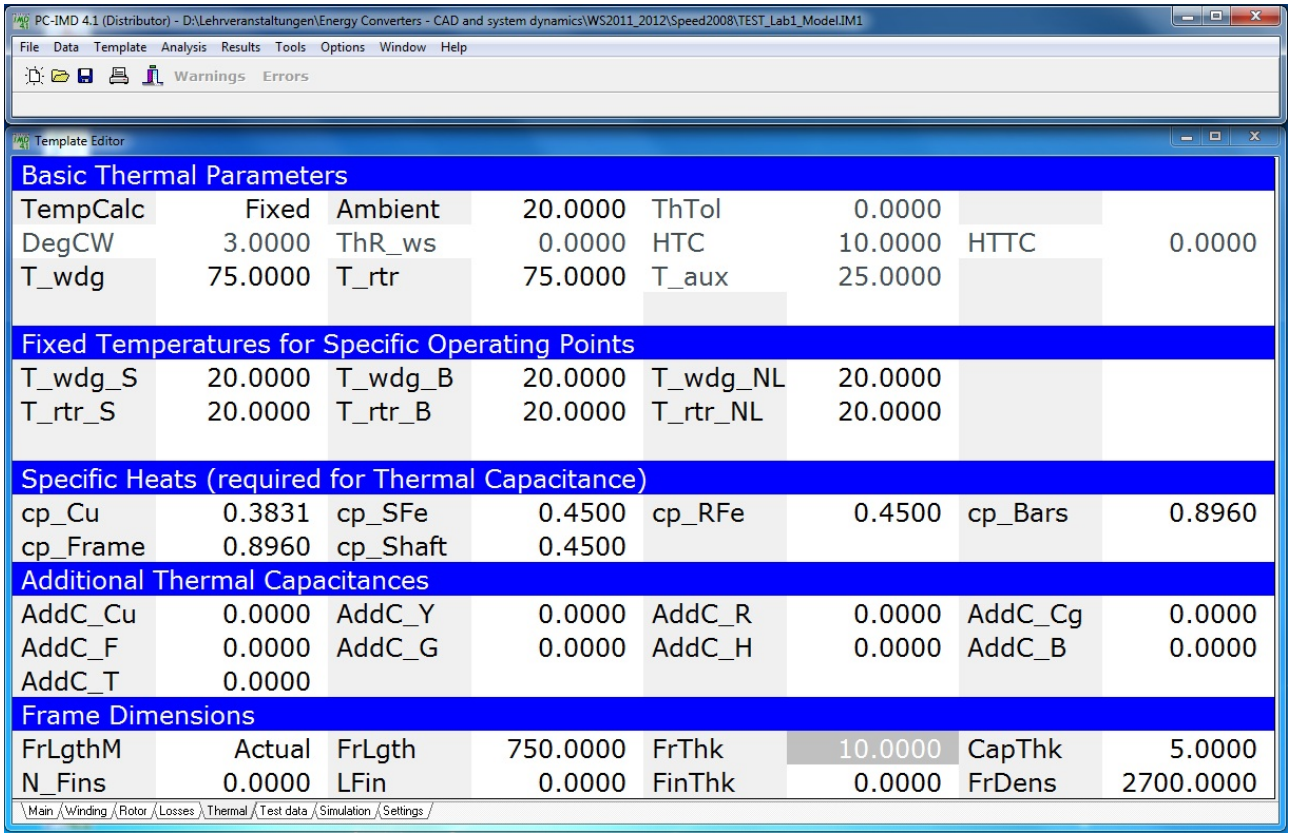

Fig. A2-7: Template editor: Thermal calculation settings

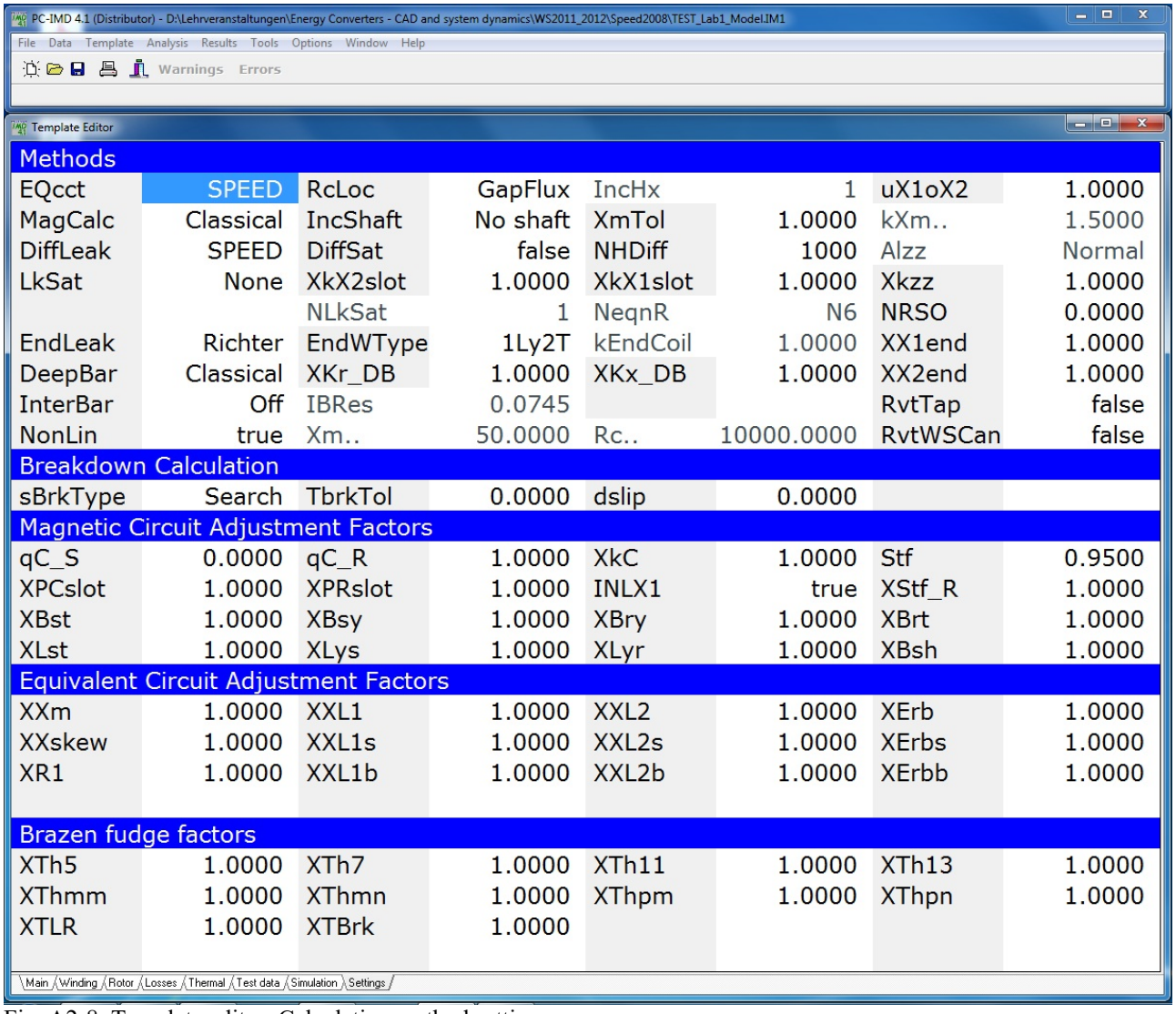

Fig. A2-8: Template editor: Calculation method settings

Make sure that the correct material curves are loaded:

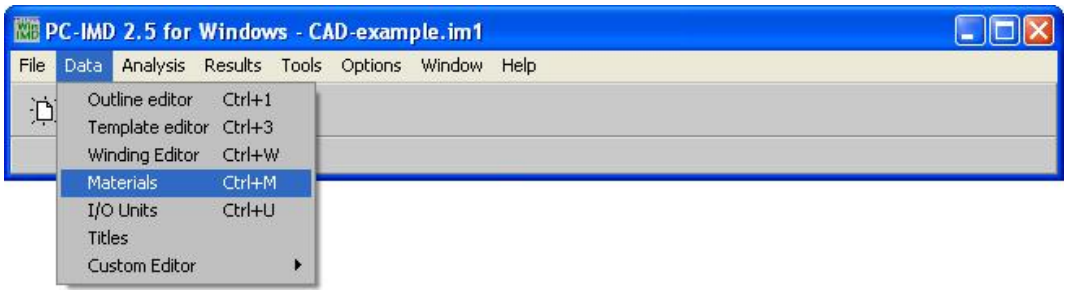

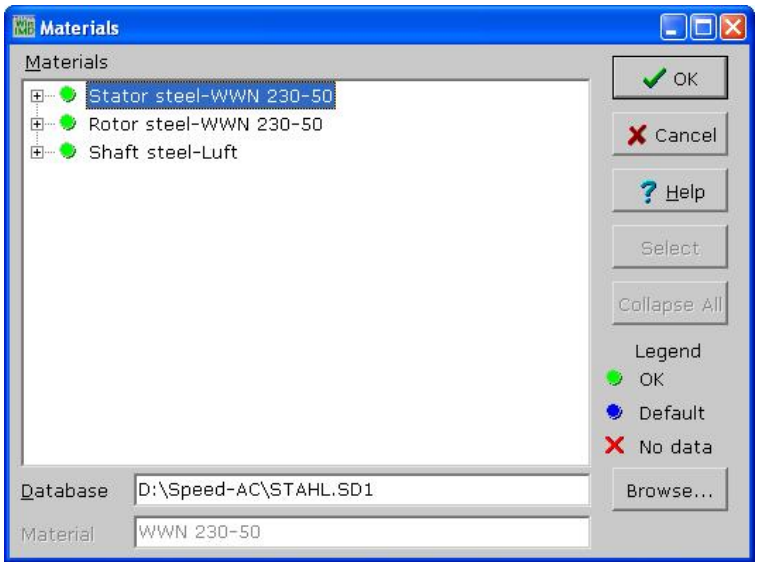

After all settings were made, start the calculation by clicking on **Steady State analysis**:

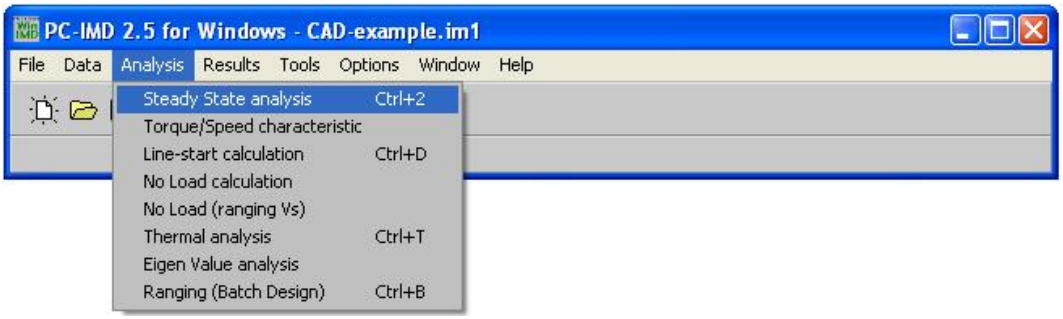

Finally see the calculation results in the **Design sheet**:

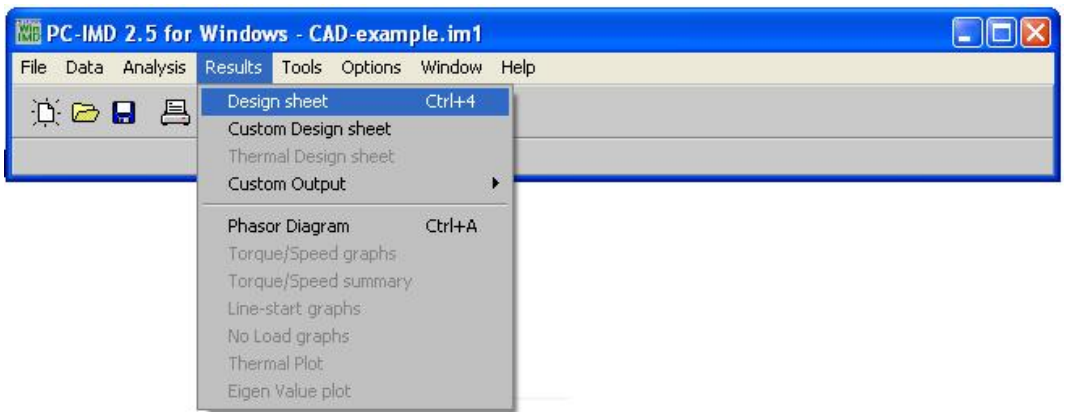

PC-IMD 4.1 (4.1.1.26) 26-Sep-2011 15:55:15
TU Darmstadt IEE

PC-IMD Design sheet

1 Dimensions : ----------

Slots	60		Poles	4		Lstk	458.0000	mm
StatorOD	750.0000	mm	RotorOD	455.2000	mm	Gap	1.4000	mm
StatorID	458.0000	mm	RotorID	200.0000	mm	MConfig	Int	

STATOR..

Rad3	375.0000	mm	R1g	229.0000	mm			
S-slot	PllSlot		ASlot	863.5539	mm^2	ASlotLL	839.0786	mm^2
SD_S	69.0000	mm	SWid	12.5000	mm	TGD_S	1.0000E-03	mm
STOH	0.0000	mm	SBWid	12.5000	mm	SYoke	77.0000	mm
NSDuct	8		WSDuct	10.0000	mm	LFeS	359.1000	mm
SWedge	NonMag		muWedge	1.0000				

ROTOR..

Rad1	227.6000	mm	Rad0	0.0000	mm	RadSh	100.0000	mm
Bar1	Type2		R_Bars	50		DblCage	false	
Skew	0.0000	SSlots	LB	458.0000	mm	BarExt	0.0000	mm
ARslot	208.7557	mm^2	Abar	200.0000	mm^2	Shrink	0.0000	
muPlug	1.0000		SBFull	false		RYoke	84.0966	mm

Rotor slot dimensions..

BarDpth	40.0000	mm	BarWdth	5.0000	mm	SO_R	2.5000	mm
SetBack	3.5000	mm						
Dbar	411.6966	mm						

Rotor end-rings and fins..

ERType1	Type C							
ERType2	Type C							
ERLedge1	0.0000	mm	ERthk1	20.0000	mm	ERID1	368.1931	mm
ERLedge2	0.0000	mm	ERthk2	20.0000	mm	ERID2	368.1931	mm
ERArea1	800.0697	mm^2	ERArea2	800.0697	mm^2	EROD	448.2001	mm
NRDuct	8		WRDuct	10.0000	mm			
ROH	0.0000	mm	LFeR	359.1000	mm			

Shaft..

RadSh	100.0000	mm	RadSh2	4.8000	mm	RadSh3	3.6000	mm
AxExSh1	0.0000	mm	AxExSh2	0.0000	mm	AxExSh3	0.0000	mm

Stacking factors..

Stf	0.9500		XStf_R	1.0000				

2 Winding Data : ----------

General

Connex	3-Ph Wye							
PC	100.0000	%Cu	TCC	0.3930	%/°C	WireDens	8900.0000	kg/m³
SFill	0.2960		SFillHBL	0.4716		ACu	255.6000	mm^2
MaxSFg	0.2960		MaxSFn	0.4716		ASlotLL	839.0786	mm^2
ACL	69006.2284	mm^2	LCL	150.6686	mm	Liner	0.1500	mm
PCSlot	1.8401		XPCslot	1.0000				
EndFill	0.5000		LaxPack	712.0051	mm	LAYERS	2.0000	
Ax1md	54.0000	mDeg	Ax2md	114.0000	mDeg	Ax3md	174.0000	mDeg

Stator winding..

WdgType	Lap		T_wdg	75.0000	°C	RLL_Amb	1.1800	ohm
Throw	12		CPP	5.0000		TC	10	
Tph	200.0000		PPaths	1		Tph1	181.9708	
MLT	2186.8835	mm	XET	1.0000		Ext	57.0000	mm

Wire_1	Rect						
wa_1	7.1000	mm					
wb_1	1.8000	mm					
NSH_1	1		EWG	40.3386			
BWDia_1	4.0339	mm	EWDia	4.0339	mm		
BWArea_1	12.7800	mm^2	ACond	12.7800	mm^2		
InsThk_1	0.1500	mm					
HBWDia_1	4.4482	mm					

Winding factors..

kw1	0.9099		kw3	-0.3804		kw5	0.0000
kw7	-0.0878		kw9	0.2351		kw11	-0.1041
kw13	-0.0601		kw15	0.0000		kw17	0.0601
kw19	0.1041		kw21	-0.2351		kw23	0.0878
ks1	1.0000		kr_RS	7947.2112		zSlot	20

Rotor cage

CgDens	8900.0000	kg/m³	ERDens	8900.0000	kg/m³	SBFull	false
PC1	100.0000	%Cu	TCC1	0.3750	%/°C	RhoBar	2.0796E-08 ohm-m
PCEndR	100.0000	%Cu	TCCEndR	0.3750	%/°C	RhoEndR	2.0796E-08 ohm-m
Kring1	0.9619		Kring2	0.9619			
PRSlot	4.1267		XPRslot	1.0000			

3 Control Data :

CalcMode	f/PowerSh						
Freq	50.0000	Hz	PowrSh..	5.0000E+05	W		
rpmS	1500.0000	rpm	rpm	1486.6834	rpm	Slip	0.0089 p.u.
Vs	6000.0000	V	Drive	AC_Volts			

4 Magnetic design :

SSteel	WWN 230-50						
RSteel	WWN 230-50						
ShSteel	Luft						
MagCalc	Classical		XBst	1.0000		XBrt	1.0000
XBsy	1.0000		XBry	1.0000		XBsh	1.0000
						IncShaft	No shaft
PPitch	359.7124	mm	Ag	0.0000	mm^2	Lge	2.7881 mm
qC_S	0.0000		qC_R	1.0000		XkC	1.0000
kC_s	1.5018		kC_r	1.0372		kC	1.9915
kC_sd	1.1307		kC_rd	1.1307			
muPlug	1.0000		PCplug	1.4000			
Bstpk	2.0330	T	ATst	733.9806	A	MMFst	0.4328 p.u.
Brtpk	1.3280	T	Atrt	35.2505	A	MMFrt	0.0208 p.u.
Bsypk	1.4496	T	ATsy	95.8747	A	MMFsy	0.0565 p.u.
Brypk	1.3273	T	ATry	28.1934	A	MMFry	0.0166 p.u.
Bshpk	0.0000	T	ATsh	0.0000	A	MMFsh	0.0000 p.u.
Bg1L	0.7643	T	ATgap	1695.8217	A	kXm	1.5268
Bgm	0.4866	T	Bgpk	0.7643	T	Phi1L	80.1649 mWb

5 Equivalent circuit parameters :

R1	0.7175	ohm	X1	6.6658	ohm	X1unsat	6.6658 ohm
R2	0.5418	ohm	X2	6.4149	ohm	X2unsat	6.4149 ohm
Rc	9207.5856	ohm	Xm0	234.8003	ohm	Xm	158.3289 ohm
Rbar	0.3791	ohm	REndRing	0.1627	ohm	Erb	0.0000 V
R_rotor	6.8174E-05	ohm	X_rotor	8.0719E-04	ohm	XErb	1.0000
EQcct	SPEED		RcLoc	GapFlux			
DeepBar	Classical		K_r	1.0016		K_x	0.9996
			XKr_DB	1.0000		XKx_DB	1.0000
EndLeak	Richter		CoilFill	1.0000		kEndCoil	1.0000
			XX1end	1.0000		XX2end	1.0000

DiffLeak	SPEED	NHDiff	1000	DiffSat	false
LkSat	None	kXL1	1.0000	kXL2	1.0000
kzz	1.0000	kX1slot	1.0000	kX2slot	1.0000
Xkzz	1.0000	XkX1slot	1.0000	XkX2slot	1.0000
XXm	1.0000	XXL1	1.0000	XXL2	1.0000

Unsaturated reactance components..

X1slot	1.8672 ohm	X1end	4.5180 ohm	X1diff	0.2806 ohm
X2slot	4.8918 ohm	X2end	1.2782 ohm	X2diff	0.2448 ohm

L-circuit parameters..

alpha_TL	1.0405	uX1oX2	1.0000	X1oX2	1.0391
XL_L	13.8811 ohm	Rc_L	9968.8143 ohm		
R2_L	0.5866 ohm	Xm_L	164.7438 ohm		

6 Performance : ----------

OpMode	Motoring				
Vt	6000.0000 V	rpm	1486.6834 rpm	Slip	0.0089 p.u.
Pshaft	4.9997E+05 W	PElec	5.2140E+05 W	Tshaft	3211.4200 Nm
PshaftHP	670.4711 h.p.	P.F.	0.8552	Effcy	95.8893 %
		WTotal	21435.0875 W	Eff_X_PF	82.0084 %

Currents..

Iph1	58.6643 A rms	IL1	58.6643 A rms	I2	52.8085 A
Imc	20.4703 A	IMag	20.4673 A	Ic	0.3519 A

Equivalent circuit voltages..

E1	3240.5650 V	VR1	42.0943 V	VX1	391.0422 V
ER2	3194.1983 V	VR2	28.6113 V	VX2	338.7613 V

Losses and related parameters..

WCuS	7408.3039 W	WCuR	4532.7666 W	WIron	3421.5033 W
SLLCalc	ANSIC50	WSLL	6072.5137 W	Wwf	0.0000 W
Jrms	4.5903 A/mm^2				
JBar1	5.7658 A/mm^2	J_ER	5.7499 A/mm^2	JRotor	5.7329 A/mm^2

Other performance parameters..

PGap	5.1058E+05 W	EMTorque	3250.4251 Nm		

Locked-rotor..

TLR	3219.1352 Nm	TLRpu	1.0024	sLR	1.0000 p.u.
ILR	343.5242 A	ILRpu	5.8558	PFLR	0.2002
PLR	7.1454E+05 W				
pTWdg	3.6533 C/sec	pTBar	9.5613 C/sec		
C_Cu	57.1755 kJ/C	C_cage	52.8862 kJ/C		
T_wdg_S	20.0000 °C	T_rtr_S	20.0000 °C		
XXL1s	1.0000	XXL2s	1.0000	XErbs	1.0000

Breakdown..

TBrk	7958.7126 Nm	TBrkpu	2.4783	sBrk	0.0363 p.u.
IBrk	187.9838 A	IBrkpu	3.2044	PFBrk	0.6809
rpmBrk	1445.6086 rpm	PBrk	1.3302E+06 W		
T_wdg_B	20.0000 °C	T_rtr_B	20.0000 °C	sBrkType	Search
XXL1b	1.0000	XXL2b	1.0000	XErbb	1.0000

No-load..

INL	22.0592 A	NLTorque	0.0000 Nm	NLPF	0.0193
INLpu	0.3760	TNLpu	0.0000	NLrpm	1500.0000 rpm
T_wdg_NL	20.0000 °C	T_rtr_NL	20.0000 °C	rpmNL	1500.0000 rpm
PNL	4418.0537 W	XLL_NL	314.0145 ohm	INLX1	true

Test data..

Wrated	0.0000 W	Irated	0.0000 A		

V_Test	6000.0000	V	I_Test	0.0000	A	P_Test	0.0000	W
s_Test	0.0000		T1_Test	20.0000	°C	T2_Test	20.0000	°C

7 Core losses, Harmonic losses, and Stray Load Losses : ----------

WFe0S	3.5086	W/kg	WFe0R	3.5086	W/kg	WFe0Sh	3.6719	W/kg
WFeS	3414.1815	W	WFeSe	884.0935	W	WFeSh	2530.0879	W
Wst	1702.4924	W	Wste	457.9210	W	Wsth	1244.5715	W
Wsy	1711.6891	W	Wsye	426.1726	W	Wsyh	1285.5165	W
WstWkg	6.0128	W/kg	WsyWkg	3.3026	W/kg			
WFeR	7.3218	W	WFeRe	0.0209	W	WFeRh	7.3009	W
Wrt	2.7773	W	Wrte	0.0079	W	Wrth	2.7694	W
Wry	4.5445	W	Wrye	0.0130	W	Wryh	4.5315	W
WrtWkg	0.0190	W/kg	WryWkg	0.0190	W/kg			
WFeCalc	SPEED		XFe	1.0000		Bd_slot	0.5951	T

8 Thermal data : ----------

TempCalc	Fixed		HeatFlux	7.7389	kW/m²	TempRise	55.0000	°C
Ambient	20.0000	°C						
T_wdg	75.0000	°C	T_rtr	75.0000	°C			

9 Miscellaneous parameters : ----------

Wt_Cu	149.2443	kg	Wt_Fe	1092.8759	kg	Wt_Tot	1301.1450	kg
WtFeS	717.0246	kg	WtFeR	375.8514	kg			
WtFesy	518.2904	kg	WtFest	198.7318	kg	WtTri	84.4109	kg
Wt_Al	59.0248	kg	WtAl_RB	40.7620	kg	WtAl_ER	18.2628	kg
WtShaft	183.7832	kg						
RotJ	13.9842	kg-m²	JL	0.0000	p.u.	JFan	0.0000	p.u.
C_cage	52.8862	kJ/C	C_main	57.1755	kJ/C			
WtFrame	54.0323	kg	WtCap	2.8416	kg			
Ecc	0.0000		UMP	2.0010E-13	kg			
FrThk	10.0000	mm	LFrame	750.0000	mm	CapThk	5.0000	mm
FrLgthM	Actual		FrLgth	750.0000	mm			
TRV	43086.1054	Nm/m3	T/Wt	2.4681	Nm/kg	P/Wt	384.2541	W/kg
Wf0	0.0000	W	RPM0	1500.0000	rpm	NWFT	1.0000	
CanStyle	None							
NumHoles	4		PCDia	286.5000	mm	HoleDia	30.0000	mm
RTC_OC	2.0256	sec	RTC_SC	0.1083	sec			

End of Design sheet----------

3. Program SPEED – Exercise example

1) The number of turns per coil will be decreased from 10 to 9. Decreasing the number of turns per coil allows increasing the cross-section of cupper (h_L from 1.8 mm to 2 mm). Calculate the new motor impedances, the starting current and the starting torque! Do the motor impedances change? How do starting torque and current vary in comparison to the initial data?

2) How do the air-gap induction, the primary current at rated slip and the electric loading change?

References:

[1] A.Binder, *Energy Converters: CAD and System Dynamics*, Text book – TU Darmstadt, 2016
[2] A.Binder, *CAD and System Dynamics of Electrical Machines*, Text book – TU Darmstadt, 2006 ÷ 2008
[3] A.Binder, *Motor Development for Electric Drive Systems,* Text book – TU Darmstadt, 2016
[4] A.Binder, *CAD and System Dynamics of Electrical Machines,* Tutorial for Exercises – TU Darmstadt, 2016
[5] A.Binder, *Energy Converters: CAD and System Dynamics,* Tutorial for Exercise – TU Darmstadt, 2009

[6] ****, *User's Manual for PC-IMD 2.5*, University of Glasgow, 1998
[7] A.Binder, M. Aoulkadi, *CAD and System Dynamics of Electrical Machines: Design of an Asynchronous Machine*, Tutorial for Exercise, 2006
[8] O.Magdun, A.Binder, *Energy Converters - Asynchronous Machine*, Guide for Computer Aided Design, 2009

Abbreviations in the Program SPEED module PC-IMD

	Symbol		Unit	Denotation	
Dimensional	BarDpth	h_r	mm	Rotorbar depth	Leiterhöhe des Rotorstabes
	BarWdth	b_r	mm	Rotorbar width	Leiterbreite des Rotorstabes
	ERLedge		mm	Additional endring length	Zusätzliche radiale Endringlänge
	Erthk		mm	Endring thickness	Endringdicke (1=linker, 2=rechter)
	Gap	δ	mm	Airgap length	Luftspaltweite
	Lstk	l	mm	Rotor and Stator stack length	Blechpaketlänge
	Poles	p	-	Number of Poles	Polzahl
	RadSh		mm	Shaft radius	Radius der Welle
	R-Bars	Q_r	-	Number of rotor bars or slots	Rotornutzahl
	SD-S	h_S	mm	Stator slot depth	Statornuttiefe
	SetBack		mm	Set-Back	Rotorstreusteghöhe
	Skew	k_{sq}	-	Rotor skew	Schrägung des Rotors um x – Nuten
	Slots	Q_s	-	Number of stator slots	Statornutzahl
	SO-R		mm	Rotor slot opening	Nutöffnung Rotor
	SO-S		mm	Stator slot opening	Nutöffnung Stator
	S-slot		-	Shape of Stator slot bottom	Statornutform
	Stf	k_{Fe}	-	Stacking factor	Stapelfaktor
	TGD-R		mm	Rotor tang depth	Streusteghöhe Rotor
	TGD-S		mm	Stator tang depth	Streusteghöhe Stator
	TW-S	b_{ds}	mm	Stator tooth width	Statorzahnbreite
Winding	Connex		-	Winding connection	Anschlussart
	Coils/P	q	-	Number of coils per pole	Nuten je Pol und Strang
	Ext		mm	Winding extension at each end	Gerader Leiter außerhalb Eisen
	LAYERS		-	Number of layers	Anzahl der Spulenlagen pro Nut
	Liner		mm	Thickness of stator slot-liner	Dicke der Nutauskleidung
	NSH	b	-	No. of strands in hand	Anzahl der parallelen Teilleiter
	PPaths	a	-	No. of parallel paths	Anzahl der parallelen Zweige
	TC	N_c	-	Turns per coil	Spulenwindungszahl
	Throw	y	-	Throw	Spulenweite
	WdgTemp	ϑ	°C	Winding temperature	Wicklungstemperatur
	WdgType		-	Type of winding	Wicklungsart
	Wire		mm	Wire size or gauge	Leiterdurchmesser
Control	Freq	f	Hz	Fundamental line frequency	Speisefrequenz
	rpm	n	min^{-1}	Actual shaft speed	Drehzahl
	rpmS	n_S	min^{-1}	Synchronous speed	Synchrondrehzahl
	Slip	s	-	Slip	Schlupf
	Vs	U	V	RMS AC line voltage	Spannung

Magnetic	Bg1L	$B_{\delta 1}$	T	Peak fundamental flux-density	Maximalwert Luftspaltflussdichte
	Bgm	$B_{\delta av}$	T	Mean airgap flux-density	Mittlere Luftspalt Flussdichte
	Bstpk	B_{ds}	T	Peak Stator tooth flux-density	Statorzahn Flussdichte
	Brtpk	B_{dr}	T	Peak rotor tooth flux-density	Rotorzahn Flussdichte
	Bsypk	B_{ys}	T	Peak stator yoke flux-density	Statorrücken Flussdichte
	Brypk	B_{yr}	T	Peak rotor yoke flux-density	Rotorrücken Flussdichte
	Bshpk	B_s	T	Peak shaft flux-density	Rotorwelle Flussdichte
	KC_s	k_{Cs}	-	Carter coefficient for stator slot	CARTER-Faktor
Equivalent	R1	R_s	Ω	Primary resistance/phase	Statorwiderstand
	R2	R_r	Ω	Secondary resistance/phase	Rotorwiderstand
	X1	$X_{\sigma s}$	Ω	Primary stray reactance	Statorstreureaktanz
	X2	$X_{\sigma r}$	Ω	Secondary stray reactance	Rotorstreureaktanz
	Xm	X_{hges}	Ω	Saturated magnetising reactance	Hauptreaktanz (gesättigt)
	Xm0	X_{hung}	Ω	Unsaturated magnetising	Hauptreaktanz (ungesättigt)
Performance	Effcy	η	%	Efficiency	Wirkungsgrad
	IL1	I	A	RMS line current	Statorstrom
	I2	I	A	Rotor current	Rotorstrom
	Imag	I_m	A	Magnetising current	Magnetisierungsstrom
	Jrms	J	A/mm^2	RMS current-density main wind.	Statorstromdichte
	Jbar1	J	A/mm^2	RMS current-density rotor cage	Rotorstabstromdichte
	P.F.	$cos\ \varphi$	-	Power factor	Leistungsfaktor cosφ
	Pelec	P_e	W	Mean electrical power	Elektrische Leistung
	PowerSh	P_m	W	Shaft power	Mech. Leistung
	TbrkR	m_b	-	Ratio Breakdown/rated Torque	Verhältnis Kipp-/Nennmoment
	WcuR	P_{Cur}	W	Rotor copper losses	Kupferverluste Rotor
	WcuS	P_{Cus}	W	Stator copper losses	Kupferverluste Stator
	Wiron	P_{Fe}	W	Iron (Core) loss	Eisenverluste
	Wwf	P_R	W	Windage and friction loss	Ventilations- & Reibungsverluste
Core Loss	WFeS	P_{Fes}	W	Stator Iron (Core) loss	Eisenverluste Stator
	WFeR	P_{Fer}	W	Rotor Iron (Core) loss	Eisenverluste Rotor
	WstWkg		W/kg	Specific stator teeth core losses	Spezifische Stator-Zahn Eisenverluste
	WsyWkg		W/kg	Specific stator yoke core losses	Spezifische Stator-Joch Eisenverluste
Miscellaneous	RPM0	n_0	min^{-1}	Shaft speed at no load	Leerlaufdrehzahl
	Wt_Al	m_r	kg	Weight of rotor cage	Gewicht Rotorkäfig
	Wt_Cu	m_s	kg	Weight of copper in stator wind.	Wicklungsgewicht Stator
	Wt_Fe	m	kg	Weight of iron stator / rotor lams	Gesamteisengewicht Stator/Rotor
	Wt_Tot	m	kg	Total active weight	Gesamtgewicht (Al+Cu+Fe)
	Wf0	P_R	W	Windage and friction loss	Ventilations- & Reibungsverluste
Thermal	Ambient	ϑ_a	°C	Ambient	Umgebungstemperatur
	RoTemp	ϑ_r	°C	Rotor cage temperature	Rotortemperatur
	TempCalc			Temperature calculating method	Temperatur-Berechnungsmethode
	WdgTemp	ϑ_{Wi}	°C	Stator winding temperature	Wicklungstemperatur Stator
	Rad1		mm	Rotor surface Radius	Außenradius des Läufers
	Rad3		mm	Stator outer radius	Außenradius Stator
	R-Cage		-	Rotor-cage	Nutform des Rotors